SHOUT
SHARE
IT

4890

HARVARD UNIVERSITY

Library of the
Museum of
Comparative Zoology

Bulletin OF THE
Museum of
Comparative
Zoology

Studies in Organismic and Evolutionary Biology in honor of A. W. Crompton

MCZ
LIBRARY

FEB 22 2002

HARVARD
UNIVERSITY

Farish A. Jenkins, Jr.,
Michael D. Shapiro,
and
Tomasz Owerkowicz
Editors

HARVARD UNIVERSITY
CAMBRIDGE, MASSACHUSETTS, U.S.A.

VOLUME 156, NUMBER 1
10 OCTOBER 2001

PUBLICATIONS ISSUED OR DISTRIBUTED BY THE MUSEUM OF COMPARATIVE ZOOLOGY HARVARD UNIVERSITY

Breviora 1952–
Bulletin 1863–
Memoirs 1865–1938
Johnsonia, Department of Mollusks, 1941–1974
Occasional Papers on Mollusks, 1945–

SPECIAL PUBLICATIONS.

1. Whittington, H. B., and W. D. I. Rolfe (eds.), 1963 Phylogeny and Evolution of Crustacea. 192 pp.
2. Turner, R. D., 1966. A Survey and illustrated Catalogue of the Teredinidea (Mollusca: Bivalvia). 265 pp.
3. Sprinkle, J., 1973. Morphology and Evolution of Blastozoan Echinoderms. 284 pp.
4. Eaton, R. J., 1974. A Flora of Concord from Thoreau's Time to the Present Day. 236 pp.
5. Rhodin, A. G. J., and K. Miyata (eds.), 1983. Advances in Herpetology and Evolutionary Biology: Essays in Honor of Ernest E. Williams. 725 pp.
6. Angelo, R., 1990. Concord Area Trees and Shrubs. 118 pp.

Other Publications.

Bigelow, H. B., and W. C. Schroeder, 1953. Fishes of the Gulf of Maine. Reprinted 1964.

Brues, C.T., A. L. Melander, and F. M. Carpenter, 1954. Classification of Insects. (*Bulletin of the M. C. Z.*, Vol. 108.) Reprinted 1971.

Creighton, W. S., 1950. The Ants of North America. Reprinted 1966.

Lyman, C. P., and A. R. Dawe (eds.), 1960. Proceedings of the First International Symposium on Natural Mammalian Hibernation. (*Bulletin of the M. C. Z.*, Vol. 124.)

Ornithological Gazetteers of the Neotropics (1975–).

Peter's Check-list of Birds of the World, vols. 1–16.

Proceedings of the New England Zoological Club 1899–1947. (Complete sets only.)

Proceedings of the Boston Society of Natural History.

Price list and catalog of MCZ publications may be obtained from Publications Office, Museum of Comparative Zoology, Harvard University, Cambridge, Massachusetts 02138, U.S.A.

This publication has been printed on acid-free permanent paper stock.

© The President and Fellows of Harvard College 2001.

STUDIES IN ORGANISMIC AND EVOLUTIONARY BIOLOGY IN HONOR OF A. W. CROMPTON

FARISH A. JENKINS, JR., MICHAEL D. SHAPIRO, AND TOMASZ OWERKOWICZ, EDITORS

CONTENTS

Introduction 1

A Probainognathian Cynodont from South Africa and the Phylogeny of Nonmammalian Cynodonts. By James A. Hopson and James W. Kitching 5

On *Microconodon*, a Late Triassic Cynodont from the Newark Supergroup of Eastern North America. By Hans-Dieter Sues 37

A Cynodont from the Upper Triassic of East Greenland: Tooth Replacement and Double-Rootedness. By Michael D. Shapiro and Farish A. Jenkins, Jr. 49

On Two Advanced Carnivorous Cynodonts from the Late Triassic of Southern Brazil. By José F. Bonaparte and Mario Costa Barberena 59

The Inner Ear and Its Bony Housing in Tritylodontids and Implications for Evolution of the Mammalian Ear. By Zhexi Luo 81

A New Specimen and a Functional Reassociation of the Molar Dentition of *Batodon tenuis* (Placentalia, Incertae Sedis), Latest Cretaceous (Lancian), North America. By Craig B. Wood and William A. Clemens 99

The Evolution of Mammalian Development. By Kathleen K. Smith 119

Skin Impressions of Triassic Theropods as Records of Foot Movement. By Stephen M. Gatesy 137

A Diminutive Pterosaur (Pterosauria: Eudimorphodontidae) from the Greenlandic Triassic. By Farish A. Jenkins, Jr., Neil H. Shubin, Stephen M. Gatesy, and Kevin Padian 151

Immature Rhizondontids from the Devonian of North America. By Marcus C. Davis, Neil H. Shubin, and E. B. Daeschler 171

How Do Mysticetes Remove Prey Trapped in Baleen? By Alexander J. Werth 189

Tongue-Jaw Linkages: The Mechanisms of Feeding Revisited. By Karen M. Hiiemae and Jeffrey B. Palmer 205

Extrinsic Versus Intrinsic Lingual Muscles: A False Dichotomy? By Kurt Schwenk 219

Electromyographic Pattern of the Gular Pump in Monitor Lizards. By Tomasz Owerkowicz, Elizabeth L. Brainerd, and David R. Carrier 237

Synchronization of Electromyographic Activity in Oral Musculature During Suckling and Drinking. By A. J. Thexton and Rebecca Z. German 249

Sonomicrometry and Kinematic Estimates of the Mechanical Power of Bird Flight. By Douglas R. Warrick, Bret W. Tobalske, Andrew A. Biewener, and Kenneth P. Dial 257

Trade-off Between Modeling and Remodeling Responses to Loading in the Mammalian Limb. By Daniel E. Lieberman and Osbjorn M. Pearson 269

Muscle Force and Stress During Running in Dogs and Wild Turkeys. By Thomas J. Roberts 283

Regulation of Skeletal Muscle Regeneration and Bone Repair in Vertebrates. By Uri Oron 297

STUDIES IN ORGANISMIC AND EVOLUTIONARY BIOLOGY IN HONOR OF A. W. CROMPTON

Fuzz Crompton

INTRODUCTION

In grateful tribute to Fuzz Crompton, this volume presents papers delivered at a symposium held in Fuzz's honor on 15 May 1999 at the Museum of Comparative Zoology, Harvard University. The seemingly eclectic array of papers spans a range of subjects and approaches that constitute a challenge to any conventionally inclusive title. And yet the diversity herein is representative of the breadth of Fuzz's interests, the scope of his inspiration, and the

extent of his influence in both teaching and research. Among this volume's authors are present and former students (and students of former students), postdoctoral fellows, colleagues, and collaborators, all of whom gladly joined to celebrate his manifold contributions to organismic and evolutionary biology. Perhaps the only aspect of these proceedings not fully conveyed in these published papers was a collegiality at the symposium that spilled over into the open joviality of a reunion, an enthusiasm for science, and a delight in professional friendships that all derive from the man we honored.

Launching a career remarkable for accomplishment, Fuzz's publication record began with a paper that appeared in *Acta Zoologica* in 1953, "The development of the chondrocranium of *Spheniscus demersus* with special reference to the columella auris of birds," a product of his graduate work at Stellenbosch University. But it was with a second doctorate, completed in a stunningly short two years and under the guidance of Francis Rex Parrington, FRS, at Cambridge University, that he redirected his investigations into vertebrate paleontology, and specifically into the morphology and relationships of mammallike reptiles, and eventually into the origins of mammals. A series of classic, oft-cited papers over the next two decades made major advances in our understanding of the intricacies of dental and cranial evolution among synapsids of the Mesozoic.

Fuzz's early interests in the tangible record of vertebrate evolution soon expanded into what is now generally known as functional morphology—understanding the mechanics and other functional integrations of structural features. In a fundamental sense, as he himself so often said, he wanted to know how animals worked. Although precedents for such an approach had previously been established in vertebrate paleontology, it was Fuzz's signal contribution that he placed his analyses in the context of experimental work on extant animals. Cineradiographic and electromyographic data from living systems provided the essential tools with which to interpret the evolutionary history and transformations embedded in fossils. From his work our understanding of the tribosphenic dentition—that once fearsome array of cusps, crests, cristi, and valleys—was forever transformed. Tribosphenic teeth, no longer the statuary marking therian beginnings, became but one expression of the functional continuum in synapsid evolution. Not content with odontology explained, Fuzz's studies with his students and collaborators became ever more complex orchestrations of experimental apparatus as he elucidated the interrelationships of jaw and tongue movements, the patterns of chewing and the mechanics of jaws, the millisecond events of swallowing, and the neurobiology of that most primal of mammalian feeding patterns, suckling. Marsupials, primates, insectivores, pigs, and goats were among his subjects, but in each case the real subject was integrative biology, with results that were invariably exemplary. This integrative approach was especially emphasized in Biology 21, Structure and Physiology of the Vertebrates, a course offered by Fuzz and the late Dick Taylor for almost three decades. At the top of the scale in terms of the required workload, the experience was consistently and enthusiastically rated by students as providing the highest of intellectual returns, and a source of genuine enjoyment.

Unless we aspire to monographic lengths, we cannot adequately recount by way of gratitude all of Fuzz Crompton's contributions to science, teaching, and promoting the careers of others. And yet there is one contribution, distinctively integrative, that must appear in this permanent record of the Museum of Comparative Zoology if we are to salute him at all. During his career, which began as Curator of Palaeontology Collections in the National Museum in Bloemfontein, South Africa, Fuzz served as Director of three major museums: first at The South African

Museum, then at Yale's Peabody Museum of Natural History, and finally at the Museum of Comparative Zoology. During the course of this extensive experience he originated the concept of Professor/Curator in face of the long-standing belief, reinforced by practice, that these were separate species with different territories. On the premise that natural history museums ought not to be simply repositories, but are justifiable to the extent that they promote research and knowledge of our natural world, the conclusion is inescapable that senior museum staff must be, first and foremost, scientists of distinction. In a university setting, as a consequence, positions supported by museum resources must be professorial, with standards and expectations no less than those held for every faculty appointment. No longer would curators exist as another class of citizenry apart from academic departments. Rather, professors with administrative appointments as curators would continue to ensure the museum's growth and participation in academic research and instruction. The concepts of Professor and Curator, once a duality, became inseparably integrated. At Harvard, this legacy from Fuzz Crompton's visionary directorship persists today, to the intellectual enhancement of the Museum of Comparative Zoology, the Department of Organismic and Evolutionary Biology, and the University.

Farish A. Jenkins, Jr.
Michael D. Shapiro
Tomasz Owerkowicz

Cambridge, Massachusetts
10 April 2001

Symposium participants, 15 May 1999. From left to right, front row: Farish Jenkins, José Bonaparte, Neil Shubin, Kathleen Smith, Fuzz Crompton, Ken Dial, Nick Hotton. Second row: Jim Hopson, Christine Janis, Craig Wood, Zhexi Luo, Rebecca German, Allan Thexton, Tomasz Owerkowicz. Third row: Steve Gatesy, Dan Lieberman, Kurt Schwenk, Alex Werth, Beth Brainerd. Fourth row: Uri Oron, Mike Shapiro, Tom Roberts, Andy Biewener (photograph by Leon Claessens).

A PROBAINOGNATHIAN CYNODONT FROM SOUTH AFRICA AND THE PHYLOGENY OF NONMAMMALIAN CYNODONTS

JAMES A. HOPSON[1] AND JAMES W. KITCHING[2]

ABSTRACT. A new small cynodont from subzone B of the *Cynognathus* Assemblage Zone (earliest Middle Triassic) of South Africa is described as *Lumkuia fuzzi*. It is represented by a nearly complete skull and lower jaw, a shoulder girdle and forelimb, and articulated dorsal and caudal vertebrae. It is placed in the eucynodont clade Probainognathia on the basis of four unequivocal synapomorphies, including absence of a parietal foramen and expanded plates on the ribs and a secondary palate extending posteriorly to the level of the orbit. *Lumkuia* is the oldest and most primitive probainognathian represented by adequate material. A cladistic analysis strongly supports the monophyly of Cynodontia, Epicynodontia (a new taxon including *Galesaurus, Thrinaxodon*, and eucynodonts), and Eucynodontia. The analysis also supports the eucynodont clades Probainognathia and Cynognathia, and Gomphodontia as a subgroup of the latter. Within Probainognathia, a chiniquodontid clade and a tritheledontid + mammaliaform clade are well supported. *Probainognathus* is sister to the latter clade, but this node breaks down in trees two steps longer than the shortest tree. Tritylodontids are deeply nested within the traversodont gomphodonts, with *"Scalenodon" hirschoni* weakly supported as their sister taxon.

INTRODUCTION

The Eucynodontia (Kemp, 1982, 1988), that is, those cynodonts more derived than the basal Triassic *Thrinaxodon*, have traditionally been divided into a carnivorous line leading to mammals and a herbivorous, or gomphodont, line leading to the Jurassic tritylodontids (Crompton and Ellenberger, 1957; Crompton, 1972b; Hopson and Kitching, 1972; Sues, 1985; Hopson and Barghusen, 1986; Hopson, 1991b, 1994). However, Kemp (1982, 1983, 1988) noted that tritylodontids and mammals share many derived features that are absent in Triassic cynodonts, which led him to suggest that tritylodontids should be separated from the herbivorous cynodonts and placed in the carnivorous line close to Mammalia; the herbivorous specializations of tritylodontids thus would be convergent on those of gomphodonts. Rowe (1986, 1988, 1993) went still further in obliterating the distinction between the carnivorous and herbivorous lineages by interleaving Middle Triassic to Early Jurassic cynodonts in a paraphyletic series of carnivorous and gomphodont taxa that lead to a terminal clade Mammaliamorpha, containing tritylodontids and traditionally defined mammals (termed Mammaliaformes by Rowe). The sister-group relationship of Tritylodontidae and Mammaliaformes has become widely accepted (Wible, 1991; Lucas and Luo, 1993; Martinez et al., 1996), although Sues (1985) and Hopson (1991b, 1994) have argued against it.

The senior author (Hopson, 1990, 1991a,b, 1994) has summarized the results of his cladistic analyses of cynodont relationships, although, to date, has not published the data on which they are based. Hopson recognizes a primarily herbivorous clade that includes tritylodontids, the Cynognathia of Hopson and Barghusen (1986), and a carnivorous clade that includes mammals, which has been designated Probainognathia (Hopson, 1990). A data matrix of synapsids as a whole was published by Sidor and Hopson (1998), but it lacks critical taxa and characters for

[1] Department of Organismal Biology and Anatomy, University of Chicago, 1027 East 57th Street, Chicago, Illinois 60637.

[2] Bernard Price Institute for Palaeontological Research, University of the Witwatersrand, Johannesburg, South Africa.

resolving lower-level relationships within nonmammalian cynodonts.

In May, 1988, while studying in the Karoo fossil collection of the Bernard Price Institute for Palaeontological Research (BPI) at the University of the Witwatersrand, Hopson noted a small skull and partial skeleton (BP/1/2669) from the *Cynognathus* Assemblage Zone. The specimen was identified in the catalog as a juvenile *Trirachodon,* but its skull morphology more closely resembled that of *Probainognathus* and the Chiniquodontidae, carnivorous eucynodonts best known from the Middle and Late Triassic of South America. A notice of the specimen, with preliminary conclusions on its phylogenetic significance, was presented at the 48th annual meeting of the Society of Vertebrate Paleontology (Hopson and Kitching, 1988).

This new cynodont is named and briefly described here. It is compared with *Thrinaxodon,* as a member of a more primitive cynodont grade; with *Probainognathus* and chiniquodontids, as members of the Probainognathia; and with *Cynognathus* and early gomphodont genera, as members of the Cynognathia. One purpose of this paper is to justify the establishment of the eucynodont clades Cynognathia (*sensu* Hopson and Barghusen, 1986) and Probainognathia (*sensu* Hopson, 1990, 1991a, 1994).

MATERIALS AND METHODS

Specimen BP/1/2669 had been partially prepared at the BPI so that portions of the skeleton were exposed on both sides of a small sandstone slab. The skull and lower jaws were subsequently removed from the slab and more fully prepared by Ms. Claire Vanderslice. Although portions of the external surface of the skull are damaged, the palate, braincase, and medial surface of the lower jaw are beautifully preserved. Because the postcranial elements are, for the most part, heavily eroded, they have been further prepared only slightly.

Comparisons with other cynodonts are based on specimens, stereophotographs, notes and drawings, and published accounts. The data matrix of cynodonts includes characters published by Sidor and Hopson (1998), with many new characters added, particularly from the dentition. The matrix was analyzed using the 3.1 version of PAUP (Swofford, 1993). In the following section, phylogenetic definitions of a number of suprageneric taxa are given, with a distinction made between node-based and stem-based definitions, as recommended by Sereno (1999).

SYSTEMATIC PALEONTOLOGY

Therapsida Broom, 1905

Cynodontia Owen, 1861

Definition. The most inclusive clade including Mammalia and excluding *Bauria.* This clade and its sister group, the Therocephalia (defined as the most inclusive clade including *Bauria* and excluding Mammalia), are stem-based members of a node-based Eutheriodontia (defined as the least inclusive clade including Mammalia and *Bauria*). (See Sereno [1999] for discussion of node-stem triplets.)

Epicynodontia new taxon

Definition. The most inclusive clade including Mammalia and excluding *Procynosuchus.* This clade includes, among others, *Galesaurus, Thrinaxodon,* and eucynodonts.

Eucynodontia Kemp, 1982

Definition. The least inclusive clade including Mammalia and *Exaeretodon.* This is a node-based taxon, with two stem-based subgroups: Cynognathia (defined as the most inclusive clade including *Exaeretodon* and excluding *Probainognathus*) and Probainognathia (defined below). Within Cynognathia is a major stem-based subgroup, the Gomphodontia (defined as the most inclusive clade including *Exaeretodon* and excluding *Cynognathus*).

Probainognathia Hopson, 1990

Definition. The most inclusive clade including *Probainognathus* and excluding *Exaeretodon.*

Family LUMKUIIDAE new family

Definition. The most inclusive clade including *Lumkuia* and excluding *Ecteninion.*

Lumkuia fuzzi new genus and species

Etymology. The generic name is from the Lumku Mission, near which the specimen was found. The species name is in honor of A. W. "Fuzz" Crompton, in recognition of his distinguished career as a student of cynodonts and early mammals.

Holotype. BP/1/2669, partial skeleton, including skull with lower jaws; left scapulocoracoid and clavicle, interclavicle, and proximal part of right clavicle; most of left forelimb; and two articulated segments of the axial skeleton; the latter consist of 10 dorsal vertebrae with associated ribs and eight caudal vertebrae.

Horizon and Locality. The specimen is from the Burgersdorp Formation, in subzone B of the *Cynognathus* Assemblage Zone. It was collected by Father Paul Reubsamen in the vicinity of the Lumku Catholic Mission, near the town of Lady Frere, Eastern Cape Province, South Africa.

Age. The *Cynognathus* Assemblage Zone in the region of Lady Frere is represented by subzone B of Hancox et al. (1995; B. S. Rubidge, personal communication), which is considered to be of early Middle Triassic (Anisian) age (Hancox and Rubidge, 1997).

Diagnosis. Lumkuia fuzzi is characterized by a unique combination of primitive and derived features. It possesses the following probainognathian features: parietal foramen absent; rear of secondary palate lies below anterior border of orbit; expanded plates on ribs absent. It is more primitive than other probainognathians in that the frontal extends down the medial orbital wall only to the level of the lacrimal foramina and an orbital process of the palatine is lacking. It is more primitive than other eucynodonts in that the dentary does not extend as far posteriorly, resulting in a longer dorsal exposure of the surangular between the rear of the dentary and the articular. At the rear of primary palate is an autapomorphic feature: the pterygoids form a deep median depression with a nearly vertical posterior wall, behind which they form a prominent median boss anterior to the interpterygoidal vacuities. The presence of interpterygoidal vacuities suggests that the type specimen may be a subadult individual.

DESCRIPTION

Skull

In dorsal view (Fig. 1), the general appearance of the skull of *Lumkuia* is similar to that of *Thrinaxodon,* although the preorbital region is shorter and the temporal fossa longer. Thus, the center of the orbits lies anterior to the middle of the skull, whereas in *Thrinaxodon* the orbits are centered exactly at midlength. The pterygoid flanges, which in *Thrinaxodon* lie below the middle of the orbits, are visible in *Lumkuia* behind the postorbital bar (as they commonly are in eucynodonts). As in *Thrinaxodon,* the sagittal crest terminates above the occiput, so that the occipital condyles are visible from above. This contrasts with *Ecteninion* and *Probainognathus* (although not chiniquodontids), in which the sagittal crest overhangs the occiput and covers the condyles. The lambdoidal crests in *Lumkuia,* as in *Thrinaxodon,* diverge at greater than 90 degrees and extend posteriorly at their outer ends only a short distance beyond the occipital condyles. In *Probelesodon* and *Chiniquodon,* and in gomphodonts, the sagittal crest terminates slightly in front of the condyles but the lambdoidal crests diverge at an acute angle and extend back well beyond the condyles. The zygomatic arches of *Lumkuia* are more flared and rounded in pro-

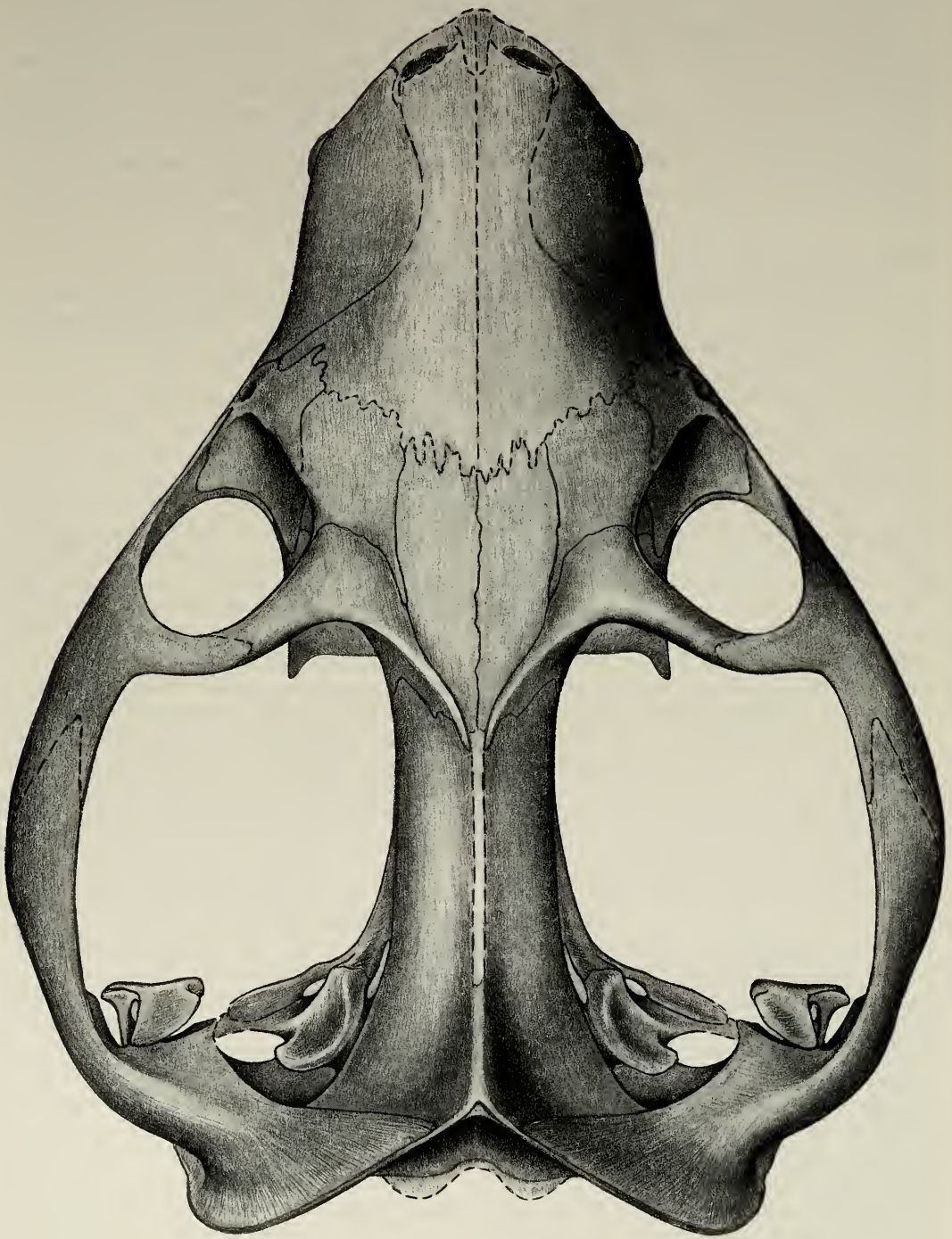

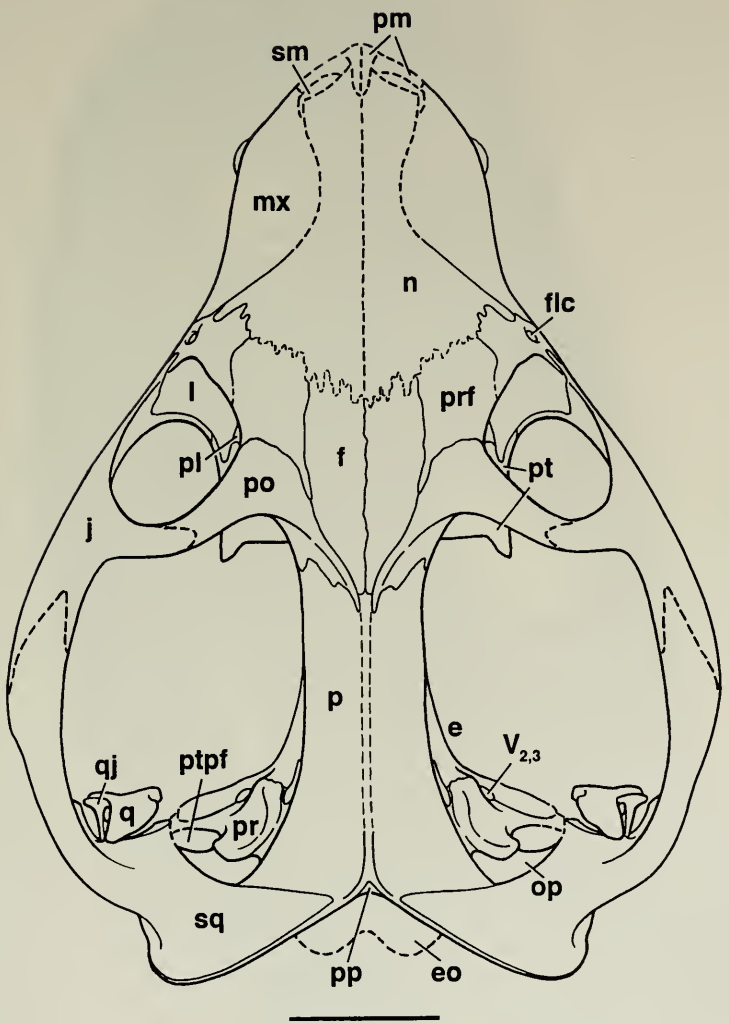

Figure 1. Skull of *Lumkuia fuzzi* (BP/1/2669) in dorsal view (on left enlarged ×3). Scale bar = 10 mm. Abbreviations: e, epipterygoid; eo, exoccipital; f, frontal; flc, foramen of lacrimal canal; j, jugal; l, lacrimal; mx, maxilla; n, nasal; op, opisthotic; p, parietal; pl, palatine; pm, premaxilla; po, postorbital; pp, postparietal; pr, prootic; prf, prefrontal; pt, pterygoid; ptpf, pterygoparoccipital foramen; q, quadrate; qj, quadratojugal; sm, septomaxilla; sq, squamosal; $V_{2,3}$, trigeminal foramen.

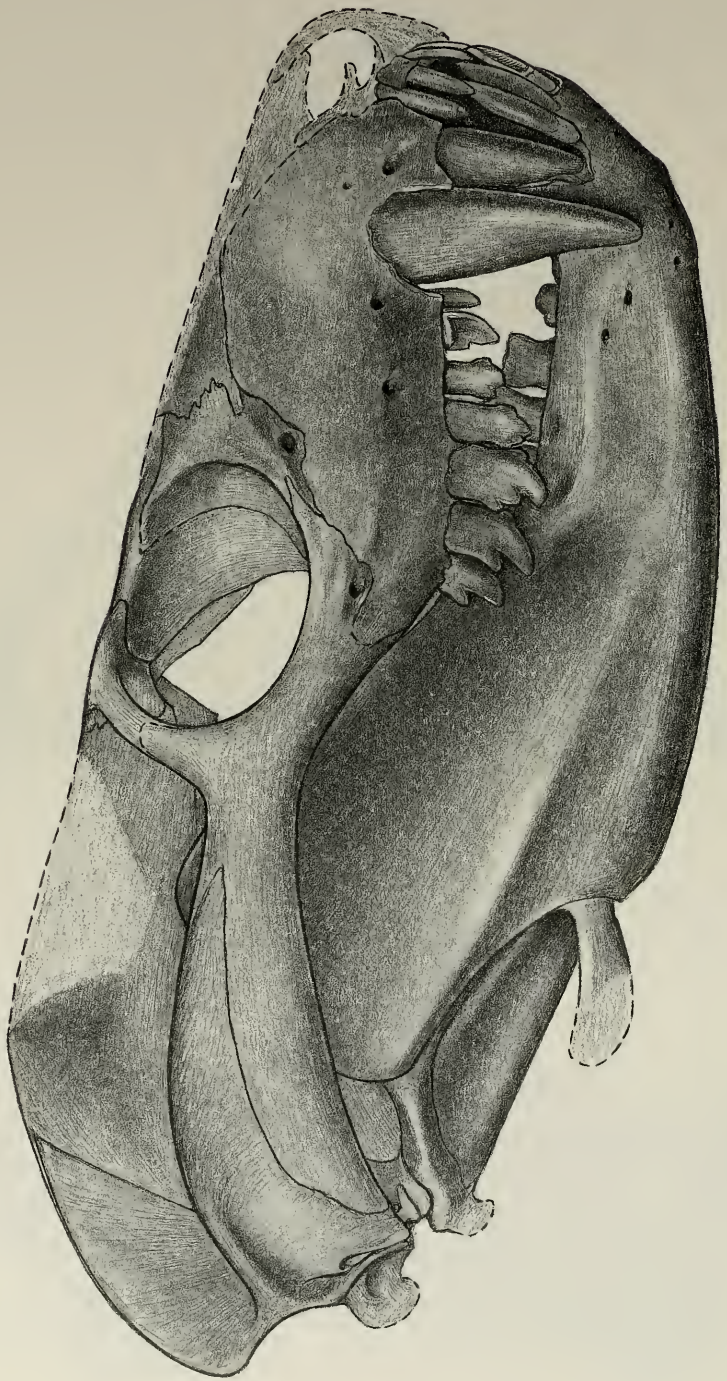

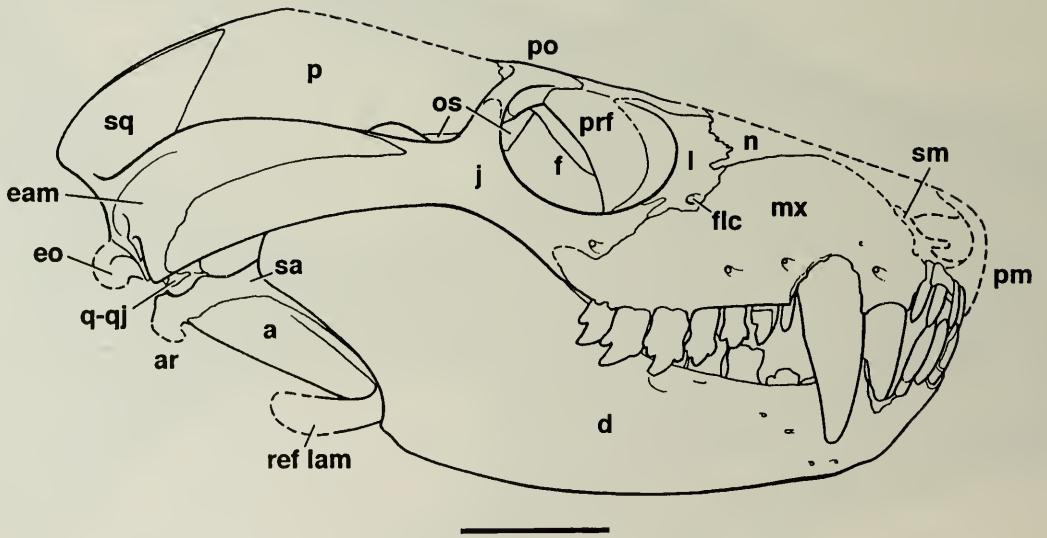

Figure 2. Skull of *Lumkuia fuzzi* (BP/1/2669) in lateral view (on left enlarged ×3). Scale bar = 10 mm. Abbreviations: a, angular; ar, articular; d, dentary; eam, external auditory meatus; eo, exoccipital; f, frontal; flc, foramen of lacrimal canal; j, jugal; l, lacrimal; mx, maxilla; n, nasal; os, orbitosphenoid; p, parietal; pm, premaxilla; po, postorbital; prf, prefrontal; q-qj, quadrate–quadratojugal; ref lam, reflected lamina; sa, surangular; sm, septomaxilla; sq, squamosal.

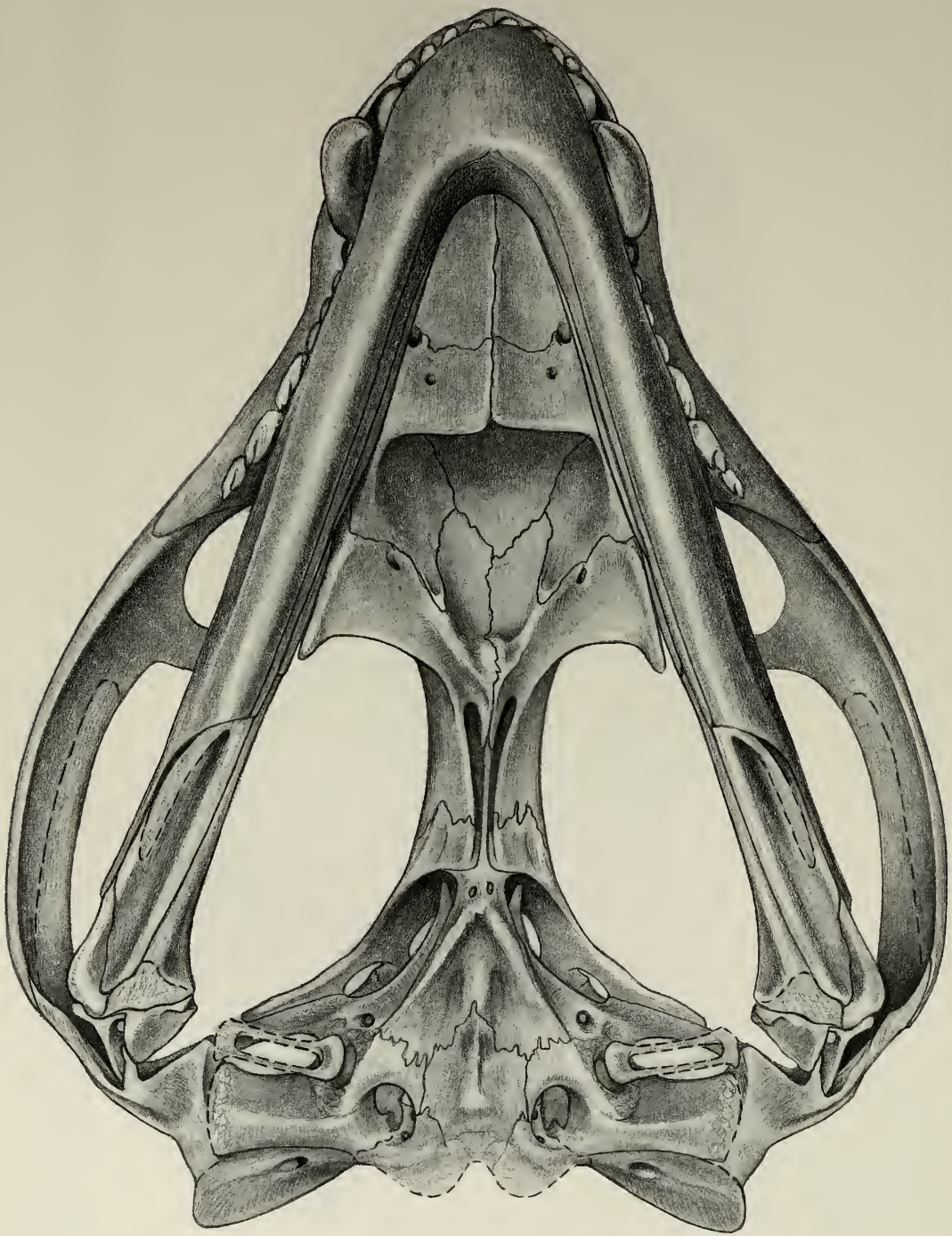

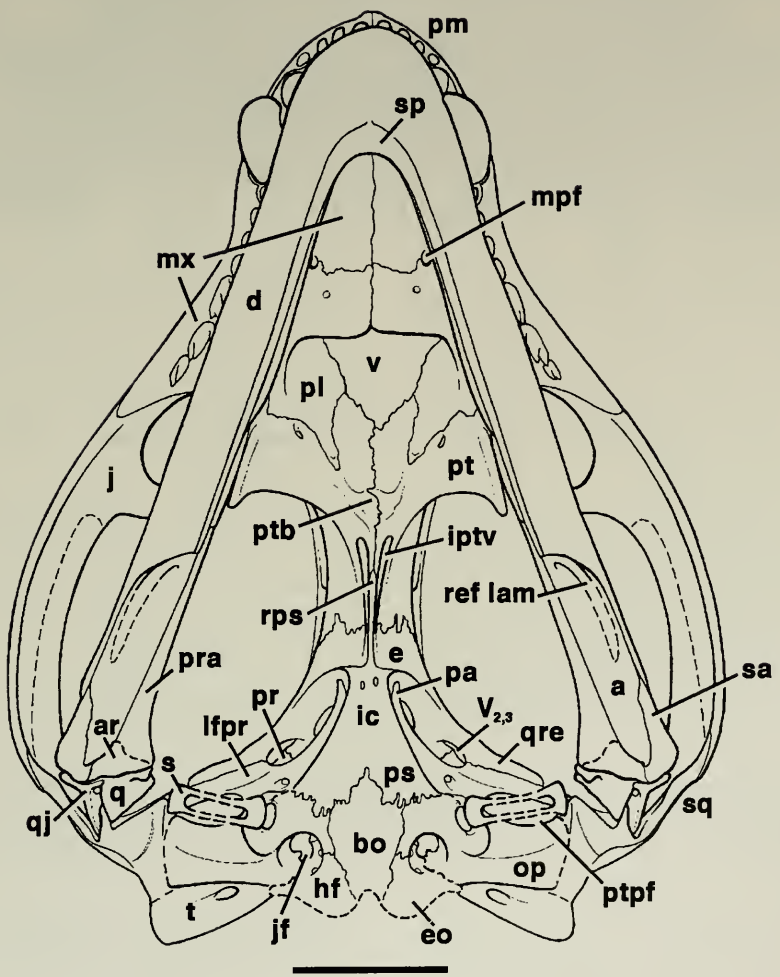

Figure 3. Skull of *Lumkuia fuzzi* (BP/1/2669) in ventral view (on left enlarged ×3). Scale bar = 10 mm. Abbreviations: a, angular; ar, articular; bo, basioccipital; d, dentary; e, epipterygoid; eo, exoccipital; hf, hypoglossal foramina; ic, internal carotid foramina; iptv, interpterygoidal vacuity; j, jugal; jf, jugular foramen; lfpr, lateral flange of prootic; mpf, major palatine foramen; mx, maxilla; op, opisthotic; pa, pila antotica; pl, palatine; pm, premaxilla; pr, prootic; pra, prearticular; ps, parasphenoid; pt, pterygoid; ptb, pterygoid boss; ptpf, pterygoparoccipital foramen; q, quadrate; qj, quadratojugal; qre, quadrate ramus of epipterygoid; ref lam, reflected lamina; rps, parasphenoid rostrum; s, stapes; sa, surangular; sp, splenial; sq, squamosal; t, tabular; v, vomer.

file than those of *Thrinaxodon,* being widest anterior to, rather than at, the level of the jaw joint; in this *Lumkuia* resembles other Triassic probainognathians and differs from cynognathians.

In lateral view (Fig. 2), the skull and lower jaw of *Lumkuia* appear to be more robust than in *Thrinaxodon* (Fig. 5A), due to the shorter snout, longer temporal region, and deeper dentary. Also, as in other eucynodonts except *Cynognathus* (Fig. 6A), the jaw joint is located more anteriorly, so that the lambdoidal crests extend well behind the articular region. The canines are more robust and the posterior cheek teeth proportionately larger than in *Thrinaxodon* and *Probainognathus* (Fig. 5C), although not in *Ecteninion* and chiniquodontids. The zygomatic arch appears to be no more robust than that of *Thrinaxodon,* except perhaps posteriorly, whereas that of *Probainognathus,* and especially of chiniquodontids and cynognathians, is much deeper.

In ventral view (Fig. 3), the symphyseal region is shorter than that of *Thrinaxodon* and the shorter jaws diverge at a greater angle. The secondary palate is only slightly more developed, with a nearly straight rather than concave posterior margin. Behind the pterygoid flanges, the basicranial axis is more transversely compressed than in *Thrinaxodon,* so that the subtemporal fossa is proportionately wider.

In occipital view (Fig. 4), the most distinctive difference from *Thrinaxodon* is in the constriction of the base of the zygomatic arch and the separation of the zygoma from the more flaring lambdoidal crest by a V-shaped notch. In noneucynodonts, such as *Procynosuchus, Galesaurus,* and *Thrinaxodon,* the lambdoidal crest is continuous with the dorsal ridge on the zygomatic arch. Only in eucynodonts, with the exception of *Cynognathus,* is there a distinct break between the two crests, with the lambdoidal crest passing back posterior to the medial end of the dorsal zygomatic ridge.

The individual skull bones are briefly described below, with only salient features noted. The facial portions of the premaxilla and septomaxilla are missing. On the palate, backwardly pointing processes of the premaxillae separate the elongate, slit-like, incisive foramina. The premaxilla forms all but the posteriormost parts of the lateral border of the incisive foramen and the fossa for the lower canine.

The alveolar border of the maxilla is straight, turning up slightly at the level of the last tooth and passing smoothly into the suborbital bar where, a short distance behind the last postcanine, it contacts the jugal. In the palate, the maxilla contributes to the rear margin of the incisive foramen and the posteriormost part of the lower canine fossa. The maxilla forms the anterior two thirds of the secondary palate, extending as far back as the gap between the third and fourth postcanines. The major palatine foramen opens anteroventrally on the maxillary–palatine suture well lateral to the midline.

The nasals have largely flaked off, leaving some bone only posterolaterally. As shown by impressions on the surface of the frontals, the nasals overlap the frontals and the nasofrontal suture lies a short distance behind the anterior border of the orbit.

The eroded dorsal surface of the frontals preserves a slightly undulating midline suture. The contact with the parietals on the skull roof is not preserved, but probably lay between the posteriormost part of the temporal crests of the postorbitals. In the medial wall of the orbit, a thin strip of frontal is exposed behind the large descending flange of prefrontal, extending ventrally about to the level of the lacrimal foramina.

Within the orbit, the prefrontal overlies the frontal and is itself overlain by the lacrimal; it extends ventrally nearly to the level of the palatine on the dorsal surface of the palate.

The lacrimal has a short exposure on the face compared with that of *Thrinaxodon* or *Probainognathus.* Within the orbit, it

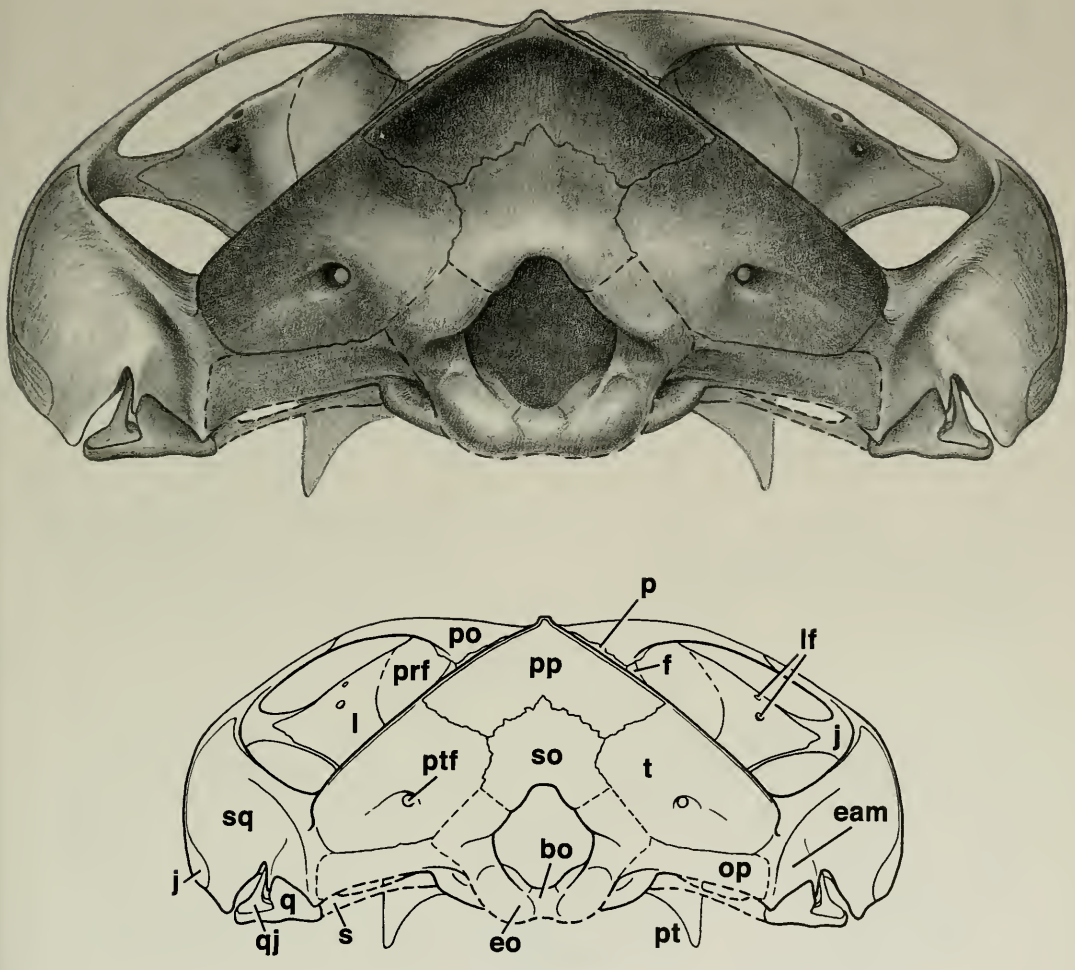

Figure 4. Skull of *Lumkuia fuzzi* (BP/1/2669) in occipital view (upper drawing enlarged ×3). Scale bar = 10 mm. Abbreviations: bo, basioccipital; eam, external auditory meatus; eo, exoccipital; f, frontal; j, jugal; l, lacrimal; lf, lacrimal foramina; op, opisthotic; p, parietal; po, postorbital; pp, postparietal; prf, prefrontal; pt, pterygoid; ptf, posttemporal foramen; q, quadrate; qj, quadratojugal; s, stapes; so, supraoccipital; sq, squamosal; t, tabular.

forms the anterior half of the orbital wall and most of its floor. Paired lacrimal foramina open forward inside the anterior rim of the orbit; a small foramen opens anterolaterally from the lower lacrimal canal on to the facial portion of the lacrimal.

A posterolaterally directed process of the postorbital forms the dorsal part of the postorbital bar; it extends down internal to the postorbital process of the jugal for an indeterminate distance. The upper, more horizontal, part of the postorbital bar is roughly triangular in cross section; its posterior face forms a flat vertical surface that is continuous posteromedially with a vertical lappet of postorbital that overlies the lateral surface of the parietal. The posterior parts of the paired postorbitals converge backwards as temporal crests and merge into the median sagittal crest on the parietals. These vertical surfaces on the postorbital mark the area of attachment of

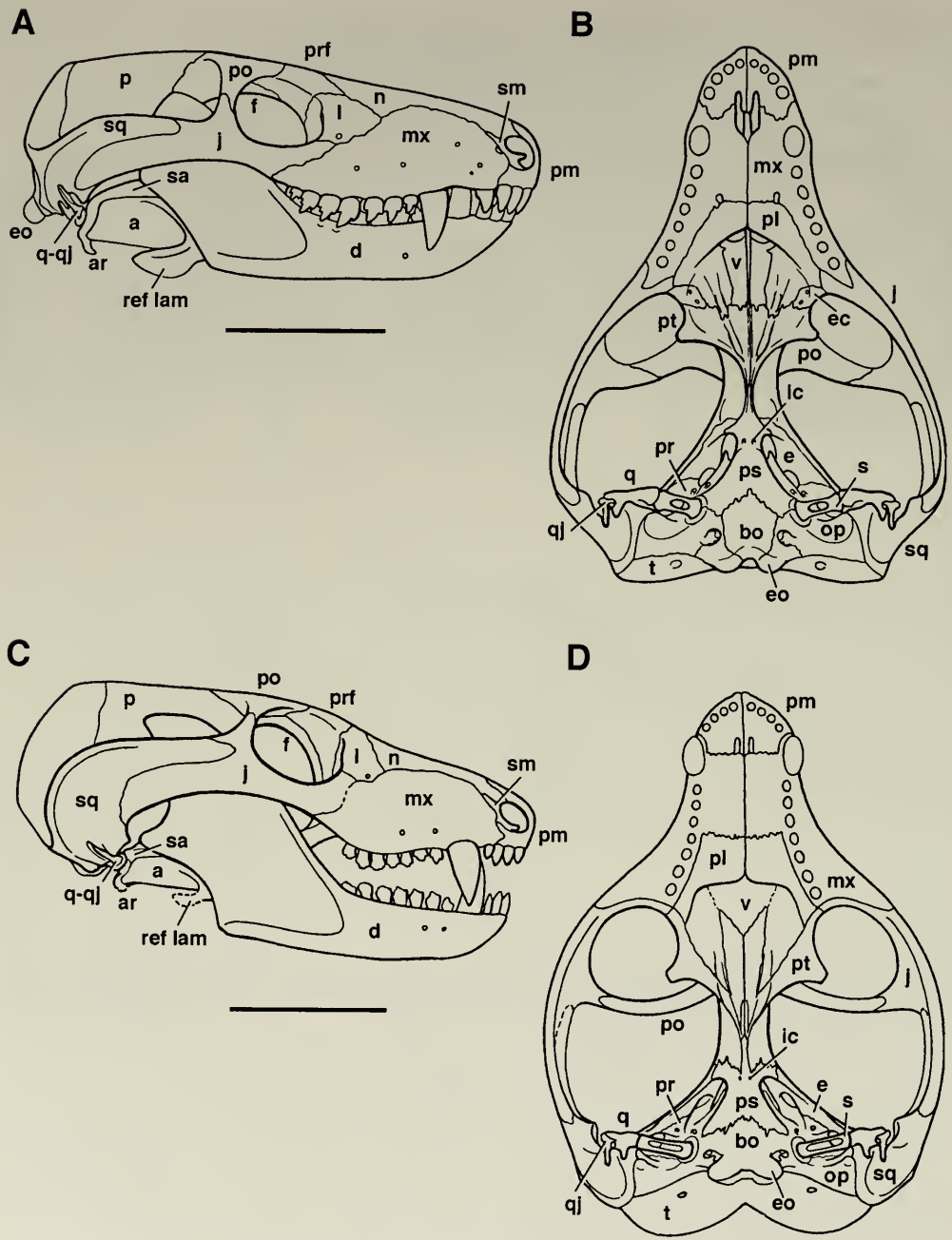

Figure 5. Skulls in lateral and ventral views of (A, B) *Thrinaxodon liorhinus*, and (C, D) *Probainognathus jenseni*. Scale bars = 20 mm. Abbreviations: a, angular; ar, articular; bo, basioccipital; d, dentary; e, epipterygoid; ec, ectopterygoid; eo, exoccipital; f, frontal; ic, internal carotid foramen; j, jugal; l, lacrimal; mx, maxilla; n, nasal; op, opisthotic; p, parietal; pl, palatine; pm, premaxilla; po, postorbital; pr, prootic; prf, prefrontal; ps, parasphenoid; pt, pterygoid; q, quadrate; qj, quadratojugal; ref lam, reflected lamina; s, stapes; sa, surangular; sm, septomaxilla; sq, squamosal; t, tabular; v, vomer.

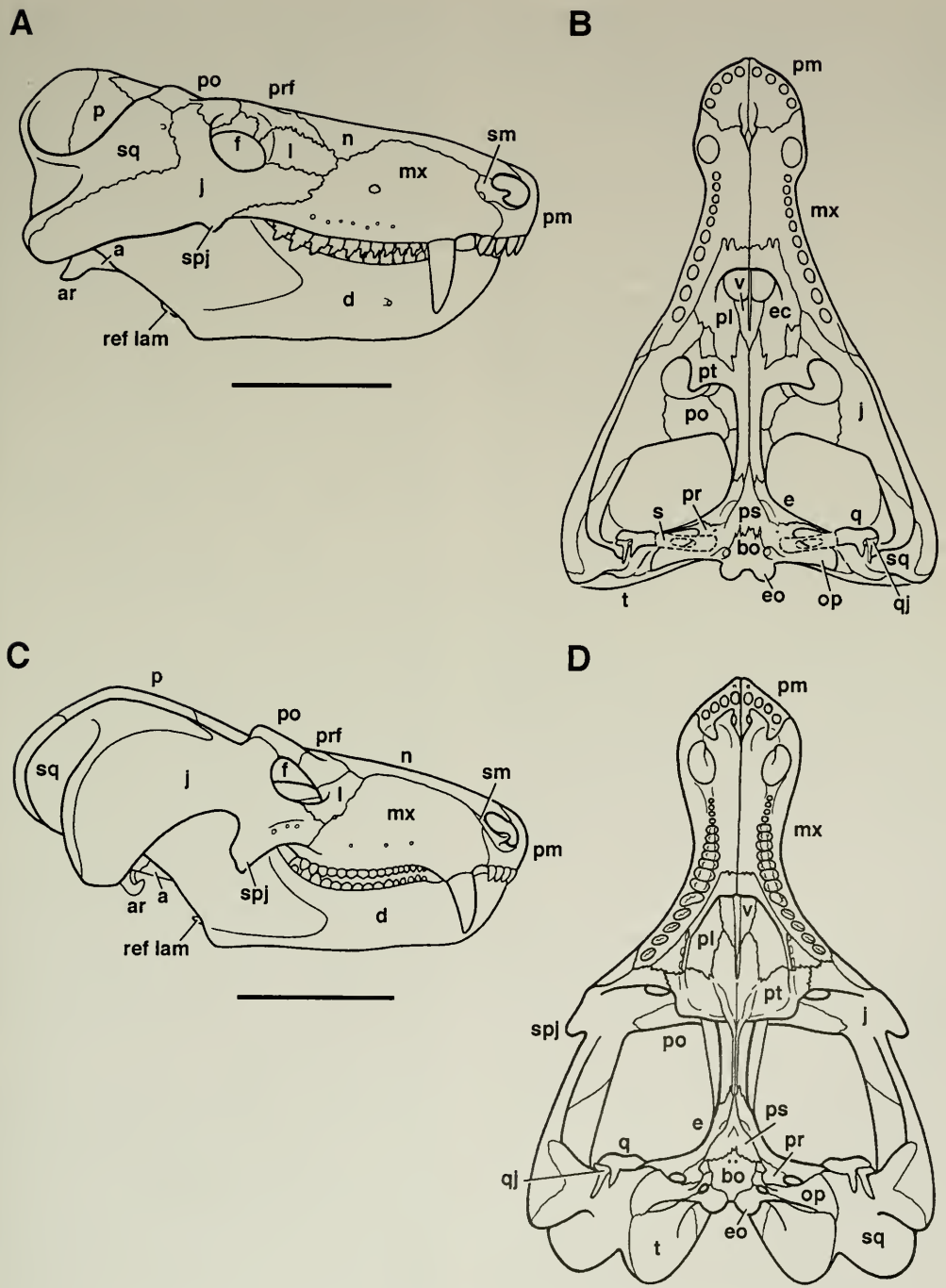

Figure 6. Skulls in lateral and ventral views of (A, B) *Cynognathus crateronotus*, and (C, D) *Diademodon mastacus*. Scale bar in A = 100 mm, in B = 90 mm. Abbreviations: a, angular; ar, articular; bo, basioccipital; d, dentary; e, epipterygoid; ec, ectopterygoid; eo, exoccipital; f, frontal; j, jugal; l, lacrimal; mx, maxilla; n, nasal; op, opisthotic; p, parietal; pl, palatine; pm, premaxilla; po, postorbital; pr, prootic; prf, prefrontal; ps, parasphenoid; pt, pterygoid; q, quadrate; qj, quadratojugal; ref lam, reflected lamina; s, stapes; sm, septomaxilla; spj, suborbital process of jugal; sq, squamosal; t, tabular; v, vomer.

the anteriormost portion of the temporalis muscle. A medially extending horizontal lappet of postorbital contacts the sliver of frontal exposed in the orbital wall.

The dorsal parts of the fused parietals are damaged, but enough is preserved to indicate that the sagittal crest was relatively low anteriorly and increased only moderately in height posteriorly. No evidence of a parietal foramen is preserved and it was almost certainly absent. The ventral margin of the parietal contacts the dorsal edge of the orbitosphenoid, behind which it is overlapped by the dorsal margin of the epipterygoid back to its midlength. Between the parietal and the dorsal margins of the epipterygoid and prootic is an elongate opening into the cranial cavity. Leading to this opening from behind, along the prootic–parietal suture, is a deeply incised groove that begins at the anterior opening of the posttemporal foramen. The groove presumably contained the supraorbital ramus of the ramus superior of the stapedial artery, with a meningeal branch entering the cranial cavity through the elongate opening (Rougier et al., 1992; Wible and Hopson, 1995). The parietals broaden posteriorly, where they are overlain by the cranial process of the squamosal, and contribute to the roof of the posttemporal foramen.

The jugal is a relatively slender bone, not unlike that of *Thrinaxodon* and *Probainognathus*. In the zygomatic arch, the jugal is overlain dorsally by the zygomatic process of the squamosal and bounded behind by a descending lappet of squamosal. A moderate-sized, anterolaterally directed foramen pierces the jugal below the orbit. A short distance behind the last postcanine, the jugal passes medial to the rear of the maxilla to contact the anterolateral margin of the pterygoid, and perhaps the palatine, at the anterior border of the subtemporal fossa. The jugal is exposed behind the lacrimal in the posterior part of the orbital floor.

The squamosal may be described as consisting of two portions, the cranial and zygomatic processes, separated at the level of the V-shaped notch. The cranial process is a relatively flat, triangular plate extending nearly to the apex of the posterior end of the sagittal crest. The cranial process overhangs the anterior opening of the posttemporal foramen and its flaring rear border forms the lambdoidal crest. The V-shaped notch has an anteroposteriorly rounded dorsal surface that separates the lambdoidal ridge from the dorsal ridge on the zygomatic process. Directly below the notch is a triangular lappet of squamosal that on its medial surface bears a depression for the incompletely ossified distal end of the paroccipital process. Anteromedially, the lappet appears to contact the lateral flange of the prootic. Laterally, it forms the medial wall of the recess for the quadrate, which is open behind as an inverted V-shaped emargination. The emargination is bounded laterally by a slender, pointed process that descends between the upper ends of the quadrate and quadratojugal. Further laterally, the zygomatic portion of the squamosal forms a descending process behind the jugal that in life presumably contacted the surangular (although here a contact is absent because the lower jaw appears to have shifted slightly forward). The zygomatic process curves forward from this level extending over the jugal nearly to the level of the postorbital bar. A shallow sulcus, the external auditory meatus, extends up and forward from the distal end of the paroccipital process on to the posterolateral surface of the zygoma.

The fused vomers form the center of the arched roof of the primary palate above the secondary palate and roof the choanal trough to a point just behind the level of the last postcanine.

The palatal plates of the palatines form the posterior third of the short secondary palate, underlying the posterior margins of the maxillae. A small foramen pierces the palatine a short distance posterointernal to the major palatine foramen. The rear margin of the secondary palate is thickened

and slightly rugose. As in other Triassic probainognathians, the lateral margin of the secondary palate curves dorsally, so that the palatine meets the maxilla in the floor of a narrow longitudinal trough internal to the posterior postcanines. This trough continues back beyond the level of the secondary palate, where it is bounded medially by slender ridges that extend back nearly to the lateral margins of the pterygoid flanges. An ectopterygoid is not present, so the posterolateralmost part of the palatine contacts the pterygoid, and perhaps the jugal, internal to the last postcanine. The palatine is here pierced by several small foramina, with a larger opening between its posterior margin and the overlying pterygoid. The palatines form the lateral walls of the choanal trough, contacting the vomer and pterygoids medially and contributing to the anterior half of the more medial palatal ridges that bound the posterior half of the trough. The palatine is exposed on the upper surface of the primary palate as a broad plate that lacks a dorsal orbital process.

The ectopterygoid is absent. Although described in other Triassic probainognathians (Romer, 1969, 1970; Martinez et al., 1996), we believe its presence has not been convincingly demonstrated.

The pterygoids form the rear of the choanal trough, which is uniquely deep and is bordered behind by a near-vertical wall. At the posterior end of the medial palatal ridges, where they converge at the rear of the choanal trough, is a prominent median boss; this feature appears to be unique among cynodonts. Lateral to the anterior end of the medial palatal ridge, adjacent to the suture with the palatine, are one or more slitlike openings that pierce the pterygoid. Laterally, the deep, triangular pterygoid flanges descend well down the inside of the lower jaws. The ridges forming their rear margins converge posteriorly and extend on to the basipterygoid rami of the pterygoids, nearly meeting where the latter contact the basipterygoid processes of the basisphenoid. An elongate gap between the ridges is divided by the long rostrum of the parasphenoid to form paired interpterygoidal vacuities. Such vacuities are present in *Dvinia* and *Procynosuchus* and in juveniles of *Thrinaxodon* (Estes, 1961), but are usually absent in postprocynosuchid cynodonts.

The orbitosphenoid is roughly the shape of an elongate half-cylinder, with a U-shaped cross section. It lies on the midline below the postorbitals and parietals in the space between the postorbital bar and the anterodorsal end of the epipterygoid.

The ascending lamina of the epipterygoid is extremely long fore to aft, being nearly twice the length of the prootic portion of the braincase sidewall. This contrasts sharply with the condition in *Probainognathus* and *Ecteninion*, in which the ascending lamina tapers anterodorsally and is much shorter than the prootic. The ascending lamina is suturally joined to the anterodorsal margin of the prootic above the anterior border of the large trigeminal foramen. The epipterygoid contacts the basicranial wing of the pterygoid ventrally and appears to have a short medial contact with the basipterygoid process. Its quadrate ramus is a shallow vertical lamina that extends back below the trigeminal foramen to meet the lateral flange of the prootic. The epipterygoid continues back for a short distance in contact with the lateral flange, terminating at the level of the anterior border of the pterygoparoccipital foramen. That portion of the epipterygoid behind the basipterygoid joint forms the lateral wall of a ventrally open space, the cavum epiptericum.

The basisphenoid consists of slightly expanded anterior basipterygoid processes that contact the pterygoids and epipterygoids, a very narrow middle portion that underlies the sella turcica and is pierced by paired carotid foramina, and an expanded posterior part that contacts the prootic dorsally and the basioccipital posteriorly. The dermal parasphenoid is fused to its ventral surface, forming a near-horizontal, triangular plate posteriorly that

covers the basisphenoid–basiooccipital contact. Further forward, the parasphenoid passes between the carotid foramina and forms an elongate midline process, the rostrum, that extends forward between the pterygoids to separate the interpterygoidal vacuities. The anterior end of the parasphenoid is suturally joined to the pterygoids immediately behind and dorsal to the median pterygoid boss.

The prootic portion of the ossified otic capsule lacks a sutural separation from the opisthotic portion, although the prootic typically contributes to the anterior part of the paroccipital process and rim of the fenestra ovalis. The lateral flange of the prootic extends posterolaterally from behind the trigeminal foramen; although the distal end of the lateral flange is damaged, it undoubtedly contacted the squamosal in life, thus enclosing the large, oval, pterygoparoccipital foramen. The lateral surface of the prootic bears a slight groove that extends between the latter opening and the trigeminal foramen. Such a groove is usual in cynodonts, although here it is unusually faint. The system of grooves and foramina in the lateral surface of the prootic are interpreted as transmitting arteries and veins (see Rougier et al., 1992; Wible and Hopson, 1995). Deep to the outer margin of the trigeminal foramen, the ossified pila antotica extends anterodorsally approximately to the level of the basipterygoid joint. Just in front of the fenestra ovalis is the small, posterolaterally directed foramen for the facial (VIIth) nerve.

The opisthotic forms the posterior half of the rim of the fenestra ovalis; most of the paroccipital process; and the anterior, anteromedial, and lateral borders of the jugular foramen. The ventral surface of the paroccipital process slopes up and forward from its rounded posteroventral margin, to form the posterodorsal wall of the middle ear cavity (Hopson, 1966). The opisthotic contacts the basioccipital medially and the exoccipital posteromedially and posterolaterally on the margins of the jugular foramen. This foramen is confluent within the opisthotic with the space occupied by the inner ear. Deep within the jugular foramen is a low ridge that extends a short distance into the opening from its posterolateral wall. This ridge in more derived cynodonts, such as *Probainognathus* (Fig. 5D) and *Massetognathus* (Rougier et al., 1992, figs. 7B, D), is a long fingerlike projection that extends toward the medial wall of the foramen. In tritheledontids, tritylodontids, and mammaliaforms, the foramen is fully subdivided, with a true jugular foramen posteriorly (transmitting nerves and vessels from the cranial cavity), and a perilymphatic foramen anteriorly (transmitting the perilymphatic duct from the inner ear cavity).

The basioccipital is exposed midventrally behind the parasphenoid, with which it has an interdigitating transverse suture. It forms the midventral part of the foramen magnum, bearing a narrow transverse articular facet for the atlas intercentrum.

The paired exoccipitals form the occipital condyles, damaged here, which extend about one third of the distance up the lateral sides of the foramen magnum. More dorsally, they meet the supraoccipital, but the sutural contact cannot be distinguished. The exoccipital contributes to the posteromedial wall of the jugular foramen, which bears a shallow depression in which lie two hypoglossal foramina, a smaller anterior one and a larger posterior one, which open into the cranial cavity shortly in front of the occipital condyle.

The median supraoccipital forms an indeterminate part of the dorsal border of the foramen magnum. The supraoccipital is overlain by the tabular laterally and the postparietal above. The postparietal occupies the upper surface of the occiput above the supraoccipital and tabulars and between the flaring lambdoidal crests. Middorsally, the postparietal has a short, pointed process that extends forward between the fused parietals. The tabulars occupy the entire occiput lateral to the supraoccipital, completely surrounding the small, circular posttemporal foramina.

The quadrate is exposed on the right side, where it has shifted slightly forward from its contact with the squamosal. The transversely oriented articular condyle of the quadrate is about as wide as the total bone is high. The flat posterior surface of its ascending process is oriented obiquely to the transverse axis and fits against a matching surface on the anterior face of the squamosal. The posterolateral third or so of the quadrate is exposed from behind in the inverted V-shaped emargination of the squamosal. The lateral end of the quadrate condyle extends well beyond the outer margin of the ascending process; its dorsal surface is clasped by the transversely expanded lower end of the quadratojugal.

The quadratojugal has a transversely compressed ascending process that fits into a narrow groove in the squamosal behind the lateral part of the ascending process of the quadrate. The quadratojugal is separated from the quadrate posteriorly by a thin descending prong of squamosal. The lower end of the bone is expanded transversely, its medial portion overlying the lateral condyle of the quadrate and its lateral portion forming a free rounded process.

An incomplete right stapes is preserved nearly in situ, its oval footplate separated slightly from the depression that houses the fenestra ovalis. The preserved posterior crus of the stapes extends anterolaterally toward the medial surface of the quadrate condyle.

Lower Jaw

The right lower jaw is essentially complete and well preserved. The large dentary consists of a deep tooth-bearing horizontal ramus and a broad ascending process (for insertion of jaw-closing muscles), each forming about one half of its length. The short, deep symphysis is fused. The anteroventral surface of the fused dentaries bears numerous tiny foramina. Two small mental foramina lie below the first and second postcanines. At the posterior end of the convex lower margin of the dentary is a slightly projecting pseudangular process, above which the lower margin of the bone curves up and back over the postdentary elements. A low outturned ridge overlies the surangular and angular and continues forward across the masseteric fossa, fading into its surface below the last upper postcanine. The masseteric fossa extends forward as a slight depression to the level of the fifth upper postcanine. The coronoid process rises slightly above the dorsal border of the zygomatic arch just behind the postorbital bar. The lateral surface of the coronoid process forms a broad, slightly concave trough between out-turned anterodorsal and posteroventral borders. The slightly convex posterior margin of the process slopes down to meet the surangular about 5 mm anterior to the articular glenoid.

As is usual in eucynodonts, the laterally exposed postdentary bones are much shallower than in *Thrinaxodon* (Fig. 5A), with their lower border sloping up and back. The surangular has less exposure behind the dentary than in *Thrinaxodon,* but more than in other eucynodonts, where the dentary nearly reaches the articular (Figs. 5C, 6A, C). On the medial surface of the jaw, the surangular has a flat dorsal surface that is buttressed by an overlying ridge on the dentary. The exposed part of the surangular behind the dentary has a transversely thickened upper margin. Anterolateral to the articular glenoid is a slightly raised area that in life may have contacted the descending flange of the squamosal; however, it lacks the prominent articular boss that contacts the squamosal in *Cynognathus* and *Diademodon* (Crompton, 1972a).

The angular covers most of the surangular laterally and has a dorsal ridge that overhangs its concave outer surface. The reflected lamina is damaged, but it appears to be more slender than that of *Thrinaxodon.* The articular is transversely narrower than in *Thrinaxodon,* more closely resembling that of *Probainognathus* and *Probelesodon.* The remaining postdentary elements are similar to those of *Thrinax-*

odon, except that the splenials are fused in the rear of the symphysis.

Dentition

The dental formula is: I4/3, C1/1, Pc7/5. The incisors are all small and closely spaced. The canines are long and broad, with extremely robust roots. The canines have a rounded anterior surface and, in the uppers at least, an unserrated ridge posteriorly.

The upper postcanines increase in size from first to sixth, with the seventh being slightly smaller than the fifth. The first three have a slightly recurved main cusp and a small posterior accessory cusp. The fourth is well preserved on the left, where it possesses a large recurved main cusp, a smaller accessory cusp behind it, and a second, much smaller, posterior accessory cusp near the base of the crown. Anterior, and slightly internal, to the main cusp is a very small accessory cusp; this cusp is absent on the right, perhaps obliterated by wear. Upper postcanine 5 is much larger than Pc^4, but is nearly identical in morphology. Upper postcanine 6 has a small anterointernal cusp, a strongly recurved main cusp, and a smaller recurved posterior accessory cusp. The rear of the crown is damaged, so the presence of a second posterior cusp is uncertain. The damaged seventh postcanine has a recurved main cusp followed by an accessory cusp, but the presence of additional cusps is uncertain. The teeth are set at a slight angle to the line of the tooth row, so that, where present, the posterior accessory cusp contacts the succeeding crown lingual to its anterior accessory cusp.

The lower postcanines are less fully exposed. The first tooth is damaged, but the well-preserved second closely resembles the fourth upper postcanine; both resemble a typical lower postcanine of *Thrinaxodon.* The crowns of Pc_{3-5} are exposed lingually; the third and fourth have an anterior accessory cusp and at least one posterior accessory cusp, whereas the fifth has two posterior accessory cusps, although the presence of an anterior accessory cusp cannot be determined. Both upper and lower postcanines appear to lack lingual cingula.

Postcranial Skeleton

The poorly preserved shoulder girdle, forelimb, and caudal vertebrae show no unusual features and will not be described. The dorsal vertebral series, although not well preserved, merits description inasmuch as it possesses features that distinguish probainognathians from cynognathians. The articulated section of the dorsal vertebral column contains 10 vertebrae exposed in ventral view. On the partially exposed left side, the last two vertebrae show a pair of articulating zygapophyses, thus establishing directionality along the column. The last nine vertebrae preserve ribs. Of these, the last two possess features that together characterize cynodont lumbar vertebrae (Jenkins, 1971): the rib attachments are entirely on the vertebral body, and these ribs are synostosed to the vertebrae with a serrate suture. In the more anterior ribs, the capitular articulation spans two adjacent centra; whether any are synostosed is uncertain, although the first rib, at least, appears to be free.

The anterior four pairs of ribs are damaged distally, but they appear to be anteroposteriorly compressed, thus resembling typical thoracic ribs. The posterior five sets of ribs appear to be short, because their more or less rounded ends retain some matrix distally. These ribs are perhaps slightly broader than those preceding them, but they do not expand distally to any noticeable degree. The last rib is broader than the preceding ones, as is the last (second) lumbar vertebra of *Cynognathus* illustrated by Jenkins (1971, fig. 15A). Also as in *Cynognathus,* the last three sets of ribs curve slightly forward. However, at a comparable distance from the proximal synostosis, the posterior ribs of *Lumkuia* show no trace of the distal expansions seen in *Galesaurus, Thrinaxodon, Cynognathus,* and *Diademodon* (Jenkins, 1971). Thus, they resemble the lumbar

ribs of the probainognathians *Probelesodon* and *Probainognathus* (Romer, 1973).

PHYLOGENETIC RELATIONSHIPS OF *LUMKUIA FUZZI*

A cladistic analysis of cynodonts was performed, with 23 cynodont taxa and the basal therocephalian *Lycosuchus* and a gorgonopsid as successive outgroups (see Appendix 2). Of 101 characters, 43 are from the skull, 9 from the lower jaw, 29 from the dentition, and 20 from the postcranial skeleton (see Appendix 1). The aims of most past phylogenetic analyses have been to order therapsid taxa with respect to mammals, hence only taxa and characters that served to do this were included. We have made a special effort to include a large sample of gomphodont taxa and to include characters, particularly from the postcanine dentition, that would specifically aid in resolving their interrelationships. The data were analyzed using a random addition sequence with 10 replicates and the tree bisection–reconnection (TBR) algorithm of PAUP 3.1 (Swofford, 1993), with the resulting character distribution optimized under delayed transformation (DELTRAN).

Although resolution of the phylogenetic relationships of tritylodontids with respect to tritheledontids and mammaliaforms is not the principal aim of this study, we have attempted to determine where these three taxa are placed under different treatments of the characters. When all characters were run unordered, the tritheledontid *Pachygenelus* and the mammaliaform *Morganucodon* were the sister group of Tritylodontidae, nested deeply within the gomphodont clade (tree length = 233; Consistency Index (CI) = 0.58; Retention Index (RI) = 0.78; Rescaled CI = 0.45). When a minimum of four multistate characters (18, 22, 63, 73) were ordered, *Pachygenelus* and *Morganucodon* shifted to a probainognathian clade, where they remained under tests of cladogram robustness (see below). This is the cladogram illustrated here (Fig. 7).

The analysis (with four ordered characters) resulted in three most parsimonious trees of 238 steps (CI = 0.57; RI = 0.77; RC = 0.44). The trees differ only in the placement of the basal cynodonts *Dvinia* and *Procynosuchus* with respect to "higher" cynodonts, either in a trichotomy with the latter, as their sister clade, or with *Procynosuchus* and *Dvinia* as their successive outgroups. The cladogram (Fig. 7) shows the last (our preferred) alternative.

Three near-basal clades are supported by large numbers of unequivocal synapomorphies: Cynodontia by 26, Epicynodontia by 14, and Eucynodontia by 11. A dichotomy within Eucynodontia includes a well-characterized Cynognathia, with eight unequivocal synapomorphies, and a less well-characterized Probainognathia, with four unequivocal (and two equivocal) synapomorphies. Within Cynognathia, the Gomphodontia are characterized by five unequivocal (and two equivocal) synapomorphies. Within the latter clade, the paraphyletic traversodonts (including Tritylodontidae as a derived subgroup) are characterized by three unequivocal (and one equivocal) synapomorphies. Characters diagnosing each clade are listed in Appendix 3.

Lumkuia is the basal member of the Probainognathia, although *Ecteninion* from the early Late Triassic is more derived in but a single feature: a frontal–palatine contact in the orbital wall. *Probelesodon, Chiniquodon,* and *Aleodon* represent a monophyletic Chiniquodontidae, characterized by a very long secondary palate and a posterior angulation of the maxilla. *Probainognathus* is allied with the tritheledontid/mammaliaform clade by two synapomorphies: the presence of postcanine lingual cingula and a medial shift of the maxillary tooth rows. *Pachygenelus* and *Morganucodon* form an extremely robust clade, supported by 18 unequivocal synapomorphies. Although this clade shares many character states with tritylodontids, the latter are deeply nested within the Gomphodontia on the basis of numerous cynognathian and gomphodont synapomorphies.

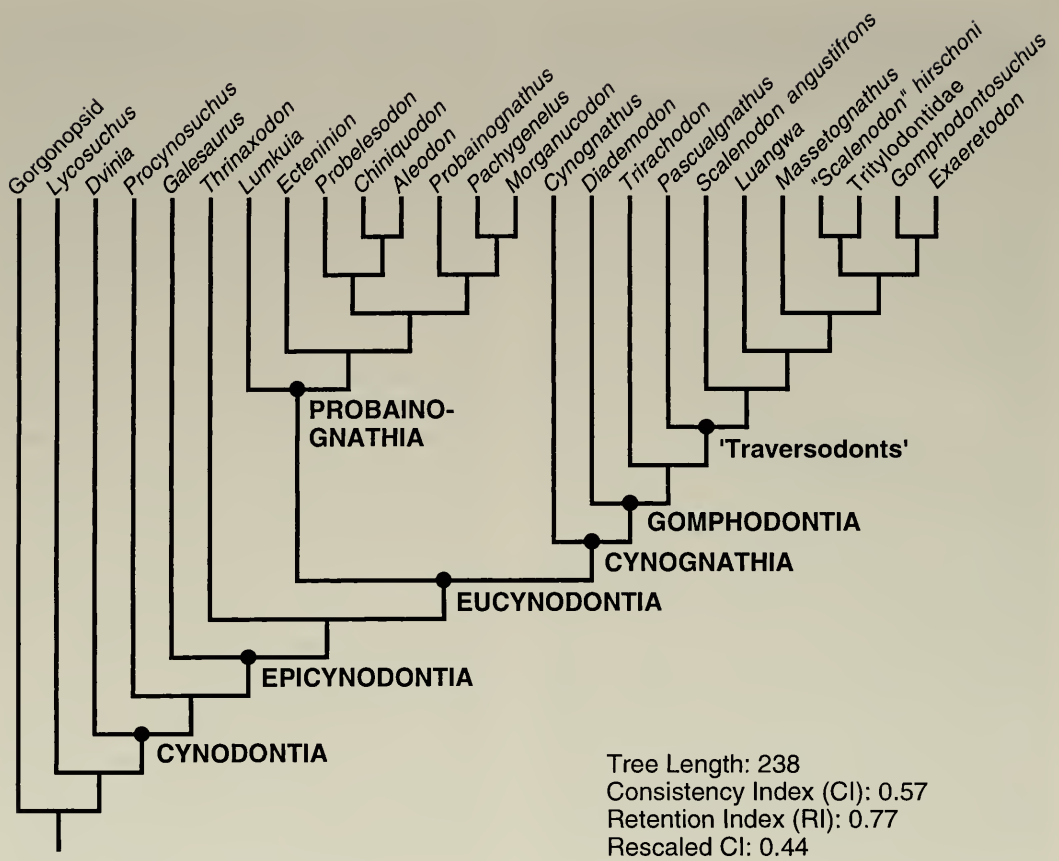

Figure 7. Cladogram of nonmammalian cynodonts. One of three shortest trees (238 steps in length), in which *Dvinia* is sister taxon to remaining cynodonts. "Traversodonts" refers to *Pascualgnathus* and more derived gomphodonts, usually designated as Traversodontidae. However, inclusion of Tritylodontidae in this "family" makes it paraphyletic, hence use of the informal term "traversodonts."

The robustness of this cladogram was tested by generating trees of incrementally greater length (up to six steps longer) to determine where specific nodes break down. At one step longer (239 steps), in the strict consensus of 59 trees, nearly all resolution within Eucynodontia breaks down, leaving only the grouping of the chiniquodontids *Aleodon* + *Chiniquodon* and of *Pachygenelus* + *Morganucodon*. However, the 50% majority-rule consensus tree has the same topology as the minimum-length tree. At two steps longer, in the 50% majority-rule consensus of 286 trees, the node between *Probainognathus* and *Ecteninion* breaks down, yielding a trichotomy with a chiniquodontid + *Pachygenelus/Morganucodon* clade. At three steps longer, in the 50% majority-rule consensus of 1,024 trees, the node between Tritylodontidae and *"Scalenodon" hirschoni* breaks down. At four steps longer (3,480 trees), the node between *Probelesodon* and the remaining chiniquodontids breaks down. Only in the 50% majority-rule consensus of 30,120 trees that are six steps longer than the minimum-length tree does the node between *Lumkuia* and the remaining probainognathians break down (Fig. 8). A probainognathian clade occurs in 75% of these trees and cynognathian and gomphodont clades both oc-

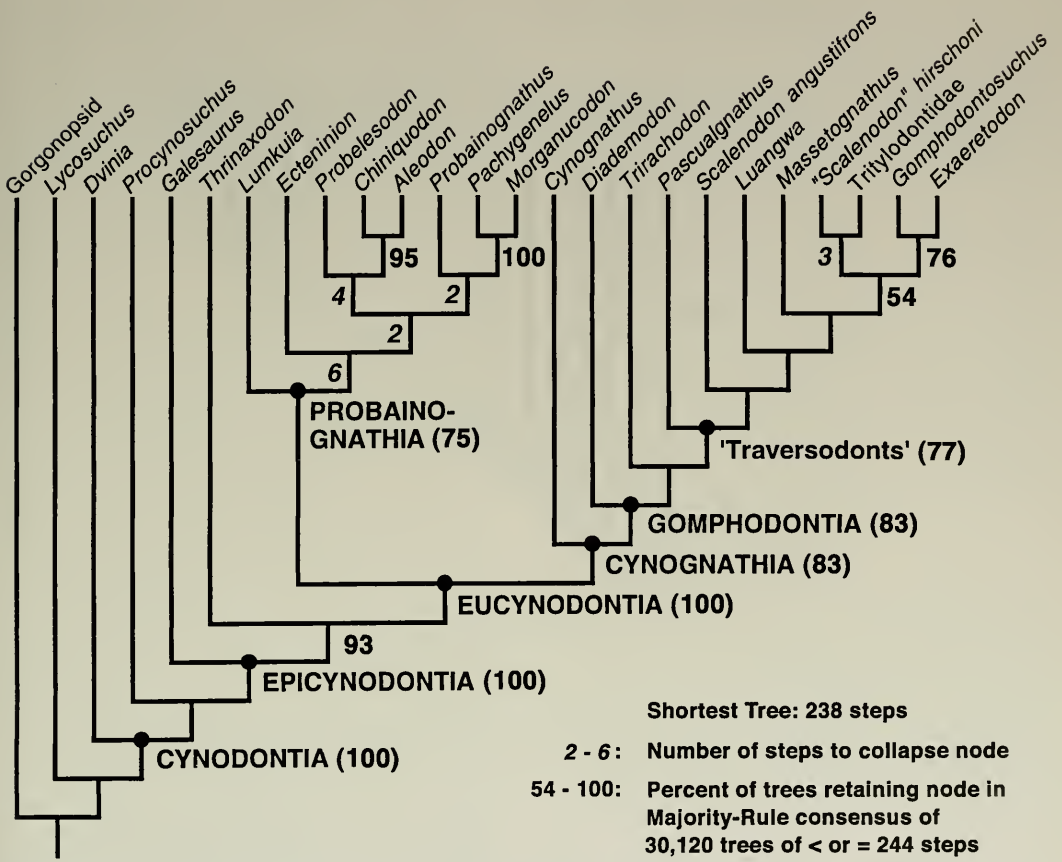

Figure 8. Cladogram of nonmammalian cynodonts. Shortest tree (238 steps) is shown, with numbers in bold italics (***2–6***) indicating the number of steps required to collapse that node, and numbers in bold (**54–100**) indicating the percentage of trees retaining that node in a 50% majority-rule consensus of 30,120 trees of less than or equal to 244 steps (six steps longer than minimum-length tree).

cur in 83% of the trees. The gomphodont genera retain the ordering seen in the minimum length tree in the great majority of trees that are six steps longer. Tritylodontids and "*S.*" *hirschoni* form a trichotomy with the *Exaeretodon/Gomphodontosuchus* clade in 54% of these trees.

In order to determine how parsimonious our preferred tree is to that of Rowe (1993, fig. 10.2), we used MacClade (Maddison and Maddison, 1992) to order our 19 eucynodont taxa in the most parsimonious tree in which the cynognathian–probainognathian dichotomy is not recognized. This turned out to duplicate the order of the far fewer taxa in Rowe's cladogram except that tritheledontids, not tritylodontids, form a clade with mammaliaforms (Fig. 9A). This tree is 267 steps long, 29 steps longer than our preferred tree. In the comparison of this tree with our preferred tree (Fig. 9B), the distribution of the internal carotid foramina is shown. Absence of these foramina in the basisphenoid is a synapomorphy of Cynognathia (Fig. 9B). When the cynognathian–probainognathian dichotomy is eliminated, the distribution of this character becomes extremely unparsimonious, with the foramina lost, regained, then lost and subsequently regained again.

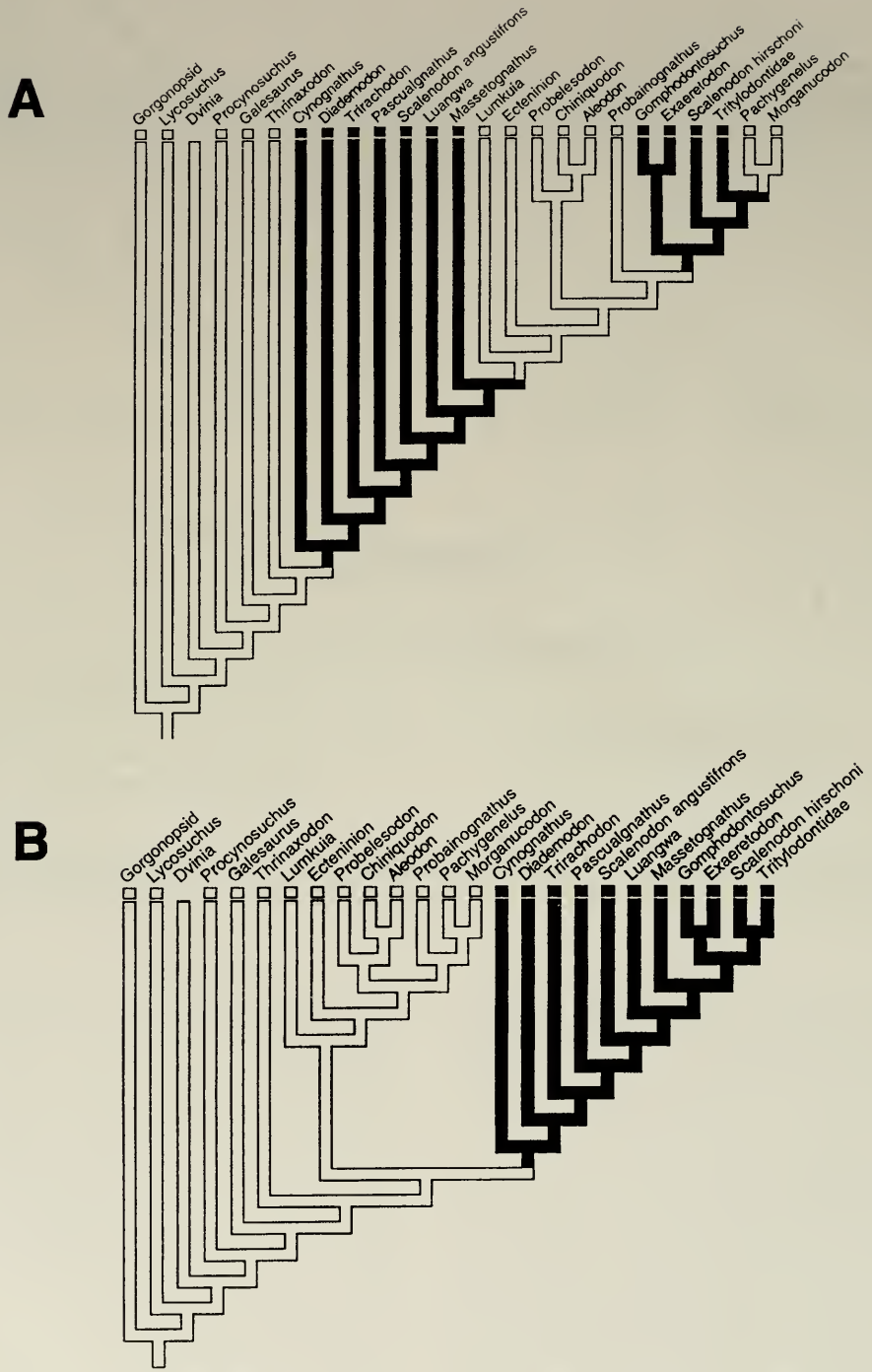

Figure 9. Cladograms constructed using MacClade showing distribution of internal carotid foramina in basisphenoid (character 26). Absence of carotid foramina is derived (black). (A) Cladogram in which 19 eucynodont taxa are ordered in the most

CONCLUSIONS

Lumkuia fuzzi is a basal member of the eucynodont clade Probainognathia. The dichotomy of eucynodonts into Probainognathia and Cynognathia is supported by this analysis, as is the placement of the Tritylodontidae within the cynognathian subgroup Gomphodontia. The sister group relationship of Tritheledontidae and Mammaliaformes is extremely well supported, although their placement in Probainognathia, rather than as sister to tritylodontids within Cynognathia, is less firm, requiring the ordering of four characters to achieve this placement. This uncertainty results from the extraordinarily large number of derived (mammallike) features shared by these three groups, features treated in other recent analyses as synapomorphies but here shown more likely to be convergences. A definitive solution to this phylogenetic problem will be found when morphologic intermediates between typical Triassic cynodonts and these primarily Jurassic (and, in the case of mammaliaforms, later) taxa are incorporated into analyses. Within the gomphodonts, *Exaeretodon* has a very mammallike postcranial skeleton and helps bridge the morphologic gap between Middle Triassic gomphodonts and tritylodontids. Bonaparte and Barberena (2001) describe two Late Triassic carnivorous cynodonts that are also very mammallike postcranially, and that appear to bridge the gap between *Probainognathus* and tritheledontids/mammaliaforms in cranial and dental morphology. We believe these newly described Late Triassic cynodonts will provide critical evidence supporting the probainognathian–cynognathian dichotomy and the occurrence of a truly extraordinary amount of homoplasy in eucynodont evolution.

ACKNOWLEDGMENTS

We thank Drs. M. A. Raath and B. S. Rubidge for the loan of material; Ms. Claire Vanderslice for preparation and illustration of specimens; and Mr. C. A. Sidor and Drs. G. W. Rougier, J. R. Wible, and J. A. Wilson for help in preparation of the manuscript. Hopson's research was supported by National Science Foundation grants BSR 86-15016 and 89-06619. We are grateful to Dr. F. A. Jenkins, Jr., and his co-organizers of the symposium for providing this opportunity to honor Fuzz Crompton. Hopson also wishes to express his pleasure at attending the symposium and enjoying the fellowship of good friends and colleagues.

LITERATURE CITED

BONAPARTE, J. F., AND M. C. BARBERENA. 2001. On two advanced carnivorous cynodonts from the Late Triassic of Southern Brazil. Bulletin of the Museum of Comparative Zoology, **156:** 59–80.

BROOM, R. 1905. On the use of the term Anomodontia. Records of the Albany Museum, **1:** 266–269.

CROMPTON, A. W. 1972a. The evolution of the jaw articulation of cynodonts, pp. 231–253. *In* K. A. Joysey and T. S. Kemp (eds.), Studies in Vertebrate Evolution. Edinburgh: Oliver and Boyd. 284 pp.

———. 1972b. Postcanine occlusion in cynodonts and tritylodontids. Bulletin of the British Museum (Natural History) Geology, **21:** 29–71.

CROMPTON, A. W., AND F. ELLENBERGER. 1957. On a new cynodont from the Molteno Beds and the origin of the tritylodontids. Annals of the South African Museum, **44:** 1–14.

ESTES, R. 1961. Cranial anatomy of *Thrinaxodon liorhinus*. Bulletin of the Museum of Comparative Zoology, Harvard, **125:** 165–180.

HANCOX, P. J., AND B. S. RUBIDGE. 1997. The role of fossils in interpreting the development of the Karoo Basin. Palaeontologia Africana, **33:** 41–54.

HANCOX, P. J., M. A. SHISHKIN, B. S. RUBIDGE, AND J. W. KITCHING. 1995. A threefold subdivision of the *Cynognathus* Assemblage Zone (Beaufort Group, South Africa) and its palaeogeographical

←

parsimonious tree that does not recognize a probainognathian–cynognathian dichotomy. Tree length is 267 steps, 29 steps longer than tree shown in (B), in which eucynodont taxa are ordered in the most parsimonious tree, determined from PAUP analysis (see Fig. 8). In this tree, the node-based Eucynodontia comprises the stem-based Probainognathia and Cynognathia. Absence of carotid foramina is a synapomorphy of Cynognathia. In tree A, CI = 0.51, RI = 0.71, RC = 0.36. In tree B, CI = 0.57, RI = 0.77, RC = 0.44.

implications. South African Journal of Science, **91:** 143–144.

HOPSON, J. A. 1966. The origin of the mammalian middle ear. American Zoologist, **6:** 437–450.

———. 1990. Cladistic analysis of therapsid relationships. Journal of Vertebrate Paleontology, **10**(3, Suppl.): 28A.

———. 1991a. Convergence in mammals, tritheledonts, and tritylodonts. Journal of Vertebrate Paleontology, **11**(3, Suppl.): 36A.

———. 1991b. Systematics of the nonmammalian Synapsida and implications for patterns of evolution in synapsids, pp. 635–693. *In* H.-P. Schultze and L. Trueb (eds.), Origins of the Higher Groups of Tetrapods: Controversy and Consensus. Ithaca, New York: Comstock Publishing Associates, a Division of Cornell University Press. xii + 724 pp.

———. 1994. Synapsid evolution and the radiation of non-therian mammals, pp. 190–219. *In* D. R. Prothero and R. M. Schoch (eds.), Major Features of Vertebrate Evolution, Short Courses in Paleontology, No. 7. Knoxville: University of Tennessee. 270 pp.

HOPSON, J. A., AND H. R. BARGHUSEN. 1986. An analysis of therapsid relationships, pp. 83–106. *In* N. Hotton III, P. D. MacLean, J. J. Roth, and E. C. Roth (eds.), The Ecology and Biology of Mammal-Like Reptiles. Washington, D.C.: Smithsonian Institution Press. x + 326 pp.

HOPSON, J. A., AND J. W. KITCHING. 1972. A revised classification of cynodonts. Palaeontologia Africana, **14:** 71–85.

———. 1988. A *Chiniquodon*-like cynodont from the Early Triassic of South Africa and the phylogeny of advanced cynodonts. Journal of Vertebrate Paleontology, **8**(3, Suppl.): 18A.

JENKINS, F. A., JR. 1971. The postcranial skeleton of African cynodonts. Bulletin of the Peabody Museum, Yale University, **36:** 1–216.

KEMP, T. S. 1982. Mammal-Like Reptiles and the Origin of Mammals. London: Academic Press. xiv + 363 pp.

———. 1983. The relationships of mammals. Zoological Journal of the Linnean Society, **77:** 353–384.

———. 1988. Interrelationships of the Synapsida, pp. 1–22. *In* M. J. Benton (ed.), The Phylogeny of the Tetrapods, Vol. 2: Mammals, Systematics Association Special Volume 35B. Oxford: Clarendon Press. 323 pp.

LUCAS, S. G., AND Z. LUO. 1993. *Adelobasileus* from the Upper Triassic of West Texas: the oldest mammal. Journal of Vertebrate Paleontology, **13:** 309–334.

MADDISON, W. P., AND D. R. MADDISON. 1992. MacClade, Version 3.01. Sunderland, MA: computer program distributed by Sinauer Associates, Inc.

MARTINEZ, R. N., C. L. MAY, AND C. A. FORSTER. 1996. A new carnivorous cynodont from the Ischigualasto Formation (Late Triassic, Argentina), with comments on eucynodont phylogeny. Journal of Vertebrate Paleontology, **16:** 271–284.

OWEN, R. 1861. Palaeontology, or a Systematic Summary of Extinct Animals and Their Geological Relations, second edition. Edinburgh: Adam and Black. xvi + 463 pp.

ROMER, A. S. 1969. The Chañares (Argentina) Triassic reptile fauna. V. A new chiniquodontid cynodont, *Probelesodon lewisi*—cynodont ancestry. Breviora, **333:** 1–24.

———. 1970. The Chañares (Argentina) Triassic reptile fauna. VI. A chiniquodontid cynodont with an incipient squamosal–dentary jaw articulation. Breviora, **344:** 1–18.

———. 1973. The Chañares (Argentina) Triassic reptile fauna. XIX. Postcranial materials of the cynodonts *Probelesodon* and *Probainognathus*. Breviora, **407:** 1–26.

ROUGIER, G. W., J. R. WIBLE, AND J. A. HOPSON. 1992. Reconstruction of the cranial vessels the early Cretaceous mammal *Vincelestes neuquenianus*: implications for the evolution of the mammalian cranial vascular system. Journal of Vertebrate Paleontology, **12:** 188–216.

ROWE, T. 1986. Osteological diagnosis of Mammalia, L. 1758, and its relationship to extinct Synapsida. Ph.D. dissertation. Berkeley: University of California. 446 pp.

———. 1988. Definition, diagnosis, and origin of Mammalia. Journal of Vertebrate Paleontology, **8:** 241–264.

———. 1993. Early mammal phylogenetic systematics, pp. 129–145. *In* F. S. Szalay, M. J. Novacek, and M. C. McKenna (eds.), Mammal Phylogeny: Mesozoic Differentiation, Multituberculates, Monotremes, Early Therians, and Marsupials. New York: Springer-Verlag. x + 249 pp.

SERENO, P. C. 1999. Definitions in phylogenetic taxonomy: critique and rationale. Systematic Biology, **48:** 329–351.

SIDOR, C. A., AND J. A. HOPSON. 1998. Ghost lineages and "mammalness": assessing the temporal pattern of character acquisition in the Synapsida. Paleobiology, **24:** 254–273.

SUES, H.-D. 1985. The relationships of the Tritylodontidae (Synapsida). Zoological Journal of the Linnean Society, **85:** 205–217.

SWOFFORD, D. L. 1993. PAUP: Phylogenetic Analysis Using Parsimony, Version 3.1. Champaign, Illinois: computer software and documentation distributed by Illinois Natural History Survey.

WIBLE, J. R. 1991. Origin of Mammalia: the craniodental evidence reexamined. Journal of Vertebrate Paleontology, **11:** 1–28.

WIBLE, J. R., AND J. A. HOPSON. 1995. Homologies of the prootic canal in mammals and non-mammalian cynodonts. Journal of Vertebrate Paleontology, **15:** 331–356.

APPENDIX 1: CHARACTER LIST

States are denoted as (0) = primitive state; (1), (2), and (3) = derived states.

Cranium

1. Premaxilla forms posterior border incisive foramen: absent (0), present (1).
2. Nasal–lacrimal contact: absent (0), present (1).
3. Prefrontal: present (0), absent (1).
4. Postfrontal: present (0), absent (1).
5. Postorbital: present (0), absent (1).
6. Prefrontal–postorbital contact: absent (0), present (1).
7. Parietal foramen: present (0), absent (1).
8. Vomer internarial shape: broad plate (0), parallel-sided keel (1).
9. Ectopterygoid: contacts maxilla (0), does not contact maxilla (1), absent (2).
10. Interpterygoid vacuity in adult between pterygoid flanges: present (0), absent (1).
11. Palatal exposure of maxilla behind canine greater than 20% distance from canine to posterior end of palatine: absent (0), present (1).
12. Secondary palatal plate on maxilla: absent (0), present, does not reach midline (1), present, reaches midline (2).
13. Secondary palatal plate on palatine: absent or low ridge (0), present, extends nearly to midline (1), present, reaches midline (2).
14. Length secondary palate relative to toothrow: shorter (0), about equal (1), longer (2).
15. Length secondary palate relative to anterior border of orbit: shorter (0), about equal (1), longer (2).
16. Teeth on pterygoid flange: present (0), absent (1).
17. Ventral surface of basisphenoid depressed below occipital condyles: less than ¼ occipital height (0), greater than ¼ occipital height (1).
18. Zygomatic arch dorsoventral height: slender (0), moderately deep (1), very deep (2).
19. Zygomatic arch dorsal extent: below middle of orbit (0), above middle of orbit (1).
20. Jugal depth in zygomatic arch relative to exposed squamosal depth: less than twice (0), greater than twice (1).
21. Jugal suborbital process: absent (0), present (1).
22. Squamosal groove for external auditory meatus: shallow (0), moderately deep (1), very deep (2).
23. Frontal–palatine contact in orbit: absent (0), present (1).
24. Tabular extends around posttemporal foramen: absent (0), present (1).
25. Descending flange of squamosal lateral to quadratojugal: absent (0), present not contacting surangular (1), present contacting surangular (2).
26. Internal carotid foramina in basisphenoid: present (0), absent (1).
27. Groove on prootic extending from pterygoparoccipital foramen to trigeminal foramen: absent (0), present and open (1), present and enclosed as a canal (2).
28. Trigeminal nerve exit: between prootic incisure and epipterygoid (0), via foramen between prootic and epipterygoid (1), via two foramina (2).
29. Quadrate contact: primarily squamosal (0), primarily crista parotica (1).
30. Quadrate ramus of pterygoid: present (0), absent (1).
31. Quadrate posteroventral process in squamosal posterior notch: absent (0), present (1).
32. Epipterygoid ascending process at level of trigeminal foramen: rodlike (0), moderately expanded (1), greatly expanded (2).
33. Epipterygoid–prootic overlap: absent (0), present (1).
34. Lateral flange of prootic: absent (0), present (1).

35. Epipterygoid–frontal contact: absent (0), present (1).
36. Separate foramina for vestibular and cochlear nerves: absent (0), present (1).
37. Double occipital condyles: absent (0), present (1).
38. Stapedial foramen orientation: anteroposterior (0), dorsoventral (1).
39. Greatest width of zygomatic arches: near middle of arch (0), at posterior end of arch (1).
40. Length of palatine relative to maxilla in secondary palate: shorter (0), about equal (1), longer (2).
41. Posterolateral end of maxilla: passes obliquely posterodorsally into suborbital bar (0), forms right angle ventral to jugal contact (1).
42. Fenestra rotunda separation from jugular foramen: confluent (0), partially separated by fingerlike projection from posterolateral wall of jugular foramen (1), completely separated (2).
43. V-shaped notch separating lambdoidal crest from zygomatic arch: absent (0), present (1).

Lower Jaw

44. Dentary symphysis: not fused (0), fused (1).
45. Dentary masseteric fossa: absent (0), high on coronoid region (1), extends to lower border of dentary (2).
46. Dentary overlap of dorsal surface of surangular: short (0). long (1).
47. Dentary coronoid process height: below middle of orbit (0), above middle of orbit (1).
48. Position of dentary–surangular dorsal contact relative to postorbital bar and jaw joint: closer to postorbital bar (0), midway between (1), closer to jaw joint (2).
49. Postdentary rod height relative to exposed length (distance between base of reflected lamina and jaw joint): greater than ½ length (0), about ½ length (1), less than ½ length (2).
50. Coronoid mediolaterally thickening: absent (0), present (1).
51. Reflected lamina of angular posterior extent relative to distance from angle of dentary to jaw joint: greater than ½ the distance (0), less than ½ the distance (1).
52. Reflected lamina of angular shape: deep corrugated plate (0), spoon-shaped plate (1), hook with depth greater than ½ length (2), hook with depth less than ½ length (3).

Dentition

53. Upper incisor number: five or more (0), four (1), three (2).
54. Lower incisor number: four or more (0), three (1), two (2).
55. Incisor cutting margins: serrated (0), smoothly ridged (1), denticulated (2).
56. Incisor size: all small (0), some or all enlarged (1).
57. Upper canine size: large (0), reduced in size (1), absent (2).
58. Lower canine size: large (0), reduced in size (1), absent (2).
59. Canine serrations: present (0), absent (1).
60. Postcanine shape: single point (0), two or more cusps in line (1).
61. Upper postcanine buccal cingulum: absent (0), present (1).
62. Postcanine lingual cingulum: absent (0), narrow (1), lingually expanded (2).
63. Number of upper cusps in transverse row: one (0), two (1), three or more (2).
64. Position of upper transverse cusp row on crown: on anterior half of crown (0), midcrown almost to posterior margin (1), at posterior margin (no posterior cingulum) (2).
65. Central cusp of upper transverse row: absent (0), midway between buccal and lingual cusps (1), closer to lingual cusp (2).
66. Longitudinal shear surface of main upper cusp: anterior and posterior

(to transverse ridge) (0), posterior only (1), anterior only (2).
67. Upper anterobuccal accessory cusp: present (0), absent (1).
68. Upper posterobuccal accessory cusp: present (0), absent (1).
69. Upper anterolingual accessory cusp: absent (0), present (1).
70. Upper anterior transverse (cingulum) ridge: low (0), high (1).
71. Upper lingual ridge: absent (0), present (1).
72. Transverse axis of crown strongly oblique to midline axis: absent (0), present (1).
73. Number of lower cusps in transverse row: one (0), two (1), three or more (2).
74. Lower anterior cingulum or cusp: absent (0), present (1).
75. Lower posterior basin: absent (0), present (1).
76. Widest lower cusp in transverse row: lingual (0), buccal (1).
77. Posterior portion maxillary tooth row inset from lateral margin of maxilla (cheek developed): absent (0), present (1).
78. Axis of posterior part of maxillary tooth row: directed lateral to subtemporal fossa (0), directed toward center of fossa (1), directed toward medial rim of fossa (2).
79. Posterior portion of maxillary tooth row extends medial to temporal fossa: absent (0), present (1).
80. Posteriormost postcanine(s) gomphodont: absent (0), present (1).
81. Postcanine replacement pattern in adult: "alternating" (0), widely spaced waves (three or more teeth/wave) (1), single wave (2).

Postcranium

82. Expanded costal plates on ribs: absent (0), present (1).
83. Lumbar costal plates with ridge overlapping preceding rib: absent (0), present (1).
84. Scapula infraspinous fossa with outturned anterior and posterior borders: absent (0), present (1).
85. Acromion process: absent (0), present (1).
86. Scapular constriction below acromion: absent (0), present (1).
87. Scapular elongation between acromion and glenoid: absent (0), present (1).
88. Procoracoid in glenoid: present (0), barely present or absent (1).
89. Procoracoid contact with scapula: greater than coracoid contact (0), equal to or less than coracoid contact (1).
90. Humerus ectepicondylar foramen: present (0), absent (1).
91. Ulna olecranon process: absent (unossified) (0), present (1).
92. Manual digit III phalanx number: four (0), three (1).
93. Manual digit IV phalanx number: five (0), four (1), three (2).
94. Length of anterior process of ilium anterior to acetabulum (relative to diameter of acetabulum): less than 1.0 (0), 1.0–1.5 (1), greater than 1.5 (2).
95. Length of posterior process of ilium posterior to acetabulum: (relative to diameter of acetabulum): between 0.5 and 1.0 (0), greater than 1.0 (1), less than 0.5 (2).
96. Dorsal profile of ilium: strongly convex (0), flat to concave (1).
97. Total length of pubis relative to acetabulum diameter: greater than 1.5 (0), between 1.5 and 1.0 (1), less than 1.0 (2).
98. Greater trochanter separated from femoral head by distinct notch: absent (0), present (1).
99. Greater trochanter joined to femoral head by ridge: present (0), absent (1).
100. Lesser trochanter position: on ventromedial surface of femoral shaft (0), on medial surface of femoral shaft (1).
101. Vertebral centra: amphicoelous (0), platycoelous (1).

APPENDIX 2: CHARACTER STATES

STATES ARE DENOTED AS 0 (PRIMITIVE); AND 1, 2, OR 3 (DERIVED). ? = STATE UNKNOWN.

Taxon	1 1234567890	1111111112 1234567890	2222222223 1234567890	3333333334 1234567890	4444444445 1234567890
Gorgonopsid	0000000000	000??00100	0000000000	000000000?	0000000020
Lycosuchus	0000000000	000??00000	0000000000	010000000?	0000000000
Dvinia	0101010010	1110010000	00010?1100	1211101100	0000110000
Procynosuchus	0101010010	1110010000	0001001100	1211101100	0000110000
Galesaurus	0101010011	1110010100	0101101100	1211101100	0000211110
Thrinaxodon	0101010111	1220010100	0101101100	1211101100	0000211110
Cynognathus	0101010111	1220010210	1201211101	1211101110	0001211220
Diademodon	0101010171	1220010211	1201211201	1211101110	0011211220
Trirachodon	0101010121	1220110211	1201212201	1211101110	0011211220
Pascualgnathus	?101010121	1220110211	1201212201	1211101110	0?11211220
Scalenodon angustifrons	0101010121	1220011211	1201212201	1211101110	0111211220
"Scalenodon" hirschoni	010101?121	122011??11	?2?121??01	1?11101170	0??1211220
Luangwa	?101010121	1220?1?211	1201212201	121110111?	0111211220
Massetognathus	1101010121	1220211211	0201212201	1211101110	0111211220
Gomphodontosuchus	?10101?121	122001??1?	?20121??01	1?111?1170	0??1211220
Exaeretodon	?101011121	122011?210	12?1212201	1211101110	0?11211220
Tritylodontidae	1111101121	1220211211	0211112211	1211111110	0210211221
Lumkuia	0101011120	1220110100	0101201101	1211101100	0011211220
Probainognathus	1101011121	1221110100	0111201101	1211101100	0111211220
Ecteninion	?101011121	1220110?00	0111201101	1211101100	0?11211220
Probelesodon	1101011121	1221210100	0111201101	1211101101	1111211220
Aleodon	1101011121	1222210?00	011120??01	1?11101102	1??1211220
Chiniquodon	?101011121	1222210100	0111201101	1211101102	1?11211220
Pachygenelus	1111101120	1222210000	0011001101	1211111102	0210211221
Morganucodon	0111101121	1222210000	001?002211	?111111100	0210211221

APPENDIX 3: SYNAPOMORPHIES OF PRINCIPAL TAXA OF CYNODONTIA

Numbers refer to characters in Appendix 1. Numbers in parentheses refer to equivocal synapomorphies under the Delayed Transformation (DELTRAN) option of PAUP.

Cynodontia

2. Nasal–lacrimal contact.
4. Postfrontal absent.
6. Prefrontal–postorbital contact.
9. Ectopterygoid does not contact maxilla.
11. Palatal exposure of maxilla behind canine greater than 20% distance from canine to posterior end of palatine.
12. Secondary palatal plate on maxilla.
13. Secondary palatal plate on palatine.
16. Teeth on pterygoid flange absent.
24. Tabular extends around posttemporal foramen.
27. Groove on prootic extending from pterygoparoccipital foramen to trigeminal foramen.
28. Trigeminal nerve exit via foramen between prootic and epipterygoid.
31. Posteroventral process on quadrate in posterior notch of squamosal.
(32). Ascending process of epipterygoid greatly expanded.
33. Epipterygoid–prootic overlap.
34. Lateral flange of prootic.
35. Epipterygoid–frontal contact.
37. Double occipital condyles.
38. Stapedial foramen with dorsoventral orientation.
45. Dentary masseteric fossa present high on coronoid region.

APPENDIX 2: EXTENDED

				1	1
5555555556	6666666667	7777777778	8888888889	9999999990	0
1234567890	1234567890	1234567890	1234567890	1234567890	1
0000000000	000?0?????	??000?000?	0000000000	0000000000	0
0000000000	000?0?????	??000?000?	0000000000	0120000000	0
0100100011	122110????	??210?000?	000?0??0??	???1001000	?
0100100011	010?00????	??010?000?	0001000000	0011001?00	0
0211100011	000?00????	??0?0?0000	0101000000	001102?00	0
0211100011	010?00????	??010?0000	0101000000	0011102000	0
1311000001	000?00????	??010?0000	?111100000	0121102?00	0
1311?000?1	0221100100	00110?0000	111110?000	0121112000	0
1311100001	0221100??0	00210?1100	1111100000	012???????	0
1311?000?1	0210010100	001?101200	2111110?00	0??1112000	0
1311000001	1221220000	0011101200	21????????	???1??????	?
1322111?11	0221221010	1011101201	2?????????	?????????0	?
13110000?1	1221221010	1011101201	2101110000	0??2112000	0
1311201111	1222221000	1010101201	2101110100	012211200?	0
1311101111	0212021011	1110111201	2?????????	?????????0	?
1321110111	0212021111	1110111211	2001110100	1122012000	0
1322112?1	0222121?10	1011??1211	2001110111	1122212111	1
1311100011	000?00????	??010?0000	10011?010?	??????????	0
1311100011	010?00????	??010?0100	1001110???	0??211?000	0
1311100001	0?0?00????	??0?0?0000	??0???????	??????????	?
1311100?1	000?00????	??010?0000	?001110100	012211?000	0
1311100?1	021?00????	??110?0000	1?0??????0	??????????	?
13111000?1	021?00????	??110?0000	??01110100	???211?000	0
1322111111	110?00????	??010?0210	0001111110	1??2212101	1
1310100111	110?00????	??010?0100	1001111111	1122212111	1

46. Dentary overlap of surangular long.
52. Reflected lamina of angular spoon-shaped plate.
55. Incisor cutting margins smoothly ridged.
59. Canine serrations absent.
60. Postcanines with two or more cusps in line.
74. Lower anterior cingulum or cusp present.
94. Length anterior process of ilium 1.0–1.5 times diameter of acetabulum.
97. Length of pubis between 1.5 and 1.0 times acetabular diameter.

Epicynodontia

10. Interpterygoidal vacuity between pterygoid flanges absent in adult.
18. Zygomatic arch moderately deep.
22. Groove for external auditory meatus moderately deep.
25. Descending flange of squamosal lateral to quadratojugal present.
45. Masseteric fossa extends to lower border of dentary.
47. Coronoid process of dentary extends above middle of orbit.
48. Dentary–surangular dorsal contact midway between postorbital bar and jaw joint.
49. Height of postdentary rod about one half the length of the laterally exposed portion of the rod (distance between base of reflected lamina and jaw joint).
52. Reflected lamina of angular hook-shaped, with depth greater than one half its length.
53. Four upper incisors.

54. Three lower incisors.
82. Expanded plates on ribs.
95. Length of posterior process of ilium greater than diameter of acetabulum.
97. Length of pubis less than diameter of acetabulum.

Eucynodontia

25. Descending flange of squamosal lateral to quadratojugal contacts surangular.
30. Quadrate ramus of pterygoid absent.
44. Dentary symphysis fused.
48. Dentary–surangular dorsal contact closer to jaw joint that to postorbital bar.
49. Height of postdentary rod less than one half the length of the laterally exposed portion of the rod.
51. Reflected lamina of angular less than one half the distance from angle of the dentary to jaw joint.
52. Reflected lamina of angular hook-shaped, with depth less than one half its length.
81. Postcanine replacement pattern of widely spaced waves (three or more teeth per wave).
85. Acromion process on scapula.
92. Manual digit III with three phalanges.
93. Manual digit IV with three phalanges.

Probainognathia

7. Parietal foramen absent.
(9). Ectopterygoid absent.
15. Rear of secondary palate lies below anterior border of orbit.
(43). V-shaped notch separates lambdoidal crest from zygoma.
82. Expanded plates on ribs absent.
88. Procoracoid barely present in or absent from glenoid.

Probainognathia Minus *Lumkuia*

23. Frontal contacts palatine in orbital wall.

Probainognathia Minus *Lumkuia, Ectinion*

(1). Premaxillae form posterior border of incisive foramina.
14. Secondary palate about equal in length to tooth row.
(42). Fenestra rotunda partially separated from jugular foramen by finger like projection.
(86). Scapula constricted below acromion process.
(94). Anterior process of ilium anterior to acetabulum greater than 1.5 times acetabular diameter.
(96). Dorsal profile of ilium flat to concave.

Probainognathus, Pachygenelus, and *Morganucodon*

62. Narrow postcanine lingual cingulum.
78. Axis of posterior part of maxillary tooth row directed toward center of temporal fossa.

Pachygenelus and *Morganucodon*.

3. Prefrontal absent.
5. Postorbital absent.
6. Prefrontal–postorbital contact absent.
(14). Secondary palate longer than tooth-row.
(15). Secondary palate extends posterior to anterior border of orbit.
18. Zygomatic arch slender.
22. Squamosal groove for external auditory meatus shallow.
25. Descending flange of squamosal lateral to quadratojugal absent.
36. Separate foramina in petrosal for vestibular and cochlear nerves.
42. Fenestra rotunda completely separated from jugular foramen.
44. Dentary symphysis not fused.
50. Coronoid mediolaterally thickened.
58. Lower canine reduced in size.
61. Upper postcanines with buccal cingulum.

87. Scapula elongated between acromion and glenoid.
(89). Procoracoid contact with scapula equal to or less than coracoid contact.
91. Ulnar olecranon process present.
95. Posterior process on ilium less than one half diameter of acetabulum.
98. Greater trochanter separated from femoral head by deep notch.
100. Lesser trochanter on medial surface of femoral shaft.
101. Vertebral centra platycoelous.

Chiniquodontidae

(15). Secondary palate extends posterior to anterior border of orbit.
41. Posterolateral end of maxilla forms right angle ventral to jugal contact.

Cynognathia

18. Zygomatic arch very deep.
19. Zygomatic arch extends above middle of orbit.
21. Suborbital process on jugal.
22. Groove for external auditory meatus very deep.
26. Basisphenoid internal carotid foramina absent.
39. Greatest width of zygomatic arches at posterior end of arch.
59. Canine serrations present.
83. Lumbar costal plates with ridge overlapping preceding rib.

Gomphodontia

20. Depth of jugal in zygomatic arch greater than twice that of exposed part of squamosal.
28. Trigeminal nerve exit via two foramina.
(43). V-shaped notch separates lambdoidal crest from zygoma.
62. Upper postcanine internal cingulum lingually expanded.
63. Upper postcanines with three cusps in transverse row.
73. Lower postcanines with two cusps in transverse row.
(96). Dorsal profile of ilium flat to concave.

Traversodonts (Incl. Tritylodontidae)

75. Posterior basin on lower postcanines.
(78). Axis of posterior part of maxillary tooth row directed toward medial rim of subtemporal fossa.
81. Adult postcanine replacement pattern consists of single wave.
86. Scapula constricted below acromion process.

"*Scalenodon*" *hirschoni* + Tritylodontidae.

(53). Three upper incisors.
54. Two lower incisors.
(56). Some or all incisors enlarged.

Gomphodontosuchus + *Exaeretodon*

63. Two cusps in transverse row on upper postcanines.
65. Central cusp of upper transverse row absent.
70. High anterior transverse ridge on upper postcanines.
72. Transverse axis of postcanine crowns strongly oblique to midline axis.
(74). Lower anterior cingulum or cusp absent.
76. Widest lower cusp in transverse row buccal.

ON *MICROCONODON*, A LATE TRIASSIC CYNODONT FROM THE NEWARK SUPERGROUP OF EASTERN NORTH AMERICA

HANS-DIETER SUES[1]

ABSTRACT. Three incomplete dentaries with teeth and several isolated postcanine teeth of a small cynodont synapsid from the Upper Triassic (Carnian) Tomahawk Member of the Vinita Formation of the Richmond basin (Newark Supergroup) in Virginia are referable to *Microconodon tenuirostris* Osborn, 1886. This taxon was previously known only from a single specimen, an incomplete right dentary with four postcanine teeth from the Upper Triassic (Carnian) Cumnock Formation of North Carolina. Once considered one of the earliest and most primitive mammals, *Microconodon* is a derived eucynodont of uncertain affinities. Its more posterior postcanine teeth have three or four anteroposteriorly aligned cusps, lack cingula, and the roots of some postcanines are incipiently divided.

INTRODUCTION

Emmons (1857) named *Dromatherium sylvestre* on the basis of three small tooth-bearing jaws from Late Triassic coals (initially thought to be Permian in age) in the Chatham coal field of central North Carolina. He interpreted these fossils as the oldest known mammalian remains. *Dromatherium* quickly became widely established as the first reputed American Mesozoic mammal and as the oldest mammal known at that time (e.g., Owen, 1871). Osborn (1886a) restudied two of the jaws; he could not trace the repository for the third specimen mentioned by Emmons, which was presumed lost. Osborn recognized the distinctive nature of one of the dentaries, housed in the collections of the Academy of Natural Sciences of Philadelphia (ANSP 10248), and made it the holotype of a new genus and species, *Microconodon tenuirostris* (see also Osborn, 1886b, 1887). Unaware of Osborn's work, Gillette (1978) still listed the holotype of *M. tenuirostris* as a "syntype" of *D. sylvestre*.

During his survey of all Mesozoic mammals then known, Simpson (1926a,b) reexamined the holotypes of *D. sylvestre* and *M. tenuirostris*. He removed both taxa from the Mammalia and referred them to the Cynodontia, as had first been suggested by Seeley (1895). In support of his reassessment, Simpson cited evidence for the presence of more than one bone in the lower jaw, the undivided roots of the lower postcanine teeth, and the resemblance of the crowns of these teeth to those of certain nonmammalian cynodonts. The first and third features are phylogenetically uninformative because they are plesiomorphic features. The second character is of questionable significance because, as Simpson (1926b) himself observed, the roots of the more posterior postcanines in the holotype of *M. tenuirostris* are incipiently divided. Since Simpson's redescription, little attention has been paid to these fossils, although doubts concerning their phylogenetic position have persisted to the present day. Hopson and Kitching (1972) classified *Dromatherium* and *Microconodon* as Cynodontia incertae sedis, but explicitly noted possible mammalian affinities for both taxa. Most recently, Hahn et al. (1994) placed both forms, together with several other problematic taxa of Late Triassic nonmammalian cynodonts in a family Dromatheriidae, which they considered the sister-taxon of Mammalia.

The holotypes of *D. sylvestre* and *M.*

[1] Department of Palaeobiology, Royal Ontario Museum, 100 Queen's Park, Toronto, Ontario M5S 2C6, Canada.

tenuirostris were collected from coal seams near the base of the Cumnock Formation, of late Carnian age (Litwin and Ash, 1993), in a now abandoned mine near Egypt, Chatham County, North Carolina. The strata belong to the Sanford subbasin of the Deep River basin of the Newark Supergroup. Simpson (1926b) provided a meticulous description of these specimens, and little can be added to his account. Both fossils have been adversely affected by early attempts at preparation and conservation. The holotype of *D. sylvestre* was originally housed in the Museum of Williams College but has recently been permanently transferred to the collections of the National Museum of Natural History. The postcanine teeth of this specimen have been badly damaged since the time of Simpson's study, and most details of his account can no longer be verified. *Dromatherium sylvestre* is quite different from *M. tenuirostris* in most comparable features (Simpson, 1926a). The holotype of *M. tenuirostris* (ANSP 10248) holds fewer teeth than the holotype of *D. sylvestre*, but the postcanines of *M. tenuirostris* are better preserved.

Three partial dentaries with teeth and several isolated postcanine teeth of a small cynodont from the Tomahawk Member of the Vinita Formation (Turkey Branch Formation *sensu* Cornet and Olsen [1990]) in the Richmond basin (Newark Supergroup) of Virginia (Sues and Olsen, 1990; Sues et al., 1994) closely resemble the holotype of *M. tenuirostris* in all comparable characters. They appear to be referable to the same taxon and exhibit significant additional anatomical detail. The new dentaries also represent different ontogenetic stages. The purpose of this paper is to describe and illustrate this material and to assess the affinities of *M. tenuirostris* within the phylogenetic framework provided by recent hypotheses of cynodont interrelationships (Rowe, 1988; Battail, 1991; Hopson, 1991). I will also briefly review the status of several possibly related but poorly known cynodont taxa from the Upper Triassic of central and western Europe (Huene, 1933; Peyer, 1956; Clemens, 1980; Hahn et al., 1984, 1987, 1994; Godefroit and Battail, 1997), New Mexico (Lucas and Oakes, 1988), and Brazil (Bonaparte and Barberena, 1975, 2001).

TABLE 1. MEASUREMENTS (IN MM) FOR THE ANTEROPOSTERIOR LENGTH (L) AND BUCCOLINGUAL WIDTH (W) OF POSTCANINE (PC) TEETH IN THE NEW SPECIMENS REFERRED TO *MICROCONODON TENUIROSTRIS*.

Specimen	Tooth	L	W
USNM 437637	Pc_3	1.4	
ROM 44300	Pc_4	1.2	0.65
	Pc_6	1.6	0.65
	Pc_7	1.9	0.7
ROM 44301	Pc_4	0.8	0.3
	Pc_5	0.9	0.4
	Pc_7	1.3	0.5

The following abbreviations for institutional names preceding catalogue numbers are used in this paper: ANSP, Academy of Natural Sciences of Philadelphia; ROM, Royal Ontario Museum, Toronto; USNM, National Museum of Natural History (formerly United States National Museum), Washington, D.C.

All dental measurements (Table 1) were made with a graded ocular scale on a Nikon SMZU stereoscopic microscope; each measurement was repeated three times.

SYSTEMATIC PALEONTOLOGY

Monophyletic Hierarchy. Amniota: Synapsida: Therapsida: Cynodontia: Eucynodontia incertae sedis.

Genus *Microconodon* Osborn, 1886

Dromatherium Emmons, 1857: 93 (in part)
Microconodon Osborn, 1886a: 540
Tytthoconus Palmer, 1903: 873 (objective junior synonym)

Type Species. Microconodon tenuirostris Osborn, 1886 (by monotypy).

Diagnosis. Dentary with very slender horizontal ramus. Angular region of dentary without distinct process. Posterior postcanine teeth with three or four anteroposteriorly aligned cusps. Postcanines

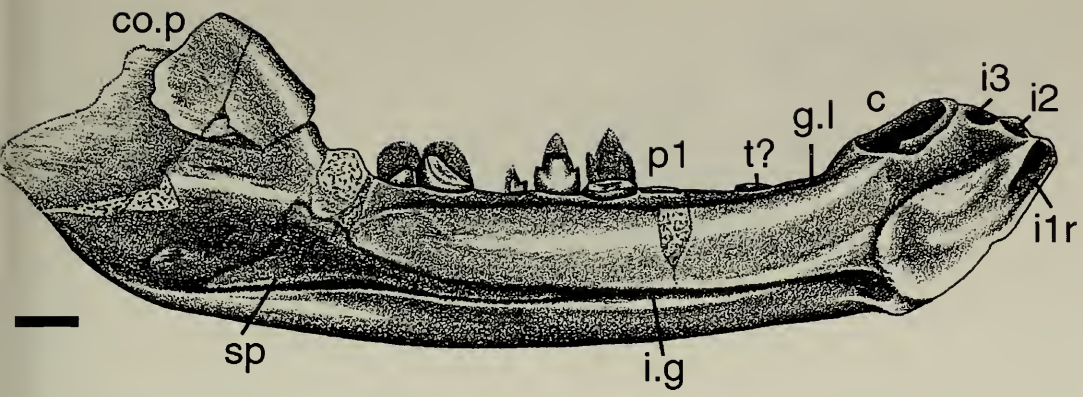

Figure 1. *Microconodon tenuirostris,* USNM 437637, left dentary (with splenial and attached symphyseal fragment of right dentary) in lingual view. Scale bar = 2 mm. Abbreviations: an, angle of dentary; ar.p, articular process of dentary; c, canine alveolus; co.p, coronoid process; co.r, coronoid ridge; f.sp., articular facet for splenial; g.l, groove for dental lamina; i1–3, alveoli for incisors 1–3; i1r, alveolus for right first incisor; i.g, internal mandibular groove; m, mental foramen; p1–8, postcanine 1–8 (tooth or alveolus); r, pit for replacement tooth; sp, splenial; t?, tooth fragment.

without cingula. Root of some postcanine teeth constricted, with figure-eight shape in transverse section.

Comment. Palmer (1903) regarded *Microconodon* Osborn, 1886 as preoccupied by *Microconodus* Traquair, 1877 and proposed *Tytthoconus* as a replacement name. Palmer's action is invalid under the rules of the *International Code of Zoological Nomenclature,* and *Tytthoconus* Palmer, 1903 is an objective junior synonym of *Microconodon* Osborn, 1886.

Microconodon tenuirostris Osborn, 1886

Dromatherium sylvestre Emmons, 1857: 93 (in part)
Microconodon tenuirostris Osborn, 1886a: 540

Holotype. ANSP 10248, right dentary with four preserved postcanine teeth, lacking the articular process and part of the coronoid process (Simpson, 1926b). The specimen is preserved on a slab of coal, and preservation of most structural details is indistinct.

Type Horizon and Locality. Basal coals of the Cumnock Formation, Sanford subbasin of the Deep River basin, Newark Supergroup; coal mine (now abandoned) at Egypt, Chatham County, North Carolina. Age: Late Triassic (late Carnian; Litwin and Ash, 1993).

Newly Referred Material. USNM 437637, incomplete left dentary lacking much of the articular and coronoid processes, with alveoli for three incisors and the canine, seven mostly broken postcanine teeth, and attached left splenial as well as fragment of the symphyseal end of the right dentary (Fig. 1). ROM 44300, incomplete left dentary with alveoli for one incisor and the canine, three postcanine teeth, and basal portions of four postcanines; mandibular symphysis for the most part preserved only as an impression (filled in with epoxy resin during preparation) and posterior portion of dentary broken and displaced anterolaterally (Fig. 2). ROM 44301, anterior portion of right dentary with alveolus for canine, five preserved postcanine teeth, and alveoli for three postcanines (Fig. 3). USNM 448579, isolated complete postcanine tooth. USNM 448600 (Sues et al., 1994, fig. 8.4) and ROM 44302, isolated postcanine teeth with most of the root broken off.

Horizon and Locality of Newly Referred Material. Tomahawk Member of Vinita Formation (Turkey Branch Formation *sensu* Cornet and Olsen [1990]), Richmond basin, Newark Supergroup; USNM locality 39981, 0.16 km (0.1 miles) east of the eastern branch of Little Tomahawk Creek along the former course of VA 652 (Old

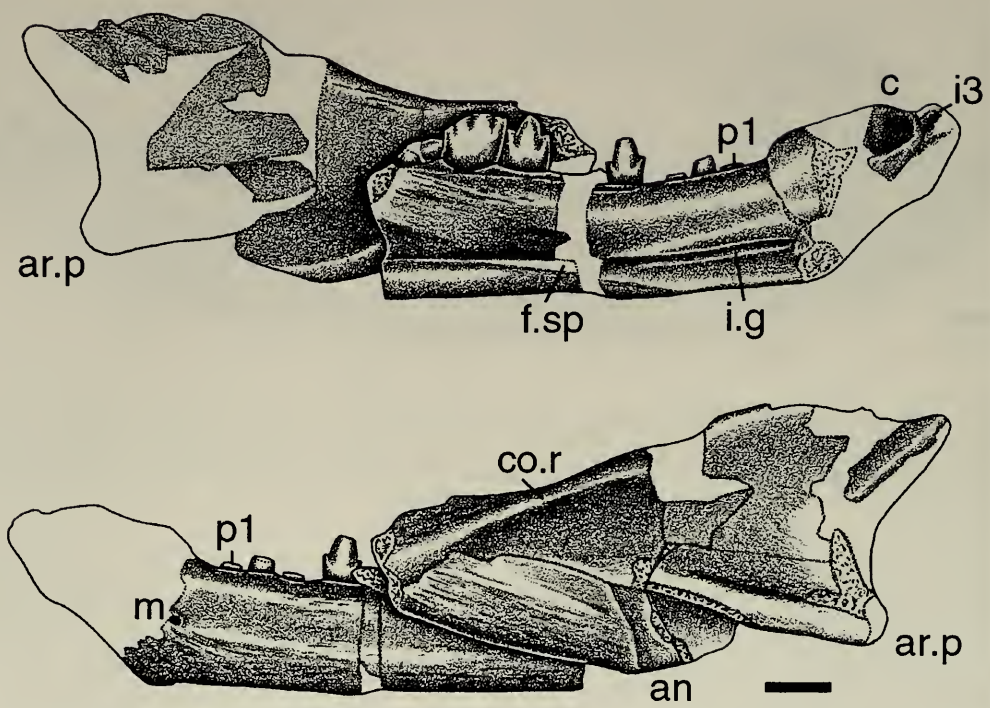

Figure 2. *Microconodon tenuirostris,* ROM 44300, left dentary in lingual (top) and buccal (bottom) views. Unshaded areas represent impressions in the matrix that were filled in with colored epoxy resin during preparation. Abbreviations as in Figure 1. Scale bar = 2 mm.

Hundred Road), near Midlothian, Chesterfield County, Virginia. Latitude 77°40′17″N, longitude 37°27′50″W, Hallsboro 7.5 Minute Quadrangle. Age: Late Triassic (late Carnian according to Lucas [1998]).

Diagnosis. Type and only known species of genus, as diagnosed above.

Discussion. The new material from the Richmond basin closely resembles ANSP 10248, the holotype of *Microconodon tenuirostris* Osborn, 1886, in most comparable features, particularly in the structure of the postcanine teeth. The only feature showing variation is the course of the internal mandibular groove, which approaches the ventral margin of the dentary in ROM 44301 but extends parallel to it in

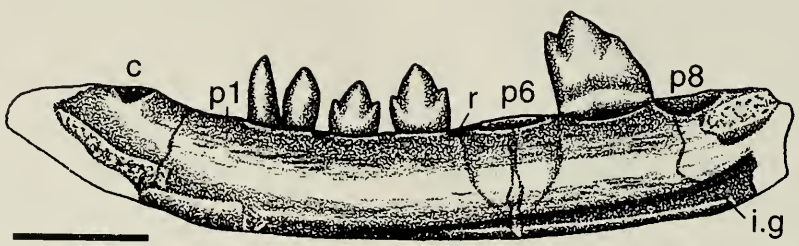

Figure 3. *Microconodon tenuirostris,* ROM 44301, anterior portion of right dentary in lingual view. Unshaded areas represent impressions in the matrix that were filled in with colored epoxy resin during preparation. Abbreviations as in Figure 1. Scale bar = 2 mm.

ROM 44300 and USNM 437637. This difference may be ontogenetic in nature, and, in the absence of other differences, I refer all specimens to the same taxon.

DESCRIPTION

Dentary

The long horizontal ramus of the dentary is slender throughout its entire length (Figs. 1–3). Behind the mandibular symphysis, the alveolar (dorsal) and ventral margins of the ramus are rather straight and extend more or less parallel to each other. The alveolar margin abruptly rises toward the canine alveolus in USNM 437637; this rise is accompanied by a lateral bulging of the dentary. Part of a mental foramen is visible on the lateral surface behind the canine alveolus in ROM 44300. Anteriorly, the ventral margin of the dentary forms a slight projection below the canine in ROM 44300 and USNM 437637 and then curves forward and upward in all specimens. The dentary is gently convex beneath the incisors. The ventral edge is rounded and thickened back to the region of the angle where it becomes sharper. The robust symphyseal portion of the dentary holds alveoli for a large canine and three apparently slightly procumbent incisors. The dentaries are fused along their long, sloping symphysis. In USNM 437637, a fragment of the symphyseal portion of the right dentary, containing the alveolus for the first lower incisor, still adheres to the left element (Fig. 1). The mandibular symphysis extends back to the level of the posterior margin of the alveolus for the canine. The buccal surface of the horizontal ramus of the dentary is convex dorsoventrally. A faint buccal groove on the horizontal ramus of the dentary ANSP 10248 noted by Osborn (1886b, 1887) appears to be the result of postmortem crushing and is not present on any of the specimens from the Richmond basin. The lingual surface of the horizontal ramus is flat near its symphyseal end but becomes gently convex below the postcanine teeth. A narrow groove, which presumably housed the dental lamina in life (Crompton, 1963), extends lingually just below and parallel to the alveolar margin and anteriorly up to the canine alveolus. The internal mandibular groove (sulcus primordialis) is developed on the lingual surface close to the ventral margin of the horizontal ramus of the dentary. This groove extends just above, and anteriorly approaches, the ventral margin on the small dentary ROM 44301 (Fig. 3), but its course is more or less parallel to and well above the margin in USNM 437637 (Fig. 1) and ROM 44300 (Fig. 2) where it reaches the posterior end of the symphysis. The internal groove forms the anterior continuation of the well-developed posterior trough for the reception of the postdentary bones. The angular region of the dentary does not form a distinct process, unlike in many other cynodonts; the ventral margin of the dentary curves gently upward and backward toward the articular process. Lateral to the last postcanine tooth, the low but anteroposteriorly broad coronoid process smoothly rises posterodorsally at an angle of about 45° relative to the long axis of the dentary. The anterior margin of the process forms a coronoid ridge, which is most pronounced anteriorly, before it merges into the horizontal ramus. The masseteric fossa is weakly defined. No distinct facet for the coronoid bone is apparent on the medial aspect of the coronoid process of the dentary. The lateral ridge on the articular process of the dentary is expanded, especially more posteriorly, but there is no indication that it contributed to a mammallike condyle posteriorly.

Splenial

A featureless, elongate-triangular bone in the posterior portion of the internal groove of the dentary in USNM 437637 (Fig. 1) represents a partial left splenial. Articular facets for the splenial on the dentary ROM 44300 (Fig. 2) indicate that this bone may have entered into the mandibular symphysis anteriorly.

Dentition

The incisors and canine are documented only by their alveoli. Three alveoli for incisors are present in USNM 437637. They indicate that the incisors were similar in size to each other and that they were slightly procumbent. The large alveolus for the canine forms an elongate oval in outline. The count of three incisors and one canine is in agreement with Simpson's (1926b) estimate based on a series of depressions on the lateral aspect of the mandibular symphysis of ANSP 10248, which he correctly interpreted as crushed alveoli.

In occlusal view, the crowns of the postcanine teeth are elliptical in outline and buccolingually narrow (Sues et al., 1994, fig. 8.4). Those of the tricuspid and tetracuspid postcanines are more than twice as long anteroposteriorly as wide buccolingually. No wear facets indicative of cusp contact resulting from tooth-to-tooth occlusion are present. The apex of the principal cusp is slightly blunted by abrasion on most teeth. The postcanine teeth preserved in situ confirm the anatomical orientations for isolated tooth crowns of possibly related cynodont taxa proposed by Peyer (1956) and Hahn et al. (1984). In buccal or lingual view, the slightly more convex cutting edge of the principal cusp faces anteriorly (mesially); in anterior or posterior view, the vertical curvature of the buccal surface is slightly more convex than that of the lingual surface.

The specimen USNM 437637 has seven postcanine tooth positions and ROM 44300 has eight (the last alveolus being incomplete). The specimen ROM 44301 preserves eight postcanine teeth or alveoli, but the posterior end of the tooth-bearing ramus of the dentary is not preserved.

The crowns of the anterior two postcanines of ANSP 10248 and of the anterior two preserved postcanines (positions 2 and 3) in ROM 44301 are simple cones. In ANSP 10248 they show a slight posterior swelling. This single-cusped type of postcanine is absent in the largest known specimen (USNM 437637).

The crowns of most of the other postcanine teeth are tricuspid. The only exceptions in the sample described here are the more posterior of the two multicuspid postcanines preserved in ANSP 10248 and the seventh postcanine in ROM 44300, both of which have one anterior and two posterior accessory cusps. The specimen ROM 44300 shows some differentiation among its multicuspid postcanine teeth: compared to the crowns of the sixth and seventh postcanines, that of the fourth is shorter anteroposteriorly and taller. The fourth postcanine also has relatively smaller anterior and posterior accessory cusps that are placed closer to the base of the crown. The crowns of the multicuspid postcanines progressively increase in length toward the posterior end of the tooth row. The buccolingually narrow cusps are aligned behind one another in a straight line and are clearly separated from each other. The median or principal cusp is much larger than the anterior (mesial) and posterior (distal) accessory cusps and dominates the tooth crown. This cusp is broad anteroposteriorly and somewhat compressed buccolingually. The subequal accessory cusps are symmetrically positioned in front and behind the principal cusp and are separated from the latter by distinct V-shaped notches. A distinct cutting edge extends down from the apex of the principal cusp along both the anterior and posterior faces; the anterior cutting edge is slightly more convex than the posterior one. Each accessory cusp bears a sharp cutting edge only on the side facing the central cusp. The accessory cusps project slightly away from the principal cusp. Neither the principal nor the accessory cusps are recurved. Cingula are absent. The enamel is completely smooth on most teeth. Fine, stained lines on the enamel of the isolated postcanine tooth USNM 448579 presumably represent postmortem fracturing (see Hahn et al., 1984). The anteroposteriorly broad and buccolingually

flattened root is not set off from the crown by an annular constriction. The specimen USNM 448579 shows a pronounced median longitudinal constriction of its root, the apical portion of which is broken. This incipient division of the root is not evident on any of the teeth preserved in situ in the referred dentaries. However, this division is visible on the two multicuspid postcanine teeth preserved in ANSP 10248. In ROM 44300 and ROM 44301, a ring of bone connects the roots of at least some functional teeth to the alveolar margin; details are not clearly visible for all tooth positions. This ankylosis is also present in basal eucynodonts such as *Thrinaxodon* (Crompton, 1963).

In ROM 44301, small pits for developing replacement teeth are present in the groove for the dental lamina anterolingual to postcanine positions 4 and 6 and lingual to tooth 7 (Fig. 3). Comparison of the four known dentaries indicates that the simple anterior postcanines were lost without replacement during growth, resulting in a progressively longer diastema in larger specimens, as in many nonmammalian cynodonts (Crompton, 1963) and in the mammaliamorph *Sinoconodon* (Crompton and Luo, 1993). However, in the latter, new teeth are added only at the posterior end of the postcanine series. The small dentaries ANSP 10248 (length: 16.5 mm) and ROM 44301 (length of preserved portion: 10.3 mm) both lack a diastema between the canine and postcanine teeth, and the postcanine tooth row begins immediately behind the canine position. On the large dentary USNM 437637, an extensive diastema separates the alveolus for the canine from the postcanine teeth (Fig. 1); a tooth fragment attached to the bone about midway probably represents a displaced fragment. The configuration of the tooth row is consistent with evidence from the pattern of bone grain for the immaturity of ROM 44300 and ROM 44301 (Figs. 2, 3); the grain on the latter two dentaries comprises fine longitudinal grooves and pores typical of immature bone (Enlow, 1969). The specimen USNM 437637 does not show this type of bone grain although it was almost identical in length to ROM 44300 (estimated lengths of 33 mm and 34 mm, respectively). The surface of ANSP 10248 is too poorly preserved to show details of texture.

DISCUSSION

Taxa Possibly Related to *Microconodon*

Lees and Mills (1983: 179) observed that "[m]any of the later small carnivorous cynodonts and early mammals had molars consisting, more or less, of a single main cusp, flattened bucco-lingually, with mesial and distal cuspules" [accessory cusps in the present paper]. This statement aptly characterizes the postcanine teeth of *Microconodon*.

Many isolated teeth resembling those of *Microconodon* as well as jaw fragments containing such teeth have been reported from the Upper Triassic of central and western Europe (Peyer, 1956; Clemens, 1980; Hahn et al., 1984, 1987, 1994; Sigogneau-Russell and Hahn, 1994; Godefroit and Battail, 1997) and New Mexico (Lucas and Oakes, 1988). These fossils have been variously referred to nonmammalian cynodonts or mammals, but, in some cases, even their synapsid affinities remain yet to be established (see below). The situation was complicated by the discovery of tricuspid teeth in the Late Triassic "rhamphorhynchoid" pterosaur *Eudimorphodon* (Wild, 1978), although Hahn et al. (1984) have provided structural criteria for distinguishing between teeth of *Eudimorphodon* and those of nonmammalian cynodonts.

Tricuspes tuebingensis Huene, 1933 from the Rhaeto–Liassic bonebed at Gaisbrunnen (Baden-Württemberg, Germany) as well as *Tricuspes sigogneauae* Hahn et al., 1994 and *Tricuspes tapeinodon* Godefroit et Battail, 1997 from the Upper Triassic (Norian) of Saint-Nicolas-de-Port (France) and Hallau (Switzerland) are known only from isolated postcanine teeth (Clemens, 1980; Hahn et al., 1994; God-

efroit and Battail, 1997). Clemens (1980) tentatively placed *Tricuspes* in the Mammalia whereas Hahn et al. (1994) referred it to the nonmammalian cynodont taxon Dromatheriidae. The tricuspid and tetracuspid postcanines of *Tricuspes* closely resemble those of *Microconodon* in most features, including the incipient division of the root. However, in occlusal view, the apex of the principal cusp in *Tricuspes* is slightly displaced so that the cusps are arranged in a broadly V-shaped pattern. Furthermore, the holotype of *T. tuebingensis*, which was identified as a right lower postcanine by Clemens (1980) and Godefroit and Battail (1997) but as a left lower postcanine by Hahn et al. (1994), bears an accessory cuspule (Hahn et al., 1994, fig. 3, m) in a posterobuccal (according to Clemens) or posterolingual (according to Hahn et al.) position. This cuspule is absent on the teeth of *T. sigogneauae* and *T. tapeinodon* from Saint-Nicolas-de-Port (Hahn et al., 1994; Godefroit and Battail, 1997).

Hahn et al. (1984) named *Pseudotriconodon wildi* on the basis of isolated postcanine teeth from a mid-Norian bonebed in Luxembourg. Some teeth referred to *P. wildi* have three cusps whereas others have four or five. The tooth crowns are devoid of cingula and closely resemble those of *Microconodon* in their overall appearance. As in *Microconodon*, the cusps are aligned directly behind one another. Both the principal and accessory cusps form distinct cutting edges anteriorly and posteriorly, unlike the condition in *Microconodon*. Incipient root division appears to be restricted to the apical portion of the root on some postcanines (Hahn et al., 1984, pl. 2, fig. 6). As in *Microconodon*, the root is not set off from the crown by an annular constriction (Hahn et al., 1984, pl. 3, figs. 1a, 2a, 6d). *Pseudotriconodon* possibly differs from *Microconodon* in that tetracuspid and pentacuspid postcanines are as common as or more common than tricuspid teeth in the currently available samples (Hahn et al., 1984).

Hahn et al. (1987) described three new cynodont taxa based on isolated postcanine teeth recovered from a Rhaetian bonebed (Sables de Mortinsart) at Gaume, southern Belgium: *Lepagia gaumensis, Gaumia longiradicata*, and ?*Gaumia incisa*. They also referred some postcanines from the Hallau bonebed to *L. gaumensis* and ?*G. incisa*. Hahn et al. (1987) assigned *Lepagia* to the Chiniquodontidae, and Sigogneau-Russell and Hahn (1994) referred it to the Chiniquodontidae or Probainognathidae on the basis of similarities in the position and shape of the splenial between *Lepagia* and *Probainognathus*. However, the phylogenetic significance of those features is uncertain (see Battail, 1991). Tooth crowns of *Lepagia* are asymmetrical in side view and have a principal cusp and one or two anterior and posterior accessory cusps. Cingula are absent. The undivided root is separated from the crown by a distinct annular constriction. Hahn et al. (1987) left the systematic position of *Gaumia* unresolved, and Sigogneau-Russell and Hahn (1994) considered it a chiniquodontoid of uncertain affinities. Teeth referable to *Gaumia* are distinguished mainly by the great length of the undivided, distally tapering root, which is set off from the crown by a slight constriction.

Lucas and Oakes (1988) described "*Pseudotriconodon*" *chatterjeei* on the basis of a tiny tooth-bearing jaw fragment and two isolated teeth from the Bull Canyon Formation (Upper Triassic: lower Norian) of New Mexico. "*Pseudotriconodon*" *chatterjeei* differs from *P. wildi* in the structure of its teeth, and indeed reference of this material to the Cynodontia remains to be confirmed by additional specimens. The cusps of "*P.*" *chatterjeei* bear numerous prominent vertical ridges buccally and lingually; similar striations are present on the teeth of the Late Triassic pterosaur *Eudimorphodon* (Wild, 1978; Hahn et al., 1984).

Therioherpeton cargnini from the Upper Triassic Santa Maria Formation of southern Brazil is based on an incomplete skull and a partial postcranial skeleton

(Bonaparte and Barberena, 1975). Cranial features shared with both Tritheledontidae and Mammaliaformes include the absence of the prefrontal and postorbital (and postorbital bar). The zygomatic arch is very slender along its entire length. The postcanine teeth lack cingula and have four cusps that are aligned directly behind one another. The root of at least one postcanine shows a median longitudinal constriction of the anteroposteriorly broad root. Kemp (1982) referred *Therioherpeton* to the Tritheledontidae, but it lacks the dental features diagnostic for the latter taxon (Gow, 1980; Shubin et al., 1991).

Lucas and Luo (1993) suggested that the possible basal mammaliaform *Adelobasileus cromptoni*, known only from an isolated braincase from the Tecovas Member of the Dockum Formation (Upper Triassic: upper Carnian) of Texas, might prove referable to *Microconodon*. However, in the absence of associated jaws and (or) postcanine teeth, this association remains untestable.

With the exception of *Therioherpeton*, the aforementioned taxa, including *Microconodon*, are poorly represented by skeletal remains. Although the similarity in the structure of the postcanine teeth in all these forms may prove to be phylogenetically significant, it is more prudent to consider them incertae sedis among the Eucynodontia until more complete specimens become available for study. *Therioherpeton* shares some apomorphic cranial features with both Tritheledontidae and Mammaliaformes, but the distribution of those characters in other derived cynodonts has yet to be fully documented. I believe that it is premature to use these features to diagnose a family-level taxon Dromatheriidae, as has been proposed by Hahn et al. (1994).

Phylogenetic position of *Microconodon*

Assessing the phylogenetic position of *Microconodon* is difficult because of the very limited set of character-states observable in the available specimens. *Microconodon* is referable to the Eucynodontia as diagnosed by Hopson (1991; see also Martinez et al. [1996]) based on the possession of the following apomorphies: dentary considerably enlarged and fused mandibular symphysis. *Microconodon* also shares with other eucynodonts a splenial reduced to a slender, thin bone covering the internal groove of the dentary and postdentary bones (articular, prearticular, and surangular) forming a rodlike complex that is lodged in a posterior trough on the lingual surface of the dentary (inferred from the shape of the trough). The material currently referable to *Microconodon* is insufficient to permit more precise determination of the phylogenetic relationships of this taxon.

Hahn et al. (1984) redefined Dromatheriidae Gill, 1872, to include *Dromatherium*, *Microconodon*, *Pseudotriconodon*, and *Therioherpeton*. Battail (1991) excluded *Therioherpeton* from the Dromatheriidae, but hypothesized a sister-group relationship between the two taxa based on the shared absence of cingula on the postcanine teeth. However, Hopson (1991) noted that cingula are also absent on the postcanines of *Probelesodon* from the Middle Triassic Chañares Formation of Argentina, and this character-state may either diagnose a more inclusive grouping or may have developed more than once. Indeed, the distribution of cingula is apparently variable among derived cynodont synapsids: the lower postcanine teeth of the mammaliamorph *Sinoconodon* have weakly developed posterolingual cingula (Crompton and Luo, 1993), whereas those of the tritheledontid *Pachygenelus* (Gow, 1980; Shubin et al., 1991) and the mammaliaform *Morganucodon* (Mills, 1971; Crompton and Luo, 1993) have well-developed lingual cingula. Battail (1991) proposed a clade including Dromatheriidae and *Therioherpeton*, which he placed as the sister-taxon of Tritheledontidae (and possibly Mammaliaformes) on the basis of several cranial and dental characters. The former cannot be determined in the

known material referable to *Microconodon*. One of the dental characters cited by Battail, the more or less oblique implantation of the postcanine teeth relative to the long axis of the tooth row, is absent in *Microconodon*. Most recently, Hahn et al. (1994) have redefined the Dromatheriidae to include *Tricuspes* and *Meurthodon* Sigogneau-Russell et Hahn, 1994, from the Upper Triassic of Saint-Nicolas-de-Port (France). They also explicitly considered Dromatheriidae the sister-taxon of "Mammalia" (Mammaliaformes *sensu* Rowe [1988]). The currently available material is insufficient for a rigorous test of this intriguing hypothesis.

The postcanine teeth of *Microconodon*, *Pseudotriconodon*, and *Therioherpeton* differ from those of other nonmammalian cynodonts (*Cynognathus*, *Probainognathus*, *Probelesodon*, and *Pachygenelus* as well as the sectorial teeth of *Diademodon* and other basal gomphodont cynodonts) in the absence of the backward curvature of the principal cusp and (with the exception of *Probelesodon*) in the lack of cingula. They also differ from the postcanines of *Cynognathus* and *Probelesodon* in the absence of serrations on the cutting edges of individual cusps. Furthermore, the postcanine teeth of *Microconodon* and *Therioherpeton* share incipient division of the roots, resulting in a figure-eight shape in transverse section. Although this feature is also present in the tritheledontid *Pachygenelus* (Shubin et al., 1991), it may well prove diagnostic for those probainognathian eucynodonts closest to Tritheledontidae + Mammaliaformes (Hopson, personal communication).

Microconodon tenuirostris is a derived eucynodont, but the currently available material does not permit a more precise placement. This uncertainty also reflects the still inadequate fossil record of small cynodonts from Mid- to Late Triassic continental strata.

ACKNOWLEDGMENTS

I am indebted to P. A. Kroehler (National Museum of Natural History), P. E. Olsen (Lamont-Doherty Earth Observatory, Columbia University), and especially E. B. Sues for their enthusiastic help in the field. W. W. Amaral (Harvard University) assisted in the preparation of the new specimens reported in this paper. E. R. Daeschler (Academy of Natural Sciences of Philadelphia) arranged for the extended loan of the holotype of *Microconodon tenuirostris*. S. G. Lucas (New Mexico Museum of Natural History) kindly provided a cast of the holotype of *"Pseudotriconodon" chatterjeei* for comparisons. D. M. Scott prepared the illustrations with her customary skill. J. A. Hopson (University of Chicago) and Z. Luo (Carnegie Museum of Natural History) offered constructive comments on a draft of the manuscript. I gratefully acknowledge financial support from the National Geographic Society (grants 3592-88 and 4232-89), National Science Foundation (NSF EAR-9016677 to H.-D. S. and P. E. Olsen), Smithsonian Institution, and the Natural Sciences and Engineering Research Council of Canada. I dedicate this paper to Fuzz Crompton who introduced me to nonmammalian cynodonts and who has made so many important contributions to our knowledge of these animals during his long and distinguished career.

LITERATURE CITED

Battail, B. 1991. Les Cynodontes (Reptilia, Therapsida): une phylogénie. Bulletin du Muséum National d'Histoire Naturelle, Série 4, Section C, **13:** 17–105.

Bonaparte, J. F., and M. C. Barberena. 1975. A possible mammalian ancestor from the Middle Triassic of Brazil (Therapsida–Cynodontia). Journal of Paleontology, **49:** 931–936.

Bonaparte, J. F., and M. C. Barberena. 2001. On two advanced cynodonts form the Late Triassic of Southern Brazil. Bulletin of the Museum of Comparative Zoology, **156:** 59–80.

Clemens, W. A. 1980. Rhaeto–Liassic mammals from Switzerland and West Germany. Zitteliana, **5:** 51–92.

Cornet, B., and P. E. Olsen. 1990. Early to Middle Carnian (Triassic) Flora and Fauna of the Richmond and Taylorsville Basins, Virginia and Maryland, U.S.A. Virginia Museum of Natural History

Guidebook Number 1. Martinsville, Virginia. 87 pp.

Crompton, A. W. 1963. Tooth replacement in the cynodont *Thrinaxodon liorhinus* Seeley. Annals of the South African Museum, **46:** 479–521.

Crompton, A. W., and Z. Luo. 1993. Relationships of the Liassic mammals, *Sinoconodon, Morganucodon oehleri,* and *Dinnetherium,* pp. 30–44. *In* F. S. Szalay, M. J. Novacek, and M. C. McKenna (eds.), Mammal Phylogeny: Mesozoic Differentiation, Multituberculates, Monotremes, Early Therians, and Marsupials. Berlin: Springer-Verlag. x + 249 pp.

Emmons, E. 1857. American Geology. Part VI. Albany, New York: Sprague and Co. x + 152 pp.

Enlow, D. H. 1969. The bone of reptiles, pp. 45–80. *In* C. Gans, A. d'A. Bellairs, and T. S. Parsons (eds.), Biology of the Reptilia. Vol. 1: Morphology A. New York: Academic Press. xv + 373 pp.

Gill, T. 1872. Arrangement of the families of mammals and synoptical tables of characters of the subdivisions of mammals. Smithsonian Miscellaneous Collections, **230:** 1–98.

Gillette, D. D. 1978. Catalogue of type specimens of fossil vertebrates, Academy of Natural Sciences, Philadelphia. Part IV: Reptilia, Amphibia, and tracks. Proceedings of the Academy of Natural Sciences of Philadelphia, **129:** 101–111.

Godefroit, P., and B. Battail. 1997. Late Triassic cynodonts from Saint-Nicolas-de-Port (northeastern France). Geodiversitas, **19:** 567–631.

Gow, C. E. 1980. The dentitions of the Tritheledontidae (Therapsida: Cynodontia). Proceedings of the Royal Society of London, Series B, **208:** 461–481.

Hahn, G., R. Hahn, and P. Godefroit. 1994. Zur Stellung der Dromatheriidae (Ober-Trias) zwischen den Cynodontia und den Mammalia. Geologica et Palaeontologica, **28:** 141–159.

Hahn, G., J. C. Lepage, and G. Wouters. 1984. Cynodontier-Zähne aus der Ober-Trias von Medernach, Grossherzogtum Luxemburg. Bulletin de la Société belge de Géologie, **93:** 357–373.

Hahn, G., R. Wild, and G. Wouters. 1987. Cynodontier-Zähne aus der Ober-Trias von Gaume (S-Belgien). Mémoires pour servir à l'Éxplication des Cartes Géologiques et Minières de la Belgique, **24:** 1–33.

Hopson, J. A. 1991. Systematics of nonmammalian Synapsida and implications for patterns of evolution in synapsids, pp. 635–693. *In* H.-P. Schultze and L. Trueb (eds.), Origins of the Higher Groups of Tetrapods: Controversy and Consensus. Ithaca, New York: Comstock Publishing Associates. xii + 724 pp.

Hopson, J. A., and J. W. Kitching. 1972. A revised classification of cynodonts (Reptilia; Therapsida). Palaeontologia Africana, **14:** 71–85.

Huene, E. von. 1933. Zur Kenntnis des Württembergischen Rätbonebeds mit Zahnfunden neuer Säuger und säugerähnlicher Reptilien. Jahreshefte des Vereins für vaterländische Naturkunde in Württemberg, **89:** 65–128.

Kemp, T. S. 1982. Mammal-like Reptiles and the Origin of Mammals. London: Academic Press. 363 pp.

Lees, P. M., and R. Mills. 1983. A quasi-mammal from Lesotho. Acta Palaeontologica Polonica, **28:** 171–180.

Litwin, R. J., and S. Ash. 1993. Revision of the biostratigraphy of the Chatham Group (Upper Triassic), Deep River basin, North Carolina, U.S.A. Review of Palaeobotany and Palynology, **77:** 75–95.

Lucas, S. G. 1998. *Placerias* (Reptilia, Dicynodontia) from the Upper Triassic of the Newark Supergroup, North Carolina, USA, and its biochronological significance. Neues Jahrbuch für Geologie und Paläontologie, Monatshefte, **1998:** 432–448.

Lucas, S. G., and Z. Luo. 1993. *Adelobasileus* from the Upper Triassic of west Texas: the oldest mammal. Journal of Vertebrate Paleontology, **13:** 309–334.

Lucas, S. G., and W. Oakes. 1988. A Late Triassic cynodont from the American South-West. Palaeontology, **31:** 445–449.

Martinez, R. N., C. L. May, and C. A. Forster. 1996. A new carnivorous cynodont from the Ischigualasto Formation (Late Triassic, Argentina), with comments on eucynodont phylogeny. Journal of Vertebrate Paleontology, **16:** 271–284.

Mills, J. R. E. 1971. The dentition of *Morganucodon,* pp. 29–63. *In* D. M. Kermack and K. A. Kermack (eds.), Early Mammals. Zoological Journal of the Linnean Society, **50**(Suppl. 1). xiv + 203 pp.

Osborn, H. F. 1886a. A new mammal from the American Triassic. Science, **8:** 540.

———. 1886b. Observations on the Upper Triassic mammals, *Dromatherium* and *Microconodon.* Proceedings of the Academy of Natural Sciences of Philadelphia, **37:** 359–363.

———. 1887. The Triassic mammals, *Dromatherium* and *Microconodon.* Proceedings of the American Philosophical Society, **24:** 109–111.

Owen, R. 1871. Monograph of the Fossil Mammalia from the Mesozoic Formations. London: Palaeontographical Society. xi + 115 pp.

Palmer, T. S. 1903. Some new generic names of mammals. Science, **17:** 873.

Peyer, B. 1956. Über Zähne von Haramiyden [sic], von Triconodonten und von wahrscheinlich synapsiden Reptilien aus dem Rhät von Hallau Kt. Schaffhausen, Schweiz. Schweizerische Paläontologische Abhandlungen, **72:** 1–72.

Rowe, T. 1988. Definition, diagnosis, and origin of Mammalia. Journal of Vertebrate Paleontology, **8:** 241–264.

Seeley, H. G. 1895. Researches on the structure, organization, and classification of the fossil Reptilia. Part IX, Section 5. On the skeleton in new

Cynodontia from the Karroo rocks. Philosophical Transactions of the Royal Society of London, Series B, **186:** 59–148.

Shubin, N. H., A. W. Crompton, H.-D. Sues, and P. E. Olsen. 1991. New fossil evidence on the sister-group of mammals and early Mesozoic faunal distributions. Science, **251:** 1063–1065.

Sigogneau-Russell, D., and G. Hahn. 1994. Late Triassic microvertebrates from central Europe, pp. 197–213. *In* N. C. Fraser and H.-D. Sues (eds.), In the Shadow of the Dinosaurs: Early Mesozoic Tetrapods. Cambridge, United Kingdom: Cambridge University Press. x + 435 pp.

Simpson, G. G. 1926a. Are *Dromatherium* and *Microconodon* mammals? Science, **63:** 548–549.

———. 1926b. Mesozoic Mammalia. V. *Dromatherium* and *Microconodon*. American Journal of Science, **12:** 87–108.

Sues, H.-D., and P. E. Olsen. 1990. Triassic vertebrates of Gondwanan aspect from the Richmond basin of Virginia. Science, **249:** 1020–1023.

Sues, H.-D., P. E. Olsen, and P. A. Kroehler. 1994. Early Late Triassic small tetrapods from the Richmond basin of Virginia, pp. 161–170. *In* N. C. Fraser and H.-D. Sues (eds.), In the Shadow of the Dinosaurs: Early Mesozoic Tetrapods. Cambridge, United Kingdom: Cambridge University Press. x + 435 pp.

Traquair, R. H. 1877. The Ganoid Fishes of the British Carboniferous Formations. Part I. Palaeoniscidae. London: Palaeontographical Society. 60 pp. [first installment only].

Wild, R. 1978. Die Flugsaurier (Reptilia, Pterosauria) aus der Oberen Trias von Cene bei Bergamo, Italien. Bollettino della Società Palaeontologica Italiana, **17:** 176–256.

A CYNODONT FROM THE UPPER TRIASSIC OF EAST GREENLAND: TOOTH REPLACEMENT AND DOUBLE-ROOTEDNESS

MICHAEL D. SHAPIRO[1] AND FARISH A. JENKINS, JR.[1]

ABSTRACT. A new genus and species of cynodont from the Upper Triassic Fleming Fjord Formation of East Greenland possesses double-rooted postcanine teeth and a nonalternate pattern of tooth replacement. The specimen represents an addition to the known diversity of Early Mesozoic taxa with multi-rooted dentitions (tritylodontids, *Sinoconodon* sp., haramiyids, morganucodontids, *Meurthodon gallicus*), and casts doubt on traditional interpretations of the interdependency of reduced tooth replacement patterns and teeth with multiple roots.

INTRODUCTION

The Upper Triassic Fleming Fjord Formation of Jameson Land, East Greenland, preserves a diverse fossil vertebrate fauna that includes mammals, theropod and prosauropod dinosaurs, plagiosaurid and cyclotosaurid amphibians, turtles, aetosaurs, phytosaurs, and pterosaurs (Jenkins et al., 1994, 2001). Mammals are represented primarily from the upper Tait Bjerg Beds and include *Kuehneotherium*, cf. *Brachyzostrodon*, and the haramiyid *Haramyavia clemmenseni* (Jenkins et al., 1994, 1997). We describe here an additional component of the fauna, a cynodont that bears double-rooted teeth, the only known specimen of this taxon. A comparable form of Late Triassic age is *Meurthodon gallicus* (Russell et al., 1976; Sigogneau-Russell and Hahn, 1994; Godefroit and Battail, 1997), represented by isolated teeth from Rhaetic deposits in France, but this taxon differs in significant details.

The following abbreviations of institutional names are used: IRSNB, Institut royal des Sciences naturelles de Belgique, Brussels; MCZ, Museum of Comparative Zoology, Harvard University, Cambridge, Massachusetts; MGUH, Geological Museum, University of Copenhagen; and MNHP, Institut de Paléontologie, Muséum National d'Histoire Naturelle, Paris.

SYSTEMATIC PALEONTOLOGY

Order Therapsida Broom, 1905

Infraorder Cynodontia Owen, 1861

Family incertae sedis

Mitredon cromptoni new genus and species

Etymology. The generic term refers to the highly peaked primary cusps, a combination of English mitre, the high-peaked ecclesiastical headdress, from Greek *mitra*, turban, and Greek *odous* (*odon*), tooth. The specific name honors A. W. Crompton for his important contributions to our understanding of the paleobiology and evolution of cynodonts.

Holotype. MGUH VP 3392, MCZ field number 11/G95 (Figs. 1A, B), a partial left dentary bearing an incomplete alveolus mesially, three unerupted postcanine teeth, roots of four other (erupted) postcanines, and an empty tooth crypt distally.

Horizon. Uppermost dolostone of Tait Bjerg Beds, Ørsted Dal Member of the Fleming Fjord Formation.

Locality. 71°32.929′N, 22°55.450′W, north of Ærenprisdal at its confluence with Pingel Dal, Jameson Land, East Greenland.

[1] Department of Organismic and Evolutionary Biology, and Museum of Comparative Zoology, Harvard University, Cambridge, Massachusetts 02138.

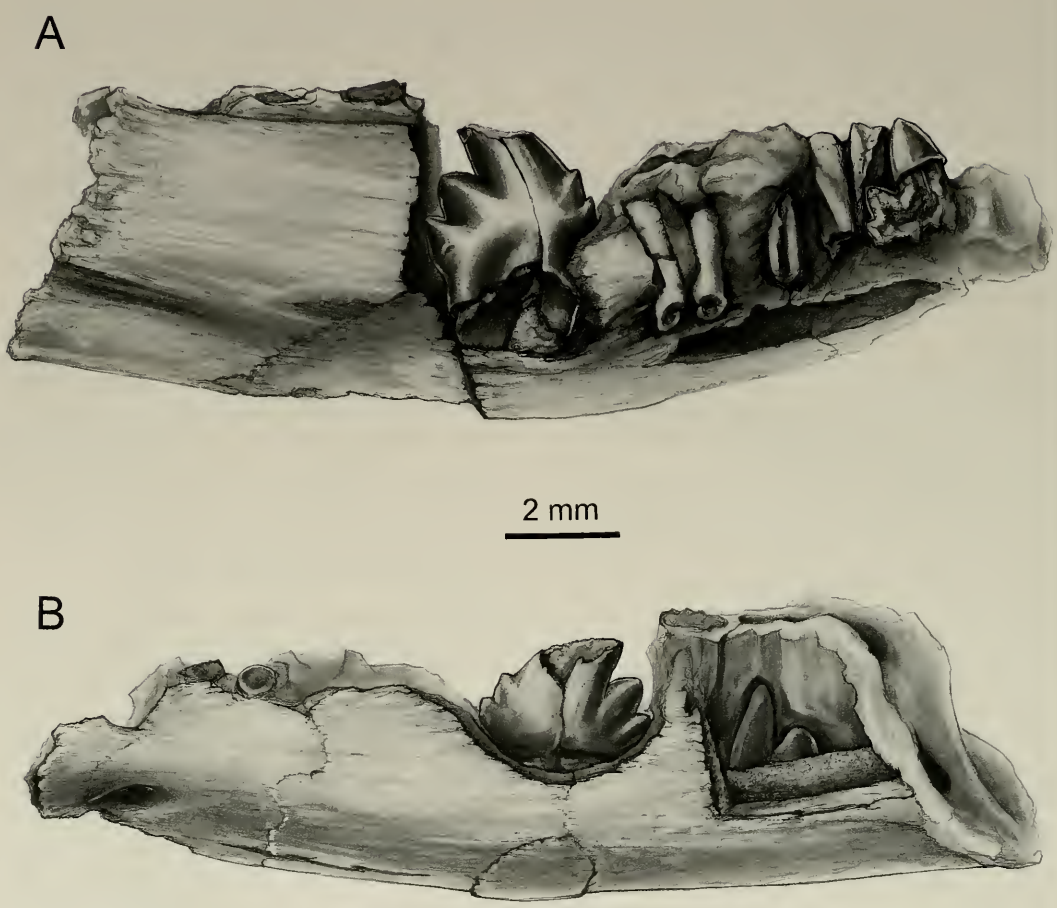

Figure 1. Left dentary of *Mitredon cromptoni,* MGUH VP 3392, in (A) lingual view and (B) occlusolabial view. In occlusolabial view, the mandibular canal is visible distally as a filled cast through a window cut in the labial aspect of the jaw; the canal obscures the basal crown of Pc_6.

Age. Late Triassic (?Norian–Rhaetic; Jenkins et al., 1994).

Diagnosis. Cingular cusps on postcanine teeth absent or lost, a derived character shared with galesaurid cynodonts, *Cynognathus,* and *Probelesodon* (Hopson and Kitching, 1972; Hopson and Barghusen, 1986). Differs from Therioherpetidae (Bonaparte and Barberena, 1975) and other nonmammalian cynodonts in possessing bifurcate postcanine tooth roots (likely convergent with multirooted tritylodontids) and lacking alternate tooth replacement. Characters shared with "chiniquodonts" are crowns of lower postcanines with laterally compressed cusps arranged in a longitudinal row and clearly separated from each other (Bonaparte and Barberena, 1975; Sigogneau-Russell and Hahn, 1994). A feature shared with *Meurthodon gallicus* (Russell et al., 1976; Sigogneau-Russell and Hahn, 1994) and some "chiniquodonts" (Kemp, 1982) is a recurved cusp *a* (following the nomenclature of Crompton and Jenkins, 1968); that is, the mesial crest is longer and more horizontal than the distal crest, which is shorter and more vertically oriented. A derived feature shared with *Meurthodon, Sinoconodon,* and Mammaliaformes (*sensu* Wible, 1991)

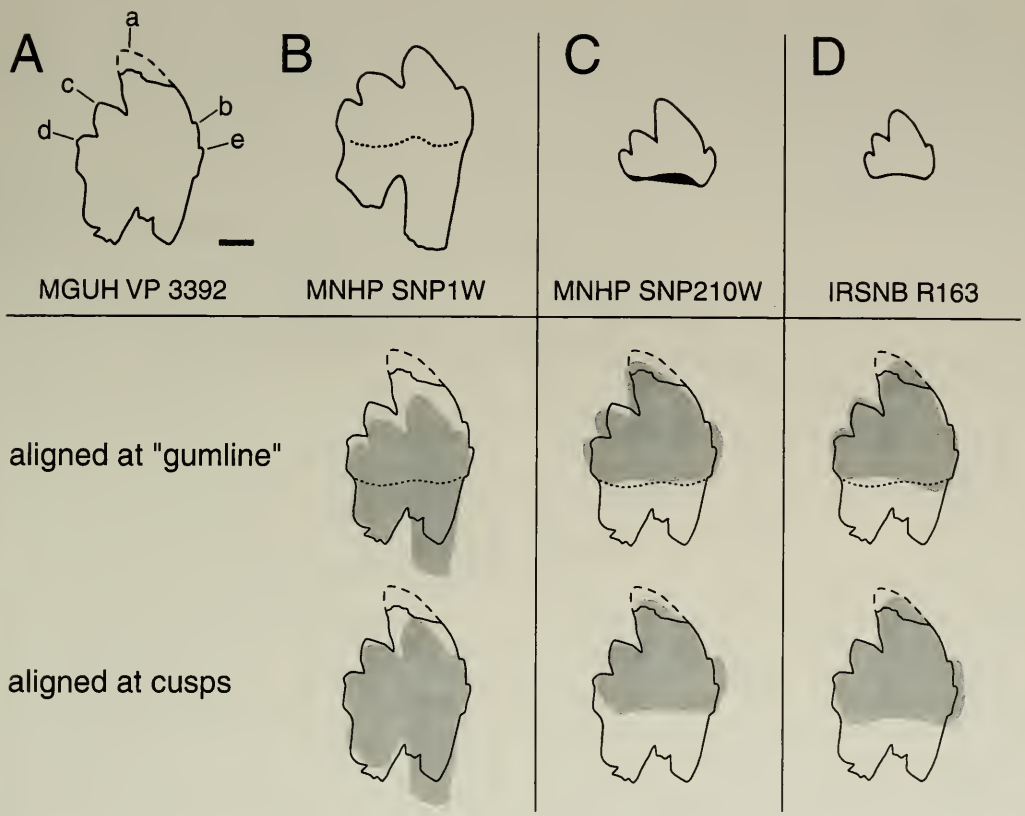

Figure 2. Comparison between (A) Pc_5 of *Mitredon cromptoni*, MGUH VP 3392, (B) the type specimen of *Meurthodon gallicus*, and (C, D) two isolated teeth referred to *Meurthodon gallicus*. Specimens MNHP SNP210W and IRSNB R163 were selected for comparison in addition to the type specimen for their gross similarity to MGUH VP 3392. In each column (B, C, and D), a *Meurthodon* tooth (shaded) is compared to Pc_5 of *Mitredon* (outline) in two ways to minimize the effects of size and completeness on morphologic comparison between specimens. First, the middle row depicts comparisons based on alignment of two teeth at the inferred gumline. Second, in the bottom row, cusps are aligned as closely as possible. Although the alignment of MGUH VP 3392 at the "gumline" with IRSNP R163 and with the cusps of MNHP SNP1W reveal overall similarities in shape, all specimens referred to *Meurthodon* lack a cusp *e*. Cusp *b* of Pc_5 in *Mitredon* is also substantially smaller than the corresponding structure in *Meurthodon*. Cusp designations in (A) after Crompton and Jenkins (1968). MNHP SNP1W redrawn from Sigogneau-Russell and Hahn (1994); MNHP SNP210W and IRSNB R163 redrawn from Godefroit and Battail (1997). For top row, scale bar = 1 mm.

is roots of lower postcanine teeth bifurcate, a character once considered diagnostic of Mammalia (e.g., Crompton and Jenkins, 1979). Distinguished from *M. gallicus* by the presence of a cuspule mesial to cusp *b* (on Pc_5); a mesiodistally longer cusp *a* (if the type specimen of *M. gallicus* and Pc_5 of *Mitredon cromptoni*, new genus and species, are scaled to the same mesiodistal length at the crown–cervical junction, the mesiodistal length of cusp *a* is approximately 60% total mesiodistal crown length in the latter, and only 40% in the former; Fig. 2); and the absolute mesiodistal length of Pc_5 is 20% smaller than that of the type specimen of *M. gallicus* (3.5 mm versus 4.2 mm). None of the three lower teeth of MGUH VP 3392 closely resembles the single isolated tooth of the type specimen of *M. gallicus* (Russell et al., 1976; Signoneau-Russell and Hahn, 1994) nor other isolated teeth that Godefroit and Battail (1997) subsequently referred to that taxon (Fig. 2).

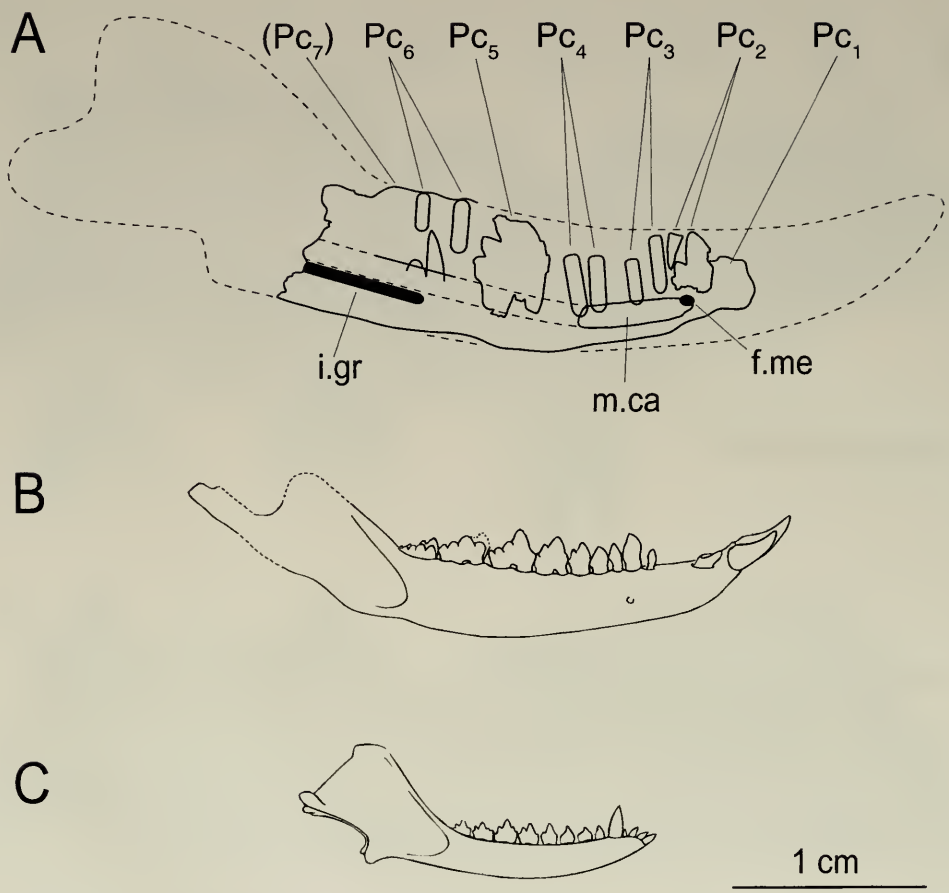

Figure 3. *Mitredon cromptoni* and contemporaneous Greenlandic mammals. (A) Schematic reconstruction of the left lower jaw of *Mitredon cromptoni*, MGUH VP 3392. Lower jaws of the Late Triassic mammals (B) *Haramiyavia* (redrawn from Jenkins et al. [1997]) and (C) *Morganucodon* (redrawn from Hopson [1994], in Bonaparte and Crompton [1994]). Abbreviations: Pc, postcanine tooth; i.gr, internal dentary groove; f.me, mental foramen; m.ca, mandibular canal.

DESCRIPTION

Lower Jaw

The specimen is a partial left dentary, slightly convex along its ventral margin, and missing the anterior and posterior ends of the ramus; erupted teeth had broken off postmortem, but several uneruptted teeth are preserved within the ramus. Although the total number of postcanine teeth is uncertain, the seven tooth positions are here referred to as Pc_1 (most mesial) through Pc_7 (most distal) (Fig. 3). The mental foramen is situated ventral and labial to Pc_2. An internal groove extends longitudinally along the inferior, lingual aspect of the dentary, indicating the presence of postdentary bones. The mandibular canal is exposed through breakage on the lingual aspect of the jaw between Pc_2 and Pc_4 (Fig. 1A). The canal passes to the labial side of Pc_5 and is preserved in cross section at the break across the posterior end of the specimen (Fig. 1B).

Teeth

Lower postcanine 1 is indicated by a partially preserved alveolus. In the next

tooth position, Pc_2, is an unerupted tooth of which the apex of cusp *a* and most of the lingual half of the crown are preserved; the apex of cusp *a* abuts a root fragment of the erupted tooth that was in the process of being replaced. Cusp *a* is laterally compressed and, unlike the recurved, asymmetrical cusp *a* of the unerupted tooth at Pc_5, appears to be nearly symmetrical. Two successively smaller cusps lie distal to cusp *a*; their apices are directed slightly distally, comparable to the distal cusps of Pc_5 but unlike the strictly dorsally directed orientation of cusp *a*. The mesial end of the tooth is not preserved and therefore the presence or absence of mesial cusps is not possible to determine. The remains of the crown of Pc_2 are sufficient to determine that the tooth is morphologically distinct from those at Pc_5 and Pc_6, the only other intact teeth in the jaw.

Lower postcanine 3 and Pc_4 are fully erupted teeth, but the crowns are lost and only the roots remain.

Lower postcanine 5, in the process of erupting from its crypt, was exposed by preparation (Figs. 1A, B). The tooth consists of a nearly complete crown bearing five cusps, and the upper parts of two roots. Mesial cusps *b* and *e* are the smallest and cusp *a* is the largest, the latter rising 2.55 mm from the base of the crown to the point at which the apex is broken. Cusps *c* and *d* are successively smaller and more distally directed than *a*. Cusp *d* supports a distinct cuspule on its lingual surface; in an examination of a cast of *Meurthodon gallicus*, J. A. Hopson (personal communication) observed a "very faint swelling" in a similar position.

Both a functional and a replacement tooth are present at the Pc_6 position. The functional tooth is preserved only by a pair of roots that straddle cusp *a* of a replacement tooth beneath. The fully divided roots are visible as ovoid cross sections at their broken surfaces in occlusal view. The replacement tooth, exposed by preparation but partially obscured in labial view by a cast of the mandibular canal (Fig. 1B), bears an elongate, tapered cusp *a*, the apex of which is directed between the roots of the predecessor tooth (Fig. 3). Cusp *c* is rounded and without a pointed apex, unlike the other *c* cusps preserved in this specimen. Much of this cusp lies on the lingual side of the mandibular canal and is best observed occlusolabially. Lower postcanine 6 is smaller than Pc_5 (Fig. 3), suggesting that Pc_6 may be the ultimate tooth in the lower dentition; however, a cryptlike depression distal to Pc_6, as well as an analysis of tooth replacement, appears to indicate that a more distal tooth position (Pc_7) may have been present.

DISCUSSION

Phylogenetic Affinities

Based on dental morphology, *Mitredon cromptoni* is likely to be closely related to *Meurthodon gallicus*. Although Sigogneau-Russell and Hahn (1994) interpreted *M. gallicus* is most closely related to *Therioherpeton cargnini*, we believe that *M. cromptoni* should be excluded from the Therioherpetidae (as originally diagnosed by Bonaparte and Barberena, 1975) on the basis of the bifurcate postcanine tooth roots and the nonalternate pattern of tooth replacement (but see below discussion of root variability in early Mesozoic cynodonts). Inasmuch as *M. gallicus* also has fully bifurcate postcanine tooth roots (unlike the incipiently double-rooted condition of *T. cargnini*, in which the cross section of the single root is in the shape of a figure 8; Bonaparte and Barberena, 1975), the inclusion of this taxon in the Therioherpetidae is questionable as well.

Mitredon cromptoni might be considered a chiniquodontid cynodont, but unresolved taxonomic issues at the familial and suprafamilial levels, as well as the incompleteness of the present specimen, make such an assignment problematic. Most taxa referred to "chiniquodonts" (Chiniquodontidae or Chiniquodontoidea) exhibit alternate tooth replacement and postcanines with three to four cusps that

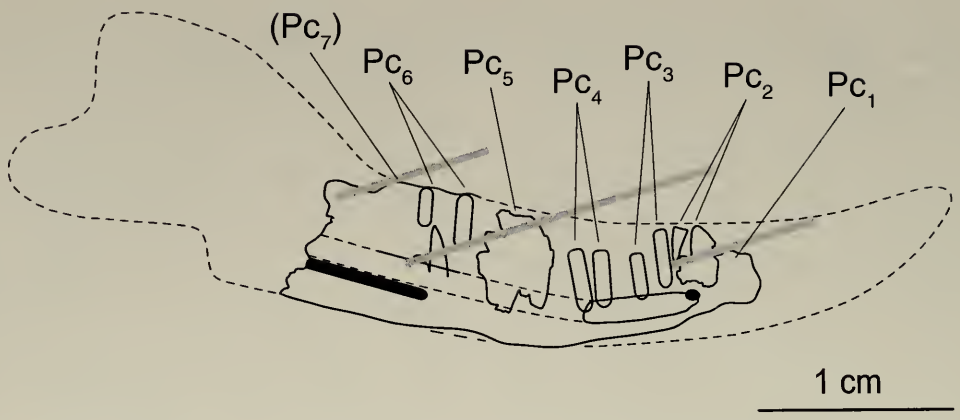

Figure 4. Schematic reconstruction of the left lower jaw of *Mitredon cromptoni*, MGUH VP 3392. Most reptiles and many cynodonts exhibit a tooth replacement pattern characterized by tooth eruption in every second tooth position. This alternate replacement pattern results from narrow spacing between *Zahnreihen* (teeth in a developmental replacement series; Hopson, 1980). As spacing between *Zahnreihen* increases, two or more teeth in a single *Zahnreihe* may be fully erupted and functional in the tooth row. Each tooth in a single *Zahnreihe* potentially may have a different crown morphology, and thus increased spacing between *Zahnreihen* may yield a heterogeneous tooth row. The dentition of *M. cromptoni* is represented by three *Zahnreihen* (heavy, shaded lines). The first *Zahnreihe* is comprised of erupting Pc_2 and probably Pc_1 (represented by an empty alveolus). The second is comprised of the erupted Pc_2 (root fragment), functional Pc_3 and Pc_4 (pairs of roots), and erupting Pc_5 and Pc_6. The roots of Pc_6 are part of the most distal *Zahnreihe*.

are labiolingually compressed and mesiodistally aligned, features that are either primitive for cynodonts or widely distributed (e.g., in galesaurids and cynognathids; Bonaparte and Barberena, 1975). Although Sigogneau-Russell and Hahn (1994: 204) assert that the teeth of "chiniquodonts" are easily distinguished from those of mammals and other therapsids, they also note that "chiniquodont" dentitions have yet to be studied in depth and therefore the "problem of subdivision of the Chiniquodontoidea into families has yet to be resolved."

Mitredon cromptoni also shares some similarities with the Early Jurassic *Sinoconodon*, which also has double-rooted teeth and likely replaced the molariform teeth (Crompton and Sun, 1985; Crompton and Luo, 1993). The postcanine teeth of *Sinoconodon*, which have four mesiodistally aligned cusps, resemble the teeth of *M. cromptoni* in lateral profile. In *Sinoconodon* postcanine teeth do not occlude, nor do upper and lower postcanines have a consistent relationship to one another; the single jaw of *M. cromptoni*, from which the erupted, functional teeth have been lost postmortem, does not permit an assessment of these features. In view of these uncertainties, we are reluctant to attempt a more precise taxonomic placement of *M. cromptoni*.

Tooth Replacement

Mitredon cromptoni possesses a lower postcanine dentition with at least three variants of crown structure. Differences in the teeth of *M. cromptoni* appear to represent different tooth replacement families, or *Zahnreihen*, comparable to those described for the cynodont *Thrinaxodon liorhinus* (Parrington, 1936; Crompton, 1963c; Osborn and Crompton, 1973; Fig. 4). However, tooth replacement in *M. cromptoni* is not comparable to the alternate pattern seen in *T. liorhinus* and allied forms. Furthermore, new generations of teeth erupt in the same sagittal plane as do previous ones (Pc_2 and Pc_6 erupt directly below the intact roots of preceding teeth; Figs. 1, 4), not in a more lingual plane as in *T. liorhinus*.

Although the number of crown variants

in each replacement series cannot be determined, we would interpret tooth replacement and variation in *Mitredon cromptoni* as representing three *Zahnreihe* (Fig. 4). The most mesial *Zahnreihe* consists of Pc_1 and the erupting Pc_2. The next *Zahnreihe* begins mesially with the root remnant of the functional tooth at the Pc_2 position. The functional teeth at positions Pc_{3-4} (represented only by roots) are part of this second *Zahnreihe*, as probably also are the replacement teeth at positions Pc_{5-6}. The last tooth in the most distal *Zahnreihe* (and thus the most distal tooth in the dentition) always erupts de novo, in a position not previously occupied by another tooth. Lower postcanine 6, which is undergoing replacement, therefore cannot be the ultimate tooth in the lower dentition of *M. cromptoni* and we would expect to see another erupting distal tooth in a more complete (and perhaps ontogenetically older) specimen. Indeed, a shallow crypt occurs distal to the roots of the functional tooth at Pc_6, evidence of yet another tooth position. The erupted Pc_6 and the potential tooth distal to it represent the most distal *Zahnreihe*.

Functional Stability of the Tooth Row and Multirooted Teeth

Before the discovery of *Mitredon cromptoni*, the fossil record appeared to provide evidence for the coevolution of stable patterns of occlusion and multirooted teeth, with the possible implication of a functional relationship. In the primitive condition, exemplified by *Thrinaxodon* and many other cynodonts, alternate replacement of single-rooted teeth resulted in continual disruption of the tooth row, and in any case there was little, if any, occlusion in the strict sense (tooth-to-tooth contact). More derived lineages (e.g., tritylodontids, *Sinoconodon*, morganucodontids, and haramiyids) developed replacement strategies to promote stability of the tooth row and, in most cases, possessed double- or multirooted postcanine teeth. An exception is the gomphodont cynodont *Diademodon*, which maintained single-rooted teeth but promoted stability within the tooth row by losing teeth mesially and adding teeth distally (Crompton, 1963a; Hopson, 1971). Tritylodontids (with up to six roots on postcanine teeth in *Oligokyphus*) and *Sinoconodon* (in which postcanines may be single- or double-rooted) possessed tooth replacement patterns comparable to that of *Diademodon*, but with a reduced number of teeth in each *Zahnreihe*. Tritylodontids did not replace mesial teeth but instead added nonreplacing, "gomphodont" teeth de novo at the distal end of the row (Hopson, 1971). Similarly, *Sinoconodon* lost anterior postcanines and added small distal teeth, which were subsequently replaced by a second generation of larger ones as jaw size increased (Crompton and Luo, 1993). Thus, *Sinoconodon* neither followed the typical "mammalian" diphyodont tooth replacement pattern nor possessed true molars (that is, *Sinoconodon* did not bear teeth that erupted de novo distally in the tooth row and were not replaced by subsequent generations of teeth).

Morganucodon was among the first mammals to possess a dentition that included true molars. Available fossils do not reveal how many times (or in what order) *Morganucodon* replaced generations of deciduous teeth, but dental wear patterns suggest that the positional relationships between upper and lower postcanine teeth were relatively consistent (Crompton and Jenkins, 1968). Fixed dental relationships were also promoted by interlocking anterior and posterior accessory cusps, maintaining alignment of the molars. Similarly, the occlusal interlocking of cusps and basins on upper and lower molariforms of the haramiyid *Haramiyavia clemmenseni* (Jenkins et al., 1997) would have required ontogenetic stasis of the tooth row. Although the exact sequence of tooth replacement cannot be ascertained for either of these mammalian taxa, their occlusal configurations are evidence that relatively precise relations were maintained between

upper and lower dentitions throughout ontogeny.

However, *Mitredon cromptoni* has a double-rooted postcanine dentition but lacks ontogenetic stasis in the lower tooth row. The tooth replacement pattern of *M. cromptoni* clearly does not retain the alternate pattern of *Thrinaxodon*, nor are teeth exclusively lost mesially and added distally, as in gomphodonts, tritylodontids, and *Sinoconodon*. Instead, *M. cromptoni* replaces mesial and distal postcanines simultaneously and thus compromises the stability of the tooth row. Of the teeth represented in MGUH VP 3392, the second and fifth were being replaced and likely lacked functional predecessors at the time of death. Thus, of the five tooth positions represented by replacement teeth or functional roots, only the third, fourth, and sixth postcanines were occupied by functional teeth. The low number of functional postcanines in MGUH VP 3392 contrasts sharply with the "uninterrupted molariform series" of mammals and gomphodont cynodonts (Hopson, 1971: 17).

The Origins of Multirooted Teeth

Teeth with multiple roots have traditionally been regarded as part of the functionally interdependent, coevolved complex of the mammalian masticatory system, which includes such diagnostic features as a dentary–squamosal jaw joint and unilateral mastication (e.g., Crompton, 1963a,b; Barghusen and Hopson, 1970; Kühne, 1973; Crompton and Parker, 1978; Crompton, 1989). However, several fossil taxa challenge the notion that "mammalian" characters are limited to the Mammalia. For example, Shubin et al. (1991) noted that unilateral occlusion may have originated not with the Mammaliaformes but with the common ancestor of trithelodontids and mammaliamorphs, or may have evolved independently in the Mammaliaformes. Likewise, the presently known structural diversity of roots within taxa, as well as the phylogenetic distribution of multirooted teeth, provide evidence that this character evolved independently more times than previously recognized. In *Morganucodon* and *Kuehneotherium*, premolar and molar roots range from incompletely divided to widely divergent; root shape also varies, from straight with a blunt or bulbous terminus, to those that are curved and tapered (Parrington, 1971, 1978). Root morphology in *Sinoconodon* also varies: some premolars (Zhang et al., 1998) and molars of *Sinoconodon* are fully divided, but at least one example is known where the two roots are confluent beneath the crown, and are only narrowly separated distally (Luo, 1994, fig. 6.6). Cui and Sun (1987) document extensive variability among tritylodontids, which until recently were the only known Early Mesozoic cynodont clade (other than mammals) with multirooted teeth. In some taxa (e.g., *Yunnanodon*) the roots are completely separated, whereas in others (*Oligokyphus* and *Lufengia*) transverse sheets of dentine connect root pairs. *Bienotherium* exhibits differences in the degree of root separation along the upper postcanine row, with unseparated roots mesially and fully separated roots distally. In general, the number of roots in tritylodont teeth varies with the number of cusps (Cui and Sun, 1987). Finally, to this spectrum of variation may be added *Mitredon cromptoni*. With a sectorial crown morphology and a tooth replacement pattern that is comparable to no known mammal, *M. cromptoni* is best interpreted as a cynodont with double-rooted teeth.

CONCLUSIONS

Advanced cynodonts may potentially exhibit a mosaic of "mammalian" and "nonmammalian" characteristics. *Mitredon cromptoni*, *Meurthodon gallicus*, tritylodontids, and mammals all possess postcanine teeth with multiple roots. Previous analyses (e.g., Sues, 1985; supported by Wible, 1991) point to an independent evolution of this character in tritylodontids. Hence, if *M. cromptoni* and *Meurthodon gallicus* are indeed "chiniquodonts" (no

recent analyses place chiniquodonts as the sister taxon of mammals), then multiple-rooted postcanines may have evolved up to three separate times in cynodonts (following the phylogenetic hypotheses of Hopson, 1994; Hopson and Kitching, 2001). This character would no longer be useful in the diagnosis of Mammaliamorpha (Rowe, 1988) or Mammaliaformes (Wible, 1991). Alternately, double-rootedness may have evolved only once, in the Mammaliaformes (Wible, 1991; Hopson and Kitching, 2001). In this scenario, *Mitredon* and *Meurthodon* would fall within the Trithelodontidae + Mammaliaformes clade, closer to mammaliaforms than to trithelodontids.

Double-rootedness did not necessarily evolve in concert with tooth row stasis during synapsid evolution. *Mitredon cromptoni* has double-rooted teeth but retains a tooth replacement pattern uncharacteristic of taxa with precise occlusion and a functionally uninterrupted postcanine tooth series.

ACKNOWLEDGMENTS

We thank W. W. Amaral, L. B. Clemmensen, W. R. Downs, S. M. Gatesy, H. E. Jenkins II, D. V. Kent, D. C. Roberts, and N. H. Shubin for their spirited collaboration in fieldwork; W. W. Amaral for his detailed preparation of the specimen; K. Brown-Wing for the precision of her renderings in Figure 1; and S. M. Gatesy and J. A. Hopson for helpful discussions. J. A. Hopson generously shared his unpublished drawings and observations of *Meurthodon gallicus* and provided useful insights in his review of the manuscript. We also thank Zhexi Luo for his thoughtful review. This work was supported by grants from the National Science Foundation, the Carlsberg Foundation, and the Putnam Expeditionary Fund of the MCZ.

LITERATURE CITED

BARGHUSEN, H. R., AND J. A. HOPSON. 1970. Dentary–squamosal joint and the origin of mammals. Science, **168:** 573–575.

BONAPARTE, J. F., AND M. C. BARBERENA. 1975. A possible mammalian ancestor from the Middle Triassic of Brazil (Therapsida–Cynodontia). Journal of Paleontology, **49:** 931–936.

BONAPARTE, J. F., AND A. W. CROMPTON. 1994. A juvenile probainognathid cynodont skull from the Ischigualasto Formation and the origin of mammals. Revista del Museo Argentino de Ciencias Naturales "Bernardino Rivadavia," Paleontología, **5:** 1–12.

CROMPTON, A. W. 1963a. The evolution of the mammalian jaw. Evolution, **17:** 431–439.

———. 1963b. On the lower jaw of *Diarthrognathus* and the origin of the mammalian lower jaw. Proceedings of the Zoological Society of London, **140:** 697–750.

———. 1963c. Tooth replacement in the cynodont *Thrinaxodon liorhinus* Seeley. Annals of the South African Museum, **46:** 479–521.

———. 1989. The evolution of mammalian mastication, pp. 23–40. *In* D. B. Wake and G. Roth (eds.), Complex Organismal Functions: Integration and Evolution in Vertebrates. Chichester: John Wiley & Sons, viii + 451 pp.

CROMPTON, A. W., AND F. A. JENKINS, JR. 1968. Molar occlusion in Late Triassic mammals. Biological Reviews of the Cambridge Philosophical Society, **43:** 427–458.

———. 1979. Origin of mammals, pp. 59–73. *In* J. A. Lillegraven, Z. Kielan-Jaworowska, and W. A. Clemens (eds.), Mesozoic Mammals: The First Two-Thirds of Mammalian History. Berkeley: University of California Press. x + 311 pp.

CROMPTON, A. W., AND Z. LUO. 1993. Relationships of the Liassic mammals *Sinoconodon, Morganucodon oehleri,* and *Dinnetherium,* pp. 30–44. *In* F. S. Szalay, M. J. Novacek, and M. C. McKenna (eds.), Mammal Phylogeny: Mesozoic Differentiation, Multituberculates, Monotremes, Early Therians, and Marsupials. New York: Springer-Verlag. x + 249 pp.

CROMPTON, A. W., AND P. PARKER. 1978. Evolution of the mammalian masticatory apparatus. American Scientist, **66:** 192–201.

CROMPTON, A. W., AND A.-L. SUN. 1985. Cranial structure and relationships of the Liassic mammal *Sinoconodon.* Zoological Journal of the Linnean Society, **85:** 99–119.

CUI, G., AND A. SUN. 1987. Postcanine root system in tritylodontids. Vertebrata PalAsiatica, **25:** 245–259.

GODEFROIT, P., AND B. BATTAIL. 1997. Late Triassic cynodonts from Saint-Nicolas-de-Port (northeastern France). Geodiversitas, **19:** 567–631.

HOPSON, J. A. 1971. Postcanine replacement in the gomphodont cynodont *Diademodon,* pp. 1–21. *In* D. M. Kermack and K. A. Kermack (eds.), Early Mammals. New York: Academic Press. xiv + 203 pp.

———. 1980. Tooth function and replacement in

early Mesozoic ornithischian dinosaurs: implications for aestivation. Lethaia, **13:** 93–105.

———. 1994. Synapsid evolution and the radiation of non-eutherian mammals, pp. 190–219. *In* D. R. Prothero and R. M. Schoch (eds.), Major Features of Vertebrate Evolution. Pittsburgh: The Paleontological Society. 270 pp.

Hopson, J. A., and H. R. Barghusen. 1986. An analysis of therapsid relationships, pp. 83–106. *In* N. Hotton III, P. D. Maclean, J. J. Roth, and C. Roth (eds.), The Ecology and Biology of Mammal-like Reptiles. Washington, D.C.: Smithsonian Institution Press. x + 326 pp.

Hopson, J. A., and J. W. Kitching. 1972. A revised classification of cynodonts (Reptilia: Therapsida). Palaeontologia Africana, **14:** 71–85.

———. 2001. A probainognathian cynodont from South Africa and the phylogeny of nonmammalian cynodonts. Bulletin of the Museum of Comparative Zoology, **156:** 5–35.

Jenkins, F. A., Jr., S. M. Gatesy, N. H. Shubin, and W. W. Amaral. 1997. Haramiyids and Triassic mammalian evolution. Nature, **385:** 715–718.

Jenkins, F. A., Jr., N. H. Shubin, W. W. Amaral, S. M. Gatesy, C. R. Schaff, L. B. Clemmensen, W. R. Downs, A. R. Davidson, N. Bonde, and F. Osbæck. 1994. Late Triassic continental vertebrates and depositional environments of the Fleming Fjord Formation, Jameson Land, East Greenland. Meddelelser om Grønland, Geoscience, **32:** 1–25.

Jenkins, F. A., Jr., N. H. Shubin, S. M Gatesy, and K. Padian. 2001. A diminutive pterosaur (Pterosauria: Eudimorphodontidae) from the Greenlandic Triassic. Bulletin of the Museum of Comparative Zoology, **156:** 151–170.

Kemp, T. S. 1982. Mammal-like Reptiles and the Origin of Mammals. London: Academic Press. xiv + 363 pp.

Kühne, W. G. 1973. The evolution of a synorgan: nineteen stages concerning teeth and dentition from the pelycosaur to the mammalian condition. Bulletin du Groupement International pour la Recherche Scientifique en Stomatologie, **16:** 293–325.

Luo, Z. 1994. Sister-group relationships of mammals and the transformations of diagnostic mammalian characters, pp. 98–128. *In* N. C. Fraser and H.-D. Sues (eds.), In the Shadow of the Dinosaurs. Cambridge: University Press. x + 435 pp.

Osborn, J. W., and A. W. Crompton. 1973. The evolution of mammalian from reptilian dentitions. Breviora, **399:** 1–18.

Parrington, F. R. 1936. On the tooth-replacement in theriodont reptiles. Philosophical Transactions of the Royal Society of London, B, Biological Sciences, **226:** 121–142.

———. 1971. On the Upper Triassic mammals. Philosophical Transactions of the Royal Society of London, B, Biological Sciences, **261:** 231–272.

———. 1978. A further account of the Triassic mammals. Philosophical Transactions of the Royal Society of London, B, Biological Sciences, **282:** 177–204.

Rowe, T. 1988. Definition, diagnosis, and origin of Mammalia. Journal of Vertebrate Paleontology, **8:** 241–264.

Russell, D., D. Russell, and G. Wouters. 1976. Une dent d'aspect mammalien en provenance du Rhétien français. Géobios, **9:** 377–392.

Shubin, N. H., A. W. Crompton, H.-D. Sues, and P. E. Olsen. 1991. New fossil evidence on the sister-group of mammals and early Mesozoic faunal distributions. Science, **251:** 1063–1065.

Sigogneau-Russell, D., and G. Hahn. 1994. Late Triassic microvertebrates from central Europe, pp. 197–213. *In* N. C. Fraser and H.-D. Sues (eds.), In the Shadow of the Dinosaurs. Cambridge: University Press. x + 435 pp.

Sues, H. D. 1985. The relationships of the Tritylodontidae (Synapsida). Zoological Journal of the Linnean Society, **85:** 205–217.

Wible, J. R. 1991. Origin of Mammalia: the craniodental evidence reexamined. Journal of Vertebrate Paleontology, **11:** 1–28.

Zhang, F. K., A. W. Crompton, Z. Luo, and C. R. Schaff. 1998. Pattern of dental replacement of *Sinoconodon* and its implications for evolution of mammals. Vertebrata PalAsiatica, **36:** 197–217.

ON TWO ADVANCED CARNIVOROUS CYNODONTS FROM THE LATE TRIASSIC OF SOUTHERN BRAZIL

JOSÉ F. BONAPARTE[1] AND MARIO COSTA BARBERENA[2]

ABSTRACT. Cranial and postcranial remains of the cynodonts *Therioherpeton cargnini* (Therioherpetidae) and a taxon originally referred to as *Thrinaxodon brasiliensis* (of indeterminate familial status) are described and compared with other advanced cynodonts and morganucodontids. Our study provides evidence that these early Late Triassic cynodonts, which possessed primitive carnivorous dentitions of the *Thrinaxodon liorhinus* type, evolved derived characters of the skull and postcranium that approximated the mammalian level of organization as represented in morganucodontids.

INTRODUCTION

Therioherpeton cargnini (Therioherpetidae) is represented by an incomplete skull and lower jaw, and most of the postcranial skeleton, but only the skull and a fragment of the lower jaw have been described (Bonaparte and Barberena, 1975). The genus *Therioherpeton* was referred to the family "Therioherpetontidae" by Bonaparte and Barberena (1975), but Battail (1991) corrected the familial name to Therioherpetidae. Likewise, *Thrinaxodon brasiliensis* (Barberena et al., 1987), of indeterminate familial status, is also represented by an incomplete skull, lower jaws, and some postcranial bones, but only the skull and jaws were described. In this paper the complete material known from both species is analyzed and compared with other advanced Triassic cynodonts and morganucodontids, and *T. brasiliensis* is assigned to a new genus. The advanced anatomical features of both taxa suggest a close proximity to the mammalian condition, not very different from that evolved by tritylodontids and tritheledontids.

Anatomical and phylogenetic issues concerning advanced cynodonts and primitive mammals have been widely analyzed (Kermack et al., 1981; Kemp, 1982; Jenkins, 1984; Crompton and Sun, 1985; Sues, 1985; Hopson and Barghusen, 1986; Battail, 1991; Hopson, 1991; Shubin et al., 1991; Crompton and Luo, 1993; Luo, 1994), but the subject is far from well understood because, as Crompton and Luo (1993: 30) remarked: "A lack of morphological information makes it difficult to interpret the relationships of advanced cynodonts and early mammals." As yet undescribed carnivorous cynodonts (recently discovered in southern Brazil in beds of early Late Triassic age), and a restudy of the advanced cynodonts *Therioherpeton cargnini* (Bonaparte and Barberena, 1975) and *Thrinaxodon brasiliensis* (Barberena et al., 1987), may advance our understanding of the complex sequence of anatomical changes that occurred in cynodonts and that foreshadow the level of mammalian organization represented by morganucodontids (Kermack et al., 1973, 1981; Crompton, 1974; Jenkins and Parrington, 1976; Gow, 1986). Unfortunately, available cranial material of neither *Thrinaxodon brasiliensis* nor *Therioherpeton cargnini* includes critical anatomical data from the basicranial region.

[1] Museo Argentino de Ciencias Naturales, Avenida Angel Gallardo 470, 1405 Buenos Aires, Argentina.

[2] Instituto de Geociencias, Universidade Federal de Rio Grande do Sul, Avenida Bento Gonçalves 9500, 91509-900 Porto Alegre, Rio Grande do Sul, Brazil.

SYSTEMATIC PALEONTOLOGY

Therapsida Broom, 1905

Cynodontia Owen, 1861

Family Therioherpetidae Bonaparte and Barberena, 1975

Diagnosis. Differs from the Thrinaxodontidae by a more extensive secondary palate. Differs from Thrinaxodontidae, Cynognathidae, Chiniquodontidae, and Probainognathidae in the following features: triangular cross section of the zygomatic arch; absence of a postorbital bar; frontal borders the orbit and bears an anterolateral projection that contacts a lateral portion of the nasal; interorbital wall more highly ossified; larger size of the neural canal in the cervical and dorsal vertebrae; parallel dorsal and ventral borders of the ilium; convex lateral surface of ilium; a narrow, elongate neck of the ischium; obturator foramen relatively large; greater trochanter of the femur extends to the same proximal level as the femoral head. Therioherpetidae differs from Tritheledontidae in the transverse narrowness of the upper postcanines. Therioherpetidae differs from gomphodont cynodonts, including Tritylodontidae, in possessing triconodont upper and lower postcanines, and in the triangular cross section of the zygomatic arch. Therioherpetids differ from basal mammals in lacking an articular condyle of the dentary and fully bifurcated roots on postcanine teeth (but see Shapiro and Jenkins, 2001).

Genus *Therioherpeton* Bonaparte and Barberena, 1975

Type Species *Therioherpeton cargnini* Bonaparte and Barberena, 1975

Holotype. An unnumbered specimen in the private collection of the Patronato Alves Ramos, Santa Maria City, State of Rio Grande do Sul, Brazil. An incomplete skull lacking the basicranium, and preserving only the right upper fifth postcanine; a fragment of the right dentary; an isolated lower postcanine (the fifth or sixth, attached to lingual surface of Pc^5); 29 articulated, incomplete vertebrae including 4 cervicals, 15 dorsals and (separated by a gap) 4 sacral and 6 caudal vertebrae; associated, incomplete ribs; left scapular blade; distal half of the right humerus; incomplete right radius and ulna; incomplete ilia; complete pubis; right ischium; complete left and incomplete right femur; fragments of tibiae and fibulae; and incomplete feet.

Revised Generic and Specific Diagnosis. The triconodont upper and lower postcanines are without cingula. The secondary bony palate extends nearly to the level of the last postcanine, as in chiniquodontids and *Probainognathus.* As in *Morganucodon,* the frontals have an extensive posterior projection, anteriorly contact the lateral aspect of the nasals, and anterolaterally project to the lacrimals. Prefrontals and postorbitals are absent. The cervical vertebrae are craniocaudally short, transversely wide, dorsoventrally low, and exhibit a very large neural canal. The iliac blade lacks a posterior projection, the lateral surface is convex, and the dorsal and ventral borders are subparallel. The obturator fenestra is large. The greater trochanter extends proximally to the level of the femoral head, with which it is connected by a sheet of bone.

Horizon and Locality. Upper Santa Maria Formation. A road cut on the BR-216 highway (outcrop BR-14 in Bortoluzzi and Barberena, 1967), 200 m northwest of Cerriquito, Township of Santa Maria, Rio Grande do Sul, Brazil.

Age. Probably early Late Triassic.

DESCRIPTION

Skull (Figs. 1–4). Only the salient characters of the type and only known skull of this species, originally described by Bonaparte and Barberena (1975), may be noted here. The more significant characters are the absence of the prefrontal and postorbital, the large lacrimal, the frontal bordering the orbit with a long posterior pro-

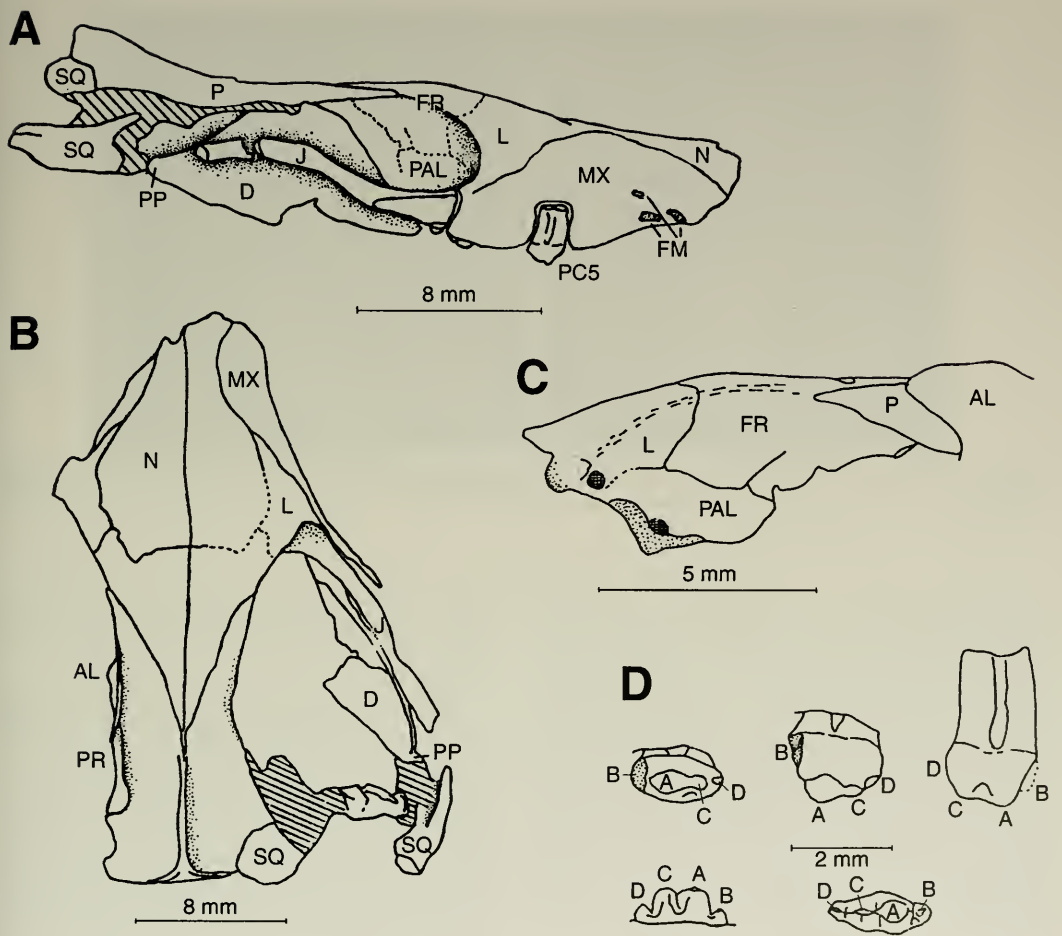

Figure 1. *Therioherpeton cargnini.* Skull and dentary fragment in (A) right lateral and (B) dorsal views. (C) Incomplete interorbital wall viewed from the left side. (D) Upper postcanine 5 in occlusal, lingual, and buccal views, and $Pc_{5 \text{ or } 6}$ in buccal and occlusal views. *Abbreviations:* AL, alisphenoid; D, dentary; FM, maxillary foramina; FR, frontal; J, jugal; L, lacrimal; MX, maxilla; N, nasal; PAL, palatine; P, parietal; PP, prearticular process; PR, prootic; SQ, squamosal.

cess, and an anterolateral projection of the frontal in dorsal view. The parietal crest is low (Fig. 1A) and the dorsal area of the braincase is large (Fig. 3); the zygomatic arch is slender with a triangular cross section (Figs. 1A, 4). The lateral surface of the maxilla bears three large foramina (Fig. 1A). The upper and lower postcanines (Fig. 1D) are of the triconodont type and lack cingula, and the upper teeth show clear indications of an incipient bifurcation of the roots.

The secondary bony palate of *Therioherpeton* was misinterpreted by Bonaparte and Barberena (1975) because an unossified, or damaged, area of the right palatine was considered as part of the internal nares. Restudy of the palatine revealed that its posterior margin is in fact complete, and thus represents the posterior border of the secondary bony palate, which is in line with the penultimate postcanine (Fig. 2).

Postcranial Skeleton (Figs. 5–8). The associated postcranium was found in nearly articulated condition lying on the external

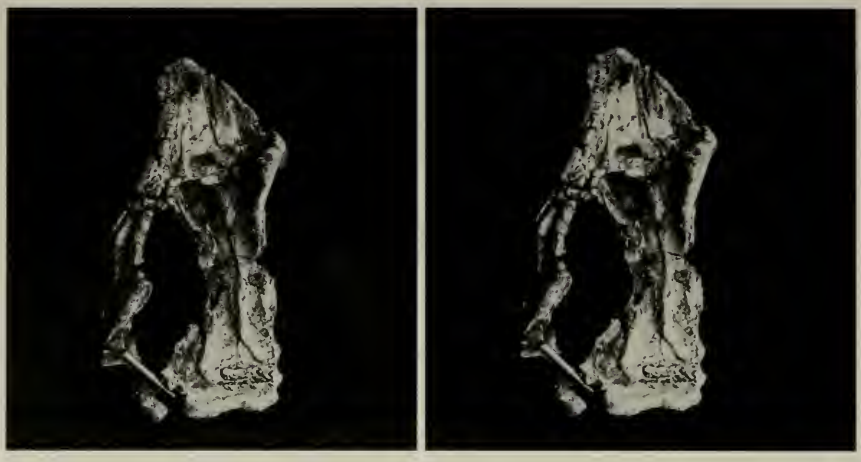

Figure 2. *Therioherpeton cargnini.* Ventral view of the incomplete skull of the holotype. The secondary osseous palate shows an unossified area of the palatine. However, the posterior border of the right palatine is well preserved. Most of the ventral side of the skull roof from nasals to parietals is shown.

side of the rib cage of a rhynchosaur, probably *Scaphonyx* sp. (Schultz, 1986). All but six vertebrae are incomplete. Three cervicals are articulated in a small, isolated block, associated with the blade of the right scapula. The centra of these vertebrae are anteroposteriorly short, transversely wide, and dorsoventrally low, and have a wide neural canal. The inferred last cervical, articulated with a series of 15 dorsals (Fig. 5A), also has a short, wide, and dorsoventrally low centrum; the neural canal is wider than the centrum because the pedicles of the neural arch project dorsolaterally.

The anteroposterior lengths of the seven anterior dorsals gradually increase; neural canals remain very large (Fig. 5A). The 8th through 10th dorsals preserve the neural spines, which are posterodorsally inclined. The centra of the 11th through 14th dorsals are longer than those of preceding vertebrae; in these vertebrae, the large neural canal is formed in part by the ven-

Figure 3. *Therioherpeton cargnini.* Dorsal view of the incomplete skull of the holotype, showing the anterolateral projection of the frontals as well as their extensive, wedge-shaped posterior projection.

Figure 4. *Therioherpeton cargnini.* Right lateral view of the incomplete skull and jaw of the holotype. Note the slender zygomatic section of the jugal, and the incipiently bifurcated root of Pc^5.

tromedial surfaces of the neural pedicles that contribute to the floor of the neural canal. The number of dorsal vertebrae is uncertain because of a gap between the fifteenth dorsal and the next group of vertebrae. The zygapophyses of the last dorsal vertebrae are anteroposteriorly robust and oriented almost horizontally, with little inclination toward the median plane. The vertebrae forming the sacrum are difficult to discern individually, although one bears fragments of sacral ribs. We infer that there might be three or possibly four sacral vertebrae. All are rather robust, and the neural canals are as wide as the centra.

Subcylindrical fragments (and many molds) preserve 15 incomplete ribs on the right side and 17 on the left side (Figs. 5A, 6). There is no evidence of overlapping uncinate processes as are known in many cynodonts. Cervical ribs, which are short, thick, and posteriorly deflected, articulate behind the anterior margins of the centra, not between adjacent centra as in *Thrinaxodon liorhinus* (Jenkins, 1971). The dorsal ribs, which in cross section are figure 8–shaped, exhibit no clear indication of a lumbar region, except that the posterior dorsal ribs gradually decrease in length.

The pectoral girdle is represented only by the blade of the right scapula (not fully prepared at present). The anterior and posterior borders of the blade project laterally, forming a deep sulcus for musculus supracoracoideus, similar to the condition in *Thrinaxodon liorhinus* (Jenkins, 1971). The distal half of the right humerus is preserved, and appears to be relatively primitive by virtue of its great distal width and the presence of an ectepicondylar foramen. The ?right radius and ulna are incompletely preserved and reveal no diagnostic characters.

Of the two incomplete ilia, the left ilium (Fig. 5B) preserves part of the blade, which has almost parallel dorsal and ventral borders and lacks a posterior process. The lateral aspect of the blade is dorsoventrally convex. The pubic pedicle is more developed and stronger than the area of ischial contact. The ischium (Fig. 5D) has an elongate, narrow neck, and forms with the pubis a large obturator fenestra. The pubis (Fig. 5C) exhibits a well-defined, "twisted" neck below the acetabulum. A thickening of the anterior margin of the pubis ventral to the neck represents a pubic process. The inferior border of the pubic ramus is rather straight, whereas the superior border is concave and forms part

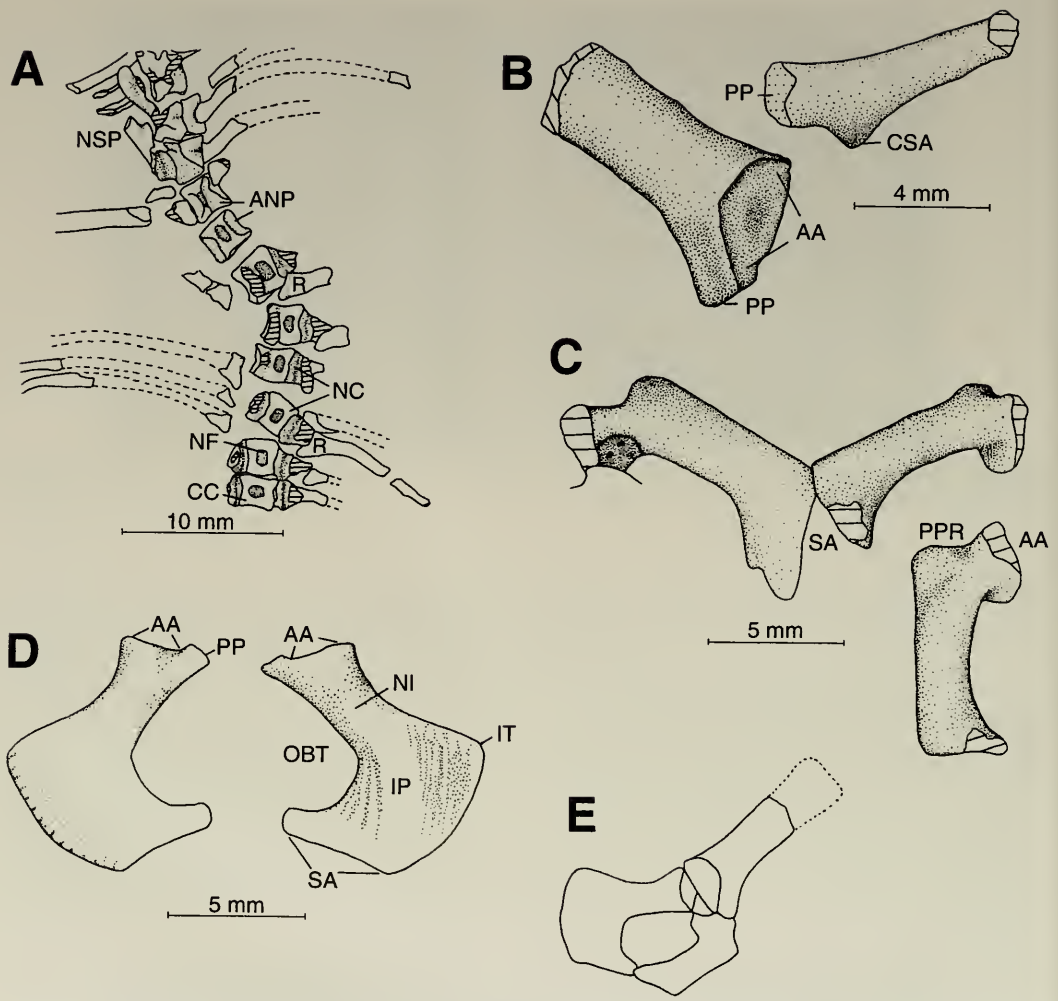

Figure 5. *Therioherpeton cargnini.* (A) Sequence of articulated incomplete vertebrae and ribs from the putative last cervical (at the bottom) to the 10th dorsal. (B) Incomplete left ilium in lateral (left) and ventral (right) views. (C) Both pubes in dorsal view as preserved, and the left pubis in lateral view. (D) Right ischium in lateral (left) and medial (right) views. (E) Reconstruction of the right half of the pelvis in lateral view. *Abbreviations:* AA, acetabular area; ANP, area for neural pedicles; CC, cervical centrum; CSA, crista supracetabularis; IP, ischial plate; IT, ischial tuberosity; NC, neural canal; NF, neural fossa; NI, neck of the ischium; NSP, neural spine; OBT, obturator foramen; PP, pubic pedicle; PPR, pubic process; R, rib; SA, symphysial area.

of the margin of the large obturator fenestra.

The left femur is nearly complete (Figs. 7A, 8). The proximal end gradually expands mediolaterally, and the trochanters are less defined than in *Oligokyphus* (Kühne, 1956) and *Morganucodon* (Jenkins and Parrington, 1976). The femoral head is anteromedially and somewhat dorsally directed, although the precise orientation is obscured by slight deformation. The proximally positioned lesser trochanter is similar to that of *Oligokyphus* and *Morganucodon*, and different from the more ventrally placed trochanters of *Probelesodon* (Romer and Lewis, 1973), *Massetognathus* (Jenkins, 1970), and *Exaeretodon* (Bonaparte, 1963). The greater trochanter is

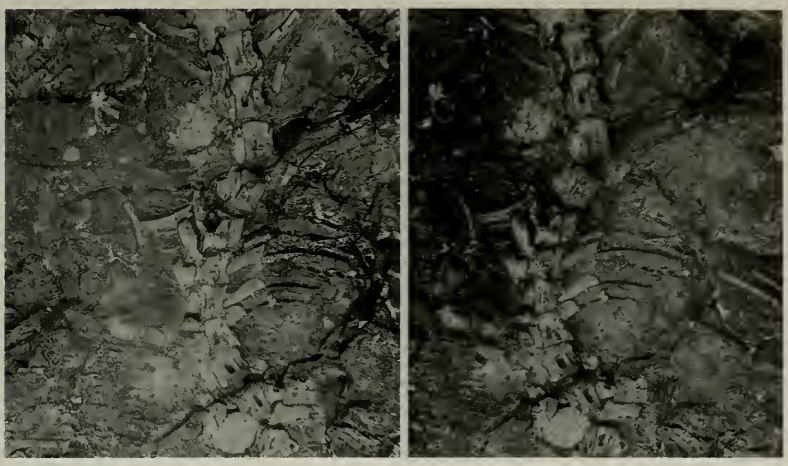

Figure 6. *Therioherpeton cargnini.* Part of the presacral vertebral column showing broad neural arches, posterodorsally directed neural spines, and ribs without overlapping processes.

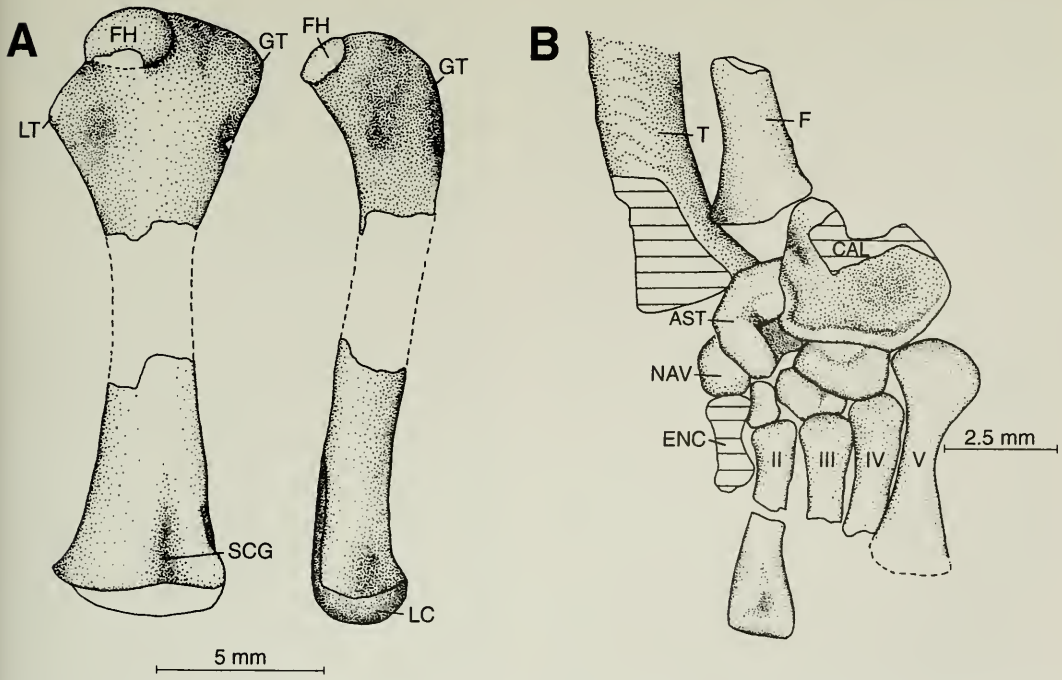

Figure 7. *Therioherpeton cargnini.* (A) Left femur in anterior and lateral views. (B) Distal portions of right tibia and fibula articulated with the incomplete foot in plantar view. *Abbreviations:* AST, astragalus; CAL, calcaneum; ENC, entocuneiform; F, fibula; FH, femoral head; GT, greater trochanter; LC, lateral condyle; LT, lesser trochanter; NAV, navicular; SCG, supracondylar groove; T, tibia; II–V, metatarsals II through V.

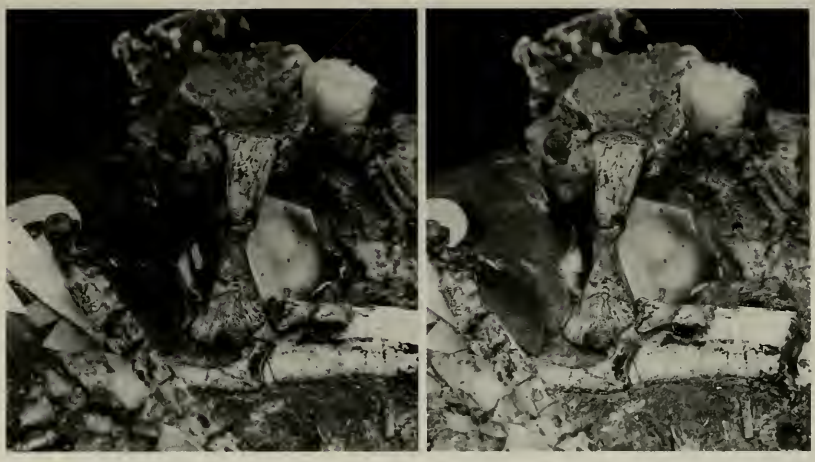

Figure 8. *Therioherpeton cargnini.* On the left is a series of incomplete sacrocaudal vertebrae in dorsal view. Also present are the left femur, left pubis, incomplete left ilium, and incomplete left foot. The ilium rests on a rhynchosaur (*Scaphonyx* sp.) rib.

proximally positioned and is united with the femoral head by a thin lamina of bone. Morphologically, the greater trochanteric structure is similar to that of *Oligokyphus* and *Morganucodon*, and very different from the condition in *Cynognathus* (Jenkins, 1971), *Probelesodon* (Romer and Lewis, 1973), *Massetognathus* (Jenkins, 1970), and *Exaeretodon* (Bonaparte, 1963). The lateral femoral condyle has a larger radius of curvature than the medial; a shallow supracondylar groove is present on dorsal surface of the distal end.

The astragalus, which is larger than the calcaneum, is only partially superimposed on the latter (Fig. 7B). Inasmuch as the calcaneum is damaged along its proximal margin, the presence or absence of a calcaneal tuber cannot be determined. The relatively elongate, slender proportions of the metatarsals resemble those of *Oligokyphus* (Kühne, 1956), rather than those of *Exaeretodon* (Bonaparte, 1963) or *"?Aleodon/?Scalenodon"* (Jenkins, 1971).

A Summary of the Distinctive Features of Therioherpeton. Although *Therioherpeton* possesses many features that are found in other Triassic cynodont families, the following assemblage is characteristic only of *Therioherpeton* and represents the degree to which this taxon approaches the morganucodontid level of organization.

1) Absence of prefrontal and postorbital bones as well as a postorbital bar (also in tritheledontids and tritylodontids).
2) Frontal bordering the orbit (also in tritheledontids and tritylodontids).
3) Frontal with anterolateral projection in dorsal view, and an elongate posterior projection.
4) Large lacrimal (also in tritheledontids and tritylodontids).

Comment. The first three characters listed above differentiate *Therioherpeton* from the Thrinaxodontidae, Cynognathidae, Chiniquodontidae, and Probainognathidae. Some of the characters are shared with the Tritylodontidae (Kühne, 1956; Sun, 1984; Sues, 1985) and Tritheledontidae (Crompton, 1958; Bonaparte, 1980), but in tritylodontids the zygomatic arch is deep and the dentition very derived, whereas in tritheledontids the specialized incisors, reduced canines, and bulbous upper postcanines differ from the corresponding features in *Therioherpeton*. The upper postcanines of the tritheledontids are transversely expanded, whereas in *Therioherpeton* they are narrow, with the

cusps in line. The structure of the frontal resembles that of *Morganucodon* (Kermack et al., 1981) in the type of contact with the nasal, a possible result of the absence of the prefrontal, as well as in the long, tapering contact with the parietals.

5) Contact between the ventral process of frontal and dorsal process of palatine (also in tritheledontids and tritylodontids; and in *Probainognathus* and chiniquodontids; J. A. Hopson, personal communication).
6) Large infraorbital foramen and two well-defined foramina for the trigeminal nerve in the maxilla (also in tritheledontids and tritylodontids).
7) Carnivorous–insectivorous dentition, similar to that of *Thrinaxodon* and *Morganucodon,* but with upper postcanines without cingula and possessing incipiently bifurcated roots.
8) Articular process of the dentary posteriorly and transversely expanded, without indication of a condyle, and set at a higher level than the alveoli (a common feature in derived cynodonts; J. A. Hopson, personal communication).
9) Cervical centra anteroposteriorly short, transversely wide and dorsoventrally low (also in *Oligokyphus,* other tritylodontids, and *Morganucodon*).
10) Neural canal of presacral vertebrae wider than the centrum.

Comment. The neural canal in *Therioherpeton* is proportionally larger than that in most cynodonts with which we were able to make a comparison. Neural canal size in the cervical, thoracic, sacral, and proximal caudal vertebrae of *Oligokyphus* (Kühne, 1956) approaches that of *Therioherpeton,* but is nonetheless proportionally smaller. The neural canal of *Therioherpeton* is in fact almost identical in proportions to that in *Morganucodon* (Jenkins and Parrington, 1976).

11) Absence of anapophyses.
12) Ribs without expanded processes (also in *Exaeretodon,* chiniquodontids, *Probainognathus,* and tritylodontids; and in tritheledontids as well; J. A. Hopson, personal communication).
13) Neural spines of presacral vertebrae posterodorsally directed (also in tritylodontids).

Comment. Short, posterodorsally directed neural spines in the posterior dorsals are known only in *Oligokyphus* and *Therioherpeton.* In *Morganucodon,* the posterior dorsals bear vertical neural spines, with fully differentiated lumbar vertebrae. The similarities between some derived axial characters in *Oligokyphus* and *Therioherpeton* suggest the probability of parallel evolution.

14) Iliac blade with dorsal and ventral borders subparallel, without posterior process (also in some tritylodontids; and tritheledontids; J. A. Hopson, personal communication).
15) Lateral side of the iliac blade dorsoventrally convex (also in tritylodontids and tritheledontids; J. A. Hopson, personal communication).
16) Ischium with narrow neck posterior to the acetabulum, and a concave dorsal border (also in *Oligokyphus* and tritheledontids; J. A. Hopson, personal communication).
17) Large obturator fenestra (also in tritylodontids and tritheledontids; J. A. Hopson, personal communication).
18) Pubis narrow with reduced distal contact with the ischium (also in tritheledontids; J. A. Hopson, personal communication).

Comment. The available parts of the ilia, the complete pubes, and the ischium show that the pelvis of *Therioherpeton* is more derived than that in any known cynodont family except the Tritylodontidae (Kühne, 1956) and Trithelodontidae (J. A. Hopson, personal communication).

19) Greater trochanter at the same level as the femoral head (also in *Oligoky-*

phus and tritheledontids; J. A. Hopson, personal communication).

20) Elongate, slender metatarsals (also in *Oligokyphus*).

SYSTEMATIC PALEONTOLOGY

Therapsida Broom, 1905

Cynodontia Owen, 1861

Family Incertae Sedis

Genus *Prozostrodon* New Genus

Type species, *Prozostrodon brasiliensis* (Barberena, Bonaparte, and Sá Teixeira, 1987).

Synonymy *Thrinaxodon brasiliensis* Barberena, Bonaparte, and Sá Teixeira, 1987.

Holotype. PV 0248T, Department of Paleontology and Stratigraphy, Universidade Federal de Rio Grande do Sul, Brazil.

Etymology. The generic designation alludes to the cingula of lower postcanine teeth (Greek, *zoster*, a girdle or band), in combination with Latin, *pro-*, before, in reference to the hypothesized antecedant phylogenetic position of the taxon.

Revised Generic and Specific Diagnosis. Reduced prefrontal and postorbital; lacrimal with large dorsal exposure; pronounced posterodorsal process of the premaxilla between septomaxilla and maxilla. Posterior projection of the frontal shorter than in *Therioherpeton*; anterolateral process of the frontal shorter than in *Therioherpeton*, and contacts the posterolateral border of the nasal, as in *Therioherpeton* and *Morganucodon*. Frontal, palatine, and orbitosphenoid extensively contact one another in the orbital wall. Five conical upper incisors; four lower incisors slightly spatulate and procumbent (as in *Morganucodon*). Triconodontlike postcanines without well-defined cingula on the uppers (except for an incipient buccal cingulum on the distal upper postcanine, as in *Thrinaxodon liorhinus* and chiniquodontids); lingual cingula on lower postcanines bear up to nine small cusps (as in *Thrinaxodon liorhinus*). Length of lower tooth row more than half the length of the dentary (as in *Morganucodon*). Secondary bony palate extends posteriorly beyond the last upper postcanine, as in chiniquodontids and tritheledontids. Neural canal of the presacral vertebrae large (as in *Oligopkyphus*), but smaller than in *Therioherpeton*. Neural spines posterodorsally inclined (as in tritylodontids). Zygapophyses of posterior dorsal vertebrae anteroposteriorly elongated, with anterior and posterior facets that are transversely concave and convex, respectively. Ribs without expanded processes. Iliac blade with a vestigial posterior process and a convex lateral surface (as in *Therioherpeton* and tritylodontids; also in tritheledontids; J. A. Hopson, personal communication).

Horizon and Locality. Facies Alemoa of the Santa Maria Formation, 200 m northwest of the hill Cerriquito, in a road cut of route BR-216, Municipio of Santa Maria, State of Rio Grande do Sul, southern Brazil.

Age. Early Late Triassic.

Material. An incomplete skull lacking most of the parietal crest, the braincase, and zygomatic arch. The orbital, preorbital, and infraorbital regions, secondary bony palate, and upper dentition are nearly complete. The right dentary and dentition are complete; the left dentary also has a complete dentition but lacks the ascending ramus and articular process. The postcranium is represented by three incomplete presacral vertebrae, 14 dorsal centra, seven dorsal neural arches, several fragmentary ribs, interclavicle, incomplete right humerus, proximal half of the left humerus, incomplete right ilium, distal halves of both femora, and a disarticulated right foot.

Comments. Significant features of the skull have been more clearly exposed through recent preparation. The skull shows some postmortem cracking and distortion.

DESCRIPTION

Skull (Figs. 9–11). The prefrontal and postorbital are reduced, and there is no indication of a postorbital bar (Fig. 9). The

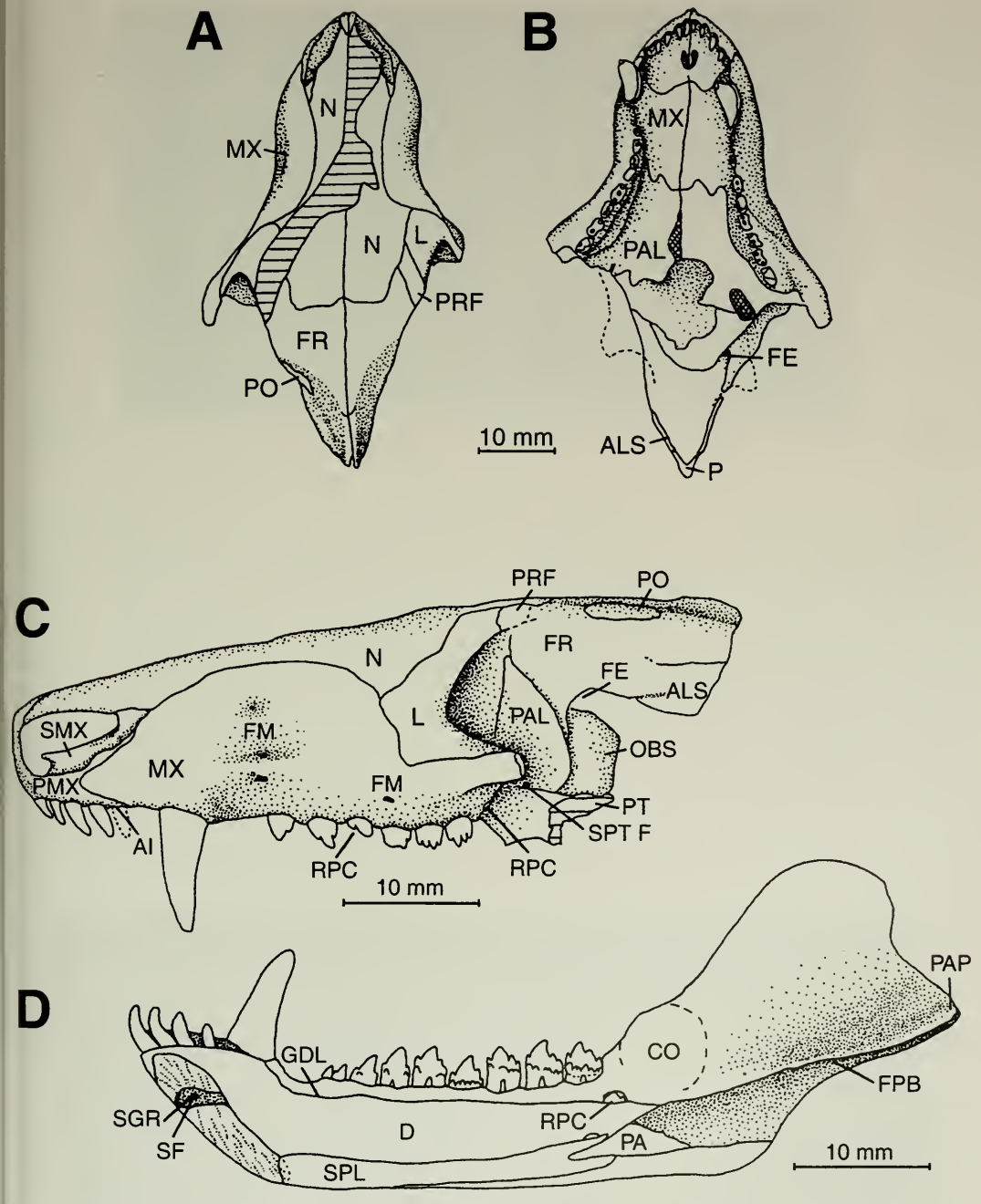

Figure 9. *Prozostrodon brasiliensis,* new genus. Incomplete skull in (A) dorsal, (B) ventral, and (C) left lateral views. (D) Incomplete right lower jaw in medial view. *Abbreviations:* AI, alveolus for incisor; ALS, alisphenoid; CO, coronoid; D, dentary; FE, ethmoidal foramen; FM, maxillary foramina; FPB, fossa for postdentary bones; FR, frontal; GDL, groove of dental lamina; L, lacrimal; MX, maxilla; N, nasal; OBS, orbitosphenoid; P, parietal; PA, prearticular; PAL, palatine; PAP, prearticular process; PRF, prefrontal; PMX, premaxilla; PO, postorbital; PT, pterygoid; RPC, replacing postcanine; SF, symphysial foramen; SGR, symphysial groove; SMX, septomaxilla; SPL, splenial; SPT F, sphenopalatine foramen.

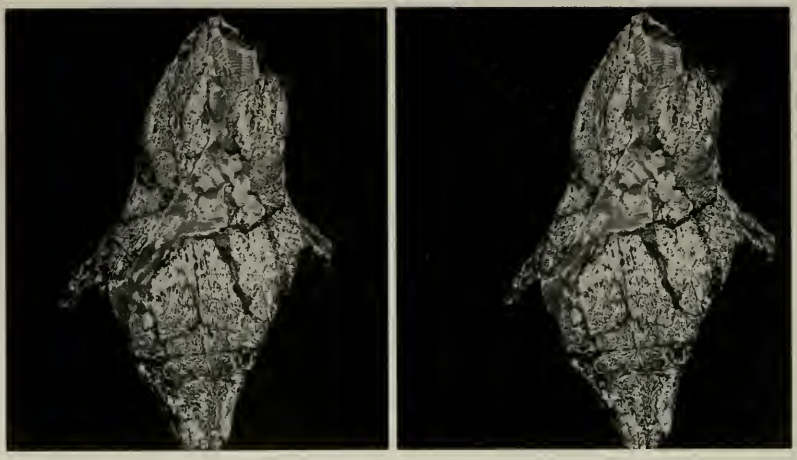

Figure 10. *Prozostrodon brasiliensis,* new genus. Dorsal view of the holotype skull. The anterolateral projection of the frontal is shown.

frontal borders the orbit and extends anterolaterally to contact the lateral, posterior portion of the nasal, as in *Therioherpeton.* The orbital process of the frontal contacts the dorsal process of the palatine and the orbitosphenoid, similar to that of *Morganucodon* (Kermack et al., 1981, fig. 96). The sphenopalatine foramen in *Morganucodon* is bordered by the palatine and orbitosphenoid (Kermack et al., 1981), whereas in *Prozostrodon* it is entirely enclosed by the palatine, possibly the primitive condition, with the orbitosphenoid in a more posterior position. Despite this difference, it is interesting to note the structural similarities of the interorbital regions of *Morganucodon* and *Prozostrodon,* with the exception that the distance between the ethmoidal foramen (Fig. 9C) and the anterior border of the orbit is proportionally shorter in *Morganucodon,* possibly representing a derived condition.

A small prefrontal is present (Fig. 9A), anteriorly reduced by the posterior expansion of the lacrimal. A small orbital process of the prefrontal is possibly present, con-

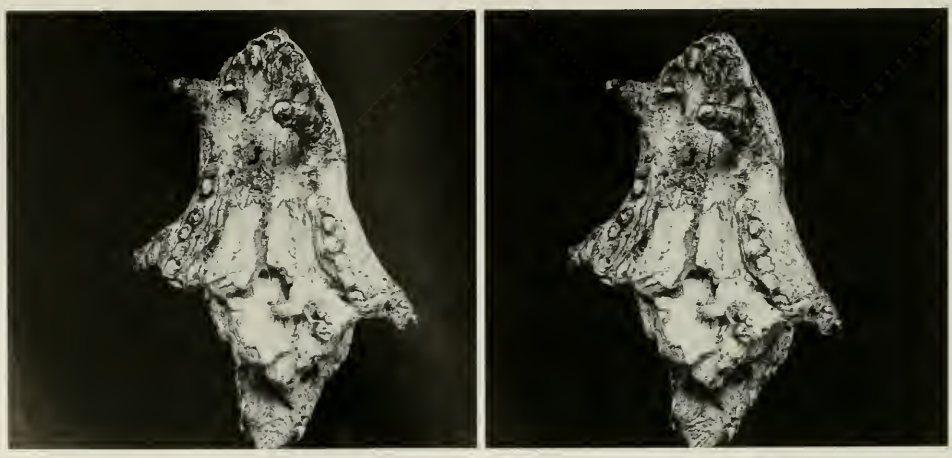

Figure 11. *Prozostrodon brasiliensis,* new genus. Ventral view of the holotype skull.

tacting a similar process of the frontal, but it cannot be positively identified because the sutures are not clear.

The postorbital is represented only on the left side (Fig. 9C) as a small plate overlapping the frontal and parietal on their dorsolateral surfaces. The bone has some external sculpturing, but there is no indication of the postorbital bar.

The premaxilla has a narial process contacting the nasal (Fig. 9C). The lateral posterodorsal process contacting the maxilla is slender and is partially covered by the maxilla. The premaxilla has a long contact with the septomaxilla and does not reach the nasal.

The slender septomaxilla of *Prozostrodon* (Fig. 9C) appears similar to that of *Sinoconodon* (Crompton and Luo, 1993), although it is uncertain whether a septomaxillary foramen is present or not.

The rather large maxilla projects laterally over the premaxilla up to the level of the third incisor (Fig. 9C). A posterior process of the maxilla forms the anterior portion of the zygomatic arch. A large infraorbital foramen lies below the anterior margin of the lacrimal, and two well-defined maxillary foramina are present above the anterior border of the first postcanine.

The anteroposteriorly elongate palatines of *Prozostrodon* (Fig. 9B) resemble a similar configuration in the bony palate of chiniquodontids and morganucodontids. Although the posterior border of the right palatine is broken, the left side is completely preserved and extends posterior to the last postcanine; this condition is similar to that in *Probelesodon kitchingi* (Sá Teixeira, 1979) and trithelodontids, and is a little more extensive than in *Therioherpeton*. The posterior half of the secondary bony palate is widest posteriorly where the tooth row diverges posterolaterally. There is a deep sulcus along the palatine–maxilla suture to accommodate the crowns of the lower postcanines when the jaw is closed. Greater and lesser palatine foramina are present.

Upper Dentition. The upper dentition comprises five incisors, one canine, and seven postcanines (Fig. 9C). The incisors are slender and posteriorly recurved. All five incisors, which are slender and slightly recurved, are present on the right; four incisors and an alveolus for the fifth incisor are present on the left.

In right upper postcanine row, the third and seventh (last) teeth were in the process of erupting. Postcanine crowns are of the "triconodont" type, with cusps aligned mesiodistally. In the three posterior postcanines, four cusps (A, B, C, and D) are present. The labial side is mesiodistally convex, whereas the lingual face is rather concave or flat, with some ill-defined wear; the lack of well-defined facets suggests that no precise occlusion was present. The mesiolingual corner of the last left postcanine bears a poorly defined, low cusp in a position that might be expected of an incipient lingual cingulum. Conversely, the last right postcanine (in the process of erupting) bears a small buccal cusp distally; there is no indication of buccal cingular development in the functional postcanines. The occurrence of cingular cuspules only on the last upper postcanine in *Prozostrodon* is perhaps comparable to the condition in *Thrinaxodon liorhinus* (Osborn and Crompton, 1973; also suggested for *Pachygenelus*; Gow, 1980) in which morphological complexity increases towards the distal end of the tooth row. The roots of the upper postcanines show evidence of incipient bifurcation, as originally indicated by Barberena et al. (1987).

Lower Jaw and Dentition (Figs. 9D, 12). The dorsal and ventral margins of the elongate body of the mandible (Fig. 9D) are subparallel as far forward as the posterior border of the symphysis. Anterior to this point, the dentary extends anterodorsally, elevating the alveolar plane of the incisors and canine above that of the postcanines.

The articular process is transversely expanded, mostly medially, without evidence of an articular condyle. The posteroventral angle of the dentary is broadly convex,

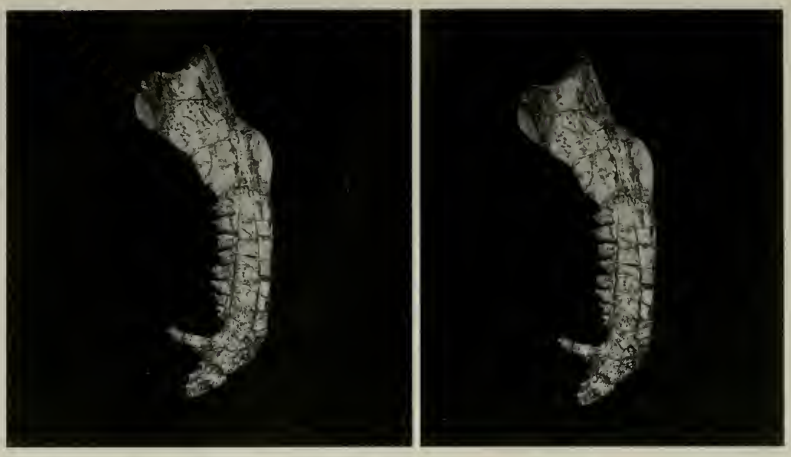

Figure 12. *Prozostrodon brasiliensis,* new genus. Right lower jaw of the holotype in medial view. Note the incipiently bifurcated postcanine roots.

lacking a posteriorly projecting angular process. A coronoid is probably present, largely fused to the medial side of the ascending ramus. The unfused symphysis exhibits rugosity indicative of ligamentous insertion, and a symphysial fossa and foramen as in *Cynognathus* (Kermack et al., 1973).

The lower dentition consists of four incisors, one canine, and 10 postcanines (Barberena et al., 1987). The incisors are slightly procumbent and recurved, with some mesiodistal expansion of the crown in the first three. The fourth incisor is shorter, mesiodistally narrow, and separated from the canine by a short diastema.

The well-preserved postcanines become more complex toward the back (as is common in carnivorous–insectivorous cynodonts; Osborn and Crompton, 1973) as well as increase in size. The following account is based on the right postcanines. Lower postcanine 1 is small, conical, and without accessory cusps. Lower postcanine 2 bears a large main cusp a with smaller cusps b (mesially) and c (distally). A slight lingual cingulum is present. On Pc_3, cusp a has a sharp distal edge, and cusps b and c are positioned on the buccal half of the tooth. Incipient division of the root is apparent in buccal aspect. Lower postcanine 4, substantially larger than preceding postcanines and also exhibiting incipient root division, possesses a (broken) lingual cingulum and a mesial and distal lingual cuspule. Lower postcanine 5 is mesiodistally longer than Pc_4 and has larger accessory cusps b and c. The lingual cingulum is not continuous mesiodistally, but has anterior and posterior sections, each bearing a cuspule. The base of the crown is larger than the root, which is well differentiated from the crown and exhibits a vertical groove. Lower postcanine 6, which is almost fully erupted, bears a conical, recurved cusp a, and a cusp d on the distal margin. Cusp c is larger than cusp b. The cingulum, which is more developed than in the preceding postcanines, extends along most of the lingual side and bears six cuspules. Cusp a is broken on Pc_7, but cusps b, c, and d are present and aligned with the base of cusp a. The lingual cingulum is continuous. The occlusal surface of the cingulum and the surface above it suggest abrasion by food while chewing. The root is deeply grooved. Lower postcanine 8 is complete, with basically the same features as in Pc_7. Lower postcanine 9, mesiodistally the longest postcanine, has a proportionally lower crown as well as the lowest cusp a (on the left side, Pc_9 appears to be in the final

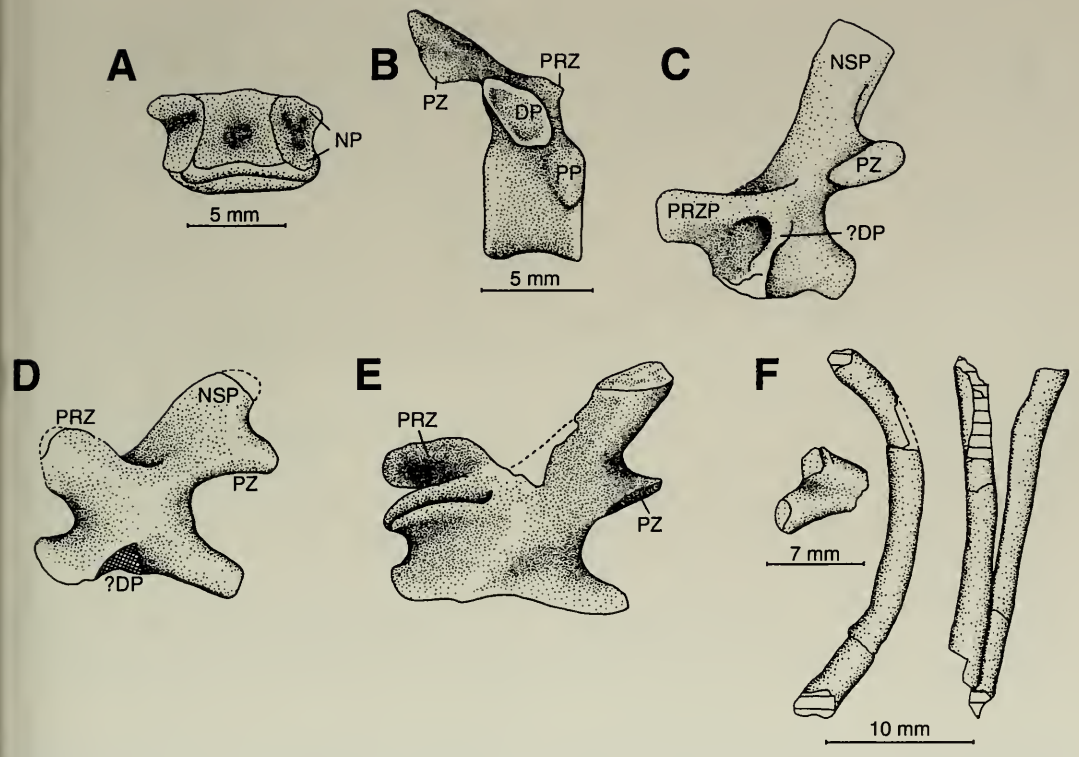

Figure 13. *Prozostrodon brasiliensis,* new genus. (A) Cervical centrum in dorsal view. (B) Anterior dorsal vertebra in lateral view. (C, D, E) Lateral views of three neural arches from the dorsal series. (F) Incomplete ribs. *Abbreviations:* DP, diapophysis; ?DP, ?diapophysis; NP, contact for neural pedicle; NSP, neural spine; PP, parapophysis; PRZ, prezygapophysis; PZ, postzygapophysis; PRZP, prezygapophysial process.

stage of eruption). Seven small cusps form the lingual cingulum. The degree of incipient root bifurcation is greater than in preceding postcanines, representing a morphological gradient that is also expressed in the increasing complexity of the cingula. The right Pc_{10} is unerupted; cusp a and part of c are exposed just below the groove for the dental lamina. The left Pc_{10} is just beginning to erupt; the position of this tooth distal to the end of the alveolar row is evidence that the individual was still growing.

Postcranium. One centrum (Fig. 13A) is tentatively considered to be cervical because it is transversely wide and anteroposteriorly short, as are the cervicals of *Therioherpeton.* The facets for the pedicles of the neural arch are in a dorsolateral position; if the pedicles were to have projected dorsolaterally, the neural canal would have been relatively wide. The parapophyseal facets are located entirely on the anteroventral margin of the centrum; there is no indication that rib heads spanned adjacent vertebrae.

A nearly complete anterior dorsal vertebra (Fig. 13B) exhibits a parapophysis on the dorsolateral region of the centrum, a large diapophysis that projects laterally from the middle of the pedicle, and a neural spine that is directed posterodorsally. The centrum is moderately amphicoelous. The neural canal is large but narrower than the centrum, differing in this respect from *Therioherpeton* (and possibly reflective of the more adult stage of *Prozostrodon*; J. A. Hopson, personal communication).

The dorsolumbar region is further rep-

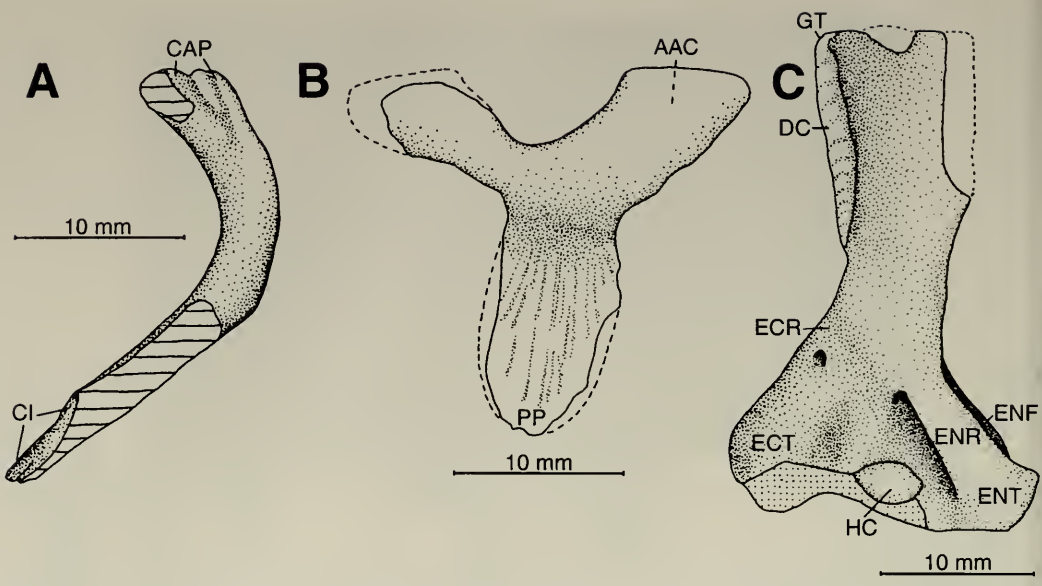

Figure 14. *Prozostrodon brasiliensis,* new genus. (A) ?Right clavicle in ?posterior view. (B) Interclavicle in dorsal view. (C) Right humerus in ventral view. *Abbreviations:* AAC, attachment area for right clavicle; CAP, contact with acromial process; CI, contact with interclavicle; DC, deltopectoral crest; ECT, ectepicondyle; ECR, ectepicondylar ridge; ENF, entepicondylar foramen; ENR, entepicondylar ridge; ENT, entepicondyle; GT, greater trochanter; HC, humeral capitulum; PP, posterior projection.

resented by an incomplete vertebra and four incomplete neural arches. The former has a massive centrum with marked amphicoely. The transverse processes are directed laterally and the broken base of the neural spine indicates that the spine was directed posterodorsally. The neural canal is large but narrower than the centrum. Structural variations in the spinous processes and zygapophyses are evidence of regional variation along the dorsolumbar column.

In one neural arch (Fig. 13C), the robust prezygapophyses are positioned more ventrally than the postzygapophyses; postzygapophyseal facets are anteroposteriorly elongate and transversely convex, possibly representing a specialization for dorsoventral flexure of the vertebral column (J. A. Hopson, personal communication). The neural spine, with almost parallel anterior and posterior borders, is posterodorsally directed, and more steeply inclined than in *Exaeretodon* (Bonaparte, 1963). Another neural arch (Fig. 13E) has a similarly elongate set of postzygapophyses with convex facets, and prezygapophyses with transversely concave facets. Jenkins and Parrington (1976, figs. 2A–D) illustrated a neural arch in *Morganucodon* with zygapophyses and a neural spine of comparable structure.

A different type of dorsal vertebra (Fig. 13D), represented by two neural arches, possibly derives from a position posterior to those described above. The zygapophyseal facets have less curvature and the damaged neural spine appears to be shorter than in the previously described neural arches.

Ribs (Fig. 13F). Eight to 10 ribs are represented by 20 fragments, and none show any indication of processes or expansions. Most are figure 8–shaped in cross section.

Clavicle (Fig. 14A). Most of the ?right clavicle is present. On the proximal end are furrowlike rugosities representing the area of attachment with the interclavicle. The wide distal end is complexly configured with surfaces representing the acro-

mial attachment. The greatest curvature of the shaft is closer to the distal end.

Interclavicle (Fig. 14B). This Y-shaped element, with broad anterolateral extensions for reception of the clavicles, is anteroposteriorly shorter (19 mm) than wide (23 mm). The ventral surface is not exposed.

Scapulocoracoid. These bones are represented only by small fragments that are too fragmentary to provide useful information on the glenoid and other features of interest.

Humerus (Fig. 14C). The left humerus is represented by the proximal half, including the deltopectoral crest and the humeral head. The right humerus is almost complete, lacking only the humeral head and part of the proximal end, and a small portion of the distal end including the articular surface for the ulna. The humerus is structurally no more derived than that of *Exaeretodon,* and is similar to that of *Probelesodon lewisi* (Romer and Lewis, 1973). The entepicondylar foramen is very large, and opens distally into a deep sulcus that continues to the entepicondylar terminus. The entepicondyle, which is larger than the ectepicondyle, terminates in a distinct projection. Near the anterior margin that extends proximally from the ectepicondyle is a small ectepicondylar foramen; this margin extends farther proximally onto the diaphysis than does the comparable margin from the entepicondyle.

Ilium (Fig. 15A). The right ilium is almost complete except for the most anterior end of the iliac blade. The neck above the acetabulum is well defined, and the posterior end of the iliac blade bears a very short process. Both of these features are derived compared with the structure seen in *Thrinaxodon* and *Cynognathus* (Jenkins, 1971) and in *Exaeretodon* (Bonaparte, 1963). The outer surface of the iliac blade is largely convex dorsoventrally, not concave as in the above cited cynodonts, and its dorsal and ventral borders are nearly parallel to one another.

Foot (Figs. 15B, C). The right hind foot is complete, except for the lateral part of the calcaneum. The superposition of astragalus and calcaneum appears to be of the type present in *Exaeretodon* (Bonaparte, 1963), defined by Jenkins (1971) as the "therapsid type of plantigrady." However, the metatarsals and phalanges are proportionally longer than in *Exaeretodon.* The phalangeal formula is 2-3-3-3-3.

Comparison of Prozostrodon *with other Cynodonts.* The referral of PV 0248T to the genus *Thrinaxodon* by Barberena et al. (1987) is untenable, as pointed out by Battail (1991), who interpreted the specimen as a chiniquodontid. The following derived characters present in the holotype of *Prozostrodon brasiliensis* are not found in specimens of *Thrinaxodon* from the Early Triassic of South Africa (Parrington, 1946; Estes, 1961) and Antarctica (Colbert and Kitching, 1977).

1) Frontal bordering the orbit (also in *Therioherpeton,* tritheledontids, and tritylodontids).
2) Contact between the ventral process of frontal and dorsal process of palatine (also in tritheledontids and tritylodontids; additionally present in *Probainognathus, Ecteninion,* and chiniquodontids; J. A. Hopson, personal communication).
3) Presence of an orbitosphenoid contacting frontal and palatine, and medially placed relative to the dorsal process of the palatine (also in *Morganucodon*; Kermack et al., 1981).
4) Secondary bony palate with large palatines that extend to the level of the last postcanine.
5) Incipient bifurcation of the roots in the upper and lower postcanines.
6) Small postorbital and prefrontal.
7) Absence of postorbital bar (also in *Therioherpeton,* tritheledontids, and tritylodontids).
8) Large infraorbital and two well-defined foramina for the trigeminal nerve in the maxilla (also in tritheledontids and tritylodontids).

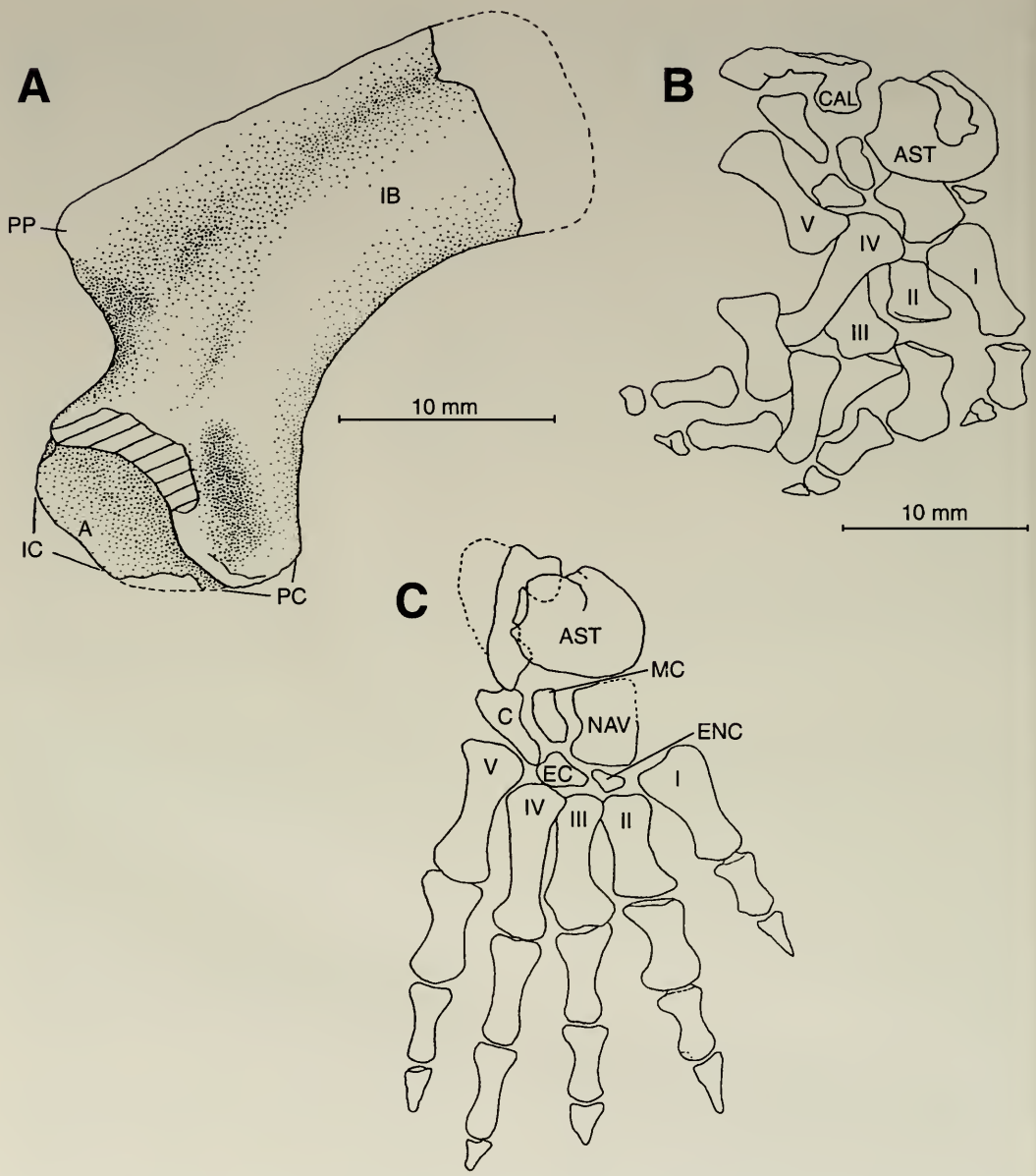

Figure 15. *Prozostrodon brasiliensis*, new genus. (A) Incomplete right ilium in lateral view. (B) Right foot as preserved. (C) Reconstruction of right foot in dorsal view. *Abbreviations:* A, acetabular area; AST, astragalus; CAL, calcaneum; C, cuneiform; EC, ectocuneiform; ENC, entocuneiform; IC, ischial contact; IB, iliac blade; MC, mesocuneiform; NAV, navicular; PC, pubis contact; PP, posterior process of the ilium; I–V, metatarsals I through V.

This combination of derived characters precludes referral of *Prozostrodon brasiliensis* not only to the Thrinaxodontidae, but also to the Cynognathidae, Chiniquodontidae, and Probainognathidae. The lack of gliriform specialization in the incisors and the transversely narrow postcanines preclude referral of the specimen to the

Tritheledontidae or to any gomphodont family, including the Tritylodontidae.

A Summary of the Distinctive Features of Prozostrodon. In addition to the characters listed above as well as in the diagnosis, *Prozostrodon* possesses other distinctive features. Although many of these features may be found among various other taxa, only in *Prozostrodon,* as far as we are aware, do they occur together. The suite is as follows.

1) Reduced unossified area between frontal, orbitosphenoid, and alisphenoid (also in tritylodontids and *Ectenion*; Martínez et al., 1996).
2) Sphenopalatine foramen within the posterior portion of the dorsal process of palatine.
3) Anteroposteriorly long palatines in the secondary bony palate (also in chiniquodontids, tritheledontids, and some tritylodontids).
4) Root of the zygomatic arch distinctly offset from the posterior margin of the maxilla (also in *Probainognathus,* chiniquodontids, tritylodontids, traversodontids, and diademodontids).
5) Carnivorous–insectivorous dentition comparable in general morphology to that of *Thrinaxodon* and *Morganucodon,* but with cingula on the upper postcanines that are either poorly developed or absent altogether.
6) Posterior portion of the upper tooth row inset from the lateral border of the maxilla (also in traversodontids, tritylodontids, tritheledontids, and *Probainognathus*).
7) Incipient bifurcation of the upper postcanine roots.
8) Incipient bifurcation of the lower postcanine roots (also in *Pachygenelus* and *Microconodon*; H.-D. Sues, personal communication; and in *Therioherpeton*).
9) Mandibular symphysis unfused, anteroposteriorly elongated, dorsoventrally narrow (as in *Thrinaxodon* [primitive], tritheledontids, and tritylodontids [derived]; J. A. Hopson, personal communication).
10) Presence of symphysial fossa and foramen in the lower jaw (also in *Cynognathus*; Kermack et al., 1973).
11) Articular process of the dentary extended posteriorly and expanded transversely, without indication of a condyle, and set above the level of the postcanine teeth (a feature of derived cynodonts; J. A. Hopson personal communication).
12) Cervical centra anteroposteriorly short, transversely wide, and dorsoventrally low (also in tritylodontids and *Morganucodon*).

DISCUSSION

The specimens of *Therioherpeton* (skull length, 38 mm) and *Prozostrodon* (skull length estimated to be 67 mm) are relatively small, and consideration should be given to whether the smaller of the two represents a juvenile individual. Four features of *Therioherpeton,* in comparison to those in *Prozostrodon,* might be interpreted as evidence of immaturity: the frontals extend further posteriorly; the anterior portion of the braincase is proportionally wider; the postcanines lack cingula; the neural canals of presacral vertebrae are proportionally larger. However, the possibility that these are juvenile characters is contradicted by the state of ossification in the postcranium of *Therioherpeton.* With the exception of the pelvis, in which the three elements are not synostosed, we find no evidence of a subadult condition. Furthermore, *Therioherpeton* does not exhibit the proportionately large orbital size that is characteristic of juvenile individuals. A juvenile skull of cf. *Probainognathus* (Bonaparte and Crompton, 1994, figs. 1, 2) of comparable length (39 mm) to that of *Therioherpeton* exhibits a skull to orbit ratio of 3.5, versus an estimated 5.0 for *Therioherpeton.* In a putatively mature skull of *Probainognathus* (Romer, 1970, fig. 2) the ratio of skull to orbital length is 6, only slightly greater than in *Therioherpeton.* Al-

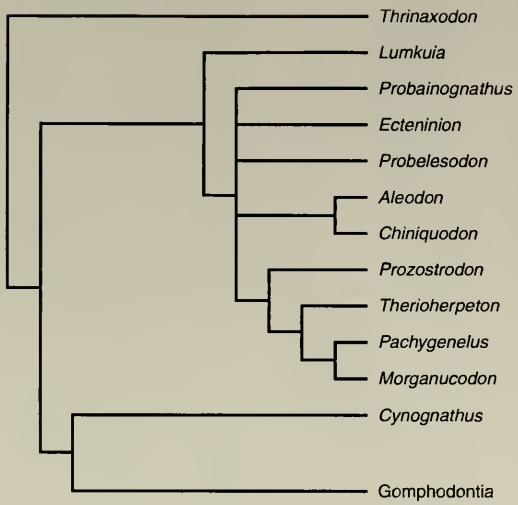

Figure 16. The hypothesized phylogenetic positions of *Therioherpeton* and *Prozostrodon*. The cladogram was generated by Dr. J. A. Hopson, who incorporated information from the Brazilian genera described in this paper into his data set of cynodont characters.

though we do not believe that the type of *Therioherpeton* represents a juvenile, we remain open to the possibility that the four characters cited above eventually might be shown to be juvenile characters retained in adulthood.

The hypothesized relationships of *Therioherpeton* and *Prozostrodon* are depicted in Figure 16. The relative positions in the cladogram of the two genera seem due to the persistence of a prefrontal and postorbital and the shorter posterior projection of the frontal in *Prozostrodon,* and to the more derived characters present in the pelvis and proximal femur of *Therioherpeton.*

The materials of *Therioherpeton* and *Prozostrodon,* although incomplete, provide new anatomical information to further elucidate the complex transition between cynodonts and primitive mammals. The taxa described here support the hypothesis that the ancestry of mammals lay among the clade of carnivorous–insectivorous cynodonts (Hopson, 1991, 1994; Hopson and Kitching, 2001), rather than among gomphodont cynodonts, and in particular the Tritylodontidae (Kemp, 1982, 1983). Sues (1985) reviewed in detail most of the synapomorphies that Kemp (1982, 1983) proposed in support of his interpretation that tritylodontids and primitive mammals were closely related, and concluded that many of these purportedly shared derived features are either superficial similarities, are symplesiomorphic, or are the result of parallel development but which, nonetheless, evidence structural differences.

We regard the dentition of *Prozostrodon* as morphologically intermediate between that of *Thrinaxodon liorhinus* from the Early Triassic and those evolved among Late Triassic and Early Jurassic morganucodontids. Although tritheledontids such as *Pachygenelus* have been considered as closely related to mammals (Hopson and Barghusen, 1986), and are represented cladistically as the sister taxon to mammals (Fig. 16; see also Shubin et al., 1991), we interpret the tritheledontid dentition as derived, particularly with respect to the buccolingual expansion of the upper postcanines. In contrast, the entire dentition of *Prozostrodon* (and what is known of that of *Therioherpeton*) is substantially similar to that in morganucodontids, with only slight differences in the development of upper postcanine cingula. During a span of time that witnessed major modifications in cranial and postcranial morphology, dental patterns were fundamentally conserved.

ACKNOWLEDGMENTS

Drafts of this paper were critically reviewed by Drs. Z. Kielan-Jaworowska, G. W. Rougier, H.-D. Sues, and J. A. Hopson. Very special thanks are accorded Dr. J. A. Hopson for his generous help and advice on improvements, and for the use of his database in the cladogram presented here. We also thank Drs. F. A. Jenkins, Jr., and M. D. Shapiro for editorial assistance. The senior author expresses gratitude to two colleagues at the Fundacao Zoobotánica de Porto Alegre, Brazil: Dr. J. Ferigolo for

interesting discussions on the subject; and Ana M. Riveiro for field and laboratory assistance. The senior author is also grateful to the CNPq. of Brazil, and to the Museo Argentino de Ciencias Naturales, Buenos Aires, for support in developing most of this research in the Museu de Ciencias Naturais de Porto Alegre, Brazil.

LITERATURE CITED

BARBERENA, M. C., J. F. BONAPARTE, AND A. M. SÁ TEIXEIRA. 1987. *Thrinaxodon brasiliensis* sp. nov., a primeira ocorrência de cinodontes galessauros para o Triásico do Rio Grande do Sul. Anais do X Congresso Brasileiro de Paleontología, Rio de Janeiro, Brazil, pp. 67–76.

BATTAIL, B. 1991. Les Cynodontes (Reptilia, Therapsida): une phylogenie. Bulletin du Museum Nationale d'Histoire Naturelle. Section C, Sciences de la Terre Paléontolgie, Géologie, Minérologie, **13:** 17–105.

BONAPARTE, J. F. 1963. Descripción del esqueleto postcraneano de *Exaeretodon* sp. Acta Geológica Lilloana, **4:** 5–52

———. 1980. El primer ictidosaurio (Reptilia–Therapsida) de América del Sur, *Chaliminia musteloides,* del Triásico Superior de La Rioja, República Argentina. Actas del II Congreso Argentino de Paleontología y Bioestratigrafía, y I Congreso Latinamericano de Paleontologia, **1:** 123–133.

BONAPARTE, J. F., AND M. C. BARBERENA. 1975. A possible mammalian ancestor from the Middle Triassic of Brazil (Therapsida–Cynodontia). Journal of Paleontology, **49:** 931–936.

BONAPARTE, J. F., AND A. W. CROMPTON. 1994. A juvenile probainognathid cynodont skull from the Ischigualasto Formation and the origin of mammals. Revista Museo Argentino de Ciencias Naturales, Paleontología, **5:** 1–12.

BORTOLUZZI, C. A., AND M. C. BARBERENA. 1967. The Santa Maria beds in Rio Grande do Sul (Brazil), pp. 169–195. *In* J. J. Bigarella, R. D. Becker, and I. D. Pinto (eds.), Problems in Brazilian Gondwana Geology. 1st International Symposium on Gondwana Stratigraphy and Paleontology. Curitiba, Brazil: Roesner Ltd. xviii + 344 pp.

COLBERT, E. H., AND J. KITCHING. 1977. Triassic cynodont reptiles from Antarctica. American Museum Novitates, **2611:** 1–30.

CROMPTON, A. W. 1958. The cranial morphology of a new genus and species of ictidosaurian. Proceedings of the Zoological Society of London, **130:** 183–216.

———. 1974. The dentitions and relationships of the Southern African Triassic mammals *Erythrotherium parringtoni* and *Megazostrodon rudnerae.* Bulletin of the British Museum (Natural History), Geology, **24:** 399–437.

CROMPTON, A. W., AND Z. LUO. 1993. Relationships of the Liassic mammals *Sinoconodon, Morganucodon oehleri* and *Dinnetherium,* pp. 30–44. *In* F. S. Szalay, M. J. Novacek, and M. C. McKenna (eds.), Mammal Phylogeny: Mesozoic Differentiation, Multituberculates, Monotremes, Early Therians and Marsupials. New York: Springer-Verlag. x + 249 pp.

CROMPTON, A. W., AND A.-L. SUN. 1985. Cranial structure and relationships of the Liassic mammal *Sinoconodon.* Journal of the Linnean Society of London, **85:** 99–119.

ESTES, R. 1961. Cranial anatomy of the cynodont reptile *Thrinaxodon liorhinus.* Bulletin of the Museum of Comparative Zoology, **125:** 165–180.

GOW, C. 1980. The dentitions of the Tritheledontidae (Therapsida: Cynodontia). Proceedings of the Royal Society of London, B, **208:** 461–481.

———. 1986. A new skull of *Megazostrodon* (Mammalia: Triconodonta) from the Elliot Formation (Lower Jurassic) of southern Africa. Palaeontologia Africana, **26:** 13–23.

HOPSON, J. A. 1991. Systematics of the non-mammalian Synapsida and implications for patterns of evolution in synapsids, pp. 635–693. *In* H.-P. Schultze and L. Trueb (eds.), Origins of the Higher Groups of Tetrapods. Ithaca, New York: Cornell University Press. xii + 724 pp.

———. 1994. Synapsid evolution and the radiation of nontherian mammals, pp. 190–219. *In* D. R. Prothero and R. M. Schoch (eds.), Major Features of Vertebrate Evolution, Short Courses in Paleontology, No. 7. Knoxville, Tennessee: University of Tennesee. 270 pp.

HOPSON, J. A., AND H. R. BARGHUSEN. 1986. An analysis of therapsid relationships, pp. 83–106. *In* N. Hotton III, P. D. McLean, J. J. Roth, and E. C. Roth (eds.), The Ecology and Biology of Mammal-like Reptiles. Washington, DC: Smithsonian Institution Press. x + 326 pp.

HOPSON, J. A., AND J. W. KITCHING. 2001. A probainognathian cynodont from South Africa and the phylogeny of nonmammalian cynodonts. Bulletin of the Museum of Comparative Zoology, **156:** 5–35.

JENKINS, F. A., JR. 1970. The Chañares (Argentina) Triassic reptile fauna. VII. The postcranial skeleton of the traversodontid *Massetognathus pascuali* (Therapsida, Cynodontia). Breviora, **352:** 1–28.

———. 1971. The postcranial skeleton of African cynodonts. Bulletin of the Peabody Museum of Natural History, **36:** 1–216.

———. 1984. A survey of mammalian origins, pp. 32–47. *In* P. D. Gingerich and C. D. Badgley (eds.), Mammals: Notes for a Short Course. Knoxville, Tennessee: University of Tennesee Department of Geological Sciences Studies in Geology 8. 234 pp.

JENKINS, F. A., JR., AND F. R. PARRINGTON. 1976. The postcranial skeletons of the Triassic mam-

mals *Eozostrodon, Megazostrodon* and *Erythrotherium.* Philosophical Transactions of the Royal Society of London B, Biological Sciences, **273:** 387–431.

KEMP, T. S. 1982. Mammal-like Reptiles and the Origin of Mammals. London: Academic Press. xiv + 363 pp.

———. 1983. The interrelationships of mammals. Zoological Journal of the Linnean Society, **77:** 353–384.

KERMACK, K. A., F. MUSSETT, AND H. W. RIGNEY. 1973. The lower jaw of *Morganucodon.* Zoological Journal of the Linnean Society, **53:** 87–175.

———. 1981. The skull of *Morganucodon.* Zoological Journal of the Linnean Society, **71:** 1–158.

KÜHNE, W. G. 1956. The Liassic therapsid *Oligokyphus.* London: Trustees of the British Museum (Natural History). x + 149 pp.

LUO, Z. 1994. Sister-group relationships of mammals and transformations of diagnostic mammalian characters, pp. 98–128. *In* N. C. Frazer and H.-D. Sues (eds.), In the Shadow of the Dinosaurs. Cambridge, United Kingdom: Cambridge University Press. x + 435 pp.

MARTÍNEZ, R. N., C. L. MAY, AND C. A. FORSTER. 1996. A new carnivorous cynodont from the Ischigualasto Formation (Late Triassic, Argentina), with comments on eucynodont phylogeny. Journal of Vertebrate Paleontology, **16:** 271–284.

OSBORN, J., AND A. W. CROMPTON. 1973. The evolution of mammalian from reptilian dentitions. Breviora, **399:** 1–18.

PARRINGTON, F. R. 1946. On the cranial anatomy of cynodonts. Proceedings Zoological Society of London, **116:** 181–197.

ROMER, A. S. 1970. The Chañares (Argentina) Triassic reptile fauna. VI. A chiniquodontid cynodont with an incipient squamosal–dentary jaw articulation. Breviora, **344:** 1–18.

ROMER, A. S., AND A. LEWIS. 1973. The Chañares (Argentina) Triassic reptile fauna. XIX. Postcranial materials of the cynodonts *Probelesodon* and *Probainognathus.* Breviora, **407:** 1–26.

SÁ TEIXEIRA, A. M. 1979. Um novo cinodonte carnívoro (*Probelesodon kitchingi*) do Triássico do Rio Grande do Sul, Brasil. Unpublished M.S. dissertation. Universidade Federal do Rio Grande do Sul, Brazil: Postgraduation in Geosciences. 71 pp.

SCHULTZ, C. L. 1986. Osteología parcial do postcránio de *Scaphonyx sulcognathus* Azevedo 1982 (Lepidosauria, Rhynchocephalia, Rhynchosauridae). Unpublished M.S. dissertation. Universidade Federal do Rio Grande do Sul, Brazil: Postgraduation in Geosciences. 139 pp.

SHAPIRO, M. D., AND F. A. JENKINS, JR. 2001. A cynodont from the Upper Triassic of East Greenland: tooth replacement and double-rootedness. Bulletin of the Museum of Comparative Zoology, **156:** 49–58.

SHUBIN, N. H., A. W. CROMPTON, H.-D. SUES, AND P. E. OLSEN. 1991. New fossil evidence on the sister-group of mammals and early Mesozoic faunal distribution. Science, **251:** 1063–1065.

SUES, H.-D. 1985. The relationships of the Tritylodontidae (Synapsida). Zoological Journal of the Linnean Society, **85:** 205–217.

SUN, A.-L. 1984. Skull morphology of the tritylodont genus *Bienotheroides* of Sichuang. Scientia Sinica, B **27:** 270–284.

THE INNER EAR AND ITS BONY HOUSING IN TRITYLODONTIDS AND IMPLICATIONS FOR EVOLUTION OF THE MAMMALIAN EAR

ZHEXI LUO[1]

ABSTRACT. The inner ear structures underwent fundamental changes during the evolution from nonmammalian cynodonts ("mammallike reptiles") to early mammals. The petrosal bone in mammals has an enlarged pars cochlearis containing an elongate cochlea. The elongation of the bony cochlear canal is usually correlated with the development of a ventral eminence of the pars cochlearis, known as the promontorium. Both cochlear canal and promontorium are regarded as apomorphies of mammals. In contrast, nonmammalian cynodonts lack the promontorium. If present at all, the bony cochlear recess is small, globular, and poorly differentiated from the vestibule in most cynodonts. The tritylodontid *Yunnanodon* has an intermediate condition. Unlike most nonmammalian cynodonts, *Yunnanodon* has a distinctive cochlear canal in an enlarged pars cochlearis, but it lacks the promontorium and retains the basisphenoid wing, a primitive feature of many cynodonts. These characters in tritylodontids suggest that a distinctive cochlear canal in an enlarged pars cochlearis probably evolved in the common ancestor to tritylodontids, tritheledontids, and mammaliaforms, and before the emergence of the petrosal promontorium in mammaliaforms. The promontorium subsequently formed by the displacement of the neighboring parasphenoid–basisphenoid complex and basioccipital bone by the pars cochlearis in the early evolution of mammaliaforms.

INTRODUCTION

The bony structure surrounding the inner ear differs between mammals and nonmammalian cynodonts. The inner ear of cynodonts is enclosed by the prootic and the opisthotic, known collectively as the periotic bones, as well as by the exoccipital and the basioccipital. The basisphenoid wing (or parasphenoid ala), which is a large component of the parasphenoid–basisphenoid complex, overlaps the prootic and indirectly contributes to the cochlear housing. The bony housing for the inner ear in cynodonts is formed by multiple bones, as documented in great detail for *Thrinaxodon* (Olson, 1944; Estes, 1961; Fourie, 1974; Rowe et al., 1993), *Probelesodon, Massetognathus* (Quiroga, 1979), and *Probainognathus* (Allin, 1986). This mosaic pattern is primitive for cynodonts because it is also present, albeit in a slightly different condition, in noncynodont therapsids (Olson, 1944; Cox, 1962; Sigogneau, 1974).

In contrast, the bony housing of the inner ear in early mammaliaforms (modified from Rowe [1988] to include *Adelobasileus* and *Sinoconodon*) is formed exclusively by the petrosal, which is the single bone composed of the fused prootic and opisthotic elements of nonmammalian cynodonts (Kermack et al., 1981; Rowe, 1988; Luo et al., 1995). The parasphenoid–basisphenoid complex, the basioccipital, and the exoccipital are excluded by an enlarged petrosal from the bony housing for the inner ear, as has been documented in a wide range of mammaliaforms and early mammals, such as *Sinoconodon* (Luo et al., 1995), morganucodontids (Kermack et al., 1981; Gow, 1985; Graybeal et al., 1989; Luo and Ketten, 1991; Crompton and Luo, 1993), triconodontids (Kermack, 1963; Crompton and Luo, 1993; Rougier et al., 1996), docodonts (Lillegraven and Krusat, 1991), monotremes (Kuhn, 1971; Zeller, 1989; Luo and Ketten, 1991; Fox and Meng, 1997), multituberculates (Miao, 1988; Luo and Ketten, 1991; Lil-

[1] Section of Vertebrate Paleontology, Carnegie Museum of Natural History, Pittsburgh, Pennsylvania 15213.

legraven and Hahn, 1993; Meng and Wyss, 1995; Fox and Meng, 1997; Hurum, 1998), and archaic therians (Wible et al., 1995; Hu et al., 1997). In mammals, the pars cochlearis that contains the cochlear canal is much larger than in cynodonts, forming a ventrolateral eminence known as the promontorium, which is a very conspicuous external feature in the mammalian basicranium (Gow, 1985; Hopson and Barghusen, 1986; Rowe, 1988; Luo et al., 1995).

Mammals and nonmammalian cynodonts differ also in features of the inner ear. In the noncynodont therapsids, such as dicynodonts (Cox, 1962) and gorgonopsids (Sigogneau, 1974), the sacculocochlear cavity (or recess) is not differentiated from the vestibular cavity (Olson, 1944; Cox, 1962; Sigogneau, 1974). At the anterior end of this sacculocochlear cavity is the fenestra vestibuli or oval window, which accommodates the stapes that transmitted sound vibrations from the middle to the inner ear. The cochlear part of the osseous inner ear is more distinctive from the vestibule in primitive cynodonts such as *Thrinaxodon* (Estes, 1961; Fourie, 1974). In advanced cynodonts (Quiroga, 1979; Allin and Hopson, 1992), the bony cochlear structure is more developed than in *Thrinaxodon* and noncynodont therapsids. The bony cochlea is represented by a small and globular cavity but is too short to be termed the cochlear canal (except for tritylodontids, and perhaps tritheledontids; see below).

In contrast, in Early Jurassic mammaliaforms, the cochlear canal is elongate and differentiated from the saccular cavity (Graybeal et al., 1989; Luo and Ketten, 1991; Luo et al., 1995). The elongate cochlear canal is a shared derived feature of diverse mammalian groups during the Mesozoic, as documented in multituberculates (Miao, 1988; Luo and Ketten, 1991; Lillegraven and Hahn, 1993; Meng and Wyss, 1995; Fox and Meng, 1997; Hurum, 1998), docodonts (Lillegraven and Krusat, 1991), and possibly in symmetrodont therians (Wible et al., 1995; Hu et al., 1997). The elongate bony cochlear canal suggests a better-developed cochlear duct, which may indicate a better sensitivity to high-frequency sound that is very important in the hearing function of all extant mammals, and probably important for at least some of the earliest mammals (Rosowski and Graybeal, 1991; Rosowski, 1992; Hurum, 1998).

Given these differences in the structure of the inner ear and its bony housing between mammals on the one hand and nonmammalian cynodonts on the other, the ear structures must have undergone extensive transformation during the early evolution of mammals after their divergence from nonmammalian cynodonts. To elucidate the pattern of this phylogenetic transformation, it is essential to obtain some detailed anatomical information on the inner ear and the surrounding bones in such derived cynodonts as tritylodontids and tritheledontids. Some earlier studies of the ear region of tritylodontids reported the presence of a cochlear canal (Kühne, 1956; Hopson, 1965). Two additional studies (Gow, 1986; Sun and Cui, 1987) offered observations on the basicranial structures surrounding the inner ear. This paper describes the inner ear and its bony housing in the tritylodontid *Yunnanodon,* and their anatomical relationships as revealed by serial sections. The new information has implications for the evolution of the ear region through the transition from nonmammalian cynodonts to mammals, given the fact that tritylodontids are considered by some to be closely related to mammals (Kemp, 1983; Rowe, 1988; Wible, 1991; Wible and Hopson, 1993; Luo, 1994; Luo and Crompton, 1994; but see the alternative phylogeny by Crompton [1972], Sues [1985a], and Hopson and Barghusen [1986]).

MATERIALS AND METHODS

Fossil remains of *Yunnanodon* (Cynodontia, Tritylodontidae) are from the Upper Red Beds of the Lower Lufeng For-

mation of Yunnan, China (Sun et al., 1985), which is considered to be Early Jurassic (Sinemurian to Pliensbachian) by recent studies (Luo and Sun, 1993; Luo and Wu, 1995). *Yunnanodon* is the smallest tritylodontid known from the Lower Lufeng Formation (Cui, 1976, 1986; Luo and Wu, 1994), with a skull length ranging from 36 to 47 mm. *Yunnanodon* has only two cusps in the lingual row of the upper postcanines, the main diagnostic character distinguishing this taxon from other tritylodontids in the Lower Lufeng, all of which have three lingual cusps on the upper teeth (Cui, 1976; Luo and Wu, 1994). *Yunnanodon* is comparable to *Dinnebitodon* from the Kayenta Formation of Arizona (Sues, 1985b) in some derived dental characters (Luo and Wu, 1995).

Several skull specimens of *Yunnanodon* (Cui, 1976; Sun and Cui, 1987) were reexamined in this study (Institute of Vertebrate Paleontology and Paleoanthropology, Beijing: IVPP 5071 [holotype]; 7204; 7205; 7219). A duplicate skull (courtesy of A.-L. Sun) was sectioned by using a Croft Grinder to expose its internal structures (Croft, 1950; Crompton, 1955). Camera lucida drawings and photographs were taken of each serial (transverse) section exposed by grinding, in the place of the original specimen. The reconstruction of the basicranial bones and the inner ear was made from the serial sections by using the Slicer Dicer™ program by Visualogic, Inc., Bellevue, Washington. Measurement of the length and internal diameters of the cochlear canal was based on the original sections (camera lucida drawing and photos, both with scales). The measurement of the internal diameter of the semicircular canal was made from the original sections. The diameter of the arc of the semicircular canal (*sensu* Hurum, 1998) was taken from the graphic models of inner ear endocasts as rendered by the Slicer Dicer program.

DESCRIPTION AND COMPARISON

Petrosal

The petrosal forms the bony housing for the entire inner ear in *Yunnanodon*. The petrosal excludes all other bones from the immediate bony housing of the inner ear. No suture marks the separation of the two periotic bones (prootic and opisthotic) in *Yunnanodon* (Figs. 1, 2). This has been documented in other tritylodontids (Kühne, 1956; Hopson, 1964, 1965; Sun, 1984; Gow, 1986; Sues, 1986). The ossification of the cartilaginous otic capsule of the chondrocranium begins in several ossification centers in amniotes (de Beer, 1937). The absence of the prootic–opisthotic suture implies that the separate embryonic ossification centers coalesced into a single bone in adult tritylodontids, instead of two separate prootic and opisthotic bones of other therapsids (Olson, 1944) and extant diapsid reptiles (de Beer, 1937). The absence of the prootic–opisthotic suture in tritylodontids is a derived condition in comparison to many other nonmammalian cynodonts, as pointed out by many authors (Kemp, 1983; Sun, 1984; Hopson and Barghusen, 1986; Sues, 1986; Rowe, 1988; Wible, 1991; Luo, 1994).

The pars cochlearis that encloses the bony cochlear canal is large relative to the rest of the petrosal, as shown in the serial sections and in the broken basicranial specimens (e.g., IVPP 5071 as described by Sun and Cui [1987]). The promontorium, defined as the ventral eminence of the pars cochlearis in extant mammals (*sensu* Williams et al. [1989] and Luo et al. [1995]), is represented by a bulging area posterior to the basisphenoid wing and anterior to the crista interfenestralis in the skull with an incomplete basisphenoid wing (Fig. 2). In a more or less intact basicranium (IVPP 7219), the medial part of the pars cochlearis is covered medially by the basioccipital, and anteriorly by the basisphenoid wing (more details below). The ventral (and external) exposure of the pars cochlearis in the intact skulls appears to be much smaller than its entire size (Fig. 1) because much of the pars cochlearis is superficially covered by the sphenoid complex and the basioccipital bone.

In some possibly juvenile skulls in which

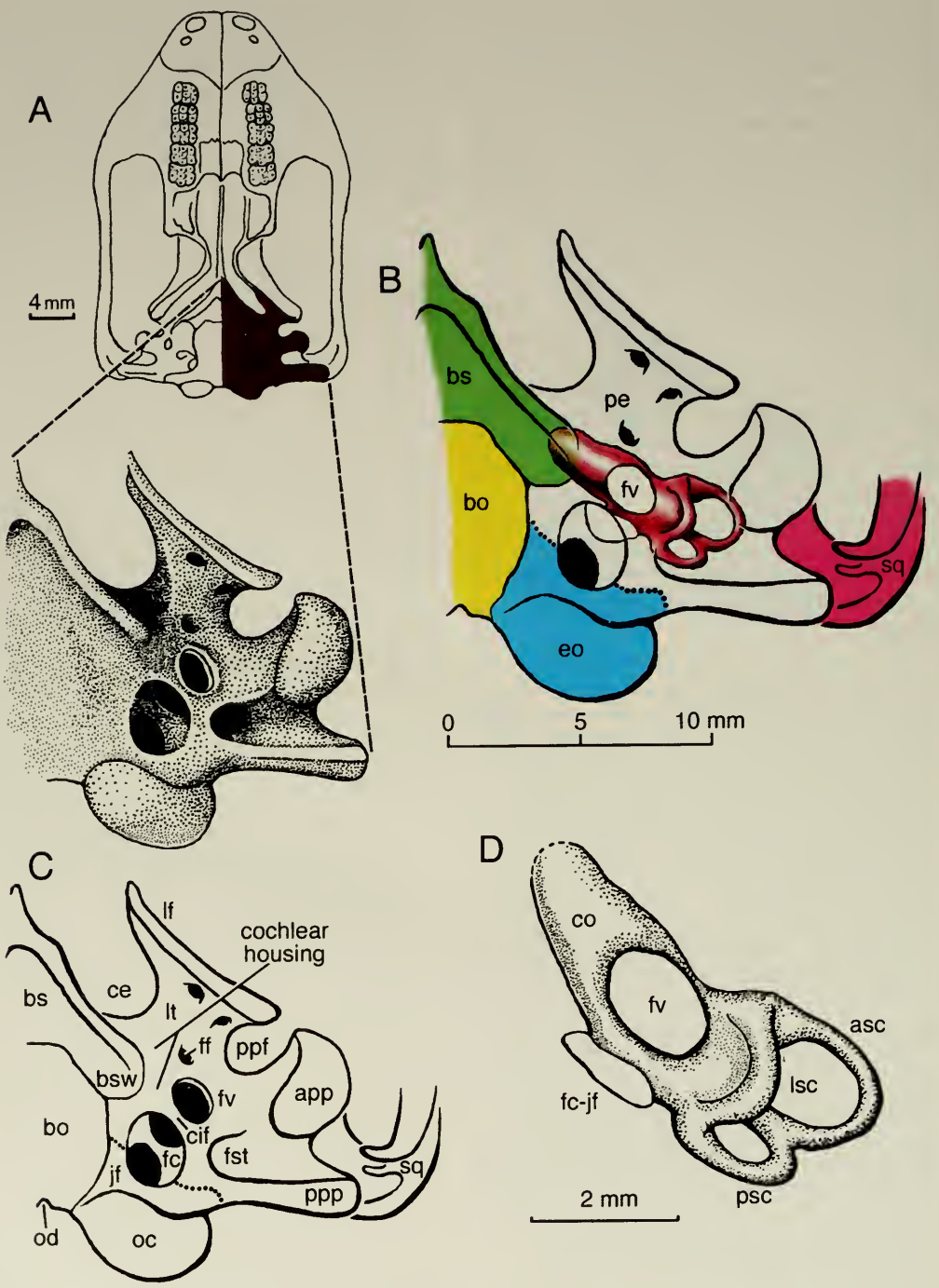

Figure 1. Basicranium and inner ear of *Yunnanodon* (Tritylodontidae, Cynodontia) in ventral views. (A) Basicranium and its position in skull (ventral view of basicranium; the squamosal is not illustrated in the stipple drawing; modified from Luo [1994]; skull outline modified from Cui [1976] and Luo and Wu [1994]). (B) Approximate position of the inner ear (purple) to the sur-

the petrosal, the basisphenoid, and the basioccipital are separated from one another, the pars cochlearis can be broadly exposed. This led Sun and Cui (1987) to suggest that *Yunnanodon* developed a promontoriumlike structure (=the pars cochlearis), an observation that is confirmed here. The medial aspect of the pars cochlearis has a flat facet that may be exposed in some specimens in which the basioccipital has become detached from the basicranium. This facet appears to be identical to the medial facet of the promontorium in *Sinoconodon* (Crompton and Luo, 1993; Luo et al., 1995). The overlap of this flat facet by the lateral lappet of the basioccipital in the intact skulls is very similar to the condition in subadult specimens of *Sinoconodon.*

The fenestra vestibuli (oval window) is oval in outline, with a long diameter of ~1.8 mm and a short diameter of ~1.5 mm (based on IVPP 7219). The fenestra vestibuli is separated by a thin crista interfenestralis from the perilymphatic foramen (round window or foramen cochleae). The latter is located in the same depression as (but separated from) the jugular foramen. The lateral trough of the petrosal is bound medially by the pars cochlearis and laterally by the lateral flange. The large ventral opening of the cavum epiptericum is anterior to the lateral trough. The facial foramen is located anterior to the fenestra vestibuli. The lateral flange is perforated by two vascular foramina. The pterygoparoccipital foramen, which probably carried the superior ramus of the stapedial artery (Wible and Hopson, 1995), is posterior to the lateral flange. The anterior paroccipital process of the petrosal is bulbous. It supports the quadrate in the intact skull. The posterior paroccipital process is represented by a horizontal ridge with a free-standing lateral (distal) end. The anterior and posterior paroccipital processes are separated by the stapedial muscle fossa and its associated groove. The dorsal aspects of the anterior and posterior paroccipital processes are in contact with the squamosal (Figs. 1, 2). These petrosal features are characteristic of all tritylodontids. The tabular bone is present on the occiput, covering much of the mastoid part of the petrosal posteriorly. This primitive feature is shared by many cynodonts but is absent in *Morganucodon* and more derived mammals.

Sphenoid Complex

The basisphenoid is an endochondral ossification whereas the parasphenoid is an intramembranous ossification that underlies the former (Goodrich, 1930; de Beer, 1937); the two elements are fused early in development to form the basisphenoid–parasphenoid complex in extant diapsids (Goodrich, 1930; de Beer, 1937; Bellairs and Kamal, 1981; Rieppel, 1993), and this complex reaches posteriorly to border on the basioccipital. In one cranial study of living diapsids (Oelrich, 1956), the unpaired anterior median element of this complex is considered to be the parasphenoid in adult diapsids, whereas the paired posterolateral parts of this complex are identified as the basisphenoid. In living mammals, the intramembranous parasphenoid ossification forms an unpaired median structure in the rostrum of the basisphenoid–parasphenoid complex (Jollie,

←

rounding basicranial bones (note that the basisphenoid [green] is superficially overlapping the petrosal [gray] but does not directly envelope the cochlea [purple]). (C) Basicranial structure. (D) Inner ear endocast (ventral view). Abbreviations (color code for bones): app, anterior paroccipital process; asc, anterior semicircular canal; bo, basioccipital (yellow); bs, basisphenoid (green); bsw, basisphenoid wing (=parasphenoid ala [green]); ce, cavum epiptericum; cif, crista interfenestralis; co, bony cochlear canal; eo, exoccipital (blue); fc, foramen cochleae; fc-jf, the confluent foramen cochleae and jugular foramen; ff, facial foramen (VII); fst, fossa for stapedial muscle; fv, fenestra vestibuli; jf, jugular foramen; lf, lateral flange of the petrosal; lsc, lateral semicircular canal; lt, lateral trough; oc, occipital condyle; od, odontoid notch of basioccipital; pe, petrosal (gray); ppp, posterior paroccipital process of the petrosal; psc, posterior semicircular canal; sq, squamosal (pink).

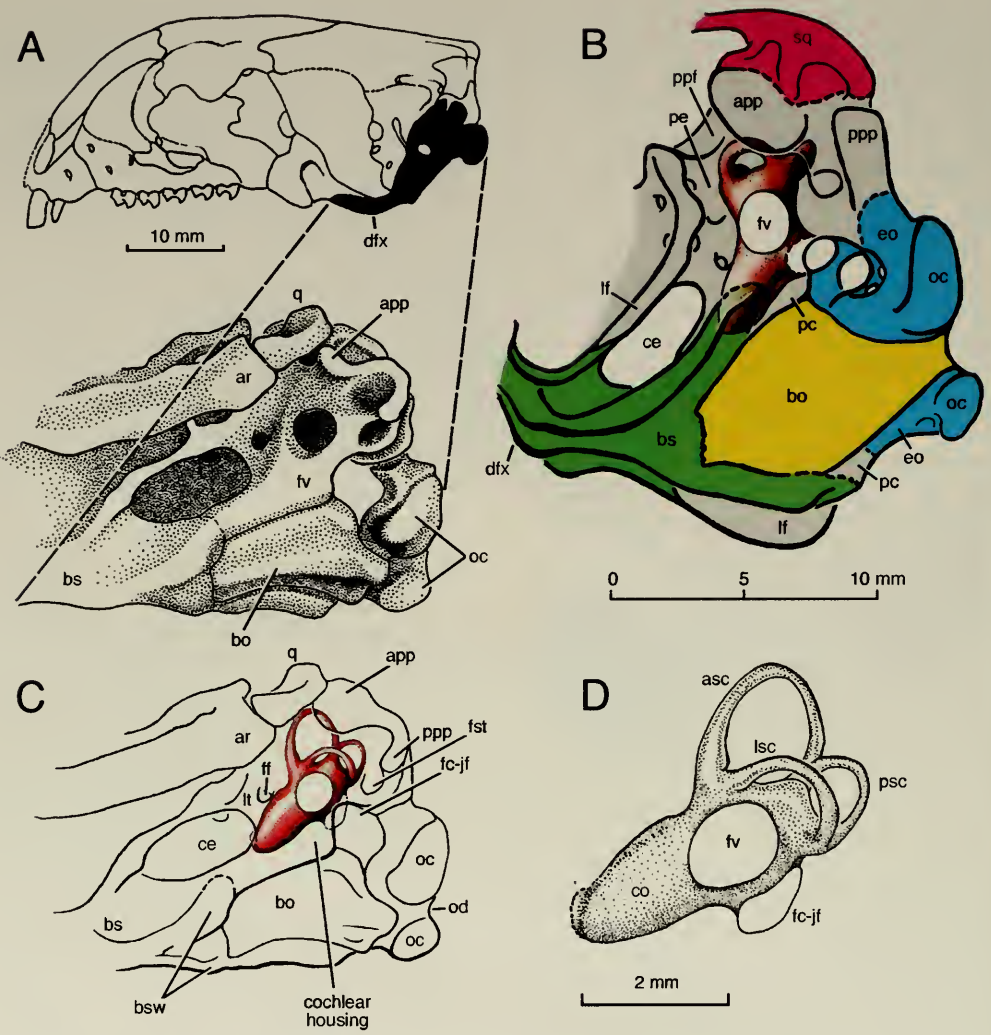

Figure 2. Basicranium and inner ear of *Yunnanodon* (Tritylodontidae, Cynodontia). (A) Basicranium (detailed features in the ventrolateral view, with skull tilted, based on IVPP 7219) and its position in skull (skull outline in lateral view, with zygoma removed). The dashed line in the stipple drawing represents the posterior limit of the preserved part of the basisphenoid wing, which is most probably incomplete in the illustrated skull. As a result, the pars cochlearis (cochlear housing) is more exposed than in the intact skull. (B) Approximate anatomical relationships of inner ear (purple) to the surrounding basicranial structures (basicranium is tilted ventrolaterally, more so than in Fig. 2A). (C) Basicranial structure. (D) Inner ear endocast (lateral view). Abbreviations (color code for bones): ar, articular bone; app, anterior paroccipital process; asc, anterior semicircular canal; bo, basioccipital (yellow); bs, basisphenoid (green); bsw, basisphenoid wing (=parasphenoid ala [green]); ce, cavum epiptericum; co, bony cochlear canal; dfx, dorsal flex of the basisphenoid; eo, exoccipital (blue); fc-jf, the confluent foramen cochleae and jugular foramen; ff, facial foramen; fst, fossa for stapedial muscle; fv, fenestra vestibuli; lf, lateral flange of the petrosal; lsc, lateral semicircular canal; lt, lateral trough; oc, occipital condyle; od, odontoid notch; pc, pars cochlearis (cochlear housing); pe, petrosal (gray); ppp, posterior paroccipital process of the petrosal; psc, posterior semicircular canal; q, quadrate; sq, squamosal (pink).

1962), whereas the posterolateral parts of this complex are formed of endochondral ossification (J. R. Wible, personal communication). The anatomical term "basisphenoid wing" (Kühne, 1956; Crompton, 1964; Luo et al., 1995) is synonymous with the "parasphenoid ala" in other studies of tritylodontids (Hopson, 1964; Gow, 1986; Sues, 1986). Both terms have been applied to the paired posterior extensions from the main body of the sphenoid complex. The basisphenoid wing is used here for cynodonts and mammaliaforms.

The basisphenoid has a strong dorsal flexion posteriorly in *Yunnanodon*, as is typical of other tritylodontids. The basisphenoid has a ventral tuberosity. Bifurcating from the ventral tuberosity are the crests of the basisphenoid wings (Fig. 1). The basisphenoid wing covers the anterior and ventral aspects of the pars cochlearis, and conceals the anterior part of the pars cochlearis from ventral view (Figs. 1C, 3B). The basisphenoid wing does not reach the rim of the fenestra vestibuli in *Yunnanodon* (Figs. 1B, C).

The development of the basisphenoid dorsal flexion and the basisphenoid wing may vary considerably in relation to overall skull size among tritylodontids. In the larger skulls of *Bienotherium* (Hopson, 1964), *Bienotheroides* (Sun, 1984), and *Kayentatherium* (Sues, 1986), the crest on the basisphenoid wing is hypertrophied and accentuates the dorsal flexion of the basicranium. The hypertrophied basisphenoid crest reaches posterolaterally near the fenestra vestibuli. In *Tritylodon*, the basisphenoid wing borders on the fenestra vestibuli and reaches the facial foramen (Gow, 1986). The basisphenoid wing is much larger and more pronounced in these larger tritylodontids than in smaller tritylodontids, such as *Yunnanodon* (Fig. 1) and *Bocatherium* (Clark and Hopson, 1985). The pars cochlearis is always present in tritylodontids. However, its external exposure as the promontorium is a variable feature in the basicranium, partly because of the allometric effect from the wide range of skull sizes in this diverse group. The pars cochlearis tends to be better exposed in small tritylodontids with a weaker basisphenoid wing, but the pars cochlearis may not have any external exposure at all if covered by a hypertrophied basisphenoid wing in large tritylodontids, such as *Bienotherium* and *Tritylodon*.

Basioccipital

The basioccipital is elongate and platelike. Its anterior part intrudes between the two basisphenoid wings (Fig. 1B). The lateral part of the basioccipital forms a lappet and overlaps the ventral surface of the pars cochlearis extensively (Fig. 3B), as evidenced by a specimen in which the suture of two bones is visible. Therefore, in the intact specimens of *Yunnanodon*, the medial part of the pars cochlearis is concealed from ventral view by the basioccipital. The overlap of the basioccipital lateral lappet on the pars cochlearis may be more extensive in large tritylodontids than in such small taxa as *Yunnanodon*. The posterior part of the basioccipital does not seem to border on the jugular foramen, which is encircled by the petrosal and the exoccipital (Fig. 1). An odontoid notch is present on the posterior border of the basioccipital.

Cochlear Housing

The serial sections of *Yunnanodon* show that the cochlear canal is entirely enveloped by the pars cochlearis, which is externally covered by the basisphenoid wing and by the lateral lappet of the basioccipital (Fig. 3B). This is consistent with an earlier observation on *Tritylodon* by Gow (1986) that the basisphenoid wing (parasphenoid ala) is a superficial part of the compound bony structure around the cochlea. However, the serial sections indicate that the basisphenoid wing and the pars cochlearis are distinctive structures in *Yunnanodon*, but not homologous to each other as suggested by Gow (1986); the basisphenoid wing does not directly envelop the cochlear canal. It should be pointed

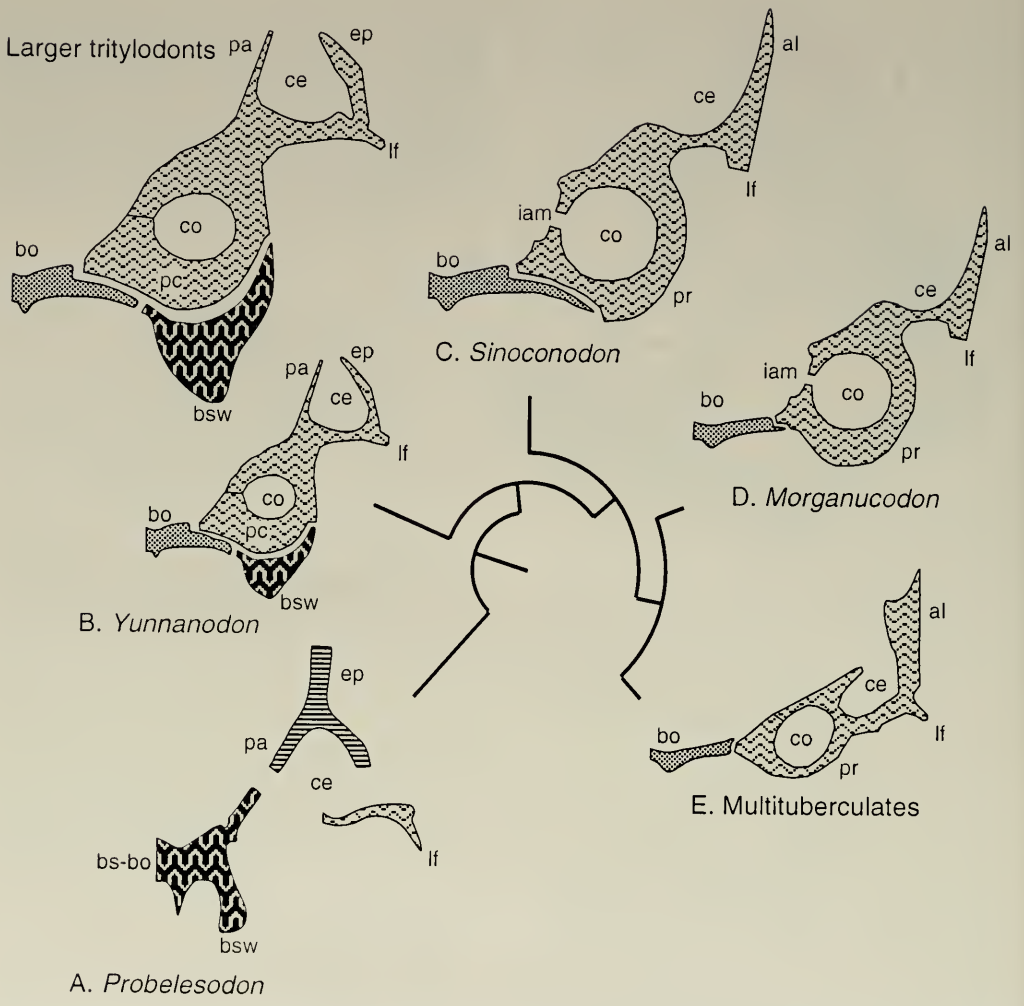

Figure 3. Comparison of the basicranial structures in cynodonts and mammals (schematic transverse section at the level of the posterior part of the cavum epiptericum and/or the anterior part of the cochlea). (A) *Probelesodon lewisi* (Romer, 1970; based on MCZ 3774, serial section 212; Museum of Comparative Zoology, Harvard University; courtesy of A. W. Crompton; the basisphenoid and basioccipital are indistinguishable in the section). (B) *Yunnanodon brevirostre* (composite sketches based on several sections of a specimen provided by A.-L. Sun) and a generalized large tritylodont (showing the proportional difference of the basisphenoid wing and the basioccipital lappet). (C) *Sinoconodon rigneyi* (based on sections of IVPP 8689; Institute of Vertebrate Paleontology and Paleoanthropology, Beijing). (D) *Morganucodon watsoni* (based on sections of MCZ 20998, Graybeal et al. [1989]). (E) *Nemegtbaatar gobiensis* (modified from Hurum, 1998, fig. 5). Abbreviations: al, anterior lamina of the petrosal; bo, basioccipital; bs, basisphenoid; bsw, basisphenoid wing (parasphenoid ala); ce, cavum epiptericum (for the trigeminal ganglion); co, cochlear canal; ep, epipterygoid (alisphenoid); lf, lateral flange of the petrosal; pa, pila antotica; pc, pars cochlearis; pr, promontorium (ventral or external eminence formed by the pars cochlearis).

out that the presence of the promontorium in *Yunnanodon*, as first noted by Sun and Cui (1987), is reconfirmed here. However, the promontorium on their specimen (IVPP 5071) is exposed because of the postmortem detachment of the basisphenoid and the basioccipital (see Fig. 2). In the intact specimens of *Yunnanodon*, the pars cochlearis is mostly concealed in ventral view. In one specimen (IVPP 7219), the basisphenoid wing seems to cover at least one half of the pars cochlearis on one

side, but its absence on the other side leaves much of the pars cochlearis exposed.

Inner Ear

The cochlear canal is a tubular structure with a bulge in the middle part (best seen in lateral view; Fig. 2). The canal is approximately 1.9 mm in length as measured from the anterior border of the fenestra vestibuli to the apex of the cochlear canal (*sensu* Luo et al. [1995]), or about 3.7 mm if measured from the posterior border of the fenestra to the apex (*sensu* Rosowski and Graybeal [1991]). The inner surface of the bony cochlear canal is simple and devoid of internal structures.

The canal is slightly constricted anterior to the fenestra vestibuli (Fig. 2A). From serial sections it appears that the cochlear canal is connected to the bony saccular cavity by a relatively narrow and short channel. This channel probably housed the ductus reuniens, the membranous structure that connects the saccule to the basal (proximal) part of the cochlear duct. On the basis of these bony features, it may be inferred that the cochlear part was better differentiated from the saccular part of the membranous labyrinth than in the primitive condition of other cynodonts. The middle portion of the cochlear canal is bulging with a maximum diameter about 1.7 mm but its anterior portion tapers towards the apex that is slightly turned in dorsolateral direction. The bulging middle portion of the cochlea is reminiscent of the globular outline of the cochleas in other advanced nonmammalian cynodonts (Quiroga, 1979). The bone near the anterior apex is fractured in serial sections (represented by dashed line on the endocasts in Figs. 1 and 2). The floor (fundus) of the internal acoustic meatus is fully ossified, as already described in *Oligokyphus* (Kühne, 1956), *Bienotherium* (Hopson, 1964), and *Tritylodon* (Gow, 1986). The cochlear and vestibular branches of the vestibulocochlear cranial nerve (VIII) had separate foramina to the inner ear.

The saccular and utricular recesses are divided in *Yunnanodon*, similar to those of *Bienotherium* as illustrated by Hopson (1965, fig. 12). The junction of the bony utricular recess and the ampullae of the anterior and lateral semicircular canals is slightly more inflated than the rest of the vestibule. All three bony semicircular canals have somewhat irregular shapes. The bony tubes of the semicircular canals range from 0.4 to 0.5 mm in diameter. The anterior semicircular canal has the largest arc with a maximum radius of ~1.7 mm. The posterior semicircular canal has a maximum radius of 1.1 mm. The posterior part of this canal is bent to form an angle. The lateral semicircular canal is the smallest, with a radius to its arc of 0.8 mm. The lateral and posterior semicircular canals are located within the petrosal deep to the fossa for the stapedial muscle (Fig. 2). The anterior semicircular canal is located within the petrosal portion of the side wall for the braincase and dorsal to the bulbous anterior paroccipital process. On the endocranial surface of the braincase, the anterior semicircular canal forms the rim of the subarcuate fossa and almost encircles the fossa.

DISCUSSION

In the primitive condition of noncynodont therapsids such as dicynodonts (Fig. 4A; Olson, 1944; Cox, 1962) and gorgonopsids (Olson, 1944; Sigogneau, 1974), the sacculocochlear cavity (="lagenar recess" of Sigogneau [1974]) is not differentiated from the rest of the bony vestibular cavity in the inner ear (Fig. 4A). The fenestra vestibuli may be either on the lateral aspect, or on the ventrolateral aspect in the sacculocochlear cavity.

A small and globular cochlear cavity is differentiated from the main part of the saccular recess in the cynodont *Thrinaxodon*. The cochlear cavity is distinctive from the fenestra vestibuli in the lateral view (Fig. 4B) and from the vestibule in the medial view (not illustrated; Fourie, 1974; Rowe et al., 1993; E. F. Allin, personal

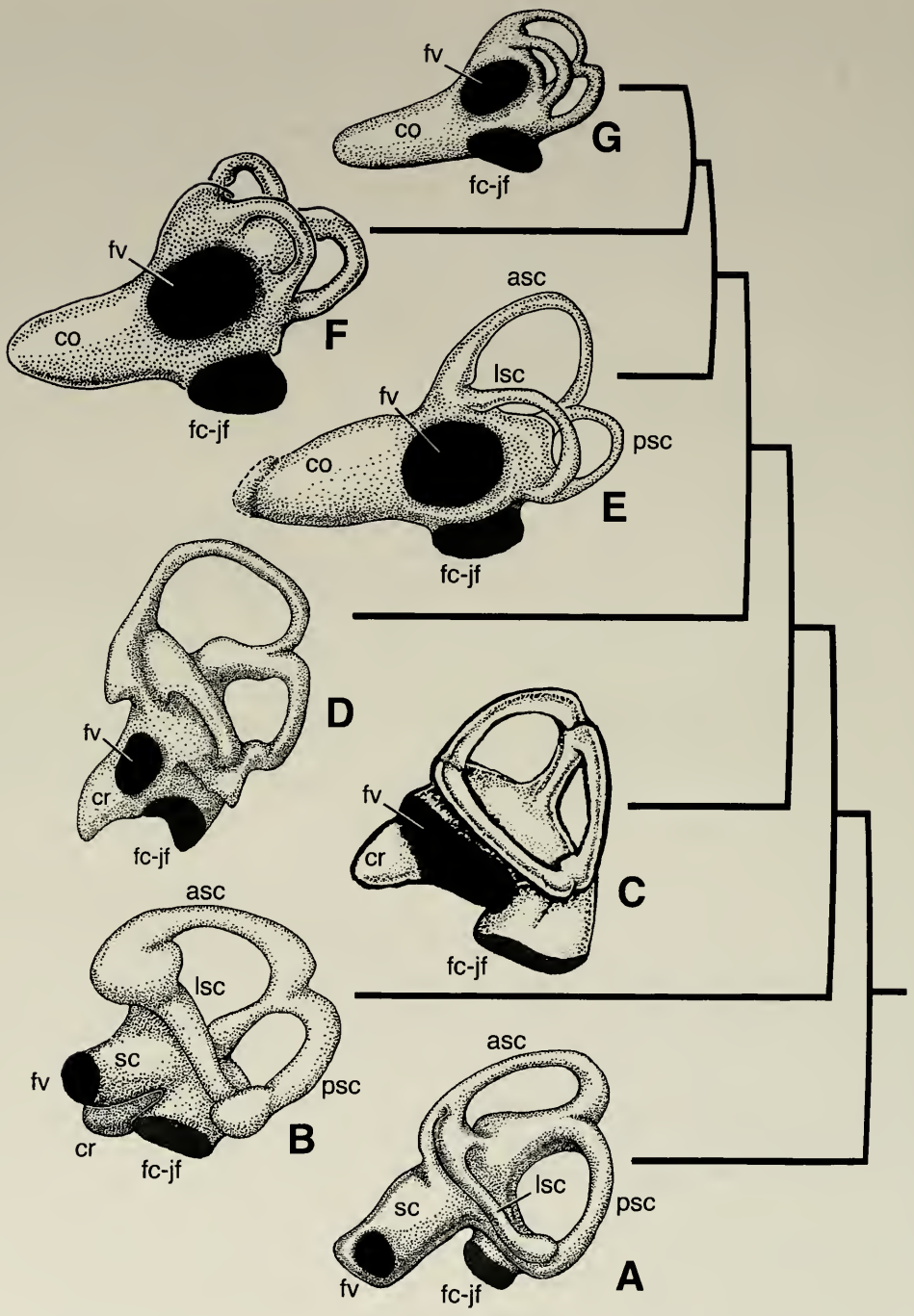

Figure 4. Comparison of inner ear endocasts of cynodonts and primitive mammals. (A) A generalized inner ear endocast of a dicynodont (modified from Olson [1944] and Cox [1962]). (B) A generalized inner ear endocast of *Thrinaxodon* (a composite figure based on descriptions and figures of Olson [1944], Fourie [1974], and illustrations by courtesy of Dr. Allin). (C) *Probelesodon* (modified and reversed from Quiroga [1979]). (D) *Probainognathus* (modified from Allin [1986]). (E) *Yunnanodon* (based

communication). However, the cochlear cavity does not extend anteriorly beyond the fenestra vestibuli. The bony housing of the inner ear has contributions from several bones: the prootic, the opisthotic, the exoccipital, and the supraoccipital, none of which are fused with one another. The cochlear component of the prootic bone is very small (Fourie, 1974). The basisphenoid wing contributes to the cochlear housing extensively. On the external surface of the basicranium, the basisphenoid wing reaches and participates in the rim of the fenestra vestibuli, concealing the prootic from the ventral view.

The more advanced *Probelesodon* and *Probainognathus* have a globular cochlear cavity that is larger in proportion to the whole inner ear (Figs. 4C, D; Quiroga, 1979; Allin, 1986). The cochlear structure also extends anterior to the fenestra vestibuli (Figs. 4C, D). A larger size and a more anterior orientation of the cochlear structure are both derived characteristics, compared to that of *Thrinaxodon*, and very different from the poorly differentiated sacculocochlear recess in dicynodonts and gorgonopsians.

Probelesodon and *Probainognathus* are more primitive than *Yunnanodon* in that their cochlear cavity is much smaller (Fig. 4), as is the pars cochlearis of the prootic. The pars cochlearis does not form an external promontorium. The cochlear cavity does not extend anteromedially, dorsal to the basisphenoid wing. The basisphenoid wing bears a prominent crest and reaches near the fenestra vestibuli. The rim of the fenestra vestibuli is formed by an elevated and thickened ring (Lucas and Luo, 1993; Luo, 1994). The prootic and the opisthotic are separate bones. All these characters are unlike those of tritylodontids and mammaliaforms.

The tritylodontid *Yunnanodon* (Fig. 4E) is more derived than other nonmammalian cynodonts including *Probelesodon, Probainognathus,* and *Massetognathus* (Quiroga, 1979; Allin, 1986) in possessing a longer and larger cochlear canal. The cochlear canal extends far beyond the anterior rim of the fenestra vestibuli. The proximal part of the canal is distinctive from the saccular region. The cast of the cochlear canal of *Yunnanodon* is similar to those of *Sinoconodon* (Luo et al., 1995) and *Morganucodon* (Graybeal et al., 1989; Luo and Ketten, 1991). The cochlear canal is even longer in *Yunnanodon* than in *Sinoconodon* in absolute size. Its proportion to the overall length of the skull is about the same as in the latter. The only feature of the cochlea that may be interpreted as a primitive character is the bulging middle part that somewhat resembles the more globular cochleas in *Probainognathus* (Allin, 1986) and *Massetognathus* (Quiroga, 1979).

The cochlear canal does not extend the entire length of the pars cochlearis in *Yunnanodon,* thus resembling those of *Sinoconodon* and *Haldanodon,* in the proportion of the cochlear canal to the pars cochlearis. Although the cochlea is housed in a pars cochlearis with an externally exposed promontorium in all known mammaliaforms and mammals, the presence of the petrosal promontorium is not necessarily correlated to a fully elongated cochlea, as evidenced by *Sinoconodon* (Luo et al., 1995) and the late Jurassic docodont *Haldanodon* (Lillegraven and Krusat, 1991). In both mammals the cochlea is short relative to the size of the pars cochlearis.

←

on reconstruction from serial sections from a specimen courtesy of A.-L. Sun). (F) *Sinoconodon* (based on sections of IVPP 8689). (G) *Morganucodon* (modified from Graybeal et al. [1989] and Luo and Ketten [1991]). Figures not to the same scale. Abbreviations: asc, anterior semicircular canal; co, cochlear canal; cr, globular cochlear recess (undifferentiated from the vestibule); fc-jf, confluent foramen cochleae and jugular foramen; fv, fenestra vestibuli (oval window); lsc, lateral semicircular canal; psc, posterior semicircular canal; sc, undifferentiated osseous sacculocochlear structure (essentially a part of the vestibule).

Yunnanodon, Sinoconodon, and *Haldanodon* share this primitive condition, in contrast to the more derived *Morganucodon,* triconodontids, and multituberculates, in which the cochlear canal extends the full length of the pars cochlearis (and the promontorium).

The overlap of the basioccipital on the flat medial facet of the pars cochlearis is present in both *Yunnanodon* and *Sinoconodon* (Figs. 3B, C). However, unlike the condition in *Sinoconodon* and other early mammaliaforms in which the basisphenoid wing is lost and the pars cochlearis is ventrally exposed (Fig. 3C), the pars cochlearis of *Yunnanodon* is not well exposed, because of coverage by the well-developed basisphenoid wing (Fig. 3B). It should be noted that the presence of a pars cochlearis may be a shared derived condition of mammals, tritylodontids, tritheledontids, and possibly probainognathids. As reported by Crompton (1994), the tritheledontid *Pachygenelus,* a taxon closely related to mammals, has a small cochlea contained within the pars cochlearis that is also concealed by the basisphenoid and the basioccipital—very similar to the configuration in *Yunnanodon* as described in this paper. A juvenile skull of a probainognathid cynodont (Bonaparte and Crompton, 1994) also has a promontoriumlike structure in the ear region. Although this structure is not known in the adult specimens of *Probainognathus, Probainognathus* possibly has a small pars cochlearis that is covered by the basisphenoid and basioccipital and not exposed as the promontorium in the fully grown skulls.

Tritylodontids and tritheledontids are both considered to belong to the mammaliamorphs (modified from Rowe [1988] to include tritheledontids; see also Wible [1991], Wible and Hopson [1993], Luo [1994], and Luo and Crompton [1994]). The characteristics of the inner ear and its bony housing in these two groups, as described by Crompton (1994) and here, offer fresh insight into the pattern of early evolution of the anatomical structures of the basicranium and the inner ear (Fig. 5).

The development of an elongate cochlear canal and change in the pattern of ossification of the basicranial bones are correlated (Fig. 5). It is hypothesized that in advanced cynodonts, such as *Probainognathus* (Allin, 1986), *Probelesodon,* and *Massetognathus* (Quiroga, 1979), an expansion of the cochlear recess occurs within the prootic. This development is related to a greater reduction of the basisphenoid wing in these derived cynodonts (Fig. 5: node B) than in *Thrinaxodon* and other basal cynodonts.

In mammaliamorphs (Fig. 5, node C, including tritheledontids), embryonic ossifications of the otic capsule must have fused into a single petrosal bone in the fully grown adults, instead of two separate ossifications (prootic and opisthotic). This change may have made the bony housing for the entire inner ear more rigid; as a result the inner ear may be better insulated and less susceptible to interference. Related to the change in ossification, a short but distinctive cochlear canal is developed within a neomorphic pars cochlearis, as described for *Yunnanodon* here, and for *Pachygenelus* by Crompton (1994). In *Sinoconodon* and more derived mammals (Fig. 5, node D), the basisphenoid wing is lost so that the pars cochlearis is exposed on the ventral surface of the basicranium. However, the ventral coverage of the pars cochlearis by the basioccipital, a primitive condition, is retained at least in part in *Sinoconodon.*

In *Morganucodon* and more derived mammals except docodonts (Fig. 5, node D), the cochlear canal is more elongate than those of *Sinoconodon* and *Yunnanodon,* and extends the full length of the pars cochlearis. Related to the elongation of the cochlear canal, the external surface of the promontorium is also more inflated. The basioccipital is shifted medially (Fig. 3). Correspondingly, the flat medial facet on the promontorium as seen in *Sinoconodon* and *Yunnanodon* is lost.

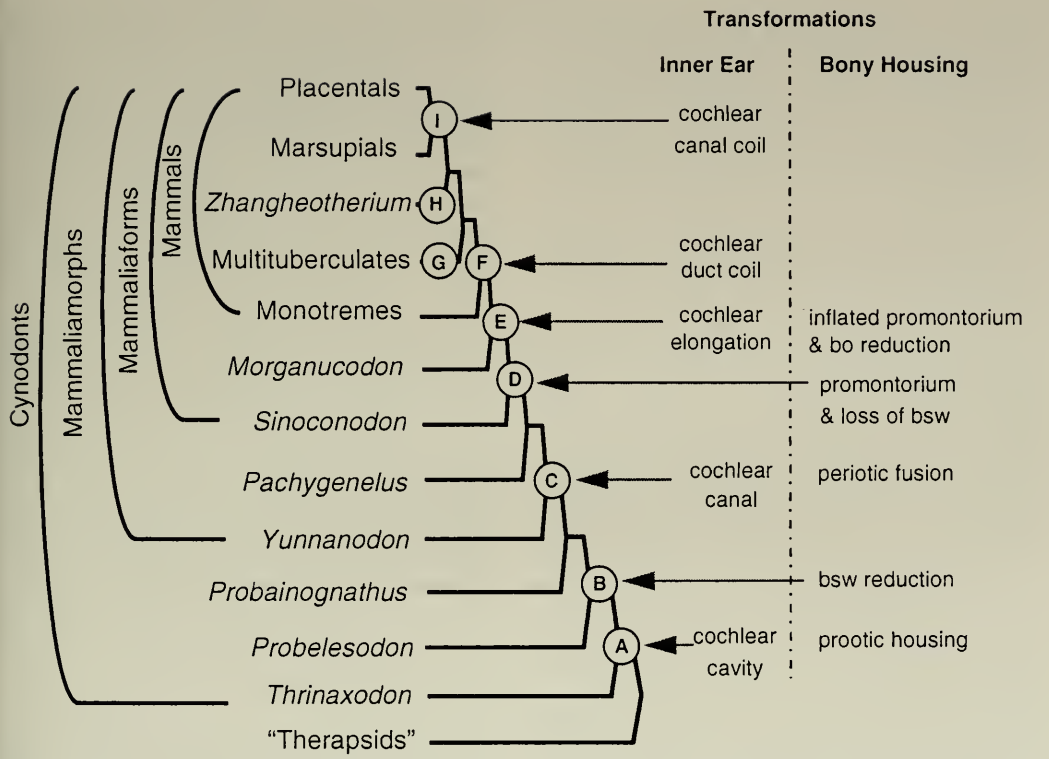

Figure 5. Stepwise transformation of the bony housing of inner ear and the cochlear structures from nonmammalian cynodonts to mammals. Phylogeny is based on Kemp (1983), Rowe (1988), Wible (1991), Wible and Hopson (1993), Luo (1994), Luo and Crompton (1994), and Hu et al. (1997). Definitions of mammaliamorphs and mammaliaforms are modified from Rowe (1988). Character evolution from nodes A through E is explained in text. The membranous labyrinth of the cochlea (cochlear duct) is coiled (node F) in all living mammals (Zeller, 1989; Luo and Ketten, 1991; Fox and Meng, 1997), although in monotremes the bony labyrinth of the cochlea (cochlear canal) lacks the corresponding coil. Multituberculates (node G) have a straight or slightly curved cochlear canal without coil (Luo and Ketten, 1991; Meng and Wyss, 1995; Hurum, 1998), as in the symmetrodont *Zhangheotherium* (node H; see Hu et al. [1997]). Only the living marsupials and placentals (node I) have a fully coiled bony labyrinth (cochlear canal) in correlation with the coiled membranous labyrinth (cochlear duct; Zeller, 1989; Luo and Ketten, 1991; Fox and Meng, 1997). Either the coiled membranous cochlear duct in living monotremes must be considered as convergent to those of living therians, or the uncoiled cochleas of multituberculates and *Zhangheotherium* (Hu et al., 1997) must be regarded as an atavistic reversal to those of mammaliaforms. The coiled cochlear structures within the pars cochlearis are homoplasic among main lineages of the mammalian crown group. Abbreviations: bo, basioccipital; bsw, basisphenoid wing.

Mammals are most specialized among living vertebrates in their hearing adaptation, much of which is attributable to their derived inner and middle ear structures. The pars cochlearis containing a cochlea is one of the most complex character systems of the mammalian skull, and is crucial for more sensitive hearing, especially for high frequency sound. The assembly of such a complex character system with significant functional adaptation occurred in several incremental steps during the morphologic evolution of nonmammalian cynodonts and early mammals (Fig. 5).

The development and the emergence of the pars cochlearis in the basicranium are correlated with the transformation of the cochlear canal. It is hypothesized that, through the transition from nonmammalian cynodonts to early mammaliaforms, the enlarged pars cochlearis with a cochlear canal had preceded the development of the petrosal promontorium. The promontorium is developed by the emergence of

the pars cochlearis on the basicranium to displace the neighboring sphenoid complex and basioccipital bone. Inflation of the external promontorium of the pars cochlearis is associated with the elongation of the cochlear canal. The seemingly drastic transformation of the ear region in the basicranium is achieved in a stepwise transformation though the phylogenetic transition from nonmammalian cynodonts to mammals.

After an elongate cochlea developed within the enlarged pars cochlearis of the petrosal in mammaliaforms, further evolution of the cochlear coiling in the crown group of mammals shows a considerable degree of homoplasy (Fig. 5). The living monotremes have a coiled cochlear duct (membranous labyrinth) but without the corresponding coil of the bony cochlear canal (bony labyrinth). Multituberculates have a straight or slightly curved bony cochlear canal without coil (Luo and Ketten, 1991; Meng and Wyss, 1995; Hurum, 1998), as in the symmetrodont *Zhangheotherium* (Hu et al., 1997). Only the living marsupials and placentals have a fully coiled membranous labyrinth (cochlear duct) that is intricately associated with the coiled bony labyrinth (cochlear canal; Zeller, 1989; Luo and Ketten, 1991; Fox and Meng, 1997). Either the coiling of the membranous cochlear duct in living monotremes must be considered as convergent to those of living therians, or the uncoiled cochleas of multituberculates and *Zhangheotherium* (Hu et al., 1997) must be regarded as an atavistic reversal to those of mammaliaforms (Fig. 5).

ACKNOWLEDGMENTS

Professor A. W. Crompton has been an inspiration for this work. I thank Professors A.-L. Sun and Z.-M. Dong, X.-C. Wu, and Mr. G. Cui for generously providing the tritylodontid specimens and their casts. For access to comparative materials, I thank Professors A. W. Crompton and F. A. Jenkins, Jr., and Mr. C. R. Schaff (Harvard University); Professor J. A. Hopson (University of Chicago); and Professor A.-L. Sun (Institute of Vertebrate Paleontology and Paleoanthropology). Professor Crompton provided the Croft grinder. Professor Sun helped with the serial sections. Mr. J. A. Georgi assisted in computerized reconstruction and Mr. M. A. Klingler assisted in illustrations. During this study, I benefited from discussion with Drs. E. F. Allin, A. W. Crompton, J. A. Hopson, T. Rowe, and J. R. Wible. Dr. Allin graciously provided his unpublished drawings of *Thrinaxodon* for this study. The manuscript benefited from the critical and editorial reviews by Drs. Allin, Hopson, Jenkins, Shapiro and Wible, and an anonymous reviewer. This research was supported by a National Science Foundation CAREER Award (DEB 9527892), the National Geographic Society, and the Netting and O'Neil Funds of Carnegie Museum of Natural History.

LITERATURE CITED

ALLIN, E. F. 1986. The auditory apparatus of advanced mammal-like reptiles and early mammals, pp. 283–294. *In* N. Hotton, III, P. D. MacLean, J. J. Roth, and E. C. Roth (eds.), The Ecology and Biology of Mammal-like Reptiles. Washington, D.C.: Smithsonian Institution Press. x + 326 pp.

ALLIN, E. F., AND J. A. HOPSON. 1992. Evolution of the auditory system in Synapsida ("mammal-like reptiles" and primitive mammals) as seen in the fossil record, pp. 587–614. *In* D. B. Webster, R. R. Fay, and A. N. Popper (eds.), The Evolutionary Biology of Hearing. New York: Springer-Verlag. li + 859 pp.

BELLAIRS, A. D'A., AND A. M. KAMAL. 1981. The chondrocranium and the development of the skull in recent reptiles, pp. 1–263. *In* C. Gans and T. S. Parsons (eds.), The Biology of Reptiles. Vol. 11. London: Academic Press. xi + 475 pp.

BONAPARTE, J. F., AND A. W. CROMPTON. 1994. A juvenile probainognathid cynodont skull from the Ischigualasto Formation and the origin of mammals. Revista del Museo Argentino de Ciencias Naturales, Paleontologia, **5:** 1–12.

CLARK, J. M., AND J. A. HOPSON. 1985. Distinctive mammal-like reptile from Mexico and its bearings on the phylogeny of Tritylodontidae. Nature, **315:** 398–400.

COX, C. B. 1962. A natural cast of the inner ear of a dicynodont. American Museum Novitates, **2116:** 1–6.

CROFT, W. N. 1950. A parallel grinding instrument for the investigation of fossils by serial sections. Journal of Paleontology, **24:** 693–698.

CROMPTON, A. W. 1955. Techniques for the study of Permo-Triassic Fossils of South Africa. South African Museums Association Bulletin, **6:** 57–60.

———. 1964. On the skull of *Oligokyphus*. Bulletin of the British Museum (Natural History), Geology, **9:** 70–82.

———. 1972. Postcanine occlusion in cynodonts and tritylodonts. Bulletin of the British Museum (Natural History), Geology, **21:** 27–71.

———. 1994. Masticatory function in non-mammalian cynodonts and early mammals, pp. 55–75. *In* J. J. Thomason (ed.), Functional Morphology in Vertebrate Paleontology. Cambridge, United Kingdom: Cambridge University Press. xi + 277 pp.

CROMPTON, A. W., AND Z. LUO. 1993. The relationships of Liassic mammals *Sinoconodon*, *Morganucodon oehleri* and *Dinnetherium*, pp. 30–44. *In* F. S. Szalay, M. J. Novacek, and M. C. McKenna, (eds.), Mammal Phylogeny: Mesozoic Differentiation, Multituberculates, Early Therians, and Marsupials. New York: Springer-Verlag. x + 249 pp.

CUI, G. 1976. *Yunnania*, a new tritylodontid from Lufeng, Yunnan. Vertebrata PalAsiatica, **25:** 1–7 (in Chinese).

———. 1986. *Yunnanodon*, a replacement name for Yunnania Cui, 1976. Vertebrata PalAsiatica, **24:** 9 (in Chinese).

DE BEER, G. R. 1937. The development of the vertebrate skull. Oxford, United Kingdom: The Clarendon Press. xxii + 552 pp.

ESTES, R. 1961. Cranial anatomy of the cynodont reptile *Thrinaxodon liorhinus*. Bulletin of the Museum of Comparative Zoology, Harvard University, **125:** 165–180.

FOURIE, S. 1974. The cranial morphology of *Thrinaxodon liorhinus* Seeley. Annals of the South African Museum, **56:** 337–400.

FOX, R. C., AND J. MENG. 1997. An X-radiographic and SEM study of the osseous inner ear of multituberculates and monotremes (Mammalia): implications for mammalian phylogeny and evolution of hearing. Zoological Journal of the Linnean Society (London), **121:** 249–191.

GOODRICH, E. S. 1930. Studies of the Structure and Development of Vertebrates. London: Macmillan. xxxiv + 837 pp.

GOW, C. E. 1985. Apomorphies of the Mammalia. South African Journal of Science, **81:** 558–560.

———. 1986. The side wall of the braincase in cynodont therapsids and a note on the homology of the mammalian promontorium. South Africa Journal of Zoology, **21:** 136–148.

GRAYBEAL, A., J. ROSOWSKI, D. R. KETTEN, AND A. W. CROMPTON. 1989. Inner ear structure in *Morganucodon*, an early Jurassic mammal. Zoological Journal of the Linnean Society (London), **96:** 107–117.

HOPSON, J. A. 1964. The braincase of the advanced mammal-like reptile *Bienotherium*. Postilla, **87:** 1–30.

———. 1965. Tritylodontid therapsids from Yunnan and the cranial morphology of *Bienotherium*. Ph.D. dissertation. Chicago: The University of Chicago. 295 pp.

HOPSON, J. A., AND H. R. BARGHUSEN. 1986. An analysis of therapsid relationships, pp. 83–106. *In* N. Hotton, III, P. D. MacLean, J. J. Roth, and E. C. Roth (eds.), The Ecology and Biology of Mammal-like Reptiles. Washington, D.C.: Smithsonian Institution Press. x + 326 pp.

HU, Y., Y. WANG, Z. LUO, AND C. LI. 1997. A new symmetrodont mammal from China and its implications for mammalian evolution. Nature, **390:** 137–142.

HURUM, J. H. 1998. The inner ear of two Late Cretaceous multituberculate mammals, and its implications for multituberculate hearing. Journal of Mammalian Evolution, **5:** 65–93.

JOLLIE, M. 1962. Chordate Morphology. New York: Reinhold Publishing Co. 478 pp.

KEMP, T. S. 1983. The interrelationships of mammals. Zoological Journal of the Linnean Society (London), **77:** 353–384.

KERMACK, K. A. 1963. The cranial structure of the triconodontids. Philosophical Transactions of the Royal Society of London, B, **246:** 83–103.

KERMACK, K. A., F. MUSSET, AND H. W. RIGNEY. 1981. The skull of *Morganucodon*. Zoological Journal of the Linnean Society (London), **71:** 1–158.

KUHN, H.-J. 1971. Die Entwicklung und Morphologie des Schädels von *Tachyglossus aculeatus*. Abhandlungen der Senckenbergischen Naturforschenden Gesellschaft, Frankfurt am Main, **528:** 1–224.

KÜHNE, W. G. 1956. The Liassic Therapsid *Oligokyphus*. London: British Museum (Natural History). x + 149 pp.

LILLEGRAVEN, J. A., AND G. HAHN. 1993. Evolutionary analysis of the middle and inner ear of Late Jurassic multituberculates. Journal of Mammalian Evolution, **1:** 47–74.

LILLEGRAVEN, J. A., AND G. KRUSAT. 1991. Craniomandibular anatomy of *Haldanodon exspectatus* (Docodonta; Mammalia) from the Late Jurassic of Portugal and its implications to the evolution of mammalian characters. Contributions to Geology, University of Wyoming, **28:** 9–138.

LUCAS, S. G., AND Z. LUO. 1993. *Adelobasileus* from the Upper Triassic of West Texas: the earliest mammal. Journal of Vertebrate Paleontology, **13:** 309–334.

LUO, Z. 1994. The sister taxon relationships of mammals and transformations of the diagnostic mammalian characters, pp. 98–128. *In* N. C. Fraser and H.-D. Sues (eds.), In the Shadow of the Di-

nosaurs—Early Mesozoic Tetrapods. Cambridge, United Kingdom: Cambridge University Press. x + 435 pp.

Luo, Z., and A. W. Crompton. 1994. Transformations of the quadrate (incus) through the transition from non-mammalian cynodonts to mammals. Journal of Vertebrate Paleontology, **14:** 341–374.

Luo, Z., A. W. Crompton, and S. G. Lucas. 1995. Evolutionary origins of the mammalian promontorium and cochlea. Journal of Vertebrate Paleontology, **15:** 113–121.

Luo, Z., and D. R. Ketten. 1991. CT scanning and computerized reconstructions of the inner ear of multituberculate mammals. Journal of Vertebrate Paleontology, **11:** 220–228.

Luo, Z., and A.-L. Sun. 1993. *Oligokyphus* (Cynodontia: Tritylodontidae) from the Lower Lufeng Formation (Lower Jurassic) of Yunnan, China. Journal of Vertebrate Paleontology, **13:** 477–482.

Luo, Z., and X.-C. Wu. 1994. The small vertebrate fauna of the Lower Lufeng Formation, Yunnan, pp. 251–270. *In* N. C. Fraser and H.-D. Sues (eds), In the Shadow of the Dinosaurs—Early Mesozoic Tetrapods. Cambridge, United Kingdom: Cambridge University Press. x + 435 pp.

———. 1995. Correlation of vertebrate assemblage of the Lower Lufeng Formation, Yunnan, China, pp. 83–88. *In* A. Sun and Y. Wang (eds.), Sixth Symposium on Mesozoic Terrestrial Ecosystems and Biotas, Short Papers. Beijing: China Ocean Press. vi + 250 pp.

Meng, J., and A. R. Wyss. 1995. Monotreme affinities and low-frequency hearing suggested by multituberculate ear. Nature, **377:** 141–144.

Miao, D. 1988. Skull morphology of *Lambdopsalis bulla* (Mammalia, Multituberculata) and its phylogenetic implications to mammalian evolution. Contributions to Geology, University of Wyoming, Special Paper, **4:** 1–104.

Oelrich, T. M. 1956. The anatomy of the head of *Ctenosaura pectinata* (Iguanidae). Miscellaneous publications, Museum of Zoology, University of Michigan, **94:** 1–122.

Olson, E. C. 1944. Origin of mammals based upon cranial morphology of therapsid suborders. Special Papers of the Geological Society of America, **55:** 1–122.

Quiroga, J. C. 1979. The inner ear of two cynodonts (Reptilia–Therapsida) and some comments on the evolution of the inner ear from pelycosaurs to mammals. Gegenbaurs morphologisches Jahrbuch, **125:** 178–190.

Rieppel, O. 1993. Patterns of diversity in the reptilian skull, pp. 344–390. *In* J. Hanken and B. K. Hall (eds.), The Skull. Vol. 2. Chicago: The University of Chicago Press. xiii + 566 pp.

Romer, A. S. 1970. The Chañares (Argentina) Triassic reptile fauna. VI. A chiniquodontid cynodont with an incipient squamosal–dentary articulation, Breviora, **344:** 1–18.

Rosowski, J. A. 1992. Hearing in transitional mammals: predictions from the middle-ear anatomy and hearing capabilities of extant mammals, pp. 615–631. *In* D. B. Webster, R. R. Fay, and A. N. Popper (eds.), The Evolutionary Biology of Hearing. New York: Springer-Verlag. li + 859 pp.

Rosowski, J. A., and A. Graybeal. 1991. What did *Morganucodon* hear? Zoological Journal of the Linnean Society (London), **101:** 131–168.

Rougier, G. W., J. R. Wible, and J. A. Hopson. 1996. Basicranial anatomy of *Priacodon fruitaensis* (Triconodontidae, Mammalia) from the Late Jurassic of Colorado, and a reappraisal of mammaliaform interrelationships. American Museum Novitates, **3183:** 1–28.

Rowe, T. 1988. Definition, diagnosis and origin of Mammalia. Journal of Vertebrate Paleontology, **8:** 241–264.

Rowe, T., W. Carlson, and W. Bottorff. 1993. *Thrinaxodon*—digital atlas of the skull. Austin, Texas: University of Texas Press (CD-ROM).

Sigogneau, D. 1974. The inner ear of *Gorgonops* (Reptilia, Therapsida, Gorgonopsia). Annals of the South African Museum, **64:** 53–69.

Sues, H.-D. 1985a. The relationships of the Tritylodontidae (Synapsida). Zoological Journal of the Linnean Society (London), **85:** 205–217.

———. 1985b. *Dinnebitodon amarali,* a new tritylodontid (Synapsida) from the Lower Jurassic of western North America. Journal of Paleontology, **60:** 758–762.

———. 1986. The skull and dentition of two tritylodontid synapsids from the Lower Jurassic of Western North America. Bulletin of the Museum of Comparative Zoology, Harvard University, **151:** 217–268.

Sun, A.-L. 1984. Skull morphology of the tritylodont genus *Bienotheroides* of Sichuan. Scientia Sinica, Series B, **27:** 270–284.

Sun, A.-L., and G. Cui. 1987. Otic region in tritylodont *Yunnanodon.* Vertebrata PalAsiatica, **25:** 1–7.

Sun, A.-L., G. Cui, Y. Li, and X.-C. Wu. 1985. A verified list of Lufeng Saurischian Fauna. Vertebrata PalAsiatica, **22:**1–12.

Wible, J. R. 1991. Origin of Mammalia: the craniodental evidence reexamined. Journal of Vertebrate Paleontology, **11:** 1–28.

Wible, J. R., and J. A. Hopson. 1993. Basicranial evidence for early mammal phylogeny, pp. 45–62. *In* F. S. Szalay, M. J. Novacek, and M. C. McKenna (eds.), Mammal Phylogeny: Mesozoic Differentiation, Multituberculates, Early Therians, and Marsupials. New York: Springer-Verlag. x + 249 pp.

———. 1995. Homologies of the prootic canal in mammals and non-mammalian cynodonts. Journal of Vertebrate Paleontology, **15:** 331–356.

Wible, J. R., G. W. Rougier, M. J. Novacek, M. C. McKenna, and D. Dashzeveg. 1995. A mammalian petrosal from the Early Cretaceous of

Mongolia: implications for the evolution of the ear region and mammaliamorph interrelationships. American Museum Novitates, **3149:** 1–19.

WILLIAMS, P. L., R. WILLIAMS, M. DYSON, AND L. H. BANNISTER. 1989. Gray's Anatomy, 37th edition. New York: Churchill Livingstone. 1,598 pp.

ZELLER, U. 1989. Die Entwicklung und Morphologie des Schädels von *Ornithorhynchus anatinus* (Mammalia: Prototheria: Monotremata). Abhandlungen der Senckenbergischen Naturforschenden Gesellschaft, Frankfurt am Main, **545:** 1–188.

A NEW SPECIMEN AND A FUNCTIONAL REASSOCIATION OF THE MOLAR DENTITION OF *BATODON TENUIS* (PLACENTALIA, INCERTAE SEDIS), LATEST CRETACEOUS (LANCIAN), NORTH AMERICA

CRAIG B. WOOD[1] AND WILLIAM A. CLEMENS[2]

ABSTRACT. *Batodon tenuis* Marsh, 1892, a rare, minute, eutherian mammal, is a member of several Late Cretaceous (Lancian North American Land Mammal Age), North American local faunas. A hitherto undescribed fragment of maxilla from the Hell Creek Formation, Garfield County, Montana, documents the association of M^2 and M^3. Analysis of the small available sample of upper and lower molars in functional orientation strengthens the basis for their association, provides a functional explanation for the enlargement of the talonid of M_3, and suggests only one species is represented. Currently, *B. tenuis*, with an estimated body mass of approximately 5 g, is the smallest known eutherian mammal from the Cretaceous. The phylogenetic position of *B. tenuis* in the poorly documented, Cretaceous radiation of eutherians is still unclear.

INTRODUCTION

In a search of University of California Museum of Paleontology (UCMP) collections to find uncataloged and fragmentary teeth of Late Cretaceous marsupials for enamel microstructure research (Wood et al., 1999), an important new specimen referable to *Batodon tenuis* came to light (Wood and Clemens, 1990). *Batodon tenuis* Marsh 1892 is a tiny, very rare, Late Cretaceous eutherian mammal previously known from isolated teeth and only three jaw fragments containing more than one tooth (see Lillegraven [1969], Clemens [1973], Archibald [1982], Storer [1991], and Lofgren [1995]). The type specimen, USNM 2139, is a dentary fragment with P_{2-4} in place. The new specimen, UCMP 136091, is a fragment of a right maxillary with almost undamaged M^{2-3} in place (Fig. 1). This specimen is only the second maxillary fragment of *B. tenuis* containing more than one tooth to be discovered and contains the first record of M^3 for the species and genus. The systematic affinities of *Batodon* are unclear, and, as discussed below, we choose to regard this rare genus as incertae sedis within the Placentalia.

Butler (1961, 1972a), Fox (1975), and Crompton and Kielan-Jaworowska (1978), among others, have advocated a functional approach to description and phylogenetic analysis of tribosphenic mammals. A great deal of this and later work (including this paper) are due to the influence of Professor A. W. Crompton's foundational work on the origin and function of tribosphenic molar teeth (see Crompton [1971] as a landmark example; also Crompton and Hiiemae [1969] and Crompton and Sita-Lumsden [1970]).

Our first goal in this study was to determine whether functional correspondence of the new specimen (UCMP 136091) with the M_{2-3} present in UA 3721 (the only known, associated last two lower molars referred to *B. tenuis* [Lillegraven, 1969]) reasonably substantiates allocation of both upper and lower molars to the same species. Furthermore, we wished to determine if the molars preserved in the new specimen show close size and morphologic similarity to all other previously referred

[1] Department of Biology, Providence College, Providence, Rhode Island 02918.

[2] Museum of Paleontology, University of California, Berkeley, California 94720.

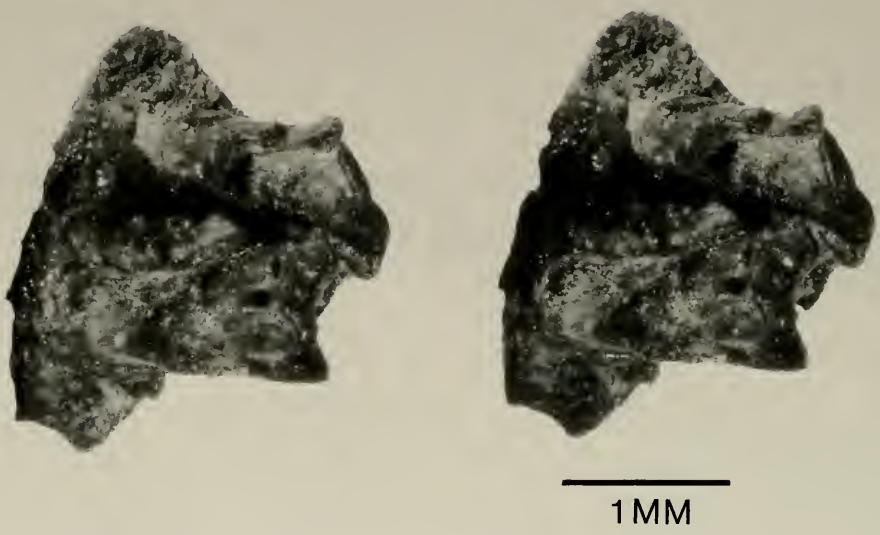

Figure 1. Stereophotograph of UCMP 136091, *Batodon tenuis*, maxillary fragment with M^{2-3}.

specimens, so that greater confidence could be expressed in their allocation to a single species. This paper perhaps may serve as a case study in the utility of functional association of isolated Mesozoic postcanine elements, an easy and yet often-neglected method. Finally, we compare the estimated body mass of *B. tenuis* to those of other small eutherians and analyze hypotheses of its phylogenetic relationships.

MATERIALS AND METHODS

Nomenclature

Here we follow McKenna and Bell (1997) in formally recognizing Placentalia as the appropriate name for the clade that frequently is dubbed Eutheria. Informally, reflecting vernacular use, the terms eutherian and placentalian are recognized as synonyms.

Provenance and History

The new maxillary fragment, UCMP 136091, described here comes from concentrates obtained in 1974 by screen washing sedimentary rocks of the Hell Creek Formation at the Flat Creek Locality 5 (V-73087) in Garfield County, Montana. Archibald (1982: 166) described four isolated teeth of *B. tenuis* from this locality. The new specimen was discovered after he completed his monographic study.

Marsh (1892) established *B. tenuis* on a fragment of a dentary (USNM 2139) containing P_{2-4} from the Lance Formation, Niobrara County, Wyoming. The type locality is UCMP locality no. V-5003 (Clemens, 1973), also referred to as Mammal locality no. 1 (Lull, 1915). Additional specimens of *B. tenuis* have been reported from Lancian North American Land Mammal Age (NALMA) local faunas of the Lance Formation, Wyoming (Clemens, 1973); the Scollard Formation, Alberta (Lillegraven, 1969); the Hell Creek Formation, Montana (Archibald, 1982); and the Frenchman Formation, Saskatchewan (Storer, 1991).

A boundary between the Lancian NALMA and the older, still poorly characterized "Edmontonian" NALMA, has not been defined. In part this reflects the presence of marine units (e.g., the Bearpaw Shale) separating the terrestrial deposits producing Lancian and "Edmontonian" local faunas (see Lillegraven and McKenna, 1986). Recently Hicks et al. (1999) esti-

mated the duration of deposition of the Hell Creek Formation in North Dakota, which has yielded Lancian local faunas, as encompassing approximately the last 1.7 million years (ca. 65.5–67.2 million years before the present) of the Cretaceous. This can be taken as a minimum duration of the Lancian NALMA and probably includes the ages of all known occurrences of *B. tenuis*.

Until recently, the genus *Batodon* had not been reported in older, Judithian NALMA local faunas of the North American Western Interior. Some of these are known from large samples obtained by screen washing (e.g., Montellano, 1992). In an abstract, Carrano et al. (1997) recently noted the discovery of *Batodon* sp. at an unspecified locality in the type area of the Judith River Formation. When fully documented, this record would greatly extend the range of the genus over approximately the last 13 million years of the Cretaceous.

Batodon tenuis was not represented in the large sample of the early Paleocene (Puercan NALMA) Hells Hollow local fauna (Archibald, 1982). Lofgren (1995) recovered four isolated teeth referable to *B. tenuis* from channel fillings in the Hell Creek Formation, McCone County, Montana, which he interpreted to have been deposited during the Puercan. Because of reworking, these channel fillings contain a mixture of fossils of Puercan and Lancian vertebrates. Sloan and Van Valen (1965) did not report the occurrence of *B. tenuis* in their collections from the Bug Creek Anthills locality in McCone County. The UCMP collections made at this locality (Bug Creek Anthills, V-87038, 87074, 87151) include four isolated molars referable to this species. The time of deposition of the channel filling at Bug Creek Anthills and the composition of its vertebrate fauna have been disputed. The strongly supported hypothesis that the Bug Creek Anthills channel filling was deposited in the Puercan and contains a mixture of latest Cretaceous and early Paleocene vertebrate fossils has not been falsified (for discussion of this problem see Lofgren et al. [1990] and Lofgren [1995]). In the following analysis we include data on the molars from Bug Creek Anthills locality and the channel fillings investigated by Lofgren (1995) but do not interpret them as documenting an extension of the range of *Batodon* into the Puercan. At least in the North American Western Interior, the genus *Batodon* appears to have become extinct at the end of the Cretaceous.

Functional Orientation

To observe their functional orientation teeth are rotated around their anterior–posterior axes until the line of sight is parallel with the direction of movement of the lower teeth as they were drawn into centric occlusion with the upper teeth. In this orientation the paracone and metacone just mask views of their respective conules. All polished wear facets on upper and lower teeth are produced by simultaneous, parallel shear in this direction ("phase one," see Kay and Hiiemae [1974]). When the proper degree of rotation has been attained, the shear facets disappear from view because they are aligned parallel with the line of sight. This orientation best illustrates the relative lengths of shearing blades and other functional elements of the crown. In this orientation, upper and lower teeth can be drawn separately on tracing paper, or as computer-based images, and then superimposed to show precise occlusal relationships of all their corresponding parts. Wood et al. (1979) used this technique to support association of rare, isolated upper and lower teeth of the Paleocene "primate," *Torrejonia*. However, in general, this technique has not enjoyed wide application in the study of tribosphenic dentitions.

In this paper our figures are labeled as "functional" when specimens are illustrated in the functionally rotated view, and "crown" in the orientation that has traditionally been labeled as "occlusal view"

(but see Crompton and Kielan-Jaworowska [1978] for additional terms).

Abbreviations

AMNH	American Museum of Natural History
NALMA	North American Land Mammal Age
P 2004.565	Specimen numbers given in this format are from the Saskatchewan Museum of Natural History
UA	University of Alberta
UCMP	University of California Museum of Paleontology
USNM	Natural History Museum, Smithsonian Institution
V-5711	Locality designations given in this format are from the UCMP locality catalog

RESULTS

Description of New Specimen

When discovered much of the new maxillary fragment (UCMP 136091) was obscured by loosely adhering sand grains. The parastylar region of M^2 was missing. During cleaning the M^2 separated from the M^3 allowing the adjacent sides of the molars to be illustrated fully. Subsequently, the maxillary fragments were rejoined and the molars exactly restored to their original positions. Figure 1 is a stereophotograph of the cleaned and restored specimen in crown view. Figure 2 is made up of line drawings of the two molars in traditional crown, lingual oblique, labial, anterior, functional, and posterior views.

M^2

The crown view of M^2 of UCMP 136091 (Fig. 2A) does not clearly illustrate some postmortem damage to the tooth. At higher magnifications of the anterior view (Fig. 2E) the enamel is obviously broken and lacking from the extremely narrow area of attachment of a parastylar lobe. The anterior root beneath the paracone is also freshly broken. The parastylar lobe is broken away from all other known upper molars except UA 4081, P 2004.565, and the M^3 of UCMP 136091. On M^2 of UA 4081 (Fig. 3), the parastylar lobe is a prominent but very thin and delicate structure; one may surmise that it survived only because it was protected by the stout metastylar blade of M^1.

Superimposed crown views (not illustrated) of the M^2 of UCMP 136091 and of UA 4081 are remarkably coincident, especially in the areas of the protocones, paracones, metacones, and conules. Differences are in a slightly more robust labial edge of the metastylar area of UCMP 136091 and its more robust precingulum. The postcingulum of UA 4081 is slightly more robust than that of UCMP 136091 and is absolutely larger in its labial extension beneath the metaconule. Although not the case on the molars of UCMP 136091, on some molars of *B. tenuis* the pre- and postcingula meet on the lingual slope of the protocone (Lillegraven, 1969). Some apical wear is apparent on the rims of the pre- and postcingula of M^2s of *B. tenuis*. Evidently they did not produce a shear. The cingula appear to have served as stops for the lower teeth as they came to their limits in centric occlusion. Perhaps selective pressures would be less for precision in shape of these structures than would have been the case for the functional shearing blades higher on the crown (but see Polly, 1998a).

The specimen UCMP 102909 lacks clearly developed internal wings of the conules. On UCMP 117649, one of the specimens described by Archibald (1982), the metaconule has a distinct internal wing; a weaker but still distinct internal wing is present on the paraconule. The stages of wear of UCMP 136091 and UA 4081 are approximately equivalent. The conules of both have distinct internal wings that are emphasized by wear, which produced chevrons of dentine within the enamel lining of the trigon basin.

In labial and lingual oblique views of *Batodon* molars, the paracones and meta-

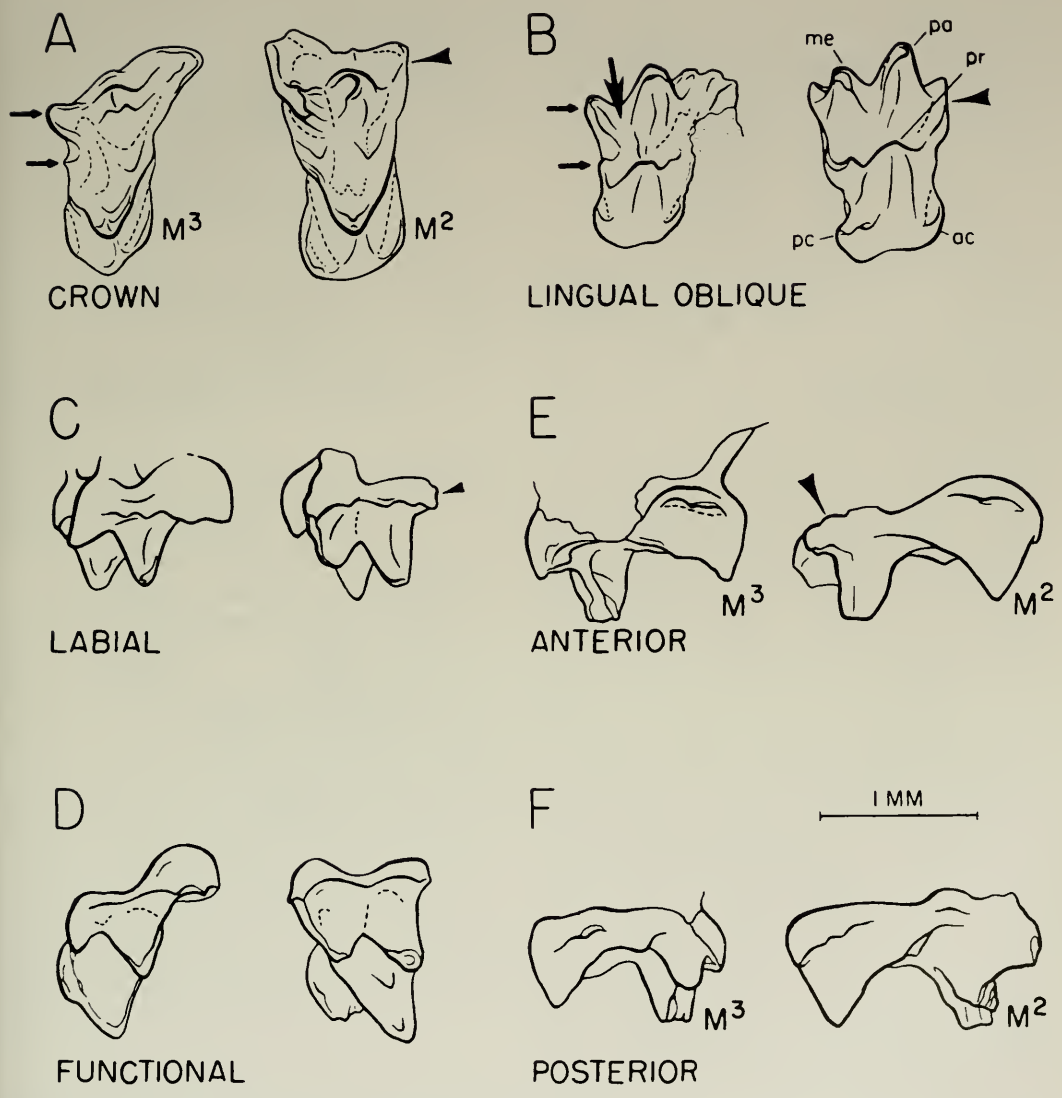

Figure 2. Line drawings of M^{2-3}, UCMP 136091, *Batodon tenuis*. (A) Crown views; arrows to M^3 indicate projecting metacone and metaconule; arrowhead to M^2 indicates damaged part of parastylar area. Posterior is to left and anterior is to right. (B) Lingual oblique views; additional large arrow on M^3 indicates heavily worn groove between metacone and paracone. (C) Labial views; arrowhead indicates damaged parastylar area of M^2. (D) Functionally rotated views. (E) Anterior views; arrowhead indicates damaged parastylar region of M^2. (F) Posterior views. Abbreviations: me, metacone; pa, paracone; pr, protocone; ac, anterior protocone cingulum (precingulum); pc, posterior protocone cingulum.

cones are closely conjoined from their bases to perhaps one half or two thirds of the distance to their apices. Such morphology might suggest that little or no shear occurred directly between the paracone and metacone. However, in worn specimens, it is evident that the hypoconid of the lower molar scraped a strong groove on the lingual surfaces of those cusps before passing between the internal conule wings and into the deeply excavated trigon basin. A comparably large hypoconid is not evident in Cenozoic genera such as *Palaeoryctes* or *Didelphodus*, but is approxi-

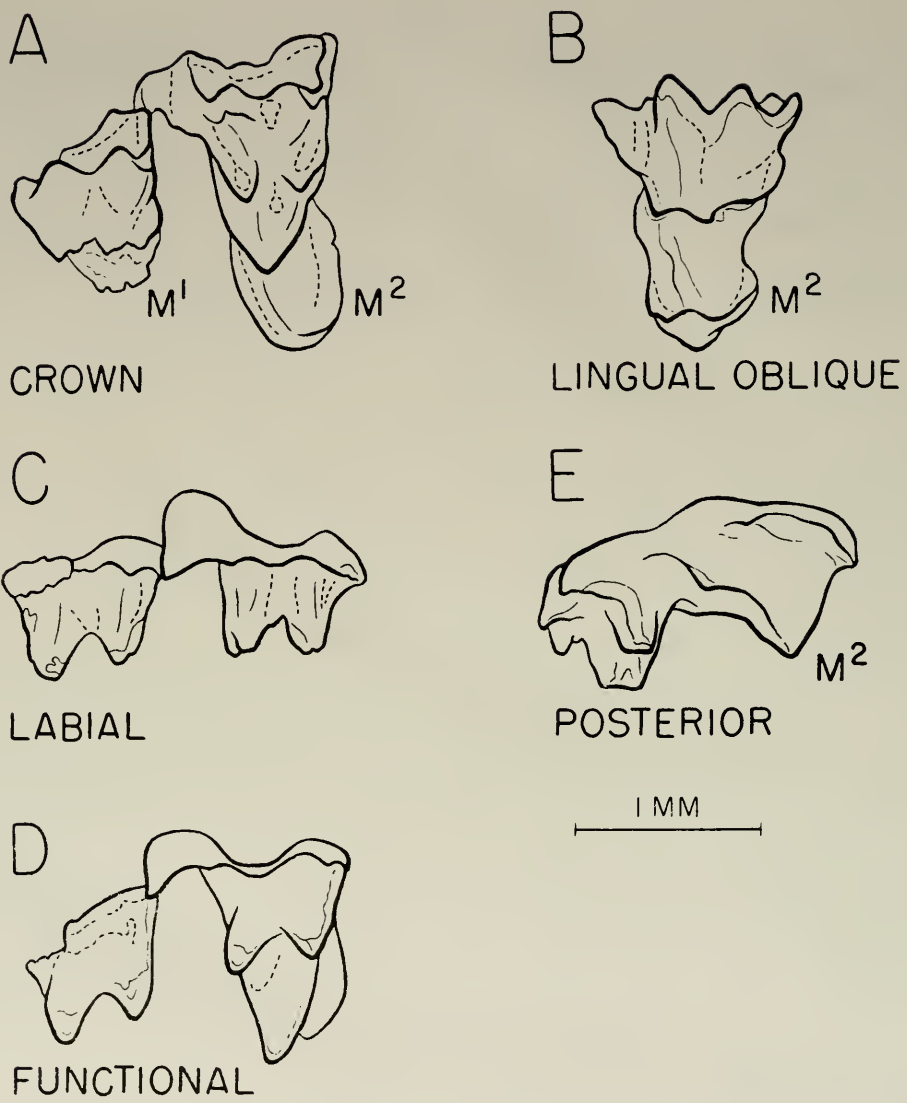

Figure 3. Line drawings of M^{1-2}, from cast of UA 4081, *Batodon tenuis,* from the Scollard Formation, Alberta, Canada (see Lillegraven [1969]). (A) Crown view. (B) Lingual oblique view of M^2 only. (C) Labial view. (D) Functional view, orientation as in Figure 2D. (E) Posterior view of M^2 only.

mated in some Lancian species of *Cimolestes.* Lipotyphlans, many condylarths, and their descendants often emphasize shearing between the hypoconid and the blades of the centrocrista that link the metacone and paracone, which usually are well separated to their bases.

Superimposed labial and lingual oblique views of M^2 of UCMP 136091 and M^2 of UA 4081 demonstrate that the former has a slightly less bowed ectoflexus and a more robust and absolutely larger metacone and metastylar blade. Slightly greater wear on the metastylar blade of UA 4081 might overemphasize the difference, but we suspect that the difference is real, yet within

the limits of individual variation. A small cuspule or expansion of the external edge of the central stylar shelf is present on both specimens. On M^2s of *B. tenuis* the paracone is taller than the metacone.

Using the cervical limit of enamel as a base line, in anterior and posterior views of M^2 the protocones of all specimens are almost as high as the paracones, and about the same height or higher than the metacones. The profile of the protocone is especially pointed and triangular. As Lillegraven (1969: 82) noted, because of the exaggerated protocone, the stylar shelf of *Batodon* appears relatively narrow, but in absolute width its proportions are comparable to the stylar shelf of *Cimolestes cerberoides*, for example.

In anterior view (Fig. 2E), the paracone is quite steep-sided and apically almost rectangular in outline. In contrast, the posterior profile of the metacone sweeps labially into the large metastylar blade. The posterior metaconule wing is clearly a strong enechelon shearing blade contacting the preprotocristid of the lower molar after it passed the metastylar blade. The anterior wing of the paraconule also forms a strong shearing blade for the postprotocristid, but the primary blade on the anterior slope of the paracone, the preparacrista, is less distinct, as often is the case in "proteutherians" (see Crompton and Kielan-Jaworowska [1978]).

M^3

The specimen UCMP 136091 is the first specimen of *B. tenuis* to preserve M^3 in association with other identifiable molars. The M^3 of the new specimen has a robust parastylar lobe with a deep groove to receive the protoconid of M_3. In anterior view, the paracone–parastylar shearing blade is more distinct than on M^2, and the shearing blade of the anterior paraconule wing is also strong. The protocone is considerably less triangular in anterior view, but is as triangular as that of M^2 in posterior view. The protocone is taller than the metacone but not as tall as the paracone. The pre- and postcingula are prominent, but the postcingulum is relatively small in comparison to those of other molars. The cingula are more widely separated by the strong lingual slope of the protocone than on M^2.

The metacone is reduced in size, but still quite prominent; it forms a distinct projection in the lingual oblique view (Fig. 2B). Metacone and paracone are closely conjoined at their bases, as on M^2, and wear emphasizes the greater angle at which they diverge. A wear facet extends down the conjoined lingual slopes of the metacone and paracone showing that the hypoconid of M_3 sheared down into the trigon basin past the distinct internal wings of the conules. The internal surface on the paraconule wall is worn flat. Resembling the metacone, the metaconule projects posteriorly. The posterior inclination of the metacone and metaconule accommodated strong hypoconid shear within the trigon.

?M^1

Storer (1991) described the mammals of the Lancian Gryde local fauna, Saskatchewan. The sample included an upper right molar, P 2004.565 (Fig. 4), that has been identified tentatively as an M^1 of *B. tenuis*. Storer (1991) noted that the specimen has a more anteriorally directed preparacrista than the M^2 of UA 4081 (Fig. 3). Also, P 2004.565 has a relatively smaller parastylar lobe. These morphologic differences support Storer's tentative identification, which is accepted here.

Lower Dentition

The type specimen of *B. tenuis*, USNM 2139, is an anterior dentary fragment containing P_{2-4}. The specimen AMNH 58777 preserves P_2, a major part of P_3, and P_4 and M_{1-2} (illustrated in Clemens, 1973). Comparable small size and morphologic similarity of P_4 to that of USNM 2139 are the basis for reference of AMNH 58777 to *B. tenuis*. Likewise small size and close morphologic similarity of the molars of AMNH 58777 and UA 3721 (Fig. 5) are the bases

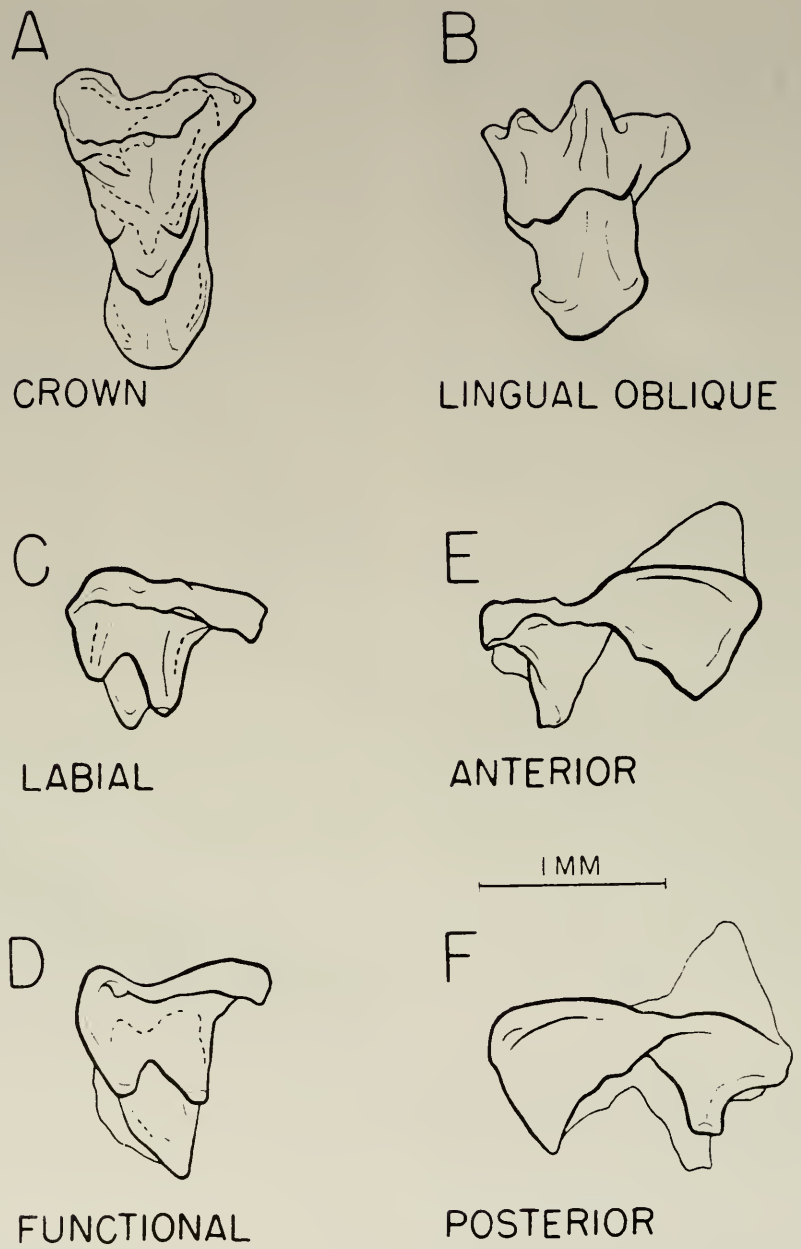

Figure 4. Line drawings of ?M¹, P 2004.565, *Batodon tenuis*, from the Gryde local fauna, Frenchman Formation, Saskatchewan, Canada (see Storer [1991]). Note that in all views the parastylar area is intact. (A) Crown view. (B) Lingual oblique view. (C) Labial view. (D) Functional view. (E) Anterior view. (F) Posterior view.

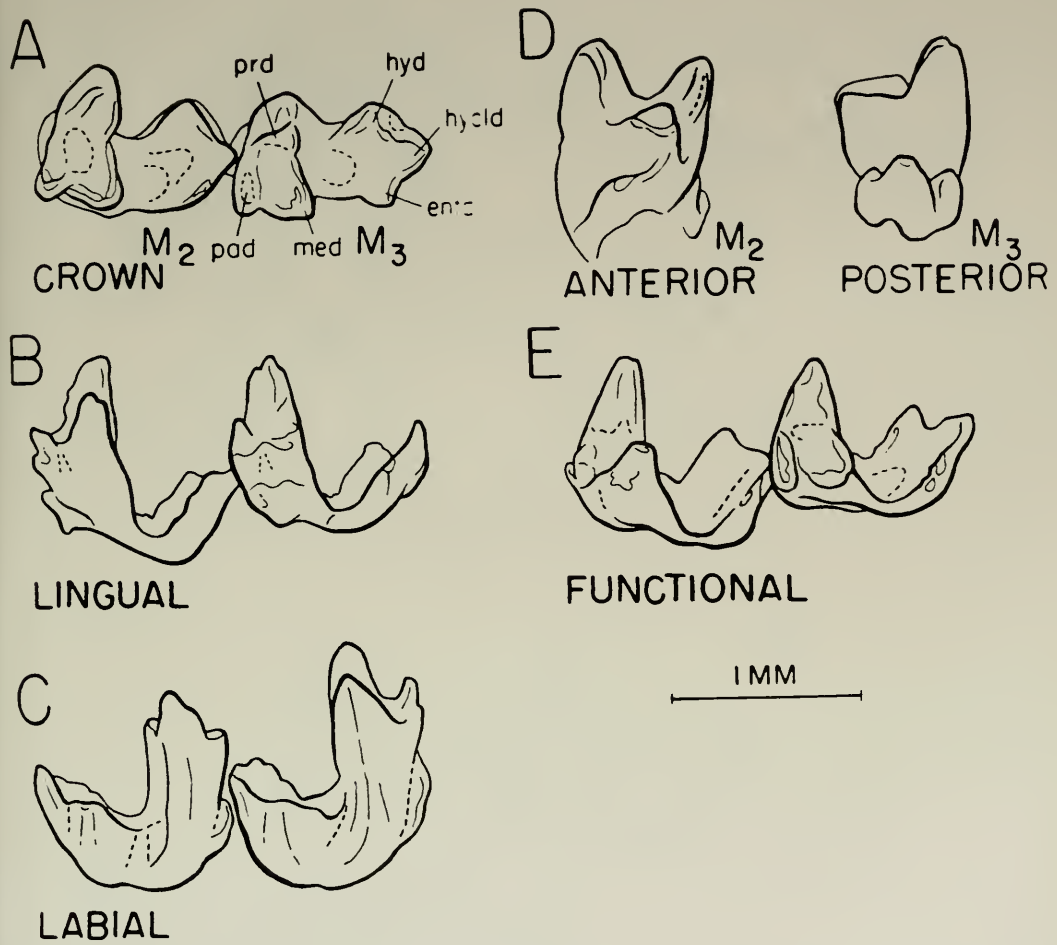

Figure 5. Line drawings of M_{2-3}, from cast of UA 3721, *Batodon tenuis*, from the Scollard Formation, Alberta, Canada (see Lillegraven [1969]). (A) Crown view. (B) Lingual view. (C) Labial view. (D) Anterior view of M_2 and posterior view of M_3. (E) Functionally rotated orientation. Abbreviations: pad, paraconid; med, metaconid; prd, protoconid; hyd, hypoconid; hycld, hypoconulid; entd, entoconid.

for reference of the latter to this species. Detailed descriptions of the morphology of these specimens can be found in Lillegraven (1969) and Clemens (1973).

Functional Relationships of Upper and Lower Molars

Figure 6 illustrates correspondingly numbered functional shear blades on upper and lower molars (after Crompton and Hiiemae [1969]). Figures 7 and 8 are composite (same-scale) drawings of the M^{2-3} of UCMP 136091 and the M^2 and fragment of M^1 of UA 4081, each shown in occlusion with M_{2-3} of UA 3721 (Fig. 5). All the teeth are illustrated in functional orientation. The occlusal fit of UCMP 136091 with UA 3721 (Fig. 7) is, overall, somewhat better than for UA 3721 and the upper molars of UA 4081 (Fig. 8). The M^{2-3} of UCMP 136091 occlude very well with M_{2-3} of UA 3721 (Fig. 7), especially in the areas between the hypoconid and paracone–metacone embrasure. With these functional units of opposing second and third molars in place, some other function-

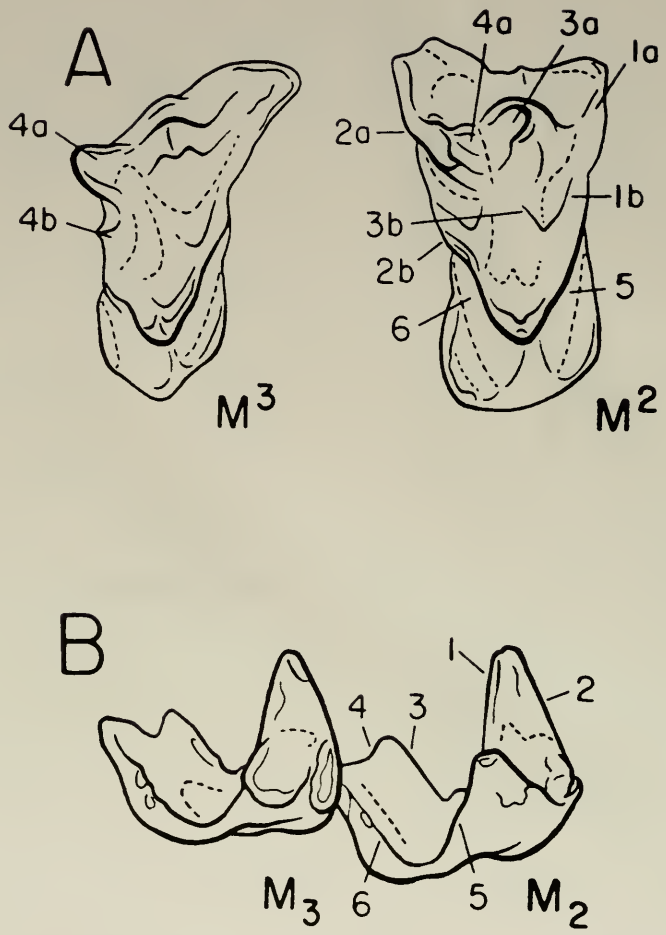

Figure 6. Line drawings of M^{2-3}, UCMP 136091, and UA 3721, *Batodon tenuis,* to indicate corresponding functional shear blades (see Crompton and Hiiemae [1969] and Crompton and Kielan-Jaworowska [1978]). (A) M^{2-3}, UCMP 136091 in crown view. Abbreviations: 1a, preparacrista; 1b, preparaconule crista (anterior wing); 2a, postmetacrista; 2b, postmetaconule crista (posterior wing); 3a, postparacrista; 3b, postmetaconule crista (posterior wing); 4a, premetacrista; 4b, premetaconule crista (anterior wing); 5, preprotocrista; 6, postprotocrista. (B) UA 3721 in functional view. Abbreviations: shear blades: 1, postprotocristid; 2, preprotocristid; 3, cristid obliqua; 4, posthypocristid; 5, postmetacristid and posterior wall of metaconid; 6, pre-entoconid cristid.

al units are not quite in perfect occlusion. The slight gap between metacone and hypoconulid of the second molar could be due to slightly greater wear on the upper tooth or simply to intraspecific variation in size. However, the protocones of M^{2-3} are slightly too extended lingually to fit comfortably into the talonid basins of M_{2-3}. This most probably indicates individual variability in size. The function of the postcingulum of M^2 as an embrasure stop is clearly reflected in the narrowed and dorsoventrally lowered configuration of the paraconid of M_3.

Lillegraven (1969: 84) and subsequent students of *B. tenuis* have commented on the posterior projection of the hypoconulid and, therefore, the "extended talonid" of M_3. The large, posteriorly projecting metacone and metaconule of M^3 are functionally related to the extended talonid of M_3. Shearing facets on the anterior face of

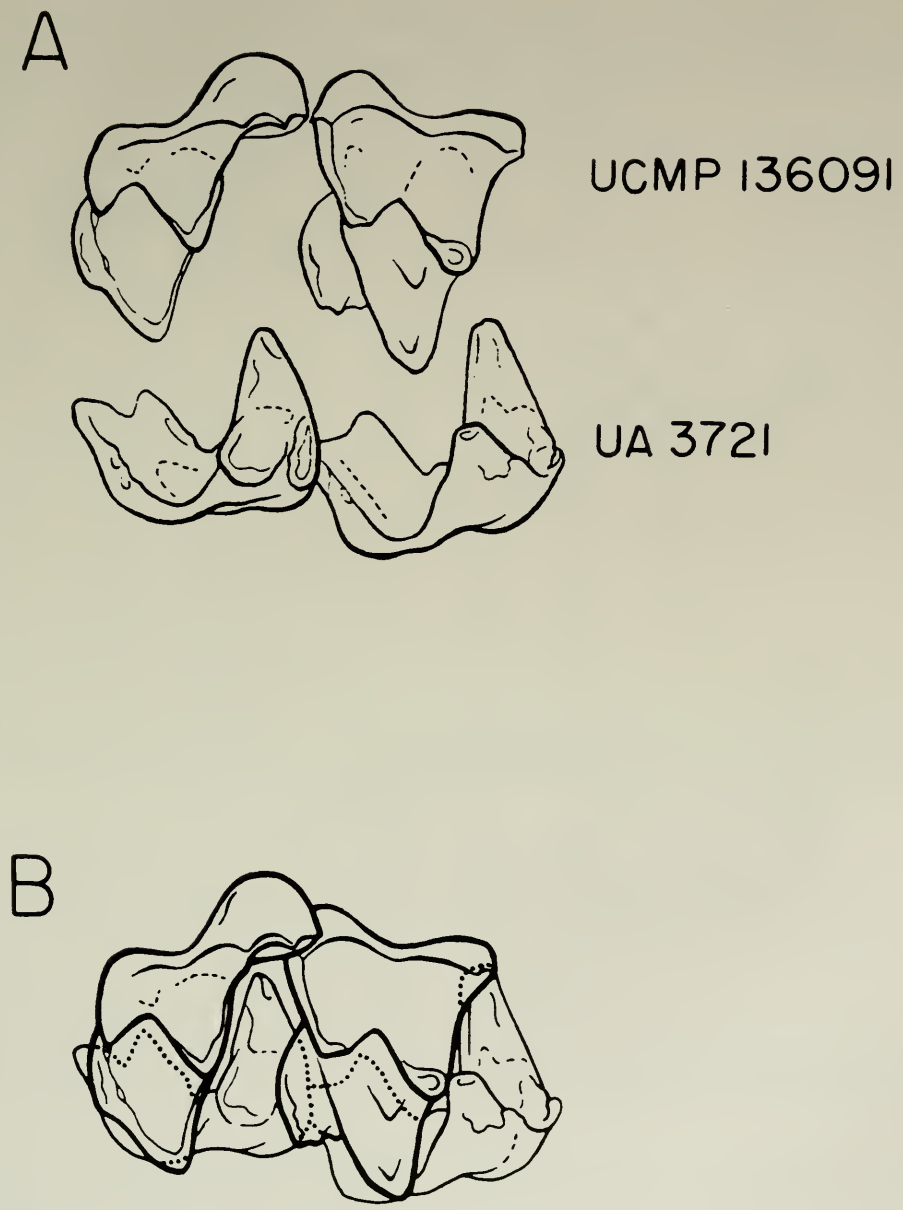

Figure 7. Functional views of M^{2-3} (UCMP 136091) and M_{2-3} (UA 3721, reversed), *Batodon tenuis*. (A) Separated views of molars. (B) Upper and lower molars shown in centric occlusion. Corresponding strong shear blades 3 and 4 on the third molar, as well as a functional postcingulum and extended hypoconulid, indicate that the upper and lower dentitions represent the same species.

the metacone (facet 4a, Fig. 6) and internal metaconule wing (facet 4b, Fig. 6) occluded against the posterior side of the hypoconid and labial side of the enlarged hypoconulid. The remainder of the hypoconulid is covered by the postcingulum of the upper molar, but it is not clear whether crushing occurred between them at full

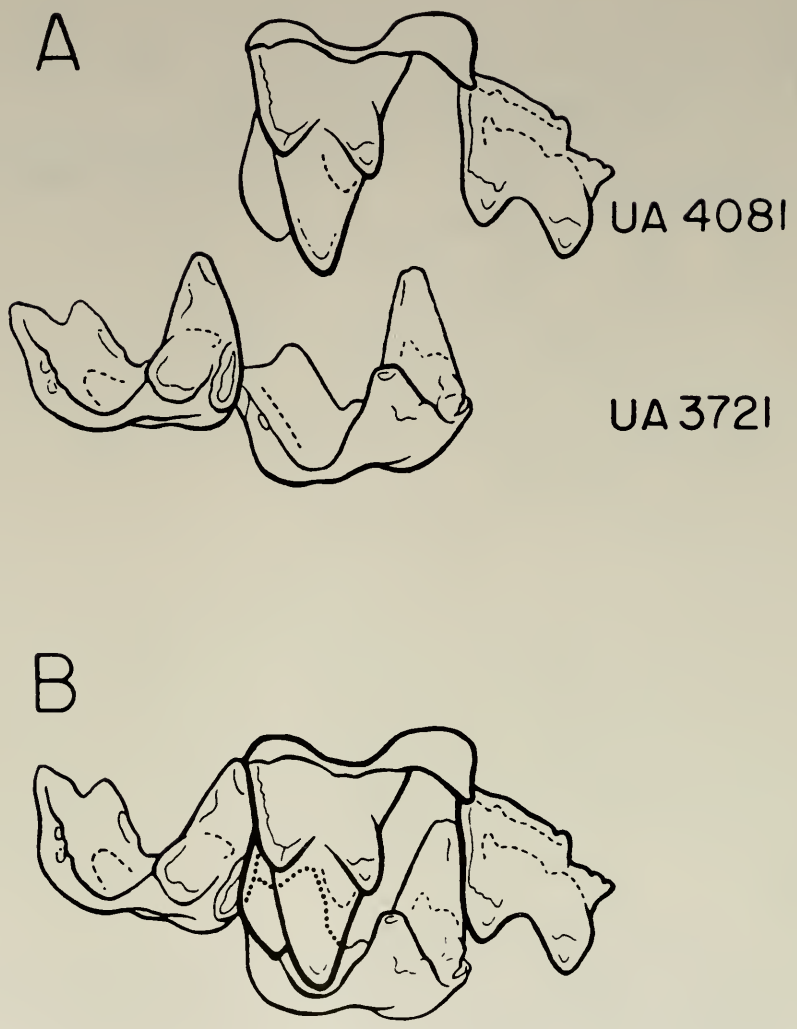

Figure 8. Functional views of fragmentary M^1 and M^2 (UA 4081, reversed) and M_{2-3} (UA 3721, reversed). (A) Separated views of molars. (B) Upper and lower molars shown in centric occlusion.

occlusion. Although not unique among eutherians, enlargement of the hypoconulid and posterior projection of metacone and metaconule are not seen in many palaeoryctids (*Cimolestes* and *Procerberus* excepted) or in undoubted lipotyphlans in which there is a trend to reduce the entire size of the last molar. This morphology could be either a plesiomorphic or an autapomorphic condition of *B. tenuis*. In *Batodontoides* (see Bloch et al. [1998]), M_3 is smaller than M_2, as is the case in the larger geolabidids (Lillegraven et al., 1981). *Paranyctoides* (Fox, 1979, 1984) has an extended M_3 talonid, and Fox (1984: 15) considered an M_3 hypoconulid "strongly developed, projecting upward in finger-like fashion" to be a primitive character state for eutherian mammals.

Although the overall fit is not as good as for UCMP 136091, M^2 of UA 4081 occludes reasonably well with M_2 of UA 3721

TABLE 1. MEASUREMENTS (MM) OF MOLARS REFERRED TO *BATODON TENUIS.**

Locality	State	Specimen	Tooth	Length	Width		Comments
Upper molars							
V73087	MT	UCMP 136091	M^2	0.97	1.64		Lacks parastyle
V73087	MT	UCMP 136091	M^3	0.99	1.45		Parastyle present
		UA 4081	M^2	1.09	1.69		Parastyle present
		UA 4081	M^2	0.82			Excluding parastyle
V73087	MT	UCMP 117649	M^2?	0.92	1.55		Lacks parastyle
V70201	MT	UCMP 102909	M^2?	0.82	1.76		Lacks parastyle
V87308	MT	UCMP 133080	M^2?	1.00 (b)	1.62		Lacks parastyle
					Width trigonid	Width talonid	
Lower molars							
V73087	MT	UCMP 117651	M_3?	1.28	0.82	0.65	
		UA 3721	M_3	1.11	0.75	0.60	
		UA 3721	M_2	1.04	0.82	0.60	
V73087	MT	UCMP 117652	M_2?			0.63	
V70201	MT	UCMP 92590	M_2?	1.33	0.77	0.70	
V70201	MT	UCMP 100638	M_2?	1.16	0.80	0.70	
V70201	MT	UCMP 98188	M_2?	1.21	0.77	0.60	
V87074	MT	UCMP 133764	M_2?	1.21	0.77	0.68	
V87151	MT	UCMP 132174	M_2?	1.26	1.09		
V5711	WY	AM 58777	M_2	1.25 (a)	0.80 (a)	0.65 (a)	
V5711	WY	AM 58777	M_1	1.30 (a)	0.75 (a)	0.70 (a)	
V73087	MT	UCMP 117650	P_4	1.21	0.60		
V87038	MT	UCMP 133081	P_4	1.21	0.60		
V5711	WY	AM 58777	P_4	1.25 (a)	0.50 (a)		
V5003	WY	USNM 2139	P_4	1.20 (a)			

* All measurements taken by C.B.W. with the exception of those taken by W.A.C. (a) and Donald Lofgren (b).

(Fig. 8). In fact, for occlusion of the protocone into the talonid basin, UA 4081 has a better size and fit. The main discrepancy is in the area of the paracone-cristid obliqua, or (if adjusted there) between protoconid and parastylar area. The differences are not great and may be as expected with an attempt to occlude the upper and lower dentitions of different individuals from the same species.

Reference of Specimens to One Species, *Batodon tenuis*

One of the purported diagnostic characters of *B. tenuis* is its diminutive size. The fossils referred to this species are the smallest eutherian teeth found in Lancian local faunas of the North American Western Interior. Geographically these sites extend from central Alberta in the north to central eastern Wyoming in the south. Making allowances for individual and possible latitudinal variation, are the patterns and ranges of variation in dimensions what might be expected for a primitive eutherian species?

Measurements and locality data for the available sample of *B. tenuis* are given in Table 1. In order to avoid introduction of variation through use of different instruments, coefficients of variation (CVs) were calculated only for specimens measured by C.B.W. In general CV values are within the ranges found in other early tribosphenic eutherian species known from much larger samples (see Polly [1998b] for a recent discussion of CVs in smaller mammals). Of course, the range of coefficients for *B. tenuis* might be the product of small sample size and uncertainty in distinguishing between isolated specimens such as those representing M_1 and M_2. Co-

TABLE 2. STATISTICAL SUMMARY FOR DIMENSIONS (MM) OF TEETH REFERRED TO *BATODON TENUIS*.*

Tooth	Dimension	Number	OR	Mean	SD	CV
M^2	Length	4	0.8–1.0	0.88	0.08	8.50
	Width	5	1.5–1.8	1.65	0.08	4.75
P_4	Length	2	1.2–1.2	1.21	0.00	0.00
	Width, trigonid	2	0.6–0.6	0.60	0.00	0.00
M_2, all specimens	Length	6	1.0–1.3	1.20	1.00	8.14
	Width, trigonid	6	0.8–1.1	0.84	0.13	15.04
	Width, talonid	6	0.6–0.7	0.65	0.05	7.29
M_2, excluding UCMP 132174	Length	5	1.0–1.3	1.19	0.10	8.79
	Width, trigonid	5	0.8–0.8	0.79	0.02	2.93
	Width, talonid	5	0.6–0.7	0.65	0.05	7.29

* OR, Observed range; SD, Standard deviation; CV, coefficient of variation.

efficients for widths are generally lower, and it is this dimension that usually is least affected by position in the tooth row. One glaring exception is in width of trigonid of M_2. However, when measurements of UCMP 132174 are removed from the calculation, the discrepancy is much less evident (see Table 2). Some reassessment of the identity of UCMP 132174, an isolated molar, may be indicated. It is evident by inspection that some of the dimensions on specimens from the Scollard Formation, Alberta, are on the small end of the size range. However, this is not consistently true for all dimensions. With these exceptions, at present, variation in dental dimensions does not demand recognition of more than one species of *Batodon* in the Lancian local faunas sampled to date.

Interestingly, measurements of the anterior and posterior margins (protocone to paracone, protocone to metacone in crown view, excluding the stylar areas) of M^2 of *B. tenuis* (Table 3) are much more uniform than standard measurements for length on the tribosphenic crown. Measurements of these nonstandard dimensions for the new specimen (UCMP 136091) and for UA 4081 are, in fact, identical. Mention was made above of the coincidence of protocone and conule outline in superimposed drawings, and of the possibility that this area could be under greater selective pressure for uniformity than would other parts of the teeth. Such a possibility would be purely hypothetical at present, of course, and is based on an inadequate sample, but extended comparative studies of better-known genera would be a worthwhile test of this idea. Although Polly (1998a) has reported that developmental factors may correlate better than functional factors in tooth crown measurements of viverravid carnivores, new data from extant *Sorex* may demonstrate different patterns of variability (D. Polly, personal communication).

In summary, reference of the smallest tribosphenic eutherian teeth from Lancian localities in the North American Western Interior to a single species, *B. tenuis*, is supported by several lines of evidence.

TABLE 3. MEASUREMENTS (MM) OF ANTERIOR AND POSTERIOR MARGINS OF M^2 OF *BATODON TENUIS* EXCLUDING THE STYLAR AREA.

Locality	Specimen	Lengths	
		Anterior	Posterior
V73087	UCMP 136091	4.1	4.0
	UA 4081	4.1	4.0
V73087	UCMP 117649	3.7	4.5
V70201	UCMP 102909	3.9	4.1
V87308	UCMP 133080	3.6	4.0

Statistical summary of dimensions of margins for M^2*

Dimension	Number	OR	Mean	SD	CV
Anterior margin	5	3.6–4.1	3.88	0.23	5.88
Posterior margin	5	4.0–4.5	4.12	0.22	5.26

* OR, Observed range; SD, standard deviation; CV, coefficient of variation.

When merged into a single, albeit small sample, observed ranges and coefficients of variation of taxonomically significant tooth dimensions are what would be expected to characterize a single species (Polly, 1998b). Sizes and configurations of cusps, basins, and shearing crests of upper and lower teeth document a common occlusal pattern. Possibly diagnostic specialization of occluding elements of the posterior parts of M^3 and M_3 add support to the proposed association of upper and lower molars.

DISCUSSION

Dentition

Analyses of patterns of occlusion using the functional orientation have strengthened the basis for association of the upper and lower dentitions of *B. tenuis*. Its upper dentition is now known from P^4 through M^3 (P^4 illustrated by Lillegraven [1969] but lost before publication; Storer [1991] offers a possible P^3, P 2004.30); the lower is known from P_2 through M_3. Although more anterior teeth are unknown or represented only by fragments, it is clear that the canine was large (USNM 2139) and that the dental formula was I?, C1, P4, M3.

Body Mass

By Cenozoic standards, Cretaceous marsupials, eutherians, and their closely related sister groups were animals of small to very small body mass. Lillegraven et al. (1987) argued that small body masses, in the context of metabolic and reproductive constraints, played a significant role in the origin and diversification of the earliest marsupials and eutherians. Because most Cretaceous and early Cenozoic mammals were known from only isolated teeth, many early estimates of body mass were, at best, educated guesses. Then, based on data from living species, Gingerich and Smith (1984) pioneered the development of a method to use the area of the crown of M_1 to estimate the body mass of extinct eutherians. Recently, Bloch et al. (1998) presented a version of this technique modified specifically to estimate the body masses of lipotyphlans and proteutherians. In their survey of the modern lipotyphlans, Bloch et al. (1998) divided the group into seven classes of body mass. The three smallest classes and the percentage of modern species included in each were 1–3 g (3%), 3–7 g (26%), and 7–20 g (35%). Bloch et al. (1998) demonstrated that, in comparison to the range of variation of body masses of extant lipotyphlans, late Paleocene (Clarkforkian) and early Eocene (Wasatchian) purported lipotyphlans occupied the lower end of the range of variation. The body mass of the extinct species, *Batodontoides vanhouteni*, from the Wasatchian of Wyoming, was estimated to have been approximately 1.3 g, and, thus, was the smallest, nonvolant, Cenozoic eutherian yet known.

Bloch et al. (1998) did not extend their study to include Cretaceous eutherians. In Table 4 we present measurements of lower first molars and estimates of body mass of the smallest eutherians or probable eutherians in several local faunas ranging from the Aptian–Albian (ca. 110 million years before the present) through the Lancian. The estimated body mass (8.05–8.53 g) of *Montanalestes keebleri* of Early Cretaceous (Aptian–Albian) age, the most primitive purported eutherian (Cifelli, 1999) from North America, falls slightly above the arbitrary boundary between the second and third modern lipotyphlan body mass classes. Similarly, *Prokennalestes minor*, the smallest known Asian eutherian, also of Early Cretaceous age, has an estimated body mass of 6.76 g, falling slightly below this boundary. The oldest (Aquilan–Judithian) and most primitive North American genus of unquestioned eutherian affinity is *Paranyctoides*, which is known from two species, *P. maleficus* (Fox, 1984) and *P. sternbergi* (Fox, 1979). Estimates of body mass of these species range between 9 and 16 g, that is, within the

TABLE 4. ESTIMATES OF BODY MASS OF SPECIES OF *BATODON, PARANYCTOIDES, PROKENNALESTES,* AND *MONTANALESTES.*

Taxon	Measurements of M_1			Estimated mass	Notes, references
	Length	Width trigonid	Width talonid		
Batodon tenuis	1.30	0.75	0.70	5.39	AMNH 58777, Clemens, 1973
Paranyctoides sternbergi	1.50	0.90	1.25	15.63	UA 14822, C.B.W. measurements
Paranyctoides maleficus	1.6	1.0	1.1	14.10	UA 16168, Fox, 1984
	1.5	0.8	0.9	9.16	UA 17170, Fox, 1984
	1.5	0.7	0.9	9.16	UA 16171, Fox, 1984
	1.5	0.9	1.0	10.87	UA 16175, Fox, 1984
	1.6	0.9	1.0	12.08	UA 16181, Fox, 1984
				11.07	Average
Prokennalestes minor	1.4	0.8	0.6	6.76	Kielan-Jaworowska and Dashzeveg, 1989
Montanalestes keebleri	1.42	0.91	0.65	8.53	Left M_1, R. Cifelli, personal communication
	1.45	0.86	0.64	8.05	Right M_1, R. Cifelli, personal communication
				8.29	Average

third class of body mass recognized by Bloch et al. (1998).

Isolated lower first and second molars of *B. tenuis* cannot be distinguished with certainty, and we have not used them for estimates of body mass. Only one M_1 of *B. tenuis* has been found in place in a dentary (AMNH 58777). The body mass of this individual is estimated as having been 5.39 g. On the basis of the estimates derived from the formula provided by Bloch et al. (1998), *B. tenuis* is the smallest known Cretaceous eutherian, but it still falls within the second class of body masses of modern lipotyphlans. *Batodon tenuis* was not as minute as the Eocene *Batodontoides vanhouteni* or the modern *Suncus etruscus.*

A variety of taphonomic and collecting biases limit the chances of recovery of the remains of very small mammals, and the available sample of Cretaceous eutherians is small in absolute number of specimens and biogeographically patchy. The possibility that even smaller Cretaceous eutherians will be discovered cannot be excluded. However, it is of interest that the smallest currently known Cretaceous eutherians have estimated body masses in the range of 3–20 g. This is the range of body masses that includes 61% of modern lipotyphlans (Bloch et al., 1998) and small members of other, more distantly related eutherian orders.

Systematic Affinities

Currently, a lively debate is swirling around the questions of the time of origin of crown-group Mammalia in general and eutherian orders in particular (see Gibbons [1998]). Several molecular phylogeneticists (for example see Springer [1997] and Kumar and Hedges [1998]) have reported data from molecular clock estimates, suggesting that modern eutherian clades may have begun to diverge as long ago as the Early Cretaceous, despite the lengthy gap in the fossil record that such dates would imply (but see Nessov et al., 1998). Studies by Foote et al. (1999) and Alroy (1999) are examples of quantitative arguments from the fossil record that cast doubt on the molecular data. Novacek (1999) has addressed this question from a phylogenetic slant. These authors argue that the major ordinal level clades of the crown-group Placentalia did not differentiate until after the extinction of the nonavian dinosaurs marking the end of the Cretaceous.

Debate over the times of origin of the major clades of eutherians is part of an extensive revision of our understanding of the pattern of the early evolution of the Mammalia. For example, eutherians and marsupials were long thought to be characterized by the synapomorphy of a tribosphenic dentition. Discoveries of many mammals with tribosphenic dentitions, which cannot be confidently referred to the crown-groups Placentalia and Marsupialia, such as *Montanalestes* (Cifelli, 1999), show that this type of dentition is a synapomorphy of a more inclusive group. A recently discovered Middle Jurassic mammal from Madagascar, *Ambondro* (Flynn et al., 1999), suggests a more ancient origin of the tribosphenic dentition than previously expected.

Other recent discoveries reveal greater complexity in the evolutionary radiation of mammals with a reversed triangular symmetry of their cheek teeth, the holotherians, during the Jurassic and Cretaceous. A newly discovered Early Cretaceous Australian mammal, *Ausktribosphenos*, exhibits a surprising combination of dental and mandibular characteristics. Rich et al. (1997, 1999) maintain that the dentition of *Ausktribosphenos* is not only fully tribosphenic but also exhibits eutherian characteristics closer to those of the Erinaceomorpha than any other group. This dental morphology is combined with very plesiomorphic mandibular structures such as a Meckelian groove and postdentary bone sulci or facets (Rich et al., 1999). Alternative interpretations suggest that *Ausktribosphenos* is a representative of an endemic Australian radiation of holotherians (Kielan-Jaworowska et al., 1998; Rich et al., 1998). An even older, isolated tribosphenic-like upper molar has been reported from Late Jurassic deposits in China (Wang et al., 1998). The authors maintain that it is probably the missing upper molar of the pseudotribosphenic genus *Shuotherium* (Chow and Rich, 1982). These and other holotherians recently discovered in both the northern and southern hemispheres demonstrate that the tribosphenic dentition was but one outcome in early experiments in the evolution of more complex triangularly symmetrical teeth (see Kielan-Jaworowska et al. [1998] and Bonaparte [1996]).

Against this background of rapidly expanding knowledge of the complexities of early mammalian evolution, interpretations of the phylogenetic affinities of *B. tenuis* play a role in discussions of the beginning of the radiation of the eutherian crown group. Is *Batodon* a member of a lineage within the crown-group Placentalia, thus favoring the hypothesis that the radiation of modern eutherian orders began in the Late Cretaceous, or is it a member of a lineage not involved in their ancestry? Lillegraven (1969) and several later workers referred *Batodon* to the Palaeoryctidae, which was classified in the order Proteutheria, an admittedly paraphyletic taxon with unclear phylogenetic affinities (see Butler, 1972b). Others opted for an even less specific reference of the Palaeoryctidae placing it in the order Insectivora, incertae sedis (Clemens, 1973) or the infraclass Eutheria, incertae sedis (Archibald, 1982; Lofgren, 1995). In contrast, Novacek (1976) and Lillegraven et al. (1981) suggested that *Batodon* is an early lipotyphlan, probably allied to or even ancestral to the Geolabididae. Fox (1984: 19) doubted these suggestions of lipotyphlan affinity. McKenna and Bell (1997) classified *Batodon* and *Batodontoides* as members of Geolabididae, within Lipotyphla.

Bloch et al. (1998) reviewed the systematic assignments of *Batodon* and *Batodontoides*. They reported a necessarily limited, computer-assisted cladistic analysis of dental characters that indicated that *Batodon* is a basal member of a monophyletic Geolabididae, with *Cimolestes*, *Palaeoryctes*, and *Asioryctes* as successive outgroups. Although a helpful beginning, this outcome may be variable depending on which and how many characters are selected, and by inclusion of other taxa such as other members of Palaeoryctidae and/or perhaps a se-

ries of additional taxa between *Palaeoryctes* and *Asioryctes*. Differences between *Batodon* and *Batodontoides* that would bear reexamination in the more extended study would be M_3 morphology, M_3 size relative to M_{1-2}, talonid cusps in all three lower molars, and presence or absence of upper molar conules.

MacPhee and Novacek (1993) summarized the issues concerning relationships between proteutherians, palaeoryctids, and lipotyphlans. An important part of the problem, perhaps presently insurmountable, is the lack of comparative cranial material for most of the earlier taxa. Known material, such as that for *Asioryctes* (Kielan-Jaworowska, 1981), is mostly devoid of apomorphic characters needed for such an analysis. Palaeoryctids (see Thewissen and Gingerich [1989]) and leptictids (see Novacek [1986]), skulls of which are known, have a few characters that can be parsimoniously interpreted as synapomorphies of the Lipotyphla. Given the limited amount of information on its dentition and the lack of cranial data, we conclude that currently *B. tenuis* is best classified as Placentalia, incertae sedis.

ACKNOWLEDGMENTS

This work would not have occurred without the encouragement and support of Professor A. W. Crompton. We sincerely thank Mr. Al Coleman, who took the stereophotograph reproduced in Figure 1, and L. Laszlo Meszoly for the drawings (Figures 2–8, based on sketches made by C.B.W. through a camera lucida attached to a Wild-Heerbrug M3 stereo microscope) that also illustrate this paper. Thanks are also due to Dr. John Storer for facilitating reillustration of P 2004.565. Financial support for this study came, in part, from the University of California Museum of Paleontology and a series of grants (most recently EAR 9505841) from the National Science Foundation. Providence College provided additional support by means of sabbatical leave and grants from its Committee to Aid Faculty Research. Finally, thanks go to P. David Polly, Richard Cifelli, an anonymous reviewer, and several other colleagues who provided data, helpful discussions of aspects of the study, or reviews of drafts of the manuscript.

LITERATURE CITED

ALROY, J. 1999. The fossil record of North American mammals: evidence for a Paleocene evolutionary radiation. Systematic Biology, **48:** 107–118.

ARCHIBALD, J. D. 1982. A study of Mammalia and geology across the Cretaceous–Tertiary boundary in Garfield County, Montana. University of California Publications in Geological Sciences, **122:** 1–286.

BLOCH, J. I., K. D. ROSE, AND P. D. GINGERICH. 1998. New species of *Batodontoides* (Lipotyphla, Geolabididae) from the early Eocene of Wyoming: smallest known mammal? Journal of Mammalogy, **79:** 804–827.

BONAPARTE, J. F. 1996. Cretaceous tetrapods of Argentina. Münchner Geowissenschaftliche Abhandlungen, **30:** 73–130.

BUTLER, P. M. 1961. Relationships between upper and lower molar patterns, pp. 117–126. *In* G. Vandebroek (ed.), International Colloquium on the Evolution of Lower and Non-specialized Mammals. Part I. Letteren en Schone Kunsten van Belgie. Brussels, Belgium: Koninklijke Vlaamse Academie voor Wetenschappen. 320 pp.

———. 1972a. Some functional aspects of molar evolution. Evolution, **26:** 474–483.

———. 1972b. The problem of insectivore classification, pp. 253–265. *In* K. A. Joysey and T. S. Kemp (eds.), Studies in Vertebrate Evolution. New York: Winchester Press. 284 pp.

CARRANO, M. T., R. W. BLOB, J. J. FLYNN, R. R. ROGERS, AND C. A. FORSTER. 1997. The mammalian fauna of the Judith River Formation type area (Campanian, Central Montana) revisited. Journal of Vertebrate Paleontology, **17**(3): 36A.

CHOW, M., AND T. H. V. RICH. 1982. *Shuotherium dongi*, n. gen. and sp., a therian with pseudotribosphenic molars from the Jurassic of Sichuan, China. Australian Mammology, **5:** 127–142.

CIFELLI, R. L. 1999. Tribosphenic mammal from the North American Early Cretaceous. Nature, **401:** 363–366.

CLEMENS, W. A., JR. 1973. Fossil mammals of the type Lance Formation, Wyoming—part III. Eutheria and summary. University of California Publications in Geological Sciences, **94:** 1–102.

CROMPTON, A. W. 1971. The origin of the tribosphenic molar, pp. 65–87. *In* D. M. Kermack and K. A. Kermack (eds.), Early Mammals. Zoological Journal of the Linnaean Society, **50**(Suppl. 1): xiv + 1–203.

CROMPTON, A. W., AND K. HIIEMAE. 1969. How mammalian teeth work. Discovery, **5:** 23–34.

CROMPTON, A. W., AND Z. KIELAN-JAWOROWSKA. 1978. Molar structure and occlusion in Cretaceous therian mammals, pp. 249–287. *In* P. M. Butler and K. A. Joysey (eds.), Development, Function, and Evolution of Teeth. New York: Academic Press. v + 523 pp.

CROMPTON, A. W., AND A. SITA-LUMSDEN. 1970. Functional significance of the therian molar pattern. Nature, **227:** 197–199.

FLYNN, J. J., J. M. PARRISH, B. RAKATOSAMIMANANA, W. F. SIMPSON, AND A. R. WYSS. 1999. A Middle Jurassic mammal from Madagascar. Nature, **401:** 57–60.

FOOTE, M., J. P. HUNTER, C. M. JANIS, AND J. J. SEPKOSKI, JR. 1999. Evolutionary and preservational constraints on origins of biologic groups: divergence times of eutherian mammals. Science, **283:** 1310–1314.

FOX, R. C. 1975. Molar structure and function in the early Cretaceous mammal *Pappotherium:* evolutionary implications for Mesozoic Theria. Canadian Journal of Earth Sciences, **12:** 412–442.

———. 1979. Mammals from the Upper Cretaceous Oldman Formation, Alberta. III. Eutheria. Canadian Journal of Earth Sciences, **16:** 114–125.

———. 1984. *Paranyctoides maleficus* (new species), an early eutherian mammal from the Cretaceous of Alberta. Special Publication of the Carnegie Museum of Natural History, **9:** 9–20.

GIBBONS, A. 1998. Genes put mammals in age of dinosaurs. Science, **280:** 675–676.

GINGERICH, P. D., AND B. H. SMITH. 1984. Allometric scaling in the dentition of primates and insectivores, pp. 257–272. *In* W. L. Jungers (ed.), Size and Scaling in Primate Biology. New York: Plenum Publishing Corporation. xiv + 491 pp.

HICKS, J. F., K. R. JOHNSON, L. TAUXE, D. CLARK, AND J. D. OBRADOVICH. 1999. Geochronology of the Hell Creek Formation of southwestern North Dakota: a multidisciplinary approach using biostratigraphy, isotopic dating, geochemistry, and magnetostratigraphy. Geological Society of America, Abstracts with Programs, **31**(7): A-71.

KAY, R. F., AND K. M. HIIEMAE. 1974. Jaw movement and tooth use in recent and fossil primates. Journal of Physical Anthropology, **40:** 227–256.

KIELAN-JAWOROWSKA, Z. 1981. Evolution of therian mammals in the Late Cretaceous of Asia. Part IV. Skull structure of *Kennelestes* and *Asioryctes*. Palaeontologica Polonica, **42:** 25–78.

KIELAN-JAWOROWSKA, Z., R. L. CIFELLI,, AND Z. LUO. 1998. Alleged Cretaceous placental from down under. Lethaia, **31:** 267–268.

KIELAN-JAWOROWSKA, Z., AND D. DASHZEVEG. 1989. Eutherian mammals from the Early Cretaceous of Mongolia. Zoologica Scripta, **18:** 347–355.

KUMAR, S., AND S. B. HEDGES. 1998. A molecular timescale for vertebrate evolution. Nature, **392:** 917–920.

LILLEGRAVEN, J. A. 1969. Latest Cretaceous mammals of upper part of Edmonton Formation of Alberta, Canada, and review of marsupial–placental dichotomy in mammalian evolution. University of Kansas Paleontological Contributions, Article **50**(Vertebrata 12): 1–122.

LILLEGRAVEN, J. A., AND M. C. MCKENNA. 1986. Fossil mammals from the "Mesaverde" Formation (Late Cretaceous, Judithian) of the Bighorn and Wind River Basins, Wyoming, with definitions of late Cretaceous North American Land-Mammal Ages. American Museum Novitates, **2840:** 1–68.

LILLEGRAVEN, J. A., M. C. MCKENNA, AND L. KRISHTALKA. 1981. Evolutionary relationships of Middle Eocene and younger species of *Centetodon* (Mammalia, Insectivora, Geolabididae) with a description of the dentition of *Ankylodon*. University of Wyoming Publications, **45:** 1–97.

LILLEGRAVEN, J. A., S. D. THOMPSON, B. K. MCNAB, AND J. L. PATTON. 1987. The origin of the eutherian mammals. Biological Journal of the Linnean Society, **32:** 281–336.

LOFGREN, D. 1995. The Bug Creek problem and the Cretaceous–Tertiary transition at McGuire Creek, Montana. University of California Publications, Geological Sciences, **140:** 1–185.

LOFGREN, D., C. HOTTON, AND A. RUNKEL. 1990. Reworking of Cretaceous dinosaurs into Paleocene channel deposits, upper Hell Creek Formation, Montana. Geology, **18:** 874–877.

LULL, R. S. 1915. The mammals and horned dinosaurs of the Lance Formation, Niobrara County, Wyoming. American Journal of Science, Series 4, **40:** 319–348.

MACPHEE, R. D. E., AND M. J. NOVACEK. 1993. Definition and relationships of Lipotyphla, pp. 13–30. *In* F. S. Szalay, M. C. McKenna, and M. J. Novacek (eds.), Mammal Phylogeny: Placentals. New York: Springer-Verlag. v + 321 pp.

MARSH, O. C. 1892. Discovery of Cretaceous Mammalia, part III. American Journal of Science, Series 3, **48:** 249–262.

MCKENNA, M. C., AND S. K. BELL. 1997. Classification of Mammals Above the Species Level. New York: Columbia University Press. xii + 631 pp.

MONTELLANO, M. 1992. Mammalian fauna of the Judith River Formation (Late Cretaceous, Judithian), northcentral Montana. University of California Publications, Geological Sciences, **136:** 1–115.

NESSOV, L. A., J. D. ARCHIBALD, AND Z. KIELAN-JAWOROWSKA. 1998. Ungulate-like mammals from the Late Cretaceous of Uzbekistan and a phylogenetic analysis of Ungulatomorpha. Bulletin of the Carnegie Museum of Natural History, **34:** 40–88.

NOVACEK, M. J. 1976. Insectivora and Proteutheria of the later Eocene (Uintan) of San Diego County, California. Los Angeles County Natural His-

tory Museum, Contributions to Science, **283:** 1–52.

———. 1986. The skull of leptictid insectivorans and the higher-level classification of eutherian mammals. Bulletin of the American Museum of Natural History, **183:** 1–112.

———. 1999. 100 million years of land vertebrate evolution: the Cretaceous–Early Tertiary transition. Annals of the Missouri Botanical Gardens, **86:** 230–258.

POLLY, P. D. 1998a. Variability, selection, and constraints: development and evolution in viverravid (Carnivora, Mammalia) molar morphology. Paleobiology, **24:** 409–429.

———. 1998b. Variability in mammalian dentitions: size-related bias in the coefficient of variation. Biological Journal of the Linnean Society, **64:** 83–99.

RICH, T. H., T. F. FLANNERY, AND P. VICKERS-RICH. 1998. Alleged Cretaceous placental from down under: reply. Lethaia, **38:** 346–348.

RICH, T. H., P. VICKERS-RICH, A. CONSTANTINE, T. F. FLANNERY, L. KOOL, AND N. VAN KLAVEREN. 1997. A tribosphenic mammal from the Mesozoic of Australia. Science, **278:** 1438–1442.

———. 1999. Early Cretaceous mammals from Flat Rocks, Victoria, Australia. Records of the Queen Victoria Museum, **106:** 1–35.

SLOAN, R. E., AND L. VAN VALEN. 1965. Cretaceous mammals from Montana. Science, **232:** 220–227.

SPRINGER, M. S. 1997. Molecular clocks and the timing of the placental and marsupial radiations in relation to the Cretaceous–Tertiary boundary. Journal of Mammalian Evolution, **4:** 285–302.

STORER, J. E. 1991. The mammals of the Gryde Local Fauna, Frenchman Formation (Maastrichtian: Lancian), Saskatchewan. Journal of Vertebrate Paleontology, **11:** 350–369.

THEWISSEN, J. G. M., AND P. D. GINGERICH. 1989. Skull and endocranial cast of *Eoryctes melanus*, a new palaeoryctid (Mammalia: Insectivora) from the early Eocene of western North America. Journal of Vertebrate Paleontology, **9:** 459–470.

WANG, Y., W. A. CLEMENS, Y. HU, AND C. LI. 1998. A probable pseudo-tribosphenic upper molar from the late Jurassic of China and the early radiation of the Holotheria. Journal of Vertebrate Paleontology, **18:** 777–787.

WOOD, C. B., G. C. CONROY, AND S. G. LUCAS. 1979. New discoveries of fossil primates from the type Torrejonian (Middle Paleocene) of New Mexico. Folia Primatologica, **32:** 1–7.

WOOD, C. B., AND W. A. CLEMENS. 1990. An undescribed upper M2–3 of *Batodon tenuis*: a functional assessment. Journal of Vertebrate Paleontology, **10**(3): 50A.

WOOD, C. B., E. R. DUMONT, AND A. W. CROMPTON. 1999. New studies of enamel microstructure in Mesozoic mammals: a review of enamel prisms as a mammalian synapomorphy. Journal of Mammalian Evolution, **6:** 177–214.

THE EVOLUTION OF MAMMALIAN DEVELOPMENT

KATHLEEN K. SMITH[1]

ABSTRACT. The developmental and reproductive strategies of marsupial mammals differ from those of placental mammals. In marsupials, most maternal nutritional support of the developing young is through lactation. The young are born at an extremely altricial state and undergo most development while attached to the teat. In order to achieve functional independence at an altricial state, the marsupial embryo accelerates the development of certain bones of the facial region, most cranial musculature, and a few additional structures. At the same time, relative to placentals, marsupials delay significantly the development of central nervous system structures, in particular the forebrain. In this paper I present preliminary results concerning the origins of these heterochronies in ontogeny and phylogeny. In ontogeny, heterochronies are initiated in marsupials by shifting the timing of neural crest differentiation and migration relative to eutherians and other amniotes. Further, early fore- and midbrain differentiation is delayed relative to the hindbrain. Preliminary data from nonmammalian amniotes and monotremes is discussed to assess phylogenetic origins. Comparisons with nonmammalian amniotes suggest that the pattern observed in marsupials is derived, and that observed in placentals is primitive. Preliminary data on monotremes suggest that the monotreme condition is somewhat intermediate between the two therian taxa. Finally, the implications of these results for controversies regarding the evolution of mammalian reproduction are discussed.

INTRODUCTION

Mammalian reproduction is characterized by distinctive adaptations for maternal nutrient provision to the young. In therian mammals this provisioning occurs via two routes. First, during a period of intrauterine embryonic development exchange of nutrient material between the mother and young occurs through a placenta. Although this adaptation is most often identified with mammals, intrauterine development and the existence of a placenta is not uncommon among vertebrates (e.g., squamate reptiles; Shine, 1985). Second, and virtually unique to mammals, nutrition is provided postnatally to the young through specialized mammary glands. The origin and evolution of these distinctive traits has been a topic of much discussion. This discussion has been enriched in part because the two clades of living therian mammals—marsupials and placentals—possess quite different strategies of reproduction, with differential emphasis on these two processes of maternal investment. (The terms marsupial–placental and metatherian–eutherian are each to some degree unsatisfactory to distinguish the two clades; however, they are used informally and interchangeably throughout the text. In particular, the characters discussed in this paper are only accessible in extant taxa, and inferences cannot be extended to members of any clade known only in the fossil record.)

Marsupials are considered lactational specialists, where a relatively short intrauterine period of maternal–fetal interchange is followed by an extended period of lactation (e.g., Renfree, 1983, 1993, 1995). In contrast, eutherians are characterized by relatively longer periods of intrauterine development, with extensive fetal–maternal interchange, and variable reliance on lactation. Because the period of organogenesis is so short in marsupials, the neonates show minimal development of most systems and are always highly altricial. Eutherian neonates exhibit a range of development from altricial to highly pre-

[1] Department of Biology, Duke University, Durham, North Carolina 27710.

cocial; however, even the most altricial eutherian is far more developed than the most precocial marsupial.

Because the reproductive mode and relative state of the neonate in marsupials and placentals is so different, a rich literature exists that contrasts these strategies and speculates on the evolutionary significance of the observed patterns. Three basic interpretations have been made. In the first interpretation the marsupial condition is seen as a primitive condition, in which significant constraints prevent long periods of intrauterine development (e.g., Lillegraven, 1975; Lillegraven et al., 1987). Hypothesized constraints have included an inability to develop an efficient maternal–fetal exchange system, physical constraints on embryo size due to the configuration of the reproductive tract, or an inability to develop immunologic protection of the fetus. At times explicitly, but always implicitly, the marsupial condition is seen as a primitive and less efficient mode of reproduction, as evidenced by the competitive difficulties marsupials face in the presence of eutherians.

A second view is that the marsupial mode has evolved in response to a number of specific selective pressures, with particular adaptive advantages (e.g., Hayssen et al., 1985; Kirsch, 1977a,b; Parker, 1977). It is argued that because little initial maternal investment occurs during intrauterine development, the female can reduce or abandon her litter in response to harsh or uncertain conditions with minimal loss of lifetime reproductive effort. This view clearly assumes that the marsupial condition is derived, and that if a competitive inferiority exists, it is due to other factors, such as the consequences of marsupials having evolved in greater isolation than have eutherians.

A third view is that marsupial and eutherian modes of reproduction are simply part of a single continuum (Tyndale-Biscoe and Renfree, 1987). Marsupials and placentals each provide nutrition to the developing young through both placental and lactational exchange. The hypothesis has been made that the primitive therian condition was characterized by an altricial neonate as a consequence of small body size in the earliest therian. During evolution, marsupials and placentals simply emphasized different ends of the maternal investment continuum. Eutherians took the strategy of greater and greater maternal investment through placentation, and because of longer periods of intrauterine development, neonates are less altricial. Highly precocial young are thought to be correlated with the evolution of large body size. In contrast, marsupials have relied on the strategy of more investment via lactation and have reduced the period of intrauterine development, resulting in a more altricial neonate. The differences between the two are simply the results of two different, but not necessarily inferior or superior, strategies of provisioning the young. Both marsupials and placentals are assumed to have diverged from a primitive condition that was somewhat intermediate.

This debate has proved difficult to resolve, in part because mammalian reproduction is so distinctive, and in part because reproductive modes are difficult to reconstruct in the fossil organisms. In this paper I will focus on the evolution of mammalian development. I argue that eutherian and marsupial reproductive strategies are reflected in distinct developmental patterns; therefore, information on the evolution of development can provide new data for phylogenetic analysis of the evolution of reproduction. I first review previously published work on organogenesis in marsupials and placental mammals. I then introduce new comparative work that extends this previously published work, to address questions about the origins of these differences in development and in evolution.

CRANIOFACIAL DIFFERENTIATION IN MARSUPIAL AND PLACENTAL MAMMALS

It has long been recognized that, relative to eutherians, marsupials accelerate

the development of certain structures such as the tongue, the bones around the oral apparatus and the bones and muscles of the forelimb (e.g., Hill and Hill, 1955; Lee and Cockburn, 1985; Klima, 1987; Maier, 1987, 1993; Tyndale-Biscoe and Renfree, 1987, and references therein; Hughes and Hall, 1988; Nelson, 1988; Filan, 1991; Clark and Smith, 1993; Gemmell and Selwood, 1994). This advancement is interpreted as an adaptive response to the functional requirements placed on the neonate by the marsupial life history. The extremely altricial neonate must independently travel to, identify, and enter the pouch or teat region, and recognize and attach to the teat. The neonate must have sufficient functional maturity to suckle and process food while it completes its development. However, by and large, no broad-based, detailed comparisons of development have been made to identify the specific heterochronies that characterize marsupials. In a series of studies I presented such an analysis for major craniofacial structures (Smith, 1996, 1997; Nunn and Smith, 1998).

In these studies, relatively complete developmental series of six placental and four marsupial mammals were examined. The placentals include the laboratory mouse, *Mus musculus* (Rodentia); the domestic cat, *Felis domestica* (Carnivora); the domestic pig, *Sus scrofa* (Artiodactyla); the pangolin, *Manis javanica* (Pholidota); the tarsier, *Tarsius spectrum* (Primates); and the tree shrew, *Tupaia javanica* (Scandentia). The four marsupials are the gray short-tailed opossum, *Monodelphis domestica* (Didelphidae); the tammar wallaby, *Macropus eugenii* (Macropodidae); the eastern quoll, a species of marsupial "cat," *Dasyurus viverrinus* (Dasyuridae); and a bandicoot, *Perameles nasuta* (Peramelidae). Care was taken to chose taxa that represent the phylogenetic breadth of their clades. Figure 1 illustrates the phylogenetic relations among these taxa. Most specimens were part of the Hubrecht Comparative Embryology collection in

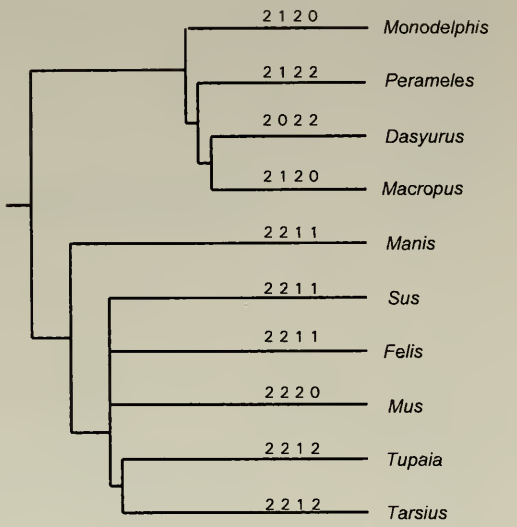

Figure 1. Phylogeny of the taxa used in the comparative studies. Phylogeny for marsupials taken from Sánchez-Villagra (1999) and Springer et al. (1998); that for placentals taken from Novacek (1990). The numbers on each line illustrate results from the event-pair analysis (Smith, 1997) and represent the character states for the following pairs of events (in order): parietal–telencephalon, dentary–telencephalon, alisphenoid–exoccipital, jugal–craniofacial muscles. Character state 0 means the first element in the pair occurs before the second; character state 1 means the first and second elements appear at same time (in the sample available); character state 2 means the first element in the pair occurs after the second. These event pairs represent a variety of phylogenetic patterns. The pair parietal–telencephalon has a uniform pattern in therians—the parietal always ossifies after the telencephalon evaginates. The pair dentary–telencephalon separates marsupials and placentals. In marsupials the dentary ossifies at the same time or before the telencephalon appears; in eutherians the dentary always ossifies after appearance of the telencephalon. The alisphenoid also separates the two clades with the exoccipital preceding the alisphenoid in all marsupials, and the alisphenoid and exoccipital ossifying at the same time in all eutherians (with the exception of *Mus*). Finally, the pair jugal–craniofacial muscles represents a case in which no phylogenetic pattern of the developmental relation of these two elements is apparent. See Smith (1997) for further discussion of these events.

The Netherlands, although others were obtained from a number of sources. For each taxon at least 10 stages were available for the period between the first and last developmental events examined. All specimens examined were serially sectioned embryos, originally embedded in paraffin and stained with common histologic stains. Details on the taxa, sources, and stages examined can be found in Smith (1997).

Each specimen was examined to deter-

mine the state of 28 elements of the cranial skeletal, muscular, and central nervous systems (CNSs), which serve as landmarks for the most critical stages in the differentiation of craniofacial structures. The kinds of events examined are briefly summarized here; further details are provided in Smith (1997). The initial ossification center of 12 bones of the dermal and endochondral skeletons was documented. Other conditions of the cranial skeleton included, for example, the first contact between the membrane bones over the cranial roof, the differentiation of cartilage in the cranial base, closure of the secondary palate, and the development of a joint capsule at the dentary–squamosal joint (see Clark and Smith [1993, and references therein] for more detail on development of the cranial skeleton).

Three stages, ranging from the first fusion in myoblasts to the age at which all craniofacial muscles were distinguishable, were used as measures of muscle development (for more detail on the assessment of muscle development see Smith [1994]). Finally, six events were examined that indicate maturation of the CNS and cranial sense organs. These included, for example, the evagination of the telencephalic vesicles, the filling of the lens vesicle by primary lens cells, and the appearance of at least four distinct layers in the cortex.

Two different approaches were taken to analyze the comparative data (see Smith [1997] and Nunn and Smith [1998] for details on methods). The first method constructs a matrix for each taxon in which the timing of each event is compared to the timing of every other event. This creates a series of pair-wise comparisons, where the timing of event A is compared to event B, C, D, and so on (forming pairs A-B, A-C, A-D, as well as B-C, B-D, and so on). The data set studied here included 28 events, which produced 378 event pairs. Each pair was assigned one of three character states, reflecting the relative timing of the two events. The three states were character state 0, when event A (the first event in the pair) occurred before event B (the second event in the pair); character state 1, when A occurred in the same stage as B; and character state 2, when A occurred after B. The character state for each pair of events was then mapped on a phylogeny, to determine whether any group of taxa (e.g., marsupials or placentals, or subsets within a major clade) had a unique character state distribution (Fig. 1; see Smith [1997]).

The second approach is quantitative. Each event in the sequence was given a rank order number between 1 and 28 (because there were 28 events), with events occurring at the same time ranked as a tie. An analysis of variance (ANOVA) was then performed to determine which events had a significantly different rank between marsupials and placentals. In addition, methods were also developed to correct for phylogenetic nonindependence in the assessment of significance (see Nunn and Smith [1998]).

Although the two analytical methods are quite different, they provide congruent results and allow a determination of which shifts in relative timing—heterochrony—characterize craniofacial organogenesis in marsupial and placental mammals. In the ANOVA the following 11 events had significantly different ranks in the two clades: the evagination of the telencephalon; contact between the olfactory bulb and the olfactory epithelium; layering in the cortex; the differentiation of the thalamus and hypothalamus; filling of the lens vesicle by primary lens cells; the initial ossification of the dentary, maxillary, premaxillary, and exoccipital bones; the closure of the secondary palate; and the meeting of the dermal bones over the cranial roof. The initial ossification of the dentary, maxillary, premaxillary, and exoccipital bones and the closure of the secondary palate occurred early in marsupials relative to placentals (i.e., they had a significantly lower rank); the other events were late in marsupials when compared to placentals. This same set of characters exhibited shifts in the

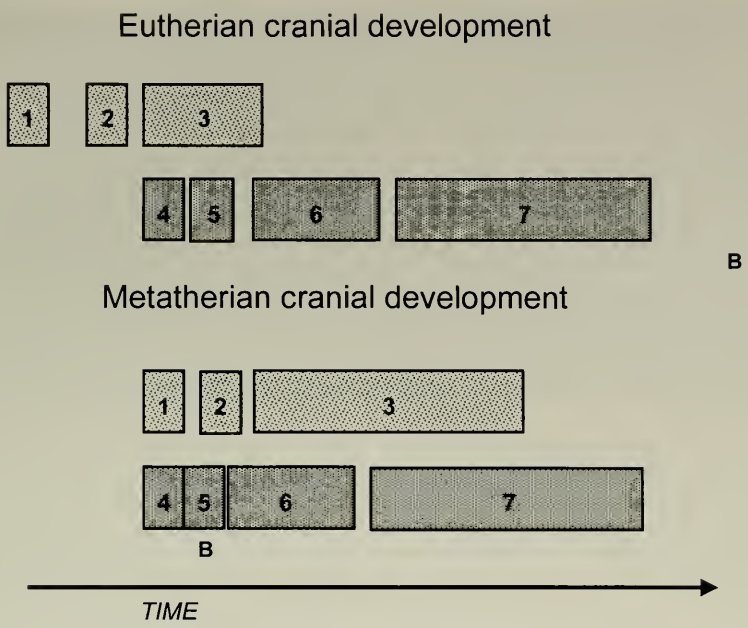

Figure 2. A summary of the relative timing of development of craniofacial features in metatherians and eutherians. The upper set of boxes (light stippling) for each clade represents events in central nervous system (CNS) development; the lower set of boxes (dark stippling) represents events in the development of skeletal–muscular systems. The arrow at the bottom represents time. The letter B represents the approximate time of birth in each group. For comparison, the two taxa were scaled and aligned relative to the timing of the events of the skeletal–muscular system; the CNS in each clade was plotted relative to the scaled skeletal–muscular system events. Key to numbers: 1, evagination of telencephalon; 2, pigment in retina; 3, connection between the olfactory epithelium and olfactory bulb, layering present in the cortex, thalamus and hypothalamus present, primary lens cells fill lens vesicle; 4, tongue muscle cells begin fusion and cartilage present in basicranium; 5, ossification of premaxillary, maxillary, and dentary bones; 6, closure of secondary palate, all major components of craniofacial muscle present, muscle maturation, differentiation of tooth buds, appearance of ear ossicles, first ossification in most membrane bones; 7, ossification of most endochondral bones, meeting of membrane bones over cranial roof, and differentiation of mandibular joint cartilage and capsule.

event-pair character analysis. In the event-pair analysis, 58 of the 378 event-pairs had character states that distinguished marsupial and placental mammals. Fifty-seven of these 58 event-pairs contained either one or two events that were found to differ in the ANOVA.

These specific results reveal that craniofacial development in marsupials and placentals is distinguished by major shifts in the relative timing of the differentiation of the somatic structures of the head relative to the differentiation of the CNS (Fig. 2). These heterochronies have two major components. First, in eutherians the onset of morphogenesis of the CNS begins long before the appearance of any cranial skeletal or muscular tissues. In marsupials cranial skeletal and muscular tissues begin development early relative to CNS differentiation. Second, in eutherians the events of CNS development examined are completed before most somatic structures begin differentiation, whereas in marsupials morphogenesis of these same elements extends long into the period of cranial skeletal development. More broadly, relative to eutherians, marsupial development can be characterized by two steep heterochronies, or shifts in developmental timing: cranial musculoskeletal tissues are highly advanced in onset and rate of development relative to the tissues of the CNS, and in the body as a whole, the rostral portion is highly advanced relative to the caudal portion (Smith, 1996, 1997; Nunn and Smith, 1998).

The early development of musculoskel-

etal tissues is almost certainly a result of the necessity for the marsupial neonate to possess certain functional abilities relatively early in its normal developmental period. The fact of this early adaptation has long been recognized. However, the adaptations of the marsupial neonate do not simply involve the advancement of the forelimbs and a few structures around the oral apparatus and birth at an altricial state. Instead, the developmental trajectory of all cranial tissues seems to be shifted. This whole-scale shift is best interpreted as the interaction of the adaptive innovations with constraints imposed by two developmental processes (Smith, 1997).

The first process involves CNS development and the constraints arising from the sensitivity of nervous tissue to energetic fluctuations during differentiation. The absence of nutrients during organogenesis of the brain can lead to long-lasting neural deficiencies (e.g., Dobbing, 1972; Winick et al., 1972; Cheek, 1975; Dodge et al., 1975; Winick, 1976, 1979; Shoemaker and Bloom, 1977; Hetzel and Smith, 1981; Dhopeshwarkar, 1983; Herschkowitz, 1989). Because of these critical requirements, Sacher and Staffeldt (1974) proposed that neurogenesis is the rate-limiting step in mammalian development. The second set of processes involves the development of mesenchymal-derived tissues and the importance of initial cell condensation size during skeletogenesis (Grüneberg, 1963; Atchley and Hall, 1991; Hall, 1991; Hall and Miyake, 1992, 1995; Dunlop and Hall, 1995; Miyake et al., 1996, 1997). This work shows that in general, condensation must be adequate before cartilage will differentiate and bone formation will begin. Therefore, it is likely that the processes of skeletogenesis require the developing embryo to allocate a sufficient number of cells, and presumably energy, to the skeletal system at the very earliest stage of differentiation.

In eutherian mammals the onset of neurogenesis and the initial period of growth of the CNS begin early, when little competition exists from other tissues, and growth and differentiation continue throughout the extended embryonic and fetal periods when nutrition is relatively constant. However, metatherians face the competing demands of the adaptations that allow function of the systems most critical to independent survival of the altricial neonate, the extremely short period from primitive streak to birth (which averages 6 days for marsupials as a group and is less than 3 days in dasyurids; Tyndale-Biscoe and Renfree, 1987), the necessity for sufficient allocation to these systems for morphogenesis, and the rate-limiting nature of neurogenesis. Marsupials apparently avoid the constraints arising from these competing demands by shifting the bulk of neural differentiation to the extended postnatal period and devoting embryonic resources to tissues that must be functional at birth (see Smith [1997] for more discussion of this hypothesis).

THE DEVELOPMENTAL ORIGINS OF HETEROCHRONY

The discussion above focused on events that occur during organogenesis, after the basic systems have appeared. These data do not address when these heterochronies originate in development. At least two competing hypotheses have been developed. First, these shifts possibly represent patterns of acceleration and deceleration of morphogenesis of cranial structures once the major elements of the embryo have differentiated. Therefore, these changes would represent relatively minor terminal shifts in development, and suggest that there is significant conservation of the basic body plan. Alternatively, it may be that these shifts occur early in development and represent major changes in patterning of the tissues of the head, and indeed the embryo as a whole. Of particular interest is the fact that the bones and connective tissues of the facial region, which are greatly accelerated relative to the CNS in marsupials, are in fact derived

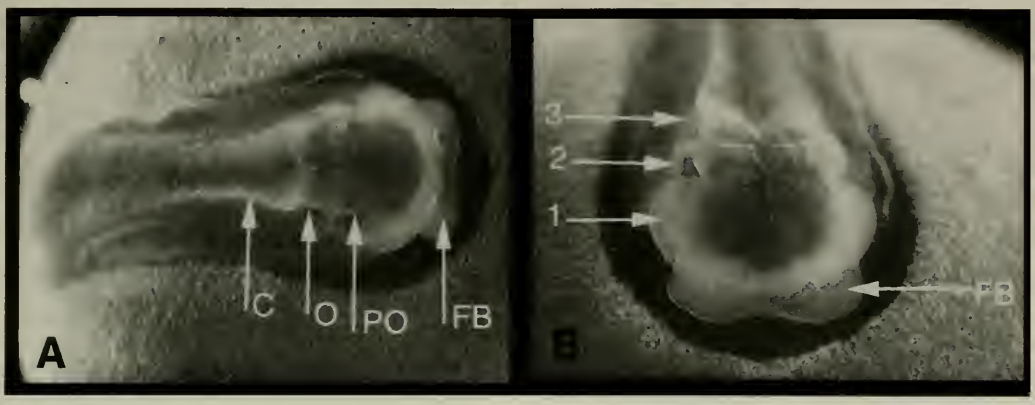

Figure 3. Photographs of a 10.5-day-gestation embryo *Monodelphis domestica* (approximately six somites); (A) is a dorsal view and (B) is an anterior-dorsal view of same specimen. Neural crest migration occurs early relative to neural tube differentiation in marsupials. Although no closure of the neural tube has occurred, streams of neural crest have migrated into the first arch region, are migrating into the second arch region, and appear to be about to migrate into posterior regions. Further, at this time the hindbrain is fairly well differentiated, with recognizable rhombomeres, yet little or no development of midbrain or forebrain regions has occurred. This is quite different from the pattern seen in eutherians. Key: C, cervical region; O, otic sulcus (region of rhombomeres 5 and 6); PO, preotic sulcus (between rhombomeres 2 and 3); FB, forebrain region; 1, the first stream of neural crest, which appears to populate the first arch and frontonasal region; 2, the second stream of neural crest, which appears to provide cells to the second arch; 3, the third stream, which appears to go to the third through sixth branchial arches.

from a neural tissue—the neural crest (reviewed in Le Douarin [1982], Noden [1983, 1987, 1991], Hall [1987], and Hall and Hörstadius [1988]). The relative timing of neural crest differentiation serves as the earliest "decision point" in embryonic allocation to neural or to mesenchymal tissues. Do these differences originate with shifts in the relative timing or pattern of neural crest migration? A positive answer would support the hypothesis that this is a fundamental change in development and that early development is potentially plastic.

Neural crest migration has been studied extensively in a number of nonmammalian vertebrates, particularly in the quail-chick system (e.g., Le Douarin, 1982; Noden, 1983, 1987, 1991; Hall and Hörstadius, 1988). The studies of mammals thus far have indicated essential similarity with other vertebrates although a few important differences exist (see, for example, Nichols [1981, 1986, 1987], Serbedzija et al. [1992], Morriss-Kay et al. [1993], Tan and Morriss-Kay [1985, 1986], Trainor and Tam [1995], and Peterson et al. [1996]). One difference is that in the mammals studied neural crest migration begins relatively early when the anterior part of the neural tube is still open, whereas in other vertebrates migration is typically after neural tube closure (e.g., Le Douarin, 1982; Hall and Hörstadius, 1988; Hanken et al., 1997). In both mice and rats neural crest appears to begin migration at the five- to six-somite stage (8 or 9 days; Nichols, 1981; Morriss-Kay et al., 1993). Other than the unpublished studies of Hill and Watson (1958), no studies of neural crest migration have been conducted in any marsupial.

Preliminary results from a study of neural crest migration in marsupials suggest that the shift in the differentiation of the CNS and somatic tissues is initiated by a shift in the relative timing of neural crest differentiation relative to neural tube differentiation. In a five- to six-somite embryo (approximately 10 days gestation) of *M. domestica* (Fig. 3), significant neural crest migration has already occurred; however, no folding has taken place in the neural plate. In marsupials substantial migration of neural crest into the first arch and future frontonasal regions has occurred

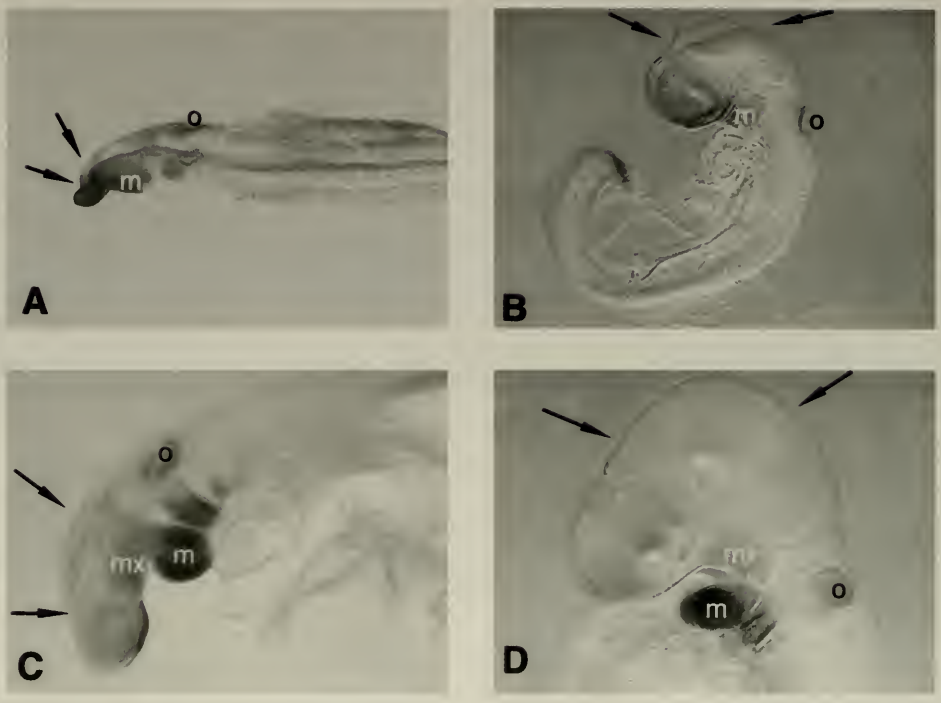

Figure 4. Whole-mount staining of embryos with antibody to Distal-less protein. Methods follow Hanken et al. (1992). (A) *Monodelphis* after 10.5 days of gestation (10–12 somites); (B) *Mus* at 10- to 12-somite stage; (C) *Monodelphis* after 10 days, 20 hours of gestation (16 somites); (D) *Mus* at 14- to 16-somite stage. (A) and (B) represent early stages in neural crest accumulation in branchial arches. Note that although the anterior neural tube is open in both embryos, the fore- and midbrain are much more robust (both in thickness of neuroepithelium and length of region) in the mouse, but that much less accumulation of neural crest has occurred in the frontonasal and first arch regions in this animal. In (C) and (D) the same pattern continues—in *Monodelphis* the neural tube is still open anteriorly, whereas in the mouse the neural tube is complete and regional differentiation is beginning. However, massive accumulations of neural crest occur in the facial region, particularly in the maxillary process, in *Monodelphis* relative to the mouse. Key: arrows represent approximate forebrain–midbrain and midbrain–hindbrain junctions; o, otic vesicle; mx, maxillary process; md, mandibular process.

before any closure of the tube occurs at any point along its length. Further, although the hindbrain is well differentiated at this stage, with evidence of all rhombomeres, little proliferation or differentiation occurs in either the fore- or midbrain regions. In eutherians significant proliferation of tissues in the fore- and midbrain regions occurs before neural crest migration begins, and rhombomere subdivision occurs after this period. These preliminary studies do indicate that the neural crest arises from the same rhombomeric segments that have been reported in other vertebrates (e.g., Noden, 1991). However, because little differentiation of fore- and midbrain regions occurs at this stage, it is difficult to assess the contribution of these regions to the neural crest in marsupials.

Migration of the neural crest was further examined using an antibody to Distal-less proteins. These proteins, produced by genes of the mammalian *Dlx* family, bind to a number of cell types, including migrating neural crest (Robinson and Mahon, 1994; Panganiban et al., 1995; Hanken et al., 1997). This antibody is not an exclusive marker of neural crest, but it does stain migrating neural crest and allows comparison of neural crest migration in marsupials and eutherians relative to other tissues (Fig. 4). Apparently, relative to neural tube development, significantly more neural crest occurs in the branchial

arch region in *Monodelphis* than in *Mus*. For example, in both the 10- to 12-somite and 16-somite stages in *Mus* (Figs. 4B, D) the neural tube is considerably advanced relative to *Monodelphis* (Figs. 4A, C) yet the relative size of the first and second arches is much smaller in *Mus*. In particular, little or no accumulation of neural crest is apparent in the maxillary region in *Mus*. Analysis of the preliminary data suggests a number of features of the pattern of neural crest migration in marsupials. In marsupials neural crest seems to migrate at a time that is earlier, relative to neural tube closure, than in eutherians, or other amniotes (and indeed, apparently other vertebrates). In addition, the neural tube seems to differentiate neural crest cells in larger populations relative to allocation to neural structures in marsupials. Finally, differentiation of the hindbrain, the region that supplies much of the neural crest to the branchial arches, seems to be advanced relative to the forebrain in marsupials, so that the major delay in CNS development is concentrated primarily in forebrain structures.

Analysis of these data on early development suggests that the differences between marsupials and placentals in the relative maturation of neural and somatic tissues occur during the early events in tissue differentiation. Therefore, the heterochronies are not shifts in the relative rates of growth or differentiation of terminal structures. These results are consistent with the hypothesis that early development is fairly plastic and may be modified to meet specific demands at a distinctive stage in development (see Raff [1996]).

THE PHYLOGENETIC ORIGINS OF HETEROCHRONY

Thus far I have considered two clades—eutherians and metatherians. Although I have implied that the marsupial condition is derived, I have not yet provided the evidence. Below, the patterns observed in marsupials and placentals first will be compared with those of nonmammalian amniotes. I will then discuss preliminary data on early development in monotremes.

Early Development of Amniotes

Marsupial development, relative to that of eutherians, was shown above to be characterized by at least three major sets of heterochronies. First, a relative delay occurs in differentiation of the CNS and in particular in the forebrain region. Second, the differentiations of the branchial arch and facial regions are advanced. These shifts seem to be effected in part by shifting forward the relative timing of neural crest differentiation and migration. Third, not discussed in detail above, is the existence in marsupials of an extreme rostral–caudal gradient of development. Although to some degree a rostral–caudal gradient exists in eutherians, so that at a given stage the forelimb is advanced relative to the hind limb, this gradient is extreme in marsupials (Fig. 5). For example, this gradient is reflected by the relative differentiation of the somites, where in marsupials posterior segments develop relatively late. However, the most striking expression of this gradient is the relative development of the fore- and hind limb buds. In marsupials the forelimb bud is massive at a time when the hind limb bud is not yet present.

These three features may be defined as three character complexes (each of which contains a multitude of individual characters) that may be examined in a broader phylogenetic context. In Figure 6 early embryos of a chicken (*Gallus*) and snapping turtle (*Chelydra*), are compared with those of *Monodelphis* and *Mus*. Eutherians share with the nonmammalian amniotes the advancement of the neural tube, the relatively small branchial arches, and the relative similarity of the rate of fore- and hind limb development. In each, the marsupial condition is quite distinct, and must be interpreted as derived. Therefore, in this context, placentals possess what must be taken as the primitive amniote condition.

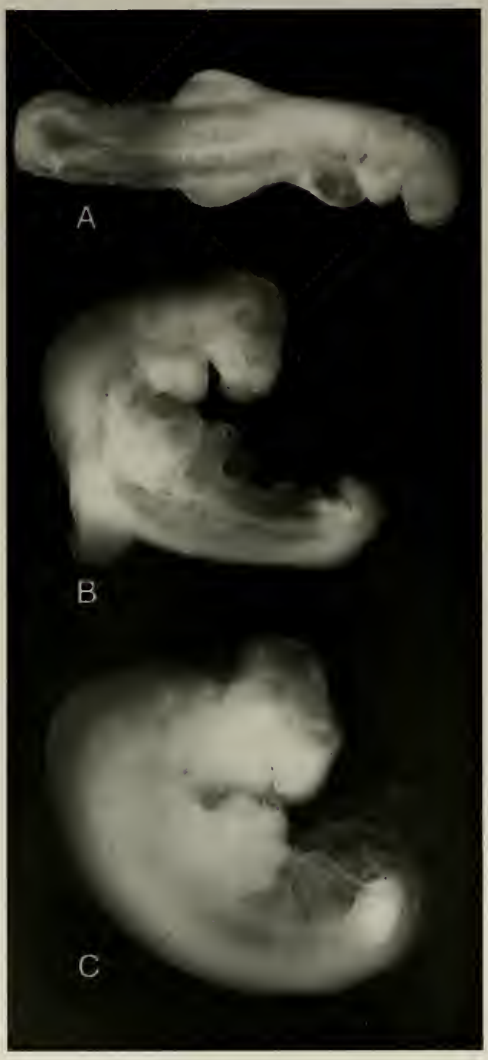

Figure 5. Three stages of development in *Monodelphis domestica*: (A) approximately 11 days of gestation; (B) approximately 12 days of gestation; (C) approximately 13 days of gestation. Note that in each specimen the anterior part of the body is greatly advanced relative to the posterior in size and relative degree of differentiation. In particular, the forelimb is highly advanced relative to the hind limb at all stages.

Comparisons Across Mammalia

To assess the condition at the node Mammalia, information on monotremes, the third major clade of extant mammals, is needed. Clear possession by monotremes of the derived elements of marsupial development would be parsimoniously interpreted as a shared derived resemblance. On the other hand, resemblance of monotremes to the eutherian condition (which is shared with nonmammalian amniotes) would further highlight the derived and specialized nature of marsupial development and reproduction.

Few monotreme embryos are available for study. Most are in the Hill Collection, part of the Hubrecht Comparative Embryology Laboratory. Preliminary evaluation of some of this material indicates that monotremes exhibit a mosaic of marsupiallike and placentallike developmental characters. First, monotremes share with marsupials and nonmammalian amniotes many primitive characteristics of the earliest embryo. For example, all develop as a flat blastodisc on a large yolk, in a manner that is quite distinct from that of eutherians (Hughes, 1993). In addition to these shared primitive characters of early development in marsupials and monotremes, monotremes and marsupials share some derived characters. For example, early in development in monotremes the branchial arches apparently are accelerated relative to the neural tube.

Somewhat later in development, monotremes seem to resemble eutherians more closely. Figure 7 shows sections of embryonic *Monodelphis* and *Mus*, and a prehatching *Ornithorhynchus* (platypus) embryo. In order to define an equivalent landmark, they are matched for the same relative stage of development of the eye. In *Mus*, the telencephalon is differentiated as distinct hemispheres and cell proliferation is well underway in both the telencephalon and diencephalon. However, the cells that will form the cartilages, bones, and muscles of the face show little or no evidence of condensation or differentiation. In contrast, in *Monodelphis* the telencephalon has just begun evagination (not shown in this section) but little or no proliferation of cells has occurred in either the telencephalon or diencephalon. Yet, at this stage cartilage is fully differentiated

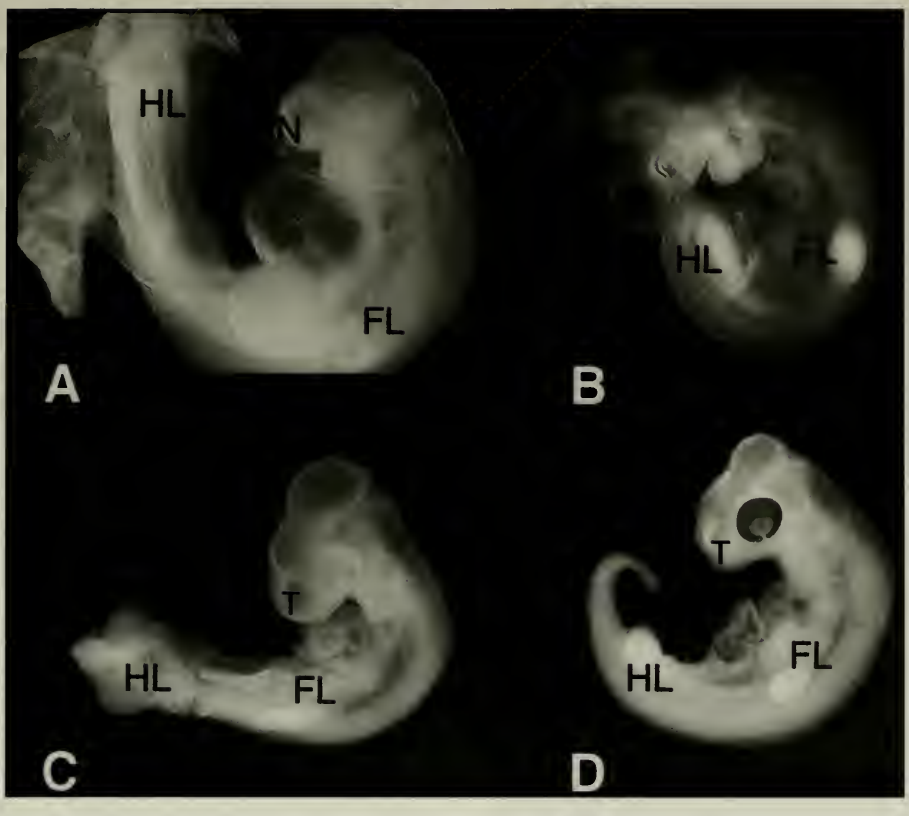

Figure 6. Embryos of (A) *Monodelphis*; (B) *Mus*; (C) *Gallus*; and (D) *Chelydra*. Note that in (B) through (D) the forelimb bud (FL) and hind limb bud (HL) are approximately the same size; in (A) the forelimb bud is massive, whereas the hind limb is not yet at the bud stage. Further note that in (B) through (D) the telencephalon (T), as well as the other regions of the brain are recognizable as distinct swellings; no such divisions yet exist in (A). Finally note that the branchial arches and frontonasal region (N) are massive in (A), and relatively small in the other taxa.

and present in the nasal and basicranial regions; bone is present in the dentary, premaxilla, and maxilla; and the tongue musculature has differentiated (see Smith [1994, 1997]). The *Ornithorhynchus* embryo is intermediate between these conditions, although it is more similar to the eutherian than metatherian condition. The major subdivisions are present in the neural tube and proliferation of the neuroepithelium is well underway in both the telencephalon and diencephalon, yet like eutherians no cartilage, bone, or muscle is present. Therefore, monotremes do not exhibit the same degree of advancement of cranial musculoskeletal tissues as marsupials.

Until more monotreme material is obtained and analyzed, the issue of the condition at the node Mammalia is obscure. Monotremes apparently share many primitive characters with marsupials, as well as some derived features of early development. However, indication also exists that aspects of the developmental trajectory of monotremes resemble that of eutherians (and nonmammalian amniotes). Understanding the mosaic of patterns is essential to our efforts to reconstruct the phylogenetic relations of mammals and model the

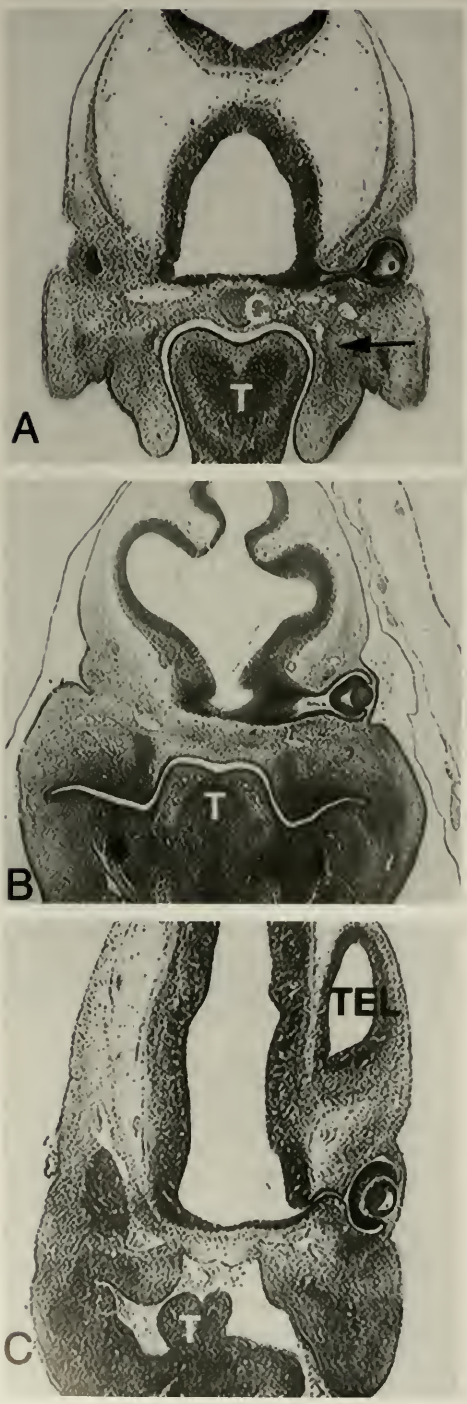

origins of mammalian developmental adaptations.

DISCUSSION

Developmental Plasticity and Conservation

The processes that distinguish marsupial and placental mammals begin at the earliest point in the differentiation of tissues of the craniofacial region. They involve fundamental shifts in early patterning events, and comprise changes in a complex series of events. These changes may be traced back to the appearance of the neural plate, where at this stage large numbers of cells differentiate into migratory neural crest cells, rather than neural tissues. Within the neural tube the hindbrain differentiates early and the midbrain and forebrain are delayed. In addition, a localized acceleration of somitic differentiation occurs in the cervical and upper thoracic regions and a marked delay occurs in caudal somites. The distinction is not a simple shifting forward in time, or speeding up the rate of development of a few features, nor is it due to the establishment of a simple anterior–posterior gradient of acceleration along the body axis. The changes involve multiple advancements and delays of sets of cells, tissues, and organs, within and between regions.

Developmental differences between mar-

←

Figure 7. Sections through the head of (A) *Monodelphis*; (B) *Ornithorhynchus*; (C) *Mus*. Specimens were chosen for approximate match in the relative development of the eye. In *Monodelphis* the neural tube is at an early stage with no significant proliferation of the neural epithelium (although the telencephalon has evaginated—not visible in this section). However, at this time the maxillary, dentary, and premaxillary bones have begun ossification; cartilage is present in the basisphenoid and basioccipital regions; and muscle has differentiated in the tongue. In *Mus* the telencephalon is evaginated, and significant proliferation of neural epithelium has occurred in all regions of the brain, but no cartilage, bone, or muscle have begun differentiation. *Ornithorhynchus* resembles *Mus*: no bone, muscle, or cartilage are present, yet the neural epithelium has started proliferation. However, unlike *Mus*, condensations for bones, muscles, and cartilages apparently have been initiated. Key: C, connective tissue in basicranium; TEL, telencephalon; arrow, ossification in the maxillary bone; T, tongue.

supials and placentals thus are not late changes or terminal additions to a conservative mammalian developmental program. Little evidence exists that development in the two groups of therians can be characterized simply as two ends of a continuum. The developmental trajectory in marsupials is highly modified from very early stages in order to produce a specific adaptive configuration of the neonate. This suggests that development, even at its earliest stages, is highly plastic.

The observation of significant early plasticity, even in animals in which the adults are quite similar, is important for understanding the ways in which development and evolution interact. If it is common for early development to be shifted in fundamental ways, with little change in adult structure, then the degree to which developmental processes impose constraints on the generation of form may have been overestimated. These issues, on relative conservation or plasticity of development, and therefore the possible severity of developmental constraints, can only be resolved by studies that are both broad phylogenetically and detailed developmentally (e.g., Richardson et al., 1977; Hall, 1984; Wray and Raff, 1991; Hanken et al., 1992, 1997; Swalla et al., 1993; Richardson, 1995; Olsson and Hanken, 1996; Raff, 1996; Lowe and Wray, 1997; Smith, 1997).

Evolution of Mammalian Development

Comparative patterns of development in marsupials and placentals can be mapped in relation to two outgroups. When monotremes are added to the comparison, very preliminary observations suggest that the primitive condition for mammals is somewhat intermediate, but probably is characterized by an altricial neonate and an early shift in the relative development of branchial arches relative to neural tissue. However, when mammals are compared with nonmammalian amniotes, the marsupial condition appears highly derived, and the pattern seen in eutherians closely resembles the outgroup, or primitive condition.

This set of observations implies one of three scenarios. First, it is possible that the primitive mammalian developmental condition was monotreme- or marsupiallike, and the resemblance of placentals to other amniotes is an evolutionary reversion. However, it must be emphasized that these are not simple shifts in growth rates of terminal structures, but instead changes in the early patterning of multiple systems. Because of the complexity of the characters, this is not a parsimonious hypothesis. Further, if this scenario is true, then several vital questions remain unanswered. Are the shared characters of marsupials and monotremes reflective of the initial adaptations of mammalian reproduction? If so, why did development change so radically in response to the initial mammalian reproductive pattern? Did this primitive reproductive pattern place the constraints on embryo resource allocation hypothesized above or are other factors in operation? Finally, why did eutherian development revert to what appears to be a primitive amniote pattern?

Second, it is possible that marsupials and monotremes share derived characters relative to eutherians + nonmammalian amniotes. This pattern would provide support for the recently revived Marsupionta, a hypothesized monophyletic group consisting of marsupial and monotreme mammals (e.g., Gregory, 1947). The existence of the Marsupionta has been supported recently by molecular data (i.e., Janke et al., 1996, 1997; Penny and Hasegawa, 1997; Kirsch and Mayer, 1998); however, virtually all morphologic and paleontological evidence firmly supports the Theria (e.g., Crompton, 1980; Rowe, 1988; Jenkins, 1990; Hopson and Rougier, 1993; Wible and Hopson, 1993; Zeller, 1993; Kirsch and Mayer, 1998). Finally, it is possible that the derived conditions that marsupials and monotremes share are independently derived. As I have argued above, this is a complex series of characters, and thus

such convergence would involve complex series of convergent changes.

The resolution of the relative merit of these scenarios requires more research on development in a variety of animals, in particular monotremes. Focus on two issues—the degree to which marsupials and monotremes share derived characters, and the complexity of the developmental processes involved—will help to assess the likelihood of reversion or convergence in the kinds of characters and processes discussed here.

To conclude, the patterns of development described here allow a number of generalizations about the evolution of mammalian reproductive strategies. First, marsupials are not simply primitive with regard to eutherians, at least in the context of amniotes as a whole. Early development in marsupials is derived when compared with other amniotes. Second, early development is quite distinct in marsupials, so that the entire developmental trajectory in marsupial and placental mammals differs. These two sets of observations seem to refute the hypothesis that marsupials and placentals are merely two ends of a continuum. The developmental data support the hypotheses that marsupials and placentals have followed two distinct paths, each derived in its own right. I hope that further detailed information will provide information on the most likely state at the node Mammalia and may allow the specific functional correlates of monotreme, marsupial, and placental developmental patterns to be assessed. Analysis of these data may help resolve phylogenetic issues as well as further efforts to reconstruct the evolution of mammalian reproduction.

ACKNOWLEDGMENTS

I thank Drs. J. Hanken, W. M. Kier, and J. A. W. Kirsch for comments; G. Panganiban for the antibody to *dll*; Alex van Nievelt for comments and technical support; the curators at the Hubrecht Comparative Embryology Collection at the National Laboratory of Developmental Biology, Utrecht, the Netherlands, and the Cornell University Comparative Embryology Collection, Ithaca, New York, for allowing me access to specimens in their care; and National Science Foundations grants IBN 9407616 and 9816985 for support. Finally, I wish to express particular gratitude to Dr. A. W. Crompton for his influence on me during my career, and his numerous contributions to our understanding of vertebrate, and particularly mammalian, evolution, function, and morphology.

LITERATURE CITED

ATCHLEY, W. R., AND B. K. HALL. 1991. A model for development and evolution of complex morphological structures. Biological Reviews, **66:** 101–157.

CHEEK, D. B. 1975. Fetal and Postnatal Cellular Growth. New York: John Wiley and Sons. xii + 538 pp.

CLARK, C. T., AND K. K. SMITH. 1993. Cranial osteogenesis in *Monodelphis domestica* (Didelphidae) and *Macropus eugenii* (Macropodidae). Journal of Morphology, **215:** 119–149.

CROMPTON, A. W. 1980. Biology of the earliest mammals, pp. 1–12. *In* K. Schmidt-Nielsen, L. Bolis, and C. R. Taylor (eds.), Comparative Physiology: Primitive Mammals. Cambridge, United Kingdom: Cambridge University Press. xiv + 196 pp.

DHOPESHWARKAR, G. A. 1983. Nutrition and Brain Development. New York: Plenum Press. viii + 326 pp.

DOBBING, J. 1972. Vulnerable periods in brain development, pp. 9–20. *In* K. Elliot and J. Knight (eds.), Lipids, Malnutrition and the Developing Brain: Ciba Foundation Symposium. Amsterdam: Elsevier. viii + 326 pp.

DODGE, P. R., A. L. PRENSKY, AND R. D. FEIGIN. 1975. Nutrition and the Developing Nervous System. St. Louis, Missouri: C. V. Mosby Company. xvi + 538 pp.

DUNLOP, L.-L., AND B. K. HALL. 1995. Relationships between cellular condensation, preosteoblast formation and epithelial-mesenchymal interactions in initiation of osteogenesis. International Journal of Developmental Biology, **39:** 357–371.

FILAN, S. L. 1991. Development of the middle ear region in *Monodelphis domestica* (Marsupialia, Didelphidae): marsupial solutions to early birth. Journal of Zoology, London, **225:** 577–588.

GEMMELL, R. T., AND L. SELWOOD. 1994. Structural development in the newborn marsupial, the stripe-faced dunnart, *Sminthopsis macroura*. Acta Anatomica, **149:** 1–12.

GREGORY, W. K. 1947. The monotremes and the palimpsest theory. Bulletin of the American Museum of Natural History, **88:** 1–52.

Grüneberg, H. 1963. The Pathology of Development. A Study of Inherited Skeletal Disorders in Animals. New York: John Wiley and Sons. xiv + 309 pp.

Hall, B. K. 1984. Developmental processes underlying heterochrony as an evolutionary mechanism. Canadian Journal of Zoology, **62:** 1–7.

———. 1987. Tissue interactions in the development and evolution of the vertebrate head, pp. 215–259. *In* P. F. A. Maderson (ed.), Developmental and Evolutionary Aspects of the Neural Crest. New York: Wiley-Interscience. xiv + 394 pp.

———. 1991. Cellular interactions during cartilage and bone development. Journal of Craniofacial Genetics and Developmental Biology, **11:** 238–250.

Hall, B. K., and S. Hörstadius. 1988. The Neural Crest. London: Oxford University Press. viii + 303 pp.

Hall, B. K., and T. Miyake. 1992. The membranous skeleton: the role of cell condensations in vertebrate skeletogenesis. Anatomy and Embryology, **186:** 107–124.

———. 1995. Divide, accumulate, differentiate: cell condensation in skeletal development revisited. International Journal of Developmental Biology, **39:** 881–893.

Hanken, J., D. H. Jennings, and L. Olsson. 1997. Mechanistic basis of life-history evolution in anuran amphibians: direct development. American Zoologist, **37:** 160–171.

Hanken, J., M. W. Klymkowsky, C. H. S. D. W. Summers, and N. Ingebrigtsen. 1992. Cranial ontogeny in the direct-developing frog, *Eleutherodactylus coqui* (Anura: Leptodactylidae) analyzed using whole-mount immunohistochemistry. Journal of Morphology, **211:** 95–118.

Hayssen, V., R. C. Lacy, and P. J. Parker. 1985. Metatherian reproduction: transitional or transcending? American Naturalist, **126:** 617–632.

Herschkowitz, N. 1989. Brain development and nutrition, pp. 297–304. *In* P. Evrard and A. Minkowski (eds.), Developmental Neurobiology. New York: Vevey/Raven Press. xix + 315 pp.

Hetzel, B. S., and R. M. Smith. 1981. Fetal Brain Disorders. Amsterdam: Elsevier/North Holland. xiii + 489 pp.

Hill, J. P., and W. C. O. Hill. 1955. The growth stages of the pouch young of the native cat (*Dasyurus viverrinus*) together with observations on the anatomy of the newborn young. Transactions of the Zoological Society, London, **28:** 349–453.

Hill, J. P., and K. M. Watson. 1958. The early development of the brain in marsupials; preliminary communication. Journal of Anatomy, **92:** 493–497.

Hopson, J. A., and G. W. Rougier. 1993. Braincase structure in the oldest known skull of a therian mammal: implications for mammalian systematics and cranial evolution. American Journal of Science, **293:** 268–299.

Hughes, R. L. 1993. Monotreme development with particular reference to the extraembryonic membranes. Journal of Experimental Zoology, **266:** 480–494.

Hughes, R. L., and L. S. Hall. 1988. Structural adaptations of the newborn marsupial, pp. 8–27. *In* C. H. Tyndale-Biscoe and P. A. Janssens (eds.), The Developing Marsupial. Models for Biomedical Research. Berlin: Springer. vii + 245 pp.

Janke, A., N. J. Gemmell, G. Feldmaier-Fuchs, A. Vhaeseler, and S. Paabo. 1996. The mitochondrial genome of a monotreme—the platypus. Journal of Molecular Evolution, **42:** 153–159.

Janke, A., X. Xu, and U. Arnason. 1997. The complete mitochondrial genome of the wallaroo (*Macropus robustus*) and the phylogenetic relationship among Monotremata, Marsupialia and Eutheria. Proceedings of the National Academy of Sciences, **94:** 1276–1281.

Jenkins, F. A., Jr. 1990. Monotremes and the biology of Mesozoic mammals. Netherlands Journal of Zoology, **40:** 5–31.

Kirsch, J. A. W. 1977a. Biological aspects of the marsupial–placental dichotomy: a reply to Lillegraven. Evolution, **31:** 898–900.

———. 1977b. The six-percent solution: second thoughts on the adaptedness of the Marsupialia. American Scientist, **65:** 276–288.

Kirsch, J. A. W., and G. C. Mayer. 1998. The platypus is not a rodent: DNA hybridisation, amniote phylogeny, and the palimpsest theory. Philosophical Transactions of the Royal Society, Series B, **353:** 1221–1237.

Klima, M. 1987. Early development of the shoulder girdle and sternum in marsupials (Mammalia: Metatheria). Advances in Anatomy, Embryology, and Cell Biology, **109:** 1–91.

Le Douarin, N. 1982. The Neural Crest. Cambridge, United Kingdom: Cambridge University Press. xi + 259 pp.

Lee, A. K., and A. Cockburn. 1985. Evolutionary Ecology of Marsupials. Cambridge, United Kingdom: Cambridge University Press. viii + 274 pp.

Lillegraven, J. A. 1975. Biological considerations of the marsupial–placental dichotomy. Evolution, **29:** 707–722.

Lillegraven, J. A., S. D. Thompson, B. K. McNab, and J. L. Patton. 1987. The origin of eutherian mammals. Biological Journal of the Linnean Society, **32:** 281–336.

Lowe, C. J., and G. A. Wray. 1997. Radical alterations in the roles of homeobox genes during echinoderm evolution. Nature, **389:** 718–721.

Maier, W. 1987. The ontogenetic development of the orbitotemporal region in the skull of *Monodelphis domestica* (Didelphidae, Marsupialia), and the problem of the mammalian alisphenoid, pp. 71–90. *In* H.-J. Kuhn and U. Zeller (eds.), Mor-

phogenesis of the Mammalian Skull. Hamburg, Germany: Verlag Paul Parey. 144 pp.

———. 1993. Cranial morphology of the therian common ancestor, as suggested by the adaptations of neonatal marsupials, pp. 165–181. *In* F. S. Szalay, M. J. Novacek, and M. C. McKenna (eds.), Mammal Phylogeny—Mesozoic Differentiation, Multituberculates, Monotremes, Early Therians and Marsupials. New York: Springer. x + 249 pp.

Miyake, T., A. M. Cameron, and B. K. Hall. 1996. Stage-specific onset of condensation and matrix deposition for Meckel's and other first arch cartilages in inbred C57Bl/6 mice. Journal of Craniofacial Genetics and Developmental Biology, **16:** 32–47.

———. 1997. Stage-specific expression patterns of alkaline phosphatase during development of the first arch skeleton in inbred C57BL/6 mouse embryos. Journal of Anatomy, **190:** 239–260.

Morriss-Kay, G., E. Ruberte, and Y. Fukuishi. 1993. Mammalian neural crest and neural crest derivatives. Annals of Anatomy, **175:** 501–507.

Nelson, J. E. 1988. Growth of the brain, pp. 86–100. *In* C. H. Tyndale-Biscoe and P. A. Janssens (eds.), The Developing Marsupial. Berlin: Springer. vii + 245 pp.

Nichols, D. H. 1981. Neural crest formation in the head of the mouse embryo as observed using a new histological technique. Journal of Embryology and Experimental Morphology, **64:** 105–120.

———. 1986. Formation and distribution of neural crest mesenchyme to the first pharyngeal arch region of the mouse embryo. American Journal of Anatomy, **176:** 221–231.

———. 1987. Ultrastructure of neural crest formation in the midbrain/rostral hindbrain and periotic hindbrain regions of the mouse embryo. American Journal of Anatomy, **179:** 143–154.

Noden, D. M. 1983. The role of the neural crest in patterning of avian cranial skeletal, connective, and muscle tissues. Developmental Biology, **96:** 144–165.

———. 1987. Interactions between cephalic neural crest and mesodermal populations, pp. 89–119. *In* P. F. A. Maderson (ed.), Developmental and Evolutionary Aspects of the Neural Crest. New York: Wiley-Interscience. xiv + 394 pp.

———. 1991. Vertebrate craniofacial development: the relation between ontogenetic process and morphological outcome. Brain, Behavior and Evolution, **38:** 190–225.

Novacek, M. J. 1990. Morphology, paleontology and the higher clades of mammals, pp. 507–543. *In* H. H. Genoways (ed.), Current Mammalogy. Vol. 2. New York: Plenum. xviii + 577 pp.

Nunn, C. L., and K. K. Smith. 1998. Statistical analyses of developmental sequences: the craniofacial region of marsupial and placental mammals. American Naturalist, **152:** 82–101.

Olsson, L., and J. Hanken. 1996. Cranial neural-crest migration and chondrogenic fate in the Oriental fire-bellied toad *Bombina orientalis*: defining the ancestral pattern of head development in anuran amphibians. Journal of Morphology, **229:** 105–120.

Panganiban, G., A. Sebring, L. Nagy, and S. B. Carroll. 1995. The development of crustacean limbs and the evolution of arthropods. Science, **270:** 1363–1366.

Parker, P. 1977. An ecological comparison of marsupial and placental patterns of reproduction, pp. 269–285. *In* B. Stonehouse and D. Gilmore (eds.), The Biology of Marsupials. London: Macmillian Press, Ltd. vii + 486 pp.

Penny, D., and M. Hasegawa. 1997. The platypus put in its place. Nature, **387:** 549–550.

Peterson, P. E., T. N. Blankenship, D. B. Wilson, and A. G. Hendrickx. 1996. Analysis of hindbrain neural crest migration in the long-tailed monkey (*Macaca fascicularis*). Anatomy and Embryology, **194:** 235–246.

Raff, R. A. 1996. The Shape of Life: Genes, Development and the Evolution of Animal Form. Chicago: University of Chicago Press. xxiii + 520 pp.

Renfree, M. B. 1983. Marsupial reproduction: the choice between placentation and lactation, pp. 1–29. *In* C. A. Finn (ed.), Oxford Reviews of Reproductive Biology. Vol. 5. Oxford, United Kingdom: Oxford University Press.

———. 1993. Ontogeny, genetic control, and phylogeny of female reproduction in monotreme and therian mammals, pp. 4–20. *In* F. S. Szalay, M. J. Novacek, and M. C. McKenna (eds.), Mammal Phylogeny—Mesozoic Differentiation, Multituberculates, Monotremes, Early Therians and Marsupials. New York: Springer, x + 249 pp.

———. 1995. Monotreme and marsupial reproduction. Reproduction, Fertility and Development, **7:** 1003–1020.

Richardson, M. K. 1995. Heterochrony and the phylotypic period. Developmental Biology, **172:** 412–421.

Richardson, M. K., J. Hanken, M. L. Gooneratne, C. Pieau, A. Raynaud, L. Selwood, and G. M. Wright. 1997. There is no highly conserved embryonic stage in the vertebrates: implications for current theories of evolution and development. Anatomy and Embryology, **196:** 91–106.

Robinson, G. W., and K. A. Mahon. 1994. Differential and overlapping expression domains of *Dlx-2* and *Dlx-3* suggest distinct roles for *Distal-less* homeobox genes in craniofacial development. Mechanisms of Development, **48:** 199–215.

Rowe, T. 1988. Definition, diagnosis and the origin of Mammalia. Journal of Vertebrate Paleontology, **8:** 241–264.

Sacher, G. A., and E. F. Staffeldt. 1974. Relation of gestation time to brain weight for placental mammals: implications for the theory of verte-

brate growth. American Naturalist, **108:** 593–615.

SÁNCHEZ-VILLAGRA, M. 1999. A Study of Cranial Evolution in Marsupials with Description of New Fossil Forms. Ph.D. thesis. Durham, North Carolina: Duke University. 538 pp.

SERBEDZIJA, G. N., M. BRONNER-FRASER, AND S. E. FRASER. 1992. Vital dye analysis of cranial neural crest cell migration in the mouse embryo. Development, **116:** 297–307.

SHINE, R. 1985. The evolution of viviparity in reptiles: an ecological analysis, pp. 605–694. *In* C. Gans and F. Billett (eds.), Biology of the Reptilia. Vol. 15, Development B. New York: John Wiley and Sons. x + 731 pp.

SHOEMAKER, W. J., AND F. E. BLOOM. 1977. Effect of undernutrition on brain morphology, pp. 147–192. *In* R. J. Wurtman and J. J. Wurtman (eds.), Nutrition and the Brain. Vol. 2. New York: Raven Press. vi + 313 pp.

SMITH, K. K. 1994. The development of craniofacial musculature in *Monodelphis domestica* (Didelphidae, Marsupialia). Journal of Morphology, **222:** 149–173.

———. 1996. Integration of craniofacial structures during development in mammals. American Zoologist, **36:** 70–79.

———. 1997. Comparative patterns of craniofacial development in eutherian and metatherian mammals. Evolution, **51:** 1663–1678.

SPRINGER, M. S., M. WASSERMAN, J. R. KAVANAGH, A. BURK, M. O. WOODBURNE, D. J. DAO, AND C. KRAJEWSKI. 1998. The origin of the Australasian marsupial fauna and the phylogenetic affinities of the enigmatic monito del monte and marsupial mole. Proceedings of the Royal Society of London, Series B, **265**: 2381–2386.

SWALLA, B. J., K. W. MAKABE, N. SATOH, AND W. R. JEFFERY. 1993. Novel genes expressed differentially in ascidians with alternate modes of development. Development, **119:** 307–318.

TAN, S. S., AND G. M. MORRISS-KAY. 1985. The development and distribution of the cranial neural crest in the rat embryo. Cell Tissue Research, **240:** 403–416.

———. 1986. Analysis of cranial neural crest cell migration and early fates in postimplantation rat chimeras. Journal of Embryology and Experimental Morphology, **98:** 21–58.

TRAINOR, P. A., AND P. P. L. TAM. 1995. Cranial paraxial mesoderm and neural crest cells of the mouse embryo: co-distribution in the craniofacial mesenchyme but distinct segregation in branchial arches. Development, **121:** 2569–2582.

TYNDALE-BISCOE, H., AND M. RENFREE. 1987. Reproductive Physiology of Marsupials. Cambridge, United Kingdom: Cambridge University Press. xiv + 476 pp.

WIBLE, J. R., AND J. A. HOPSON. 1993. Basicranial evidence for early mammal phylogeny, pp. 45–62. *In* F. S. Szalay, M. J. Novacek, and M. C. McKenna (eds.), Mammal Phylogeny—Mesozoic Differentiation, Multituberculates, Monotremes, Early Therians and Marsupials. New York: Springer. x + 249 pp.

WINICK, M. 1976. Malnutrition and Brain Development. New York: Oxford University Press. xv + 169 pp.

———. 1979. Nutrition, Pre- and Postnatal Development. New York: Plenum Press. xx + 496 pp.

WINICK, M., P. ROSSO, AND J. A. BRASEL. 1972. Malnutrition and cellular growth in the brain: existence of critical periods, pp. 200–206. *In* K. Elliot and J. Knight (eds.), Lipids, Malnutrition and the Developing Brain: Ciba Foundation Symposium. Amsterdam: Elsevier. viii + 326 pp.

WRAY, G. A., AND R. A. RAFF. 1991. The evolution of developmental strategy in marine invertebrates. Trends in Ecology and Evolution, **6:** 45–50.

ZELLER, U. 1993. Ontogenetic evidence for cranial homologies in monotremes and therians, with special reference to *Ornithorhynchus,* pp. 95–107. *In* F. S. Szalay, M. J. Novacek, and M. C. McKenna (eds.), Mammal Phylogeny—Mesozoic Differentiation, Multituberculates, Monotremes, Early Therians and Marsupials. New York: Springer. x + 249 pp.

SKIN IMPRESSIONS OF TRIASSIC THEROPODS AS RECORDS OF FOOT MOVEMENT

STEPHEN M. GATESY[1]

ABSTRACT. A sample of 20 Late Triassic theropod footprints from Greenland preserves evidence of pedal integument. Skin impressions range from dimples, valleys, peaks, and ridges, to parallel striations. These features were created by the scale-covered digital pads as the skin–sediment interface was broken. Therefore, skin impressions document aspects of both the direction and timing of skin motion, allowing foot movements during the stance phase of locomotion to be inferred. Skin impressions represent a previously unrecognized source of functional data for reconstructing theropod locomotion.

INTRODUCTION

Dinosaur footprints vary widely in the amount of detail they preserve. The majority of tracks show diffusely contoured imprints of each digit, although some are more clearly defined by digital pad and claw impressions. Very few preserve the finest level of detail—evidence of integumentary structures (Lockley, 1989). Many factors are responsible for the relative rarity of tracks bearing traces of minute features. Almost all of these factors relate to scale, which can range over two orders of magnitude from the entire foot to an individual epidermal tubercle. For example, larger features permanently deform substrates of widely differing properties, whereas smaller features require much more stringent conditions to leave their mark (Allen, 1997; Currie et al., 1991). Imprints of gross structures are also more likely to be preserved and discovered as underprints or overprints (Langston, 1986; Lockley, 1989). In contrast, fine details are only visible if the "true" track survives and is directly exposed. Finally, large imprints are more resistant to erosion than are small ones, both before burial and after exposure.

Reports of skin impressions in fossil dinosaur tracks are uncommon in the ichnological literature. Classic works include only brief references to "papillae", "tubercles", and "pits" (Hitchcock, 1858; Lull, 1953), and one illustration (Hitchcock, 1858, plate X). "Striations", "striae", and "furrows" are also described in passing (Baird, 1957; Hitchcock, 1858; Woodhams and Hines, 1989). The most thoroughly documented pedal skin imprints have been attributed to ornithischians (Currie et al., 1991). In this study I report on Late Triassic theropod tracks from Greenland that preserve evidence of integumentary detail. I analyze skin impressions as records of foot movement and discuss their contribution to reconstructing theropod locomotion.

MATERIALS AND METHODS

In 1989, extensive horizons containing dinosaur tracks were discovered in the Ørsted Dal Member of the uppermost Fleming Fjord Formation of Jameson Land, East Greenland (Gatesy et al., 1999; Jenkins et al., 1994). These cyclically bedded siliciclastic and carbonate-bearing strata were deposited in an extensive rift lake system of Norian–Rhaetic age (Clemmensen et al., 1998). Herein, I report on 20 tracks with skin impressions that were collected from four localities (see map in Jenkins et al., 1994): eight prints at Tait

[1] Department of Ecology and Evolutionary Biology, Box G, Brown University, Providence, Rhode Island 02912.

Bjerg (L layer), two at Macknight Bjerg (S layer), one at Sydkronen (SS layer), and nine at Wood Bjerg (C layer). These specimens are, with one exception, isolated prints. Individual trackways were either too poorly exposed or impossible to identify because of a high density of similarly sized tracks. Specimens will be housed at the Geological Museum at the University of Copenhagen; herein, temporary identification numbers are used.

All tracks were exposed by natural weathering; excavation and mechanical preparation have proven largely unsuccessful. Original material was collected and analyzed for this study, but silicone (Silastic) or alginate molds were made of one half of the tracks and some were cast in plaster. Impressions on tracks, molds, and casts were studied using a Wild M7-S binocular dissecting microscope and fiber-optic illuminators. An axis drawn along the length of the imprint of digit III was used as a reference to measure the relative mediolateral orientation of features within a track. The distribution of skin imprints within and among specimens was tabulated by dividing each track into 22 subregions (see below, Fig. 3, and Table 1). Unfortunately, it is typically extremely difficult to discern whether a region lacks skin impressions because of a true absence rather than incomplete exposure or localized damage. Therefore, distribution frequencies represent raw percentages that were not adjusted to compensate for differential preservation.

All figures show impressions as if they were made by right feet; left footprints were reversed to ease comparison among tracks. Illustrations of skin impressions (Fig. 1) were made from camera lucida drawings. Stipple density was varied to represent depth, rather than shadow. Track outlines and regions of skin impression were traced over digitized video images. Stereo images of skin impressions (Fig. 2) were created by image processing digitized video images in Adobe Photoshop 2.5. Three-dimensional vectors were modelled and rendered in Studio 8.5 software from Alias|Wavefront using data measured from striations with a protractor and ruler.

RESULTS AND DISCUSSION

Ichnology

Skin impressions are only found in relatively shallow tracks (maximum depth 4–21 mm). All preserve imprints of digital pads and claws, but lack evidence of the manus or hallux (Gatesy et al., 1999; Jenkins et al., 1994). Tracks in the sample range from 15 to 23 cm in length (Table 1; estimated in nearly complete specimens), with a mean of 18.8 ± 2.7 cm (N = 19). Such prints are referable to the ichnogenus *Grallator* (*Anchisauripus*; Hitchcock, 1858; Lull, 1904; Olsen and Galton, 1984), which has been attributed to small to medium-sized theropod dinosaurs (e.g., Farlow and Lockley, 1993; Olsen et al., 1998).

Identification of Skin Impressions

Tracks with skin impressions were recognized in the field by their distinctive reticulate texture (Figs. 1, 2). The floor, and less frequently the walls, of digital pad im-

→

Figure 1. Examples of skin impressions in Late Triassic theropod prints from Greenland. Reticulate patterns are found on the floor and walls of digital pad impressions; micromorphology varies from hexagonally arranged dimples (a, L.04) to bumps, ridges, and valleys (b, L.00). Striations are found on the borders of depressions. Entry striations (c, L.01) were formed by scales plowing down and forward in early stance, whereas exit striations (d, L.00) were created as digital pads were withdrawn in late stance. All tracks are drawn as those made by right feet. Shaded areas designate preservation of skin impressions. Illustrations of skin impressions show depth, not shadow; deeper areas are darkly stippled relative to lighter, elevated areas. Textures in a–d are drawn from a perspective perpendicular to the impressed sediment, rather than the horizontal bedding plane.

Scale bar: 5 cm for track outlines and 2 mm for skin impression details.

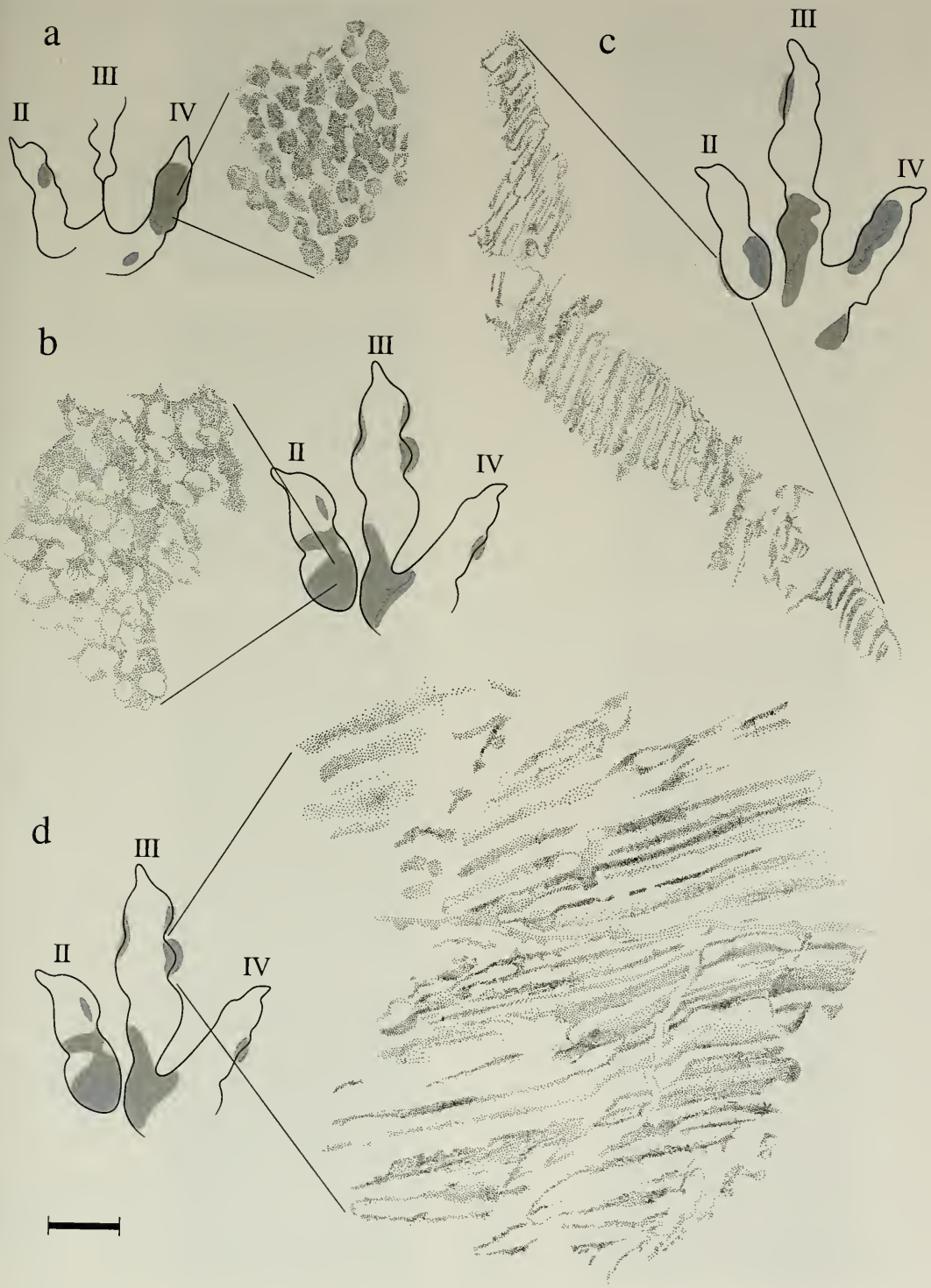
a
II
III
IV
b
II
III
IV
c
II
III
IV
d
II
III
IV

pressions bear structures forming densely packed, loosely hexagonal arrays. The specific microtopography of these arrays is variable within and among tracks. In some, concave dimples are separated by raised laminae (Figs. 1a, 2a). This morphology may represent a relatively accurate mold of convex reticulate scales (Lucas and Stettenheim, 1972) covering the digital pads. In others, arrays are formed from convex peaks of sediment. Between these two extremes are less regular patterns of peaks, ridges, dimples, and troughs (Figs. 1b, 2b). The size of components making up all arrays is relatively consistent, both within and among tracks. Dimples are approximately 1 mm in diameter and peaks are spaced approximately 1 mm apart. These characteristic reticulate patterns are not found on sediment outside of dinosaur tracks.

Along the borders of digital pad depressions, and more rarely within them, are regions bearing parallel grooves. Grooves are spaced 0.5–1.5 mm apart. In some cases these furrowed areas abut reticulate arrays, but many are isolated patches. Grooved sediment is found within parabolic tracts (Figs. 1c, 2c, 3) posterior to pad imprints of digits II and IV. These are likely entry striations that formed as the scale-covered digital pads plowed through the sediment before settling into their deepest position. Similar grooves are located along the medial and lateral walls of the impression of digit III (Figs. 1d, 2d, 3). Such grooves are interpreted as exit striations, which were created by scales scraping the sediment as the digital pads of digit III were lifted from the substrate. In two specimens, claw scrapes and striations sweep posteriorly; these were formed when the foot slipped backward before breaking ground contact (Thulborn and Wade, 1984, 1989).

Distribution of Skin Impressions

Reticulate arrays are found within all nine digital pad depressions (two for II, three for III, and four for IV), as well as in the area around the base of the toes. However, skin impressions are unequally distributed within and among prints; some regions preserve skin imprints much more frequently than others (Fig. 3; Table 1). Arrays produced by the proximal pad of digit II, proximal pad of digit III, and proximal-middle pad of digit IV are present in 60%, 65%, and 70% of the tracks sampled, respectively. Impressions tend to decrease in frequency distally, with the exception of the proximal pad of digit IV. Overall, reticulate imprints of skin are relatively common for each digit (II, 50%; III, 38%; IV, 51%) as well as for the toe base area (50%).

Striations are much less widespread (Fig. 3). Entry striations are lacking from digit III, but present at low frequencies (5–25%) posterior to pad imprints of digits II and IV. The impression of digit III can bear exit striations medially, laterally, or both; medial grooves produced by the withdrawal of the distal pad are most common (20%). Evidence of backward slipping is relatively rare.

The uneven distribution of skin impressions within tracks likely stems from an interaction among several influences. Each portion of every pad depression exhibits skin texture in at least one of the 20 tracks, showing that the entire plantar surface was capable of leaving reticulate arrays. However, the timing or magnitude of pressure could have differentially altered the sediment's cohesiveness and adhesion, affect-

→

Figure 2. Stereophotographs of skin impressions showing variety of reticulate (a, L.04 and b, L.00) and striated (c, L.01 and d, L.00) textures. In all cases the lighting is from the upper left.

Scale bars: 5 mm.

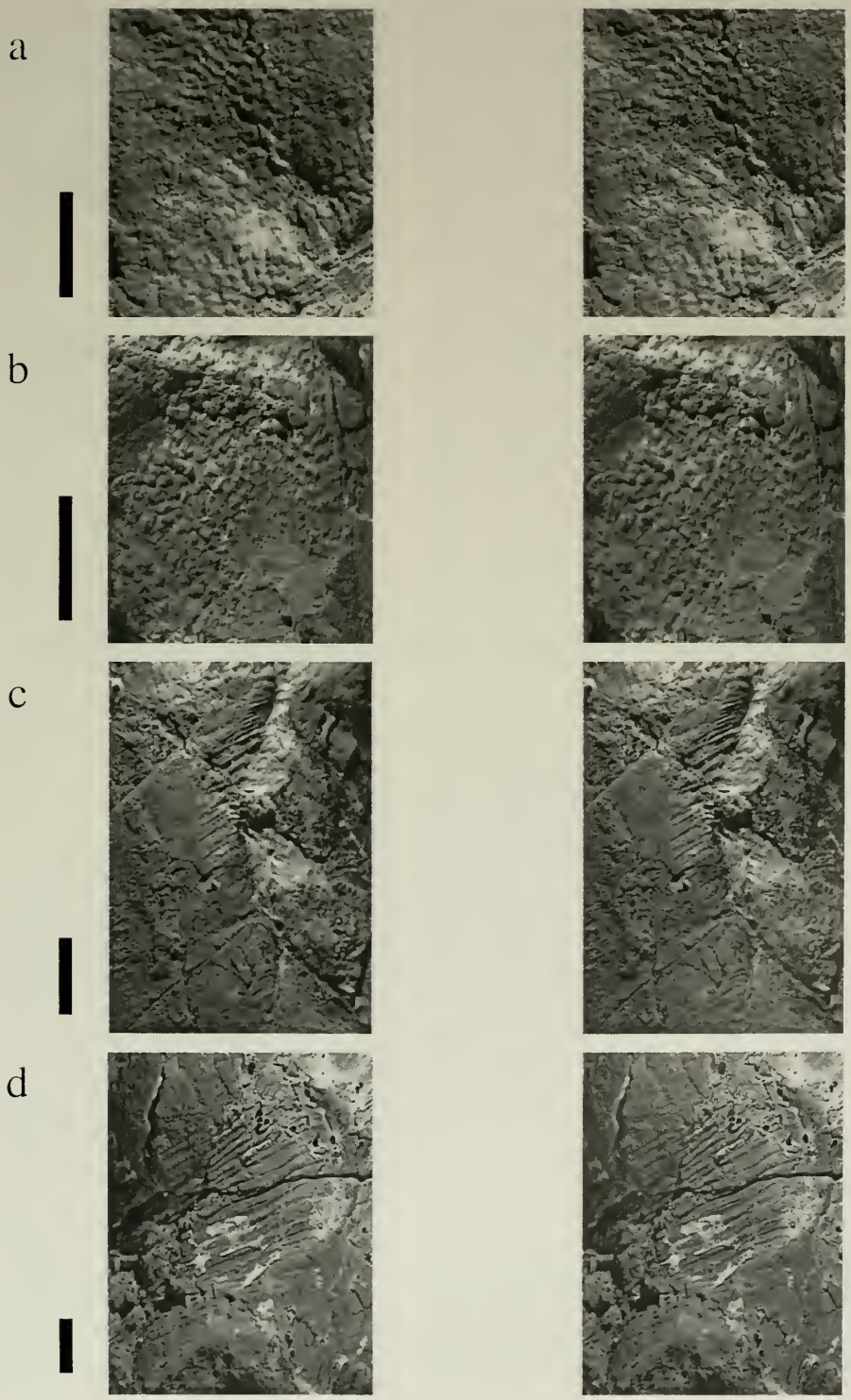
a
b
c
d

Table 1. Distribution of skin impressions in 20 theropod footprints. Presence of reticulate texture (R) and entry or exit striations (S) is indicated for the nine toe pads and the toe base. Entry and exit tracts not bearing striations are designated by t.

Track	Side	Length (cm)	Digit II Proximal	Digit II Distal	Digit III Proximal	Digit III Middle	Digit III Distal	Digit IV Proximal	Digit IV Proximal–Middle	Digit IV Distal–Middle	Digit IV Distal	Toe Base
L.00	L	21	R	R	R	S	S	R t	S	t	t	R
L.01	R	23	R S		R	t	S	S	R t	R S	R	R
L.02	R	21	R	R	R	R	R		R	R	R S	R
L.03	R	16	R	R	R		R	R		R	R	
L.04	R	inc.						R	R	R	R	
L.05	R	20		R				R	R	R	R	
L.06	L?	17			R	R	R		R			
L.07	L	22	R	R S	R			R	R	R	R	
S.01	L	21	R S	R S	R S	R S	R S	R	R S	S		R
S.02	L	18	R	R	R	R			R	R	R	
SS.00	R	19	R	R								
C.I	R	19	S	t	R			t	R t	R t	t	
C.III	R	21	S	t				R t	R			R
C.A	L	18			R			t	R t	R S	R S	R
C.B	R	17	t	t	R	R		t	R t	S	t	R
C.01	R	16	R t	t		R			t			
C.02	R	16	t		R							R
C.03	L	23	R t		R			R	R t	t		R
C.04	R	15	R				S		t	S	t	
C.05	R	15	R t	t					R	R	R	R
Percent of sample			60 20	40 10	65 5	30 10	20 20	40 5	70 10	50 25	45 10	50

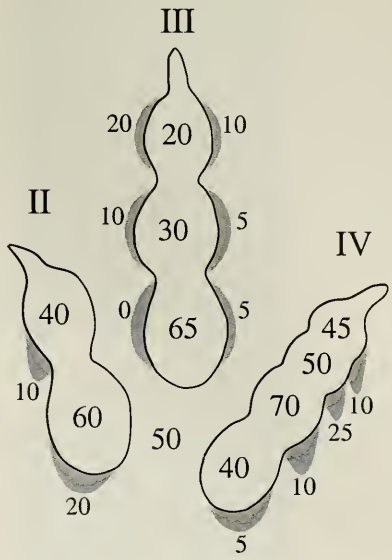

Figure 3. Relative frequency of skin impressions within prints. Numbers show the percentages of the track sample (N = 20) having reticulate arrays or striations in each of 22 subregions. Shaded areas posterior to the impressions of digits II and IV represent entry tracts, many of which bear striations (see Table 1). Shaded areas medial and lateral to the impression of digit III are exit tracts.

ing the likelihood of skin leaving a mark (Currie et al., 1991). Intraprint depth variation may also play a role. The distal portions of each toe often left the deepest, narrowest depressions. Such contour might make skin imprints from distal pads less likely to be freed from overlying matrix by natural erosion. Field identification and collection could impose an additional bias, because a reticulate texture was more easily recognized than entry or exit striations. An analysis of variation within a single trackway could elucidate the relative contribution of these factors, but such data are as yet unavailable from Greenland.

Formation Dynamics

With every step, walking theropods applied forces against the ground. On a receptive substrate, sediment conformed to the plantar surface of the penetrating foot. However, skin impressions were only created as the integument moved off the substrate. If the skin–sediment interface di-

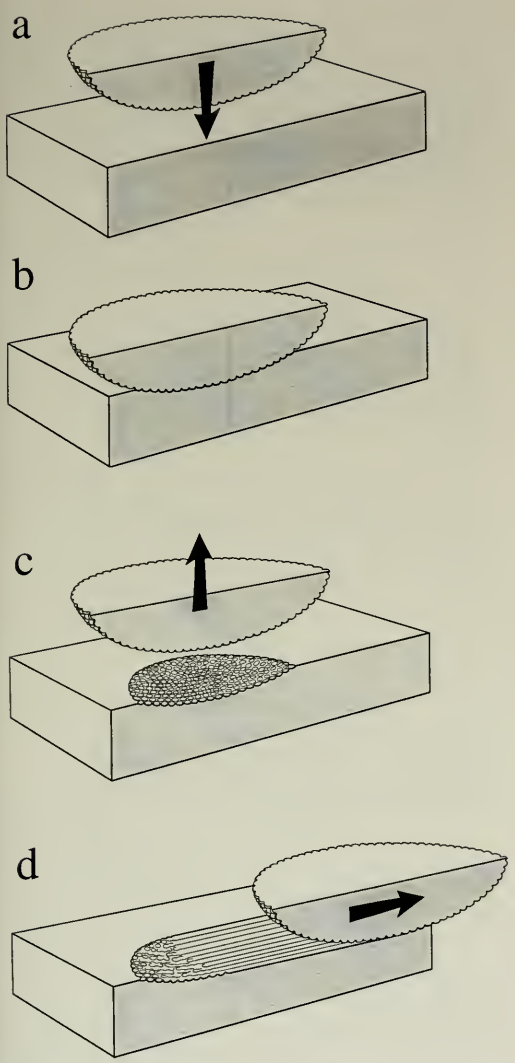

Figure 4. Simplified depiction of skin impression formation. As a section of a digital pad is driven vertically into the ground (a to b), the receptive substrate molds itself to the reticulate scales, creating a skin–sediment interface (b). If the pad is withdrawn at a steep angle, a relatively accurate representation of the integument is exposed (c). In contrast, if the pad plows through the sediment, scales on the skin tangential to the direction of motion will create striations (d). Therefore, skin impressions can act as three-dimensional records of skin movement.

vided cleanly, each subregion of the track would reflect the integumentary structure it last apposed. This perspective, emphasizing the dynamic nature of skin impression formation, has both spatial and temporal connotations.

Motion of the skin relative to the sediment during separation strongly influences skin impression morphology (Fig. 4). This relationship is easily visualized by two examples, both starting with a patch of skin in contact with a receptive substrate (Fig. 4b). If the patch is lifted normal to the skin–sediment interface, it will have a good chance of leaving behind a relatively accurate mold of its integumentary surface (Fig. 4c). Clear impressions of a reticulate scale pattern are indicative of skin withdrawn relatively steeply up and away from the sediment. In contrast, if the patch is dragged through the sediment, its scales will leave behind a series of parallel striations (Fig. 4d). The last scales to contact the substrate will plow furrows along the path of skin movement. Thus, the dynamics of separation allow skin impressions to act as three-dimensional records of integumentary motion.

Time is also represented, because all skin imprints in a track are not formed simultaneously. The moving toes generate skin impressions sequentially as localized subregions of the pedal integument vacate their underlying area of substrate. For the remainder of the discussion, I focus on the breaking of the skin–sediment interface and the formation of skin impressions in specific portions of the track. Based on such evidence, I analyze aspects of theropod foot movement in three periods within the stance phase.

Early Stance: Entry Tracts and Entry Striations

The stance phase of the stride cycle begins with ground contact. In early stance ("touch-down" of Thulborn and Wade, 1989), the area of skin–sediment contact increased as the digital pads penetrated the substrate. However, Triassic theropod feet did not follow a simple vertical path. The convex plantar surface of most digital pads entered the substrate obliquely, forming a teardrop-shaped impression.

Such parabolic entry tracts, primarily produced by digits II and IV, are preserved in 70% of the prints. In 50% of the sample, entry tracts bear striations that were formed as scales plowed through the sediment. Specifically, striations are furrows made by the last scales to vacate the substrate. Such scales are located on those portions of a pad's surface tangential to the direction of penetration (Figs. 4d, 5b). Thus, entry striations are three-dimensional motion vectors, which verify that the digital pads moved down and forward immediately after ground contact.

An oblique penetration is expected if theropods walked using the same general mechanism employed by living tetrapods (e.g., Alexander 1977). A stance limb initially pushes both down and forward against the substrate, causing the animal to decelerate. Under such a loading regime, the direction and distance a theropod's digital pads move after contact depend on substrate consistency. Entry striations reveal that feet penetrated at relatively shallow slopes (Fig. 6). Of the 12 specimens measured, the average slope was only 16°.

Digital pad movements also vary in their mediolateral direction with respect to the long axis of the footprint. Striation orientations vary from −39° (intorted) to +15° (extorted) with respect to the long axis of digit III. Entry striations produced by the proximal pad of digit II are intorted (mean −19°) in all four specimens showing this detail (Fig. 6). If the impression of digit III lies parallel to the theropod's direction of travel, digit II's proximal pad would have moved forward and laterally in early stance. Alternatively, if the entire foot was medially rotated (toed-in) at the time of contact (e.g., Padian and Olsen, 1989; Thulborn and Wade, 1989), the proximal pad of digit II may have slid primarily forwards. The sequence of pad touchdown and relative movement among pads could potentially be recorded in prints with a complete complement of entry striations. Unfortunately, only three prints have striae documenting the entry path of more than one pad. Spreading (abduction) of digits II and IV can be inferred from one print (S.01), but is not clearly supported by another (L.01). Again, trackways bearing multiple prints with skin impressions could test these hypotheses, but await discovery in the Ørsted Dal.

Digit III must have followed a down and forward trajectory similar to digits II and IV, but clear entry tracts are only preserved in a single specimen (C.A). One possible explanation is overprinting, caused by motion nearly parallel to the long axis of digit III in early stance. The distal pad of digit III may have produced an entry tract that was quickly obliterated by the advancing middle pad, which in turn had its entry tract erased by the proximal pad. A similar mechanism could explain the variation in entry tracts and striations made by digits II and IV. Motion of the foot parallel to the long axis of digit III would minimize overprinting in the divergent side digits. For example, two specimens with entry striation angles of −1° (C.B) and −2° (C.I) preserve entry tracts from all six pads of digit II and IV. In contrast, a more oblique trajectory would tend to obliterate all but the most proximal entry tract of a digit oriented parallel to foot movement. A specimen (C.A) showing entry striations made by distal pads of digit IV angled medially shows entry tracts from the middle and distal pads of digit III, but very little signs of entry from digit II. In this case, the foot was likely laterally rotated (toed-out) at impact, possibly during a sharp turn.

Mid Stance: Pad Deformation

As the limb force increased and became more vertically oriented, each digital pad ceased moving forward. Loading would have caused a theropod's pads to deform and settle into their mid stance ("weight-bearing" of Thulborn and Wade, 1989) positions (Figs. 5a–c). Although the amount of deformation that took place is difficult to quantify, the presence of at least some vertical compression and horizontal expan-

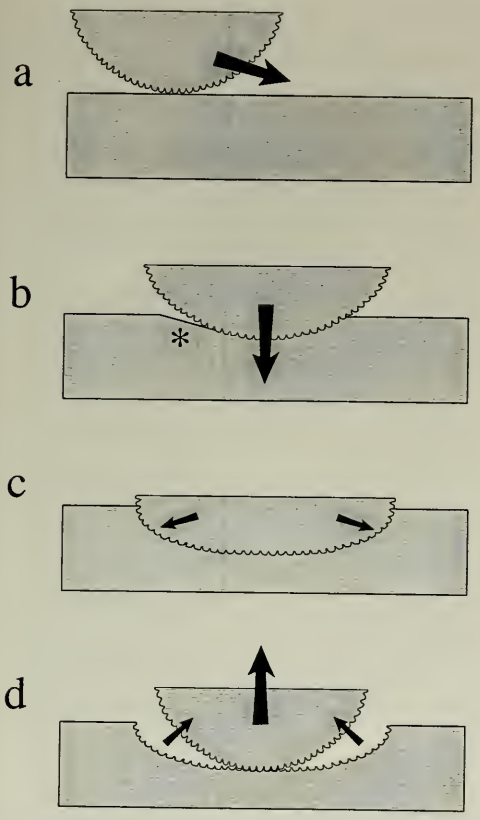

Figure 5. Effects of pad deformation and recoil on skin impressions. A digital pad entering the substrate obliquely in early stance (a to b) creates an entry tract with entry striations (*). In mid stance the limb drives the pad down vertically (b to c), flattening the pad and obliterating the entry tract as new skin is forced against the substrate (small arrows). In late stance the load is reduced, allowing the viscoelastic pad to return to its unflattened shape before liftoff (d). Peripheral skin is peeled off at a relatively steep angle (small arrows), leaving reticulate arrays. In most cases the pad can exit its depression without contacting the walls. Pad deformation has been exaggerated for clarity.

sion can be inferred. The viscoelastic paw pads of living mammals have been found to reduce impact forces (Alexander et al., 1986); avian digital pads also deform in early stance (Gatesy, personal observation).

In Triassic theropods, the profile of digital pad depressions in Greenlandic tracks is direct evidence of pad flattening. Some prints have almost horizontal floors, despite having entry tracts with a fluted, U-shaped profile. Such impressions are best explained by pad deformation, rather than toes with a flat plantar surface (Lockley and Hunt, 1994: 38). As a pad compressed, new skin around the periphery would contact the substrate. This increase in depression diameter could partially or even completely obliterate entry tracts and striations made earlier in stance (Figs. 5b, c). In tracks retaining such traces of entry, the pads must have plowed forward far enough to escape mid-stance overprinting. Thus, pad deformation may explain the relative size of entry tracts from digits II and IV and their absence in some prints.

Movements of the proximal pad of digit III, for which an entry tract has never been found, are difficult to infer. One possibility is that this pad made an entry tract that it subsequently overprinted during mid-stance deformation. Alternatively, the proximal pad of digit III may not have contacted the substrate in early stance. The pad could have descended and deformed only after forward motion of the foot was complete. The toe base region, which also never shows signs of oblique entry, likely delayed contact as well. Thus, mid stance was a period during which skin contact was maximized, leading to the destruction of earlier skin impressions rather than the creation of new ones.

Late Stance: Reticulate Arrays, Exit Striations, and Backward Scrapes

During the second half of stance, the limb's force against the ground decreased and was directed down and backwards. In late stance ("kick-off" of Thulborn and Wade, 1989), the foot was withdrawn, thereby breaking skin–sediment interfaces and creating all skin impressions other than entry striations. Three main types of imprints were left behind: reticulate arrays, exit striations, and backward slips.

Reticulate arrays were exposed on the walls and floors of the digital pad depressions. In the formation of most tracks in the sample, regions of skin moved up and away from the indented sediment at an angle steep enough to prevent striations.

Figure 6. Summary stereo renderings of the three-dimensional orientation of entry and exit striations for 17 pads from nine different specimens. Vectors represent the direction of the striations only, not their length, and have been placed around a diagrammatic track outline adjacent to their appropriate pads. Entry striations are roughly parallel with the long axis of the track and slope downwards at a low angle, indicating that the pads of digits II and IV mostly slid forward after contact. In contrast, exit striations created by the middle and distal pads of digit III have a very small forward component; most motion was upward upon toe withdrawal.

This scenario is reasonable for the central regions of the floor of each pad impression, but what about the peripheral areas and walls? Could skin have moved normal to all surfaces simultaneously? One possible explanation is pad recoil. If a pad was deformed in mid stance, a decreased load would allow pad soft tissues to rebound, thereby vacating the walls and outer portions of its depression's floor first (Fig. 5d). Skin abutting the center of the floor of the pad depression would rise slightly later. Such a mechanism could explain the absence of exit striations for most pads. Re-

coil would reduce a pad's transverse diameter enough to allow a clean withdrawal without wall contact.

Not all pads avoided scraping the walls of their depression upon withdrawal. In some relatively deep tracks, pads of digit III intersected with sediment, creating striation-bearing exit tracts. The three-dimensional orientation of exit striations is based on a small sample (Fig. 6), but some patterns can be discerned. The distal and middle pads of digit III left relatively vertical striations upon withdrawal at the very end of stance (Figs. 1d, 2d, 6). When measured in the horizontal plane, skin movement was primarily transverse with respect to the long axis of the print. These trajectories are consistent with digit III being lifted up and out of its depression rather than being dragged forward (Fig. 6). However, neither medial nor lateral exit striations predominate; both are present in two specimens. In most cases the third toe seems to have been removed without significant transverse deviation.

At least two prints show evidence of backward movement of toes before liftoff. Such slippage occurred when the down and backward limb force overcame friction between skin and sediment. In one case (L.06) slipping produced an elongate claw scrape ("retro-scratches" of Thulborn and Wade, 1989) as well as scale-induced striations. These marks converge posteriorly, indicating adduction of digits II–IV upon flexion of the metatarsophalangeal joints (Baird, 1957; Gatesy et al., 1999).

Previous Work and Future Directions

Study of vertebrate tracks has increased dramatically in the past two decades (e.g., Farlow and Chapman, 1997; Gillette and Lockley, 1989; Lockley, 1991, 1997, 1998; Thulborn, 1990). Along with this revival has been a heightened awareness of the contribution footprints can make to understanding dinosaur locomotion. Many workers have applied Alexander's (1976) method to calculate speed (e.g., Farlow, 1981; Russell and Belland, 1976; Thulborn, 1982), or interpreted trackways as evidence of limb posture (e.g., Lockley and Hunt, 1995; Padian and Olsen, 1989). A wealth of locomotor information has been gleaned from the two-dimensional position of prints with respect to one another (stride length, step angle, trackway width, and toed-in versus toed-out), but little emphasis has been given to the morphology of single prints. One exception is Thulborn and Wade (1984, 1989), who were able to explain much of the variation in their large sample by relating specific features of a track to events during the stance phase. Walking dynamics have also been inferred from subsurface sediment deformation (Avanzini, 1998). Most recently, deep tracks have been shown to preserve the three-dimensional foot movements of Late Triassic theropods from Greenland (Gatesy et al., 1999). One concern with these data is the possible effects of sinking on locomotion. Did theropods walk differently on soft and firm substrates?

Data from skin impressions may help answer this question, because they are found in relatively shallow tracks. Evidence of pad movement during locomotion on a firm substrate can be compared to foot trajectories preserved in deep prints. The effects of sinking on stance phase movements, if any, can then be assessed in order to discern locomotor function under a variety of substrate conditions. Results from this analysis of skin impressions of 20 Greenlandic tracks must be considered preliminary, but they contribute to a more detailed documentation of foot movements in basal theropods. Pedal function may have been very similar to that seen in living ground-dwelling birds, but this hypothesis requires testing and verification.

Clearly, much more work is needed. Trackways with skin impressions would be particularly informative about the effects of speed, turning, and preservational variation. A broader survey of theropod tracks with skin impressions from other localities

and ages is sorely needed. Analyses of fossils will also benefit from a better understanding of track formation in living animals, particularly birds. Surprisingly, a complete description of avian foot motion during terrestrial locomotion is unavailable (for preliminary accounts see Cracraft, 1971; Gatesy, 1999; Gatesy et al., 1999). Techniques such as high-speed film or video should allow features such as tracts and striations to be related directly to skin motion. Simple manipulations may elucidate variation in reticulate patterns and permit a more precise interpretation of reticulate arrays in fossil tracks. Extant forms also allow the magnitude, direction, and position of the limb's force against the substrate to be measured (e.g., Roberts, 2001) and related to foot movement. Finally, a more sophisticated analysis of substrate properties and their effects on track formation dynamics (e.g., Allen, 1997) is needed for dinosaurs. In time, a combination of such approaches may delineate both general features of theropod locomotion as well as more specific details of its evolutionary history.

ACKNOWLEDGMENTS

Footprints were collected as part of a joint Harvard University and University of Copenhagen expedition, with support from the National Science Foundation, the Carlsberg Foundation, and the Putnam Expeditionary Fund of Harvard University. I particularly thank F. A. Jenkins, Jr., N. H. Shubin, W. W. Amaral, K. M. Middleton, and other members of the field crew for their help, and J. O. Farlow for comments and advice. Skin impressions in Figure 1 were drawn by Peggy Price. This paper is dedicated to my advisor, Fuzz Crompton, who taught me that variation is often information, not just noise to be averaged out.

LITERATURE CITED

Alexander, R. McN. 1976. Estimates of speeds of dinosaurs. Nature, **261:** 129–130.

———. 1977. Mechanics and scaling of terrestrial locomotion, pp. 93–110. *In* T. J. Pedley (ed.), Scale Effects in Animal Locomotion. London: Academic Press. xx + 545 pp.

Alexander, R. McN., M. B. Bennett, and R. F. Ker. 1986. Mechanical properties and function of the paw pads of some mammals. Journal of Zoology, London, **209:** 405–419.

Allen, J. R. L. 1997. Subfossil mammalian tracks (Flandrian) in the Severn Estuary, S. W. Britain: mechanics of formation, preservation and distribution. Philosophical Transactions of the Royal Society of London B, Biological Sciences, **352:** 481–518.

Avanzini, M. 1998. Anatomy of a footprint: bioturbation as a key to understanding dinosaur walk dynamics. Ichnos, **6:** 129–139.

Baird, D. 1957. Triassic reptile footprint faunules from Milford, New Jersey. Bulletin of the Museum of Comparative Zoology, **117:** 449–520.

Clemmensen, L. B., D. V. Kent, and F. A. Jenkins, Jr. 1998. A Late Triassic lake system in East Greenland: facies, depositional cycles and palaeoclimate. Palaeogeography, Palaeoclimatology, Palaeoecology, **140:** 135–159.

Cracraft, J. 1971. The functional morphology of the hind limb of the domestic pigeon, *Columba livia*. Bulletin of the American Museum of Natural History, **144:** 171–268.

Currie, P. J., G. C. Nadon, and M. G. Lockley. 1991. Dinosaur footprints with skin impressions from the Cretaceous of Alberta and Colorado. Canadian Journal of Earth Sciences, **28:** 102–115.

Farlow, J. O. 1981. Estimates of dinosaur speeds from a new trackway site in Texas. Nature, **294:** 747–748.

Farlow, J. O., and R. E. Chapman. 1997. The scientific study of dinosaur footprints, pp. 519–553. *In* J. O. Farlow and M. K. Brett-Surman (eds.), The Complete Dinosaur. Bloomington, Indiana: Indiana University Press. xi + 752 pp.

Farlow, J. O., and M. G. Lockley. 1993. An osteometric approach to the identification of the makers of early Mesozoic tridactyl dinosaur footprints, pp. 123–131. *In* S. G. Lucas and M. Morales (eds.), The Nonmarine Triassic. New Mexico Museum of Natural History and Science Bulletin, **3.** 478 pp.

Gatesy, S. M. 1999. Guineafowl hind limb function 1: cineradiographic analysis and speed effects. Journal of Morphology, **240:** 127–142.

Gatesy, S. M., K. M. Middleton, F. A. Jenkins, Jr., and N. H. Shubin. 1999. Three-dimensional preservation of foot movements in Triassic theropod dinosaurs. Nature, **399:** 141–144.

Gillette, D. D., and M. G. Lockley. 1989. Dinosaur Tracks and Traces. Cambridge, United Kingdom: Cambridge University Press. xvii + 454 pp.

Hitchcock, E. 1858. Ichnology of New England: A Report on the Sandstone of the Connecticut Val-

ley, Especially its Fossil Footmarks, Made to the Government of the Commonwealth of Massachusetts. Boston, Massachusetts: W. White. xii + 220 pp.

JENKINS, F. A., JR., N. H. SHUBIN, W. W. AMARAL, S. M. GATESY, C. R. SCHAFF, L. B. CLEMMENSEN, W. R. DOWNS, A. R. DAVIDSON, N. BONDE, AND F. OSBAECK. 1994. Late Triassic continental vertebrates and depositional environments of the Fleming Fjord Formation, Jameson Land, East Greenland. Meddelelser om Grønland, Geoscience, **32:** 1–25.

LANGSTON, W. 1986. Stacked dinosaur tracks from the Lower Cretaceous of Texas—a caution for ichnologists, p. 18. *In* D. D. Gillette (ed.), First International Symposium on Dinosaur Tracks and Traces, Abstracts with Program. Albuquerque, New Mexico: New Mexico Museum of Natural History. 31 pp.

LOCKLEY, M. G. 1989. Summary and prospectus, pp. 441–447. *In* D. D. Gillette and M. G. Lockley (eds.), Dinosaur Tracks and Traces. Cambridge, United Kingdom: Cambridge University Press. xvii + 454 pp.

———. 1991. Tracking Dinosaurs: A New Look at our Ancient World. Cambridge, United Kingdom: Cambridge University Press. xii + 238 pp.

———. 1997. The paleoecological and paleoenvironmental utility of dinosaur tracks, pp. 554–578. *In* J. O. Farlow and M. K. Brett-Surman (eds.), The Complete Dinosaur. Bloomington, Indiana: Indiana University Press. xi + 752 pp.

———. 1998. The vertebrate track record. Nature, **396:** 429–432.

LOCKLEY, M. G., AND A. P. HUNT. 1994. Fossil footprints of the Dinosaur Ridge area. Publication of the Friends of Dinosaur Ridge and the University of Colorado at Denver Dinosaur Trackers Research Group, **2:** i–53.

———. 1995. Ceratopsid tracks and associated ichnofauna from the Laramie Formation (Upper Cretaceous: Maastrichtian) of Colorado. Journal of Vertebrate Paleontology, **15:** 592–614.

LUCAS, A. M., AND P. R. STETTENHEIM. 1972. Avian Anatomy: Integument. 2 vols. Agriculture Handbook 362. Washington, D.C.: U.S. Department of Agriculture. 750 pp.

LULL, R. S. 1904. Fossil footprints of the Jura-Trias of North America. Memoirs of the Boston Society of Natural History, **1904:** 461–557.

———. 1953. Triassic life of the Connecticut Valley. Connecticut State Geological and Natural History Survey, Bulletin, **81:** 1–336.

OLSEN, P. E., AND P. M. GALTON. 1984. A review of the reptile and amphibian assemblages from the Stormberg of southern Africa, with special emphasis on the footprints and the age of the Stormberg. Palaeontologia Africana, **25:** 87–110.

OLSEN, P. E., J. B. SMITH, AND N. G. MCDONALD. 1998. Type material of the type species of the classic theropod footprint genera *Eubrontes*, *Anchisauripus*, and *Grallator* (Early Jurassic, Hartford and Deerfield Basins, Connecticut and Massachusetts, U.S.A.). Journal of Vertebrate Paleontology, **18:** 586–601.

PADIAN, K., AND P. E. OLSEN. 1989. Ratite footprints and the stance and gait of Mesozoic theropods, pp. 231–241. *In* D. D. Gillette and M. G. Lockley (eds.), Dinosaur Tracks and Traces. Cambridge, United Kingdom: Cambridge University Press. xvii + 454 pp.

ROBERTS, T. J. 2001. Muscle force and stress during running in dogs and wild turkeys. Bulletin of the Museum of Comparative Zoology, **156:** 283–295.

RUSSELL, D. A., AND P. BELLAND. 1976. Running dinosaurs. Nature, **264:** 486.

THULBORN, R. A. 1982. Speeds and gaits of dinosaurs. Palaeogeography, Palaeoclimatology, Palaeoecology, **38:** 227–256.

———. 1990. Dinosaur Tracks. London: Chapman and Hall. xvii + 410 pp.

THULBORN, R. A., AND M. WADE. 1984. Dinosaur trackways in the Winton Formation (mid-Cretaceous) of Queensland. Memoirs of the Queensland Museum, **21:** 413–517.

———. 1989. A footprint as a history of movement, pp. 51–56. *In* D. D. Gillette and M. G. Lockley (eds.), Dinosaur Tracks and Traces. Cambridge, United Kingdom: Cambridge University Press. xvii + 454 pp.

WOODHAMS, K. E., AND J. S. HINES. 1989. Dinosaur footprints from the Lower Cretaceous of East Sussex, England, pp. 301–307. *In* D. D. Gillette and M. G. Lockley (eds.), Dinosaur Tracks and Traces. Cambridge, United Kingdom: Cambridge University Press. xvii + 454 pp.

A DIMINUTIVE PTEROSAUR (PTEROSAURIA: EUDIMORPHODONTIDAE) FROM THE GREENLANDIC TRIASSIC

FARISH A. JENKINS, JR.,[1] NEIL H. SHUBIN,[2] STEPHEN M. GATESY,[3] AND KEVIN PADIAN[4]

ABSTRACT. A diminutive eudimorphodontid pterosaur, from the Late Triassic Fleming Fjord Formation of East Greenland, possesses relatively short wings, short ulnae and tibiae, and long metatarsals. The new species, smaller than any known individual of *Eudimorphodon*, is unique among known pterosaurs in having proximal limb segments (humerus, ulna, femur, tibia) of nearly equal length. Although the Greenlandic pterosaur is probably a juvenile, as indicated primarily by the lack of synostosis of axial and limb girdle components, the appendicular proportions of the specimen are too different from those in other known pterosaurian taxa to be accounted for solely by immaturity. The bicondylar fourth metacarpophalangeal joint, in which the dorsal condyle has a larger radius of curvature and a more extensive articular surface than the ventral condyle, appears to be intermediate between a primitive unicondylar joint and the asymmetric trochlea common among pterosaurs. This spectrum of joint configurations represents increasing mechanical stability, consonant with the interpretation that the mechanism evolved among basal pterosaurs to accommodate wing folding during the upstroke in flapping flight.

INTRODUCTION

The earliest well-documented records of pterosaurs are from Late Triassic (Norian) deposits in Italy. *Eudimorphodon ranzii*, first described from a single, nearly complete skeleton from the Zorzino limestones (Middle to Upper Norian) near Bergamo (Zambelli, 1973), is now known from four additional specimens, including juveniles (Wild, 1978, 1994). Another specimen, designated as a different species (*E. rosenfeldi*), derives from the lower part of the Dolomia di Forni (Middle Norian) in Udine Province (Dalla Vecchia, 1995). Other contemporaneous taxa from Bergamo Province include *Peteinosaurus zambellii* (represented by two specimens; Wild, 1978), also from the Zorzino limestones, and *Preondactylus buffarinii* (known from a single specimen; Wild, 1984; Dalla Vecchia, 1998) from the Dolomia di Forni. A compacted assemblage of pterosaur bones, interpreted as a gastric pellet, was referred to *P. buffarinii* by Dalla Vecchia et al. (1989) principally on the basis of estimated limb length ratios. The specimen derives from a fossiliferous, Middle Norian zone in the Dolomia di Forni (Roghi et al., 1995), 150–200 m lower in the section that yielded the type of *P. buffarinii* (Dalla Vecchia et al., 1989).

Some pterosaurs of the Late Triassic already had attained moderate size. Padian (1980) described a partial wing skeleton from a pterosaur with a wingspan of 1.5 m that he recognized was neither *Eudimorphodon* nor *Peteinosaurus*. Wild (1984), in his description of the type of *Preondactylus buffarinii*, referred the wing skeleton to this taxon on the basis of phalangeal proportions, although the type of *P. buffarinii* is smaller, with a wingspan estimated at 45 cm (Wellnhofer, 1991) or "a little less than 50 cm" (Dalla Vecchia, 1998:

[1] Department of Organismic and Evolutionary Biology, and Museum of Comparative Zoology, Harvard University, Cambridge, Massachusetts 02138.

[2] Department of Organismal Biology and Anatomy, University of Chicago, Chicago, Illinois 60637.

[3] Department of Ecology and Evolutionary Biology, Brown University, Providence, Rhode Island 02912.

[4] Department of Integrative Biology, and Museum of Paleontology, University of California, Berkeley, California 94720.

358). Adult *Eudimorphodon ranzii* had a wingspan of 1 m (Wild, 1978).

Here we describe a tiny pterosaur, which we interpret as a young individual of a new species of *Eudimorphodon,* with an estimated 24-cm wingspan, from the Late Triassic Fleming Fjord Formation, Jameson Land, East Greenland (Jenkins et al., 1994).

The following abbreviations of institutional names are used: MCSNB, Museo Civico di Scienze Naturali, Bergamo; MCZ, Museum of Comparative Zoology, Harvard University, Cambridge, Massachusetts; MFSN, Museo Friulano di Storia Naturale, Udine; and MGUH, Geological Museum, University of Copenhagen.

SYSTEMATIC PALEONTOLOGY

Class Reptilia Laurenti, 1768

Subclass Archosauria Cope, 1869

Order Pterosauria Kaup, 1834

Family Eudimorphodontidae Wellnhofer, 1978

Genus *Eudimorphodon* Zambelli, 1973

Eudimorphodon cromptonellus new species

Holotype. MGUH VP 3393 (MCZ field no. 13/91G; Fig. 1).

Etymology. The specific epithet combines a patronym honoring A. W. Crompton for his contributions to our understanding of the evolution of vertebrate structure and function, with Latin *-ellus,* diminutive in reference to the small size of the type.

Diagnosis. A very small pterosaur that shares with *Eudimorphodon ranzii* (as diagnosed by Wild, 1978: 179, and later emended by Wild, 1994: 97–102) a heterodont dentition composed of uni-, tri-, and quinticuspid teeth (unknown in any other pterosaurian taxon); additionally, some teeth are quadricuspid. *Eudimorphodon rosenfeldi* (Dalla Vecchia, 1995) also has quinticuspid teeth but the dentition is incompletely known. The tooth count is estimated at 11 or 12 postpremaxillary teeth, which is 14 or 15 fewer than the type of *E. ranzii* and three or four fewer than the number reconstructed for the Milano juvenile specimen of *E. ranzii* (Wild, 1978, figs. 25, 27). The tibia is relatively shorter than in any known pterosaur (104% of the femur); the ulna is relatively shorter than in most other pterosaurs (111% of the humerus; some specimens of *Campylognathoides zitteli* have comparable humero-ulnar proportions, see Table 2). As in the Milano juvenile, no evidence is found of the two enlarged, fanglike maxillary teeth situated beneath the ascending process that are characteristic of adult *E. ranzii.* Differs from the juvenile specimen (MCSNB 8950) referred to *E. ranzii* by Wild (1994) in that the metatarsals are approximately 25% longer, whereas all other limb bone lengths are substantially shorter. The new taxon differs from *E. rosenfeldi* (Dalla Vecchia, 1995) in having a humerus that is shorter than the femur.

Horizon and Locality. Lower part of the Carlsberg Fjord beds in the Ørsted Dal Member of the Fleming Fjord Formation, Scoresby Land Group, Jameson Land, East Greenland. On the southern flank of Macknight Bjerg (Geodætisk Instituut, Grønland series 1:250,000, Carlsberg Fjord Quadrangle), a localized bone assemblage was discovered in 1989 by William W. Amaral at 71°22.277′N, 22°33.341′W (the Macknight Bjerg quarry; the latitude and longitude coordinates given here, taken in 1995 by averaging multiple global positioning system readings to reduce anomalies due to drift, differ slightly from those reported by Jenkins et al. (1994) based on a single reading from a hovering helicopter). Excavated in 1991 and 1992, this locality presented a rich taphocoenosis of vertebrate remains, predominantly the plagiosaurine *Gerrothorax* cf. *pulcherrimus* but also the capitosaur *Cyclotosaurus* cf. *posthumus* (Jenkins et al., 1994). In addition to the pterosaur, the only other associated skeletal material of a terrestrial tetrapod found at this

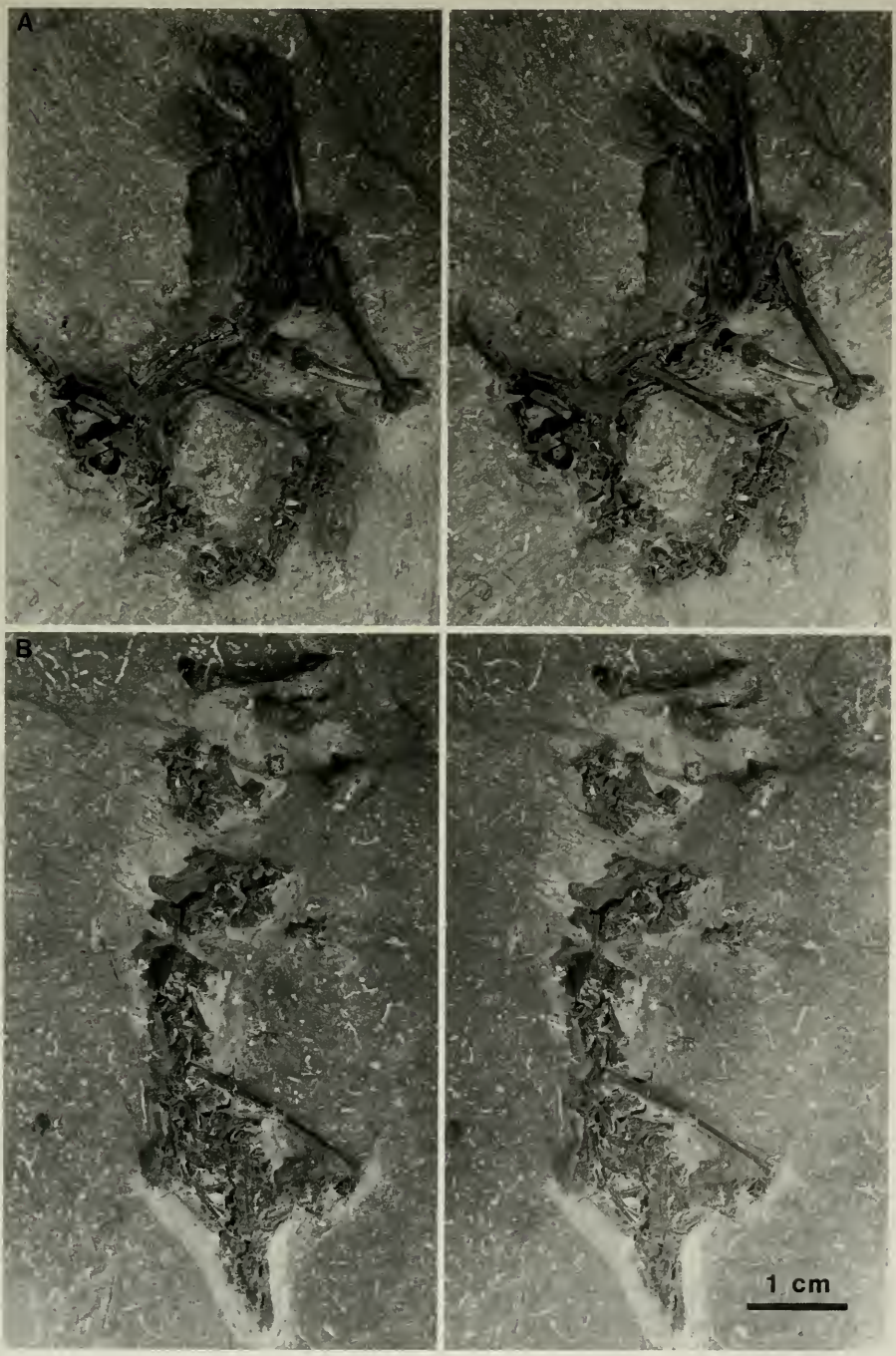

Figure 1. Stereophotographs of *Eudimorphodon cromptonellus* (MGUH VP 3393), new species, preserved in two matrix blocks (A, see Fig. 3 for details; B, see Fig. 2).

site was that of a ?lepidosauromorph represented by a partial postcranial skeleton and lower jaws.

Age. Late Triassic (?Norian–Rhaetian) (Jenkins et al., 1994; Clemmensen et al., 1998).

Material. A fairly complete but largely disarticulated and partly crushed skeleton. Identifiable cranial bones include both mandibles and maxillae, as well as a nasal, lacrimal, jugal, quadrate, and squamosal. Other cranial elements are too damaged to offer a basis for useful description. Postcranial remains include numerous cervical and dorsal vertebrae (most neural arches are disassociated from centra), several caudal vertebrae, and rib fragments. Appendicular elements include the right scapula; a partial coracoid; the right humerus, radius, ulna, fourth metacarpal, and wing phalanges; both femora, a tibia, and a fibula; metatarsals; and numerous pedal phalanges.

Comments. The specimen was discovered in the process of splitting coarsely bedded matrix in the Macknight Bjerg quarry; parts of the skeleton are thus preserved on part and counterpart blocks (Figs. 1–3). Postmortem tissue maceration resulted in disarticulation of most of the bones, but transport was minimal and some natural associations are preserved (skull, cervical vertebrae, right manus, right hind limb).

DESCRIPTION

Skull

Maxilla. The right maxilla (Figs. 2, 4), largely complete except for some damage to its rostral and caudal ends, is 13.5 mm in length. A posteriorly recurved ascending process is preserved, which in *Eudimorphodon ranzii* separates the antorbital fenestra from the external naris (Wild, 1978, fig. 1). The maxilla bears 11 teeth with an apparent diastema between the third and fourth. The diastema, which is situated anteroventral to the ascending process of the maxilla approximately in the locus of the enlarged fanglike teeth of adult *E. ranzii* (Wild, 1978, fig. 25b), shows no evidence of alveoli. The last seven teeth are posterior to the ascending process of the maxilla. The left maxilla (in medial aspect, Fig. 2), partly overlain and obscured by the right maxilla, is fractured and deformed but is complete posteriorly where it lies in contact with the jugal. Nine teeth are present, but most are incompletely preserved; a gap (?diastema) between the fourth (in the process of eruption) and fifth is sufficient to have accommodated three tooth positions.

Other Cranial Bones. Most cranial bones are obscured by postmortem collapse, crushing, and disarticulation of the skull. However, a few can be identified, but offer little detail that warrants further description beyond that illustrated (Figs. 2, 3). Crushed bone superorostral to the anterior ends of the maxillae represents part of the right nasal, and possibly the posterior part of the premaxilla. No evidence is found of premaxillary teeth. The slender right lacrimal lies behind the ascending process of the maxilla. The jugal is represented by a postorbital process. Both the right squamosal and quadrate lie separate from the skull. The squamosal has a deep notch that represents the superior border of the inferior temporal fenestra. The quadrate bears a large, bulbous articular condyle.

Dentition. The teeth are buccolingually narrow and vary in mesiodistal length from 0.42 to 1 mm. The relatively simple, unicuspid mesial teeth, exemplified by the most mesial tooth preserved in the right maxilla (Fig. 4) and left mandible (Fig. 2), are the smallest (0.42, 0.48 mm in length, respectively); the mesial crest that descends from the apical cusp is slightly more convex than the distal crest. The remainder of the dentition comprises multicusped teeth structurally similar to those of *Eudimorphodon ranzii* (Wild, 1978) but unlike that in any other known pterosaur. The enamel is smooth and without surficial grooves; Wild (1978, fig. 28) regarded

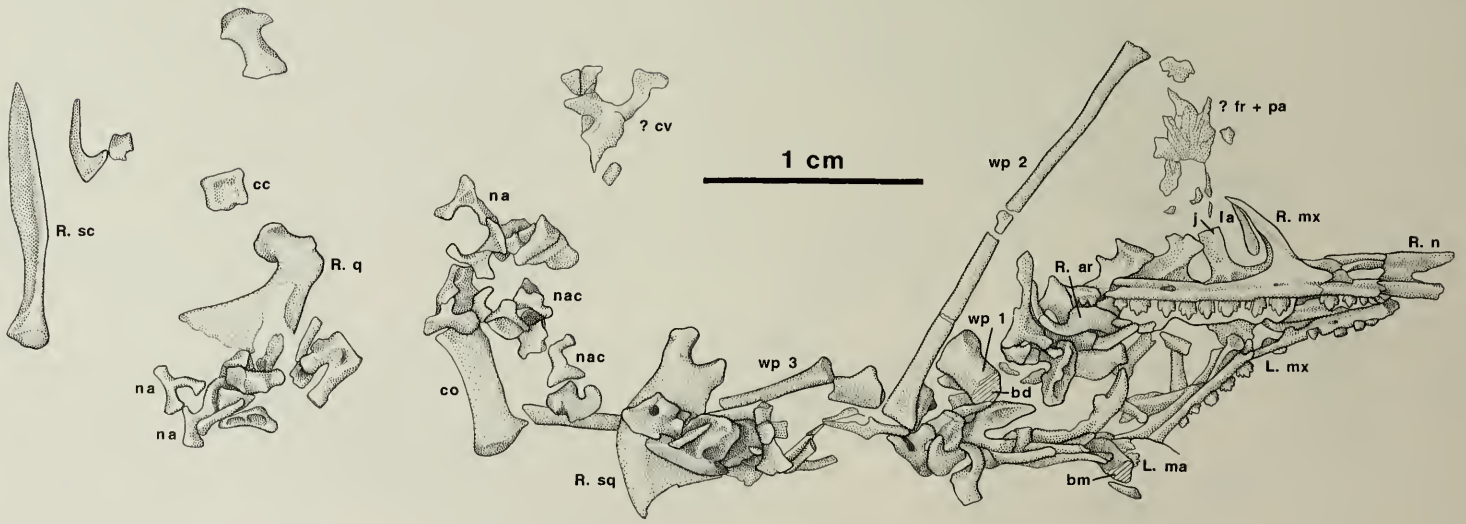

Figure 2. Part of the skeleton of *Eudimorphodon cromptonellus* (MGUH VP 3393), new species, as preserved on one of two matrix blocks (see Fig. 3). Abbreviations: ar, articular; bm, break in mandible, the two pieces of which are preserved in the part and counterpart blocks (Figs. 2, 3); bd, break in diaphysis of wing phalanx 1, the two pieces of which are preserved in the part and counterpart blocks (Figs. 2, 3); cc, cervical centrum; cdv, caudal vertebra; co, coracoid; cv, cervical vertebra; cva, cervical vertebra, anterior series; cvp, cervical vertebra, posterior series; dv, dorsal vertebra; f, femur; fi, fibula; fr, frontal; h, humerus; j, jugal; L., left; la, lacrimal; ma, mandible; mdt, medial distal tarsal; mc, metacarpal; mph, manual phalanx; mt, metatarsal; mx, maxilla; n, nasal; na, neural arch; nac, neural arch, cervical; op, opisthotic; pa, parietal; pph, pedal phalanx; q, quadrate; R., right; ra, radius; sc, scapula; sq, squamosal; st, sternum; t, tibia; ul, ulna; up, ungual phalanx; Vi, Vii, proximal, distal phalanges of pedal digit V; wp, wing phalanx.

Figure 3. The remainder of the skeleton of *Eudimorphodon cromptonellus* (MGUH VP 3393), new species, as preserved on the counterpart block. See Figure 2 legend for abbreviations.

the textural difference in enamel among specimens of *E. ranzii* as ontogenetic (adults possess grooves that run apicobasally; juveniles lack them). Accessory cuspules are developed along the mesial and distal crests descending from the primary, or apical, cusp; comparable to the variability illustrated by Wild (1978, fig. 7) for the Milano juvenile specimen of *E. ranzii,* teeth may bear a single accessory cuspule (along the distal crest), or two, three, or four cuspules. Mesial teeth (ranging in mesiodistal length from 0.54 to 0.78 mm) tend to be tricuspid, with the accessory cuspules situated at the mesial and distal base of the crown. Teeth in the distal part of the row (ranging in mesiodistal length from 0.83 to 1.08 mm) tend to be quinticuspid. Accessory cuspules, particularly the basal ones, tend to be oriented in palmate fashion, splaying from the central (apical) axis; in adult *E. ranzii,* cuspules either parallel the central axis or converge slightly (Wild, 1978, fig. 8). One tricuspid tooth illustrated by Wild (1978, fig. 7) of a juvenile *E. ranzii* (the Milano specimen) exhibits a similar splaying of accessory cuspules.

Eleven teeth are present in the left mandible (nine shown in Fig. 3; the two most distal in Fig. 2). The most mesial, unicuspid tooth is followed by a bicuspid (with a minute accessory cuspule on the distal crest). Most of the remaining left mandibular teeth, insofar as preserved, appear to be tricuspid, with the exception of the penultimate, which is quinticuspid.

The 11 teeth of the right mandible, better preserved than those of the left, all exhibit three or more accessory cuspules; the mesial dentition appears to be unrepresented because there are no uni- or bicuspid teeth. The most mesial tooth bears two accessory cuspules mesially, and at least one distally (the basal part of the crown, where a second distal cuspule would be positioned, is obscured by the next overlying tooth). The second tooth is tricuspid. The third tooth is at least quadricuspid; the obliquity of its position in the alveolus possibly conceals a second distal accessory cuspule at the base of the crown. The fourth tooth, in the process of eruption, displays three cusps, but the basal mesial and distal cuspules, if present, would be obscured. The fifth tooth has two accessory cuspules mesially, but only one distally. Of the six most distal teeth, all appear to be quinticuspid, except for the relatively small eighth tooth (mesiodistal length, 0.45 mm), which appears to be tricuspid.

The 11 teeth of the right maxilla (Fig. 4) are the best preserved of the entire dentition. A diastema between the third and fourth teeth is evidence that the maxillary tooth count could have been 12 or more. The most mesial tooth is unicuspid and relatively small (mesiodistal length, 0.42 mm); the second also appears to be unicuspid, but the third is clearly tricuspid (respective lengths, 0.54, 0.72 mm). The remaining eight teeth (4th–11th) vary in mesiodistal lengths from 0.8 to 1 mm, with the exception of the most distal tooth (0.6 mm). The fourth and very probably the fifth are quinticuspid. However, the sixth and seventh are quadricuspid, with a single accessory cuspule on the distal crest of the sixth and mesial crest of the seventh. The 9th is tricuspid, the 10th quinticuspid, and the most distal a small tricuspid. As in the smaller, Milano juvenile specimen of *Eudimorphodon ranzii* (Wild, 1978, figs. 25, 27), no evidence is found of the two enlarged, fanglike maxillary teeth situated beneath the ascending process that are characteristic of adult *E. ranzii.* Few of the 10 left maxillary teeth preserve any details of the crowns; the fifth, sixth, and seventh are certainly quinticuspid.

A definitive tooth count cannot be ascertained because of postmortem damage; neither the premaxillary teeth, nor the fanglike, mesialmost teeth of the lower jaw known in presumably ontogenetically older specimens of *Eudimorphodon ranzii* are preserved. Nonetheless, the tooth counts in both maxillae and both mandibles are sufficiently comparable to estimate 11 or 12 postpremaxillary teeth, two to three

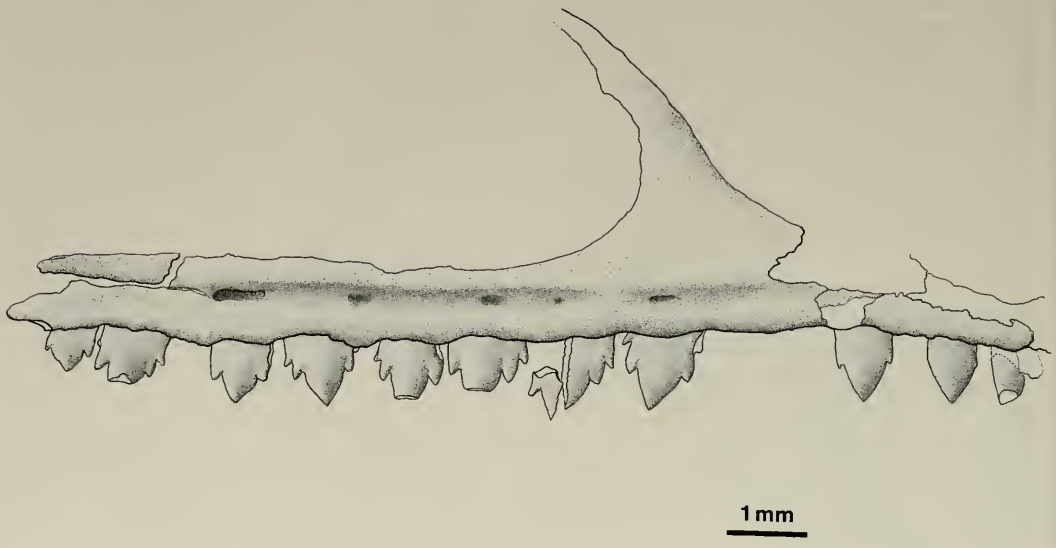

Figure 4. Lateral view of the right maxilla of *Eudimorphodon cromptonellus* (MGUH VP 3393), new species.

fewer than the number reconstructed for the Milano juvenile (Wild, 1978, figs. 25, 27).

Postcranial Skeleton

Vertebrae. Approximately six cervical, eight dorsal, one ?sacral, and one (possibly two) caudal vertebrae are represented. However, postmortem disturbance considerably obscures vertebral details. Although some vertebrae are more or less associated in a series, most are disarticulated from one another. Furthermore, in most cases the neural arches and centra themselves are disarticulated; the only complete vertebra is an elongate midcaudal (Fig. 3; centrum length 5.7 mm; overall length, 7.6 mm). Reconstruction is further hampered by the overlap of bones that have collapsed one on the other. Of the eight isolated centra that appear undistorted and are sufficiently exposed for measurement, all are of uniform length (1.7–1.75 mm). The most complete neural arch (Fig. 3), which is isolated, is 1.6 mm in length (including the small pre- and postzygapophyses), lacks transverse processes, has a neural canal width of 1.25 mm, and has a spinous process height of 0.8 mm. The arch's lack of transverse processes and relatively restricted neural canal, considered with its proximity to the hind foot and a midcaudal vertebra, are evidence that the element is derived from the proximal caudal series. Two neural arches (also separated from their respective centra; Fig. 2) are interpreted as representing dorsal vertebrae by virtue of their association with elements of the shoulder girdle and the presence of transverse processes (approximately 1 mm in length) that project horizontally from the junction of the laminae and pedicles. The breadth of the neural canal is 1.5 mm in the smaller, and 2.25 mm in the larger specimen; likewise, the respective distances between the distal ends of the transverse processes are 4.1 and 4.75 mm. However, these measurements are only approximate because of slight postmortem

displacement between the left and right halves of the arches.

Shoulder Girdle. A dissociated scapula and partial coracoid are the only shoulder elements preserved. The evidence of a sternum is equivocal. A comminuted, sheetlike expanse of bone associated with the humeral head (?st, Fig. 3) may be sternal, and at one end is a process that resembles a cristospine. The coracoid (presented in medial aspect, Fig. 2) is 6.5 mm long as preserved, but the sternal end has disintegrated beneath vertebral remains. The acrocoracoid process is partly visible. The scapula (in dorsomedial aspect, Fig. 2) is 12.6 mm in length as preserved; degradation of the caudal end of the blade raises the likelihood of somewhat greater length (at least 13 mm).

Forelimb. The right humerus, 18.2 mm long, has a slightly sigmoidal, dorsoventral curvature; the proximal end as a whole is reflected dorsally, and the distal end is reflected ventrally. The deltopectoral crest is subtriangular, comparable to that in juvenile *Eudimorphodon ranzii* but unlike the shape in adults, which is quadrangular (Wild, 1978, fig. 29). The humeral head is oriented dorsally, and possesses the typically pterosaurian sellar shape (Padian, 1983). The diaphysis at midshaft, which is slightly flattened, is 1.4 mm in width. The distal end, 3.3 mm in width, lacks cortical bone; radial and ulnar condyles are not distinct.

The right radius and ulna (Fig. 3; estimated lengths, 19.5 and 20.1 mm, respectively) lie approximately parallel to each other. The proximal shaft of the ulna is crushed; the proximal shaft of the radius is broken, with the fragmented ends overlapping. Much of the distal ulnar and radial shafts lie beneath the humerus, posterior skull, and other bones. The proximal end of the ulna overlaps that of the radius; neither is well preserved in this region. The distal ulna, preserved in lateral view, exhibits a bicondylar, typically pterosaurian shape, and the distal radius has the characteristic ventral process that broadens the articulation with the proximal carpals.

Metacarpals and manual phalanges lie beneath the distal ends of the radius and ulna and the adjacent jaw. The right fourth or wing metacarpal (8.4 mm length) is presented in medial view (R.mc 4, Fig. 3). The well-ossified distal articular surface is bicondylar (Fig. 5A), unlike the trochlear form that is conventional among pterosaurs (Fig. 5B). However, as in other pterosaurs, the dorsal (=extensor side) condyle has a radius of curvature greater than that of the ventral (=flexor side) condyle. Metacarpal I (5.6 mm length) lies parallel to IV (Fig. 3). In most pterosaurs these two bones are nearly equal in length (I is slightly shorter than IV), whereas in this specimen metacarpal I is only 67% of IV, comparable to the ratio that can be estimated for the adult holotype of *Eudimorphodon ranzii* (MCSNB 2888; Wild, 1978, fig. 17). Metacarpals I and IV are separated by a phalanx (2.7 mm) and two incomplete elements (3.8 and 3.9 mm) that are probably also phalanges (Fig. 3). The third metacarpal (8.3 mm), which lies beneath the adjacent jaw, overlies another metacarpal (here interpreted as a right metacarpal II; 7.4 mm length; R.mc 2, Fig. 3) that became fully exposed when metacarpal IV was removed. Associated with these bones is a small, rounded, flat bone that may be a distal carpal. No manual claws are evident.

Parts of a proximal (first) wing phalanx are associated with the distal end of a wing metacarpal on one block (Fig. 3) and the posterior end of the skull on the counterpart block (Fig. 2). The bone was broken when the matrix containing the entire specimen was first cleaved during quarrying. Mid-diaphyseal diameter is 1.1 mm, but the shaft broadens at both ends; the shaft closest to the occiput (presumably the distal end) has a diameter of about 2 mm. As preserved, the restored length of the bone is 12.2 mm. However, cross-sectional diameters of the two broken ends differ (1.56, 1.05 mm versus 1.1, 0.9 mm),

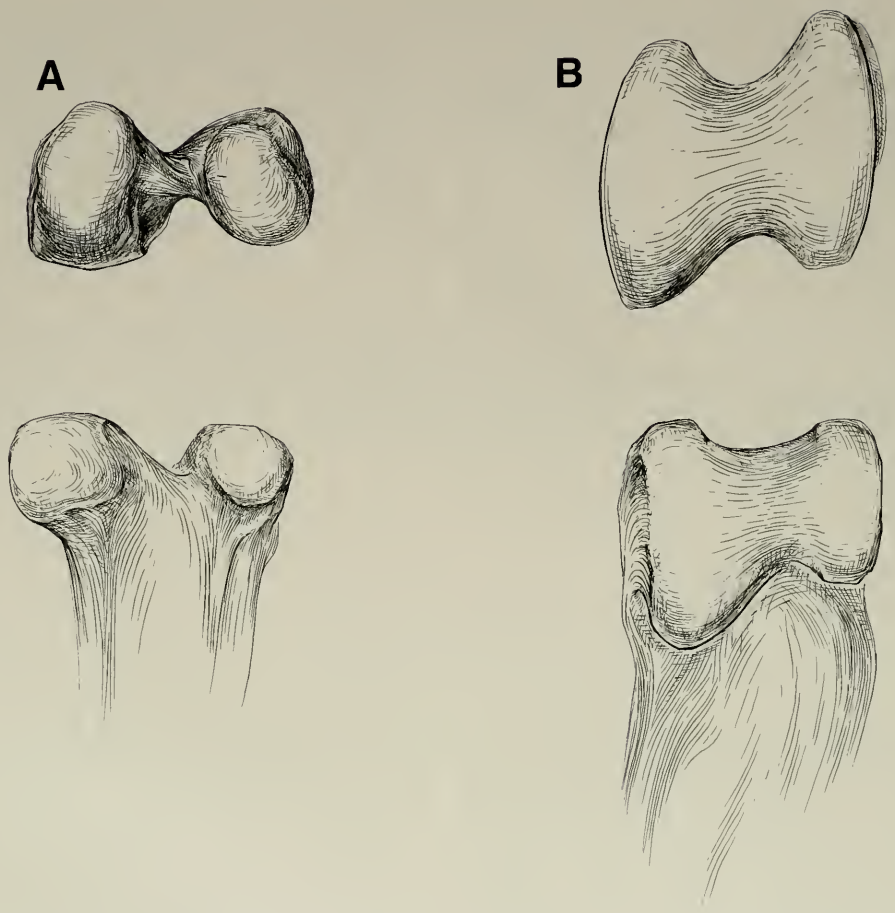

Figure 5. The distal end of right metacarpal IV of (A) *Eudimorphodon cromptonellus,* new species, and (B) *Rhamphorhynchus* sp. (after Wellnhofer, 1975a, fig. 13c) in distal (above) and medial, or ulnar, views. Not to scale.

and thus a diaphyseal section appears to be missing. The other proximal wing phalanx overlies the humeral head and is complete (18 mm length) although broken at midshaft and crushed distally (Fig. 3).

Other wing phalanges are identified on the basis of the dimensions of their articular ends. A second wing phalanx (20.5 mm length) lies behind the skull (Fig. 2); the breadth of the proximal and distal ends are respectively 1.5 and 1.2 mm. The proximal half of the other second wing phalanx protrudes from beneath the metatarsals (Fig. 3); its proximal end (1.35 mm breadth) contacts the distal end of a proximal wing phalanx. The proximal two thirds of a third wing phalanx (Fig. 2) is tentatively identified on the basis of the breadth of its proximal end (1.15 mm). Several fragmentary bones may represent fourth wing phalanges, but are too incomplete to assess.

Hind Limb. Both femora are preserved in close association (Fig. 3). The complete right femur (19.7 mm length) is presented in dorsolateral view, with only the distal end partially obstructed by overlying bone. The left femur, represented by the diaphysis and distal end (fragment length, 15.75 mm), was removed for histologic exami-

nation (see below), as was another fragment (length, 4.5 mm), possibly representing the proximal end. Some distortion of the femora is apparent, but nonetheless both preserve indications of the curvature (i.e., dorsal deflection of the proximal end, and lateral deflection of the distal end) that is characteristic of pterosaurs and dinosaurs (Padian, 1986). The proximal end expands into a distinct head that is slightly upturned and inflected medially; a plane normal to the broadly convex articular surface would intersect the longitudinal axis of the shaft at about 45°. The distal end of the femur bears two contiguous condyles separated only by a slight sulcus; the larger medial condyle is more hemispheroidal in comparison to the ovoid, less convex lateral condyle.

A tibia is preserved, and a fibula is tentatively identified (Fig. 3). Unlike the condition in adult *Eudimorphodon ranzii* (Wild, 1978: 214) and most pterosaurs, no tibiofibular synostosis is apparent; the bones have been completely separated postmortem. The right tibia, contiguous with the distal end of the right femur, is complete, although its proximal end lies beneath vertebrae. The length of the exposed bone is 19 mm; inasmuch as a proximal expansion is evident, the extent of the obscured part is probably no more than 1–2 mm, giving an estimated length of 20.5 mm. The narrowest diameter of the cylindrical shaft is 1.1 mm. Distally the tibia is expanded (2.3 mm width) to support an astragalar facet that is set transversely to the shaft. Identification of the fibula, usually established on the basis of tibial association, cannot be made unambiguously in the present specimen. The presumed fibula (fi, Fig. 3) is incomplete; as preserved, the bone is 13.8 mm in length (and thus longer than the closely associated metatarsals). The ?proximal end diameter is 1.3 mm. A displaced fragment near its ?distal end, if fibular, would indicate an overall fibular length of about 15 mm.

No tarsal bones can be identified, with the possible exception of a medial distal tarsal associated with the phalanges of ?digit V (Fig. 3). However, four complete but disarticulated metatarsals are preserved among the hind limb bones (Fig. 3). Midshaft diameters vary from 0.4 to 0.5 mm. The distal ends, adjacent to pedal phalanges, bear articular surfaces that are relatively flat, as in *Dimorphodon weintraubi* (Clark et al., 1998). The lengths of the metatarsals (12, 11.35, 11.25, and 10.5 mm) would correspond to the relative proportions of the second, third, first, and fourth metatarsals in the juvenile specimen of *Eudimorphodon ranzii* (MCSNB 8950 B) described by Wild (1994) in which II > III > I > IV. In pterosaurs generally, either metatarsal II or III is the longest (Wellnhofer, 1978). The series of four metatarsals in the Greenlandic specimen may represent bones from different feet, and the identifications here are suggested on the basis of relative lengths. Specimen MCSNB 8950 B is in every comparable feature a larger individual than the Greenlandic form except in metatarsal lengths, which are (I) 8.1 mm, (II) 8.85 mm, (III) 8.6 mm, and (IV) 7.4 mm (Wild, 1994, fig. 4).

At least 15 disarticulated pedal phalanges, including a claw, are preserved in the region of the metatarsals. Inasmuch as there are primitively only 12 nonungual phalanges in a pterosaur foot (excepting pterodactyloids, which have only 10), the probability that elements of both feet are comingled is increased still further.

DISCUSSION

The Greenlandic pterosaur is smaller than any known individual of *Eudimorphodon* or any other Triassic pterosaur (Table 1); only some small (ostensibly juvenile) specimens of *Pterodactylus* spp. are of comparable size (Wellnhofer, 1970). However, a precise, quantitative comparison of size is limited by disarticulation, and especially the lack of any reliable indication of axial length. Although the specimens of *Eudimorphodon* with which the Greenlandic form may be compared are

Table 1. Long-bone lengths (mm). Data from (a) Wild, 1978; (b) Wild, 1994; (c) Dalla Vecchia, 1998; (d) Dalla Vecchia, 1995; (f), Wild, 1984.

	Eudimorphodon cromptonellus, new species MGUH VP 3393	*E. ranzii* juvenile MCSNB 8950 (b)	*E. ranzii* juvenile Milano (a)	*E. ranzii* subadult MCSNB 2887 (a)	*E. ranzii* adult (type) MCSNB 2888 (a)	*E. rosenfeldi* ?adult MFSN 1797 (d)	*Peteinosaurus zambellii* MCSNB 3359 (a)	*Preondactylus buffarinii* MFSN 1770 (c, f)
Humerus	18.15	26	26	28	47	40.5	38.5	32
Ulna	20.1	33.5	35	38	65	55	48	42
Metacarpal IV	8.4	9.3	9.8	14e	29	21	17	14.25
Wing phalanx 1	18e*	33	38.5	39.5	80+ (100e)	64	43	35.5
Wing phalanx 2	20.5	35	33e	40e	—	58.2	43	39
Wing phalanx 3	20.5e	35	36	—	—	63.2	46.5	39
Wing phalanx 4	—	32	35e	—	—	51.5	34.8	28
Femur	19.7	19.6	19e	22	41	37	37	32.5
Tibia	20.5e	25.5	25e	28.5	50e	54.2	49	44
Metatarsal I	11.25	8.06	—	—	—	—	17.6	16e
Metatarsal II	12	8.85	—	—	—	—	18.5	16e
Metatarsal III	11.35	8.58	—	—	—	21	17.9	16e
Metatarsal IV	10.5e	7.43	—	—	—	—	17.3	16e
Σ h + u + mc IV + wp 1 + f + t $\approx$	102	147	153	170	312	272	233	200

* e, estimated.

h, humerus; u, ulna; mc IV, metacarpal IV; wp 1, wing phalanx 1; f, femur; t, tibia.

articulated, none is complete and the lengths of some limb elements can only be estimated. Nonetheless, the size range represented by the available sample of *Eudimorphodon* may be approximated by summing the lengths of the humerus, ulna, metacarpal IV, wing phalanx 1, femur and tibia (Σ h + . . . t, Table 1). By this index, MGUH VP 3393 is one-third the size of the type and largest specimen of *E. ranzii,* and two-thirds the size of two juvenile specimens (Fig. 6).

Taxonomic Assignment

The distinctive dentition in MGUH VP 3393 offers secure evidence on which to assign the specimen to the genus *Eudimorphodon,* but allocation to a known species is problematic. Conspecificity with *E. ranzii* appears improbable on the basis of two proportional disparities. First, the lengths of the metatarsals in the juvenile *E. ranzii* (MCSNB 8950 B) described by Wild (1994) from Ponte Giurino are on the order of 25% shorter than those in MGUH VP 3393 (Table 1), although almost all other long bone lengths indicate that MCSNB 8950 is larger (Fig. 6). Although the Ponte Giurino *Eudimorphodon* lacks a skull, Wild (1994: 112–115) expressed confidence in referring the specimen to *E. ranzii* based primarily on the close correspondence of limb bone lengths and proportions to those of the Milano juvenile. Second, femoral lengths in the Greenlandic specimen and the two juvenile but larger *E. ranzii* are essentially the same (Table 1), with the improbable implication for conspecificity that all long bones, except the femur, increased in length during early development.

Differences in limb proportions obviate the possibility that the Greenlandic pterosaur might be an immature conspecific of *Eudimorphodon rosenfeldi. Eudimorphodon rosenfeldi,* decribed by Dalla Vecchia (1995) on the basis of a single, smaller specimen than the type of *E. ranzii,* was differentiated in part from *E. ranzii* by the comparable lengths of the tibia and ulna, and the greater length of the tibia relative to the humerus; these proportions are more or less shared by the Greenlandic specimen (Table 1). However, unlike the condition in *E. rosenfeldi,* the humerus is shorter than the femur in the Greenlandic specimen, a primitive condition known among pterosaurs only in *Preondactylus buffarinii* (Dalla Vecchia, 1998, table 5). Furthermore, the hypothesis that the Greenlandic specimen is an immature *E. rosenfeldi* entails seemingly improbable allometric reversals in comparison to those known in congeners. In *E. ranzii,* the humeral/femoral index decreases from juvenile to adult stages (from about 135% to 115%; Table 2), but the same index increases when the Greenlandic specimen (92%) and *E. rosenfeldi* (109%) are compared. A comparable reversal is seen in the ulnar/femoral index (Table 2). Finally, the femoral/tibial index in *E. ranzii* increases slightly from juvenile to adult stages, whereas an approximately 30% decrease occurs in the same index between MGUH VP 3393 and *E. rosenfeldi* (Table 2).

Assessment of Ontogenetic Stage

Various criteria have been employed to differentiate immature from adult pterosaurs: relative body size, degree of ossification, and osteometric ratios (Wellnhofer, 1970, 1975a–c); synostosis, epiphyseal ossification, and bone histology (Bennett, 1993); and a combination of morphometric and histologic features (Padian et al., 1995).

Insofar as these criteria may be applied, the Greenlandic pterosaur would appear to be neither a hatchling nor an adult, and is most probably a juvenile. The lack of intracranial fusion, as well as the lack of synostosis between vertebral arches and centra, and between scapula and coracoid, are indicative of a preadult stage. The diminutive size of the individual is suggestive of immaturity, but not conclusive. The limb proportions may be interpreted as ontogenetically immature, or phylogenetically primitive, or both. In the series of

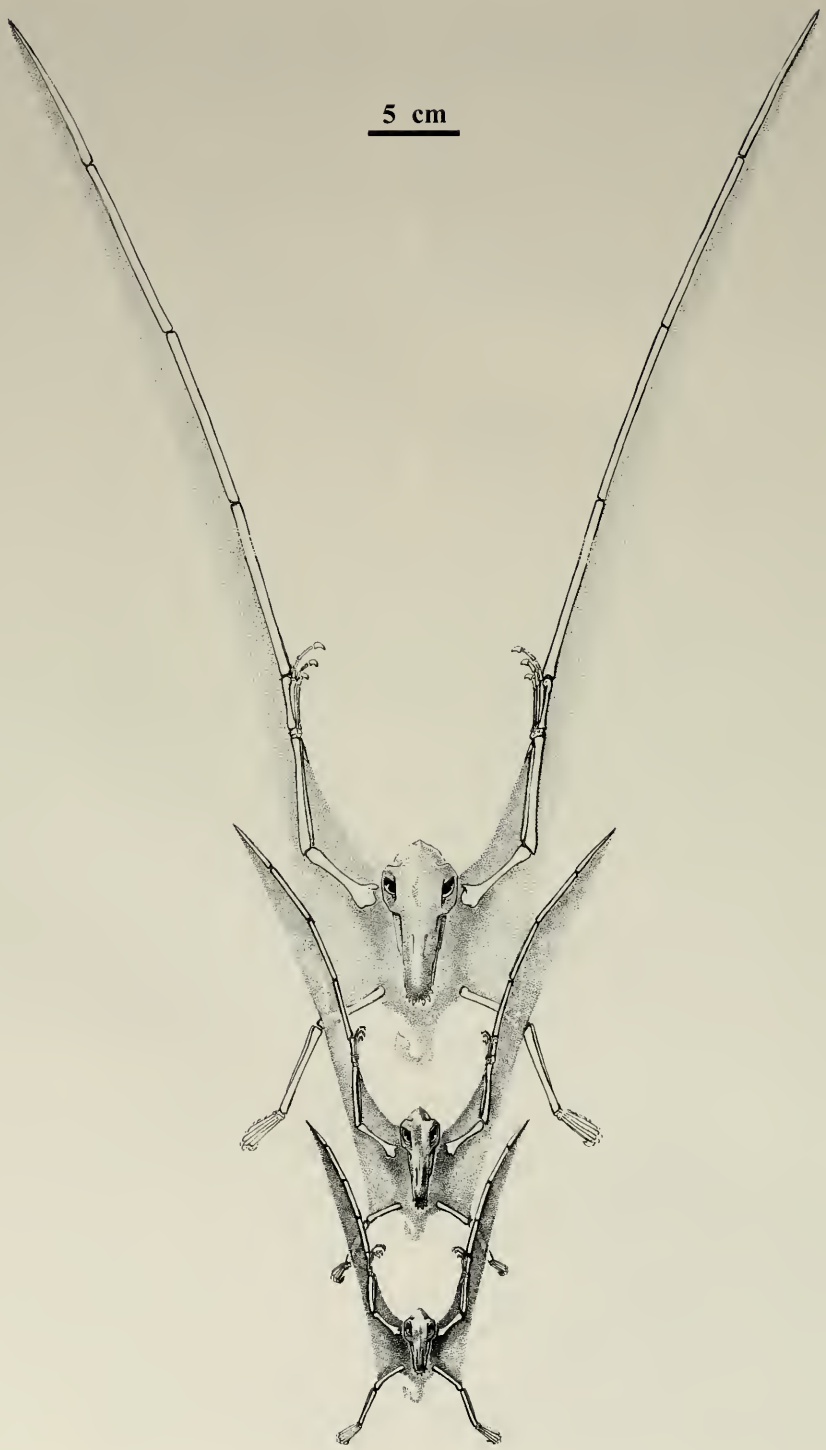
5 cm

Pterodactylus spp. studied by Wellnhofer (1970), juveniles generally possess more comparable humeral/radial and femoral/tibial lengths than do adults. Although the limb proportions of the Greenlandic pterosaur represent the juvenile end of this allometric spectrum, these proportions are also intermediate between various basal pterosaurs and nonpterosaurians (Table 2).

Histologic sections of the the left femur yielded less than definitive results because of extensive diagenetic alteration and resultant artifacts. As in pterosaurs and birds, the diaphyseal cortex is thin (about 15–20% of shaft diameter). The wide medullary cavity, infilled with calcite, shows no trace of trabecular projections that have been identified in chelonian, crocodilian, and dinosaurian embryos (Horner et al., 2001). The bone cortex is mostly parallel fibered, with only indistinct indications of localized lamellar deposition; the osteocytic spaces are variably distributed. No features are present that might be expected in an embryo or rapidly growing neonate, nor are indicators present of growth stasis and maturity. The parallel-fibered matrix differs from the fibrolamellar architecture known in later pterosaurs, which has been interpreted as indicative of rapid growth (Bennett, 1993). Vascular canals are nearly all longitudinally oriented; the canals appear to be primary, but no evidence is present of primary osteonal development. The bone is less vascularized than that of embryonic and hatchling dinosaurs, and is more comparable to that in hatchling alligators (see Horner et al., 2001). Longitudinal sections through the epiphysis reveal endosteo-endochondral trabeculae, most of which are diagenetically altered to ghost images; evidence of calcified cartilage is preserved in a few areas. Although no trace is found of a subchondral bone plate or transphyseal canals, a delineation is visible between the diaphyseal and epiphyseal–metaphyseal regions. Histology thus provides primarily negative evidence with which to assess the ontogenetic stage of the Greenlandic pterosaur.

Appendicular Proportions

Certain appendicular proportions of the tiny Greenlandic form lie within the range known among other pterosaurs (Table 2). The humerus is slightly shorter (92%) than the femur, a condition unusual among pterosaurs; comparable proportions are known only in *Preondactylus buffarinii* (Dalla Vecchia, 1998, table 5) and in *Pterodactylus antiquus, P. suevicus,* and *P. micronyx* (Wellnhofer, 1970; see Bennett, 1996, for a taxonomic reallocation of *P. suevicus* to the genus *Cycnorhamphus*). In both juvenile and adult *Eudimorphodon ranzii* as well as in other pterosaurs, these proportions are reversed. In other appendicular proportions the Greenlandic pterosaur is distinctive (Table 2). Relative to the humerus or femur, the ulna is shorter than in any known pterosaur. Similarly, relative to the femur, the tibia is shorter than in any known pterosaur. Among pterosaurs, the Greenlandic pterosaur is distinctive in having the relative lengths of brachium to antebrachium, and femur to crus, both nearly equal.

The length of the metatarsus also appears to be unusual. Metatarsals in the Greenlandic pterosaur vary from 132 to 156% of the lengths represented in a juvenile eudimorphodontid (MCSNB 8950 B), which is particularly notable because

←

Figure 6. Limb proportions of the adult, type specimen of *Eudimorphodon ranzii* (MCSNB 2888), top, compared with a juvenile *E. ranzii* (MCSNB 8950), middle, and *E. cromptonellus,* new species (MGUH VP 3393), bottom. The limbs are positioned in the same transverse plane to permit graphic illustration of the relative lengths of the long bones; no postural or kinematic representation is intended. Data on *E. ranzii* are from Wild (1978, 1994). Appendicular bone lengths are estimated for the metatarsus of MCSNB 2888; the wing phalanges distal to the break in the proximal wing phalanx of MCSNB 2888; and the first and fourth wing phalanges of MGUH VP 3393.

Table 2. Limb segment proportions. Data from (a) Ewer, 1965; (b) Sereno and Arcucci, 1994; (c) Padian, personal observation; (d) Dalla Vecchia, 1998; (e) Wild, 1978; (f) Wild, 1994; (g) Dalla Vecchia, 1995; (h) Unwin, 1988, and Padian, personal observation (i) Wellnhofer, 1978, and Padian, personal observation.

	N	Humerus/ femur (%)	Humerus/ ulna (%)	Femur/ tibia (%)	Ulna/ femur (%)	Humerus/ tibia (%)
Euparkeria capensis	1 (a)	68	112	117	60	79
Marasuchus lilloensis	1 (b)	69	107	80	64	55
Scleromochlus taylori	7 (c)	62	91	93	69	57
Eudimorphodon cromptonellus, new species, MGUH VP 3393	1	92	90	96	102	89
Preondactylus buffarinii, MFSN 1770	1 (d)	98	76	74	129	73
Peteinosaurus zambellii, MCSNB 3359	1 (e)	104	80	76	130	79
Eudimorphodon ranzii, juvenile, Milano specimen	1 (e)	137	74	76	184	104
Eudimorphodon ranzii, juvenile, MCSNB 8950	1 (f)	133	78	77	171	102
Eudimorphodon ranzii, adult, type, MCSNB 2888	1 (e)	115	72	82	159	94
Eudimorphodon rosenfeldi MFSN 1797	1 (g)	109	74	68	149	75
Dimorphodon macronyx	1–5 (h)	104–109	77	64–72	130–134	67–75
Dorygnathus banthensis	15 (i)	120–138	59–71	65–81	191–210	82–105
Campylognathoides liasicus	6 (i)	123–141	78–86	75–94	153–169	100–132
Campylognathoides zitteli	1–2 (i)	108	85–94	74	126	80–100

every other limb dimension (with the exception of femoral length) indicates that MCSNB 8950 is a larger animal (Table 1; Fig. 6). Similarly, even the shortest metatarsal of the Greenlandic pterosaur (ca. 11 mm) is longer than the longest metatarsals of *Pterodactylus* specimens that, in other limb dimensions, appear to be otherwise comparably sized or even larger (*P. elegans*, no. 49, 7.8 mm; *P. elegans*, no. 12, 9.5 mm; *P. micronyx*; no. 42, 8.8 mm; Wellnhofer, 1970, fig. 19). In most pterosaurs, the average length of metatarsals I–IV is less than that of metacarpal IV. Exceptions are *Peteinosaurus zambellii* (Wild, 1978, pl. 14) and *Campylognathoides zitteli* (Plieninger, 1895: 216–217; Wellnhofer, 1978: 38), in which average metatarsal lengths are greater (105%, 129%, respectively). The Greenlandic form is even more exceptional, having metatarsals that average 141% of metacarpal IV length.

Wild (1978) interpreted *Peteinosaurus zambellii* as the most primitive pterosaur then known on the basis of the relative shortness of the wing compared to the length of the hind limb. Wild (1984: 54) later cited various limb segment ratios in support of his observation that *Preondactylus buffarinii* is unique among pterosaurs for "... an unproportionally long hind-limb," and a wing that is "extraordinarily short." More recently, a reanalysis of *Pr. buffarinii* led Dalla Vecchia (1998: 365) to conclude that *Pe. zambellii*, *Pr. buffar-*

inii, and *Dimorphodon macronyx* are "probably the most primitive of all known pterosaurs." Direct comparison of these taxa with the Greenlandic pterosaur is limited because the fourth wing phalanx in MGUH VP 3393 is unknown, and the lengths of various phalanges can only be estimated. Nonetheless, a restricted comparison may be made on the basis of summed lengths of the propodial, mesopodial, and metapodial elements (Σ humerus + ulna + metacarpal IV/Σ femur + tibia + average metatarsal length). The proportionate lengths of the proximal forelimb to proximal hind limb, thus defined, are 90% in the Greenlandic pterosaur, 95% in *Pr. buffarinii,* and 100% in *Pe. zambellii.* In *D. macronyx* the proportion is 104%, in *Campylognathoides liasicus* 124%, in juvenile *Eudimorphodon ranzii* and *Dorygnathus banthensis* 130%, but in *Campylognathoides zitteli,* with its unusually short hind limb, 94%.

The Pterosaurian Wingbeat Cycle

Most reconstructions of pterosaurs in flight depict the wings fully extended in a position that is suggestive of soaring, although general agreement exists that all except the largest pterosaurs were capable of sustained, flapping flight. The only attempt to illustrate the excursion of an entire wing is by Wellnhofer (1991: 153), but his diagram of a pterodactyloid only depicts the downstroke, and shows major flexion at the wrist and little at the metacarpophalangeal joint. Subsequently, Padian and Rayner (1993: 143, fig. 13C) suggested that the pterosaurian ". . . metacarpophalangeal joint is ideally adapted for sweeping the wingtip during the upstroke in a movement analogous to that in birds. With their long, thin wings the pterosaur wingbeat would have appeared very similar to that of long-winged birds such as gulls or albatrosses."

As a first-order approximation, an avian model of a pterosaurian wingbeat cycle fulfills fundamental aerodynamic requirements: upon downstroke the wing is fully extended to promote maximum thrust, and during upstroke the effective wingspan is shortened. Nonetheless, the analogy is limited by anatomical differences. Birds possess a multiaxial carpometacarpal joint complex with numerous degrees of freedom and movement possibilities (Vazquez, 1992). Reduction of aerofoil drag of the distal wing during upstroke in birds may be further promoted by a rotation of the feathers that opens slots between them (the valve function of Norberg, 1985), or by a closure of the imbricating fan of feathers. The fiber-stiffened distal patagium of pterosaurs (i.e., distal to the metacarpophalangeal joint; Padian and Rayner, 1993; see also Unwin et al., 1993) has no comparable intrinsic mechanisms for changes in shape, and thus shortening effective wingspan would appear to be the only alternative mechanism for reducing aerofoil drag during upstroke. The joint that permits the largest range of excursion is the metacarpophalangeal joint. However, the pterosaurian metacarpophalangeal joint is a uniaxial joint, with one degree of freedom; the asymmetrical form of this joint, which entails a screwlike motion (Wellnhofer, 1978), provides for radial deviation of the wing finger upon wing extension, and ulnar deviation and flexion upon wing folding.

The bicondylar form of the metacarpophalangeal joint in *Eudimorphodon cromptonellus* appears to be intermediate between a primitive, unicondylar joint and the trochlear form of later pterosaurs. This spectrum of joint configurations represents increasing mechanical stability, consonant with the interpretation that the joint was actively employed in flapping flight. As in other pterosaurs, the joint in *Eudimorphodon cromptonellus* is structurally asymmetric: the dorsal condyle has a larger radius of curvature, and a more extensive articular surface, than the ventral condyle (Fig. 5). However, the joint surfaces at their extensor end are evenly aligned. Thus, during the downstroke, the extended distal wing (supported by the four pha-

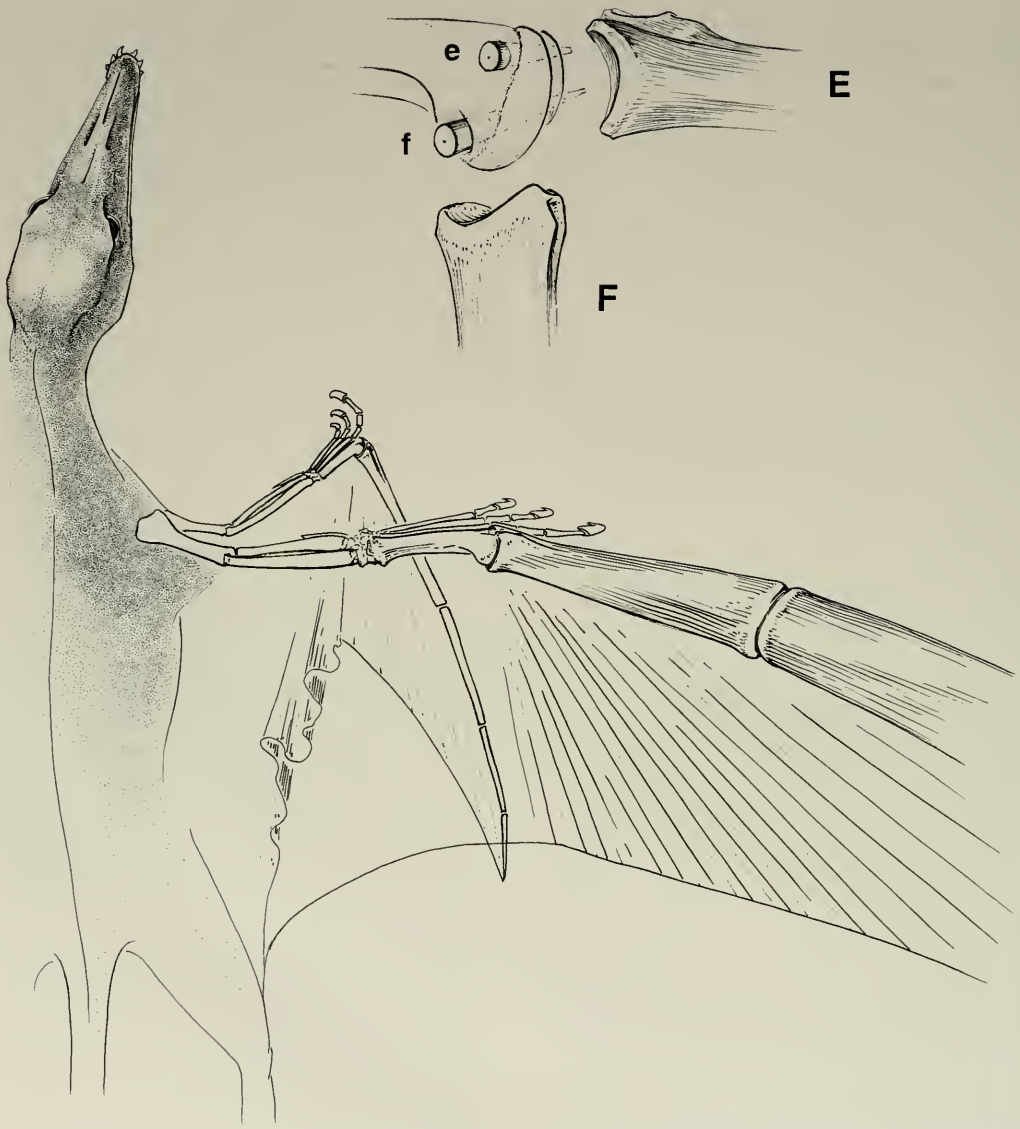

Figure 7. Reconstruction of metacarpophalangeal (mp) joint function in *Eudimorphodon cromptonellus,* new species, during flapping flight. The wing, in dorsolateral view, is shown in an extended position during early downstroke and in a flexed position in early upstroke. The inset above depicts mp joint relations, disarticulated for illustrative purposes, in the extended (E) and flexed (F) positions. The axis of the mp joint in an extended position (e) is normal to the metacarpal shaft because of the symmetry of the condyles in this region; the proximal phalanx is thus aligned with metacarpal IV. The mp joint axis in a flexed position (f) is oblique to the metacarpal shaft because of condylar asymmetry, resulting in a slight rotation and flexion of the distal wing as the mp joint undergoes ulnar deviation. The excursion of the mp joint during the upstroke of flapping flight is consonant with the distribution of fibers as interpreted by Wild (1994: 109) for the congener *E. ranzii* (MCSNB 8950). Elongate, membrane stiffening fibers occur in the distal wing, whereas short fibers in the proximal wing allow flexibility.

langes) is aligned with the proximal wing (Fig. 7) because the joint's axis at the extensor end of the metacarpophalangeal joint is perpendicular to the plane of the entire wing (Fig. 7, top inset). Were the metacarpophalangeal joint to be flexed during upstroke, the shift in the joint's axis (Fig. 7, top inset), which results from condylar asymmetry, engenders a rotation and flexion of the distal wing out of the plane of the proximal wing. Thus, during upstroke, the distal wing would be directed ventrally and somewhat everted (i.e., the ventral surface turned to face slightly laterally). On this interpretation, the trailing position of the distal wing relative to the proximal wing during the upstroke would be comparable to that seen in birds, but the rotation and flexion would seem uniquely pterosaurian.

ACKNOWLEDGMENTS

Field work, supported by grants from the National Science Foundation, the Carlsberg Foundation, and the Putnam Expeditionary Fund of the Museum of Comparative Zoology, was initiated on the basis of geological studies by L. B. Clemmensen (University of Copenhagen). We thank W. W. Amaral for preparation of the specimen; A. H. Coleman and P. Chandoha for photography; L. L. Meszoly for drawing Figures 2 and 3; and K. Brown-Wing for rendering Figures 5, 6, and 7. For histologic examination of the femur, we are grateful to M. Goodwin (University of California Museum of Paleontology) and E. Lamm (Museum of the Rockies) for technical assistance, A. Paulsen for photography, and J. R. Horner and A. de Ricqlès for consultation. Finally, we thank S. C. Bennett, F. M. Dalla Vecchia, K. M. Middleton, P. Wellnhofer, and R. Wild for authoritative, helpful reviews.

LITERATURE CITED

BENNETT, S. C. 1993. The ontogeny of *Pteranodon* and other pterosaurs. Paleobiology, **19:** 92–106.

———. 1996. On the taxonomic status of *Cycnorhamphus* and *Gallodactylus* (Pterosauria: Pterodactyloidea). Journal of Paleontology, **70:** 335–338.

CLARK, J. M., J. A. HOPSON, R. HERNÁNDEZ R., D. E. FASTOVSKY, AND M. MONTELLANO. 1998. Foot posture in a primitive pterosaur. Nature, **391:** 886–889.

CLEMMENSEN, L. B., D. V. KENT, AND F. A. JENKINS, JR. 1998. A Late Triassic lake system in East Greenland: facies, depositional cycles and palaeoclimate. Palaeogeography, Palaeoclimatology, Palaeoecology, **140:** 135–159.

DALLA VECCHIA, F. M. 1995. A new pterosaur (Reptilia, Pterosauria) from the Norian (Late Triassic) of Friuli (northeastern Italy). Preliminary note. Gortania—Atti del Museo Friulano di Storia Naturale, **16:** 59–66.

———. 1998. New observations on the osteology and taxonomic status of *Preondactylus buffarinii* Wild, 1984 (Reptilia, Pterosauria). Bollettino della Società Paleontologica Italiana, **36:** 355–366.

DALLA VECCHIA, F. M., G. MUSCIO, AND R. WILD. 1989. Pterosaur remains in a gastric pellet from the Upper Triassic (Norian) of Rio Seazza Valley (Udine, Italy). Gortania—Atti del Museo Friulano di Storia Naturale, **10:** 121–131.

EWER, R. F. 1965. The anatomy of the thecodont reptile *Euparkeria capensis* Broom. Philosophical Transactions of the Royal Society of London B, **248:** 379–435.

HORNER, J. R., K. PADIAN, AND A. DE RICQLÈS. 2001. Comparative osteohistology of some embryonic and perinatal archosaurs: developmental and behavioral implications for dinosaurs. Paleobiology, **27:** 39–58.

JENKINS, F. A., JR., N. H. SHUBIN, W. W. AMARAL, S. M. GATESY, C. R. SCHAFF, L. B. CLEMMENSEN, W. R. DOWNS, A. R. DAVIDSON, N. BONDE, AND F. OSBÆCK. 1994. Late Triassic continental vertebrates and depositional environments of the Fleming Fjord Formation, Jameson Land, East Greenland. Meddelelser om Grønland, Geoscience, **32:** 1–25.

NORBERG, R. Å. 1985. Function of vane asymmetry and shaft curvature in bird flight feathers; inferences on flight ability of *Archaeopteryx*, pp. 303–318. *In* M. K. Hecht, J. H. Ostrom, G. Viohl, and P. Wellnhofer (eds.), The Beginnings of Birds. Eichstätt, Germany: Freunde des Jura-Museums. 382 pp.

PADIAN, K. 1980. Note of a new specimen of pterosaur (Reptilia: Pterosauria) from the Norian (Upper Triassic) of Endenna, Italy. Rivista del Museo Civico di Scienze Naturali "E. Caffi," **2:** 119–127.

———. 1983. A functional analysis of flying and walking in pterosaurs. Paleobiology, **9:** 218–239.

———. 1986. On the type material of *Coelophysis* Cope (Saurischia: Theropoda) and a new specimen from the Petrified Forest of Arizona (Late Triassic: Chinle Formation), pp. 45–60. *In* K. Padian (ed.), The Beginning of the Age of Dinosaurs: Faunal Change across the Triassic–Jurassic

Boundary. New York: Cambridge University Press. xii + 378 pp.

PADIAN, K., AND J. M. V. RAYNER. 1993. The wings of pterosaurs. American Journal of Science, A, **293:** 91–166.

PADIAN, K., A. J. DE RICQLÈS, AND J. R. HORNER. 1995. Bone histology determines identification of a new fossil taxon of pterosaur (Reptilia: Archosauria). Comptes Rendus de l'Académie des Sciences, Sciences de la Terre et des Planetes, série IIa, **320:** 77–84.

PLIENINGER, F. 1895. *Campylognathus Zitteli.* Ein neuer Flugsaurier aus dem Oberen Lias Schwabens. Palaeontographica, **41:** 193–222.

ROGHI, G., P. MIETTO, AND F. M. DALLA VECCHIA. 1995. Contribution to the conodont biostratigraphy of the Dolomia di Forni (Upper Triassic, Carnia, NE Italy). Memorie di Scienze Geologische Università di Padova, **47:** 125–133.

SERENO, P. C., AND A. B. ARCUCCI. 1994. Dinosaurian precursors from the Middle Triassic of Argentina: *Marasuchus lilloensis,* gen. nov. Journal of Vertebrate Paleontology, **14:** 53–73.

UNWIN, D. M. 1988. New remains of the pterosaur *Dimorphodon* (Pterosauria: Rhamphorhynchoidea) and the terrestrial ability of early pterosaurs. Modern Geology, **13:** 57–68.

UNWIN, D. M., D. M. MARTILL, AND N. N. BAKHURINA. 1993. The structure of the wing membrane in pterosaurs. Journal of Verebrate Paleontology, **13**(3, Suppl.): 61A.

VAZQUEZ, R. J. 1992. Functional osteology of the avian wrist and the evolution of flapping flight. Journal of Morphology, **211:** 259–268.

WELLNHOFER, P. 1970. Die Pterodactyloidea (Pterosauria) der Oberjura-Plattenkalke Süddeutschlands. Abhandlungen bayerische Akademie der Wissenschaften, mathematisch-naturwissenschaftliche Klasse, **141:** 1–133.

———. 1975a. Die Rhamphorhynchoidea (Pterosauria) der Oberjura-Plattenkalke Süddeutschlands. Teil 1. Allgemeine Skelettmorphologie. Palaeontographica A, **148:** 1–33.

———. 1975b. Die Rhamphorhynchoidea (Pterosauria) der Oberjura-Plattenkalke Süddeutschlands. Teil II. Systematische Beschreibung. Palaeontographica A, **148:** 132–186.

———. 1975c. Die Rhamphorhynchoidea (Pterosauria) der Oberjura-Plattenkalke Süddeutschlands. Teil III. Palökologie und Stammesgeschichte. Palaeontographica A, **149:** 1–30.

———. 1978. Pterosauria, pp. 1–81. *In* P. Wellnhofer (ed.), Handbuch der Paläoherpetologie, Teil 19. Stuttgart, Germany: G. Fischer. 81 pp.

———. 1991. The Illustrated Encyclopedia of Pterosaurs. London: Salamander Books. 192 pp.

WILD, R. 1978. Die Flugsaurier (Reptilia, Pterosauria) aus der Oberen Trias von Cene bei Bergamo, Italien. Bollettino della Società Paleontologica Italiana, **17:** 176–256.

———. 1984. A new pterosaur (Reptilia, Pterosauria) from the Upper Triassic (Norian) of Friuli, Italy. Gortania—Atti del Museo Friulano di Storia Naturale, **5:** 45–62.

———. 1994. A juvenile specimen of *Eudimorphodon ranzii* Zambelli (Reptilia, Pterosauria) from the Upper Triassic (Norian) of Bergamo. Rivista Museo civico di Scienze Naturali "E. Caffi," **16:** 95–120.

ZAMBELLI, R. 1973. *Eudimorphodon ranzii* gen. nov., sp. nov., uno pterosauro Triassico. Istituto Lombardo Rendiconti Scienze, B **107:** 27–32.

IMMATURE RHIZODONTIDS FROM THE DEVONIAN OF NORTH AMERICA

MARCUS C. DAVIS,[1] NEIL H. SHUBIN,[1,2]* AND E. B. DAESCHLER[2]

ABSTRACT. New fossils from the Duncannon Member of the Catskill Formation provide material for hypotheses about the evolution of fin development and function in extinct sarcopterygians. The rhizodontid affinity of these specimens is supported by the pattern of overlap between the clavicle and cleithrum, the robustness of the pectoral girdle, the presence of unjointed and elongate lepidotrichia in the pectoral appendage, and the presence of multiple lateral line canals. The small body size and weakly ossified endochondral skeletons indicate that these individuals are immature. The pectoral fin includes both dermal and endochondral elements; massive, unjointed dermal rays that compose the bulk of the appendage envelop the endochondral bones. The emphasis on both dermal and endochondral elements in rhizodontids is an unexpected intermediate condition between ray-finned and lobe-finned designs that could not be predicted from current models of dermal fin development. The large size of rhizodontids and, perhaps, aspects of their locomotor and feeding strategies, may have necessitated fins with large surface areas. Expansion of the surface area of the fins was accomplished by elaboration of the dermal radials. The evolution of an extensive endochondral skeleton in rhizodontids may relate to the role of the endochondral skeleton in the control of movements and shape of this expanded fin.

INTRODUCTION

Rhizodontid sarcopterygians are large, predatory fish that have a variety of unique features of the skull, pectoral girdle, fins, and lateral line systems (Andrews, 1985). Many of these features, such as the unjointed and elongate lepidotrichia in the pectoral fins, suggest that rhizodontids may have been specialized for modes of locomotion and predation unseen in other sarcopterygian taxa. Represented by eight or nine genera from the Devonian and Carboniferous, these fish typically attain lengths greater than 3 m. Because of the many similarities between the endochondral skeletons of rhizodontid fins and tetrapod limbs, these taxa have figured prominently in studies of the origin of tetrapod limbs (e.g., Gregory and Raven, 1941).

Remains of rhizodontid sarcopterygians are major components of Late Devonian and Early Carboniferous nonmarine fossil assemblages (Andrews, 1985; Young et al., 1992). Scales, isolated vertebrae, and teeth are the most common rhizodontid elements encountered; these are usually assigned to the genera *Rhizodus* and *Strepsodus*. However, more complete material is rare. The most complete specimens are known from the Dinantian of Foulden, United Kingdom (*Strepsodus,* several partially articulated specimens [Andrews, 1985]), the Lower Carboniferous of Australia (*Barameda,* an articulated partial skeleton preserved as a natural mold [Long, 1989]), the Frasnian of Antarctica (*Notorhizodon,* isolated cranial and girdle elements [Young et al., 1992]), and the Famennian of New South Wales, Australia (*Gooloogongia,* articulated individuals preserved as natural molds [Johanson and Ahlberg, 1998]) and of North America (*Sauripterus*, isolated pectoral fins and scales [Hall, 1843; Daeschler and Shubin, 1998]).

A number of features, particularly in the paired fins and associated girdles, distin-

* Corresponding Author

[1] Department of Organismal Biology and Anatomy, University of Chicago, 1027 East 57th Street, Chicago, Illinois 60637.

[2] Department of Vertebrate Biology, Academy of Natural Sciences of Philadelphia, 1900 Benjamin Franklin Parkway, Philadelphia, Pennsylvania 19103.

guish rhizodontids as a clade. Rhizodontid pectoral girdles are unique in both their massive relative size as well as the nature of the internal articulations between constituent bones. The ventral laminae of the clavicles and cleithra are broad, ornamented plates that extend cranially, enclosing the caudal portion of the gular region (Andrews, 1985, fig. 10b). In porolepiforms and osteolepids (for example see *Eusthenopteron* [Andrews and Westoll, 1970, fig. 1]), the dorsal lamina of the cleithrum is overlapped medially by the clavicle, whereas the ventral lamina of the clavicle is overlapped medially by the cleithrum. In rhizodontids the pattern of overlap is reversed: the dorsal lamina of the cleithrum is overlapped laterally by the clavicle, and the ventral lamina of the clavicle is overlapped laterally by the cleithrum. The function of this massive shoulder girdle, with its unusual pattern of overlap between constituent elements, is unknown.

Although rhizodontid pectoral girdles are readily distinguished from those of other sarcopterygians, the pectoral fins of rhizodontids share a number of similarities with the limbs of tetrapods. The best-known rhizodontid fins are isolated appendages that have been assigned to the genus *Sauripterus*. *Sauripterus* possesses a limblike arrangement of endochondral bones, including distal radials that have been compared to tetrapod digits (Gregory and Raven, 1941; Daeschler and Shubin, 1998). Despite differences in the size and shape of corresponding elements in *Sauripterus* and tetrapods, the pattern of endochondral bones is extremely similar. The phylogenetic significance of these similarities is muddled by the fact that recent cladistic studies do not support a sister-group relationship between tetrapods and rhizodontids. Missing data are problematic in the cladistic analysis of the higher level relationships of rhizodontids because few overlapping characters occur between taxa such as *Sauripterus* (consisting of isolated fins and scales) and *Gooloogongia* (consisting of a relatively complete skull and body, but with poorly preserved fins).

Here we describe immature rhizodontid specimens, which we refer to the genus *Sauripterus*, from the Famennian Catskill Formation of North America. The relative completeness of the skeletons provides an opportunity to examine the morphology of rhizodontids in greater detail and to assess hypotheses on the ontogeny of the paired fin skeleton in nontetrapod sarcopterygians.

GEOLOGICAL SETTING

The new rhizodontid material was recovered from the Late Devonian Red Hill locality in Clinton County, Pennsylvania (Fig. 1). Red Hill is a road-cut exposure of the Duncannon Member of the Catskill Formation. During the Late Devonian, the Catskill Delta extended from the foothills of the Acadian highlands within the Old Red Continent (Euramerica) to the epicontinental Catskill Sea that lay to the west (Woodrow, 1985). The fossiliferous horizons at Red Hill have been interpreted to represent channel margin and overbank deposits of a wide river flowing across a low-gradient floodplain under a subtropical climate (Woodrow et al., 1995). The 2-m-thick fossiliferous zone at Red Hill has produced the most abundant and well-preserved vertebrate fossils discovered to date from the Catskill Formation.

The rhizodontids were recovered from a grayish-red, poorly bedded sandy siltstone unit within the fossiliferous zone. Their degree of articulation is exceptional, even for Red Hill, and suggests that the specimens were quickly buried, did not undergo significant postmortem transport, and were not subsequently reworked. The two specimens on which this study is based are preserved on opposite sides of the same block of matrix. Remarkably, these specimens are the only rhizodontids known from Red Hill.

Red Hill has yielded a diverse assemblage of freshwater vertebrates, terrestrial plants, and invertebrates. Among the ver-

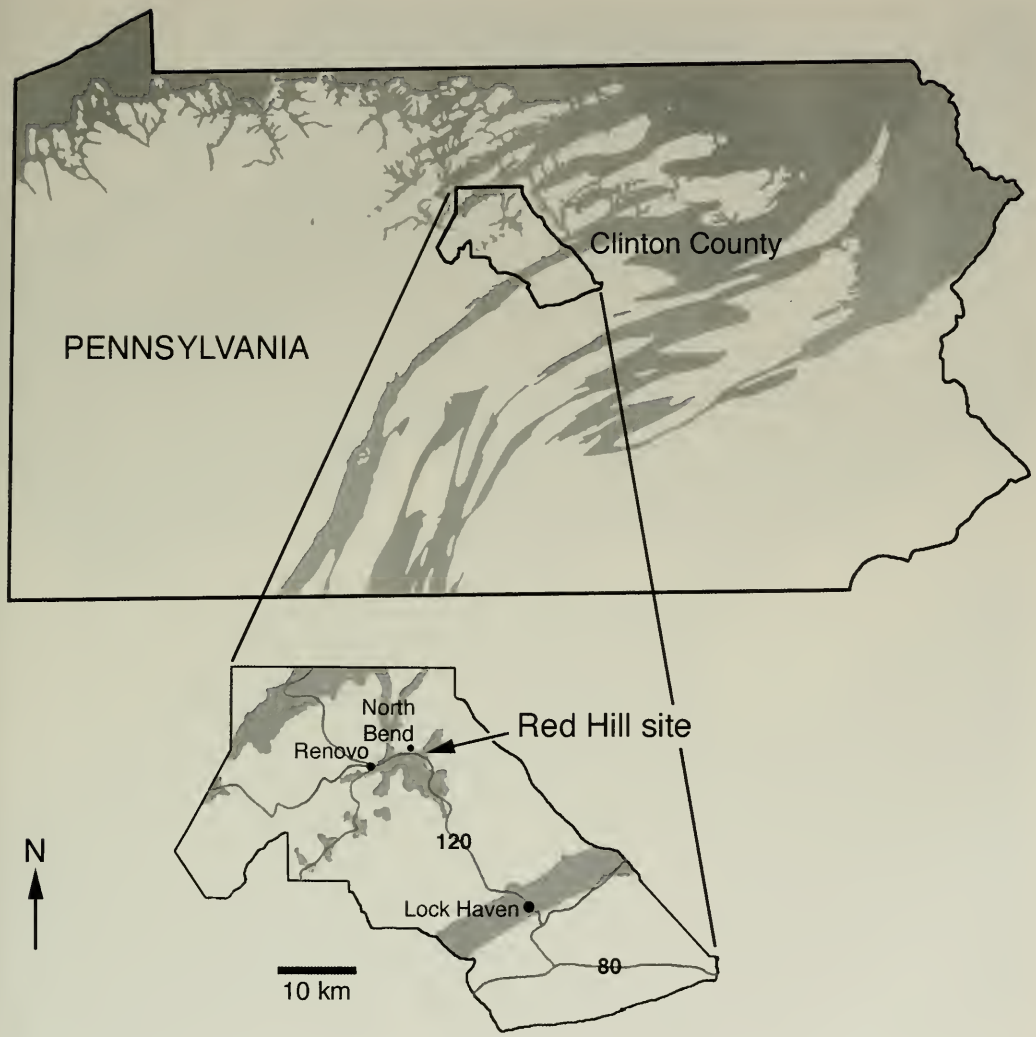

Figure 1. Location of Red Hill site, Clinton County, Pennsylvania, USA. Shaded areas represent Devonian age sediments. Abbreviations: 80, Interstate 80; 120, Pennsylvania State Route 120.

tebrates from the fossiliferous zone are two early tetrapod taxa, at least three taxa of osteolepiform sarcopterygians, an early actinopterygian, groenlandaspidid and phyllolepid placoderms, gyracanthid acanthodians, and chondrichthyans. This vertebrate fauna is associated with progymnosperm and lycopsid plants as well as palynomorphs. In addition, trigonotarbid arthropods are preserved both as body fossils and traces.

SYSTEMATIC PALEONTOLOGY

Sarcopterygii Romer, 1955

Rhizodontida Andrews and Westoll, 1970

cf. *Sauripterus* Hall, 1843

Diagnosis. Rhizodontid affinities are supported by the following features: cleithrum overlaps dorsal lamina of clavicle medially and ventral lamina of clavicle laterally (reversed from the condition seen

in osteolepiforms); laterally expanded ventral lamina of clavicle and cleithrum; rostrally expanded ventral lamina of cleithrum relative to the condition seen in osteolepiforms; scapulocoracoid sits dorsal to the junction of dorsal and ventral laminae of cleithrum; dermal skeleton of the paired fins composed of elongate, unjointed lepidotrichia; no postaxial process on the ulnare; accessory lateral lines. Assigned to the genus *Sauripterus* based on the following: radius anteroposteriorly broader than ulna relative to the condition seen in *Barameda* (Long, 1989) and *Strepsodus* (Andrews, 1985); ventral laminae of cleithra meet at midline.

These specimens also have unique characters seen in no other known rhizodontid: no entepicondyle on the humerus; no distal radials in the pectoral fin; no articulations between fin endochondral elements; disproportionally large pectoral fins relative to body size (when compared to all rhizodontids and osteolepids for which this can be measured); elongate interclavicle (craniocaudal length greater than that of ventral laminae of clavicle). Many of these characters can be interpreted as being related to the ontogenetic stage of ossification in the fin endoskeleton. Therefore, these specimens are referred to the genus *Sauripterus* as immature individuals.

Horizon and Locality. The Duncannon Member of the Catskill Formation. USA, Pennsylvania, Clinton County, Red Hill (coordinates 41°20.645′N, 77°40.800′W).

Age. Late Devonian; late Famennian stage (Fa2c substage); *Rugospora flexuosa–Grandispora cornuta* palynomorph zone (Traverse, in press).

Material. All specimens are housed in the Academy of Natural Sciences of Philadelphia (ANSP): ANSP 20980, a well-preserved skeleton lacking most cranial elements and median fins, preserved as part and counterpart (Figs. 2, 3); ANSP 20981, a smaller individual consisting of a left dentary, paired gulars, pectoral girdle and fins, preserved on the reverse side of the ANSP 20980 counterpart block (Fig. 4).

DESCRIPTION

Operculogular Series. Lateral gulars, a left operculum, and portions of the submandibular series are preserved on ANSP 20981. The lateral gulars are preserved in internal view, with the left gular, which is relatively more complete, overlapping the right. Both sides lack the rostral margin. It is difficult to determine whether a median gular was present. The ornamentation on the internal surface consists of shallow grooves that radiate caudally from the rostrolateral margin. Medial to this margin, two small teeth are preserved in cross section (Fig. 4, f. vom). These teeth may have been derived from the left dermopalatine or vomer, both of which are not preserved. A recessed edge along the lateral margin of the left gular marks the contact for the submandibulars. The submandibular series lies medial to the labial margin of the dentary and lateral to the left gular. The bone in this area appears very thin and broken, making it impossible to identify sutures.

A left opercular is preserved in ANSP 20981 (Fig. 4). The external surface is sparsely ornamented with a series of shallow, parallel grooves that extend dorsoventrally across the bone. The margins of the opercular lack this ornamentation and appear relatively smooth. The opercular is narrow rostrocaudally and deep dorsoventrally. This shape is similar to that of *Gooloogongia* (Johanson and Ahlberg, 1998, fig. 2g), but unlike the rounded operculars of *Barameda* (Long, 1989, fig. 5b) and *Strepsodus* (Andrews, 1985, fig. 1b). In porolepiforms and osteolepids the opercular extends caudally to contact the cranial margin of the dorsal lamina of the cleithrum. The proportions of the opercular in ANSP 20981 make it unlikely that it abutted against the dorsal lamina of the cleithrum. The resulting gap was likely filled by soft tissue, as in *Latimeria* (Jarvik, 1980). A preopercular lies rostral to the opercular. The poor preservation of the sutures

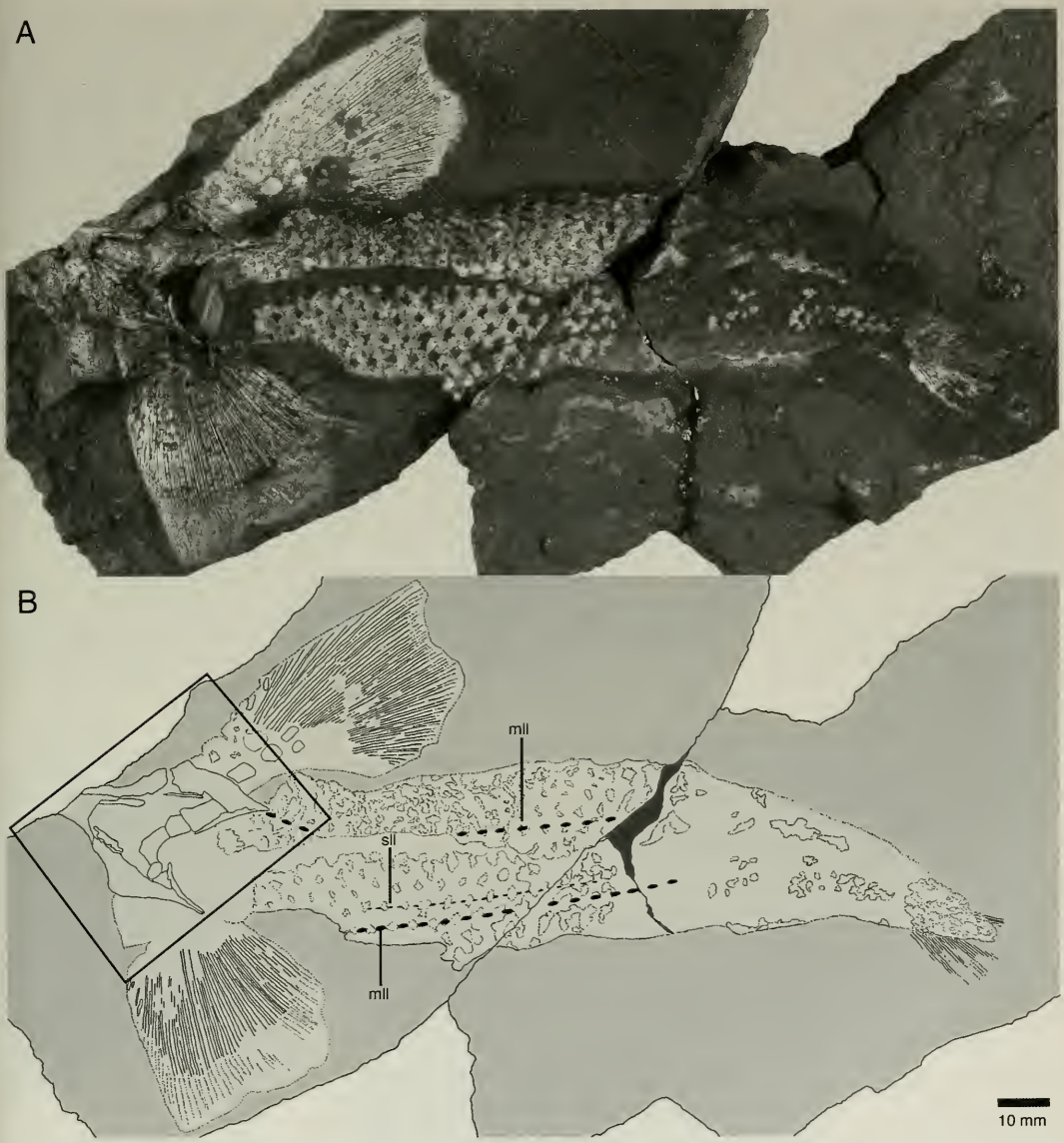

Figure 2. ANSP 20980 in part. (A) Photograph of specimen. (B) Labeled drawing: light shading represents fossil or fossil impression, dark shading represents matrix. Boxed area refers to Figure 5.

Abbreviations for Figs. 2–7: ano, anocleithrum; bo, internal boss of scale; cen, centra; clm, cleithrum; clm. dl, dorsal lamina of cleithrum; clm. vl, ventral lamina of cleithrum; clv. dl, dorsal lamina of clavicle; clv. vl, ventral lamina of clavicle; d1, d8, digits 1, 8; de, dentary; epi, epicaudal lobe; f. par, parasymphysial fang; f. vom, vomerine fang; gul, gular; H, humerus; hyp, hypocaudal lobe; iclv, interclavicle; i, intermedium; j. lep, jointed lepidotrichia; lbw, lateral body wall; m. ex, median extrascapular; mll, main lateral line; op, opercular; pcf, pectoral fin; plf, pelvic fin; pop, preopercular; pot, posttemporal; R, radius; subm, submandibular series; sll, secondary lateral line; su, supracleithrum; U, ulna; u, ulnare; unj. lep, unjointed lepidotrichia.

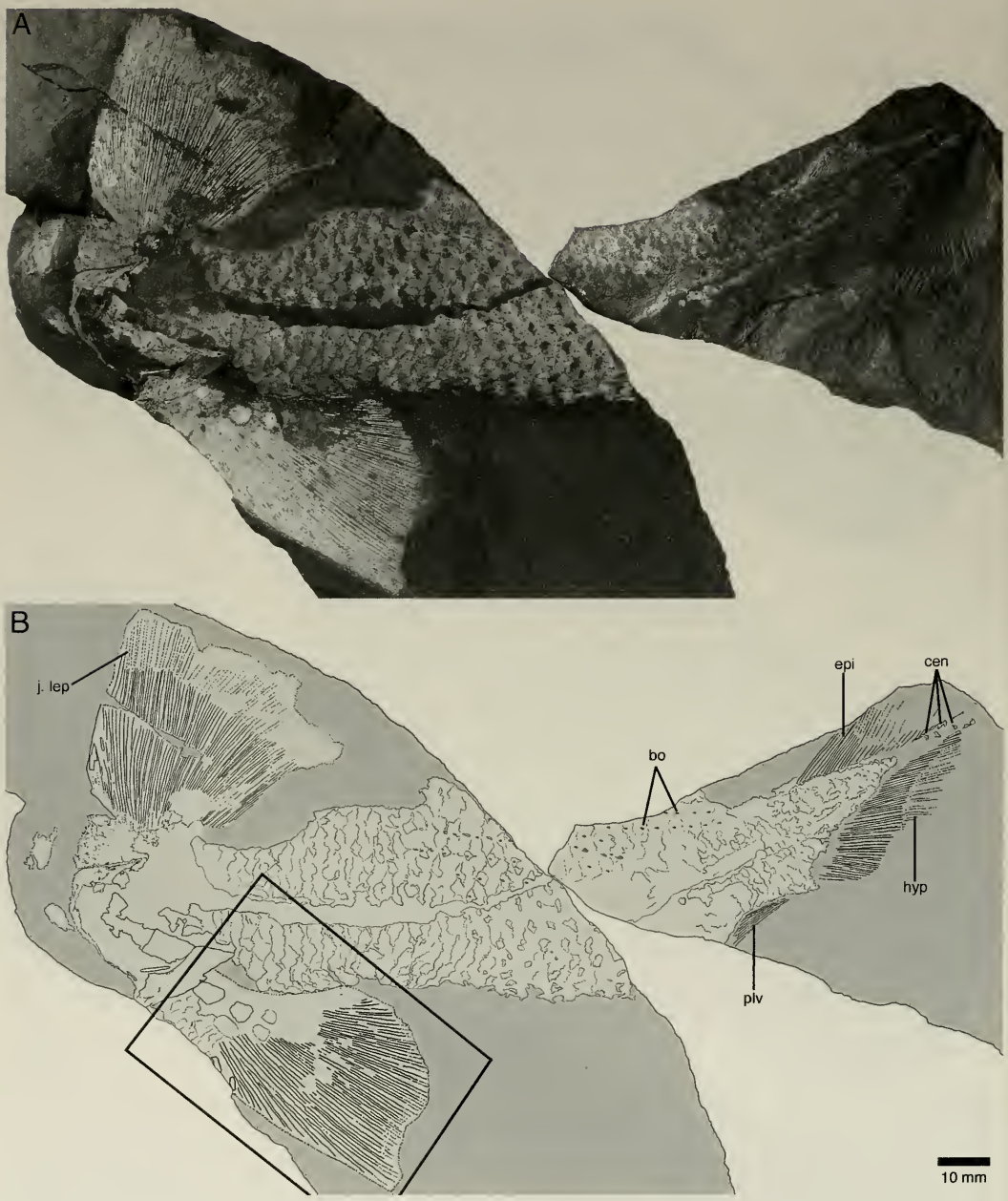

Figure 3. ANSP 20980 in part. (A) Photograph of specimen. (B) Labeled drawing. Boxed area refers to Figure 6.

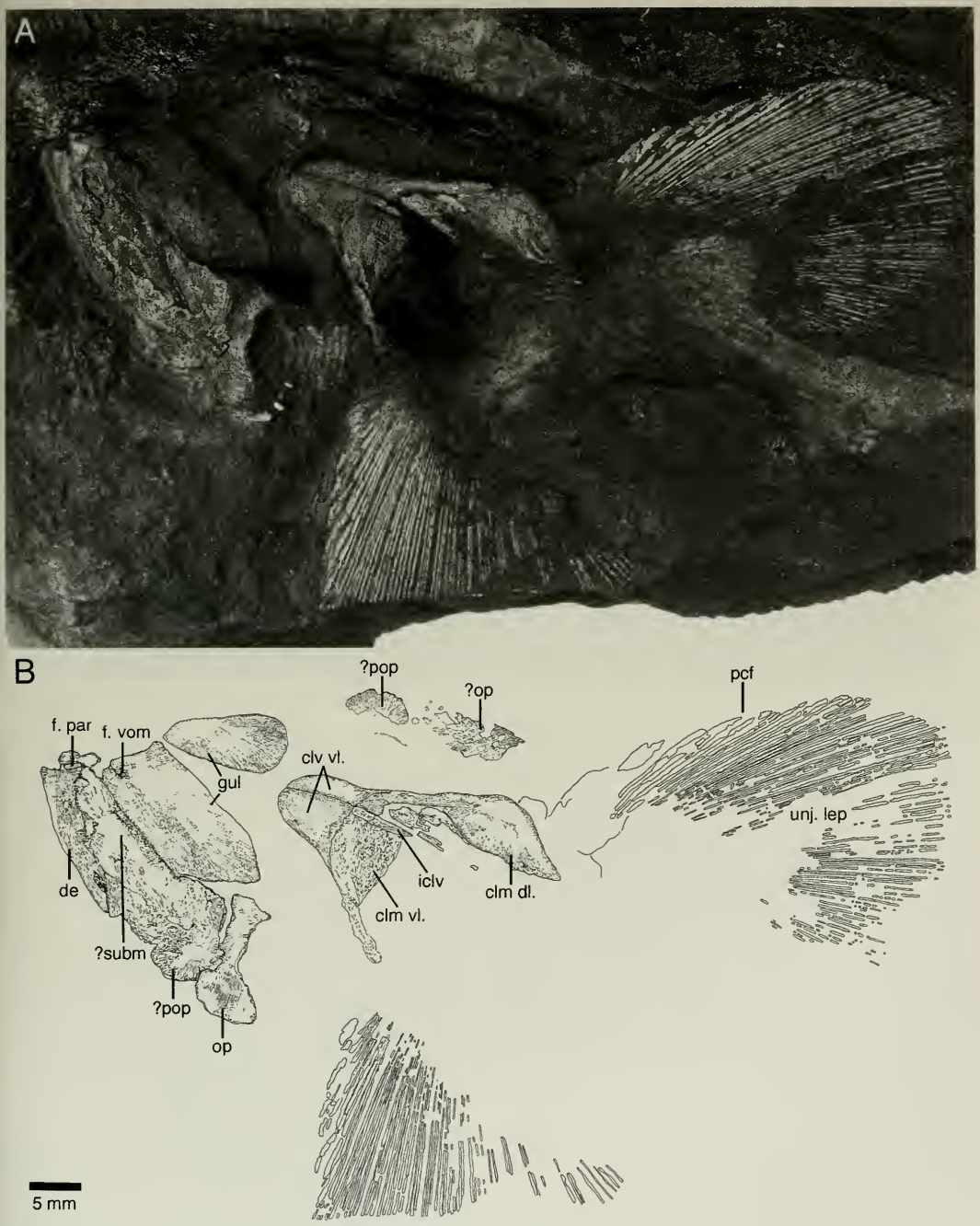

Figure 4. ANSP 20981 in visceral view. (A) Photograph of specimen. (B) Labeled drawing.

makes it impossible to identify the rostral and dorsal margins of this bone.

Dentary. On ANSP 20981, a left dentary is preserved lateral to the left gular and submandibulars (Fig. 4). The distal portion of the dentary is obscured. A series of mesiodistally oriented striations ornament the labial surface of the dentary. No sutures are visible that would indicate the presence of infradentary bones, nor is it possible to identify coronoids or coronoid teeth. Total dentary length is estimated to be approximately 20 mm.

Four incomplete teeth are preserved on the dentary. These teeth are oval in cross section and are buccolingually compressed. The largest and most mesial of the four is a parasymphysial fang (Fig. 4, f. par). Rhizodontid teeth are generally sigmoid in shape and possess lingual striations (see Andrews, 1985; Long, 1989). The extreme small size of the teeth and state of preservation make it difficult to determine whether ANSP 20981 possesses these tooth characters. The dentary of ANSP 20981 is similar to that ascribed to *?Strepsodus anculonamensis* (RSMGY 1980.40.36 [Andrews 1985, figs. 9b, c]) in the overall proportion of the dentary and the position of the parasymphysial fang.

Extrascapular Series. An incomplete median extrascapular is the only cranial element that can be identified with confidence on ANSP 20980. The bone is roughly trapezoidal in shape, narrowing craniomedially. A craniolaterally directed occipital commissural canal crosses the center of the median extrascapular (Fig. 5). In *Gooloogongia* and *Barameda,* only a small area of contact is present between the median extrascapular and the postparietals (Johanson and Ahlberg, 1998, figs. 2d, f). It is not possible to determine the nature of this contact on ANSP 20980 because the rostral margin of the median extrascapular is incomplete and postparietals are not preserved.

Pectoral Girdle. The articulation between the dorsal laminae of the clavicle and cleithrum is preserved on both left and right sides of ANSP 20980 and on the right side of ANSP 20981. The rostral and caudal margins of the dorsal lamina of the cleithrum are subparallel to each other (Fig. 5). This condition is also seen in the specimen of *Sauripterus* described by Daeschler and Shubin (1998) and in *Gooloogongia* (Z. Johanson, personal communication). In other rhizodontids the dorsal lamina tends to narrow at midlength before expanding to meet the ventral lamina.

Rhizodontid cleithra possess a depressed flange that extends along the caudal margin of the dorsal lamina; this flange is absent on ANSP 20980 and ANSP 20981. The right cleithrum associated with the fin of *Sauripterus* described by Daeschler and Shubin (1998) also lacks this flange, as does that of *Gooloogongia* (Z. Johanson, personal communication).

The cleithra are split internally between part and counterpart, leaving cancellous bone exposed in many places. However, the dorsal lamina of the right cleithrum is completely preserved in internal view. The external surface is exposed at the intersection of the dorsal and ventral laminae. Both the internal and external surfaces are ornamented with subparallel ridges that extend dorsoventrally (Fig. 5).

On ANSP 20980 the ventral laminae of the right clavicle and cleithrum overlap those of the left as a result of postmortem inturning and compression of the entire girdle (Fig. 5). In ANSP 20981, the reverse is true with the left ventral laminae of both the cleithrum and clavicle overlapping the right. The lateromedially directed ventral contact between clavicle and cleithrum is preserved in ANSP 20981 (Fig. 4).

An interclavicle lies in association with the ventral laminae of the clavicles and cleithra in both ANSP 20980 and ANSP 20981. The interclavicles have been displaced dorsocaudally from the position they were likely to have occupied in life (Figs. 4, 5). In both specimens the rostrocaudal length of the interclavicle appears to be greater than that of the ventral cla-

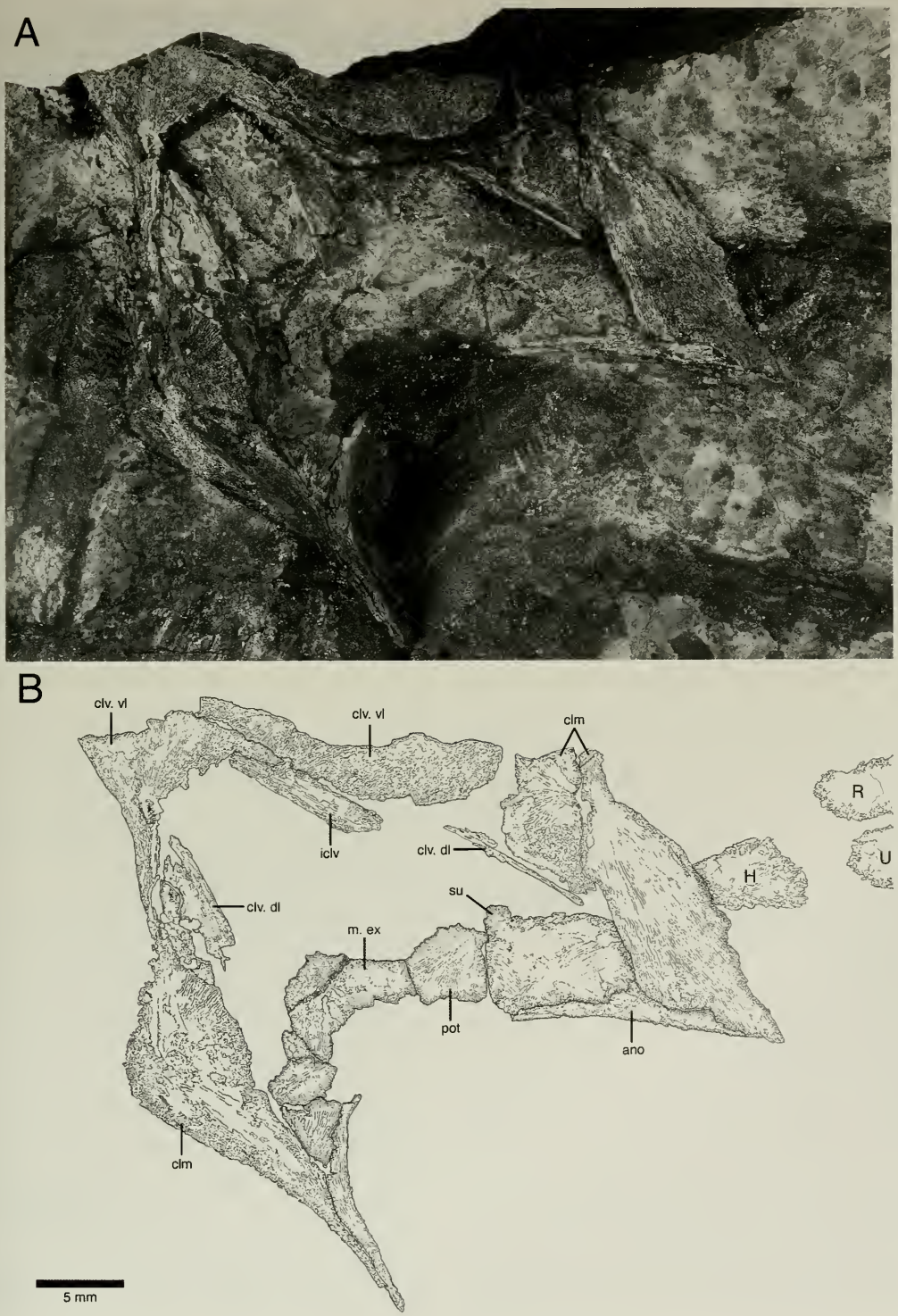

Figure 5. Shoulder girdle of ANSP 20980 in ventral view. (A) Photograph of specimen. (B) Labeled drawing.

vicular lamina. This condition suggests that the interclavicle may have been incorporated into part of the contact between ventral cleithral laminae. The elongation of the interclavicle caudally is a unique condition that is not seen in other rhizodontids or sarcopterygians. An interclavicle is not preserved with either known specimen of *Sauripterus* (Hall, 1843; Daeschler and Shubin, 1998), making it impossible to determine whether the elongation of the interclavicle is a characteristic of ANSP 20980 and ANSP 20981 only or of *Sauripterus* in general. ANSP 20981 is also unusual in possessing cleithra that meet at the ventral midline, lending further support to the possibility that the interclavicle was fused to the symphysis of the cleithra. Contact between the ventral cleithra laminae is also preserved in the adult *Sauripterus* specimen.

On ANSP 20980, a poorly preserved right scapulocoracoid is present medial to the caudal margin of the broken cleithrum. The scapulocoracoid is preserved as a small section of diaphanous bone, similar in texture to the endochondral elements of the pectoral fin. The lack of any diagnostic morphology on the scapulocoracoid is most likely due to the ontogenetic stage of the specimen, as the endochondral elements of the pectoral fin are also weakly ossified (see below). The scapulocoracoid appears to lie dorsal to the curvature formed by the intersection of the dorsal and ventral cleithral laminae. This relatively dorsal position of the scapulocoracoid is seen in other rhizodontids such as *Strepsodus* (Andrews, 1985) and *Sauripterus* (personal observations). In osteolepids, the scapulocoracoid assumes a more ventral position than in rhizodontids and rests in the curvature formed by the intersection of the cleithral laminae.

All bones of the supercleithral series are preserved in articulation on the left side of ANSP 20980. Corresponding elements are present on the right side, but are disarticulated and partially obscured by the dorsal lamina of the right cleithrum. The supracleithrum is a rectangular bone that contacts the posttemporal rostrally and the rostrodorsal margin of the cleithrum caudally. The posttemporal is somewhat smaller and more triangular in shape than the supracleithrum. The posttemporal contacts the median extrascapular rostrolaterally and the supracleithrum caudally. The anocleithrum is subdermal, a condition shared with porolepiformes, actinistia, and dipnoi (Ahlberg, 1989). In osteolepiformes (e.g., *Eusthenopteron* [Jarvik, 1980]) the anocleithrum contacts the supracleithrum rostrally and the cleithrum caudally, preventing contact between the supracleithrum and cleithrum.

Paired Fins. In ANSP 20980, the leading edge of the pectoral fin forms a gentle arc, with the greatest degree of curvature at midlength (Fig. 6). The trailing edge of the fin is composed of poorly preserved lepidotrichia that appear jointed. The bulk of the fin is supported by lepidotrichia that are unjointed for most of their length. The lepidotrichia are arranged in two layers, one forming the dorsal surface of the fin and one forming the ventral surface. All endochondral elements, except for the humerus, thus are enveloped dorsally and ventrally by unjointed lepidotrichia. These layers span all but the most proximal region of the fin, with preaxial lepidotrichia extending more proximally than do those on the postaxial edge.

The endochondral elements of the fin are weakly ossified; the central region of each element consists of relatively dense bone matrix, whereas the cortical regions are thin and translucent. The five elements that are present correspond to the humerus, radius, ulna, intermedium, and ulnare of derived sarcopterygians. The humerus of ANSP 20980 lacks postaxial processes, and thus differs from those of all other rhizodontids. The radius is anteroposteriorly broader than the ulna. The overall proportions of the radius of ANSP 20980, relative to the ulna and humerus, are very similar to those of *Sauripterus* (Daeschler and Shubin, 1998). Other rhizodontids,

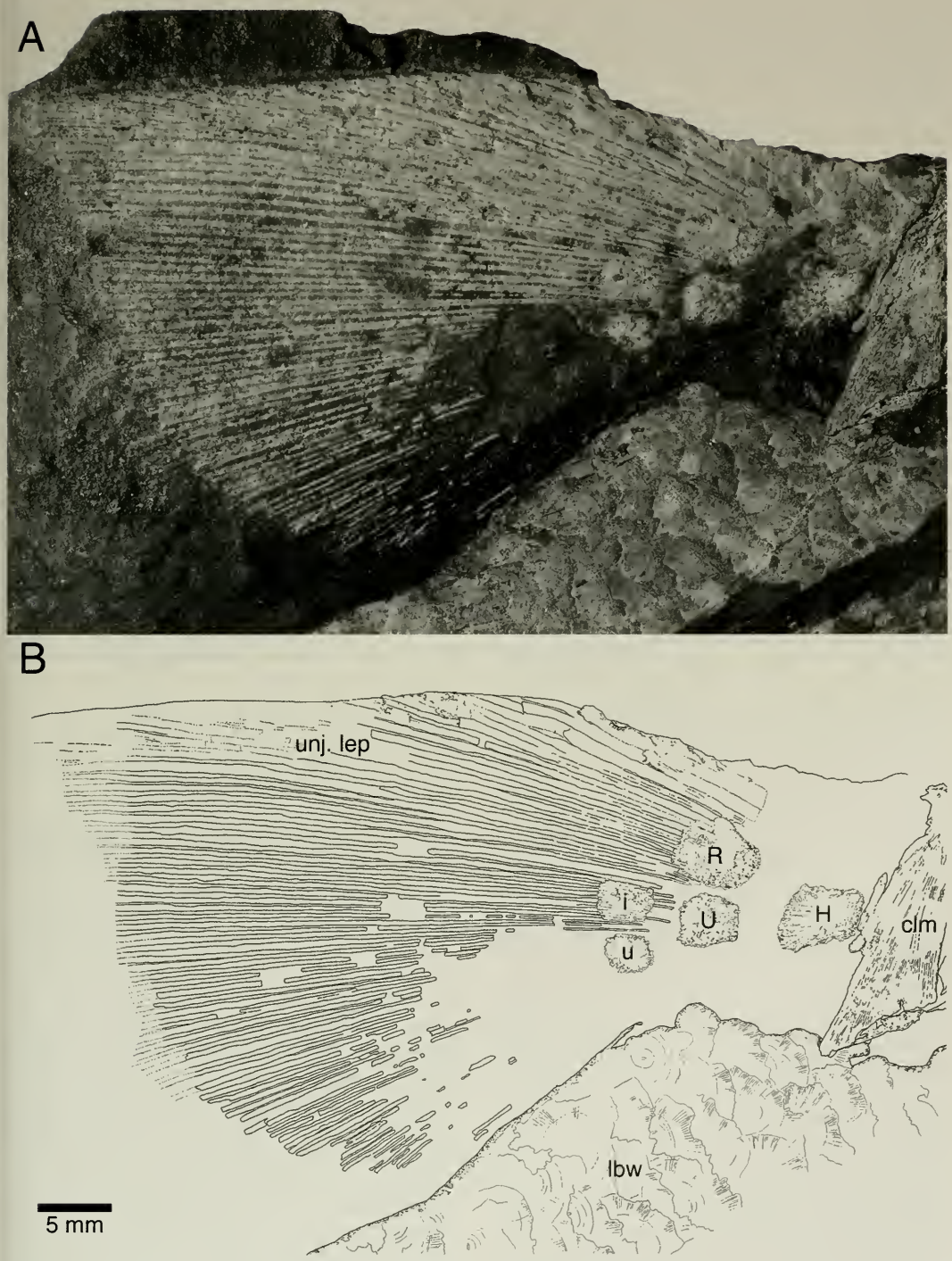

Figure 6. Left pectoral fin of ANSP 20980 showing endoskeletal and dermal elements. (A) Photograph of specimen. (B) Labeled drawing.

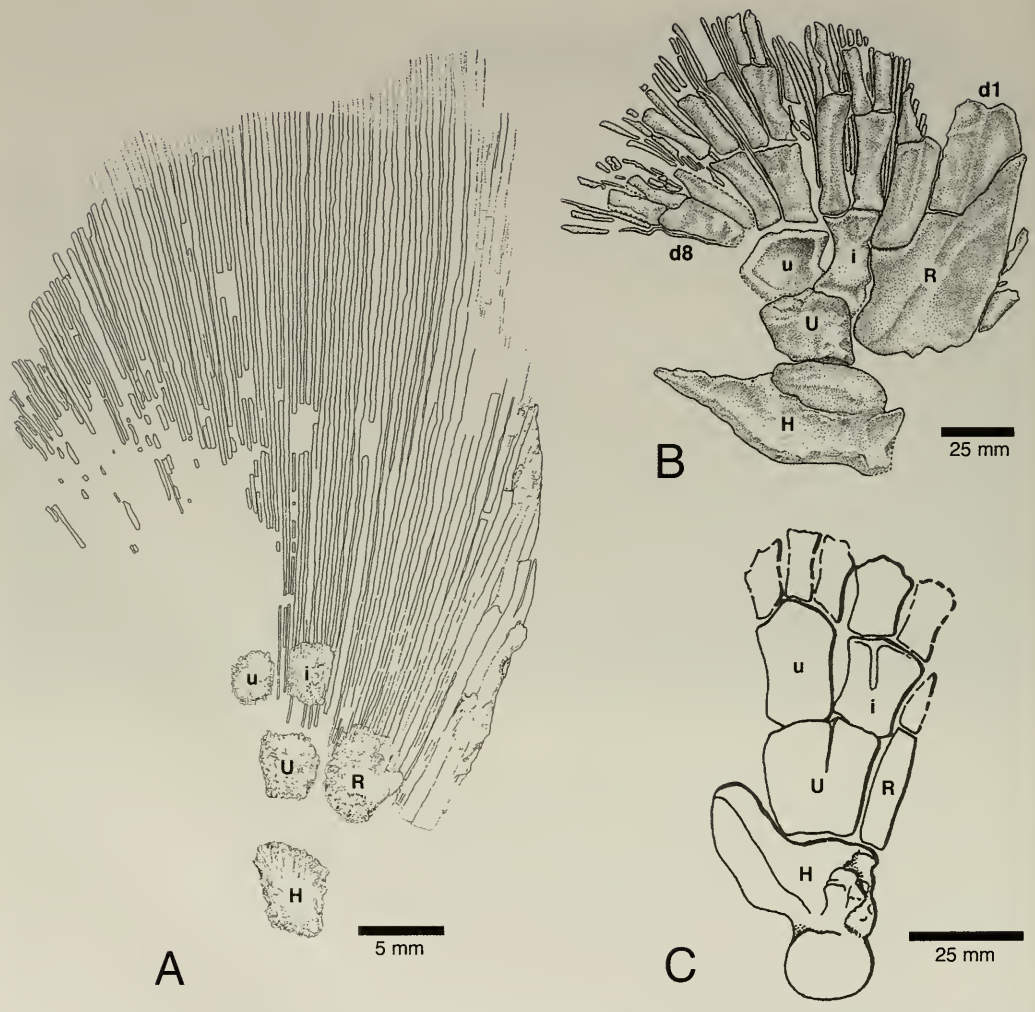

Figure 7. Comparison of the pectoral fins of (A) ANSP 20980, (B) *Sauripterus*, and (C) *Barameda*. *Barameda* modified from Long (1989).

such as *Barameda*, possess a radius that is narrower than the ulna (Fig. 7). Furthermore, a relatively narrow radius is also seen in osteolepids, including derived taxa such as *Panderichthys* (Vorobyeva and Schultze, 1991). Like *Barameda* and *Sauripterus*, the ulnare also lacks postaxial processes. In addition, the ulnare and intermedium terminate at the same distal level, a feature shared with *Sauripterus*, *Barameda*, and basal tetrapods.

The richly branched series of preaxial radials that distinguish the fins of *Barameda* and *Sauripterus* are not observed in the pectoral fins of ANSP 20980. Furthermore, there are no articulations between any of the endochondral elements, despite the fact that all bones appear to be preserved in situ. The distinct separations between adjacent endochondral bones may reflect the immaturity of the specimens, as all bones are also weakly ossified. The lack of distal radials may also be attributed to ontogeny given that they are the most dis-

tal elements of the fin. If ossification of the endoskeleton proceeded proximally to distally, then distal radials may not have ossified by this stage. ANSP 20981 represents a smaller individual and, indeed, there is no evidence of endochondral ossification in either pectoral fin. The entire fin is composed of long, unjointed lepidotrichia. The absence of endochondral elements may be due to lack of preservation, but it suggests that ANSP 20981 may be ontogenetically younger than ANSP 20980. Both specimens indicate that ossification of the fin dermal skeleton preceded that of the fin endoskeleton.

The pectoral fins of ANSP 20980 are disproportionally large for a sarcopterygian. Ratios of fin length to body length for ANSP 20980 can be compared to the type of *?Strepsodus anculonamensis* (RSMGY 1980.40.36 [Andrews, 1985]) and other osteolepids. The proximodistal length of the pectoral fin of *Strepsodus* is approximately 15% of the total body length (50 mm fin/345 mm estimated total length). This ratio is not unusual for a sarcopterygian: *Eusthenopteron* (14.9%, based on Jarvik's 1980 reconstruction), *Osteolepis* (15.3% [Jarvik, 1980]), and *Panderichthys* (16.5%, based on Vorobyeva and Schultze's 1991 reconstruction) all share similar proportions. ANSP 20980 has a pectoral fin that is nearly one fourth of the animal's body length (62 mm fin/254 mm estimated total length, or 24.4%). When corrected for body length, the fin surface area of the new rhizodontid is 2.4 times that of *Strepsodus*. The type of *?Strepsodus anculonamensis* is also considered to be an immature specimen, yet its fin proportions are similar to those of adult rhizodontids, as well as other sarcopterygians. The proportionally enlarged fin of ANSP 20980 may, in part, correlate to its ontogenetic stage, but may also be a unique characteristic of either the genus *Sauripterus*, or of this specimen.

A series of small, unjointed lepidotrichia are the only pelvic fin elements that are preserved (Fig. 3). Whether the lack of endochondral elements in this area is due to the preservation or ontogenetic stage of the specimen cannot be determined. Rhizodontids may have exhibited a high degree of variation in the timing and degree of endochondral ossification. For example, Foulden rhizodontids *Strepsodus* and *Rhizodus* show variation in the degree of ossification of the axial skeleton that is independent of body size.

Unpaired Fins. Vertebrae and the pelvic girdle are not preserved and presumably were unossified. The central lobe of the caudal fin contains a linear series of incompletely developed centra (Fig. 3B). These ossifications cover the dorsal and ventral surfaces of small impressions in the central axis of the fin. Although lepidotrichia are present for both the epaxial and hypaxial lobes of the caudal fin, they are incomplete distally. Dorsal and anal fins are not preserved.

Body Scales. Body scales are split between part and counterpart leaving most scales exposed in internal view. Like other rhizodontids, cosmine is absent. Scales are thin, roughly circular in shape, and have a series of bony ridges that radiate from an unornamented central plateau (Fig. 6). Concentric rings of bone connect these ridges, giving the surface a woven appearance. There are none of the breaks or gaps in these ridges that have been hypothesized to be the growth lines described for other species such as *Strepsodus* (Andrews, 1985). Internally, scales possess a fusiform boss with the rounded caudal end underlying the growth center. The suggestion has been made that these bosses are either points of scale attachment to underlying tissues or structural supports for the nonoverlapping part of the scale (Andrews, 1985).

The thin scales that cover the ventral and dorsal surfaces of the pectoral fin conform to the shape of the underlying lepidotrichia without any sign of fracture. The most distal fin scales extend approximately 15 mm beyond the distal edge of the intermedium (approximately three fifths of total fin length from base to tip). This pat-

tern of overlap contrasts with the specimen of *?Strepsodus anculonamensis* described by Andrews (1985: 73) where scales extend "almost" to the fin margin.

Lateral Lines. Rhizodontids are highly derived in that they have multiple lateral line canals. On ANSP 20980, sensory pores of the main lateral line canal extend along the dorsal body wall from the cleithrum to the caudal fin (Figs. 2, 3). These oval-shaped pores possess no discernible internal morphology, and are flanked dorsally and ventrally by elongate ridges of elevated bone. Faint traces of accessory lateral line canals can be seen along the scale rows that lie dorsal and ventral to the main lateral line. Although no sensory pores can be identified, accessory lines can be inferred from the presence of a furrow that runs craniocaudally along the center of the scale rows adjacent to the main line. Indeed, this furrow corresponds in appearance to the accessory lines described for *Strepsodus* (Andrews, 1985, fig. 5c). The presence of multiple lateral lines may be a synapomorphy of Rhizodontida, as all rhizodontids for which articulated scale rows can be identified (*Sauripterus, Gooloogongia,* and *Strepsodus*) possess accessory lateral lines. The only other evidence of sensory structures on ANSP 20980 is the occipital commissural canal on the median extrascapular.

ONTOGENETIC STATUS

The small size and incomplete ossification of the skeletons suggest that ANSP 20980 and ANSP 20981 are immature individuals. Indeed these features account for most of the differences between the fins of ANSP 20980 and ANSP 20981 and those of other specimens of *Sauripterus.* These differences are most profound in the endochondral portion of the fin skeleton, where these elements are poorly ossified, lack articulations between corresponding bones, and lack any processes. In ANSP 20980 the cortex of each endochondral element is less ossified than the medullary regions. Furthermore, the lack of articulations between endochondral elements differs greatly from other rhizodontids; larger specimens of *Sauripterus* and *Barameda* possess well-defined articulations between all endochondral bones. Likewise, the absence of both distal radials and a postaxial process on the humerus may be ontogenetic features that relate to the degree of ossification of the specimen. All rhizodontids, and virtually all sarcopterygians, have postaxial processes on the humerus. In addition, all rhizodontids possess numerous preaxial radials, many of which are richly branched (Fig. 7).

The degree of ossification of the axial skeleton could also be used to assess the ontogenetic stage of the new specimens. In ANSP 20980, no hemal or neural arches are observed in any portion of the axial skeleton. Although trunk centra are absent in the caudal fin, there are the impressions of three segmented units, whose dorsal and ventral surfaces are ossified. We interpret these ossifications to represent partially ossified ring centra. Ring centra are known from the Foulden material, from *Barameda,* and are associated with the type of *Sauripterus.* However, axial ossification does not always correlate to body size. Small, presumed immature, individuals of *Rhizodus* and *Strepsodus* possess partially ossified neural and hemal arches caudal to the first dorsal fin. Similarly, the large rhizodontids described from Foulden do not possess ossified ring centra (Andrews, 1985). The complete lack of neural arches, hemal arches, and caudal fin supports, and the partially ossified caudal ring centra are suggestive, although not definitive, evidence of an immature condition.

DISCUSSION

The discovery of immature *Sauripterus* provides new material for hypotheses about the evolution of fin development and function in extinct sarcopterygians. Three stages of growth are currently known for fin development in *Sauripterus.* In the earliest stage, represented by ANSP 20981, unjointed lepidotrichia are promi-

nent and no endochondral ossifications are present in the fin. In a later stage, such as that seen in ANSP 20980, the endochondral skeleton is weakly ossified and lacks the distal preaxial radials seen in adults. Adults, such as those of *Sauripterus*, contain fins with pronounced lepidotrichia and endochondral radials. The endochondral skeleton does not play a role in support and locomotion until later stages of growth, after the animal reaches a body size of at least 25 cm. By the time the animal is an adult, dermal and endochondral fin supports are both greatly expanded and ossified. Therefore, the ossification and elaboration of endochondral fin supports may correlate with the functional demands placed on these large predatory fish.

This emphasis on both dermal and endochondral elements in rhizodontids is an unexpected intermediate condition between ray-finned and lobe-finned designs and would not be predicted from current models of dermal fin development. Thorogood (1991) proposed that the differences between ray-finned and lobe-finned designs are due to a heterochronic shift during development. The relative amounts of dermal skeleton and endoskeleton in the fin are hypothesized to relate to the timing of the shift between an apical ectodermal ridge and apical ectodermal fold during early fin bud development (Fig. 8). The hypothesis suggests that ray-finned fishes, such as teleosts, have an early shift from ridge to fold, leading to a greater proportion of the skeleton being of dermal origin. A developmentally later shift from ridge to fold, or the extreme case of no shift whatsoever, would result in an appendage that is primarily or exclusively endochondral in design. The new specimens, and the previously described *Sauripterus* fins, represent a mosaic between these morphological and developmental extremes. With an extensively developed dermal skeleton, and interleaved endochondral elements, *Sauripterus* does not fit in a model based solely on comparisons between teleosts and derived sarcopterygians. Indeed, a great development of the dermal skeleton seems to occur in rhizodontids, even in immature forms. The dermal skeleton, both within the fin and across the entire pectoral girdle, is well ossified, whereas endochondral elements are weakly developed.

It would seem paradoxical that the expansion of the endochondral radials in rhizodontids is correlated with the origin of large and unjointed dermal rays. After all, the endochondral elements would not interact with the substrate: the main surfaces of the fin would be entirely defined by the lepidotrichia. Why expand endochondral skeletal elements that do not seem to play a direct role in support and locomotion? The answer to this question may lie in the fact that in adult *Sauripterus* the endochondral bones provide surfaces for the attachment of muscles. The humerus and radius, in particular, contain crests and processes for muscles that presumably would have played a role in motions at the shoulder and elbow. The enhancement of the endochondral skeleton in rhizodontids may be correlated to their increased role as control elements for the dermal fin skeleton. The large size of rhizodonts and, perhaps, aspects of their locomotor and feeding strategies, may have called for fins with large surface areas. The enlarged surface area was established by the expansion of the dermal fin supports, whereas the control of movements was provided by elaboration of the endochondral radials.

ACKNOWLEDGMENTS

This paper is dedicated to Fuzz Crompton in recognition of his pathbreaking synthesis of experimental morphology and expeditionary paleontology. We would like to thank Doug Rowe for many years of diligent excavation at Red Hill, C. Frederick Mullison for his skillful preparation of the specimens, and Robert Carroll and Richard Cloutier for their generous access to *Eusthenopteron* specimens for comparative purposes. We also wish to thank Zerina Johanson and Farish A. Jenkins, Jr., for helpful

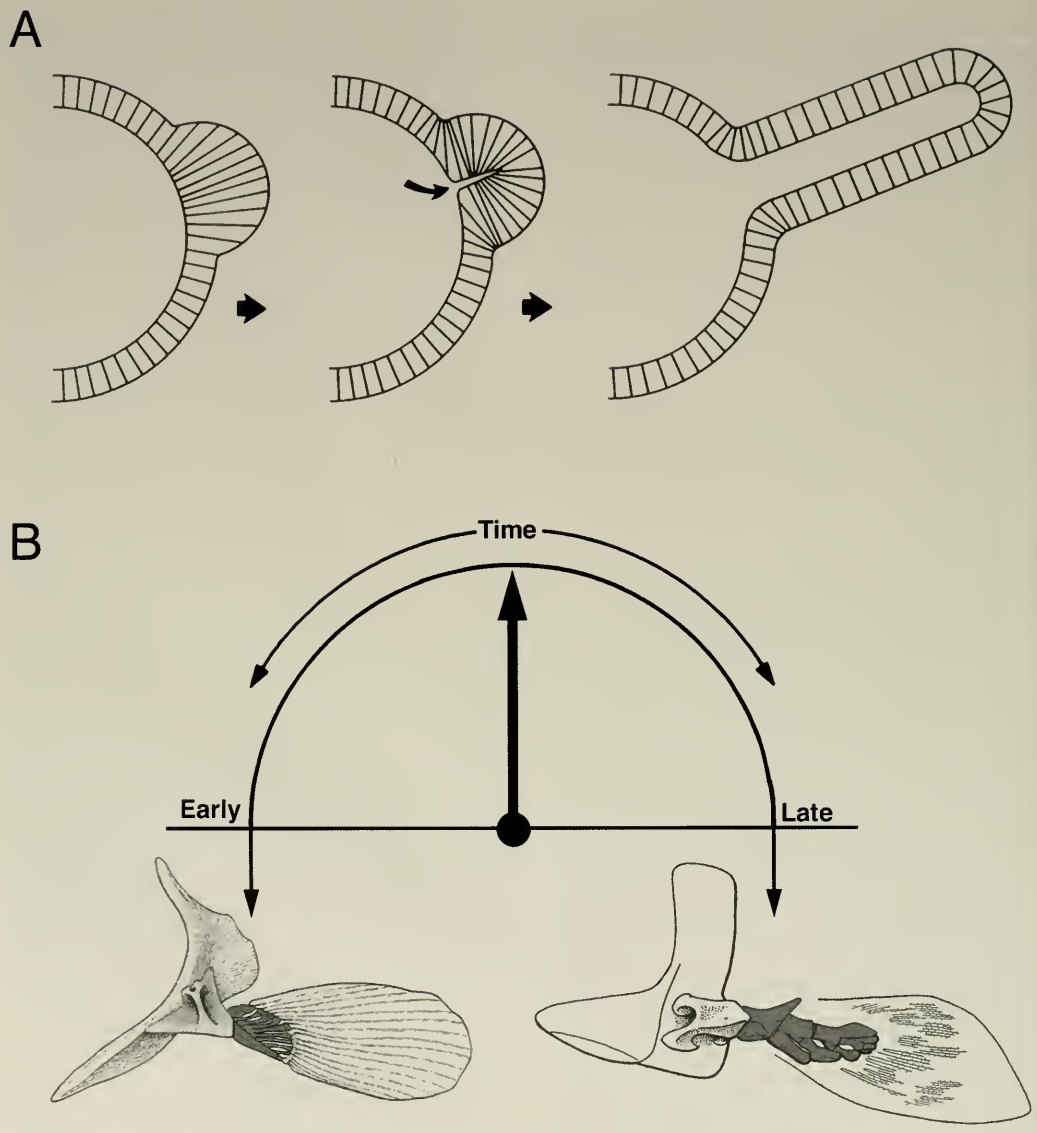

Figure 8. (A) Transition from apical ectodermal ridge (AER, left) to apical ectodermal fold (AEF, right) during early fin development. Cross section along proximodistal axis. (B) "Clock model" of heterochrony and phenotype. A developmentally early transition from AER to AEF would result in an "actinopterygian" phenotype (here represented by the pectoral fin of *Amia*). A developmentally later transition from AER to AEF would result in a "sarcopterygian" phenotype (here represented by *Eusthenopteron*). A and B modified from Thorogood (1991). Fins modified from Jarvik (1980; Early) and Andrews and Westoll (1970; Late).

discussions. Kalliopi Monoyios provided editorial assistance. This research was supported by the Academy of Natural Sciences of Philadelphia and the National Science Foundation (EAR 9628163 to N. H. S.).

LITERATURE CITED

Ahlberg, P. E. 1989. Paired fin skeletons and relationships of the fossil group Porolepiformes (Osteichthyes: Sarcopterygii). Zoological Journal of the Linnean Society, **96:** 119–166.

ANDREWS, S. M. 1985. Rhizodont crossopterygian fish from the Dinantian of Foulden, Berwickshire, Scotland, with a re-evaluation of this group. Transactions of the Royal Society of Edinburgh, **76:** 67–95.

ANDREWS, S. M., AND T. S. WESTOLL. 1970. The postcranial skeleton of rhipidistian fishes excluding *Eusthenopteron.* Transactions of the Royal Society of Edinburgh, **68:** 391–489.

DAESCHLER, E. B., AND N. H. SHUBIN. 1998. Fish with fingers? Nature, **391:** 133.

GREGORY, W. K., AND H. C. RAVEN. 1941. Studies of the origin and early evolution of paired fins and limbs. Annals of the New York Academy of Science, **42:** 273–360.

HALL, J. 1843. Geology of New-York. Part IV. Comprising the Survey of the Fourth Geological District. Natural History of New York. Vol. 4. Albany, New York: Carroll and Cook. 683 pp.

JARVIK, E. 1980. Basic Structure and Evolution of Vertebrates. 2 vols. London: Academic Press. xvi + 575 pp. and xiii + 337 pp.

JOHANSON, Z., AND P. E. AHLBERG. 1998. A complete primitive rhizodont from Australia. Nature, **394:** 569–573.

LONG, J. A. 1989. A new rhizodontiform fish from the Early Carboniferous of Victoria, Australia, with remarks on the phylogenetic position of the group. Journal of Vertebrate Paleontology, **9:** 1–17.

ROMER, A. S. 1955. Herpetichthyes, Amphibiioidei, Choanichthyes or Sarcopterygii?. Nature, **176:** 216.

THOROGOOD, P. 1991. The development of the teleost fin and implications for our understanding of tetrapod limb evolution, pp. 347–354. *In* J. R. Hinchcliffe, J. M. Hurle, and D. Summerbell (eds.), Developmental Patterning of the Vertebrate Limb. New York: Plenum Press. xi + 452 pp.

TRAVERSE, A. (in press). Dating the earliest tetrapods: a Catskill palynological problem in Pennsylvania. Courier Forschungsinstitut Senckenberg.

VOROBYEVA, E. I., AND H.-P. SCHULTZE. 1991. Description and systematics of panderichthyid fishes with comments on their relationship to tetrapods, pp. 68–109. *In* H.-P. Schultze and L. Trueb (eds.), Origins of the Higher Groups of Tetrapods: Controversy and Consensus. Ithaca, New York: Cornell University Press. xii + 724 pp.

WOODROW, D. L. 1985. Paleogeography, paleoclimate, and sedimentary processes of the Late Devonian Catskill Delta, pp. 51–63. *In* D. L. Woodrow and W. D. Sevon (eds.), The Catskill Delta, Special Paper 201. Boulder, Colorado: Geological Society of America. vii + 246 pp.

WOODROW, D. L., R. A. J. ROBINSON, A. R. PRAVE, A. TRAVERSE, E. B. DAESCHLER, N. D. ROWE, AND N. A. DELANEY. 1995. Stratigraphic, sedimentologic, and temporal framework of Red Hill (Upper Devonian Catskill Formation) near Hyner, Clinton County, Pennsylvania: site of the oldest amphibian known from North America, pp. 1–8 *In* J. Way (ed.), 1995 Field Trip Guide, 60th Annual Field Conference of Pennsylvania Geologists. Lock Haven, Pennsylvania.

YOUNG, G. C., J. A. LONG, AND A. RITCHIE. 1992. Crossopterygian fishes from the Devonian of Antarctica: systematics, relationships and biogeographic significance. Records of the Australian Museum, **14**(Suppl): 1–77.

HOW DO MYSTICETES REMOVE PREY TRAPPED IN BALEEN?

ALEXANDER J. WERTH[1]

ABSTRACT. Mysticete whales trap prey in a sieve of baleen, the structure of which varies in such parameters as the number of plates, their overall dimensions, and the number and density of hairlike fringes that form on the medial surface, creating filters of different mesh size. Many prey items presumably entangle in the mat of interwoven fringes, necessitating that they be freed for oral transport and swallowing. Although the tongue is commonly implicated in such removal, this has never been studied. Three hypotheses for prey release are presented: mechanical scraping or shaking of baleen by the tongue, shaking of the head or lips to dislodge prey with the aid of gravity, and use of a rapid flushing "backwash" current to draw water into the mouth through baleen. Previously unpublished data on mysticete tongue structure and function support all hypotheses; behavioral observations of foraging whales and morphologic findings such as baleen growth and wearing also aid in their evaluation. All three mechanisms are likely to be used depending on the type of baleen and size, type, and density of prey.

INTRODUCTION

For as long as whales have been distinguished from fishes, the role of baleen or "whalebone" in trapping prey has been recognized. Indeed, given this singular, highly derived tissue's unique construction and arrangement in rows of serial plates, baleen's sievelike function—filtering large quantities of small prey from high volumes of seawater—seems obvious, all the more so with cursory examination of mysticete diet and foraging behavior.

Yet for all that has long been known about prey capture in the mammalian suborder Mysticeti ("mustached" whales), one aspect is only dimly understood: how are entangled prey removed from the filter before transport and deglutition? The tongue is commonly implicated in this function, but this is a grossly inadequate and vague answer. Because of manifest logistical limitations a clear, Jonah's-eye view inside a live whale's closed mouth is unattainable. The experimental techniques of cineradiography and electromyography that have greatly elucidated precise mechanisms of lingual function in other mammals are, regrettably, inapplicable. Hence the best (and indeed perhaps only) way to address this question is to rely on speculative inference based on the functional anatomy of the tongue and associated oral structures. This paper introduces and compares, on the basis of morphological and ecological evidence, three hypotheses concerning removal of trapped prey from mysticete baleen.

PREY CAPTURE

Before proceeding to a discussion of plausible prey removal mechanisms it is necessary to consider briefly the mechanisms by which prey are captured. Mysticetes vary dramatically in foraging methods. Variation occurs mainly along family lines, and is reflected in the baleen itself as well as in other oral structures and (concomitantly) in diet and foraging ecology, all of which have consequences for prey removal.

Foraging and Diet

Right whales (Balaenidae) utilize a type of suspension feeding similar to that of more primitive vertebrates, which pump or push water constantly and unidirectionally through the mouth (Sanderson and Wassersug, 1993). Balaenid skim feeders

[1] Department of Biology, Hampden–Sydney College, Hampden–Sydney, Virginia 23943.

cruise slowly through swarms of minute zooplankton, primarily copepods, amphipods, and euphausiids (Lowry and Frost, 1984; Carroll et al., 1987). Skim feeding is most commonly observed at the ocean's surface (Watkins and Schevill, 1979; Mayo and Marx, 1990), yet stomach content data and scratched, muddy rostra indicate that skim feeding occurs at all levels of the water column, including the bottom. The enormous head, constituting one third of an adult balaenid's 15- to 20-m length, functions as an immense plankton tow net (as in other continuous filter feeders such as manta rays and whale and basking sharks), although the "seine" is not pulled along but rather propelled by the whale's forward locomotion at leisurely speeds of approximately 4 km per hour during foraging (Reeves and Leatherwood, 1985; Carroll et al., 1987; Lowry, 1993). A constant current of prey-laden water enters anteriorly, passes through baleen "racks" on either side of the mouth, and exits lateral to the pharyngeal orifice at the trailing edge of the lips. Tiny zooplankton in the steady stream of incurrent water are caught in the finely fringed baleen, and field observations suggest that right whales (*Eubalaena glacialis*) graze for hours with few interruptions for breathing or closing the mouth (Watkins and Schevill, 1979; Mayo and Marx, 1990), leading to anecdotal speculation that they may spend long periods skimming before gathering enough prey to swallow.

In contrast, other mysticetes are not continuous filter feeders but are intermittent filter feeders that ingest discrete mouthfuls of water and separate food from this water before expelling it. A single mouthful is engulfed either by ram feeding in rorquals (Balaenopteridae) such as fin and humpback whales (Jurasz and Jurasz, 1979; Watkins and Schevill, 1979; Hain et al., 1982) or by intraoral suction in the gray whale (*Eschrichtius robustus*, Eschrichtiidae), whose tongue is rapidly depressed and retracted to expand the oral cavity and create negative pressure, stirring the bottom and sucking in muddy water from which prey are winnowed (Klaus et al., 1990; Weitkamp et al., 1992). Ram gulping necessitates forward lunges parallel to or through the surface; the gray whale can feed while stationary. In both cases prey are filtered as the mouth closes to expel engulfed water (and, in the gray whale, sediment). As Pivorunas noted (1979), baleen does not actually catch prey; it merely retains prey as water is expelled from the oral cavity.

As expected, the type, size, and abundance of preferred prey correlate with foraging ecology. For example, the sei whale (*Balaenoptera borealis*) occasionally eats schooling fish as do other rorquals, yet more commonly feeds on copepods or other zooplankton and hence engages in skim feeding much like that employed by balaenids (Kawamura, 1974). The gray whale primarily uses suction to ingest benthic macroinvertebrates (e.g., gammarid amphipods, mysids, and molluscs; Murison et al., 1984; Nerini, 1984) yet has been observed feeding on shoals of fish in midwater (Sund, 1975). Although well-documented ecological partitioning exists within mysticetes, opportunism is the rule. Variation in type, size, and abundance of prey might alter the behavior of prey capture as well as removal of trapped prey in any mysticete species.

Oral Morphology

The differences between continuous and intermittent (ram and suction) filter-feeding mysticetes are manifested not only in diet but more aptly in key features of oral anatomy. Unlike other mysticetes, balaenids possess no throat grooves yet have a large anterior cleft (the subrostral gap) between baleen racks. The high, arched skull accommodates extremely long, narrow baleen plates (Fig. 1), and the huge semicircular lower lips, which extend far above the mandible (like the arched, deep-sided lower jaw of flamingos; Milner, 1981), cover the baleen laterally and enfold the narrow rostrum when the mouth

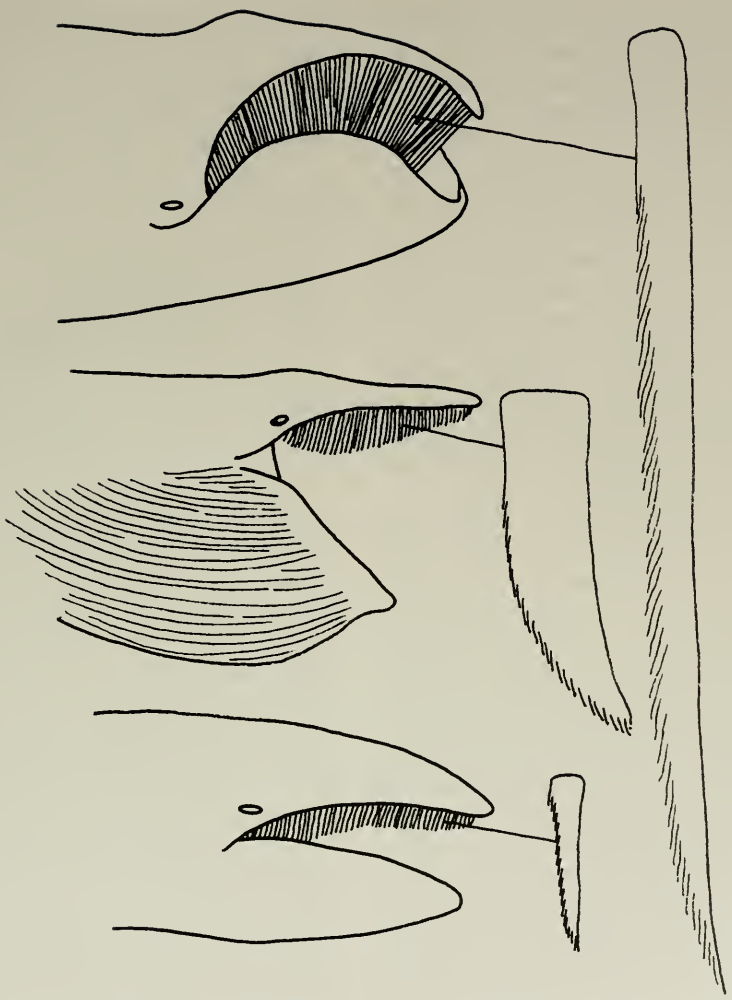

Figure 1. Baleen size, shape, and fraying correlate with prey type and size. Right whales (top) skim microplankton with narrow, finely fringed baleen ≥4 m in length. Rorquals (center) gulp schooling shrimp and fish with shorter (≤1 m), wider, coarser baleen. The gray whale (bottom) sucks in benthic invertebrates and filters them with short (≤40 cm), coarsely fringed baleen.

is closed. Like the subrostral gap, the orolabial sulcus—a gutterlike groove medial to the lip—promotes continuous, unidirectional flow as filtered water passes to an "exhaust port" at each lip's trailing edge, lateral to the pharyngeal opening. The tongue is firm, muscular, and extraordinarily large; it is estimated to average 4–6% of total body mass (Omura, 1958), so that in a standard 50-ton or 50,000-kg whale, the tongue weighs 2,000–3,000 kg and measures several meters in length. Cervical vertebrae are fused, yet the mandibular symphysis is loose and the lips highly mobile, controlled by labial musculature (Lambertsen et al., 1989). The gray whale's tongue is also firm and muscular and this whale has a small subrostral gap, although this is far less pronounced than the gap found in balaenids (Wolman, 1985). The scarred, abraded jaws of *Eschrichtius* disclose its benthic suction feeding, as do mud plumes trailing behind feeding whales and suction-generated pits

that scar the ocean floor (Oliver and Slattery, 1985; Nelson and Johnson, 1987).

Likewise, rorquals possess singular morphologic features for lunge feeding. Positive inertial pressure opens the mouth just as a bag is opened by pulling it through air; water and prey are passively enveloped rather than displaced forward or sucked internally (Orton and Brodie, 1987). Key innovations include the flaccid and deformable tongue and oral floor with intermuscular fascial cleft; the cavum ventrale, which receives engulfed water and the displaced baglike tongue (von Schulte, 1916; Pivorunas, 1979); accordionlike longitudinal throat pleats and elastic throat wall (Orton and Brodie, 1987); wide-opening jaws with locking temporomandibular joint to prevent opening during rapid locomotion and frontomandibular stay to store kinetic energy for jaw closure (Lambertsen, 1983; Lambertsen et al., 1995); unfused mandibular symphysis with fibrocartilage arms extending to mandibular rami (Pivorunas, 1977); and flat, streamlined rostrum (Gaskin, 1976). Storro-Patterson (1981) speculated that a blue whale (*Balaenoptera musculus*) might engulf 1,000 tons of water in a single gulp. Pivorunas (1979) gave a more conservative estimate of at least 60 m^3 (approximately 70 tons) of water, still a huge amount of water equal to roughly 50% of a blue whale's total body volume. Lambertsen's recent calculations from computer modeling (Zackowitz, 2000) suggest an almost identical engulfment volume of 15,000 gallons (56.85 m^3) in humpbacks. Specialized behaviors of rorqual lunge feeding, including ingenious bubble entrapment devices emitted by the blowholes (Gormley, 1983; Würsig, 1988) or lobtailing, flipper slapping, and flick feeding to concentrate prey (Evans, 1987; Clapham et al., 1995), are as remarkable and resourceful as the mechanics of engulfment.

Baleen

More important than these divergences in oral morphology and ecology, the baleen filter itself varies substantially in numerous ways (Fig. 1), including the number of flexible triangular laminae or plates in each rack, which ranges from 100 in *Eschrichtius* to 480 in the fin whale (*Balaenoptera physalus*), although the bowhead (*Balaena mysticetus*) and most large rorquals generally have about 300–350 plates per rack (Leatherwood et al., 1983). Plates are arranged transversely like teeth of a comb and suspended from the maxillae at intervals of roughly 1 cm. Plates are generally only a few millimeters thick (anteroposteriorly) yet vary greatly between species in other dimensions, notably length, measuring just 5–25 cm in *Eschrichtius* yet often exceeding 4 m in *Balaena* (requiring that they fold posteriorly as the mouth closes). However, baleen seldom grows wider than 35 cm in any species, so that the shape of the triangle varies markedly. Baleen also differs in such characteristics as lateromedial curvature (Lambertsen et al., 1989), flexibility (very stiff in *Eschrichtius*; said to be most pliable in the pygmy right whale, *Caperea marginata*; Leatherwood et al., 1983), and less consequential factors such as color, although the latter may relate to prey capture, as has been supposed for jaw and flipper color (Mitchell, 1970; Brodie, 1977).

Certainly most significant from the standpoint of prey retention is the variation in type and density of baleen fringes. Although the plates themselves form a sort of rudimentary sieve, the true task of filtration is accomplished by the many thin, hairlike projections that develop on each plate's medial side, forming a network of meshed fibers (Tomilin, 1957; Williamson, 1973). All baleen develops as a dermal–epidermal interaction in which conical dermal papillae extend ventrally from an underlying basal plate of connective tissue through an epidermal layer, at which time the papillae are enveloped in a horny layer of keratin to form long bristles called horn tubes (Slijper, 1962). These tough, fibrous strands are likewise surrounded and cemented together by a layer of compacting

horn, while a soft cushioning layer of intermediate horn provides a dense cortex covering the anterior and posterior faces of the plate. Friction abrades the matrix medially, wearing away compacting horn to reveal the hollow horn tubes that remain as the frayed fibers comprising the sieving apparatus, whereas the long side of the scalene triangle facing the lip remains smooth. Cells in the rubbery, pliant epithelium of the gums anchor baleen to the palate and proliferate to replenish abraded gingival tissue, just as all papillae grow at a uniform rate to replace worn horn tubes. The visible portions of baleen consist exclusively of dead cornified cells, but the dermal process remains a living tissue, so that baleen is analogous to the part-living tissue in an ungulate hoof (Slijper, 1962). Baleen's anisotropic nature, with a homogeneous cortical layer surrounding free, hollow, cylindrical tubes, affords maximal strength with minimal mass (Slijper, 1962). Baleen is tough yet elastic, a suitable material to meet the demands of constant friction. Sadly, the exceptional physical characteristics of this material also rendered it an extremely valuable commodity that fueled the whaling industry.

The hairlike bristles that fray on the medial side intertwine to form a fibrous mat. The slender, springy plates of the skim-feeding balaenids and sei whale possess 35–70 fine filamentous fringes per square centimeter (Leatherwood et al., 1983). Microscopic examination of bowhead baleen reveals several distinct histologic units, including simple (bristle) and compound (hair) filaments, according to their gingival origin (Haldiman et al., 1981; Haldiman and Tarpley, 1993). In contrast, fibers of rorqual and gray whale baleen are much shorter, coarser (thicker in diameter), and fewer in overall number and density (about 30 fringes per plate; Watson, 1981); they are more like rough scrub-brush bristles than fine hairs, and are typically more wavy than the fine strands of skim feeders. However, these rough bristles are sufficiently long that they may link with other fibers from the same and adjacent plates to form an interwoven, loosely braided mesh. In a mathematical model correlating plate and fringe features, Pivorunas (1976) suggested that the angle at which fringes develop from the medial surface seems more critical for prey retention than fringe density, and that shorter fringes alleviate drawbacks of having fewer fringes. Where plates angle laterally, as in rorquals (Fig. 2), many fringes are exposed on the medial surface by friction, so that the coarse fibers in this tangled, brushlike mat need not have such small diameter, whereas in balaenids fewer fringes can be exposed on the relatively straighter medial side. In any event the most fundamental distinction between baleen of different species is the spacing between fringes, and thus the porosity of the filter.

Because baleen is not a rigid material, its filter porosity varies according to hydrodynamic factors such as the swimming velocity of ram feeders; size and density of retained prey; and direction, rate, and pressure of water flow (Sanderson and Wassersug, 1990). The mysticete filter-feeding apparatus acts simply as a sieve—no active adjustment of filter porosity according to prey size or density is made before engulfment—with filter elements (baleen fringes) spaced more closely than the sizes of items to be captured. However, although no particles are directly intercepted by adhering to a sticky surface, it is possible although unlikely that tiny prey (smaller than the filter spacing) may be trapped by other methods of aerosol filtration, such as inertial impaction or gravitational deposition (Rubenstein and Koehl, 1977). Although small suspension feeders must contend with the constraints inherent in moving in a dense, viscous fluid, mysticete filtration may depend more on inertial forces that prevail at high Reynolds numbers (Vogel, 1994).

Baleen whales consume whole organisms, whereas small filtering organisms often feed on detritus (fragmented organic debris; Sanderson and Wassersug, 1993).

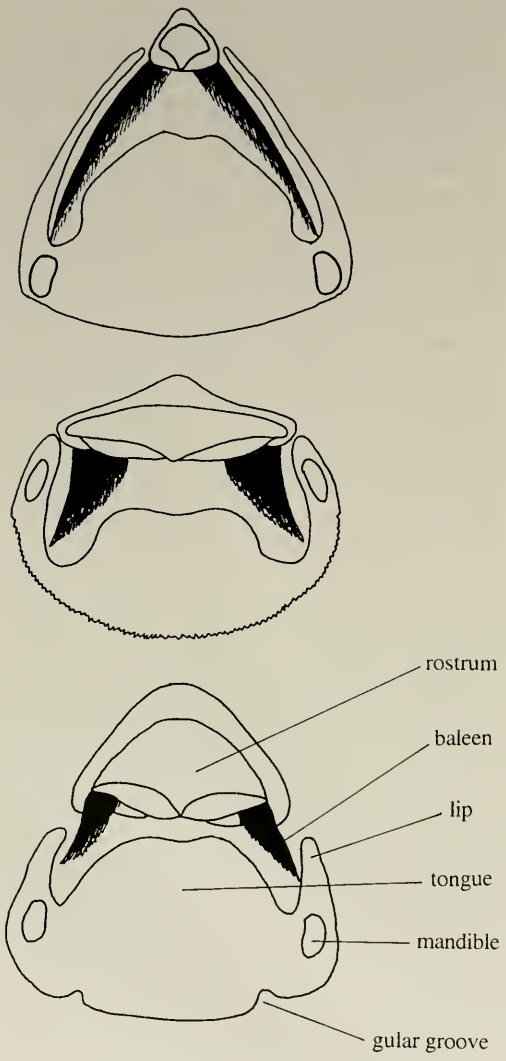

Figure 2. Diagrammatic cross sections through the closed mouth of a right whale (top), rorqual (middle), and gray whale (bottom), showing the different dimensions and relations of oral features (baleen, lips, tongue, and mouth floor) that affect prey prehension and extrication in these families.

Yet as with other suspension feeders, mysticetes feed in abbreviated trophic chains and thus reap great energy input, a critical factor in their attainment of huge body size and (before their decimation by hunting) wide distribution. Each whale consumes gigantic quantities of prey, with estimates ranging from 200–1,000 kg per meal and 200,000–600,000 kg annually (Gaskin, 1982). Like other strainers mysticetes are not selective; they locate patchy food sources and trap whatever is there. Although the filter porosity determines the smallest prey retained, fine filters catch large prey as well as small and hence may be more versatile (Gaskin, 1982). However, dietary studies indicate that coarse-fringed mysticetes are less selective (Nemoto, 1959, 1970), ingesting items ranging from plankton and fish to hapless seabirds, whereas balaenids are specialized feeders with more restrictive diets. In fact, it may be unnecessarily costly to use a finer filter than is needed to trap preferred prey, particularly during continuous filtration, because this increases pressure drag, slowing an animal and preventing capture of large or evasive prey. Watkins and Schevill (1976) noted that the water level inside the mouth of a right whale during surface skim feeding is higher than that of the surrounding sea (although gravity would then force water out through baleen). A photogrammetric study of bowhead baleen curvature by Lambertsen et al. (1989) suggested that hydrodynamic rather than passive hydraulic forces may develop, creating Bernoulli and Venturi effects within the mouth to improve filtering efficiency. Werth (1995) devised mathematical and physical models of the bowhead mouth to test these predictions and confirmed that both hydrodynamic effects might reduce turbulent flow and avoid creation of an anterior pressure wave so that balaenids could capture elusive prey even at slow swimming speeds. Foraging in tight formation may achieve the same effect (Würsig, 1988, 1989).

PREY REMOVAL

The process of prey removal from the mysticete filter is an intriguing question that has not yet been satisfactorily addressed, much less resolved. Given the fine porosity of the filter (because it involves baleen strands rather than simple laminae) in all species and the small prey

size of many species, prey may become trapped not only on but actually in this filter, necessitating that they be freed before they can be swallowed.

Consider an analogy with a dip net used to clean a swimming pool. One way to remove debris that accumulates on the net would be to scrape the mesh or employ some other direct mechanical means to brush off collected material. Alternatively, the net might be shaken vigorously so that debris falls off with the aid of gravity. A third method relies on hydrodynamic rather than mechanical forces: by rapidly jerking the net backwards, a backwash flow would filter through the net and free trapped items. Undoubtedly additional ways exist to clean the net, yet these are the simplest and most obvious methods.

Just as a clogged dip net must be cleaned periodically for effective filtration, so too the baleen sieve must be cleared for it to continue removing planktonic or nektonic prey from ingested water. Clearly the mysticete filter is more complex than a dip net screen, for its pore size is not fixed and is likely pressure dependent. Although only continuous skimmers appear routinely to ingest items small enough to be deeply ensnared in fringes (i.e., copepods 1–5 mm in length), the rapid, explosive expulsion of water in intermittent filter feeders might serve to drive prey further into the meshwork of fringes, as a huge volume of water exits the mouth at high velocity and pressure. Still, the relationship between filter element spacing and prey size in most intermittent filter feeders—namely their coarser fringes and attendant trend toward larger prey (10- to 50-cm schooling fish and squid)—means that much of their food accumulates on rather than within the sieve during collection (and is unlikely to penetrate it during water expulsion). Yet euphausiids (10 cm) are a favored prey of most rorquals and the gray whale eats many small invertebrates (1–15 cm), all of which could easily become enmeshed in fringes. Clearly, ingestion of any prey (large or small) in large quantities would mean that many items (not all, yet enough to be swallowed) simply fall onto the tongue upon water expulsion. Also, most macroscopic prey are negatively rheotropic (i.e., preferring to swim against a current); if still alive they will attempt to swim away from the expulsive flow, out of the ensnaring mesh and into the center of the mouth.

Baleen, unlike some dip nets, is not meant to gather debris, although *Eschrichtius* might be expected occasionally to collect sediment along with intended prey from the benthic substrate. Inorganic material must be removed from the filter so as to prevent clogging of the baleen, as well as separated from food so as to prevent its ingestion, although sand and pebbles have been found in gray whale stomachs (Tomilin, 1954; Pike, 1962). Unfortunately, although baleen could easily become fouled with spilled oil (Geraci and St. Aubin, 1990; Loughlin, 1994), this material is unlikely to be removed effectively by any means, such that not only the toxic effects of its ingestion but also the obviation of filtration would pose dire consequences for all mysticetes.

The combination of coarse brushlike baleen and large prey commonly ingested by rorquals means that their food is far less likely to become entangled than in species with fine fringes and correspondingly smaller prey, particularly sei and right whales. The large prey of intermittent filter feeders might simply fall onto the tongue or swim out of baleen without need of any removal mechanisms. Accumulations of minute prey might also drop in this manner, leaving some organisms remaining in the baleen yet creating a sufficiently large bolus to be swallowed. Recurrent dislodging of enmeshed items, especially tiny prey, may be metabolically costly. However, such costs must be balanced with the need for periodic baleen cleaning to present the freest, least clogged filter for optimal prey capture and/or to preclude swallowing of too large a bolus or too thick a slurry of prey. Do microplankton that gather on gill rakers of

filter-feeding sharks eventually migrate to the pharynx in similarly large masses? As with mysticetes, the act of filtration has received much more attention than the topic of how collected prey are processed intraorally. However, even if large prey and accumulated small prey drop off baleen spontaneously, small prey clearly become enmeshed in the filter, necessitating that they be removed for transport and swallowing (as well as to restore the filter's porosity and efficiency).

By extension from the dip-net analogy, I propose three hypotheses to explain the most likely mechanisms for removal of prey trapped in baleen fringes. Two are mechanical—direct dislodging of items via lingual scraping and indirect release by vigorous head shaking, whereas one is hydrodynamic, relying on a powerful, rapid reversed-flow backwash to flush items. These options need not be mutually exclusive: a species might use all three processes to "cleanse the palate" depending on prey type and density or other circumstances. Additionally, the extent to which individuals might devise unique methods of prey removal ought not to be discounted.

Although no discussion of baleen cleaning has been published previously, superficial references implicate the tongue in passing. Indeed the tongue plays a central role in two of the baleen cleaning strategies presented and analyzed here on the basis of anatomical and observational evidence. Specifically, those mechanisms involving the tongue depend predominantly on changes in its position rather than shape, which is supported by preliminary study of lingual myology.

Prey Removal Via Direct Lingual Scraping or Shaking

The most common supposition is that the tongue is applied directly to scrape baleen and free trapped items. Although this is mainly presumed to involve lingual elevation and retraction, it might entail any motion—anteroposterior, dorsoventral, or lateral—that could abrade, shake, or otherwise disturb or wear the mat of interwoven fringes and thereby release entangled prey. According to this idea, prey either fall onto the tongue's central furrow and are subsequently transported to the rear of the oral cavity for swallowing via lingual elevation and retraction and depression, or else prey removal and transport steps occur concurrently with such lingual movements, perhaps in a cyclic series controlled by a central pattern generator.

A major drawback of this mechanism is that the tongue might push prey more deeply into fringes, furthering entanglement. Other potential disadvantages include inefficient clearing of prey from fringes that do not directly contact the tongue as well as rapid abrasion and, ultimately, removal of baleen. Baleen's occasional presence in whale feces is offered as evidence that it regularly wears away, providing compelling circumstantial support for this hypothesis. Isotopic studies of bowhead baleen confirm that its growth varies with age (Schell and Saupe, 1993), exceeding 50 cm of growth in the first year, then decreasing by about 10 cm per year until stabilizing at about 20 cm or less in older animals. Whether the bowhead's annual addition of this much baleen is sufficient to offset potential loss from abrasive prey removal can only be addressed in theory. Yet, although abrasion might be hypothesized to be reduced in nonskimming mysticetes that need not release tiny prey from fine fringes, Ruud's (1940, 1945) studies of fin whale baleen growth provide data comparable to those from bowheads, suggesting a constant level of abrasion not correlated with diet and foraging method.

A more serious fault of this line of reasoning is that lingual scraping would abrade baleen's medial surface far more than its lateral surface, resulting in differential wear and continually narrowing plates. However, not only does plate shape not change with age, but growth is uniform along the entire base of the plate

(Ruud, 1940, 1945), so that such differential wear could not be countered by differential growth. Nor could baleen be scraped solely from below to wear evenly, because baleen angles laterally in all mysticetes and the tongue contacts only its medial surface (Fig. 2). Still, support for the lingual scraping hypothesis might come from another type of differential baleen wear seen in gray whales: they seem predominantly right handed, with significantly shorter baleen on this side (Kasuya and Rice, 1970). This asymmetry has been ascribed to friction from benthic suction ingestion on the right side (head scarring and barnacle placement are likewise asymmetrical), yet the wear might be incurred not during prey capture but during subsequent scraping removal of prey and sediment that is trapped chiefly in the right rack.

The effect of such scraping on the tongue must also be considered, and at least in the case of *Balaena* the dorsum is covered by a thick, keratinized stratified squamous epithelium with a well-developed stratum corneum (Tarpley, 1985; Haldiman and Tarpley, 1993). A horny, cornified corium is similarly present on the tongue of *Eubalaena* (Werth, 1990, 1993), yet no data are available for other mysticetes. Unfortunately, although comparative mysticete lingual myology would shed light on the ability of the tongue to perform the movements necessary for the scraping motions outlined above, few published data exist.

The lingual movements necessary for this manner of prey removal involve changes in the tongue's position rather than its shape. Use of the human tongue to remove food particles trapped between teeth or on the palate is familiar. Yet, although the mysticete tongue might deform to shorten or curl and thereby contact localized regions of baleen, it is likely that prey become uniformly distributed throughout the filter, so that displacement of the entire tongue organ via protraction and retraction, elevation and depression, and lateral shifting would probably be more effective in prey removal than lingual shape deformation. This view accords with myologic findings of balaenid tongues (Werth, 1990, 1993), which have extrinsic muscles (originating outside the tongue) that appear to be greater contributors to its body (by mass and cross-sectional area) than are intrinsic muscles, which exist solely within the tongue. Analysis of unpublished data (Werth, in preparation) from fresh, frozen, and preserved fetal, neonate, and adult right and bowhead whales suggests that although scattered fibers of the musculus (m.) lingualis proprius, especially verticalis (perpendiculares) and transversus fibers, are found on the dorsum of the tongue root and tip as they intergrade with plentiful adipose tissue (presumably for nutritional storage or thermoregulation), the m. genioglossus is a much larger contributor to the tongue body, based on gross examination and calculation of relative cross-sectional area. The m. hyoglossus and m. styloglossus, although significantly smaller than the m. genioglossus, nonetheless are well developed in all age classes (see also Lambertsen et al., 1989). Taken together, analysis of these data on component muscles (similar to data from an odontocete "great whale," the sperm whale; Werth, 1998) suggests that although the balaenid tongue possesses a limited ability for shape change, it is well suited to the elevation, retraction, and depression that underlie the lingual scraping hypothesis.

Although gray whales also possess a large, firm, elevated, muscular tongue, the conspicuous flaccidity of the adult rorqual tongue would seem to preclude much of the activity described here. Pivorunas (1979) noted major changes in the balaenopterid tongue as it transformed from a solid, muscular structure used in suckling to the deformable, flaccid sheet seen in adults. From birth until around weaning muscle fiber is replaced with adipose and elastic connective tissues as the increasingly saccular organ flattens and spreads lat-

erally. Intrinsic muscle fibers are scattered and poorly developed; as in balaenids, the tongue may serve as a seasonal store of adipose tissue (Howell, 1930; Tarpley, 1985). The tongue is thought to play a role in expelling water from the oral cavity in all mysticetes, yet the elastic recoil of gular closure may accomplish much of this function in rorquals and obviate the need for a muscular tongue in this family.

A related yet alternative notion is that the tongue could simply slap or shake prey free, perhaps by vibrating plates or waving them anteroposteriorly. This could alleviate baleen abrasion (and to a lesser extent lingual abrasion, although it would involve similar muscle actions), as well as the inability of the tongue to free prey from fringes not directly contacting the tongue. Any motion that might jostle plates or knock them together could release prey, although this would likely be less efficient with minute prey trapped in fine, filamentous fringes. However, the fact that skimmers continuously filter might obligate them to purge their filter continuously, instead of at long intervals as was suggested earlier. This is especially crucial in light of the fact that the filter is at best inefficient and at worse useless when clogged with prey or other items. Balaenids' long plates might also clean themselves to some extent by rubbing or squeezing together when they fold posteriorly as the mouth closes; however, this is not feasible for the much shorter plates of the skim feeding sei whale.

Prey Removal Via Head or Lip Shaking

A second hypothesis, also mechanical in nature, stems from observations of occasional head-shaking behavior in southern right whales (Payne, in press). Whales have been seen shaking their heads rapidly from side to side above the surface with a sound audible from a great distance. This sound is not unlike the "baleen rattle" of right whale skim feeding (Watkins and Schevill, 1976), produced by water lapping over partially submerged plates, and, possibly, plates rapping together, although the rattle is presumably associated with skim foraging, not prey release. Although observation of lateral head movement has been limited, any degree and direction of motion (including dorsoventral shaking, which has not been documented) might dislodge prey. Unfortunately, fine baleen fringes might adhere together closely (the way gill lamellae clump) in air, impeding proper prey removal. Head shaking underwater might resolve this problem, yet because many prey are neutrally buoyant in seawater gravitational forces would not prove effective; prey would more likely float or even swim off fringes in water currents inside the oral cavity generated by head shaking.

As with the lingual scraping hypothesis, a serious shortcoming of this plan is that it might not release prey adequately, yet because balaenids skim for hours with little apparent swallowing (at least with sparsely distributed prey), a good head shake would likely dislodge sufficient food to swallow. A major disadvantage of head shaking would seem to be the metabolic cost of moving the entire head, which, although it need not be particularly rapid nor vigorous, would certainly require more energy than simply moving the tongue. Yet simpler ways may exist to move the head. In one of the few published mentions of prey release, Gaskin (1982) postulated that the short, lunging rushes of right whales during bouts of skim feeding could agitate and remove clinging food particles.

Another solution, at least in balaenids whose large lower lips abut the baleen's lateral edge (Fig. 2), would be to flap the lips or shake only the lower jaw rather than the entire head. Lambertsen et al. (1989) described the bowhead's strong labial musculature, particularly the temporalis and deep masseter, which have extensive insertions on the coronoid process. Although these muscles, like the specialized mysticete temporomandibular articulations and mandibular symphysis, have been implicated in mandibular adduction for balaen-

id feeding (especially to establish the orolabial sulcus and support baleen; Eschricht and Reinhardt, 1866), they could play a further role in prey removal. Preliminary study also discloses the presence of small slips of labial musculature arising solely from the lower jaw of *Balaena* (Lambertsen et al., 1989; Werth, 1993); the extent to which these control the lips is unknown. A combination of surface and submerged head shaking, forward lunging, mandibular rotation, and cheek flapping in right whales might allow for mechanical removal of trapped prey without direct contact between tongue and baleen and substantial wear on either. The study of Ray and Schevill (1974) of benthic suction feeding in a young captive gray whale confirmed that each lip could be moved independently and curled away from the baleen. Mandibular rotation has also been associated with enhanced gape and enlargement of the oral cavity for improved water engulfment in balaenopterids (Lillie, 1915; Howell, 1930), yet the ability of rorqual lips to knock baleen is doubtful, for although the lips contact the short baleen, they protrude little above the mandible and are likely far less mobile than those of gray and right whales.

Prey Removal Via Hydrodynamic Flushing

A third cleaning strategy entails backwashing a small amount of water into the mouth to remove items from baleen and deposit them on the tongue for transport and swallowing. As in the first hypothesis, the tongue is directly involved, although it would not contact baleen. By rapidly depressing and/or retracting the tongue, the oral space would enlarge, briefly generating a suction pressure to draw water through baleen into the mouth. Just as a dip net can be rinsed by rapidly jerking it back to reverse the flow through it, so water might momentarily enter a whale's mouth from the sides and thereby release captured items, so long as gape was sufficiently closed to prevent water from entering ventral to the baleen racks. Rapid abduction of the jaws might be coupled with lingual depression to create sufficient negative pressure to pull water in. The ensuing current need not be strong, merely sufficient to reverse the water flow and deliver prey into the center of the oral cavity. Note that this idea differs from the preceding two in that it depends on hydrodynamic rather than mechanical forces, with water (rather than a solid object) supplying the cleaning mechanism.

Not only would this flushing method require substantial lingual (and likely labial) mobility, but its efficacy would vary depending on such mobility as well as other factors—namely prey size and type and coarseness of baleen strands—that determine how likely items are to lodge in fringes. Although rorquals might not possess a sufficiently firm and muscular tongue to achieve even weak intraoral suction pressures, their coarser fringes and typically larger prey (with the exception of the sei whale) ought to ensure that even euphausiids would not become entangled, but would simply drop onto the tongue once the mouthful of engulfed water was expelled. Certainly the suction-feeding gray whale could generate sufficient negative pressure to flush baleen effectively. In essence the sole difference between suction-generated prey capture and release would be gape and, to a minor extent, lip position: although a wide gape would allow for prey ingestion, a narrow gape would simply result in a stream of cleansing water through baleen plates. A foraging gray whale could right its body or remain in a side-swimming position (although not contacting the substrate) for this backflushing. Just as the mouthful of engulfed water is expelled from the mouth through baleen, the mouthful of water for prey flushing could likewise be expelled by intermittently filter-feeding mysticetes, either before or after deglutition of accumulated prey. However, note that although whales can handle the osmotic load of swallowed seawater, they do not drink seawater (Slijper, 1962). The potential for increased

seawater ingestion from this rinsing flow might pose a serious problem for baleen cleaning via backwash.

Although balaenid tongues should also prove adequate to generate backwash flow, their delicate hairlike baleen fringes might preclude prey release. Indeed, any extra water flow (in any direction) might only serve to ensnare items further. Such hydrodynamic considerations are crucial, for recall that this is a nonstatic three-dimensional filter with porosity dependent on flow (Sanderson and Wassersug, 1990). The higher the water pressure, the denser the filter becomes (i.e., the smaller the pores), promoting prey capture and allowing ever smaller prey to be captured. As flow through the filter slows, the compacted mesh expands, so that it can be rinsed much more easily. Hence, a backwash flow should not be notably rapid or powerful. However, the fact that most swimming prey are negatively rheotropic further complicates matters; live prey would tend to swim upstream and burrow deeper into baleen during backwashing.

Although comparative mysticete tongue muscle studies are sorely lacking, myologic studies of right whales suggest that the tongue is capable of undergoing the movements needed to generate backwash flow. The rapid mouth closure and water expulsion observed in right whales by Mayo and Marx (1990) may relate to such prey removal. Although this behavior (which was observed to occur roughly once an hour) is described as flushing, no direct evidence exists to confirm that it indeed frees trapped prey. Limited observation of "nodding behavior," in which a right whale quickly dips its head and jerks it back (Gaskin, 1982; Mayo and Marx, 1990), might likewise be construed as supporting the backwash hypothesis, although this behavior might also support the claim of prey removal via head shaking or brief forward lunging described previously.

CONCLUSIONS

Baleen cleaning is not so simple as might initially be assumed, with many factors to be taken into consideration, chief among these the relation between the filtration apparatus and filtered items. Given the respective strengths and weaknesses of the three prey removal hypotheses, all seem equally likely to occur, especially in skim feeders. Confirmation of baleen wearing and replenishment, along with the purported actions of tongue musculature, support the claim of baleen cleaning by tongue scraping—although the lack of differential wear calls this into serious question—or by gentler rubbing, which would minimize abrasive loss of baleen. Limited observations of lateral head shaking and nodding in *Eubalaena* provide indirect support for the other hypotheses. Morphologic evidence seems to sustain rather than preclude each conjectural means of prey removal. It may well be that different species and individuals in different situations use all three mechanisms.

ACKNOWLEDGMENTS

I am greatly indebted to Laurie Sanderson, whose critical comments greatly improved the content and clear expression of the ideas presented here. Richard Wassersug and Jim Mead also provided many useful insights in their careful reviews of this paper. Discussions with Scott Kraus, Tom Albert, Larry Barnes, Roger Payne, Tom Ford, Butch Rommel, Dan Hillmann, Stormy Mayo, and Craig George helped me to formulate and develop the hypotheses of prey removal and their respective strengths and weaknesses. The ongoing anatomical study of bowhead tongues described in this paper was supported financially and logistically by the North Slope Borough, Department of Wildlife Management, Barrow, Alaska (contract C2189) and Alaska Eskimo Whaling Commission, which generously permitted me to use data from harvested whales and examine specimens housed at the Lousiana State University School of Veterinary Medicine.

LITERATURE CITED

Brodie, P. F. 1977. Form, function, and energetics in Cetacea: a discussion, pp. 45–58. *In* R. J. Har-

rison (ed.), Functional Anatomy of Marine Mammals. Vol. 3. New York: Academic Press. x + 428 pp.

CARROLL, G. M., J. C. GEORGE, L. L. LOWRY, AND K. O. COYLE. 1987. Bowhead whale (*Balaena mysticetus*) feeding near Point Barrow, Alaska, during the 1985 spring migration. Arctic, **40:** 105–110.

CLAPHAM, P. J., E. LEIMKUHLER, B. K. GRAY, AND D. K. MATTILA. 1995. Do humpback whales exhibit lateralized behaviour? Animal Behaviour, **50:** 73–82.

ESCHRICHT, D. F., AND J. T. REINHARDT. 1866. On the Greenland right whale (*Balaena mysticetus* L.), with special references to its geographical distribution and migration in times past and present, and to its external and internal characteristics. Ray Society Publications, **40:** 3–150.

EVANS, P. G. H. 1987. The Natural History of Whales and Dolphins. New York: Facts on File. xvi + 343 pp.

GASKIN, D. E. 1976. The evolution, zoogeography, and ecology of Cetacea. Oceanography and Marine Biology Annual Review, **14:** 247–346.

———. 1982. The Ecology of Whales and Dolphins. Portsmouth, New Hampshire: Heinemann Educational Books. xii + 459 pp.

GERACI, J. R., AND D. J. ST. AUBIN (EDS.). 1990. Sea Mammals and Oil: Confronting the Risks. Toronto: Academic Press. xvi + 282 pp.

GORMLEY, G. 1983. Hungry humpbacks forever blowing bubbles. Sea Frontiers, **29:** 258–265.

HAIN, J. H. W., G. R. CARTER, S. D. KRAUS, C. A. MAYO, AND H. E. WINN. 1982. Feeding behavior of the humpback whale, *Megaptera novaeangliae*, in the western North Atlantic. Fishery Bulletin, **80:** 259–268.

HALDIMAN, J. T., Y. Z. ABDELBAKI, D. W. DUFFIELD, W. G. HENK, AND R. W. HENRY. 1981. Determination of the gross and microscopic structure of the lung, kidney, brain and skin of the bowhead whale, *Balaena mysticetus* (RU 1380), pp. 305–662. *In* T. F. Albert (ed.), Tissue Structural Studies and Other Investigations on the Biology of Endangered Whales in the Beaufort Sea. Final Report to the Bureau of Land Management from the Department of Veterinary Science, University of Maryland, College Park, Maryland. NTIS PB86-153583/AS. iv + 953 pp.

HALDIMAN, J. T., AND R. J. TARPLEY. 1993. Anatomy and physiology, pp. 71–156. *In* J. J. Burns, J. J. Montague, and C. J. Cowles (eds.), The Bowhead Whale. Lawrence, Kansas: Society for Marine Mammalogy. xxxvi + 787 pp.

HOWELL, A. B. 1930. Aquatic Mammals. Springfield, Illinois: Charles C. Thomas. xii + 338 pp.

JURASZ, C. M., AND V. P. JURASZ. 1979. Feeding modes of the humpback whale, *Megaptera novaeangliae*, in southeast Alaska. Scientific Reports of the Whales Research Institute, **31:** 69–83.

KASUYA, T., AND D. W. RICE. 1970. Note on baleen plates and on arrangement of parasitic barnacles of gray whale. Scientific Reports of the Whales Research Institute, **22:** 39–43.

KAWAMURA, A. 1974. Food and feeding ecology in the southern sei whale. Scientific Reports of the Whales Research Institute, **26:** 25–144.

KLAUS, A. D., J. S. OLIVER, AND R. G. KVITEK. 1990. The effects of gray whale, walrus, and ice gouging disturbance on benthic communities in the Bering Sea and Chukchi Sea, Alaska. National Geographic Research, **6:** 470–484.

LAMBERTSEN, R. H. 1983. Internal mechanism of rorqual feeding. Journal of Mammalogy, **64:** 76–88.

LAMBERTSEN, R. H., R. J. HINTZ, W. C. LANCASTER, A. HIRONS, K. J. KREITON, AND C. MOOR. 1989. Characterization of the functional morphology of the mouth of the bowhead whale, *Balaena mysticetus*, with special emphasis on feeding and filtration mechanisms. Report to the Department of Wildlife Management, North Slope Borough, Barrow, Alaska. xiii + 134 pp.

LAMBERTSEN, R., N. ULRICH, AND J. STRALEY. 1995. Frontomandibular stay of Balaenopteridae: a mechanism for momentum recapture during feeding. Journal of Mammalogy, **76:** 877–899.

LEATHERWOOD, S., R. R. REEVES, AND L. FOSTER. 1983. The Sierra Club Handbook of Whales and Dolphins. San Francisco: Sierra Club Books. xviii + 302 pp.

LILLIE, D. G. 1915. Cetacea. British Antarctic (Terra Nova) Expedition, Zoology, **1:** 85–125.

LOUGHLIN, T. R. (ED.). 1994. Marine Mammals and the Exxon Valdez. London: Academic Press. xix + 395 pp.

LOWRY, L. F. 1993. Foods and feeding ecology, pp. 201–238. *In* J. J. Burns, J. J. Montague, and C. J. Cowles (eds.), The Bowhead Whale. Lawrence, Kansas: Society for Marine Mammalogy. xxxvi + 787 pp.

LOWRY, L. F., AND K. J. FROST. 1984. Foods and feeding of bowhead whales in western and northern Alaska. Scientific Reports of the Whales Research Institute, **35:** 1–16.

MAYO, C. A., AND M. K. MARX. 1990. Surface foraging behaviour of the North Atlantic right whale, *Eubalaena glacialis*, and associated zooplankton characteristics. Canadian Journal of Zoology, **68:** 2214–2220.

MILNER, A. 1981. Flamingos, stilts, and whales. Nature, **289:** 347.

MITCHELL, E. D. 1970. Pigmentation pattern and evolution in delphinid cetaceans: an essay in adaptive coloration. Canadian Journal of Zoology, **48:** 717–740.

MURISON, L. D., D. J. MURIE, K. R. MORIN, AND J. DA SILVA CURIEL. 1984. Foraging of the gray whale along the west coast of Vancouver Island, British Columbia, pp. 451–463. *In* M. L. Jones, S. L. Swartz, and S. Leatherwood (eds.), The

Gray whale *Eschrichtius robustus*. Orlando, Florida: Academic Press. xxiv + 600 pp.

NELSON, C. H., AND K. R. JOHNSON. 1987. Whales and walruses as tillers of the sea floor. Scientific American, **256:** 112–117.

NEMOTO, T. 1959. Food of baleen whales with reference to whale movements. Scientific Reports of the Whales Research Institute, **14:** 149–241.

———. 1970. Feeding pattern of baleen whales in the ocean, pp. 241–252. *In* J. H. Steele (ed.), Marine Food Chains. Edinburgh: Oliver and Boyd. viii + 552 pp.

NERINI, M. 1984. A review of gray whale feeding ecology, pp. 423–450. *In* M. L. Jones, S. L. Swartz, and S. Leatherwood (eds.), The Gray whale *Eschrichtius robustus*. Orlando, Florida: Academic Press. xxiv + 600 pp.

OLIVER, J. S., AND P. N. SLATTERY. 1985. Destruction and opportunity on the sea floor: effects of gray whale feeding. Ecology, **66:** 1965–1975.

OMURA, H. 1958. North Pacific right whale. Scientific Reports of the Whales Research Institute, **13:** 1–52.

ORTON, L. S., AND P. F. BRODIE. 1987. Engulfing mechanics of fin whales. Canadian Journal of Zoology, **65:** 2898–2907.

PAYNE, R. S. (In press). Behavior of Southern Right Whales (*Eubalaena australis*). Chicago: University of Chicago Press.

PIKE, G. C. 1962. Migration and feeding of the gray whale (*Eschrichtius gibbosus*). Journal of the Fisheries Research Board of Canada, **19:** 815–838.

PIVORUNAS, A. 1976. A mathematical consideration on the function of baleen plates and their fringes. Scientific Reports of the Whales Research Institute, **28:** 37–55.

———. 1977. The fibrocartilage skeleton and related structures of the ventral pouch of balaenopterid whales. Journal of Morphology, **151:** 299–314.

———. 1979. The feeding mechanisms of baleen whales. American Scientist, **67:** 432–440.

RAY, G. C., AND W. E. SCHEVILL. 1974. Feeding of a captive gray whale, *Eschrichtius robustus*. Marine Fisheries Review, **36:** 31–38.

REEVES, R. R., AND S. LEATHERWOOD. 1985. Bowhead whale, pp. 305–344. *In* S. H. Ridgway and R. J. Harrison (eds.), Handbook of Marine Mammals. Vol. 3: The Sirenians and Baleen Whales. San Diego: Academic Press. xviii + 362 pp.

RUBENSTEIN, D. I., AND M. A. R. KOEHL. 1977. The mechanisms of filter feeding: some theoretical considerations. American Naturalist, **111:** 981–994.

RUUD, J. T. 1940. The surface structure of the baleen plates and a possible clue to age in whales. Hvalradets Skrifter, **23:** 1–24.

———. 1945. Further studies on the structure of the baleen plates and their application to age determination. Hvalradets Skrifter, **29:** 1–69.

SANDERSON, S. L., AND R. WASSERSUG. 1990. Suspension-feeding vertebrates. Scientific American, **262**(3): 96–101.

———. 1993. Convergent and alternative designs for vertebrate suspension feeding, pp. 37–112. In J. Hanken and B. K. Hall (eds.), The Skull. Vol. 3: Functional and Evolutionary Mechanisms. Chicago: University of Chicago Press. x + 460 pp.

SCHELL, D. M., AND S. M. SAUPE. 1993. Feeding and growth as indicated by stable isotopes, pp. 491–509. *In* J. J. Burns, J. J. Montague, and C. J. Cowles (eds.), The Bowhead Whale. Lawrence, Kansas: Society for Marine Mammalogy. xxxvi + 787 pp.

SLIJPER, E. J. 1962. Whales. New York: Basic Books. 475 pp.

STORRO-PATTERSON, R. 1981. Great gulping blue whales. Oceans, **14:** 16.

SUND, P. N. 1975. Evidence for feeding during migration and of an early birth of the Californian gray whale (*Eschrichtius robustus*). Journal of Mammalogy, **56:** 265.

TARPLEY, R. J. 1985. Gross and microscopic anatomy of the tongue and gastrointestinal tract of the bowhead whale (*Balaena mysticetus*). Ph.D. dissertation. College Station, Texas: Texas A&M University. xiv + 141 pp.

TOMILIN, A. G. 1954. Adaptive types of the order Cetacea. Zoologicheskii Zhurnal Moscow, **33:** 677–691.

———. 1957. Mammals of the USSR and Adjacent Countries. Vol. IX: Cetacea. Jerusalem: Israel Program for Scientific Translations. xxi + 717 pp.

VOGEL, S. 1994. Life in Moving Fluids: The Physical Biology of Flow, second edition. Princeton: Princeton University Press. xiii + 467 pp.

VON SCHULTE, H. W. 1916. The sei whale (*Balaenoptera borealis* Lesson). Anatomy of a foetus of *Balaenoptera borealis*. Monographs of the Pacific Cetacea. Memoirs of the American Museum of Natural History (New Series), **1:** 389–499.

WATKINS, W. A., AND W. E. SCHEVILL. 1976. Right whale feeding and baleen rattle. Journal of Mammalogy, **57:** 58–66.

———. 1979. Aerial observation of feeding behavior in four baleen whales: *Eubalaena glacialis*, *Balaenoptera borealis*, *Megaptera novaeangliae*, and *Balaenoptera physalus*. Journal of Mammalogy, **60:** 155–163.

WATSON, L. 1981. Whales of the World. London: Hutchinson. 302 pp.

WEITKAMP, L. A., R. A. WISSMAR, C. A. SIMENSTAD, K. L. FRESH, AND J. G. ODELL. 1992. Gray whale foraging on ghost shrimp, *Callianassa californiensis*, in littoral sand flats of Puget Sound, USA. Canadian Journal of Zoology, **70:** 2275–2280.

WERTH, A. J. 1990. Functional anatomy of the right whale tongue [abstract]. American Zoologist, **30:** 21A.

———. 1993. Functional morphology of balaenid whale tongues [abstract], p. 112. *In* G. A. J. Worthy (ed.), Proceedings of the Tenth Biennial

Conference on the Biology of Marine Mammals, Galveston, Texas. 130 pp.

———. 1995. Models of hydrodynamic flow in the bowhead filter feeding apparatus [abstract]. American Zoologist, **35:** 59A.

———. 1998. Functional anatomy of the sperm whale tongue [abstract]. American Zoologist, **38:** 66A.

WILLIAMSON, G. R. 1973. Counting and measuring baleen and grooves of whales. Scientific Reports of the Whales Research Institute, **25:** 279–292.

WOLMAN, A. A. 1985. Gray whale, pp. 67–90. *In* S. H. Ridgway and R. J. Harrison (eds.), Handbook of Marine Mammals. Vol. 3: The Sirenians and Baleen Whales. San Diego: Academic Press. xviii + 362 pp.

WÜRSIG, B. 1988. The behavior of baleen whales. Scientific American, **258:** 102–107.

———. 1989. Cetaceans. Science, **244:** 1550–1557.

ZACKOWITZ, M. 2000. Doing a whale of a research job. National Geographic, **197:** 140.

TONGUE–JAW LINKAGES: THE MECHANISMS OF FEEDING REVISITED

KAREN M. HIIEMAE[1] AND JEFFREY B. PALMER[2]

ABSTRACT. Since the first description of cyclical tongue movements in feeding (opossum and cat), studies on a range of mammals (fruit bat, tenrec, rabbit, hyrax, macaque, and man) have been completed. This review examines those data to determine whether a pattern of tongue–jaw linkage in feeding is common to all mammals. Major directional changes in hyoid and tongue surface movement occur at comparable points in the jaw movement cycle regardless of craniofacial anatomy and dietetic specialization. In all cases, the hyoid and tongue surface move forward during the early part of jaw opening, with a return movement during later jaw opening and closing. The role of this cyclical tongue movement in the transport and manipulation of food is common to all mammals studied, save that triturated food is moved through the palatoglossal–palatopharyngeal arches for bolus formation earlier in the tongue cycle in macaque and man. New data on swallowing in man suggest that *Homo* has a specialized pattern for liquid bolus formation but otherwise retains the basic mammalian pattern.

INTRODUCTION

In a letter to *Nature*, Crompton et al. (1975) reported that the hyoid bone moves continuously in feeding in the American opossum (*Didelphis virginiana*). This simple observation refuted the then conventional wisdom, based on limited human studies, that the hyoid only moves in swallowing. Attention has since focused on the interrelationships between jaw and hyoid movement, jaw movement, and hyoid and tongue surface movement, and the role of these movements in the acquisition, processing, and transport of food in mammals. In 1978, Hiiemae, Thexton, and Crompton posited that cyclical movements of the tongue, by facilitating the intraoral management of food, including its transport to the pharynx for bolus accumulation and swallowing, were integral to the feeding process. A sufficient body of evidence has now accumulated from experimental studies (listed in the Appendix) examining feeding behavior in representative terrestrial mammals with very different dietetic adaptations to make a synthesis possible. This review examines the proposition that a pattern of linked jaw and hyoid–tongue movement is common to all terrestrial mammals with type I tongues (Doran, 1975).

Although the craniofacial anatomy of terrestrial mammals has a common Bauplan, anatomical details vary widely both among and within orders (Hiiemae, 2000; Turnbull, 1970). However, the basic physiological functions performed by the teeth, jaws, tongue and associated soft tissues do not vary (Hiiemae, 2000). These functions are associated with the acquisition, reduction (if needed), transport, and swallowing of food for chemical digestion. It follows that because all mammals have the same Bauplan, subserving the same biological functions, it is reasonable to postulate that the mechanisms used to fulfill these physiological functions will be essentially the same. If a patterned linkage exists between the cyclical movements of the jaws and the cyclical movements of both the tongue surface and the hyoid, that linkage should be expressed by a consistent relationship

[1] Institute for Sensory Research, and Department of Bioengineering and Neuroscience, Syracuse University, Syracuse, New York 13244-5290.

[2] Department of Physical Medicine and Rehabilitation, The Johns Hopkins University School of Medicine, Good Samaritan Hospital, Baltimore, Maryland 21239.

between jaw and tongue–hyoid movement events in all feeding cycles in all species examined.

Bramble and Wake (1985) developed a theoretical model for a generalized feeding cycle in nonmammalian terrestrial tetrapods, largely based on a synthesis of kinesiological and electromyographic (EMG) data from terrestrial salamanders, turtles, and lizards. This model had features, such as rate change and direction of jaw and hyolingual motion, similar to those reported in mammals (Bramble and Wake 1985, fig. 13.3). They suggested that there might be homologies between mammalian feeding mechanisms, especially intraoral transport, and those observed in nonmammalian vertebrates, such that the patterns seen in mammals might have evolved in earlier terrestrial tetrapods. While acknowledging the absence of experimental data, they extended their analysis to suggest that the central pattern generator (CPG) maintaining the rhythmic jaw movements of feeding identified in mammals (Bremer, 1923; Dellow and Lund, 1971), might be present in antecedent forms, and that the output of such a CPG was regulated by sensory modulation from oral receptors. Smith (1994: 294) argued, for that to be true, neuromotor patterns had to be homologous, that is, despite changes in peripheral anatomy, the neuromotor output from the central nervous system (CNS) had to be conserved. She observed that similarities in movement patterns (or, functional behaviors, our term) had been extended "to hypotheses of neuromotor conservatism, to assertions of evolutionary constraints." Taking a broad-brush approach using examples from a broad range of vertebrate taxa to test the hypothesis that terrestrial vertebrates have a conservative feeding program, she found little evidence for its support.

The purpose of this review is to examine what is now known about tongue–jaw movements in feeding in mammals, including man; to determine whether there is a basic mammalian pattern; and to briefly revisit the issue of whether the mammalian pattern could have its antecedents in the mechanisms for food transport developed in phylogenetically earlier terrestrial tetrapods.

EXPERIMENTAL STUDIES

Intraoral behavior is particularly difficult to study. The only techniques that allow the concurrent recording of jaw movement, hyoid movement, tongue surface movement (provided radiopaque markers are used), and food position (if treated with barium sulfate) are cinefluorography (CFG) or videofluorography (VFG). It must be emphasized that any CFG or VFG record is a 2D projection or image of 3D events. If a structure, such as the hyoid, has little mediolateral movement, then the 2D image seen in lateral projection probably accurately represents its movement pattern. Data for macaque and man confirm that no such confidence can be attached to tongue surface movement data. Although CFG and VFG have been used in many studies of feeding in mammals representative of omnivores (including the Pecora), carnivores, herbivores, rodents, and primates, relatively few (see Hiiemae, 2000; and the Appendix) have examined the temporal relationships between jaw and tongue–hyoid movements during feeding sequences. Comparison and synthesis of those reports to address the question of whether a common pattern exists is complicated by the rate of experimental data acquisition, the methods used for analysis, the form in which data were presented, and the need to reconcile the underlying behavioral patterns regardless of the terminology used.

THE ANATOMY OF THE TONGUE–HYOID–JAW COMPLEX

Although the proportions of the skull and lower jaw, as well as the general position of the hyoid and the shape of the tongue, differ markedly between mammals (Hiiemae, 2000), the muscles producing

jaw, hyoid, or tongue movement are generally homologous. Hyoid position is known to be controlled by the interplay of activity in three groups of muscles. The anterior suprahyoids (anterior belly of digastric and geniohyoid) pull the hyoid forward and can depress the lower jaw. The mylohyoid can also elevate the hyoid, synchronously raising the floor of the mouth and so the tongue body. The hyoid is connected to the skull base by the posterior belly of digastric and the stylohyoid (posterior suprahyoids), which can pull the hyoid backward and upward. The infrahyoids connect the hyoid to the sternum (sternohyoid), the scapula (omohyoid), and the thyroid cartilage (thyrohyoid). The major infrahyoids (sternohyoid and omohyoid) act to pull the hyoid back, down, or both.

The biomechanics of the hyoid complex are poorly understood. Using EMG and movement data, Crompton et al. (1977) demonstrated the mechanism by which jaw and hyoid movements were produced in *Didelphis*, whether divergent (i.e., the hyoid traveling backward, away from the symphysis, in jaw closing, lengthening the tongue base) or convergent (the hyoid traveling forward, toward the symphysis, in jaw opening, shortening the tongue base). No comparable study has been conducted for any other mammal. However, the changing pattern of shortening and lengthening in these muscles regulates hyoid position and so the length of the tongue base.

Nonanthropoid mammals have anteroposteriorly (AP) elongate and vertically shallow tongues. However, the evolution of the anthropoid primates resulted in progressive change in tongue shape, with concomitant changes in the anatomy of the oropharynx. As described by Thexton and Crompton (1998), the shape of the tongue in macaque has changed from that seen in *Didelphis* and most other mammals: it is shorter anteroposteriorly but has greater vertical height. In man, the tongue is still shorter with much greater height, such that the hyoid is widely separated from its oral surface, creating a long, vertically oriented pharyngeal surface (Hiiemae, 2000; Hiiemae and Palmer, 1999). If a basic mammalian pattern exists, it follows that these morphological changes should not affect its expression, although the mechanical outcomes may be different.

Doran (1975) identified two types of mammalian tongues, both with oral and pharyngeal parts. Type I, found in most mammals (and all those mammals in which its movement has been studied), can be protruded to a maximum of 50% of its resting length. Type II tongues are found in a few mammals, such as the anteaters, and can be extensively protruded outside the mouth for food gathering. Livingstone (1956) argued, first, that the movement of the tongue depends largely on the movement of the hyoid; second, that change of position, coupled with a change of form results from extrinsic muscle action, and, last, that the intrinsic muscles provide for a great deal of mobility. It follows that if the tongue base shortens (geniohyoid, mylohyoid), carrying the hyoid and the body of the tongue forward, then the effect of contraction of the genioglossus, which protrudes the tongue, will be augmented. Similarly, the action of hyoglossus or styloglossus, either of which can pull the tongue backward, will be augmented by retraction of the hyoid. However, given the pattern of insertion of both genioglossus (medially) and hyoglossus (laterally), contraction of either will affect the overall shape of the tongue body. Nevertheless, as Kier and Smith (1985) and Smith and Kier (1989) have emphasized, the tongue has constant volume, such that a change in any dimension must be accompanied by changes in the other two. This makes the distinction between extrinsic and intrinsic muscles, while anatomically convenient, somewhat arbitrary with respect to function. Schwenk (2001) further advances this argument.

To summarize, it follows that movements of the lower jaw are linked to hyoid position; movements of the body of the tongue are linked to the length of its base,

itself affected by hyoid position and lower jaw movements; and the working surfaces of the tongue (oral and pharyngeal) have their shape affected by both of the above, but augmented by the activity of the intrinsic muscles.

ISSUES IN SYNTHESIS

The rhythmic movements of the jaw in feeding, especially chewing, are well described. Those movements are now known to be associated with rhythmic hyoid movements. At the same time, the tongue not only changes its gross position but also changes shape depending on the condition of the food in the mouth and stage in sequence: ingestion with stage I transport; processing; bolus formation with stage II transport; and deglutition (see Hiiemae, 2000; Hiiemae and Palmer, 1999). We also now know that the overall jaw cycle time varies between species studied, and also within each sequence in a given species, such that the time spent in closing (Fast Close [FC], Slow Close [SC]/Power Stroke [PS]), Intercuspal Phase (IP), and opening (Slow Open [SO] or O1, O2, Fast Open [FO]) also varies, based on the changing rate of jaw movement. It follows that if jaw, hyoid, and tongue movements are linked, that is, their movements are interdependent, then there should be some consistent relationship, regardless of separation in time, between specific events in jaw, hyoid, and tongue movement cycles. For such linkage to exist, synchrony is not essential, rather events should occur in a consistent sequence.

If the hypothesis that there is such linkage and that same linkage will be found in all mammals is to be exhaustively tested, then a rigorous comparative analysis using a set of uniform event criteria and techniques such as interval analysis is required. Clearly this is infeasible for the full range of mammals so far studied given the issues in data collection and reduction alluded to above. Instead, we are forced to examine the available qualitative (behavioral) data and attempt to determine whether the patterns of activity within cycles and within sequences for those mammals studied show any commonality across species and orders.

PATTERNS OF TONGUE AND HYOID MOVEMENT

All jaw movement cycles have closing and opening strokes separated by an IP phase of variable duration (very short in some carnivores and insectivores, longer in most omnivores and herbivores with a substantial lateromedial or posteroanterior lower molar traverse in occlusion on the working side). For all mammals studied, the hyoid moves from its most backward and downward position, at about minimum gape, to its most forward and upward position during opening, reversing direction before maximum gape (Fig. 1). Tongue marker orbits also demonstrate this reversal (Fig. 2).

To test the hypothesis that all mammals show the same jaw and tongue movement patterns, regardless of cycle duration, or phase duration within cycles, and tongue shape, the available data were analyzed using distinct movement turnpoints as event markers (Palmer et al., 1997). The jaw movement event markers were maximum and minimum gape. For the tongue–hyoid, they were maximum forward (MF for hyoid or TF for tongue); maximum down (MD or TD), maximum back (MB or TB), and maximum up (MU or TU), relative to the upper occlusal plane. The available data were brought to a consistent time scale (normalized) and these turnpoints (hyoid–tongue marker), as reported, were established relative to maximum and minimum gape and entered into a bar chart as accurately as possible. The results are shown in Figure 3.

In every species, TF occurs before maximum gape in opening. In all these mammals, including tenrec and opossum (data limited to text descriptions), the tongue marker (anterior tongue marker, ATM, or middle tongue marker, MTM) reaches its most backward position concurrent with or

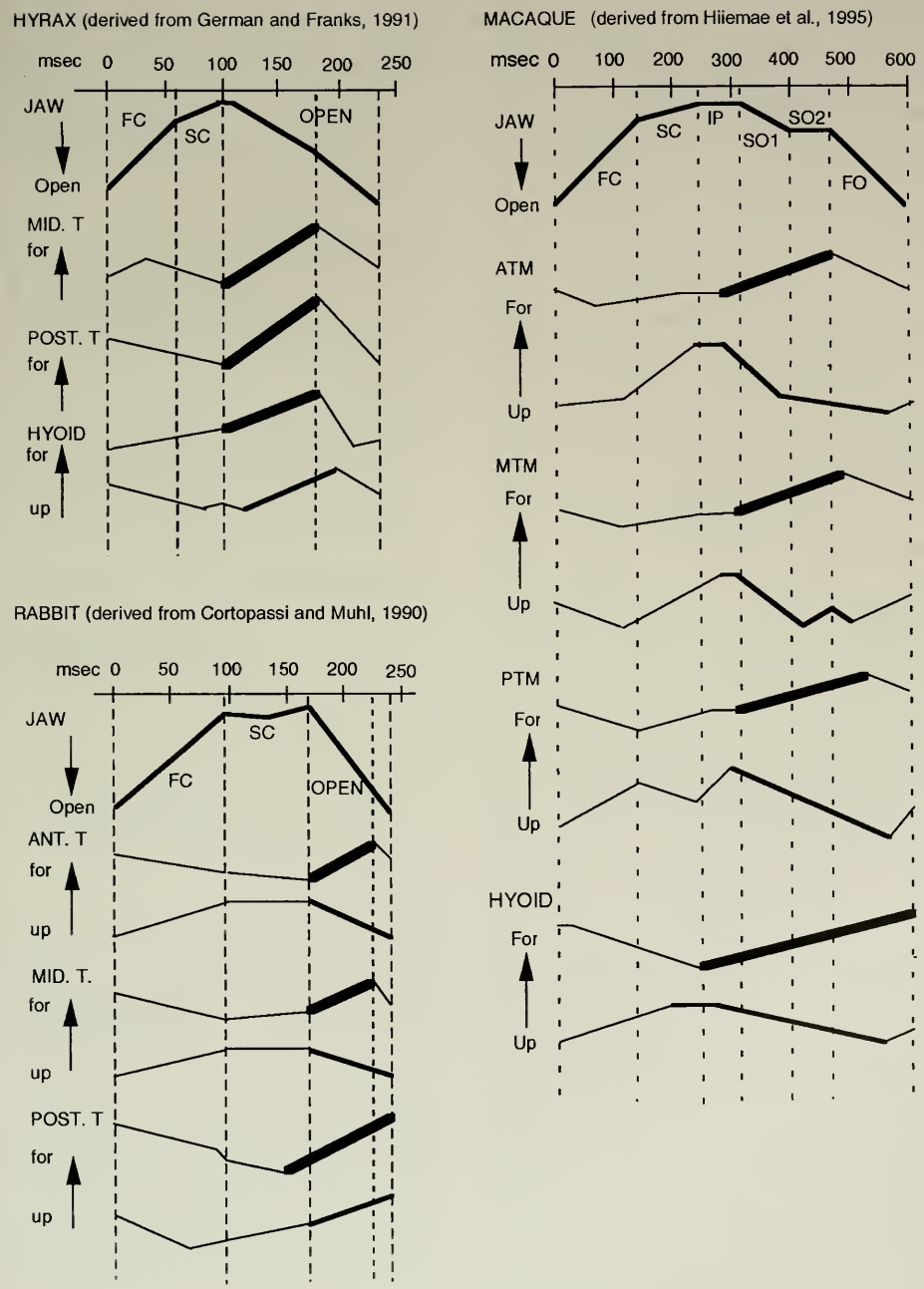

Figure 1. Gape-time (GT) plots for a single cycle of jaw, tongue, and hyoid movement in hyrax, rabbit, and macaque redrawn from data in the papers cited (no attempt has been made to represent actual distances traveled in any direction). The pattern of upward and forward movement of the tongue surface in the first part of opening is shown by the extra thick lines, the synchronous downward movement by thick lines. The hyrax and rabbit records (published figures, or text) provide no basis for dividing the opening jaw movement into O1, O2, or FO/O3 phases; however, the macaque cycle (a composite) shows the pattern of jaw movement when the SO phase has two components. The reversal of ATM and MTM movement at the SO2–FO transition is clearly shown (see text).

Abbreviations: ANT. T, anterior tongue; ATM, anterior tongue marker; MID. T, middle tongue; MTM, middle tongue marker; POST. T, posterior tongue; PTM, posterior tongue marker.

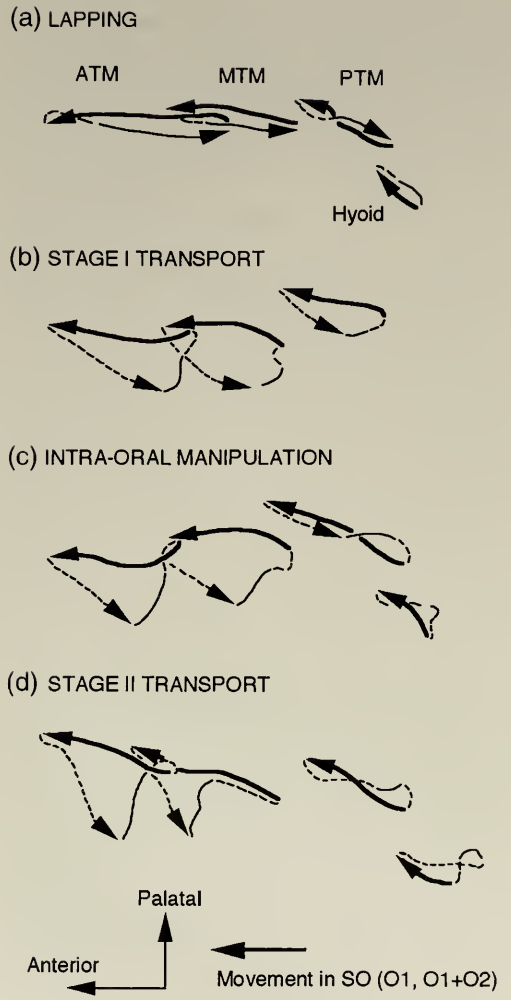

Figure 2. The trajectory, shown as loops, of anterior (ATM), middle (MTM), and posterior (PTM) tongue markers, and the hyoid, in opossum. (a) Lapping (a low-amplitude jaw movement without FO or FC); (b) stage I transport (movement of food from an extraoral position or from the front of the oral cavity to the molar region); (c) chewing (processing) cycles where food has to be repositioned on the occlusal surfaces of the postcanines (manipulation); and (d) stage II transport, in which triturated food is moved through the palatoglossal arches for bolus formation and deglutition. Although the tongue and hyoid movements in lapping show long elliptical loops, the introduction of the FO and FC phases when feeding on solid food increases their vertical dimension. (FO dashed line, FC thin solid line, SC longer dotted line). Regardless of stage in sequence, the tongue surface (ATM, MTM) is moving from a maximum tongue back (TB) to a maximum tongue forward (TF) position during early opening, reaching its most forward position in opening, but before maximum gape. Redrawn from Hiiemae and Crompton (1985, fig. 14–12).

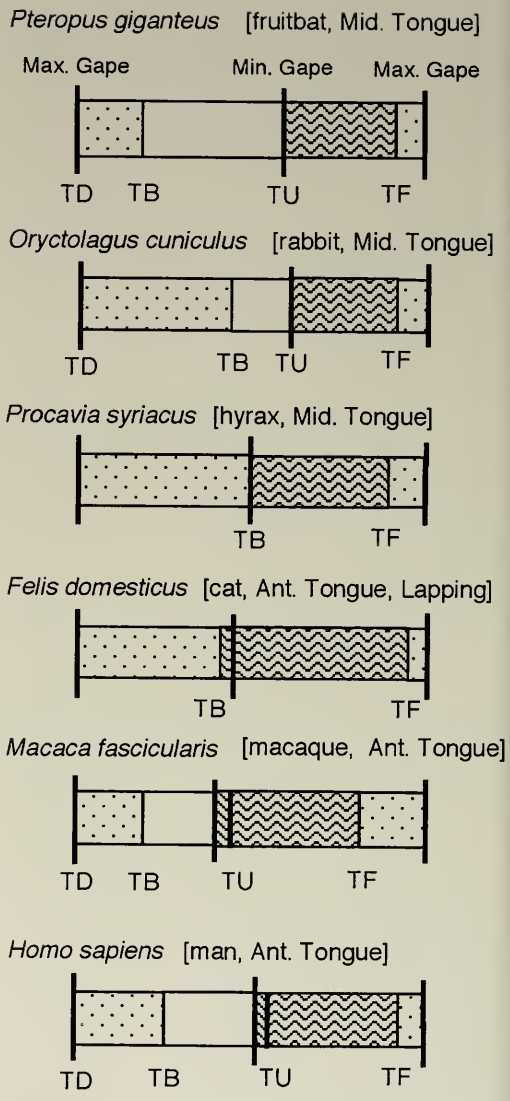

Figure 3. Tongue turnpoints (TB and TF, with TD and TU where available, see text) for chewing cycles in mammals where time data is available (no data for opossum are included because the gape-time plot data from which Fig. 2 was prepared were not published). Cycle times have been normalized to express the time of events within cycles expressed as the percentage of time after initial maximum and before terminal maximum gape. The common rhythmic pattern of AP tongue movement is shown.

Vertical bars mark start maximum gape, minimum gape, and terminal maximum gape. Forward tongue movement in opening is shown by the wavy stippling; backward movement is shown by the dots. The blank periods (fruit bat, rabbit, macaque, and man) indicate the time in which the tongue surface is rising.

before minimum gape. The exceptions appear to be hyrax and opossum, where a very short IP often occurs. However, the time compressed data in German and Franks (1991, fig. 2) show a short forward–backward oscillation before the computed minimum gape in stereotypical chewing cycles. If TB is taken as the first of these backward positions, then the pattern for hyrax is consistent with that for the other species (as shown in Fig. 3). In some records for the opossum (Hiiemae and Crompton, 1985), TB occurs before minimum gape. Unfortunately, because the orbits shown in the published figures are examples of actual cycles, rather than a statistically derived norm based on analysis of large numbers of cycles, this result has to be taken as strongly supportive, rather than confirmatory, of a generalized pattern.

It should also be noted that there is little likelihood that the tongue markers were in comparable positions in these separate experiments, because the published data used for each analysis referred to mid-tongue or anterior tongue. Further, strong evidence exists that although markers in the anterior and middle parts of the tongue tend to move in synchrony, forward movement of the posterior tongue and hyoid may be slightly delayed (Hiiemae et al., 1995). This suggests that were the original data to be revisited, a much clearer demonstration of a common pattern might be obtained. However, we consider it significant that an analytical approach developed to describe tongue–hyoid–jaw movements in macaque and man shows the same pattern when applied to other mammals.

The jaw movement cycle is designed to assure food reduction in a chewing stroke (SC/PS). The remainder of the jaw movement cycle serves to reposition the lower jaw for the next such stroke. Concurrently, there is a tongue movement cycle with its major activity occurring during opening and the FC phase of closing. German and Franks (1991) analyzed the temporal relationships between minimum gape and the start of tongue and hyoid protrusion in hyrax. They found that the tongue and hyoid turnpoints for the onset of forward movement were synchronized to within one frame of the computed minimum gape, but that no predictable linkage occurred between tongue–hyoid movement events and maximum gape. This study provides a convincing demonstration of the existence of a possible switch from the jaw movement cycle required for food reduction to a tongue movement cycle functioning to control intraoral food position and food transport in hyrax at minimum gape. However, this study cannot be readily extrapolated to other mammals, especially anthropoids, where no minimum gape is clearly visually identifiable given a long IP phase.

Although there is no stereotypical jaw movement cycle in macaque (Thexton and Hiiemae, 1997), Hiiemae et al. (1995) were able to show that TF (ATM and MTM), always occurred within 30 milliseconds (usually less) of the last rate change in opening, that is, with the initiation of FO. Furthermore, when O2 was present, the amplitude of forward tongue movement was greatest. However, gape at the O2–FO transition was always small. If, as Thexton and Crompton (1989) argue, the O1 and O2 phases of lapping (cat, opossum) correspond to SO (O1 ± O2) in chewing, then the extensive tongue protrusion involved in lapping exemplifies the anatomical relationship between tongue–hyoid movement and gape amplitude, leading to the hypothesis that extensive tongue protrusion can only occur within a relatively narrow range of gape, because additional jaw opening (FO) requires hyoid retraction. It also explains the EMG data, which show low-level activity in the adductors (masseter or medial pterygoid) during O2, suggesting an antagonist function that resists jaw opening and promotes protraction of the hyoid bone and the tongue body.

It must be emphasized that these results

must not be construed as implying that tongue and jaw movements are invariably time and movement linked. Quite the reverse is true. The interdependence between jaw–hyoid–tongue movement demonstrated here applies only to chewing, lapping, and food transport. Even in chewing sequences, albeit in man, the rhythm may be disrupted during the collection and aggregation of food particles (clearance) for bolus formation (Hiiemae et al, 1996; Hiiemae and Palmer, 1999; Palmer et al., 1997).

Intrinsic Tongue Movement. Cortopassi and Muhl (1990) described AP movements of the rabbit tongue surface as undulating. This could be explained as a function of the time delay between the initiation of an anteriorly or posteriorly directed movement between the various parts of the tongue. Where comparative data are available, such a sequential pattern with the anterior tongue leading seems to be present. However, there is no doubt that in the fruit bat (de Gueldre and de Vree, 1984), cat (Thexton and McGarrick, 1988, 1989), and macaque (Hiiemae et al., 1995), there is differential expansion and contraction of the tongue surface, as measured by lengthening or shortening of the Euclidean distance between tongue markers.

These studies show that the tongue can be considered as having three distinct components: the anterior tongue (tip to anterior postcanines), the mid-tongue (related to the cheek teeth), and the posterior tongue (the postfaucial, or pharyngeal, surface). As might be expected, the amplitude of possible expansion and contraction is greatest in the anterior tongue and least in the posterior. However, in chewing cycles (macaque) when little or no anteroposterior food transport is occurring, expansion–contraction (measured in lateral projection) is restricted to the middle segment. This may be illustrative not only of the 2D representation of 3D events mentioned above, but also of the tongue's capacity to respond, independently of jaw and hyoid movement, to functional (food processing) needs cycle to cycle within sequence.

To summarize, as the jaw movement cycle (close, IP, open) proceeds, there are concomitant movements of both the hyoid and the tongue surface. The hyoid and tongue move forward and variably upward, starting at minimum gape or within IP, and reverse direction during opening, before maximum gape, or at the small maximum gape used in lapping (end O2).

MECHANISMS IN FEEDING

Vertical and AP tongue movements during feeding cycles have a common pattern across all the adult mammals studied regardless of dietary specialization, stage in sequence, and type of food. The question arises: how does this apparent common pattern subserve the physiological processes required for transmission of swallowable food to the gastrointestinal tract for chemical digestion? The corollary has to be addressed: how is the linkage between forward tongue movement in early jaw opening correlated with the backward movement of food within and through the oral cavity? How does the tongue, acting against the hard palate, and with the cheeks (variably developed in mammals), produce the documented aggregation and distal movement of swallowable food?

Feeding sequences are now considered to have four stages: stage I transport (movement of food from the anterior oral cavity to the postcanines); processing (food reduction in chewing or by tongue–hard palate compression, or both); stage II transport (movement of swallowable food through the palatoglossal–palatopharyngeal arches with bolus formation), and, last, deglutition. Tongue movements in processing are poorly understood, but clearly involve rotation of the working (gustatory) surface of the tongue about its long (AP) axis to position food, or maintain food position, in readiness for the next chewing cycle (Hiiemae, 2000; Hiiemae and Crompton, 1985).

Tongue and hyoid movement patterns for stage I and II transport have been described for most of the mammals studied (see the Appendix; Hiiemae and Crompton, 1985). In all cases, food, whether liquid or solid, is carried backward through the mouth to the postcanines, or from the oral cavity to the pharynx, on a backwardly traveling tongue surface or by virtue of a backwardly traveling tongue–palate contact. For stage I transport, the only differences in the mechanism, between mammals studied, can be directly correlated with the length of the tooth row. The process may take several cycles in macaque (German et al., 1989) but can be accomplished in a single cycle in man (Hiiemae and Palmer, in preparation). Superficially, the mechanisms of stage II transport show the greatest differences. In the mammals studied, except macaque and man, aliquots of swallowable food are moved through the palatoglossal arches (fauces) during the upward and backward movement of the tongue in late FO (O3) and FC (Hiiemae and Crompton, 1985). This is described as the squeeze-wedge mechanism. In macaque (Franks et al., 1984, see also Thexton and Crompton, 1998) and man (Hiiemae and Palmer, 1999) the upward and forward movement of the tongue in IP brings the anterior surface of the tongue into contact with the anterior palate, and that contact rapidly spreads backward (middle and posterior tongue) forcing the food mass through the fauces. This mechanism, squeeze-back, depends on forward movement of the tongue coupled with a posteriorly traveling tongue–palate contact.

All nonanthropoid mammals form the bolus in the oropharynx (piriform fossae–valleculae). Without prejudice to the airway, given an intranarial larynx, the bolus is moved into the esophagus from the oropharynx (see Thexton and Crompton, 1998). It has long been axiomatic that man is different because in *Homo sapiens,* the bolus is formed in the oral cavity and propulsively expelled across the oropharynx, to avoid the risk of aspiration into a respiratory tract whose aditus (true vocal folds) lies well below the oral cavity. We find (Hiiemae and Palmer, 1999) that in *H. sapiens,* boli formed from natural bites (e.g., 6–8 g of normal foods) normatively form in the oropharynx. In short, man is a mammal. Equally, we argue that for ingested liquids, the bolus is formed, contained, and organized within the oral cavity, and swallowed therefrom. We argue that the pivotal evolutionary change in hominid development has been the development of a behavioral mechanism for process management of liquids, which can flow, in contrast to solids, which, even when triturated, probably cannot.

CONCLUSIONS

Jaw, hyoid, and tongue movements, during the rhythmic cycles of normal feeding in mammals including man, are interdependent, that is, there is a consistent event order relationship between movements of the jaw and the hyoid, and the grosser movements of the tongue. This should occasion no surprise given the physiological and gross anatomical homologies among the structural elements involved. That said, the available data cannot support any detailed conclusions about the actual behavior of the tongue surface during feeding sequences for mammals in general. However, if food is to be of metabolic utility, it has to reach the gastrointestinal tract for chemical digestion. A primary role of the tongue–hyoid complex is the movement of swallowable food into the pharynx for bolus formation and then deglutition. Although the mechanisms of stage I and stage II transport are now well documented (at least for representative species, see Hiiemae, 2000; Hiiemae and Crompton, 1985; Hiiemae and Palmer, 1999), the precise role of the pattern of complex and poorly understood changes in tongue surface position and shape during intraoral food management are not.

The available data do support a generic mammalian model that posits that two cy-

clical, linked but not interlocked mechanisms are operative during feeding sequences in mammals. Cyclical jaw movements position the teeth for food reduction in SC, and then complete a cycle to reposition the teeth for the next chewing stroke. Concomitantly, the hyolingual system is also cycling. Tongue movements, facilitated by changes in gross tongue position as a function of hyoid movement, and implemented by changes in tongue surface–palate contacts, manipulate and transport food within and through the oral cavity during the SO-FO and FC phases of the jaw movement cycle. Although the order of events is the same for all the mammals studied, the temporal linkages between them seem tighter in opossum and hyrax, where the start of tongue and hyoid protrusion is closely associated with minimum gape. In macaque and man, both of which have more vertically oriented tongues, the definitive (functional) forward movement begins during IP and, at least in macaque, ends with the last rate change in opening. Rate changes do occur in opening in man, but are only clearly associated with cycles in which stage II transport is occurring (work in progress).

These conclusions are, of necessity, based largely on qualitative data. What inferences can be drawn as to why this pattern is present and whether it evolved from an antecedent premammalian pattern? For most mammals, solid food has to be processed before it can be swallowed, requiring powered tooth–food–tooth contact, that is, the jaws have to separate and then close with the food positioned between the teeth. The tongue, given the variable development of highly mobile cheeks in nonanthropoid mammals, is the primary agent for food manipulation and positioning. Clearly, food positioning must occur in advance of a power stroke if such is to be effective and the tongue not be traumatized. The amplitude of jaw movement must be such as to allow large bites of material to be properly positioned. It is possible that the rotational movements of the tongue surface associated with food positioning are a mammalian adaptation.

Equally, we argue that, both ontogenetically and phylogenetically, the fundamental functional mammalian behavior is food transport. Liquids, requiring no processing, are simply moved through the mouth, into the oropharynx, and swallowed. The rhythmic cycle of hyolingual movement is the conveyor belt moving material backward. Tongue contacts with the hard palate act as the stop to ensure the unidirectional (posterior) movement of food. In mammalian lapping, the amplitude of jaw movement is minimal, sufficient to protrude the tongue, allow it to collect an aliquot, and then retract. This low-amplitude gape (O2) is maintained as the tongue completes its aliquot collection. The jaw cycle is modified when solid food requiring processing is introduced. The FO phase, with a longer close (FC and SC) appears. The underlying hyolingual cycle remains the same, its reversal from forward to backward movement occurring at a gape in the range associated with lapping.

What is significant is that every mammal studied adopts, within and between sequences, a cyclical behavior that can, post hoc, be correlated with the initial consistency of the food, and by inference, with the effect of its processing. This, given that functional behavior can change from cycle to cycle, implies continuous sensory feedback to the CNS, which regulates the output from the CPG(s) producing rhythmic jaw and hyolingual movement.

As Bramble and Wake (1985) observed, mammals are by no means unique in having jaws and a hyolingual complex. Their model for solid food transport in generalized terrestrial tetrapods looks, as they stated, functionally very similar to that documented for solid food transport in mammals: the hyolingual complex is protruded as the jaws open and retracted during jaw closure. Does a commonality of outcome (food delivered to the digestive

tract) require a commonality of mechanism? This is the issue at the core of the question posed by Smith (1994) when she addressed the question: is this consistent pattern reflective of a 'conserved neuromotor system'? Two issues must be addressed. The first, given phylogenetically old osseocartilaginous and soft tissue elements, connected by muscle blocks arranged to generate movement in specific directions, is biomechanical. What muscle blocks contract in what way to produce what result temporally and spatially? Do they do so in a predictable and patterned order? If viewed simply as jaw elevators and depressors, and hyolingual protractors and retractors, then the activity of those muscle blocks, as modeled by Bramble and Wake (1985), could represent the substrate on which the more complex mammalian pattern evolved.

We argue that, given our current knowledge of the CNS control of rhythmic jaw–hyolingual behaviors in mammals and in nonmammalian tetrapods, it is premature to focus on neuromotor systems *per se*. (Given the foregoing, one might ask "what is a neuromotor system": anatomically or functionally homologous structures?) It is now clear that complex CNS linkages form the CPGs for rhythmic jaw movement and swallowing in mammals (Dellow and Lund, 1971; Jean, 1990), although how linked tongue rhythmic behavior fits into those identified CPGs is not yet known. However, we do know that there is a complex, and probably itself experientially modulated, web of interconnectivity between the sensory and motor nuclei in the pons and medulla for all the cranial nerves (CN V, VII, IX, X, XI, XII) involved. The importance of smell and taste in the selection of foods for transport and processing (Gilbertson, 1998) cannot be ignored: input from those sensors clearly affects feeding behavior. At a time when the sources of sensory input from the mammalian orofacial complex modulating rhythmic motor output are a matter of dispute, broader-brush inferences for the evolution of these functional behaviors and their control in terrestrial tetrapods are intriguing. Nevertheless, as such, they hopefully can serve as a stimulus to further, and difficult, research focused on the CNS rather than on the qualitative analysis of functional behaviors as the basis for modeling CNS control mechanisms.

ACKNOWLEDGMENTS

This review is dedicated to A. W. Crompton (A. W. C.), without whose support and encouragement (especially for K. M. H. in the late 1960s through early 1970s) much of this body of research could never have been accomplished. Almost all of the authors cited in the Appendix were participants or beneficiaries of the Yale and then the Museum of Comparative Zoology research effort that A. W. C. oversaw. Since 1991, Syracuse University Bioengineering undergraduates electing Senior Thesis Research in K. M. H.'s laboratory at the Institute for Sensory Research have made much of the analysis reported here possible (1992–1999). We also acknowledge the superb technical support afforded by Xuezhen Wu and Chune Yang in Jeffrey Palmer's laboratory at Johns Hopkins University. U.S. Public Health Service Awards, first NIH DE 05738, and later NIH DC 02123, augmented by institutional resources (Syracuse University and Johns Hopkins University), supported this research.

LITERATURE CITED

ANAPOL, F. 1988. Morphological and videographic study of the hyoid apparatus and its function in the rabbit (*Oryctolagus cuniculus*). Journal of Morphology, **195:** 141–157.

BRAMBLE, D. M., AND D. B. WAKE. 1985. Feeding mechanisms of lower vertebrates, pp. 230–261. *In* M. Hildebrand, D. M. Bramble, K. F. Liem, and D. B. Wake (eds.), Functional Vertebrate Morphology. Cambridge, Massachusetts: Belknap Press of Harvard University Press. 430 pp.

BREMER, F. 1923. Physiologie nerveuse de la mastication chez le chat et lapin. Archives Internationale Physiologique, **21:** 309–352.

CORTOPASSI, D., AND Z. MUHL. 1990. Videofluorographic analysis of tongue movement in the rab-

bit (*Oryctolagus cuniculus*). Journal of Morphology, **204:** 139–146.

CROMPTON, A. W. 1989. The evolution of mammalian mastication. *In* D. B. Wake and G. Roth (eds.), Complex Organismal Function: Integration and Evolution in Vertebrates. New York: John Wiley. xiii + 451 pp.

CROMPTON, A. W., P. COOK, K. M. HIIEMAE, AND A. J. THEXTON. 1975. Movement of the hyoid apparatus during chewing. Nature, **258:** 69–70.

CROMPTON, A. W., A. J. THEXTON, P. PARKER, AND K. M. HIIEMAE. 1977. The activity of the hyoid and jaw muscles during chewing of soft food in the opossum, pp. 287–305. *In* B. Stonehouse and D. Gilmore (eds.), The Biology of Marsupials. London: Macmillan. viii + 486 pp.

DELLOW, P., AND J. LUND. 1971. Evidence for the central timing of rhythmical mastication. Journal of Physiology (London), **215:** 1–13.

DE GUELDRE, G. D., AND F. D. DE VREE. 1984. Movements of the mandible and tongue during mastication and swallowing in *Pteropus giganteus* (Megachiroptera). Journal of Morphology, **179:** 95–114.

DORAN, G. 1975. Review of the evolution and phylogeny of the mammalian tongue. Acta Anatomica, **91:** 118–129.

FRANKS, H. A., A. W. CROMPTON, AND R. Z. GERMAN. 1984. Mechanism of intraoral food transport in macaques. American Journal of Physical Anthropology, **65:** 275–282.

FRANKS, H. A., A. W. CROMPTON, R. Z. GERMAN, AND K. M. HIIEMAE. 1985. Mechanisms of intraoral transport in a herbivore, the hyrax (*Procavia syriacus*). Archives of Oral Biology, **30:** 539–544.

GERMAN, R. Z., AND H. A. FRANKS. 1991. Timing in the movements of the jaws, tongue and hyoid during feeding in the hyrax (*Procavia syriacus*). Journal of Experimental Zoology, **257:** 34–42.

GERMAN, R. Z, S. SAXE, A. W. CROMPTON, AND K. M. HIIEMAE. 1989. Mechanism of food movement through the anterior oral cavity in anthropoid primates. American Journal of Physical Anthropology, **80:** 765–775.

GILBERTSON, T. 1998. Peripheral mechanisms of taste, pp. 1–28. *In* R. W. A. Linden (ed.), The Scientific Basis of Eating. Frontiers of Oral Biology. Vol. 9. Basel, Switzerland: Karger. vii + 244 pp.

HIIEMAE, K. M. 2000. Feeding in Mammals, pp. 399–436. *In* K. Schwenk (ed.), Feeding: Form, Function, Phylogeny in Tetrapod Vertebrates. San Diego, Califonia: Academic Press. xv + 537 pp.

HIIEMAE, K., AND A. CROMPTON. 1985. Mastication, food transport and swallowing, pp. 262–290. *In* M. Hildebrand, D. M. Bramble, K. Liem, and D. B. Wake (eds.), Functional Vertebrate Morphology. Cambridge, Massachusetts: Belknap Press of Harvard University Press. 430 pp.

HIIEMAE, K. M., M. R. HEATH, G. HEATH, E. KAZOGLU, J. MURRAY, D. SAPPER, AND K. HAMBLETT. 1996. Natural bites, food consistency and feeding behaviour in man. Archives of Oral Biology, **41:** 175–189.

HIIEMAE, K. M., AND J. B. PALMER. 1999. Food transport and bolus formation during complete feeding sequences on foods of different initial consistency. Dysphagia, **14:** 31–42.

HIIEMAE, K. M., A. REESE, AND S. HAYENGA. 1995. Patterns of tongue and jaw movement: a cinefluorographic study of feeding in the macaque. Archives of Oral Biology, **40:** 229–246.

HIIEMAE, K. M., A. J. THEXTON, AND A. W. CROMPTON. 1978. Intra-oral food transport: a fundamental mechanism of feeding?, pp. 181–208. *In* D. S. Carlson and J. A. McNamara, Jr. (eds.), Muscle Adaptation in the Craniofacial Region. Ann Arbor, Michigan: Center for Human Growth and Development, The University of Michigan. x + 252 pp.

JEAN, A. 1990. Brainstem control of swallowing: localization and organization of the central pattern generator, pp. 294–321. *In* A. Taylor (ed.), Neurophysiology of the Jaws and Teeth. London: Macmillan. xii + 397 pp.

KIER, W., AND K. K. SMITH. 1985. Tongues, tentacles and trunks: the biomechanics of movement in muscular hydrostats. Zoological Journal of the Linnean Society, **83:** 307–324.

LIVINGSTONE, R. 1956. Some observations on the natural history of the tongue. Annals of the Royal College of Surgeons of England, **19:** 185–200.

ORON, U., AND A. W. CROMPTON. 1985. A cineradiographic and electromyographic study of mastication in *Tenrec ecaudatus*. Journal of Morphology, **185:** 155–182.

PALMER, J. B., K. M. HIIEMAE, AND J. LUI. 1997. Tongue–jaw linkages in feeding: a preliminary videofluorographic study. Archives of Oral Biology, **42:** 429–441.

PALMER, J. B., N. RUDIN, G. LARA, AND A. W. CROMPTON. 1992. Coordination of mastication and swallowing. Dysphagia, **7:** 187–200.

SCHWENK, K. 2001. Intrinsic versus extrinsic lingual muscles: a false dichotomy? Bulletin of the Museum of Comparative Zoology, **156:** 219–235.

SMITH, K. K. 1994. Are neuromotor systems conserved in evolution? Brain, Behavior and Evolution, **43:** 293–305.

SMITH, K. K., AND W. KIER. 1989. Trunks, tongues and tentacles: moving with skeletons of muscle. American Scientist, **77:** 29–35.

THEXTON, A. J., AND A. W. CROMPTON. 1989. Effect of sensory input from the tongue on jaw movement in normal feeding in the opossum. Journal of Experimental Zoology, **250:** 233–243.

———. 1998. The control of swallowing, pp. 168–222. *In* R. W. A. Linden (ed.), The Scientific Basis of Eating. Frontiers of Oral Biology. Vol. 9. Basel, Switzerland: Karger. vii + 244 pp.

THEXTON, A. J., AND K. M. HIIEMAE. 1997. The effect of food consistency on jaw movement in the macaque: a cineradiographic study. Journal of Dental Research, **76:** 552–560.

THEXTON, A. J., K. M. HIIEMAE, AND A. W. CROMPTON. 1980. Food consistency and particle size as regulators of masticatory behavior in the cat. Journal of Neurophysiology, **44:** 456–474.

THEXTON, A. J., AND J. D. MCGARRICK. 1988. Tongue movement of the cat during lapping. Archives of Oral Biology, **33:** 331–339.

———. 1989. Tongue movement in the cat during the intake of solid food. Archives of Oral Biology, **34:** 239–248.

THEXTON, A. J, J. D. MCGARRICK, K. M. HIIEMAE, AND A. W. CROMPTON. 1982. Hyomandibular relationships during feeding in the cat. Archives of Oral Biology, **27:** 793–801.

TURNBULL, W. 1970. Mammalian masticatory apparatus. Fieldiana: Geology, **18:** 153–356.

APPENDIX

The following lists those mammals for which data on tongue and hyoid movement in feeding are available, with the sources used in preparing this review. The order represents the approximate chronology of these studies.

Opossum (*Didelphis virginiana*)

CFG (lateral projection), EMG, tongue and hyoid markers.

Sources. Crompton, 1989; Crompton et al., 1977; Hiiemae and Crompton, 1985; Thexton and Crompton, 1989, 1998.

Cat (*Felis domesticus*)

CFG (lateral projection), tongue and hyoid markers.

Sources. Hiiemae et al., 1978; Thexton and McGarrick, 1988, 1989; Thexton et al., 1980, 1982.

Fruit bat (*Pteropus giganteus*)

CFG (lateral and dorsoventral projection), tongue (10) and hyoid markers.

Source. de Gueldre and De Vree, 1984.

Macaque (*Macaca fascicularis*)

CFG (lateral projection), EMG, tongue and hyoid markers.

Sources. Franks et al., 1984; German et al., 1989; Hiiemae and Crompton, 1985; Hiiemae et al., 1995.

Tenrec (*Tenrec ecaudatus*)

CFG (lateral and dorsoventral projections), EMG, tongue and hyoid markers.

Source. Oron and Crompton, 1985.

Hyrax (*Procavia syriacus*)

CFG (lateral projection), tongue and hyoid markers.

Sources. Franks et al., 1985; German and Franks, 1991.

Rabbit (*Oryctolagus cuniculus*)

VFG (lateral and dorsoventral projection), hyoid marker, tongue and hyoid markers.

Sources. Anapol, 1988; Cortopassi and Muhl, 1990.

Man (*Homo sapiens sapiens*)

VFG (lateral and posteroanterior projection), EMG, tongue and hyoid markers.

Sources. Hiiemae and Palmer, 1999; Palmer et al., 1992, 1997.

EXTRINSIC VERSUS INTRINSIC LINGUAL MUSCLES: A FALSE DICHOTOMY?

KURT SCHWENK[1]

ABSTRACT. The muscular tongue of amniote vertebrates is traditionally described as a composite of two muscle types: extrinsic muscles originate outside the tongue and insert within it; intrinsic muscles arise and insert completely within the tongue. Whole-tongue movements are attributed to the former, lingual shape change to the latter. This dichotomous view of tongue structure and function has endured since the mid-19th century, despite persistent indications of its inadequacy. A histologic analysis of the musculi genioglossus and verticalis in mammals and the musculus (m.) hyoglossus in lepidosaurian reptiles finds that the "extrinsic" m. genioglossus contributes extensively to the "intrinsic" m. verticalis; the verticalis "muscle" is composed of fibers from at least three nominally separate muscles, both extrinsic and intrinsic (genioglossus, longitudinalis inferior, intrinsic verticalis fibers); and the "extrinsic" m. hyoglossus in lepidosaurs comprises both extrinsic and intrinsic parts, which may be histochemically differentiated. Current models of the tongue as a muscular hydrostat suggest that it functions as an integrated functional unit and that the traditional atomistic, dichotomous view is inaccurate and misleading. The notion of individuated "muscles" is inapplicable within the tongue and should be replaced by reference to "fiber systems."

> Apart from simplifying matters to the student of anatomy, the division of the lingual muscles into extrinsic and intrinsic groups is of no proper scientific significance (Abd-El-Malek, 1938: 26)

INTRODUCTION

The evolution of tetrapod vertebrates from piscine ancestors was attended by the appearance of a mobile, muscular tongue. The tongue, in effect, assumed the ancestral role of water in the dynamics of feeding and is used by tetrapods today to capture, support, manipulate, transport, and swallow prey in the terrestrial environment. These functions depend on the capacity of the tongue, and the associated hyobranchial apparatus, to generate complex movements in three dimensions, within the mouth and without. The form and internal anatomy of the tongue vary widely among tetrapods, as does the nature and extent of its movements (e.g., Livingston, 1956; Schwenk, 2000a). Mammals, lepidosaurian reptiles and terrestrial turtles possess the most muscular and architecturally intricate tongues among tetrapods, and these evince the greatest complexity of motion. Contradictions about the muscular constituents of these amniote tongues and their role in generating tongue movement is the subject of this paper.

The tongue of most nonarchosaurian amniotes is a large, muscular mass, often with little or no internal skeletal support. The corpus of the tongue comprises orthogonal arrays of interweaving muscle fibers, the pattern of which is taxonomically variable. Despite extensive comingling of muscle fibers within the tongue, early anatomists treated the tongue like any other part of the musculoskeletal system and partitioned it into nominally discrete muscles. Initially, virtually all tongue muscles were thought to arise from elements of the skeleton outside the tongue (e.g., the mandible, hyobranchium, and styloid process of the skull in mammals) and the muscles were divided on the basis of their separate origins (Barnwell, 1976). However, by the early 19th century it was recognized that some muscle fibers arise and insert entire-

[1] Department of Ecology and Evolutionary Biology, University of Connecticut, Storrs, Connecticut 06269-3043.

ly within the tongue and several "intrinsic muscles" were thus recognized in addition to the better known "extrinsic muscles" (Barnwell, 1976). Intrinsic muscles were identified on the basis of their direction (transverse, longitudinal, or circular) and position (superior/dorsal or inferior/ventral) within the tongue.

The distinction between extrinsic and intrinsic muscles was formalized by Salter (1852; in Barnwell, 1976) who, in addition, attributed different kinds of tongue movement to the two muscle types: extrinsic muscles were said to move the whole tongue by virtue of their external skeletal attachments, whereas intrinsic muscles were thought to "move the tongue on itself." Thus, by the mid-19th century, two parallel dichotomies were established in the literature: an anatomical division of the tongue into extrinsic and intrinsic muscles, and a functional division relating the former to whole tongue movements and the latter to changes in tongue shape.

Remarkably, this dichotomous view of tongue form and function has endured in the literature to the present time (e.g., Sonntag, 1925; McGregor, 1938; Bennett and Hutchinson, 1946; Cooper, 1953; Livingston, 1956; Oelrich, 1956; Sondhi, 1958; Bowman, 1968; Perkell, 1969; Warwick and Williams, 1973; Miyawaki, 1974; Barnwell et al., 1978b; Langdon et al., 1978; Hellstrand, 1980, 1981; Tanner and Avery, 1982; Schwenk, 1986; Smith, 1988; Delheusy et al., 1994; Herrel et al., 1995). For example, in describing a lizard tongue, Oelrich (1956: 54) stated: "The extrinsic muscles, genioglossus and hyoglossus, control the motions of the tongue; the intrinsic muscles control its shape." Hellstrand (1980: 187) began his paper on the cat tongue by pointing out that it "is provided with muscles termed *extrinsic* or *intrinsic* according to whether they run partly or totally within the tongue. Functionally, the extrinsic muscles are usually classified as protruders or retractors and the intrinsic as shaping or modeling agents." In *Gray's Anatomy* (Warwick and Williams, 1973: 1239, 1240) it is noted that within the human tongue, "there are two sets of muscles, extrinsic and intrinsic; the former have attachments outside the tongue, the latter are contained within it." Each extrinsic muscle is said to move the tongue in some way, that is, retract, depress, or elevate it. In contrast, it is held that the intrinsic muscles, in toto, are "mainly concerned in altering the shape of the tongue."

Despite the persistence of the dichotomous descriptive convention, those who have investigated tongue anatomy in some detail have often questioned the accuracy or appropriateness of the dichotomy—anatomically, functionally, or in both ways (e.g., Bennett, 1935; Abd-El-Malek, 1938; Bennett and Hutchinson, 1946; Sondhi, 1958; Barnwell et al., 1978a; Langdon et al., 1978; Cave, 1980; Lowe, 1980; Kier and Smith, 1985; Schwenk, 1986; Smith, 1986, 1992; Smith and Kier, 1989; Sokoloff and Deacon, 1992; Napadow et al., 1999). Some authors have expressed doubt, even while beginning with the conventional view. Oelrich (1956: 55), for example, noted that extrinsic and intrinsic fibers interlace within the tongue and admitted that the intrinsic muscles "do not maintain their integrity throughout, but at some levels are intermingled to such an extent that their identity is obscured." Schwenk (1986: 137) pointed out that in tuatara (*Sphenodon*), the "distinction is not always demonstrable in every part of the tongue because both intrinsic and extrinsic fibers interlace complexly." Barnwell et al. (1978a: 8) concluded that the nominally intrinsic musculus (m.) longitudinalis superior of the human tongue "is comprised of both intrinsic and extrinsic fiber groups." It is telling that many writers seem compelled to state the conventional view, despite their evident dissatisfaction. This ambivalence is clear, for example, in a textbook account that virtually contradicts itself within the space of two sentences: "Generally, 'movements' other than those that basically alter the shape of

the tongue are the result of contractions of the extrinsic muscles, though one group seldom functions alone. The overlapping, intermingling, and decussating nature of the intrinsic and extrinsic muscle groups permit the fine coordinated effort so necessary in speech" (Hiatt and Gartner, 1982: 239–240).

Others have rejected the traditional dichotomy altogether. For example, in his study of cat tongue anatomy and function, Abd-El-Malek (1938) concluded with the remark quoted at the outset of this paper, suggesting that the dichotomy is no more than a convenience, without scientific merit. He particularly rejected the functional dichotomy, suggesting that "most, if not all, of the intrinsic muscles are involved in every movement of the tongue. Indeed, in many movements both intrinsic and extrinsic muscles so called, are working together." Other authors take the radical view that all putative intrinsic muscle fibers are nothing more than extensions of extrinsic muscles (Lesbre [1922] in Cave [1980] for the horse, *Equus*; Cave [1980] for the rhinoceroses, *Rhinoceros*, *Ceratotherium*, and *Diceros*; and Sondhi [1958] for the monitor lizard, *Varanus*). According to Cave (1980: 128): "The so-called intrinsic tongue muscles are not therefore, morphological entities but merely continuations of the extrinsic muscles." Sondhi (1958: 175) concluded: "While there can be no doubt that the 'intrinsic muscles' can be distinguished from each other in certain regions of the tongue, the fact that they arise directly as a result of the change in course of certain bundles of the [extrinsic] hyoglossus fibres indicates that they do not deserve the status of independent muscles." It is worth noting that the studies of Lesbre and Cave were based on gross dissection without the benefit of histologic sections, and Sondhi's sections were of poor quality.

The purpose of this paper is to explore the anatomical relationship between "extrinsic" and "intrinsic" lingual muscles in representative mammals and lepidosaurian reptiles. The mammalian genioglossus and verticalis muscles, and lepidosaurian hyoglossus muscle are investigated in detail and used as exemplars. Results of the morphologic investigation are considered in light of current models of tongue function in order to assess the structural and functional validity of the dichotomous view. Based on this analysis, a synthetic view of tongue form and function is proposed.

MATERIALS AND METHODS

Reference material included complete, serial paraffin sections of tongues from two mammalian species (domestic cat, *Felis catus*, three specimens; crab-eating macaque, *Macaca fascicularis*, three specimens) and more than 100 lepidosaurian reptile species (one to three specimens each), including tuatara (*Sphenodon punctatus*; Schwenk, 1986) and representatives of every major squamate clade (Schwenk, 1988, 2000b, unpublished data). The emphasis here is on the cat (Carnivora, Felidae) and generalized lizards (Squamata, Iguanidae) that putatively retain the plesiomorphic condition (Schwenk, 1986, 1988, 2000b). Histologic results were compared to literature accounts of tongue anatomy.

Sections were prepared using standard paraffin techniques (Presnell and Schreibman, 1997). Whole-tongue specimens were sectioned whenever possible to facilitate fiber tracing. Some previous studies have suffered from the myopic view offered by partial or fragmented specimens.

Both transverse and sagittal sections (6–10 μm) were prepared for most species, but only transverse sections were available for *Sphenodon* and some squamates (note that transverse tongue sections correspond to 'coronal' sections in the parlance of human anatomy). Sections were stained with hematoxylin and picro-ponceau or hematoxylin and eosin (Presnell and Schreibman, 1997).

In addition to paraffin sections, frozen tissue sections were available for several squamate species. These were stained for

myosin adenosine triphosphatase and succinic dehydrogenase using standard techniques, as part of an ongoing histochemical study of tongue muscle fiber types (Schwenk and Anapol, in preparation). These data are preliminary and referred to here only in passing.

RESULTS

Genioglossus and Verticalis Muscles in the Cat

Preliminary observations indicate that the findings reported here for the cat are equally valid for the macaque. Based on consideration of the literature, the findings are likely to apply as well to many mammals with generalized tongues, including other carnivorans, opossums, and humans. However, with the exception of humans, detailed information is lacking for these and other species, including many with highly divergent tongue forms (e.g., monotremes: Doran and Baggett, 1970; Doran, 1973; and nectar-feeding bats: Greenbaum and Phillips, 1974; T. Griffiths, 1978). Therefore, the results of this study cannot necessarily be extrapolated to mammals as a whole.

When viewed in transverse section, most mammalian tongues are divisible into cortical and medullary regions. The cortex is distinguished by the presence of longitudinal fibers, whereas the core of the tongue is filled with transverse and vertical fibers. "Transverse" and "vertical" are convenient descriptors for these more-or-less perpendicular sets of fibers, but fibers of both groups are often quite oblique. Throughout most of the medullary zone, vertical and transverse fibers are organized into thin sheets of muscle that run across the width of the tongue, alternating one after the other along the tongue's length (Fig. 1). Tracing individual verticalis sheets through serial sections confirmed that in most of the tongue each sheet runs across the full width of the medullary core. However, in the anteriormost part of the tongue, a verticalis sheet may be interrupted across its width by invading bands of transversus. However, interpreting sections here is difficult because the sheets apparently do not run in a plane, becoming curved or cup-shaped, instead. Finally, some vertical fibers cross anteroposteriorly between adjacent sheets to form anastomoses (especially evident in the free, anterior part of the tongue; e.g., Fig. 3). Despite these complications, throughout most of the tongue the extreme regularity of the alternating vertical and transverse sheets is its most striking feature. The sheets of vertical and transverse fibers constitute the nominal intrinsic muscles, m. verticalis and m. transversus, respectively. In the cat they are separated into left and right moieties by a complete median septum.

The m. transversus fibers originate from the median septum and run radially across the width of the tongue to insert into the lamina propria of the lingual tunic dorsally, laterally, and ventrolaterally. Some m. verticalis fibers originate from the lamina propria of the tongue's ventral surface and run dorsomedially to the lamina propria of the dorsal surface (but see below). In the lateral part of the tongue, dorsolaterally running transversus fibers cross dorsomedially running verticalis fibers in an X-like pattern (i.e., perpendicular, but approximately 45° to the vertical). Toward the midline verticalis fibers become more nearly vertical (see below).

The m. genioglossus is one of the major extrinsic muscles of the tongue and is assumed to be its principal protractor and protruder. In the cat, the m. genioglossus originates medially from two heads on the mandible near the symphysis. A ventral head gives rise to fibers that run posteriorly, inserting onto the anteroventral surface of the basihyal. Fibers from a larger dorsal head run posterodorsally in a fanlike array, penetrating the tongue midventrally along the posterior two thirds of its length. The most anterior of these fibers curve sharply dorsad as they enter the tongue's medullary core and run vertically to the

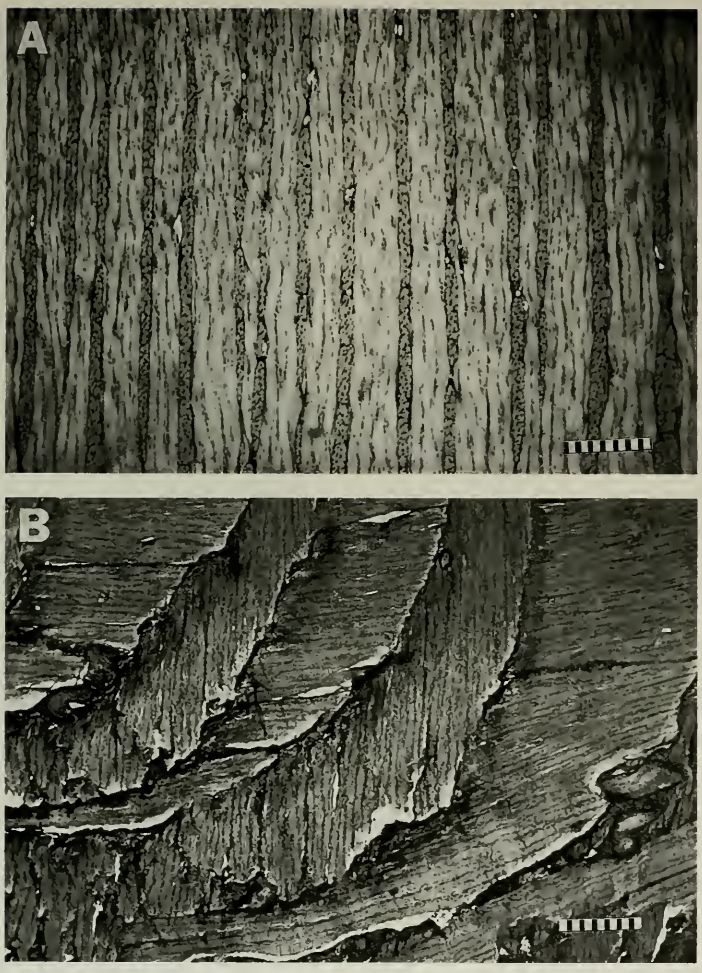

Figure 1. Alternating sheets of vertical (musculus [m.] verticalis) and transverse (m. transversus) muscle fibers in the medullary core of the cat midtongue. Note extreme regularity of alternating sheets. (A) Parasagittal section; verticalis sheets are thicker than transversus sheets in this region. Anterior is to the left. Scale bar = 0.2 mm. (B) Transverse section near the midline, in the ventromedial portion of the tongue's right half; medial septum to the right. Section is slightly oblique relative to plane of transversus and verticalis sheets so that it passes through several adjacent layers. As for (A), note extreme regularity of alternating pattern. Darker-staining tissue at the margins of each sheet is collagenous connective tissue of the thin fascial plane separating each sheet. Note that the ventralmost transverse fibers run ventrolaterally and the dorsalmost fibers run laterally. Dorsal to these, out of the photographic frame, the transverse fibers run dorsolaterally, that is, the transverse fibers radiate laterally from their midline origin on the median septum. Scale bar = 0.2 mm.

lamina propria of the dorsal surface, but posteriorly the fibers become progressively more longitudinal, curving gently dorsad at their distal ends to meet the posterior surface of the tongue as it slopes downward to the root of the tongue. In (fetal) humans, the anteriormost fibers form a third bundle that turns sharply anterior as it enters the tongue, running to the tip (Langdon et al., 1978), but in the cat (Abd-El-Malek, 1938; this study) and several other mammals (Doran and Baggett, 1972), no comparable bundle is found and the most anterior genioglossus fibers run more or less vertically. The unattached, anterior part of the tongue is therefore devoid of genioglossus fibers.

In reconstructions of the genioglossus,

its fibers are often shown in sagittal view to end at the base of the tongue before penetrating the medullary core, or to run obliquely across the alternating sheets of vertical and transverse fibers toward the dorsal and posterior surfaces of the tongue (e.g., Kallius, 1910; Abd-El-Malek, 1938; Warwick and Williams, 1973; Crouch, 1978; Walker and Homberger, 1992). Independence of the genioglossus from the medullary, intrinsic fiber system is implied in these and other descriptions. In actuality, as genioglossus fibers turn dorsally into the tongue, they become confluent with the serially arranged sheets of verticalis fibers (Fig. 2A). As such, for most of the tongue's length, the medial portion of the verticalis muscle comprises genioglossus fibers. In other words, a large portion of the "intrinsic" verticalis muscle is composed of "extrinsic" fibers.

Although the previous observations seem to support the radical position of Cave (1980) and others suggesting that intrinsic fibers are merely extensions of extrinsic muscles, this view is vitiated by a full consideration of m. verticalis anatomy. Although the medial portion of each verticalis sheet comprises extrinsic genioglossus fibers, its lateral portion derives from purely intrinsic fibers that originate on the lamina propria of the ventral surface (Fig. 2B). Although medial genioglossus fibers are relatively vertical and lateral intrinsic fibers are oblique (running dorsomedially; see above), fibers of both sorts blend insensibly across the breadth of a single verticalis sheet to form a continuous structural unit. These units are repeated serially along the length of the tongue, alternating with sheets of m. transversus. Extrinsic and intrinsic components of the verticalis are also clearly evident in the opossum, *Monodelphis* (Smith, 1994, fig 2a).

Given the absence of genioglossus fibers in the anterior, free part of the tongue, one might expect the sheets of verticalis in this region to be uniformly intrinsic. Indeed, this is true laterally, as elsewhere in the tongue (Fig. 3A). However, in place of ge-

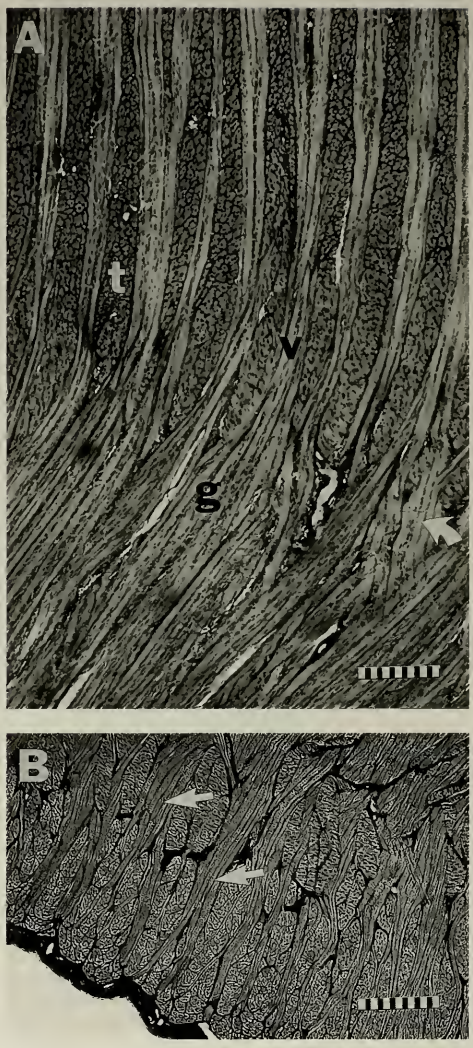

Figure 2. The relationship between musculus (m.) verticalis and m. genioglossus fibers in the cat tongue. (A) Parasagittal section near the midline, anterior to the left. Ventrally, the genioglossus muscle (g) penetrates the tongue's medullary core where it curves dorsad and is separated into separate layers by intervening sheets of transversus fibers (t). Thus, in this medial portion of the tongue the vertical fibers of the medulla, nominally m. verticalis (v), are actually contributed by the extrinsic genioglossus. However, note that some verticalis fibers continue a more vertical descent through the genioglossus to an intrinsic point of origin (curved arrow). Scale bar = 0.2 mm. (B) Transverse section through the ventrolateral part of the tongue's right side showing longitudinal fibers of lingual cortex and the origin of intrinsic verticalis fibers from the ventrolateral lamina propria (arrows). These lateral, purely intrinsic fibers, form an uninterrupted continuum within a single verticalis sheet with the medial genioglossus fibers. Scale bar = 0.2 mm.

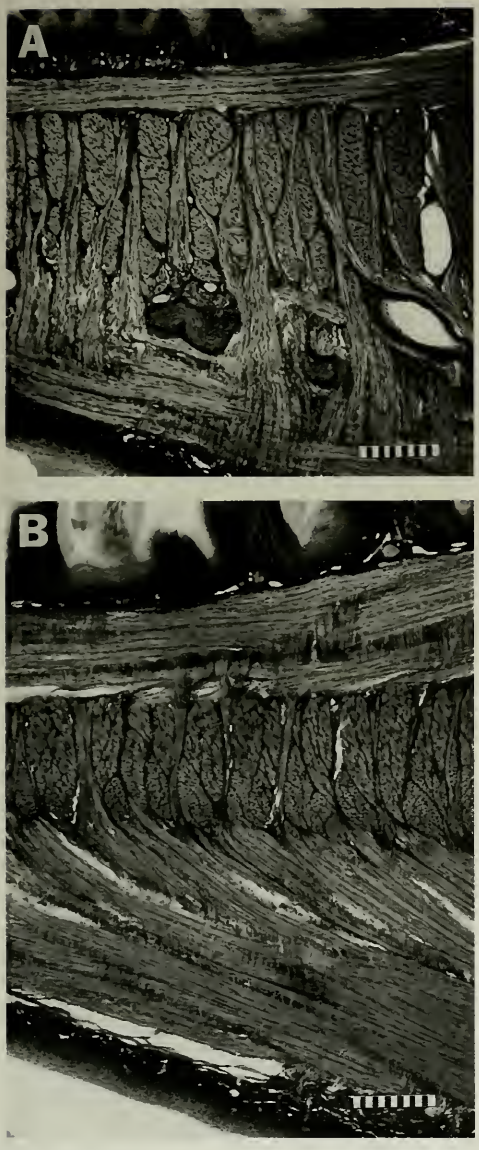

Figure 3. The free, anterior portion of the cat tongue in sagittal section. The tongue tip is toward the left. Note that longitudinal fibers run beneath the tongue's dorsal and ventral surfaces forming the cortex, whereas the medulla is filled by the alternating sheets of vertical and transverse fibers. These sheets are not so regularly disposed as they are posteriorly (Fig. 1) and anastomoses between verticalis sheets are frequent. (A) Section through lateral part of the tongue. Note that vertical fibers penetrate the cortex to arise and insert from dorsal and ventral laminae propria, that is, they are intrinsic fibers. The dark-staining structure just above the ventral longitudinal fibers is a nerve, kinked to permit extension during hydrostatic tongue elongation. The white areas are vascular spaces slightly distended by perfusion of the tongue. Scale bar = 0.2 mm. (B) Section more medial to (A), near to midline. In contrast to

nioglossus fibers, the medial portion of each verticalis sheet is here occupied by ventral longitudinal fibers that turn dorsad into the verticalis (Fig. 3B). The ultimate origin of all ventral longitudinal fibers has not been traced with certainty, but most clearly belong to the intrinsic m. longitudinalis inferior. Among the ventral longitudinal fibers of the lingual cortex, longitudinalis inferior fibers are generally the most median (e.g., Barnwell et al., 1978b). Nonetheless, longitudinal fibers of the cortex are notoriously difficult to segregate according to source and it remains possible that some of the fibers contributing to the verticalis in the anterior part of the tongue derive from the extrinsic styloglossus muscle. Sections show that styloglossus fibers course anteroventrally along the sides of the tongue, joining the ventral longitudinal system anteriorly, but it is not certain that these fibers extend far enough anteriorly and medially to contribute to the verticalis in the free part of the tongue. Although (extrinsic) m. hyoglossus fibers are said to run within the ventral longitudinal system of some mammals (e.g., humans, Barnwell et al., 1978b), my sections (and those of Abd-El-Malek, 1938) indicate that in the cat, all hyoglossus fibers run anterodorsally into the dorsal longitudinal system.

In conclusion, the extrinsic genioglossus muscle makes a substantial contribution to the putatively intrinsic verticalis muscle. Anteriorly, the verticalis also includes fibers of a second intrinsic muscle, the longitudinalis inferior, and possibly extrinsic fibers of the styloglossus. The verticalis "muscle" thus includes fibers from three, or possibly, four different sources: intrinsic vertical fibers; intrinsic longitudinal fibers; extrinsic genioglossus fibers; and possibly,

←

(A), vertical fibers are here contributed by the extensively developed ventral longitudinal system. These fibers represent musculus longitudinalis inferior, although it is possible that extrinsic styloglossus fibers also contribute. Compare to Figure 2A. Scale bar = 0.2 mm.

Figure 4. Transverse section through the midtongue of a lizard (*Holbrookia texana,* Iguanidae). The circular structure in the center is the lingual (entoglossal) process of the hyobranchium, which is surrounded by fibers of the midline intrinsic muscle, musculus (m.) verticalis (V). Dorsal to the verticalis is the m. transversalis (T) and on either side are the paired hyoglossus bundles (H); the lateral part of each bundle is cut off in the figure. Note that within each hyoglossus bundle the fibers are separated into two parts: a dense, more vertically oriented dorsolateral portion (1) and a more loosely organized, more longitudinally oriented ventromedial portion (2). Scale bar = 0.2 mm.

extrinsic styloglossus fibers. An individual sheet of verticalis occupies a transverse plane across the width of the tongue comprising a continuum of vertically oriented muscle fibers, yet within a given sheet, a large proportion of the fibers are contributed by a nominally separate muscle, usually from outside the tongue. Furthermore, the muscles making this contribution vary along the length of the tongue. Thus, the nominal m. verticalis satisfies neither the definition of "intrinsic," nor even the usual notion of a "muscle." Nonetheless, the serial coherence of the verticalis is maintained throughout the medullary core, despite the disparate sources of its constituent fibers.

The Hyoglossus Muscle in Lepidosaurian Reptiles

Lepidosaurs include the tuatara of New Zealand (*Sphenodon*) and the squamates, comprising lizards, snakes, and amphisbaenians. The lepidosaurian tongue, with few exceptions, is a highly mobile organ that rivals that of mammals in its internal complexity. However, unlike mammals, the principal longitudinal muscles of the tongue lie within its core and not its periphery. These are the hyoglossus muscles, evident in transverse section as two large, cylindrical or subcylindrical bundles (Fig. 4). In a few taxa (notably gekkotans) they subdivide anteriorly into multiple bundles, but in the vast majority of species they remain paired for the length of the tongue (Schwenk, 1988, 2000b).

As in mammals, the hyoglossus is one of the major extrinsic muscles of the lepidosaurian tongue. It is traditionally described as originating on the first ceratobranchial of the hyobranchial apparatus and inserting within the tongue near its tip (e.g., Gnanamuthu, 1937; Oelrich, 1956; Delheusy et al., 1994; Herrel et al., 1997, 1999) and is regarded as the principal retractor of the tongue.

Some studies have indicated that hyoglossus anatomy is more complex than suggested by conventional descriptions. In his figures of transversely sectioned *Sphenodon* embryos, Edgeworth (1935) identified a separate ventromedial bundle within the hyoglossal mass, which he called the

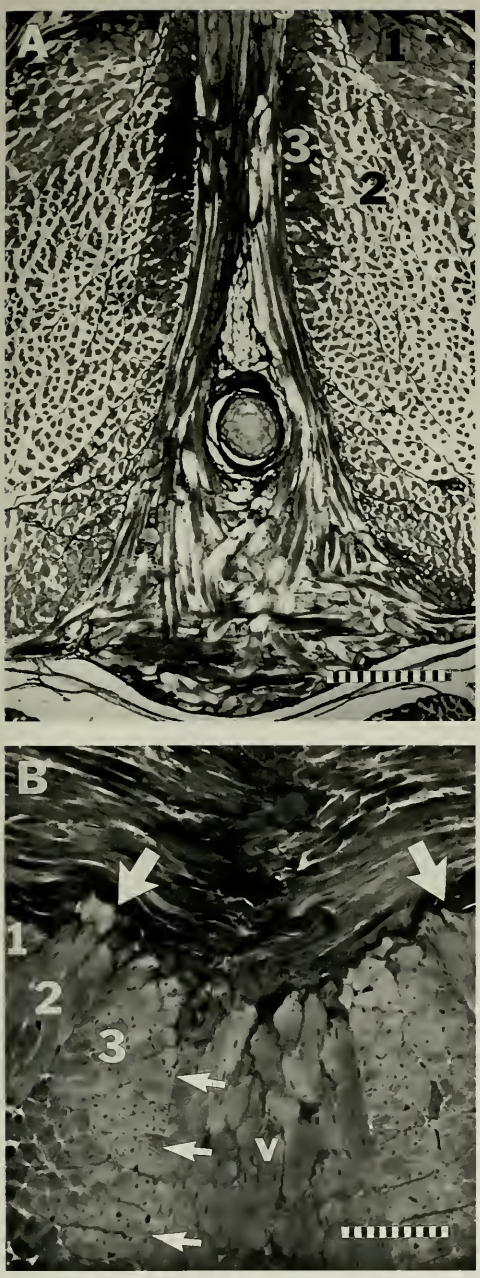

Figure 5. Transverse section through the midtongue of two iguanid lizards. (A) *Oplurus sebae,* showing the lingual process and musculus (m.) verticalis medially, as in Figure 4. On either side of the verticalis are the hyoglossus bundles (truncated laterally by the photograph) showing subdivision of the muscle into three portions (1, 2, 3) indicated by differences in fiber density and orientation. Dorsally, parts 1 and 2 appear to be separated by a thin fascial plane, but ventrally the three zones blend insensibly. Scale bar = 0.4 mm. (B) *Stenocercus*

longitudinalis linguae. Schwenk (1986) did not report such a division in his study of an adult specimen, but the sections reveal different fiber orientations in the ventromedial and dorsolateral portions of the hyoglossus bundle, supporting the notion of a subdivided hyoglossus in *Sphenodon.* Smith's (1988) transverse sections of agamid lizard tongues show distinct partitioning of the hyoglossus into two or three divisions. Smith (1986) suggested that each hyoglossus bundle within the highly modified tongues of monitor lizards (*Varanus*) comprises a series of shorter fibers running obliquely within the longitudinal bundle, possibly spiraling, and inserting into the surrounding epimysium along the length of the bundle. She disagreed with Sondhi's (1958) suggestion that hyoglossus fibers in this genus turn within the tongue to form the circular fibers surrounding the hyoglossus bundles. Indeed, she showed that the circular muscles were, themselves, composed of shorter, oblique fibers arrayed helically around each hyoglossus bundle.

A cursory survey of tongue sections from a variety of species indicates that internal hyoglossus partitioning is commonplace among lepidosaurs. Transverse sections of iguanian lizards, in particular, often reveal two (Fig. 4) or even three (Figs. 5A, B) different moieties, as indicated by fiber orientation and, sometimes, fascial planes. The number and distinctness of the hyoglossus divisions vary among species and, notably, along the length of the tongue. In some sections it is evident that one division contains vertically oriented fi-

←

sp., showing three-part subdivision of the hyoglossus, as in (A). The dark-staining band separating transverse fibers from the verticalis (v) and hyoglossus (1, 2, 3) is the collagenous connective tissue of the dorsal transverse septum. The division between verticalis and hyoglossus fibers is indicated on one side by three small arrows. Fibers of the middle hyoglossus subdivision (2) in this part of the tongue are vertically oriented and originate on the dorsal transverse septum (large arrows). These fibers represent an intrinsic component of the putatively extrinsic m. hyoglossus in lepidosaurs. Scale bar = 0.1 mm.

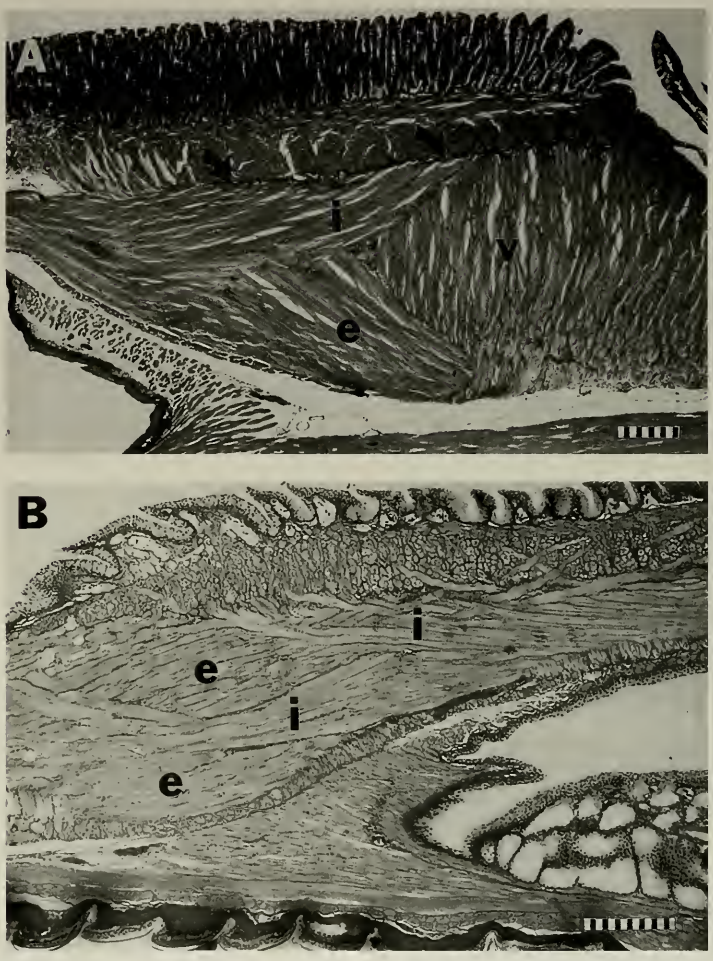

Figure 6. Parasagittal sections of the tongues in two lizards. (A) *Sceloporus* sp. (Iguanidae). Anterior to the left. The dorsal surface of the tongue is covered by long, filamentous papillae. Beneath the papillary surface is a layer of intrinsic longitudinal and transverse fibers. Directly beneath the latter is the dark-staining connective tissue band of the dorsal transverse septum (arrows). The plane of section passes through the verticalis (v) posteriorly and the hyoglossus (i and e) anteriorly. Note that the longitudinal hyoglossus bundle occupies the depth of the tongue from the transverse septum dorsally to the base of the tongue ventrally (compare Figs. 4 and 5). The extrinsic hyoglossus is shown here to consist of an intrinsic component (i), originating on the dorsal transverse septum and running anteroventrally toward the tongue tip, and an extrinsic component (e), running anterodorsally from the hyobranchium (the posterior extent of this muscle is not evident in this section). Scale bar = 0.2 mm. (B) *Gonatodes antillensis* (Gekkonidae). Anterior to the right. In gekkotans and other scleroglossan squamates, the dorsal transverse septum is weakly developed or absent. Nonetheless, the hyoglossus bundle comprises fibers with an intrinsic origin (i) and an extrinsic origin (e), as in (A). Scale bar = 0.2 mm.

bers taking origin from the connective tissue plane of the dorsal transverse septum (Fig. 5B). Sagittal sections reveal that these fibers form a substantial bundle running anteroventrally from the dorsal transverse septum to the tongue tip, joining anterodorsally directed fibers arriving from the hyobranchium (Fig. 6). In transverse section these separate groups of fibers are evident as the aforementioned subdivisions within the hyoglossus bundle. In other words, the hyoglossus muscle in most lepidosaurs minimally includes two distinct components: an intrinsic part, origi-

nating within the tongue from the dorsal transverse septum, and an extrinsic component, originating from the hyobranchium.

This brief characterization does not capture the full complexity of the hyoglossus muscle. Changes in cross-sectional shape of individual fibers along the length of the tongue suggest some degree of spiraling within the bundle so that extrinsic and intrinsic fibers are interwoven. As such, the number, form, and distinctness of the hyoglossus divisions vary anteroposteriorly. However, no matter how great its internal complexity, conservatively two different sources of fibers contribute to the hyoglossus muscle, including one that is fully intrinsic.

Analysis of preliminary data indicates that the intrinsic component of the hyoglossus is histochemically distinct in iguanids (*Sceloporus graciosus* and *Phrynosoma platyrhinos*) and a gecko (unidentified species), but not in a teiid (*Ameiva undulatus*). In *Varanus niloticus,* the hyoglossus is neither subdivided nor does it show histochemically distinct compartments (Schwenk and Anapol, in preparation). This is consistent with Smith's (1986) interpretation of hyoglossus anatomy in *Varanus.* The tongues of *Ameiva* and *Varanus* are both specialized for rapid lengthening of the tongue for chemosensory tongue-flicking (Smith, 1984, 1986; Schwenk, 2000b), whereas iguanids and gekkotans exhibit more variable and complex lingual shape changes associated with feeding and other behaviors. It is tempting to relate the different histochemical profiles to these functional differences, but this is highly speculative at this point.

In summary, the putatively extrinsic hyoglossus muscle includes both an extrinsic and an intrinsic component in many, if not most, lepidosaurian reptiles. The intrinsic component originates from the dorsal, transverse septum in the posterior and midtongue and runs anteroventrally to the tongue tip. The extrinsic component arises from the first ceratobranchial of the hyobranchium and runs anterodorsally to the tongue tip. It is likely that these fiber groups spiral and are complexly interwoven, changing orientation along the length of the tongue. The intrinsic fiber component is histochemically distinct in basal lizards with functionally generalized tongues.

DISCUSSION

The Anatomical Dichotomy

The results of this study clearly indicate the inadequacy of segregating tongue muscles into "extrinsic" and "intrinsic" types. Indeed, the traditional notion of what constitutes a "muscle," based as it is on more typical components of the musculoskeletal system, may be inapplicable within the tongue. Only three muscles were considered here in any detail, but comparable issues arise for nearly every nominal muscle in the amniote tongue. The genioglossus is putatively an extrinsic muscle, but it contributes substantially to the vertical fiber system of the tongue's medullary core, presumed to consist of intrinsic fibers. Conversely, the putatively intrinsic verticalis muscle is largely composed of extrinsic (genioglossus) fibers, as well as fibers from one to two other nominally separate muscles (longitudinalis inferior and styloglossus). The lepidosaurian hyoglossus is putatively an extrinsic muscle, but a large portion of its fibers arises intrinsically. Thus, the dichotomous view of tongue musculature is falsified.

The Functional Dichotomy

Tongue movement derives from one or a combination of three different mechanisms evident among tetrapods: (1) whole-tongue movement coupled to hyobranchial movement; (2) whole-tongue movement independent of hyobranchial movement; or (3) length or shape changes intrinsic to the tongue and independent of hyobranchial movement (e.g., Livingston, 1956; Schwenk, 2000a,b). In the traditional view, mechanism two is attributed to the action of the extrinsic muscles and mechanism

three to the intrinsic muscles. To exemplify the differences among mechanisms, consider tongue protrusion. The tongue can be protruded if it is "pushed" beyond the jaw margins by protraction of the hyobranchial apparatus. Alternatively, the tongue can be "pulled" out of the mouth by muscles linking it to the mandible. In this case, movement of the tongue relative to a fixed hyobranchium must be possible, as occurs, for example, in many lizards when the tongue slides along the lingual process of the basihyal (Schwenk, 2000b). Finally, the tongue can protrude beyond the jaw margins if it elongates anteriorly by changing its shape, despite being fixed to a stationary hyobranchium posteriorly. Obviously, these mechanisms might be combined to effect tongue protrusion.

The first two types of tongue movement conform to traditional models of musculoskeletal movement, but the third implies a far more complex mechanism. The nature of this mechanism and its relationship to the tongue's internal architecture were appreciated by Owen (1868: 394), who described it in reference to the giraffe and its ability to strip an acacia tree of leaves with its highly protrusible tongue:

> The muscular fibres in the free and flexible part of the tongue present an arrangement adequate to all its movements. The stylo-glossi and inferior linguales expand into a layer of longitudinal fibres . . . these longitudinal muscles inclose a mass of fibres, which run in the transverse direction. The action of the transverse, combined with that of several short vertical, fibres near the margins, and of those forming the thin circular stratum surrounding the stylo-glossi at the middle part of the tongue, serves to attenuate or diminish the transverse diameter of the tongue and increase its length; while thus rigidly extended the apex of the tongue can be curved upward or downward by the superficial longitudinal fibres . . . .

The intrinsic mechanism of tongue elongation outlined by Owen (1868) and others (e.g., M. Griffiths, 1968, 1978; Winkelmann, 1971, in T. Griffiths, 1978) was formalized by Kier and Smith (1985) in their "muscular hydrostat" model of tongue movement (also Smith and Kier, 1989). They modeled the tongue (and similar organs) as a constant-volume cylinder filled with incompressible fluid (intracellular water). They recognized that a reduction in one dimension must cause a compensatory increase in another and showed that muscular hydrostats are characterized by orthogonal arrays of muscle fibers arranged to modulate the tongue's diameter and length. In addition, superficial longitudinal fibers cause bending and helical or oblique fibers cause torsion. Differential, localized activity of these fiber systems can potentially create a vast range of complex shape changes in tongue form.

In light of the muscular hydrostat model of tongue function, it is clear that the serial, orthogonal arrangement of muscle fibers in the medullary region of the mammalian tongue serves to lengthen the tongue by decreasing its diameter, regardless of whether individual fibers originate intrinsically or extrinsically. Likewise, longitudinal fibers of the cortex participate in tongue shortening, retraction, bending, and torsion, regardless of nominal origin. In other words, within the tongue, muscle fibers behave as organized systems that do not correspond to the extrinsic–intrinsic dichotomy: within the vertical fiber system, both intrinsic and extrinsic fibers function together to reduce the vertical dimension of the tongue. Furthermore, the serial vertical system must often act in concert with the serial transverse system to reduce tongue diameter uniformly along its length. By implication, a relatively "simple" action, such as tongue elongation, involves minimally four nominal "muscles," including both "extrinsic" and "intrinsic" types.

Similarly, the lepidosaurian tongue is capable of hydrostatic shape change. Although the m. hyoglossus is assumed to be a tongue retractor, its internal complexity, as described here, suggests that it may be active during "intrinsic" shape changes as well. Schwenk (2000b) suggested that the foretongue in lizards is somewhat independent of the hind tongue, with the for-

mer more specialized for hydrostatic elongation independent of the hyobranchium and the latter more tightly coupled to the hyobranchium. If so, it is possible (but speculative) that the traditional notion of whole-tongue retraction attributed to the hyoglossus resides in its extrinsic component and the anterior, intrinsic component functions predominantly to retract the foretongue after it is hydrostatically elongated (as during tongue-flicking behavior or lapping). This interpretation implies a functional heterogeneity within the hyoglossus muscle, which is consistent with its histochemical partitioning in some species—a hypothesis that could be tested electromyographically.

The Tongue as a Functional Unit

Based on the traditions of musculoskeletal anatomy, our expectation for muscles is that they are discrete entities with an origin, an insertion, and an action. Although we accept that individual fibers might not run the full course of a muscle (e.g., Loeb et al., 1987), the muscle, as a whole, is clearly delimited by its origin and insertion, coherence, and separation from adjacent muscles. Furthermore, the clear relationship between these anatomical attributes and a muscle's action(s) reinforces our sense that muscles are discrete morphologic units whose homologous counterparts can be identified in other species. As such, muscles satisfy the requirements of a "character" in the traditional neo-Darwinian sense: they are "quasi-independent" (Lewontin, 1984) and "quasi-autonomous" (Wagner, 1999) parts of the phenotype. In other words, they are capable of evolutionary change somewhat independent of change in other characters and are developmentally autonomous units individuated from other such units.

There is no denying that several lingual "muscles" have "typical" origins outside the tongue, but once within the tongue they deviate from the traditional conception of a muscle and seem to be subject to a different set of rules. These rules are dictated by the muscular hydrostat model of tongue movement. Fibers are arrayed within the tongue to generate global or local reductions in diameter, reductions in length, lateral bending, dorsoventral bending, torsion, and a nearly infinite variety of shape changes—all by virtue of the incompressibility of intracellular fluid and the principle of compensatory deformation in a constant volume structure—regardless of the extrinsic or intrinsic origin of the fibers.

In light of muscular hydrostatic function, the atomization of the tongue into individuated muscles is insupportable. Instead, the tongue is better viewed holistically as a single functional unit (Schwenk, 2001). This does not imply that the tongue is a single evolutionary character, but rather emphasizes that the components of the tongue are more tightly integrated functionally with each other than they are with other parts of the oral apparatus. As such, proper tongue function depends on the closely coordinated action of its many parts acting in concert to achieve a given functional output. An action such as tongue elongation emerges as the instantaneous manifestation of countless vertical and transverse muscle fiber contractions, regardless of their point of origin or nominal affiliation. Indeed, the highly organized internal architecture of the tongue is literally the incarnation of this extreme functional coherence, a coherence that belies its disparate anatomical components. In a mammal, for example, it is important that sheets of vertical fibers are arranged along the length of the tongue; it is not important whether the fibers within each sheet derive extrinsically from the genioglossus, or intrinsically from the lamina propria or the longitudinalis inferior. Similarly, Barnwell et al. (1978a) noted that, despite extrinsic and intrinsic contributions, the dorsal longitudinal muscle layer functions as "a whole." Thus, rather than "muscles," within the tongue it is more accurate (and I believe preferable) to refer to fiber systems. Vertical and transverse fiber systems

contribute to reduction in tongue diameter, regardless of which "muscles" provide them with fibers.

A holistic view of tongue form and function is further supported by tongue development in mammals. From the earliest stages, orientations of all muscle fibers within the tongue are evident (Smith, 1994). In *Monodelphis,* Smith (1994: 158) observed, "adjacent cells simultaneously orient into one of the three mutually perpendicular planes, so that the three-dimensional arrangement of muscle fibers in the tongue is present at the earliest stages observed." As such, sheets of vertical and transverse fibers begin to organize within the tongue in situ without regard to the subsequent connection or insertion points of their constituent fibers. For example, a given vertical fiber, ultimately connects to the lamina propria within the tongue, whereas an adjacent cell connects extrinsically within the genioglossus. Another nearby cell orients transversely and contributes to the adjacent sheet of transverse fibers (K. K. Smith, personal communication).

I have here focused on the anatomy of the tongue and completely neglected the issue of motor control. Such a discussion is beyond the scope of this paper. However, it is worth noting that, although a muscle such as the genioglossus is morphologically continuous from its origin on the mandible to its insertion into the lamina propria of the tongue's dorsal surface, individual fibers may not run its full length. As such, some fibers might have an intrafascicular origin within the muscle mass (Loeb et al., 1987). Thus, the fiber population actually penetrating the tongue possibly has an intrafascicular origin within the genioglossus. Such an arrangement would allow segregation of the muscle into extrinsic and intrinsic motor units, thereby simplifying control. Strain mapping data from the human tongue in vivo are consistent with this hypothesis (Napadow et al., 1999), although simplifying assumptions of the analysis somewhat weaken its support. The ability of the tongue to form localized deformations and to protrude, for example, in cylindrical, spatulate and cupped conformations (personal observation) strongly implies separate motor control of both vertical and transverse fiber systems, as well as regional control of these systems along the length of the tongue. As such, functional integrity of lingual fiber systems need not imply coarseness of control. Finally, finite element analyses that model the tongue as a series of regional elements with certain contractile and viscoelastic properties, regardless of fiber source, are effective in predicting patterns of tongue shape change (Wilhelms-Tricarico, 1995; Sanguineti et al., 1997), further supporting a holistic conception of tongue functionality.

CONCLUSIONS

The results of this study refute the dichotomous view of the lingual musculature, both anatomically and functionally. The distinction of "intrinsic" from "extrinsic" muscles may serve as a convenience for description or instruction, as suggested by Abd-El-Malek (1938), but our current understanding of tongue function suggests that the convention is no longer tenable. It acts only to reinforce an outmoded, atomistic view of the tongue that deflects us from a more complete conception of this remarkable organ. The muscular hydrostat model dictates that the tongue acts as a functional unit and as such, internal tongue form manifests functional unity rather than the separate contributions of individuated muscles. Thus, within the tongue there is a blurring of distinctions among muscles, even those arising from outside the tongue, so that muscle individuality is lost. In this context, the notion of a lingual "muscle" is not meaningful and reference to "fiber systems" more accurately, if still inadequately, represents the tongue's inner workings. Therefore, a holistic view of tongue form and function highlights coherence over separability and

the precedence of functional integrity over anatomical atomization.

ACKNOWLEDGMENTS

I am deeply indebted to Fuzz Crompton, to whom this contribution is dedicated, for his friendship, mentorship, and support. My two years as a postdoctoral fellow in his lab were among the most enjoyable and instructive of my career. I thank Farish A. Jenkins, Jr., for organizing the symposium in honor of Fuzz and for inviting me to participate. I am grateful for the support and guidance of Karen Hiiemae, who first introduced me to mammal tongues. Kathleen Smith shared her extensive knowledge of tongue structure, function, and development. Elizabeth Jockusch, Kathleen Smith, and an anonymous reviewer critically read the manuscript. Various phases of this work were supported by Marvalee Wake, University of California, Berkeley; the Graduate College and Department of Oral Anatomy, University of Illinois at Chicago; A. W. Crompton, the Department of Organismic and Evolutionary Biology, and the Milton Fund, Harvard University; the University of Connecticut Research Foundation; and grants NIH F32 DE05467 and NSF IBN-9601173 to the author.

LITERATURE CITED

ABD-EL-MALEK, S. 1938. A contribution to the study of the movements of the tongue in animals, with special reference to the cat. Journal of Anatomy, **73:** 15–30.

BARNWELL, Y. M. 1976. Human lingual musculature: an historical review. International Journal of Oral Myology, **2:** 31–41.

BARNWELL, Y. M., K. KLUEBER, AND H. L. LANGDON. 1978a. The anatomy of the intrinsic musculature of the tongue in the early human fetus: Part I, M. longitudinalis superior. International Journal of Oral Myology, **4**(3): 5–8.

BARNWELL, Y. M., H. L. LANGDON, AND K. KLUEBER. 1978b. The anatomy of the intrinsic musculature of the tongue in the early human fetus: Part II. M. longitudinalis inferior. International Journal of Oral Myology, **4**(4) 5–8.

BENNETT, G. A. 1935. Die anatomische Grundlage der halbseitigen Zungenlähmungen. Sitzungsbericht der Gesellschaft für Morphologie und Physiologie (München), **44:** 1–6.

BENNETT, G. A., AND R. C. HUTCHINSON. 1946. Experimental studies on the movements of the mammalian tongue. II. The protrusion mechanism of the tongue (dog). Anatomical Record, **94:** 57–83.

BOWMAN, J. P. 1968. Muscle spindles in the intrinsic and extrinsic muscles of the rhesus monkey's (*Macaca mulatta*) tongue. Anatomical Record, **161:** 483–488.

CAVE, A. J. E. 1980. The rhinoceros lingual intrinsic musculature. Mammalia, **44:** 123–128.

COOPER, S. 1953. Muscle spindles in the intrinsic muscles of the human tongue. Journal of Physiology, **122:** 193–202.

CROUCH, J. E. 1978. Functional Human Anatomy, third edition. Philadelphia: Lea & Febiger. xxi + 663 pp.

DELHEUSY, V., G. TOUBEAU, AND V. BELS. 1994. Tongue structure and function in *Oplurus cuvieri* (Reptilia: Iguanidae). Anatomical Record, **238:** 263–276.

DORAN, G. A. 1973. The lingual musculature of the echidna, *Tachyglossus aculeatus*. Anatomischer Anzeiger, **133:** 468–476.

DORAN, G. A., AND H. BAGGETT. 1970. The vascular stiffening mechanism in the tongue of the echidna (*Tachyglossus aculeatus*). Anatomical Record, **167:** 197–204.

———. 1972. The genioglossus muscle: a reassessment of its anatomy in some mammals, including man. Acta Anatomica, **83:** 403–410.

EDGEWORTH, F. H. 1935. The Cranial Muscles of Vertebrates. Cambridge, United Kingdom: Cambridge University Press. viii + 493 pp.

GNANAMUTHU, C. P. 1937. Comparative study of the hyoid and tongue of some typical genera of reptiles. Proceedings of the Zoological Society of London, Series B, **1937:** 1–63

GREENBAUM, I. F., AND C. J. PHILLIPS. 1974. Comparative anatomy and general histology of tongues of long-nosed bats (*Leptonycteris sanborni* and *L. nivalis*) with reference to infestation of oral mites. Journal of Mammalogy, **55:** 489–504.

GRIFFITHS, M. 1968. Echidnas. Oxford: Pergamon. ix + 282 pp.

———. 1978. The Biology of the Monotremes. New York: Academic Press. viii + 367 pp.

GRIFFITHS, T. A. 1978. Muscular and vascular adaptations for nectar-feeding in the glossophagine bats *Monophyllus* and *Glossophaga*. Journal of Mammalogy, **59:** 414–418.

HELLSTRAND, E. 1980. Morphological and histochemical properties of tongue muscles in cat. Acta Physiologica Scandinavica, **110:** 187–198.

———. 1981. Contraction times of the cat's tongue muscles measured by light reflection. Innervation of individual tongue muscles. Acta Physiologica Scandinavica, **111:** 417–423.

HERREL, A., P. AERTS, J. FRET, AND F. DE VREE. 1999. Morphology of the feeding system in agamid lizards: ecological correlates. Anatomical Record, **254:** 496–507.

HERREL, A., J. CLEUREN, AND F. DE VREE. 1995. Prey capture in the lizard *Agama stellio*. Journal of Morphology, **224:** 313–329.

———. 1997. Quantitative analysis of jaw and hyolingual muscle activity during feeding in the lizard *Agama stellio*. Journal of Experimental Biology, **200:** 101–115.

HIATT, J. L., AND L. P. GARTNER. 1982. Textbook of Head and Neck Anatomy. New York: Appleton-Century-Crofts. xiv + 350 pp.

KALLIUS, E. 1910. Beiträge zur Entwickelung der Zunge. III. Teil. Säugetiere. 1. *Sus scrofa* dom. Anatomische Hefte. Arbeiten aus Anatomischen Instituten. **123/124:** 176–337.

KIER, W. M., AND K. K. SMITH. 1985. Tongues, tentacles and trunks: the biomechanics of movement in muscular-hydrostats. Zoological Journal of the Linnean Society, **83:** 307–324.

LANGDON, H., K. KLUEBER, AND Y. BARNWELL. 1978. The anatomy of m. genioglossus in the 15-week human fetus. Anatomy and Embryology, **155:** 107–113.

LEWONTIN, R. 1984. Adaptation, pp. 234–251. *In* E. Sober (ed.), Conceptual Issues in Evolutionary Biology. Cambridge, Massachusetts: MIT Press. xiv + 725 pp.

LIVINGSTON, R. M. 1956. Some observations on the natural history of the tongue. Annals of the Royal College of Surgeons, England, **19:** 185–200.

LOEB, G. E., C. A. PRATT, C. M. CHANAUD, AND F. J. R. RICHMOND. 1987. Distribution and innervation of short, interdigitated muscle fibers in parallel-fibered muscles of the cat hindlimb. Journal of Morphology, **191:** 1–15.

LOWE, A. A. 1980. The neural regulation of tongue movements. Progress in Neurobiology, **15:** 295–344.

MCGREGOR, G. 1938. Comparative anatomy of the tongue. Annals of Otology, Rhinology and Laryngology, **47:** 196–211.

MIYAWAKI, K. 1974. A study on the musculature of the human tongue. Annual Bulletin (Research Institute of Logopedics and Phoniatrics, University of Tokyo), **8:** 23–50.

NAPADOW, V. J., Q. CHEN, V. J. WEDEEN, AND R. J. GILBERT. 1999. Intramural mechanics of the human tongue in association with physiological deformations. Journal of Biomechanics, **32:** 1–12.

OELRICH, T. M. 1956. The anatomy of the head of *Ctenosaura pectinata* (Iguanidae). Miscellaneous Publications of the Museum of Zoology, University of Michigan, **94:** 1–122.

OWEN, R. 1868. On the Anatomy of Vertebrates, vol. 3. Mammals. London: Longmans, Green, and Co. x + 915 pp.

PERKELL, J. S. 1969. Physiology of Speech Production: Results and Implications of a Quantitative Cineradiographic Study. Cambridge, Massachusetts: MIT Press.

PRESNELL, J. K., AND M. P. SCHREIBMAN. 1997. Humason's Animal Tissue Techniques, fifth editon. Baltimore: The Johns Hopkins University Press. xi + 572 pp.

SANGUINETI, V., R. LABOISSIÈRE, AND Y. PAYAN. 1997. A control model of human tongue movements in speech. Biological Cybernetics, **77:** 11–22.

SCHWENK, K. 1986. Morphology of the tongue in the tuatara, *Sphenodon punctatus* (Reptilia: Lepidosauria), with comments on function and phylogeny. Journal of Morphology, **188:** 129–156.

———. 1988. Comparative morphology of the lepidosaur tongue and its relevance to squamate phylogeny, pp. 569–598. *In* R. Estes and G. Pregill (eds.), Phylogenetic Relationships of the Lizard Families. Stanford, California: Stanford University Press. xiv + 631 pp.

———. 2000a. An introduction to tetrapod feeding, pp. 21–61. *In* K. Schwenk (ed.), Feeding in Tetrapods: Form, Function, Phylogeny. San Diego, California: Academic Press. xv + 537 pp.

———. 2000b. Feeding in lepidosaurs, pp. 175–291. *In* K. Schwenk (ed.), Feeding in Tetrapods: Form, Function, Phylogeny. San Diego, California: Academic Press. xv + 537 pp.

———. 2001. Functional units and their evolution, pp. 165–198. *In* G. P. Wagner (ed.), The Character Concept in Evolutionary Biology. San Diego, California: Academic Press. xxiii + 622 pp.

SMITH, K. K. 1984. The use of the tongue and hyoid apparatus during feeding in lizards (*Ctenosaura similis* and *Tupinambis nigropunctatus*). Journal of Zoology, London, **202:** 115–143.

———. 1986. Morphology and function of the tongue and hyoid apparatus in *Varanus* (Varanidae, Lacertilia). Journal of Morphology, **187:** 261–287.

———. 1988. Form and function of the tongue in agamid lizards with comments on phylogenetic significance. Journal of Morphology, **196:** 157–171.

———. 1992. The evolution of the mammalian pharynx. Zoological Journal of the Linnean Society, **104:** 313–349.

———. 1994. Development of craniofacial musculature in *Monodelphis domestica* (Marsupialia, Didelphidae). Journal of Morphology, **222:** 149–173.

SMITH, K. K., AND W. M. KIER. 1989. Trunks, tongues, and tentacles: moving with skeletons of muscle. American Scientist, **77:** 29–35.

SOKOLOFF, A. J., AND T. W. DEACON. 1992. Musculotopic organization of the hypoglossal nucleus in the cynomolgus monkey, *Macaca fascicularis*. Journal of Comparative Neurology, **324:** 81–93.

SONDHI, K. C. 1958. The hyoid and associated struc-

tures in some Indian reptiles. Annals of Zoology, **2:** 155–239.

SONNTAG, C. F. 1925. The comparative anatomy of the tongues of Mammalia. XII. Summary, classification and physiology. Proceedings of the Zoological Society of London, **21:** 701–762.

TANNER, W. W., AND D. F. AVERY. 1982. Buccal floor of reptiles, a summary. Great Basin Naturalist, **42:** 273–349.

WAGNER, G. P. 1999. A research programme for testing the biological homology concept, pp. 125–140. *In* G. R. Bock and G. Cardew (eds.), Homology (Novartis Foundation Symposium No. 222). Chichester, United Kingdom: John Wiley & Sons. viii + 256 pp.

WALKER, W. F., JR., AND D. G. HOMBERGER. 1992. Vertebrate Dissection, eighth edition. Fort Worth, Texas: Saunders College Publishing. xii + 459 pp.

WARWICK, R., AND P. L. WILLIAMS. 1973. Gray's Anatomy, 35th edition. Edinburgh: Longman. xvi + 1471 pp.

WILHELMS-TRICARICO, R. 1995. Physiological modeling of speech production: methods for modeling soft-tissue articulators. Journal of the Acoustical Society of America, **97:** 3085–3098.

ELECTROMYOGRAPHIC PATTERN OF THE GULAR PUMP IN MONITOR LIZARDS

TOMASZ OWERKOWICZ,[1] ELIZABETH L. BRAINERD,[2] AND DAVID R. CARRIER[3]

ABSTRACT. Gular pumping in monitor lizards is known to play an important role in lung ventilation, but its evolutionary origin has not yet been addressed. To determine whether the gular pump derives from the buccal pump of basal tetrapods or is a novel invention, we investigated the electromyographic activity associated with gular pumping in savannah monitor lizards (*Varanus exanthematicus*). Electrodes were implanted in hyobranchial muscles, and their activity patterns were recorded synchronously with hyoid kinematics, respiratory airflow, and gular pressure. Movement of the highly mobile hyoid apparatus effects large-volume airflows in and out of the gular cavity. The sternohyoideus and branchiohyoideus depress, retract, and abduct the hyoid, thus expanding the gular cavity. The omohyoideus, constrictor colli, intermandibularis, and mandibulohyoideus elevate, protract, and adduct the hyoid, thus compressing the gular cavity. Closure of the choanae by the sublingual plicae precedes gular compression, allowing positive pressure to be generated in the gular cavity to force air into the lungs.

The gular pump of monitor lizards is found to exhibit a neuromotor pattern similar to the buccal pump of extant amphibians, and both mechanisms involve homologous muscles. This suggests that the gular pump may have been retained from the ancestral buccal pump. This hypothesis remains to be tested by a broad comparative analysis of gular pumping among the amniotes.

INTRODUCTION

Monitor lizards (genus *Varanus*) have recently been found to supplement their lung ventilation with gular pumping during locomotion (Brainerd and Owerkowicz, 1996). In a gular pump cycle, a monitor lizard first draws fresh air into its large pharyngeal (gular) cavity and then contracts its throat muscles to create positive pressure, thus forcing air into the lungs. Multiple gular pumps may occur in succession between costal breaths. Gular pumping has been shown to significantly increase both minute ventilation and aerobic capacity of savannah monitor lizards (*Varanus exanthematicus*) during exercise (Owerkowicz et al., 1999).

Little is known about the actual mechanism of gular pumping and its evolution. A highly expandable pharynx, supported by an elaborate hyobranchial basket, is a characteristic feature of monitor lizards. The large size and compressibility of the pharynx make it ideally suited for pumping large volumes of air. Smith (1986) studied the function of throat musculature in *V. exanthematicus* during feeding, and recorded hyobranchial muscle activity and hyoid movements. Bels et al. (1995: 99) provided a kinematic analysis of the throat threat display in *Varanus griseus*, "a ventilatory bucco-pharyngeal breathing pump (VBPBP)," consisting of alternating expansions and compressions of the gular cavity. These studies have documented the extreme excursions of the hyoid apparatus during a wide repertoire of monitor behaviors. However, the electromyographic (EMG) signature of the gular pump, as a ventilatory mechanism, has not been reported.

This study aims to determine how throat muscle activity is coordinated during gular pumping in *V. exanthematicus*. Which

[1] Museum of Comparative Zoology, Harvard University, 26 Oxford Street, Cambridge, Massachusetts 02138.

[2] Department of Biology and Organismic and Evolutionary Biology Program, University of Massachusetts, Amherst, Massachusetts 01003.

[3] Department of Biology, University of Utah, Salt Lake City, Utah 84112.

muscles are responsible for gular expansion, and which ones are responsible for compression? How is pressure generated in the gular cavity? What controls the airflow pattern?

The evolutionary origin of the gular pump also presents an interesting dilemma. Squamates have been presumed to ventilate their lungs solely by means of costal aspiration (Gans, 1970; Carrier, 1987; but see Deban et al., 1994); they rely on contraction of intercostal muscles to create negative pressure in the pleural cavity to suck air into the lungs. The use of a pressure pump was thought to be reserved for air-breathing fish and amphibians (Liem, 1985; Brainerd et al., 1993). In this mechanism, air is gulped into the buccal (mouth) cavity, and subsequently the hyoid apparatus generates positive pressure, forcing air into the lungs. The gular pump of monitor lizards clearly qualifies as a pressure pump and therefore breaks with this traditional phylogenetic separation of breathing mechanisms. However, the gular pump differs from the buccal pump because the hyoid apparatus of monitor lizards is positioned posteriorly in the throat, whereas the hyoid apparatus of amphibians resides in the mouth cavity between mandibular rami. The presence of gular pumping behavior has not been rigorously investigated in other lizard genera, and it is unclear whether gular pumping is a uniquely derived trait of monitor lizards or whether its ancestry can be traced back to buccal pumping of basal tetrapods.

Therefore, this study attempts to address the origin of gular pumping from a functional perspective. How similar is the EMG pattern of the gular pump to that of the amphibian buccal pump? Is the gular pump a case of neuromotor conservatism in evolution, or has it evolved de novo in monitor lizards?

MATERIALS AND METHODS

Animals

Experiments were performed on four savannah monitor lizards (230–2,400 g) during and immediately after locomotion on a motorized treadmill at speeds of 1–5 km/h. The animals were maintained at 25–40°C on a 14:10 hour light:dark photoperiod and were fed a diet of mice.

Terminology

This study follows the terminology of Smith (1986) in her description of the osteology and myology of the varanid gular region.

Videoradiography

Videos of the lizards were taken with a Sony DCR VX1000 digital camcorder (60 fields/s at 1/250 s shutter speed) and the Siemens X-ray fluoroscope at the Museum of Comparative Zoology Laboratories at Harvard University. Video recordings were made separately in lateral and dorsoventral projections. Select video fields were imported into Adobe Photoshop on a Power Macintosh computer.

To better visualize movements of the floor of the mouth relative to the skull and hyoid, lead markers (1.6 × 0.5 mm) were placed unilaterally in the left sublingual plica and in the anterior epithelial border of the left choana. Marker implantation was performed percutaneously with a 20-gauge needle and plunger while the animals were under 1–2% halothane anesthesia.

Pneumotachography

Two animals were used to measure airflow during gular pumping. A lightweight mask, fashioned from clear acetate and epoxy, was custom-fitted and taped over the lizard's snout to enclose the mouth and nostrils. A bias flow of humidified air (1,200 ml/min) was drawn through the mask. A pneumotachograph (8421 series 0-5 LPM, H. Rudolph, Kansas City, Missouri), connected to a differential pressure transducer (MP 45-1-871, Validyne, Northridge, California) downstream from the animal, measured airflow through the mask. The system was calibrated against

repeated injections of measured aliquots of air into the mask.

Pressure Recordings

Two animals (not used for airflow recordings) were instrumented to measure gular pressure during gular pumping. With the animal under 1–2% halothane gas anesthesia, a skin incision was made between the ceratohyal and ceratobranchial. The underlying muscles were carefully blunt-dissected and a 13-gauge needle was inserted through the pharyngeal epithelium into the gular cavity. A 20- to 30-cm-long polyethylene cannula (1.14-mm inner diameter, 1.57-mm outer diameter), previously sterilized and heat-flared at the distal end, was threaded through the hole and securely sutured to the lateral wall of the gular cavity. Before each recording session, the cannula was cleared of mucus to prevent capillarity artefacts and connected to a differential pressure transducer (PX138-0.3D5V, Omega Engineering, Inc., Stamford, Connecticut). The pressure transducer was calibrated against 10 cm H_2O after each recording session.

Electromyography

Electromyographic activity was recorded in the following muscles: constrictor colli, intermandibularis, mandibulohyoideus, omohyoideus, sternohyoideus, and branchiohyoideus. Patch and sew-through bipolar electrodes, as detailed by Loeb and Gans (1986) and Carrier (1996), respectively, were constructed of 0.28-mm-diameter Teflon-coated stainless steel wire (Cooner Wire Co., Chatsworth, California) and silastic-reinforced sheeting (Specialty Manufacturing, Inc., Saginaw, Michigan). In each electrode, the exposed portions of wires were 2 mm long and 1 mm apart. With the animal anesthetized, electrodes were surgically implanted and firmly anchored in the desired muscles. The electrode wires were then passed subcutaneously under the pectoral girdle to a single exit on the trunk's dorsum and soldered to connectors (Microtech, Inc., Boothwyn, Pennsylvania). The signals were amplified 5,000–20,000 times (as appropriate for each channel) with Grass P511J amplifiers (Quincy, Massachusetts), with a bandpass of 100–1,000 Hz (with the 60-Hz notch filter in). The signals were acquired at 5,000 Hz and analyzed on a Power Macintosh computer using AcqKnowledge (BioPac Systems, Santa Barbara, California) and Igor Pro (WaveMetrics, Inc., Lake Oswego, Oregon) software. Electromyographic and pressure signals were temporally synchronized with video recordings by means of a light-emitting diode trigger (Thexton Unlimited, London, United Kingdom).

RESULTS

Kinematics

Four stages of hyobranchial movement characterize each gular pumping cycle (Fig. 1): resting, active expansion, early closure, and compression. The cycle usually begins with the expansion of the hyobranchial basket. From its resting position (Fig. 1A), the basihyoid and the lingual process are drawn slightly ventrad and caudad. The anterior processes are abducted and, pivoting on the basihyoid, swung laterad. The ceratohyals and ceratobranchials rotate to assume a more vertical orientation (Fig. 1B).

The compressive phase of the pump cycle begins with the elevation of the buccal floor to abut the palate, thereby closing off the mouth and nostrils. As highlighted by radiopaque markers, each choana is occluded by its ipsilateral sublingual plica. The glottis is located in the gular cavity, while the hyoid remains in a retracted and expanded configuration (Fig. 1C). Finally, the basihyoid is protracted and elevated, while the trachea slides rostrad in the gular cavity. The anterior processes are adducted, and the ceratohyals and ceratobranchials fold horizontally (Fig. 1D). The hyobranchium then relaxes and passively returns to its resting state (Fig. 1A); another pumping cycle may follow.

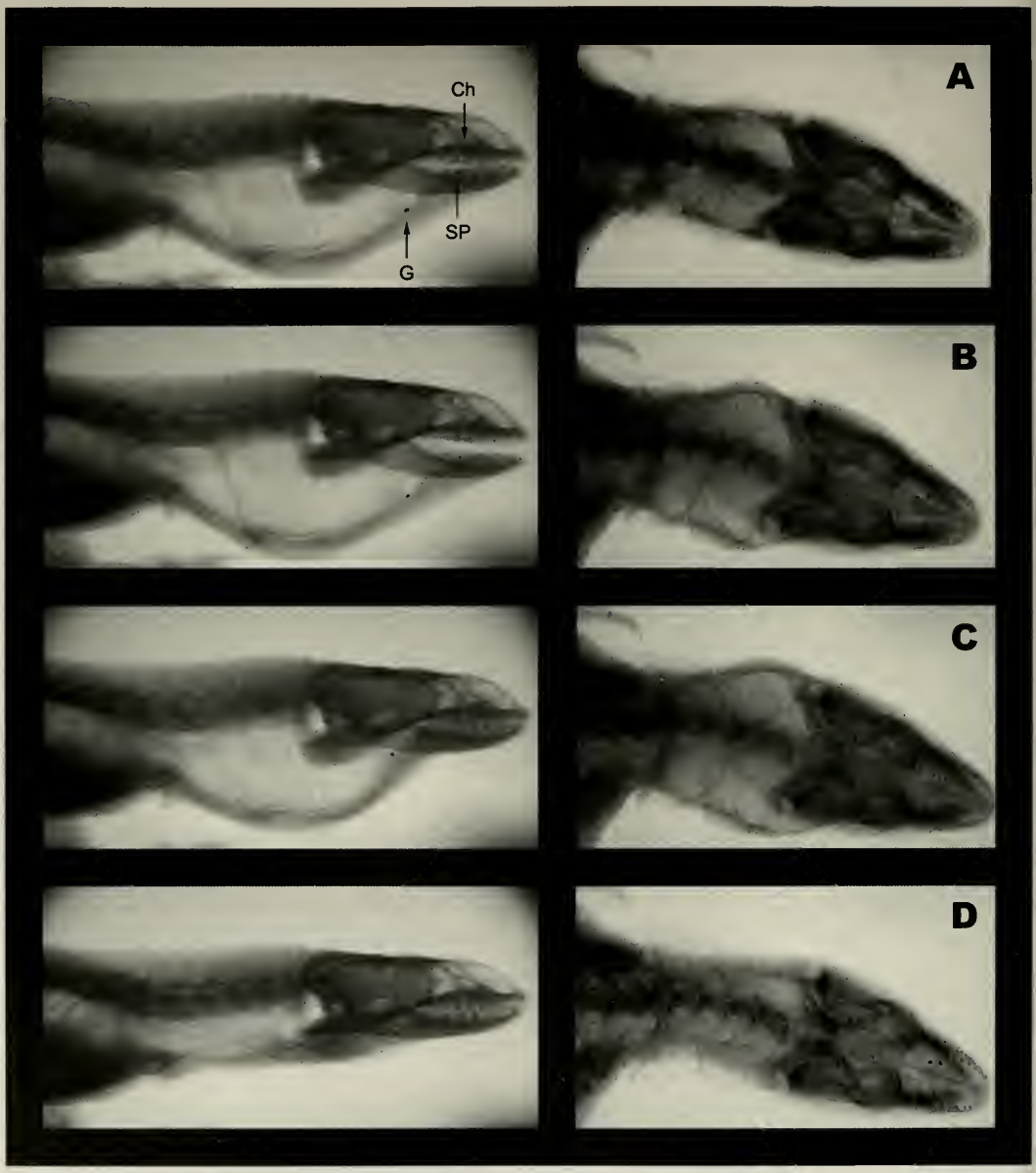

Figure 1. Still frames from an X-ray positive video (shutter speed 1/250 s) showing one gular pump cycle in *Varanus exanthematicus* (body mass = 600 g). The left column shows the animal in lateral projection, the right column in dorsoventral projection. Although not recorded simultaneously, frames in each row portray corresponding stages of a pump cycle. (A) Gular cavity relaxed. (B) Gular cavity expanded. (C) Buccal floor elevated. (D) Gular cavity compressed. Radiopaque markers (arrows) are placed at the choana (Ch), the sublingual plica (SP), and the glottis (G). Note the closure of the mouth and nares, which seals the gular cavity, as demonstrated by proximity of markers Ch and SP in (C).

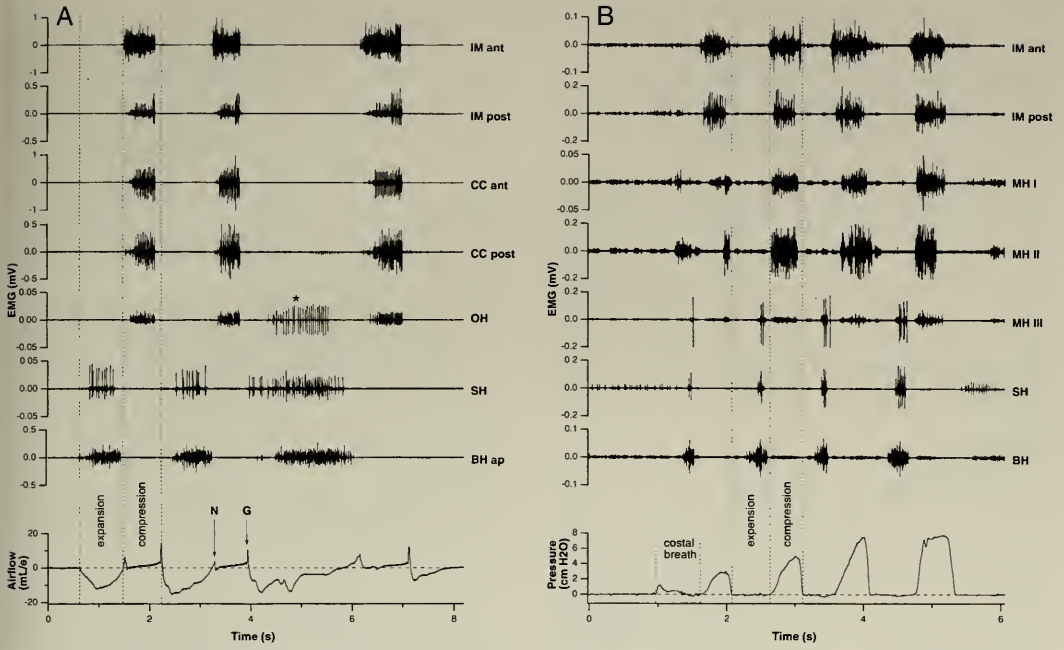

Figure 2. Raw electromyograms of hyobranchial muscles during gular pumping in *Varanus exanthematicus*. (A) Three gular pump cycles recorded simultaneously with airflow at the snout. Gular expansion (negative airflow) is initially passive because of the gravitational drop of the hyoid, and then active as the branchiohyoideus and sternohyoideus begin to contract. Gular compression occurs during the zero-flow plateau, as air is pressed into the lungs. Minimal air leakage occurs—note the spikes showing early closure of the nares (N) and the late closure of the glottis (G). The asterisk indicates unanticipated activity of the omohyoideus due to neck bending. (B) A costal breath followed by four successive gular pump cycles, recorded simultaneously with gular pressure. Gular expansion generates little negative pressure, but peak compressive pressures up to 15 cm H_2O have been recorded. *Abbreviations:* CC, m. constrictor colli; IM, m. intermandibularis; MH, m. mandibulohyoideus; BH, m. branchiohyoideus (ceratohyoid head); BH ap, m. branchiohyoideus (coruhyoid head); SH, m. sternohyoideus; OH, m. omohyoideus; ant, anterior; post, posterior.

Active expansion was not observed in every pump cycle. The animals often chose to proceed to closure and compression directly from the resting stage, in which case the volume of air pumped was not as great as when preceded by active expansion. Furthermore, resting gular volume was dependent on the positioning of the hyobranchial apparatus in the neck of the animal, which varied with the animal's posture and muscle tone of associated pectoral musculature (sternohyoideus and omohyoideus—see below).

Airflow

The airflow pattern at the animal's mouth and nostrils (Fig. 2A) is consistent with a biphasic nature of each gular pump, whereby a filling (expansive) phase is immediately followed by an emptying (compressive) phase. Average filling volumes ranged from 6 to 15 ml, but individual gular inspirations up to 33 ml were also recorded. Early in the pump cycle, animals were observed to rely on passive filling of the gular cavity by gravitational drop of the hyoid (correspondent to the return of the hyoid from compressed to resting stage). Passive filling was followed by active expansion, as indicated by concomitant activity in the branchiohyoideus and sternohyoideus, which resulted in faster (more negative) airflow and greater filling volumes.

Early in the filling phase, airflow into the gular cavity was rapid, as shown by the steep descent of the airflow trace to its minimum value. Late in the filling phase, inspiratory airflow gradually diminished to

nil. A slight overshoot of the zero-flow line (N in Fig. 2A) marked early closure of the mouth and nostrils, and the beginning of the emptying phase. A zero-flow plateau was recorded for the duration of the emptying phase, as air was forced from the gular cavity into the lungs. The emptying phase terminated in a small expiratory spike (0.5–1.0 ml), after the inferred closure of the glottis (G in Fig. 2A) and opening of the mouth and nares. Unless another pumping cycle occurred immediately afterwards, passive filling followed and a longer apnoeic period ensued.

Pressure

Each costal breath was followed by as many as five gular pumps, with successive pump cycles generating increasingly positive gular pressures (Fig. 2B). Peak pressures up to 15 cm H_2O were recorded. With the onset of each compressive phase, gular pressure climbed steeply and reached peak pressure within 200 milliseconds. For most pumping cycles, gular pressure hovered within 5% of peak value for less than 100 milliseconds, although gular pressure would sometimes remain elevated at peak for up to 400 milliseconds. Thereafter, gular pressure dropped rapidly (within 100 milliseconds), often dipping to subatmospheric levels, and then equilibrated with the atmospheric pressure.

Gular pressure varied little from atmospheric pressure during the filling phase of a pump cycle. Active gular expansion generated only slightly subatmospheric pressures (-0.2 to -0.4 cm H_2O).

Electromyographic Activity

Recordings from hyobranchial muscles produced a consistent activity pattern during gular pumping (Fig. 2A, B). Although they remained quiescent during passive filling, branchiohyoideus (both cerato- and cornuhyoid heads), sternohyoideus, and mandibulohyoideus III were turned on during active gular expansion. Onset of the branchiohyoideus was followed in 50–200 milliseconds by almost simultaneous activation of the sternohyoideus and mandibulohyoideus III. The intensity of their firing remained roughly constant while these muscles were active. All three muscles were turned off before the end of the filling phase, with activity in the branchiohyoideus persisting for up to 150 milliseconds after the offset of the sternohyoideus and mandibulohyoideus III.

Gular compression began with a burst of activity in the intermandibularis anterior, which was followed within 100 milliseconds by contraction of the constrictor colli, intermandibularis posterior, and all three heads of mandibulohyoideus. The intensity of their firing generally increased from onset to offset. Activity ceased in all muscles together, once gular pressure had peaked.

The activity of the mandibulohyoideus III was biphasic; it contracted during gular expansion and compression, but not continuously (Fig. 2B). It was briefly (50–100 milliseconds) silent between the two phases of the pumping cycle.

The omohyoideus was usually quiescent during gular pumping. When participating in gular pumping, the omohyoideus was predominantly active during gular compression. However, it might occasionally fire during gular expansion (* in Fig. 2A), which tended to decrease the gular filling volume. In such instances, activity of the omohyoideus was correlated with changes in posture and/or neck bending by the animal.

During locomotion, regular phasic activity was observed in most hyobranchial muscles, but was especially prominent in the sternohyoideus and omohyoideus. The rate of discharge was the same as the footfall frequency, and in the latter two muscles the signal amplitude was greater than in stationary animals.

DISCUSSION

Hyobranchial Muscle Function

The role of individual muscles involved in the gular pump can be inferred by con-

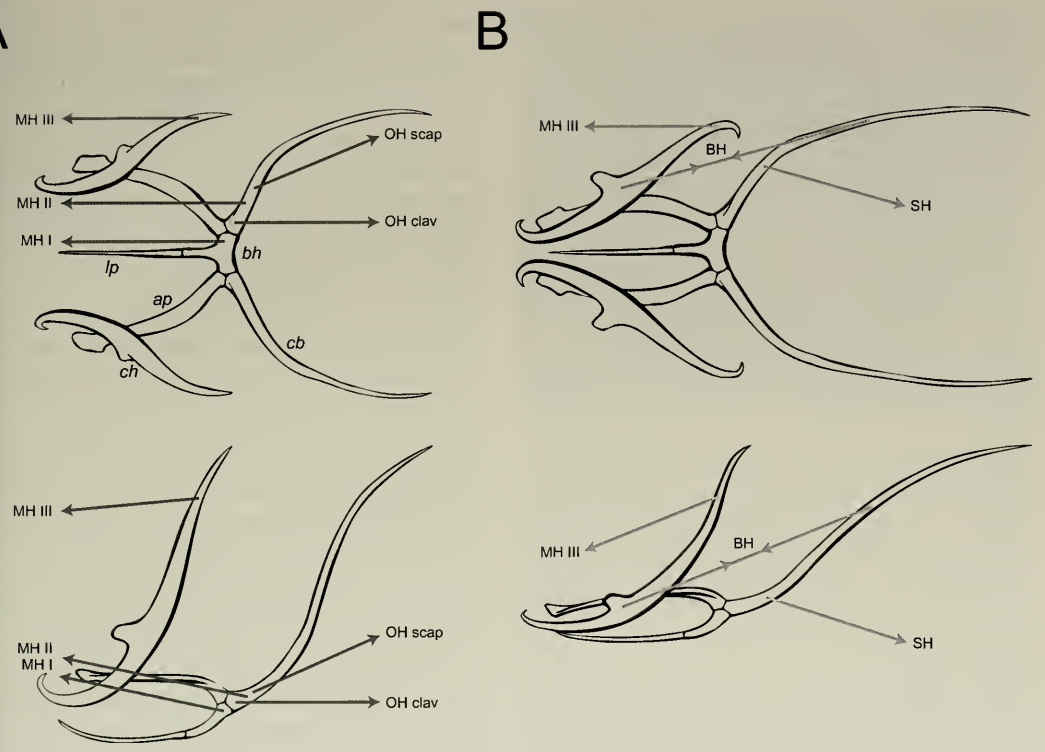

Figure 3. The hyobranchial apparatus of *Varanus exanthematicus*, in ventral (top row) and lateral (bottom row) views. Force vectors (gray arrows) show the sites of insertion and lines of action of the hyobranchial muscles, as measured in dissected specimens. (A) The hyoid in its expanded configuration; contraction of musculi (mm.) mandibulohyoideus and omohyoideus will result in hyoid compression. Constrictor colli and intermandibularis are not shown, because they do not insert directly on the hyoid. (B) The hyoid in its compressed configuration; contraction of the branchiohyoideus, sternohyoideus, and mandibulohyoideus III will result in hyoid expansion. *Abbreviations:* ap, anterior process; bh, basihyoid; cb, ceratobranchial; ch, ceratohyal; clav, clavicular; lp, lingual process; scap, scapular; others as in Figure 2.

sidering their insertion sites on the hyoid apparatus (Fig. 3), the patterns of their EMG activity, and the kinematics of the hyoid elements during each gular pump cycle.

Gular expansion results from the coordinated activity of the sternohyoideus, branchiohyoideus, and mandibulohyoideus III. The sternohyoideus pulls the ceratobranchial in a caudoventrad direction, giving it a more vertical orientation. This action tends to retract and depress the basihyoid, while pointing the lingual process ventrad. With the ceratobranchial stabilized by the sternohyoideus, the branchiohyoideus tends to abduct the anterior process and retract the ceratohyal. However, the proximal end of the anterior process pivots about the basihyoid, and the ceratohyal has its distal end anchored to the lower jaw by the mandibulohyoideus III. The broad, loose nature of articulation between the ceratohyal and the anterior process allows sliding to occur between these two elements. Thus, as the anterior process swings laterad, it pushes against the ceratohyal, the angle between these two elements increases, and the ceratohyal assumes a more vertical orientation. Altogether, these muscles tend to expand the gular cavity in the lateral and dorsoventral dimensions.

Gular compression begins with the early closure of mouth and nostrils. The intermandibularis anterior, positioned under the sublingual plicae, contracts to elevate

Figure 4. Cross section of the snout of *Varanus exanthematicus* at the anterior border of the choanae. Each nasal passage connects to its ipsilateral choana just posterior to this plane. Elevation of the mouth floor allows the sublingual plica to plug the choana above. The congruent outlines of the lower and upper jaws allow an airtight closure of the mouth, sealed with saliva from labial and sublingual glands. *Abbreviations:* Ch, choana; LG, labial gland; LJ, lower jaw; N, nasal passage; SG, sublingual gland; SP, sublingual plica; UJ, upper jaw.

the buccal floor and push the plicae against the choanae (SP → Ch in Fig. 4), thus blocking airflow through the nasal passages. Although no recordings were taken from the adductor mandibulae, this muscle is most likely to be responsible for keeping the mouth closed, while the thick, fleshy gums (Auffenberg, 1981) seal the oral margins with secretion of salivary glands lining both lingual and labial aspects of the lower jaw. The gular cavity is effectively made airtight for the duration of gular compression.

Muscles responsible for gular compression include the omohyoideus, constrictor colli, intermandibularis posterior, and mandibulohyoideus. The clavicular and scapular heads of the omohyoideus attach the ceratobranchials to the respective parts of the pectoral girdle, and their contraction retracts and elevates the basihyoid. The constrictor colli encircles the floor and sides of the gular cavity, forming a sleeve in which the hyobranchial basket is suspended. Together with its anterior extension, the intermandibularis posterior, this superficial transverse muscle elevates the hyoid apparatus. On the other hand, the mandibulohyoideus connects the hyoid to the lower jaw and, along with the sternohyoideus and omohyoideus, controls its anteroposterior position in the neck. As the basihyoid is protracted, the ceratohyals and ceratobranchials assume a more horizontal orientation, in effect folding the hyobranchial basket. The orthogonal orientation of muscle fibres in the constrictor colli and intermandibularis to the mandibulohyoideus means that their synchronous activity will squeeze the air out of the gular cavity.

With the onset of locomotion, most hyobranchial muscles show bursts of activity in phase with the footfall pattern. This is particularly pronounced in the sternohyoideus and omohyoideus; their firing intensity during locomotion is several times greater than at rest. Yet it is hard to imagine their acting as locomotor muscles. It is more likely that with every retraction of the forelimb these muscles are stretched and fire reflexively to stabilize the hyoid, keeping it in position for pumping. Low-intensity phasic activity detected in other hyobranchial muscles is probably an artefact of cross-talk from the underlying axial muscles of the neck, participating in the lateral bending of the neck during locomotion.

Airflow and Pressure Changes

The pneumotachograph and the pressure transducer provide complementary information about the patterns of airflow and pressure generation outside and inside the gular cavity. During gular expansion, pressure drops only slightly below the atmospheric level. The lizard's mouth and nares are wide open (Fig. 1B) and provide little resistance to airflow into the gular cavity. Gular expansion, whether passive or active, is too slow for gular pressure to turn more negative; instead, it quickly equilibrates with atmospheric pressure.

Inspiratory airflow ceases when the mouth and nares are shut (see above). The "corking" of the choanae by the sublingual

plicae expels an aliquot of air from the narial passages (N in Fig. 2A). The gular pressure increases from this point on and air is pressed through the open glottis into the trachea and lungs. The plateau at zero-flow indicates the efficacy of the oral seal.

Only at the very end of compression does a puff of air leak out of the mouth and nares at a high flow rate (G in Fig. 2A). The hyobranchial muscles have already turned off by this time, yet their contraction clearly persists for approximately 120 milliseconds (a reasonable time period for slow-twitch fibers in isometric contraction) and gular pressure remains elevated. This expiratory "gular leakage" possibly represents excess air, which was not pressed into the lungs. The fact that this occurs at the end of every pumping cycle indicates that the glottis always closes before the nares open. Such carefully coordinated timing suggests that this may be a hard-wired mechanism designed to prevent air escaping from the lungs, which have been pressurized by gular pumping.

Origin of Gular Pumping

The gular pump of monitor lizards bears striking resemblance to the buccal pump of extant amphibians, in function and in mechanism. Both pumps generate positive pressure to force air from the pharyngeal cavity into the lungs. Both employ the hyobranchial apparatus to produce volumetric changes of the buccal and gular cavities. This similarity suggests that buccal pumping and gular pumping may be homologous behaviors. However, the derived morphology of the monitor lizards and their deeply nested position in the squamate phylogeny (Estes et al., 1988) suggest the possibility that gular pumping, as ventilatory behavior, may have evolved independently in monitor lizards. This alternative hypothesis would be supported by finding that the gular and buccal pumps are powered by nonhomologous muscles, or that the patterns of their activation are markedly different.

Lepidosaurs, especially the highly derived varanids, do not necessarily possess the same ensemble of hyobranchial muscles found in Lissamphibia, and even among the latter, the muscular organization of the throat is highly variable. However, muscle homologies can be established with a fair degree of certainty by determining their anatomical relations and motor nerve supply (Fürbringer, 1888, in Cunningham, 1890). The constrictor colli of lizards and the interhyoideus of amphibians seem to be homologous, by virtue of having a common precursor in the constrictor hyoideus, as found among the Dipnoi (Edgeworth, 1935). Except for its lateralmost third head with a disparate motor innervation and therefore origin (Rieppel, 1978), the mandibulohyoideus is clearly a highly differentiated version of the geniohyoideus, ubiquitous among the vertebrates. The rectus cervicis of caecilians is homologous with the sternohyoideus in both frogs and monitor lizards. Lacking a pectoral girdle, caecilians lack an omohyoideus.

The branchiohyoideus is found in neither anurans nor caecilians. Its putative homologue, subarcualis rectus I (not the larval branchiohyoideus externus; Edgeworth, 1935, contra Smith, 1920), is present in urodeles, but the EMG activity of this muscle during buccal pumping is yet to be investigated. Nevertheless, EMG evidence from feeding studies in *Ambystoma* (Lauder and Shaffer, 1985; Reilly and Lauder, 1991) shows that the subarcualis rectus I is active during buccal expansion in aquatic and terrestrial prey capture, and its role in generating buccal expansion during suction feeding has been deduced from its anatomical position and fiber orientation in various salamanders (Erdman and Cundall, 1984; Lauder and Shaffer, 1988; Lorenz-Elwood and Cundall, 1994). This suggests that the subarcualis rectus I functions in much the same way in the buccal pump of salamanders as does the branchiohyoideus in the gular pump of lizards.

Having established the homology of hyobranchial muscles of amphibians and

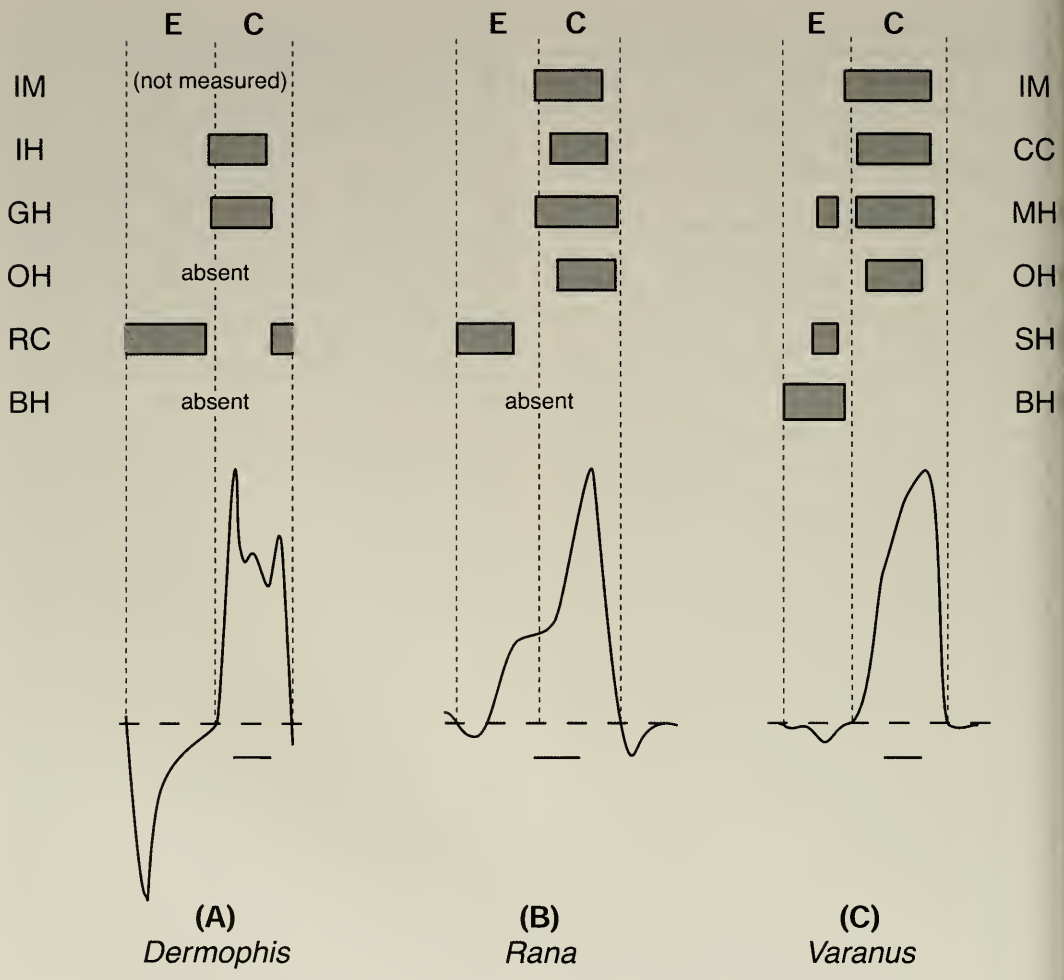

Figure 5. Comparison of hyobranchial muscle activity patterns during a single pressure pump cycle in (A) a caecilian (*Dermophis*), (B) a frog (*Rana*), and (C) a monitor lizard (*Varanus*). Homologous muscles are shown in the same row. Each pumping cycle (E + C) has been scaled to the same duration time (the scale bars are 0.2 seconds). Pressures (bottom trace) have been scaled to the same peak value; maximum peak pressures range from 4 cm H_2O (frog) to 15 cm H_2O (caecilian and monitor lizard). *Abbreviations:* E, active expansion; C, compression; GH, m. geniohyoideus; IH, m. interhyoideus; RC, m. rectus cervicis; others as in Figure 2. (A) is modified from Carrier and Wake (1995); (B) is a composite of de Jongh and Gans (1969) and West and Jones (1974); and (C) is from this study.

lizards, it is possible to directly compare their activity patterns in the gular pump of *V. exanthematicus* and in the buccal pump of a caecilian (Carrier and Wake, 1995) and an anuran (de Jongh and Gans, 1969; West and Jones, 1974). Differences in pressure profiles aside, all three neuromotor patterns clearly are similar (Fig. 5). This suggests that homologous hyobranchial muscles function in much the same way in these distantly related clades. Therefore, the homology of the gular and buccal pumping behaviors cannot be rejected.

Nevertheless, analysis of the present data does not allow us to conclude with confidence that the gular and buccal pumps are homologous behaviors. Neuromotor similarity is not sufficient to claim that a behavioral mechanism has been

conserved in evolution (Smith, 1994). Unlike other situations in which the neuromotor pattern is conserved despite functional divergence (e.g., in the evolution of terrestrial and aerial locomotion; Goslow et al., 1989), the gular pump may represent functional convergence with the buccal pump by using homologous structures. The question of homology in the case of the gular pump is made even more complex by the fact that cycles of gular expansion and compression are also used in feeding (Smith, 1986), gular flutter (Heatwole et al., 1973), and throat displays (Bels et al., 1995). One or more of these behaviors could have retained the ancestral motor pattern for hyobranchial movement and this pattern could have been co-opted for lung ventilation (with appropriate modification of narial and glottal valving). The next study undertaken to explore the homology of buccal and gular pumping should be a broad comparative analysis to map the character of gular pumping (its presence or absence) on the phylogeny of Amniota. Preliminary investigations within Squamata indicate that gular pumping is widespread among nonserpentine squamates (Deban et al., 1994; Al-Ghamdi et al., 2001; Brainerd and Owerkowicz, personal observation). This result, combined with our finding of neuromotor similarity in the pumping mechanisms of monitor lizards and amphibians, suggests that the gular pump of lizards may have been retained continuously from a buccal pumping ancestor.

ACKNOWLEDGMENTS

Fuzz Crompton provided the original inspiration for this study by explaining the nuance between "gular" and "buccal." Under Fuzz's guidance, T. O. honed his experimental skills in radiographic, electromyographic, and histologic techniques used in this study. T. O. wishes to express his gratitude to Fuzz for his mentorship and support over the last decade. We thank C. Farmer and L. Claessens for lending a hand with the surgeries, K. Schwenk for his invaluable critique of the early version of the manuscript, and the Festschrift editors F. A. Jenkins, Jr., and M. D. Shapiro for their infinite patience. We appreciate L. Meszoly for his rendering of the hyoid apparatus, and C. Musinsky for applying finishing touches to the figures. This work was supported by the Chapman Fellowship (Harvard University) to T. O., and by National Science Foundation grants IBN-9875245 to E. L. B. and IBN-9807534 to D. R. C.

LITERATURE CITED

Al-Ghamdi, M. S., J. F. X. Jones, and E. W. Taylor. 2001. Evidence of a functional role in lung inflation for the buccal pump in the agamid lizard, *Uromastyx aegyptius microlepis*. Journal of Experimental Biology, **204:** 521–531.

Auffenberg, W. 1981. The Behavioral Ecology of the Komodo Dragon. Gainesville, Florida: University Presses of Florida. x + 406 pp.

Bels, V. L., J.-P. Gasc, V. Goosse, S. Renous, and R. Vernet. 1995. Functional analysis of the throat display in the sand goanna *Varanus griseus* (Reptilia: Squamata: Varanidae). Journal of Morphology, **235:** 95–116.

Brainerd, E. L., J. S. Ditelberg, and D. M. Bramble. 1993. Lung ventilation in salamanders and the evolution of vertebrate air-breathing mechanisms. Biological Journal of the Linnaean Society, **49:** 163–183.

Brainerd, E. L., and T. Owerkowicz. 1996. Role of the gular pump in lung ventilation during recovery from exercise in *Varanus exanthematicus*. American Zoologist, **36:** 88.

Carrier, D. R. 1987. The evolution of locomotor stamina in tetrapods: circumventing a mechanical constraint. Paleobiology, **13:** 325–341.

———. 1996. Function of the intercostal muscles in trotting dogs: ventilation or locomotion? Journal of Experimental Biology, **199:** 1455–1465.

Carrier, D. R., and M. H. Wake. 1995. Mechanism of lung ventilation in the caecilian *Dermophis mexicanus*. Journal of Morphology, **226:** 289–295.

Cunningham, D. J. 1890. Value of nerve supply in the determination of muscular homologies and anomalies. Journal of Anatomy, **25:** 31–40.

Deban, S. M., J. C. O'Reilly, and T. Theimer. 1994. Mechanism of defensive inflation in the chuckwalla, *Sauromalus obesus*. Journal of Experimental Zoology, **270:** 451–459.

de Jongh, H. J., and C. Gans. 1969. On the mechanism of respiration in the bullfrog, *Rana catesbeiana*: a reassessment. Journal of Morphology, **127:** 259–290.

Edgeworth, F. H. 1935. The Cranial Muscles of

Vertebrates. Cambridge, United Kingdom: Cambridge University Press. viii + 493 pp.

ERDMAN, S., AND D. CUNDALL. 1984. The feeding apparatus of the salamander *Amphiuma tridactylum*: morphology and behavior. Journal of Morphology, **181:** 175–204.

ESTES, R., K. DE QUEIROZ, AND J. GAUTHIER. 1988. Phylogenetic relationships within Squamata, pp. 119–281. *In* R. Estes and G. Pregill (eds.), Phylogenetic Relationships of the Lizard Families. Stanford, California: Stanford University Press. xii + 631 pp.

GANS, C. 1970. Strategy and sequence in the evolution of the external gas exchangers of ectothermal vertebrates. Forma et Functio, **3:** 61–104.

GOSLOW, G. E., JR., K. P. DIAL, AND F. A. JENKINS, JR. 1989. The avian shoulder: an experimental approach. American Zoologist, **29:** 287–301.

HEATWOLE, H., B. T. FIRTH, AND G. J. W. WEBB. 1973. Panting thresholds of lizards. Comparative Biochemistry and Physiology, A, **46:** 711–826.

LAUDER, G. V., AND H. B. SCHAFFER. 1985. Functional morphology of the feeding mechanism in aquatic ambystomatid salamanders. Journal of Morphology, **185:** 297–326.

———. 1988. Ontogeny of functional design in tiger salamanders (*Ambystoma tigrinum*): are motor patterns conserved during major morphological transformations? Journal of Morphology, **197:** 249–268.

LIEM, K. F. 1985. Ventilation, pp. 185–209. *In* M. Hildebrand, D. M. Bramble, K. F. Liem, and D. B. Wake (eds.), Functional Vertebrate Morphology. Cambridge, Massachusetts: Belknap Press. 430 pp.

LOEB, G. E., AND C. GANS. 1986. Electromyography for Experimentalists. Chicago, Illinois: University of Chicago Press. xx + 373 pp.

LORENZ-ELWOOD, J. R., AND D. CUNDALL. 1994. Morphology and behavior of the feeding apparatus in *Cryptobranchus alleganiensis* (Amphibia: Caudata). Journal of Morphology, **220:** 47–70.

OWERKOWICZ, T., C. G. FARMER, J. W. HICKS, AND E. L. BRAINERD. 1999. Contribution of gular pumping to lung ventilation in monitor lizards. Science, **284:** 1661–1663.

REILLY, S. M., AND G. V. LAUDER. 1991. Experimental morphology of the feeding mechanism in salamanders. Journal of Morphology, **210:** 33–44.

RIEPPEL, O. 1978. The throat musculature of *Sphenodon*, with comments on the primitive character states of the throat muscles in lizards. Anatomischer Anzeiger, **144:** 429–440.

SMITH, K. K. 1986. Morphology and function of the tongue and hyoid apparatus in *Varanus* (Varanidae, Lacertilia). Journal of Morphology, **187:** 261–287.

———. 1994. Are neuromotor systems conserved? Brain, Behavior and Evolution, **43:** 293–305.

SMITH, L. 1920. The hyobranchial apparatus of *Spelerpes bislineatus*. Journal of Morphology, **33:** 527–583.

WEST, N. H., AND D. R. JONES. 1974. Breathing movements in the frog *Rana pipiens*. I. The mechanical events associated with lung and buccal ventilation. Canadian Journal of Zoology, **53:** 332–344.

SYNCHRONIZATION OF ELECTROMYOGRAPHIC ACTIVITY IN ORAL MUSCULATURE DURING SUCKLING AND DRINKING

A. J. THEXTON[1] AND REBECCA Z. GERMAN[2,3]

ABSTRACT. Suckling and drinking are rhythmic activities, with an electromyographic pattern that is characterized by a significant coactivation of multiple muscles that are not obvious synergists. If the rhythm and coactivation were due to conventional excitation of motor neurons by a single, central source of rhythm generation then, within the periods of coactivation, there should also be a degree of synchronization of muscle action potentials, similar to that established for respiration. Both respiration and suckling are activities that can persist in the absence of the cerebral hemispheres. However, in a preliminary study of suckling, evidence for synchronization was not characteristic of most of the coactive muscles. Marked rhythmic coactivation of muscles is also characteristic of the cerebrally directed, more mature activity of drinking. Synchronization of action potentials in other conscious movements suggests that cerebrally directed drinking might differ from suckling with respect to the level of synchronization. We tested this hypothesis in miniature pigs by cross-correlation analysis of the electromyographic activity recorded in multiple oral and submandibular muscles during suckling and drinking in the same animals. Evidence of intraburst synchronization was found in only a few muscles (sternohyoid, omohyoid, and geniohyoid) during suckling, but that evidence was absent in drinking in exactly the same muscles in the same animals. A tentative explanation for the paucity of evidence for synchronization in suckling, despite the coactivation of muscles, is that the rhythmic muscle activity is generated by plateau potentials in individual motor neurons; this is a phylogenetically primitive mechanism with respect to mammals. The absence of evidence for synchronization in drinking may reflect the fact that the neural mechanisms for drinking precede those for suckling phylogenetically, although not ontogenetically.

INTRODUCTION

Rhythmic oral movements can be generated by brainstem mechanisms alone. Suckling occurs in the anencephalic human infant (Hall, 1833; Gamper, 1926; Monnier and Willi, 1953) and rhythmic chewing or lapping movements can be elicited in decerebrate animals (Bremer, 1923). These reports are consistent with the subsequent localization of a central pattern generator (CPG) for rhythmic oral movements within the brainstem (Dellow and Lund, 1971). Nevertheless, cerebrocortical centers have been described for both mastication and for suckling (Iriki et al., 1988). When these higher centers are functional, they may simply supply drive to the CPG (Bremer, 1923; Lund and Dellow, 1971) but their activity may also interact with the brainstem mechanisms in other ways, including direct monosynaptic connections to trigeminal motor neurons (Mishima et al., 1982; Moriyama, 1987; Ohta et al., 1989; Ohta and Saeki, 1989). The pattern of activity of cortical motor neurons can, in the case of the limbs, be directly related to the amplitude and to the direction of a resultant limb movement (Georgopoulos, 1995) so that a similar action in directing oral activity towards extraorally located food is to be expected in, for example, drinking.

When the infant pig locates on an artificial teat, rhythmic suckling is only triggered when milk is present (German et al., 1997) and suckling then continues as a re-

[1] Physiology Department, Kings College London (School of Biomedical Sciences of Guy's, King's and St. Thomas's Hospitals), St. Thomas's Campus, Lambeth Palace Road, London SE1 9RT.

[2] Department of Biological Sciences, University of Cincinnati, Cincinnati, Ohio 45221-0006.

[3] To whom correspondence should be addressed.

sponse to the intraoral delivery of the liquid. Conversely, drinking is directed to the acquisition of an extraorally located liquid and the maintained direction of this activity is likely to involve cortical activity. The postnatal maturation of cerebral functions might then relate to the ability to change from suckling to drinking.

Consequently, the aim of this study was to test the proposition that some aspect of the generation or control of the pattern of electromyographic (EMG) activity in drinking differed from that in suckling. As a first stage in this investigation, a form of analysis was adopted that had originally been developed in relation to the rhythmic activity of respiration (Sears and Stagg, 1976). Respiration is a similar activity to suckling and drinking in the sense that respiration is generated by a CPG and as such involves a number of different muscles that exhibit simultaneous bursts of EMG activity. Each of these bursts of EMG activity consists of a number of individual spikes or muscle action potentials, henceforth referred to as intraburst spikes. Some of these intraburst spikes occur at the same time in the muscles of different intercostal spaces, that is, the different muscles are not only coactivated but show synchronous firing within the periodic bursts, indicating that some of the motor neurones receive identical synchronous activation.

The demonstration of synchronization of spikes within bursts of EMG activity occurring at the same time (in two different but coactive or synergistic muscles) only indicates that a proportion of the action potentials arriving presynaptically at the motor neurons are also synchronous. Cortically originating activity acting on two synergistic muscles is often associated with a degree of such synchronization in the EMGs. Similarly, a CPG supplying two synergistic muscles will also produce synchronization of a proportion of the spikes in the two EMGs.

In contrast, pilot studies on infant pigs (Banks and Thexton, 1999) indicated that the drive to the motor neurons during suckling does not produce simultaneous intraburst spikes during EMG activity in most of the coactive muscles (but does in just a few hyoid muscles). This contrasts with studies of rhythmic somatic activity (Sears and Stagg, 1976) in adult animals and with studies of cortically directed activity (Datta and Stephens, 1990) where synchronization can be regularly demonstrated. Consequently, the initial hypothesis was that, in drinking, action potentials within bursts of EMG activity of some pairs of muscles might show greater degrees of synchronization, compared to the more immature activity of suckling.

MATERIALS AND METHODS

Three miniature pigs (*Sus scrofa*), each 3 weeks old, were trained to feed in a box from an artificial teat. At this age pigs are at the start of weaning; some individuals will repeatedly change their mode of ingestion from suckling to drinking and back again within a few minutes (depending upon how the food is made available). Consequently, data comparisons can be made in which there is no significant time delay during which electrodes can move or deteriorate or during which other longer-term maturational changes can confuse the picture.

The methods used in these experiments have been described in detail elsewhere (Thexton et al., 1998) so that only a brief description is given here. Under general anesthesia (halothane/oxygen), the submandibular musculature was exposed and individual muscles identified. Bipolar fine wire electrodes were then inserted into the muscles and the leads passed via a subcutaneous tunnel to a multipole connector on the back. After recovery, the animals were again fed in the box, allowing the multipole connector to be connected to amplifiers. The amplified signals were then recorded on tape for off-line digitization. All analysis was carried out on the digitized data.

The EMG activity in the relevant mus-

cles was first half-wave rectified and the spike peaks identified. The spike peaks were then converted to point events and all events, with an amplitude less than 10% of the maximum, were eliminated as being due largely to noise, that is, they were set to zero; all the other events were given a value of one. A pairwise correlation between the two series of point events was then calculated. This was then repeated for different time shifts of one data set relative to the other, for example, from t_0 − 40 milliseconds to t_0 + 40 milliseconds, where t_0 is zero time shift between the two data sets (Fig. 1). If any tendency exists for intraburst spikes to occur either synchronously in the two data streams or with a regular time lag in one data stream with respect to the other, they come to correspond with each other at one of the time shifts and so produce a larger correlation at that time shift.

The EMG activities were analyzed to determine if any difference existed in the level of synchronization occurring in suckling and drinking. The hypothesis was that if the two activities arose or were centrally influenced in different ways, as indicated in the Introduction, there might be different levels of synchronization.

RESULTS

The data analyzed in this study were the multichannel EMG activities recorded in a variety of muscles during suckling and during drinking. The EMG activity recorded during a short period of drinking is shown in Figure 2. The period contained just over six cycles of movement including three cycles in which swallowing was present; the three swallowing cycles were associated with the three higher-amplitude bursts of activity in the hyoglossus. Simultaneous bursts of EMG activity occurred in a number of muscles that are innervated by different motor nuclei, for example, digastric (V), stylohyoid (VII), and hyoglossus (XII). This coactivation of sets of muscles is characteristic of the activity in feeding in the weaning pig, whether suckling or drinking (Thexton et al., 1998).

When the EMG signals obtained from the submandibular muscles during suckling were processed, they produced a series of correlograms that, for the most part, were flat (Figs. 3A–C). Across all three animals the expected central peaks, indicative of short- or medium-term synchronization, were generally absent, as previously reported (Banks and Thexton, 1999). The only cross-correlograms with visible central peaks, which were consistent with synchronization, were those that were obtained by the crosscorrelation of geniohyoid, sternohyoid, and omohyoid activity (Figs. 3D, E); of these, the cross-correlation between sternohyoid and omohyoid activity provided the clearest evidence (in two out of three animals).

When the same analyses were applied to drinking data, the results were similar in so far as the cross-correlograms were generally flat. However, the results differed in that no obvious central peaks occurred in the cross-correlations derived from the geniohyoid, sternohyoid, or omohyoid signals. Direct intra-animal comparisons were also made between the cross-correlations of omohyoid, sternohyoid, and geniohyoid activity in suckling and the same cross-correlations in drinking. In two animals (that within minutes would change from suckling to drinking and back again) the evidence for intraburst synchronization, which was clearly evident in muscles such as sternohyoid and omohyoid during suckling (Fig. 3E), was always absent in drinking (Fig. 3F).

DISCUSSION

One of the earliest studies that provided evidence of intraburst synchrony among the motor units of cocontracting muscles (Sears and Stagg, 1976) was carried out on the respiratory system, that is, on a rhythmic activity produced by a brainstem pattern generator. Suckling and drinking similarly involve cocontracting muscles and, on current evidence, are also generated by

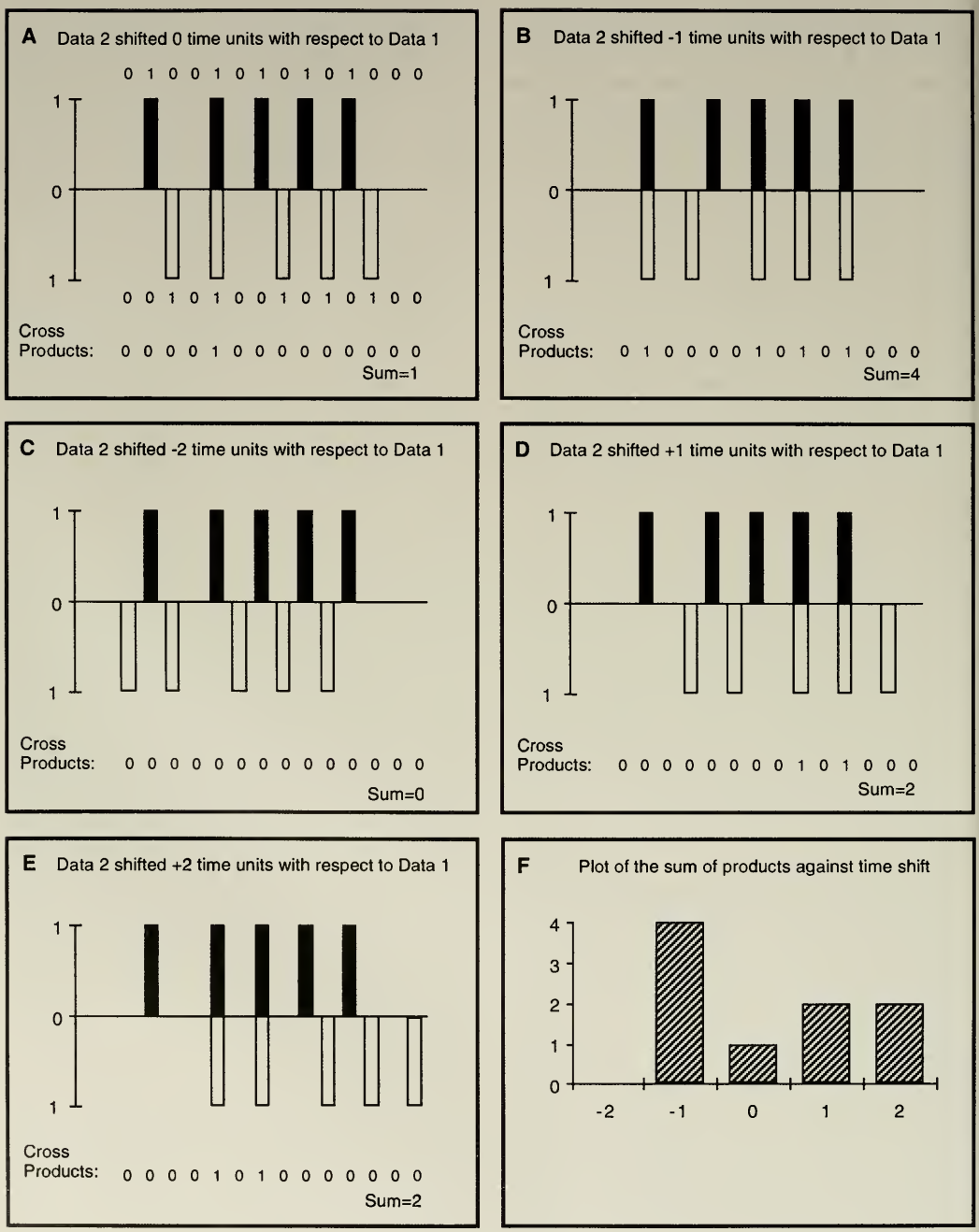

Figure 1. Cross-correlation using two ultrashort sections of synthetic data in binary form. Such data sets are produced if the peaks of half-wave rectified electromyographic (EMG) activity are reduced to point processes indicating the presence or the absence of a spike peak; the example shown could represent the spikes in a single burst of EMG activity. In (A), the two data series (shown both as binary and as graphical data) are initially correctly aligned in time (zero time shift or t_0). At each point in time, the product of the values in the two series is obtained and this is then summed. In (B), data set 2 is moved one unit back

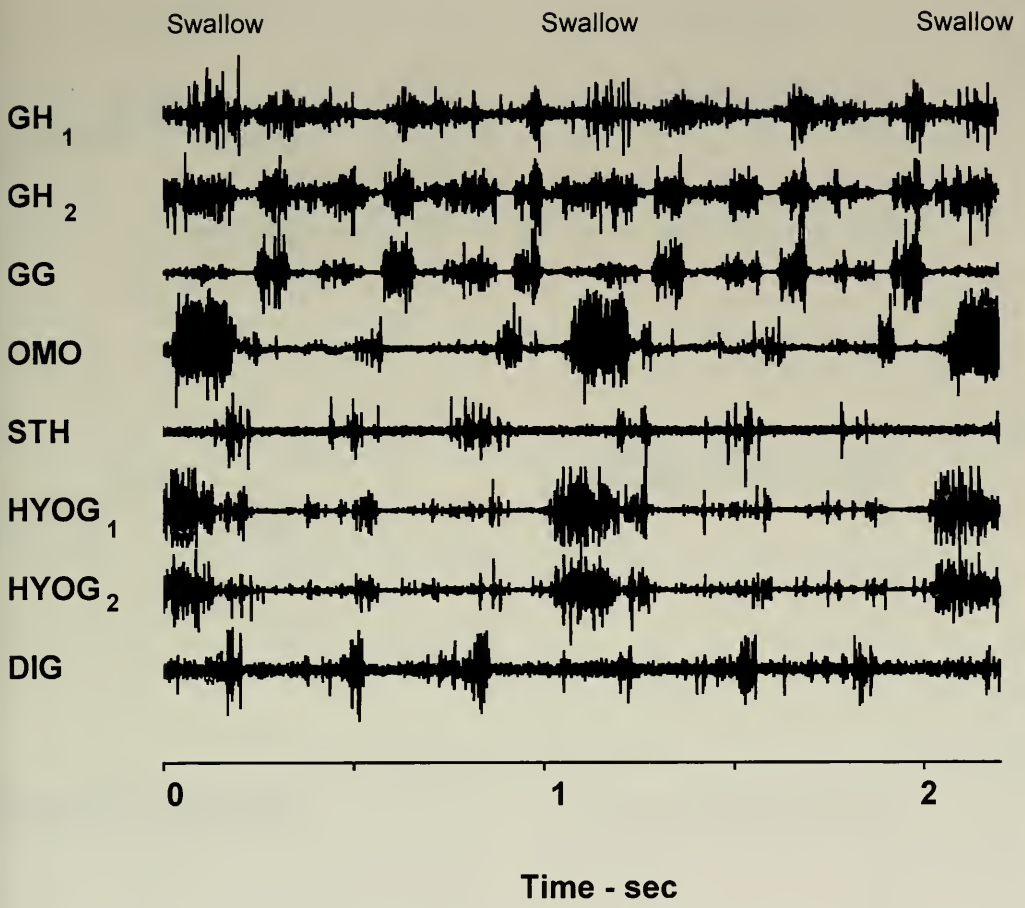

Figure 2. Raw electromyogram (EMG) signals recorded from representative muscles during drinking. In several muscles two sets of electrodes were inserted to establish that the signals recorded were not obviously site dependent within the muscle. Abbreviations used: GH, geniohyoid; GG, genioglossus; OMO, omohyoid; STH, sternohyoid; HYOG, hyoglossus; DIG, digastric; subscript numbers identify two electrodes in the same muscle. All muscles are unilateral.

a brainstem pattern generator. Consequently, the assumption was that synchrony would also be present between coactivated muscles during suckling and drinking. However, most cross-correlograms between muscle activities showed no evidence for intraburst synchronization during either suckling or drinking (Fig. 3; Banks and Thexton, 1999). Nevertheless, peaks that were consistent with synchronization were evident in the cross-correlograms of sternohyoid, geniohyoid, and omohyoid activities, with the cross-correlation between sternohyoid and omohyoid

←

in time (t_{-1}) relative to data set 1; again the products of the values in the two series are obtained and summed. In (C), the process is repeated with data set 2 moved back two units back in time (t_{-2}) relative to data set 1. In (D), the process is repeated with a time shift of +1 time units (t_1) and in (E) with a time shift of +2 time units (t_2). In (F), the sum of cross products (a count of those spikes that coincided at a particular time shift) is plotted against the time shift. In these synthetic data, the maximum correspondence between spikes in the two data sets occurred with a shift of t_{-1}. In practice two data sets each at least 15,000 time units long, containing many hundreds of spike locations, are cross-correlated.

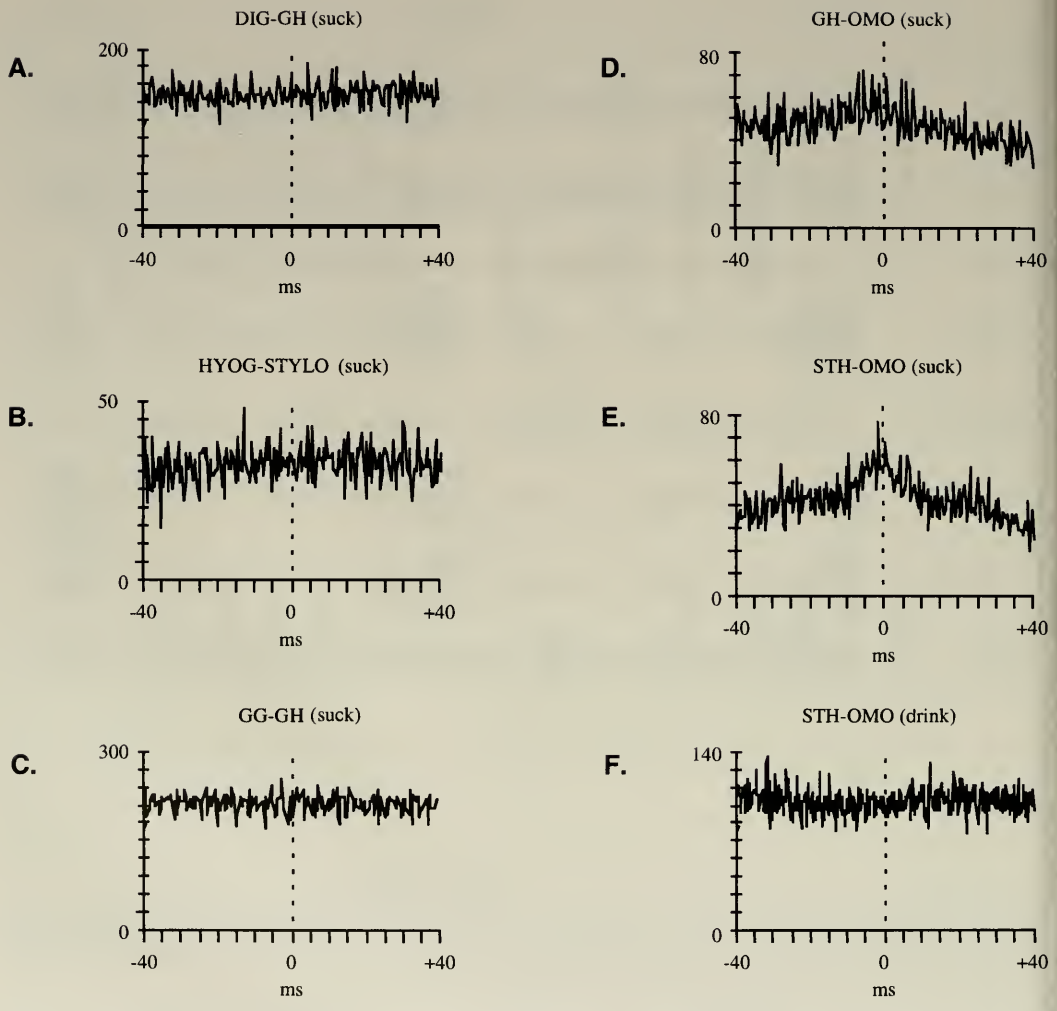

Figure 3. Cross-correlations between signals detected by different pairs of electrodes in one animal. Abbreviations used: DIG, digastric; GH, geniohyoid; HYOG, hyoglossus; STYLO, styloglossus; GG, genioglossus; OMO, omohyoid; STH, sternohyoid. The horizontal axis indicates time shift relative to zero time shift (t_0). Examples of cross-correlations that were commonly found in suckling are shown in (A), (B), and (C). Some evidence of short-term synchronization (elevation of central region ± 2 milliseconds) in suckling is present in (D) and stronger evidence is present in (E). In (F), the activities in the same muscles as in (E) were recorded during drinking and were cross-correlated but with no sign of a central peak.

providing the clearest evidence of the presence of synchronization.

Before dealing with the significance of this finding, it is necessary to comment briefly on its validity. First, the results shown in Figure 3E indicate that the cross-correlation method used in this paper was intrinsically capable of detecting synchronization within the recorded EMG signals. However, motor neurons are activated from multiple sources within the central and peripheral nervous systems and not all the motor neurons supplying units in a given muscle are subject to the same neural influences. Consistent with this, some motor units have different tasks from others within the same muscle. If EMG activity is recorded with an intra-

muscular wire electrode (which only records from a limited number of motor units) the record will represent a restricted sample of the different motor units within that muscle. If, by chance, the sample from one of the two muscles being cross-correlated does not include motor units that receive drive synchronous with the sample in the other muscle, then the cross-correlograms will be flat. This suggests that those motor units, the activity of which generated flat correlograms, were essentially firing randomly in time. However, such correlograms do not prove that other motor units within the muscles would not exhibit synchrony. Therefore, the general failure to detect signs of synchrony in this study is best interpreted as indicating a scarcity of synchronized units in most coactive muscles, with synchronized units simply being more frequently found in the coactive geniohyoid, sternohyoid, and omohyoid muscles during suckling.

One possible scenario is that a large number of neurons and synapses intervene between the CPG neurons generating the rhythmic activity and most of the motor neurons receiving that rhythmic drive. Because of the nonlinear input–output relations at each synapse, considerable temporal dispersion of the signals would then occur and the original synchronous drive would become diluted by other influences also acting at those synaptic relays. Thus, although the rhythmic drives to the motor neurons of the different coactive muscles would still be expected to wax and wane together, little of the intraburst spike generation would still be synchronous in the coactive muscles. However, this mechanism would not be consistent with the abrupt "on" and "off" of the bursts seen in the recorded EMG activity (Fig. 2).

Thus, a problem may exist with the concept of a CPG producing the activities of suckling or drinking purely by supplying a rhythmically fluctuating drive to the different motor neuron groups producing the EMG pattern seen in Figure 2. In fact, the absence of consistent evidence for synchrony (Fig. 3) suggests that the drive from the CPG may not directly supply series of action potentials that produce a cumulative depolarization of most of the motor neurons and, therefore, most of the spike production in the coactive muscles. However, if the central pattern generator functioned as an on–off switch, simply triggering the motor neurons into becoming their own independent burst generators, no synchronization would occur between intraburst spikes in coactive muscles. That situation can arise when motor neurons are simply triggered to produce long-lasting depolarizations known as plateau potentials. Although such potentials are well known in invertebrates (Croll et al., 1985), they have only relatively recently been described as occurring in mammals. It is of particular interest that these potentials have been found in mammalian motor nuclei involved in generating the movements of feeding (Mosfeldt Laursen and Rekling, 1989; Rekling and Feldman, 1997).

Whatever the mechanisms involved in generating the rhythmic movements, the results clearly do not support the initial ontogenetic hypothesis, that the EMG signals in the more mature and probably cortically directed activity of drinking would show more synchronization than in suckling. However, suckling is an evolutionary novelty (Clark and Smith, 1993; German and Crompton, 2000), whereas mammalian drinking is probably a substantially older evolutionary trait, functionally resembling drinking in other nonmammalian tetrapods. Consequently, the neural basis of drinking could reflect the evolutionary heritage of mammals and, in that sense, be less derived than suckling. The limited evidence for synchrony during suckling, which is absent in drinking, might reflect the contemporaneous evolution of suckling and the more developed central nervous system that characterizes mammals.

LITERATURE CITED

BANKS, D., AND A. J. THEXTON 1999. Evidence for pre-synaptic synchronization of electromyographic activity in oral musculature during suckling in mini pigs. British Neuroscience Association Abstracts, **15:** 44.

BREMER, F. 1923. Physiologie nerveuse de la mastication chez le chat et le lapin. Archive internationale de Physiologie, **21:** 309–352.

CLARK, C. T., AND K. K. SMITH. 1993. Cranial osteogenesis in *Monodelphis domestica* (Didelphidae) and *Macropus eugenii* (Macropodidae). Journal of Morphology, **215:** 103–114.

CROLL, R. P., M. P. KOVAC, AND W. J. DAVIS. 1985. Neural mechanisms of motor program switching in the mollusc Pleurobranchaea. II. Role of the ventral white cell, anterior ventral, and B3 buccal neurons. Journal of Neuroscience, **5:** 56–63.

DATTA, A. K., AND J. A. STEPHENS. 1990. Synchronization of motor unit activity during voluntary contraction in man. Journal of Physiology, **422:** 397–419.

DELLOW, P. G., AND J. P. LUND. 1971. Evidence for central timing of rhythmical mastication. Journal of Physiology, **215:** 1–13.

GAMPER, E. 1926. [In the film of:] The Human Mid-Brain. British Film Institute. London.

GEORGOPOULOS, A. P. 1995. Current issues in directional motor control. Trends in Neurosciences, **18:** 506–510.

GERMAN, R. Z., AND A. W. CROMPTON. 2000. Ontogeny of feeding in mammals, pp. 449–457. *In* K. Schwenk (ed.), Feeding: Form, Function and Evolution in Tetrapod Vertebrates. San Diego, CA: Academic Press. xv + 537 pp.

GERMAN, R. Z., A. W. CROMPTON, D. W. HERTWECK, AND A. J. THEXTON. 1997. Determinants of rhythm and rate in suckling. Journal of Experimental Zoology, **278:** 1–8.

HALL, M. 1833. On the reflex function of the medulla oblongata and medulla spinalis. Philosophical Transactions of the Royal Society, London, **132:** 635–665.

IRIKI, A., S. NOZAKI, AND Y. NAKAMURA. 1988. Feeding behavior in mammals: corticobulbar projection is reorganised during conversion from sucking to chewing. Developmental Brain Research, **44:** 189–196.

LUND, J. P., AND P. G. DELLOW. 1971. The influence of interactive stimuli on rhythmical masticatory movements in rabbits. Archives of Oral Biology, **16:** 215–223.

MISHIMA, K., K. SASAMOTO, AND M. OHTA. 1982. Amygdaloid or cortical facilitation of antidromic activity of trigeminal motoneurons in the rat. Comparative Biochemistry and Physiology. A, Comparative Physiology, **73:** 355–359.

MONNIER, M., AND H. WILLI. 1953. Die integrative Tätigkeit des Nervensystems beim mesorhombenspinalen Anencephalus (Mittelhernwesen). Monatsschrift der Psychiatrie und Neurologie, **126:** 239–273.

MORIYAMA, Y. 1987. Rhythmical jaw movements and lateral ponto-medullary reticular neurons in rats. Comparative Biochemistry and Physiology. A, Comparative Physiology, **86:** 7–14.

MOSFELDT LAURSEN, A., AND J. C. REKLING. 1989. Electrophysiological properties of hypoglossal motoneurons of guinea-pigs studied in vitro. Neuroscience, **30:** 619–637.

OHTA, M., S. ISHIZUKA, AND K. SAEKI. 1989. Corticotrigeminal motor pathway in the rat—II. Anterio- and retrograde HRP labeling. Comparative Biochemistry and Physiology. A, Comparative Physiology, **94:** 405–414.

OHTA, M., AND K. SAEKI. 1989. Corticotrigeminal motor pathway in the rat—I. Antidromic activation. Comparative Biochemistry and Physiology. A, Comparative Physiology, **94:** 99–104.

REKLING, J. C., AND J. L. FELDMAN. 1997. Calcium-dependent plateau potentials in rostral ambiguus neurons in the newborn mouse brain stem in vitro. Journal of Neurophysiology, **78:** 2483–2492.

SEARS, T.A., AND D. STAGG. 1976. Short term synchronization of intercostal motoneurone activity. Journal of Physiology, **263:** 357–381.

THEXTON, A. J., A. W. CROMPTON, AND R. Z. GERMAN. 1998. Transition from suckling to drinking at weaning: a kinematic and electromyographic study in miniature pigs. Journal of Experimental Zoology, **280:** 327–343.

SONOMICROMETRY AND KINEMATIC ESTIMATES OF THE MECHANICAL POWER OF BIRD FLIGHT

DOUGLAS R. WARRICK,[1] BRET W. TOBALSKE,[2] ANDREW A. BIEWENER,[2] AND KENNETH P. DIAL[1,3]

ABSTRACT. To improve our measurements of mechanical power output of flying birds, we examined the congruency between two recording techniques of pectoralis muscle-length change (sonomicrometric and kinematic) used in empirical measures of the mechanical power output of black-billed magpies flying over their full range of flight speeds (0–14 m/s) in a variable-speed wind tunnel. Simultaneous recordings of pectoralis muscle force (obtained from strain gauges attached to the muscle's humeral insertion) were integrated with the two recording techniques to generate a work-loop for each wingbeat. Although the overall shapes of the power curves obtained by the two techniques were similar, estimates of muscle length change using sonomicrometric data were, on average, very similar to those obtained by one-axis kinematics and slightly lower than those obtained by two-axis kinematics. Given these small differences, our sonomicrometry measurements indicate that kinematic estimates of muscle length change, when combined with humeral strain measurements, can provide an accurate estimate of pectoralis work and power output during bird flight. However, a key advantage of sonomicrometry is that it provides a direct measure of the lengthening and shortening of the muscle's fascicles relative to their rest length, which is not possible to derive from wing motion alone.

INTRODUCTION

The cost of flight is central to understanding the biology of any flying animal. In particular, without knowing the metabolic costs of flight, conclusions obtained from time and energy budget studies of birds regarding selection for migration habits, optimal foraging behaviors, and reproductive strategies will remain unclear (Welham and Ydenberg, 1993; Hedenström and Alerstam, 1995).

Various approaches have been taken to address the metabolic power requirements of flight. The mechanical cost of flight may be modeled using aerodynamic theory (Pennycuick, 1975; Rayner, 1979), and the metabolic cost of flight can then be inferred using estimates of the muscular efficiency of converting metabolic energy to mechanical work (Pennycuick, 1989; Thomas and Hedenström, 1998). Metabolic power has been measured directly over a limited midrange of flight speeds by means of oxygen consumption studies of birds flying in a wind tunnel (Tucker, 1968, 1972; Berger et al., 1970; Torre-Bueno and LaRochelle, 1978; Rothe et al., 1987). Other methods have included measurements of doubly-labeled water (Hails, 1979; Flint and Nagy, 1984) and heart rate (Berger et al., 1970; Butler et al., 1977) of birds in flight. More recently, infrared imaging has also been used to assess metabolic power (Speakman et al., 1997; Ward et al., 1997). However, many of these studies have been restricted to a narrow range of flight speeds and flight behavior, preventing a complete picture of metabolic cost versus flight speed. Thus, models of mechanical power are the most useful means currently available for predicting flight costs over a wide range of speeds. The wide acceptance and use of such mechanical power models (Welham and Ydenberg, 1993; Pennycuick, 1997) suggests that it may prudent to provide an independent test of their accuracy.

In a previous study (Dial et al., 1997),

[1] Division of Biological Sciences, University of Montana, Missoula, Montana 59812.

[2] Concord Field Station, Harvard University, Bedford, Massachusetts 01730.

[3] To whom reprint requests should be addressed.

the mechanical power output of black-billed magpies (*Pica pica*) was measured using force-calibrated strain gauges attached to the deltopectoral crest (DPC), which serves as the insertion site of the primary downstroke flight muscle (musculus pectoralis) on the humerus. These force measurements were integrated with kinematics of the wing to estimate the mechanical power output of the pectoralis and, hence, the whole bird. When appropriate kinematic parameters (Tobalske and Dial, 1996; Tobalske et al., 1997) are incorporated in models based on aerodynamic theory, predicted power output agrees reasonably well with our earlier measurements of mechanical power output of magpies (Rayner, 1999). Our previous measurements used kinematic estimates of pectoralis length change. However, some questions remain regarding estimates of the magnitude and timing of pectoralis length change inferred from distal wing movement in the work of Dial et al. (1997). In the present study, we reassess the mechanical power output of magpies based on direct sonomicrometric measurements of pectoralis fascicle length changes and compare these data directly with corresponding kinematic estimates based on wing excursion.

MATERIALS AND METHODS

Bird Training and Wind Tunnel Trials

Three black-billed magpies were trained to fly in a wind tunnel (Tobalske and Dial, 1996) over a range of flight speeds (0–14 m/s) that represented the full extent that the animals were willing to fly. Birds were housed in the University of Montana's animal facility and given food and water ad libitum. The protocol for all facilities, care, and surgical procedures was approved by the Institutional Animal Care and Use Committee established at the University of Montana.

Force–Strain Measurements

Birds were anesthetized (25 mg/kg ketamine and 2 mg/kg xylazine, supplemented as needed) and the feathers removed over the left shoulder and the middle of the back between the scapulae. A 15-mm incision was made in the skin overlying the DPC, which was then exposed by gently parting the fascicles of the deltoid muscle. The dorsal surface of the DPC was prepared by lightly scraping away the periosteum and then swabbing the underlying bone surface with methyl-ethyl ketone to remove any residual tissue and to dry the site. A strain gauge (single-element metal foil type FLE-05-11, Tokyo Sokki Kenkyujo, Ltd., Tokyo, Japan) was then attached to the dorsal surface of the DPC using self-catalyzing cyanoacrylate adhesive, with its principal axis aligned approximately 15° proximal to the perpendicular axis of the humeral shaft (Dial and Biewener, 1993). Strain gauge lead wires (36 gauge, Teflon insulated; Micromeasurements Inc.) ran beneath the deltoid and subcutaneously to a miniature connector plug (Microtech FG-6 [×2]) that was mounted on the back of the bird by suturing the plug's epoxy base securely to the intervertebral ligaments using 0 silk. The skin was drawn snugly around the protruding connector plug, and the surrounding skin was covered with elastic surgical tape.

The DPC strain signals were transmitted to bridge amplifiers (Vishay model 2120A, Micromeasurements Inc.) via two light-weight shielded cables running through a small hole in the top of the wind tunnel test section. Raw in vivo DPC strains, sonomicrometry signals, and electromyograms (see below) were sampled at 5,000 Hz by a Keithley Instruments A/D converter and stored in a computer. To monitor the quality of the recordings during the experiment, live data from each trial were printed on a Gould 2400 chart recorder.

In past studies, the tensile strains experienced by the DPC during flight were calibrated to pectoralis force in situ after flight trials. However, in all three birds, after flights at all eight speeds had been recorded, either the bonding of the strain

gauge to the bone or the strain gauge itself failed. Rather than attempting to reattach the strain gauge to the DPC in the same position or use another strain gauge for calibration, we chose to leave the DPC strain data uncalibrated as raw voltages. Although this precluded a quantification of pectoralis force and calculation of muscle work, relative work-loops derived from raw DPC strain voltages coupled with fascicle length changes (from sonomicrometry, next section) provide valuable information concerning the relative change in mechanical power as a function of flight speed (henceforth "uncalibrated power"). To average the data for all three birds, the uncalibrated power required for flight at all speeds was normalized relative to the maximum ("relative") power recorded for each individual, which for all three birds was observed during hovering flight.

Sonomicrometry

Sonomicrometry crystals (2-mm SL-2, Triton Inc.) were implanted in the anterior region of the left pectoralis muscle of each bird in a position thought to represent best the contraction of the entire muscle (as suggested in Shigeoka [1999]). Each crystal was mounted on a stainless steel wire featuring two anchoring points ("loops"). After a skin incision was made to expose the pectoralis muscle, the muscle's fascicles were parted using surgical scissors, creating two openings into which the crystals were inserted. Once aligned, the crystals were held in place by suturing the two anchoring loops to the surrounding muscle tissue and fascia. The wires for the crystals were passed subcutaneously to the dorsal side of the bird and connected to the back plug. After closing the incision, the birds were allowed to recover from the anesthesia for approximately 24 hours. The resting length between the crystals (resting fascicle length, L_r) was taken while the bird was standing at rest, with its wings held against its body. To compensate for the faster transmission of the ultrasound pulse through the epoxy lens of each crystal, a 0.74-mm offset was added to all length measurements. Total fascicle length change (L) for the pectoralis was calculated as:

$$L = L_l/L_{lr} \cdot L_r, \quad (1)$$

where L_l is the change in distance between the sonomicrometry crystals, L_{lr} is the local resting length between the crystals, and L_r is the total (average) resting length of the pectoralis muscle fascicles measured to with 0.5 mm using digital calipers.

Work-loops

The work done throughout one wingbeat cycle (W_{wb}) was calculated by integrating the change in DPC strain with the change in fascicle length:

$$W_{wb} = [F_n(L_n - L_{n+1})] \quad (2)$$

where F is the DPC strain voltage and L is the pectoralis fascicle length at the same point in the time series n. Only that part of the wingbeat cycle during which positive strain voltages were recorded (i.e., when the gauge measured tensile strain, rather than the compressive strain experienced by the DPC during upstroke) was used to calculate relative pectoralis work. Relative work (volt × mm) was then divided by the cycle time (t) for each individual work-loop to obtain an estimate of relative muscle power (Fig. 1). Measurements of relative power were obtained over a range of speeds, based on averages at each speed obtained from a minimum of two wingbeats (for magpie 3 during hovering flight) and a maximum of 23 wingbeats (magpie 3 at 8 m/s).

Kinematics

Each trial was videotaped from lateral (Panasonic S-VHS) and caudal (Sony Hi-8 Handicam) views. Video from each trial was captured on computer (Iomega Buz Video Capture), and bitmap still images (60 fields per second [fps]) were digitized using NIH Image. The x and y coordinates of the bird's eye, tail base, and wing tip were scaled using a 2-cm grid background

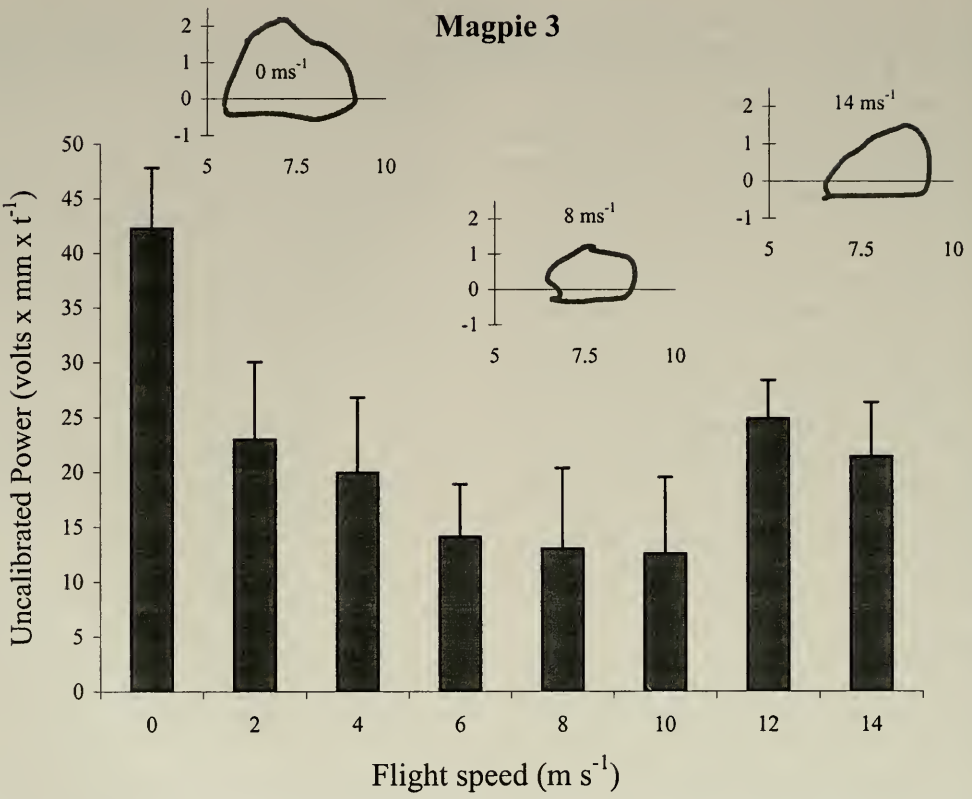

Figure 1. Work-loops (insets) created by plotting the change in tensile strain (y axis, in volts not calibrated to force) of the deltopectoral crest by the fiber length (*x* axis, mm). The area of the work-loop above zero volts was integrated to calculate work done by the pectoralis. Dividing this area by the wingbeat cycle time yields a measure of relative power. The mean relative power output (± SDs) of magpie 3 is shown over the range of flight speeds.

located behind the bird, adjusted for camera parallax, and imported into Microsoft Excel. The eye and base of the tail were used to establish the orientation of the body from which the excursion of the wing tip was measured (Fig. 2). From lateral views, the excursion of the wing tip was calculated both one dimensionally (in the dorsoventral plane, following Dial et al. [1997]; Fig. 2A) and two dimensionally (dorsoventral and anteroposterior planes; Fig. 2B). Wing-tip excursion was used to estimate DPC excursion and, hence, change in pectoralis fiber length by the formula $L = \sin^{-1}(h/b)r$, where h is the wing-tip excursion (either one or two dimensionally), b is wing length measured from the wing tip to the glenoid, and r is the distance from the glenoid to the DPC. For those wingbeats in which simultaneous sonomicrometric and kinematic data were available ($n = 20$; magpie 1, $n = 9$; magpie 2, $n = 7$; magpie 3, $n = 5$), fascicle length changes obtained using the two methods were compared using reduced major axis regression.

RESULTS

Sonomicrometry and strain-gauge data were obtained from magpies 2 and 3 over the entire speed range, whereas, because of equipment failure, measurements of magpie 1 were only obtained over speeds from 0 to 8 m/s.

As was the case in our earlier study (Dial et al., 1997), all three birds exhibited

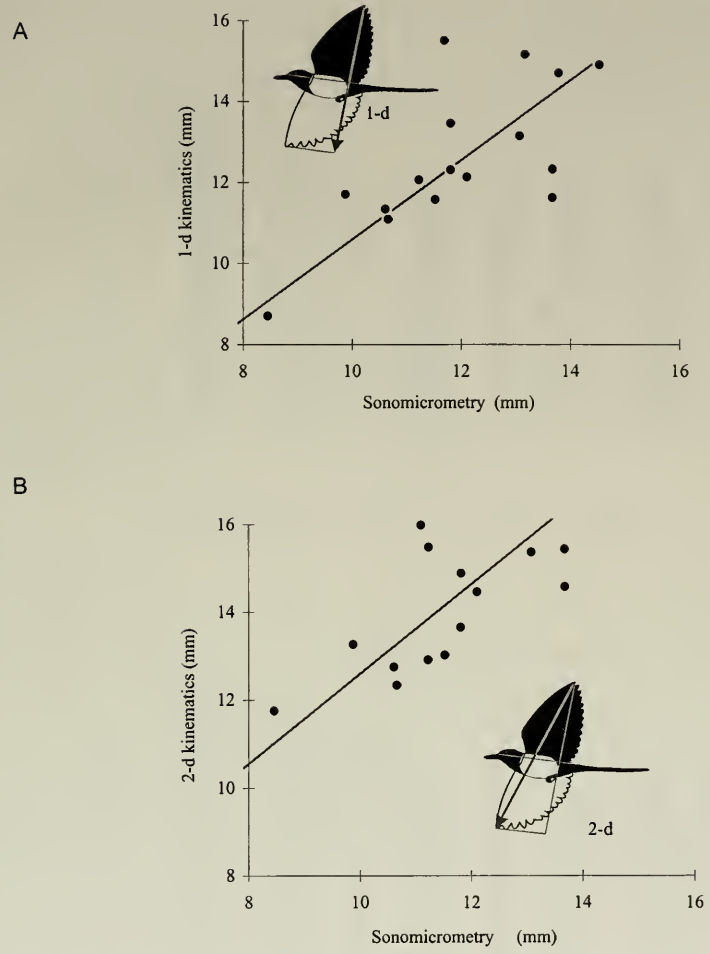

Figure 2. Wing kinematics (insets) as measured from lateral video images (60 fields per second). The one-axis (dorsoventral excursion only) wingbeat amplitude (2A inset) was measured as in Dial et al. (1997), whereas the two-axis excursion (2B inset) also incorporated the anteroposterior movement of the wing. (A) Correlation of one-axis kinematic estimate of fiber length change (i.e., deltopectoral crest excursion) with fiber length change as measured by sonomicrometry. (B) Correlation of two-axis kinematic estimate of fiber length change with fiber length change as measured by sonomicrometry.

the greatest muscle power output during hovering flight (Fig. 1). Minimum power speeds differed between the three birds, being 6 m/s, 4 m/s, and 10 m/s, respectively, for magpies 1, 2, and 3. However, the low power output of magpie 3 at 10 m/s was probably due to a ceiling effect, because this bird insisted on flying close (<30 cm) to the ceiling of the test chamber. This likely resulted in the disruption of tip vortices and consequent reduction in drag, causing the low observed power output.

Strain estimated from single-axis kinematics was positively correlated with strain measured for the same muscle contraction using sonomicrometry. Although significant, the correlation was not strong (r^2 = 0.36; $y = 0.98x + 0.78$; $P = 0.003$, df = 18; Fig. 2A). Fiber length changes estimated from two-axis kinematics and sonomicrometry exhibited a stronger correla-

tion (r^2 = 0.52, y = 1.02x + 2.4; P < 0.0001, df = 18; Fig. 2B).

Our sonomicrometric measurements of fascicle strain reported here were 10% greater than those estimated in our previous study of magpie flight based on wingbeat kinematics (Dial et al., 1997). Across all speeds, mean fascicle strain ($L/L_r \cdot 100$) obtained from sonomicrometry averaged 27.6% for magpie 1, 36.2% for magpie 2, and 35.0% for magpie 3. The greatest fascicle strain was recorded during hovering flight for magpies 1 and 3 (32.2 ± 1.1% and 46.0 ± 0.9%, respectively), whereas magpie 2 exhibited the greatest strain at 14 m/s (43.5 ± 0.3% [SE]).

Averaging the relative muscle power among birds (by first normalizing each individual's uncalibrated relative power output at each speed to the maximum for that individual) yielded relative power curves similar to those that we previously reported (Figs. 4A, B). When the maximum relative power obtained for magpies in this study is set to the maximum power (W) reported in Dial et al. (1997), Figure 4B reveals a similar shape for the power curves derived from the two approaches (sonometric versus kinematic). This is particularly the case over the intermediate speed range (8–12 m/s), where a marked increase in mean power output at 8 m/s is observed in both sets of data. In the present study two of the three birds exhibited this increase, whereas power increased at 8 m/s for all three individuals in the previous study.

DISCUSSION

Our new results for magpies, obtained from direct measurements of muscle length change using sonomicrometry, but relying on a relative estimate of pectoralis force and, thus, power output, generally agree well with the measurements of mechanical power output that we obtained in our previous study using kinematic estimates of muscle length change (Dial et al., 1997). For both data sets, power output was highest during hovering, dropped rapidly (~40%) at 2 m/s, reached minimum values at intermediate speeds, and then increased again modestly (~20%) at the fastest speeds (12 and 14 m/s). As was the case in our earlier study (Dial et al., 1997), minimum power speed varied among birds (6, 4, and 10 m/s for magpies 1, 2, and 3, respectively), and no bird exhibited minimum power at 8 m/s (Fig. 3A). Consequently, our sonomicrometry measurements provide support for the use of kinematic data (accounting for both humeral elevation–depression and protraction–retraction) to estimate muscle length change and, when combined with DPC strain measurements, to calculate muscle work and power output.

Given that all three birds possessed fairly uniform wing and tail dimensions, the variance in power curves among birds was most likely due to differences in flight behavior. As noted above, differences in the birds' flight positions in the test section of the wind tunnel also likely affected our estimated power output. For example, the low power obtained at 10 m/s for magpie 1 may well have resulted from its flying in close proximity to the ceiling of the tunnel. Individual differences may also reflect differing behavioral reactions that the birds exhibited having to fly at a fairly uniform speed because of the space restrictions of the wind tunnel. Magpies (or any bird, for that matter) rarely fly at steady speeds in the wild, instead exhibiting gait modulation and intermittent flight; when flying in a wind tunnel, magpies adopt a more regular pattern of gait modulation than they exhibit outdoors (Tobalske et al., 1997). It is likely that some birds are more adept (i.e., capable of assuming body postures and wing presentations that reduce their flight power requirement) than others at flying with greater modulation of their normal flight pattern. Nevertheless, our findings of a fairly flat power curve over much of this species' speed range are generally consistent with aerodynamic theory (Rayner, 1999; Fig. 4B; Appendix), existing

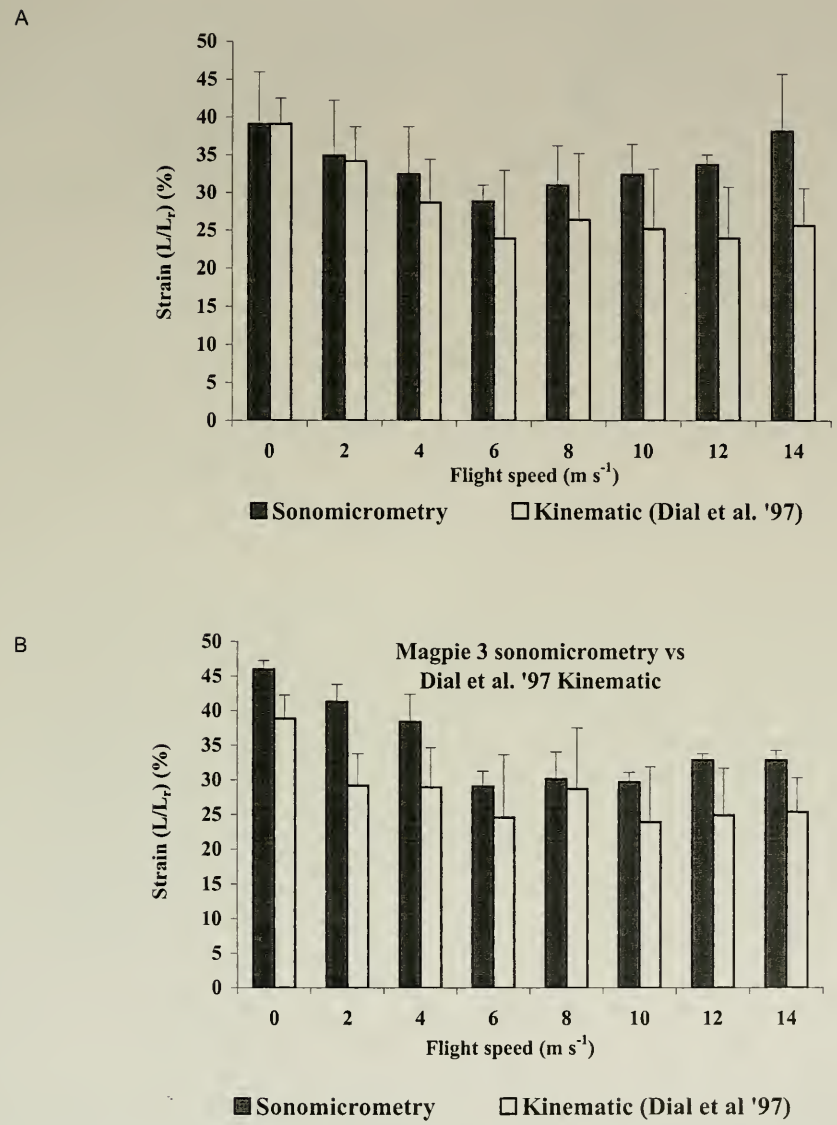

Figure 3. (A) Mean percent (standard deviations) pectoralis muscle strain (change in fiber length/resting fiber length × 100) of the three magpies over the range of flight speeds. (B) Mean pectoralis muscle strain for magpie 3 compared with pectoralis muscle strain estimated from distal wing kinematics from our previous study.

metabolic data (Ellington, 1991), and our earlier findings based on force measurements and wing kinematics.

Despite the general consistency of our measurements of pectoralis length change with those based previously on wing kinematics, sonomicrometry has a clear advantage by providing a direct measure of the lengthening and shortening of the muscle's fascicles relative to their resting length. This enables an assessment of the fractional length change of the muscle associated with active lengthening versus active shortening. Consistent with earlier ki-

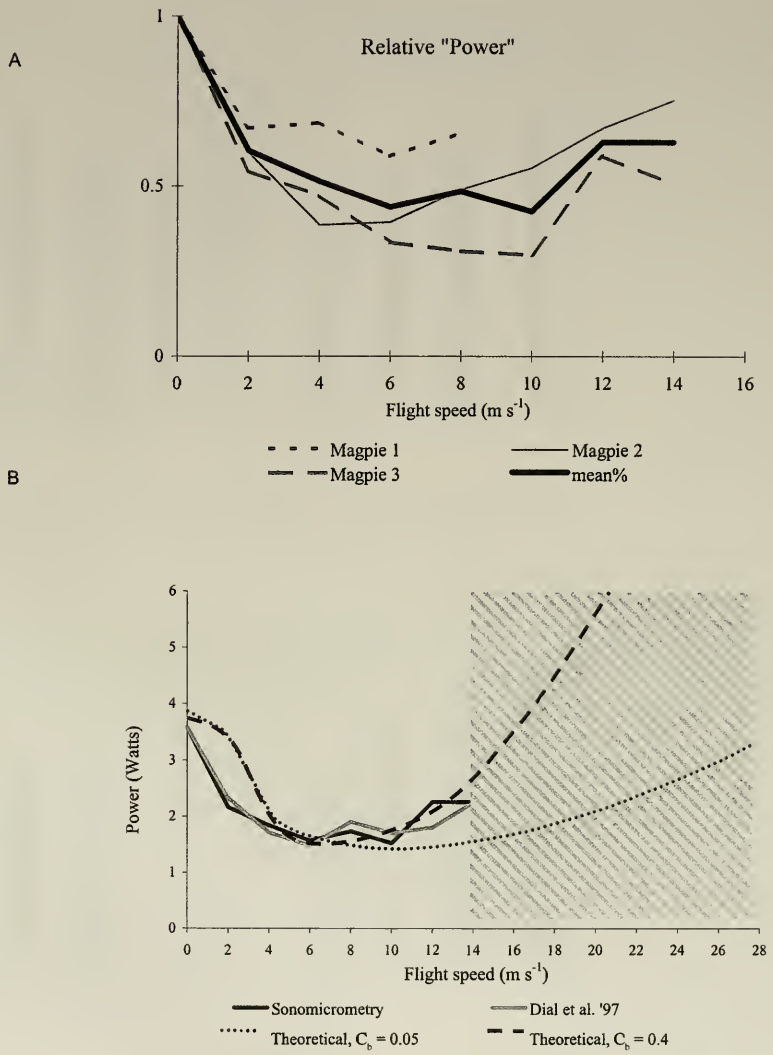

Figure 4. (A) Mean relative power (mean uncalibrated power for a bird at a flight speed normalized to the bird's maximum power output speed, which was 0 m/s in all cases) of all three magpies over the range of flight speeds. (B) Mean power output of magpies flying over the same range of speeds from Dial et al. (1997) and the present study. For purposes of comparing the shapes of the power curves, the uncalibrated relative power at hovering was set to equal the mean power at hovering from Dial et al. (1997). The theoretical power curve was derived from modified momentum jet theory, using a C_b coefficient of either 0.4 (dashed line upper; Pennycuick, 1989) or 0.05 (dashed line lower; Pennycuick et al., 1996) and an induced power factor of 1.2 (see Appendix). Note that although magpies seem to possess sufficient power to fly at speeds well above 20 m/s, their top sustainable speed in the wind tunnel was 14 m/s.

nematic estimates (Dial and Biewener, 1993) and recent sonomicrometry measurements of length changes in pigeons (Biewener et al., 1998), we find that pectoralis force development during the downstroke of magpies is achieved over a surprisingly large range of muscle length change (35–50% of resting length, over the range of recorded speeds). Moreover, this is achieved primarily by the muscle being lengthened (mean: 28%) versus being shortened (mean: 10%) relative to its rest-

ing length. This large length change is clearly linked to the pectoralis's function in generating considerable mechanical power by moving the wing through a broad range (approximately 80–110°) during the downstroke.

Classical aerodynamic theory predicts a U-shaped power curve for any flying object. Under steady-state conditions, the underlying physics of this relationship is inevitable. However, one conclusion suggested by analysis of our empirical data relative to theoretical power curves (Fig. 4B) is that magpies may not be able to fly fast enough to achieve the speeds necessary to incur a significant rise in power requirement, such as a U-shaped curve would predict. Our measurements of mechanical power output at 0 and 2 m/s might seem to suggest that magpies should be able to attain speeds of up to 18–28 m/s (Fig. 3B). However, the greater power output achieved at these very low speeds likely reflects nonsustainable flight performance and a significant anaerobic energy supply. Consistent with this interpretation, we found that well-trained birds (before surgery) rarely achieved, and could never sustain, 16 m/s in the tunnel. This is also consistent with observations of the maximum flight speeds recorded for magpies in the field being only 11 m/s (Tobalske et al., 1997), as well as our observation of a low variance in power output at higher speeds (Dial et al., 1997). We have argued that decreased variation in wingbeat kinematics and power output suggests a more constrained flight style as an animal approaches its limit of sustainable performance. Consequently, we interpret 14 m/s as this species' maximum sustained flight speed.

An alternative explanation for the observed maximum flight speed may be that the magpies were unable to generate sufficient thrust at speeds greater than 14 m/s. A bird engaged in flapping flight generates lift with its wings that provides both weight support (vertical component of aerodynamic force) and thrust (horizontal component). For lift to be produced, a portion of the wing must have a positive angle of attack relative to incident air. If, at faster speeds, the angular velocity of the wing during downstroke is not sufficient to maintain a positive angle of attack while directing the net aerodynamic force forward (i.e., providing thrust), the animal will be unable to sustain flight.

It is noteworthy that the empirical curve of mechanical power was generally similar to predicted curves at slow and intermediate speeds (Fig. 3B), particularly given that we used published values for induced power factor and drag coefficients in predicting the mechanical power required for flight in the magpie (Appendix). We assumed an induced power factor of 1.2, which gives an estimate of induced power during hovering that is approximately 30% lower than that that would result from vortex theory (Rayner, 1979; Ellington, 1984). However, a magpie flying in the closed-section flight chamber could have enjoyed a 27–31% reduction in power costs because of lift recirculation (Rayner, 1994; Tobalske and Dial, 1996). Thus, it would be unwise to use our data to address the validity of momentum jet theory versus vortex theory as applied to slow flight in birds. Further research into mechanical power output during free flight, in the absence of ground effects, therefore, would be worthwhile.

At fast speeds, our empirical data are less than predicted values obtained from a model using a coefficient of body drag = 0.4 (Pennycuick, 1989) and greater than those from a more recent model using a coefficient of body drag = 0.05 (Pennycuick et al., 1996). Assuming our estimates of induced and profile power are correct, this comparison suggests that the coefficient of body drag for the magpie should be somewhere between 0.4 and 0.05, and that the magpie has a relatively "dirty" or nonstreamlined shape compared to some bird species (Pennycuick et al., 1996). With regard to predictions of minimum cost of transport (work per unit distance,

or power divided by flight speed), which is generally expected by ecologists and others to define maximum range speed, or v_{mr}, it can be inferred from Figure 4B that predicted v_{mr} would differ greatly depending upon parasite drag. Using our empirical data, we calculate v_{mr} to be 12 m/s. In contrast, v_{mr} was 10 m/s using a coefficient of body drag of 0.4 and 18 m/s using a coefficient of body drag of 0.05. This brief analysis shows that a specific prediction of v_{mr} for a given bird species should be regarded with caution, if not distrust, unless direct measures of mechanical or metabolic power are used to support the prediction.

ACKNOWLEDGMENTS

K. P. D. and A. A. B. would like to thank A. W. "Fuzz" Crompton for his input and extraordinarily positive attitude toward our research efforts and life in general. We thank F. A. Jenkins, Jr., for the invitation to the Crompton Symposium and for the review by his editorial staff of this manuscript for publication. This project was funded by NSF-IBN-9507503 to K. P. D.

LITERATURE CITED

Berger, A. J., J. S. Hart, and O. Z. Roy. 1970. Respiration, oxygen consumption and heart rate in some birds during rest and flight. Zeitschrift für Vergleichende Physiologie, **66:** 201–214.

Biewener, A. A., W. R. Corning, and B. W. Tobalske. 1998. In vivo pectoralis muscle force—length behavior during level flight in pigeons (*Columba livia*). Journal of Experimental Biology, **201:** 3293–3307.

Butler, P. J., N. H. West, and D. R. Jones. 1977. Respiratory and cardiovascular responses of the pigeon to sustained level flight in a wind tunnel. Journal of Experimental Biology, **71:**7–26.

Dial, K. P., and A. A. Biewener. 1993. Pectoralis muscle force and power output during different modes of flight in pigeons (*Columba livia*). Journal of Experimental Biology, **176:** 31–54.

Dial, K. P., A. A. Biewener, B. W. Tobalske, and D. R. Warrick. 1997. Mechanical power output of bird flight. Nature, **390:** 67–70.

Ellington, C. P. 1984. The aerodynamics of hovering insect flight. V. A vortex theory. Philosophical Transactions of the Royal Society of London, Series B, Biological Sciences, **305:** 115–144.

———. 1991. Limitations on animal flight performance. Journal of Experimental Biology, **160:** 71–91.

Flint, E. N., and K. P. Nagy. 1984. Flight energetics of free-living sooty terns. Auk, **101:** 288–294.

Hails, C. J. 1979. A comparison of flight energetics in hirundines and other birds. Comparative Biochemistry and Physiology A, **6:** 581–585.

Hedenström, A., and T. Alerstam. 1995. Optimal flight speed of birds. Philosophical Transactions of the Royal Society of London, Series B, Biological Sciences, **48:** 471–487.

Norberg, U. M. 1990. Vertebrate Flight. Berlin: Springer-Verlag. 291 pp.

Pennycuick, C. J. 1975. Mechanics of flight, pp.1–75. *In* D. S. Farner and J. R. King (eds.), Avian Biology 5. London: Academic Press. xxii + 523 pp.

———. 1989. Bird Flight Performance: A Practical Calculation Manual. Oxford, United Kingdom: Oxford University Press. 153 pp.

———. 1997. Actual and "optimum" flight speeds: field data reassessed. Journal of Experimental Biology, **200:** 2355–2361.

Pennycuick, C. J., M. Klaassen, A. Kvist, and A. Lindstrom. 1996. Wingbeat frequency and the body drag anomaly: wind tunnel observations on a thrush nightingale (*Luscinia luscinia*) and a teal (*Anas crecca*). Journal of Experimental Biology, **199:** 2757–2765.

Rayner, J. M. V. 1979. A new approach to animal flight mechanics. Journal of Experimental Biology, **80:** 17–54.

———. 1994. Aerodynamic corrections for the flight of birds and bats in wind tunnels. Journal of Zoology, London, **234:** 537–563.

———. 1999. Estimating power curves for flying vertebrates. Journal of Experimental Biology, **202:** 3449–3461.

Rothe, H.-J., W. Biesel, and W. Nachtigall. 1987. Pigeon flight in a wind tunnel. II. Gas exchange and power requirements. Journal of Comparative Physiology B, **157:** 99–109.

Shigeoka, C. 1999. Regional muscle activity and contraction dynamics of the avian pectoralis during flight. M.S. thesis. University of Montana, Missoula. 83 pp.

Speakman, J. R., S. Ward, U. Möller, D. M. Jackson, J. M. V. Rayner, and W. Nachtigall. 1997. Thermography: a novel method for measuring the energy cost of flight? Journal of Morphology, **232:** 326.

Thomas, A. L. R., and A. Hedenström. 1998. The optimum flight speeds of flying animals. Journal of Avian Biology, **29:** 469–477.

Tobalske, B. W., and K. P. Dial. 1996. Flight kinematics of black-billed magpies and pigeons over a wide range of speeds. Journal of Experimental Biology, **199:** 263–280.

Tobalske, B. W., N. E. Olson, and K. P. Dial. 1997. Flight style of the black-billed magpie: variation in wing kinematics, neuromuscular con-

trol, and muscle composition. Journal of Experimental Zoology, **279:** 313–329.

TORRE-BUENO, J. R., AND J. LAROCHELLE. 1978. The metabolic cost of flight in unrestrained birds. Journal of Experimental Biology, **75:** 223–229.

TUCKER, V. A. 1968. Respiratory exchange and evaporative water loss in the flying budgerigar. Journal of Experimental Biology, **48:** 67–87.

———. 1972. Metabolism during flight in the laughing gull, *Larus atricilla*. American Journal of Physiology, **222:** 237–245.

VAN DEN BERG, C., AND J. M. V. RAYNER. 1995. The moment of inertia of bird wings and the inertial power requirement for flapping flight. Journal of Experimental Biology, **198:** 1655–1664.

WARD, W., U. MOELLER, J. M. V. RAYNER, D. M. JACKSON, W. NACHTIGALL, AND J. R. SPEAKMAN, 1997. Metabolic power requirement for starling *Sturnus vulgaris* flight. Journal of Morphology, **232:** 338.

WELHAM, C. V. J., AND R. C. YDENBERG. 1993. Efficiency-maximizing flight speeds in parent black terns. Ecology, **74:** 1893–1901.

APPENDIX 1.

Numerous assumptions are intrinsic to mathematical models of mechanical power in animal flight, and it is beyond the scope of this paper to compare the family of curves that could be generated using different aerodynamic theories (Pennycuick, 1975; Rayner, 1979; Ellington, 1984) and their associated estimates of lift and drag on a body and flapping wings. As an alternative, we modeled aerodynamic power using equations and simplifying assumptions in Norberg (1990), which were modified from the work of Pennycuick (1975) and Rayner (1979). Total power was calculated as the sum of induced, parasite, and profile power; thus, we neglected inertial power (Van den Berg and Rayner, 1995) and ventilation and circulation factors (Pennycuick, 1975). We selected an induced power factor of 1.2 (Pennycuick, 1975, 1989) even though induced power factors of 1.5 or 1.7 are predicted from vortex theory (Rayner, 1979; Ellington, 1984). For drag coefficients on the body and wings, we employed values from published sources (Pennycuick, 1975, 1989; Pennycuick et al., 1996; Rayner, 1979), and we treated the body as a flat plate (Pennycuick, 1975) rather than a tilted-cylinder (Rayner, 1979). Our predicted mechanical power curves should not be interpreted to represent the only, or best, curves that can be synthesized from existing theory.

Symbols and assumed values:

b = wing span = 0.573 m
C_b = drag coefficient for body, 0.4 (Pennycuick, 1989) or 0.05 (Pennycuick et al., 1996)
C_w = drag coefficent for wings, 0.02 (Rayner, 1979)
g = gravitational acceleration, 9.805 m s^{-2}
k = induced power factor, 1.2 (Pennycuick, 1975, 1989)
m = body mass = 0.174 kg
P_i = induced power during forward flight
P_{ih} = induced power during hovering
P_{pa} = parasite power
P_{pro} = profile power, assuming constant wing area and mean resultant velocity (Norberg, 1990).
P_f = total mechanical power during forward flight
P_h = total mechanical power during hovering
S = combined surface area of both wings = 0.064 m^{-2}
S_b = frontal area of body, 0.00238 m^{-2} (Pennycuick, 1989)
S_d = disk area, 0.2578 m^2
S_r = strip area at distance r from wing root
T = wingbeat duration, s, assumed wingbeat frequency of 7.5 Hz
t = proportion of wingbeat in downstroke (assumed 0.55)
V = flight velocity
V_i = induced velocity
V_r = resultant velocity on wing at strip distance r from wing root
W = body weight, 1.706 N
ϕ = wing amplitude in radians, assumed to be 1.57 (=90°)

ρ = air density, 1.115 kg m^{-3}.

To calculate total mechanical power during hovering flight:

$$P_h = P_{ih} + P_{pro} + P_{pa} \quad (3)$$

And during forward flight:

$$P_f = P_i + P_{pro} + P_{pa} \quad (4)$$

To calculate induced, parasite, and profile powers:

$$P_i = kW^2/2\rho v S_d \quad (5)$$

$$P_{ih} = kW^{3/2}/(2\rho v_i S_d)^{1/2} \quad (6)$$

$$P_{pa} = 0.5\rho v^3 S_b C_b \quad (7)$$

$$P_{pro} = \sum_{r = 0.01}^{0.25} [(1.77 \cdot 10^{-3})\ \rho b^3 \phi S_r v_r^3/t^2 T^3] \quad (8)$$

TRADE-OFF BETWEEN MODELING AND REMODELING RESPONSES TO LOADING IN THE MAMMALIAN LIMB

DANIEL E. LIEBERMAN[1] AND OSBJORN M. PEARSON[2]

ABSTRACT. This paper tests the hypothesis that cortical bone growth (modeling) and repair (Haversian remodeling) responses to exercise-induced mechanical loading vary according to loading and position within the skeleton. Higher rates of modeling and Haversian remodeling are predicted to occur in response to loading, but a trade-off is predicted between modeling and Haversian remodeling, with proportionately higher Haversian remodeling rates at distal than proximal midshafts, and proportionately higher modeling rates at proximal than distal midshafts. The hypothesis is tested with cross-sectional and histologic data from juvenile sheep (*Ovis aries*) who trotted at low speed (4 km/h) for 60 min/d on a treadmill for 90 days, compared with sedentary controls. Exercised sheep had higher periosteal modeling and Haversian remodeling rates than controls. In both groups, midshaft periosteal growth rates were higher in proximal than distal elements in inverse proportion to the area-normalized inertial cost of accelerating mass; midshaft Haversian remodeling rates were higher in distal than proximal elements in proportion to the same energetic cost. The results suggest that growing animals modulate modeling versus remodeling responses to loading at different skeletal locations in order to optimize cross-sectional strength relative to the kinetic energy cost of accelerating added mass.

INTRODUCTION

This paper tests a hypothesis initially proposed by Lieberman and Crompton (1998) about the processes by which bones optimize in vivo responses to mechanical loading. The observation that bones adjust dynamically to their functional environment (Wolff's law) has been well substantiated over the last 100 years despite a poor understanding of the high degree of variability that characterizes osteogenic responses to mechanical loading (see Lanyon and Rubin, 1985; Bertram and Swartz, 1991). Such variations are of special interest for understanding the general trend among most cursorially adapted mammals for distal limb elements to have smaller diameters than proximal elements, which gives the limb a tapered shape (Smith and Savage, 1956; Alexander, 1980, 1996; Currey, 1984). Limb tapering is almost certainly an adaptation to minimize the kinetic energetic cost of limb acceleration. At a given angular velocity, this cost for a limb segment is proportional to the product of its mass and the square of its moment arm (Hildebrand, 1985). However, limb tapering has a structural cost. By reducing bone mass, limb tapering decreases the second moment area (I) available to counteract bending forces that may account for approximately 75–95% of midshaft strains (Bertram and Biewener, 1988). If applied forces are similar in proximal and distal elements, then tapered distal elements will experience higher strains than proximal elements, potentially leading to the generation and propagation of microcracks and other structural damage that ultimately contribute to mechanical failure (Currey, 1970, 1984; Carter et al., 1981a,b; Martin and Burr, 1982, 1989; Burr et al., 1985; Burr, 1993; Mori and Burr, 1993). As a result, distal elements may have lower safety factors than proximal elements (Currey, 1984; Alexander, 1998).

Some mammals, most notably equids, have evolved structural adaptations to

[1] Department of Anthropology, Harvard University, Cambridge, Massachusetts 02138.

[2] Department of Anthropology, University of New Mexico, Albuquerque, New Mexico 87131.

avoid the potentially higher stresses that may result from limb tapering, including orientating distal elements in line with ground reaction forces to decrease bending (Gambaryan, 1974; McMahon, 1975; Biewener, 1983a, 1989, 1990; Biewener et al., 1988), shortening of distal elements to reduce their bending moments (Gambaryan, 1974; Alexander, 1977), and decreased curvature of distal elements to minimize compressive bending and buckling (Biewener, 1983a,b; Pauwels, 1980; Bertram and Biewener, 1992). However, many cursorially adapted mammals, including most ungulates, are characterized by tapered limbs with long distal elements that have high excursion angles (Gambaryan, 1974). These species are predicted to experience high functional strains in their distal elements and must compensate through other means.

The two most important in vivo processes by which distal and proximal elements can adapt differentially to functional loading are growth (referred to as modeling) and repair (Haversian remodeling). Modeling responses are the best studied. Modeling increases resistance to bending stresses by augmenting I so that a given force generates less strain (Wainwright et al., 1976). Bones model in response to mechanical loads through increases in periosteal apposition (Chamay and Tchantz, 1972; Goodship et al., 1979; Lanyon et al., 1982; Lanyon and Rubin, 1984; Rubin and Lanyon, 1984a,b, 1985; Biewener et al., 1986; Raab et al., 1991), and through inhibition of endosteal resorption (Woo et al., 1981; Ruff et al., 1994). The optimal way for bones to minimize mass and maximize I (which is a fourth-power function of bone radius), is to add mass periosteally and remove mass endosteally. Because marrow is 50% as dense as bone, the optimum diameter to thickness (D/t) ratio in mammals is predicted to be 4.6 (Alexander, 1981; Currey, 1984). One study of terrestrial mammals (Currey, 1984: 109–111) found the median D/t ratio to be approximately 4.4 (albeit with considerable variation), with a higher median value for the femur (5.6) and correspondingly lower values for the humerus and other more distal limb elements.

The other mechanism by which bones adapt to high functional loads is to increase the frequency of bone repair responses through Haversian remodeling. Haversian remodeling is a sequential activation of vascularborne osteoclasts on a resorption surface that cuts a channel through old bone, followed by circumlamellar deposition of new bone by osteoblasts around a central neurovascular channel (Frost, 1963; Martin and Burr, 1989). Haversian remodeling was once thought to be a mechanism for maintaining calcium homeostasis (de Ricqlès et al., 1991), but most calcium exchange occurs in osteocyte canaliculi and through remodeling of trabecular bone (Parfitt, 1988b). Instead, Haversian remodeling in cortical bone is probably an adaptation to strengthen bone by removing weakened tissue or reorienting its structure (Currey, 1970, 1984; Carter and Hayes 1976a,b, 1977a,b; Carter et al., 1981a,b; Martin and Burr, 1982; Schaffler et al., 1989, 1990). Although secondary osteonal (Haversian) bone is weaker in vitro than young primary osteonal bone (Currey, 1959; Carter et al., 1976; Carter and Hayes 1977a,b; Vincentelli and Grigorov, 1985; Schaffler and Burr, 1988), secondary osteonal bone is stronger than microcrack-damaged primary bone (Schaffler et al., 1989, 1990). Haversian remodeling may also increase elasticity and halt microfracture propagation (Currey, 1984). Several studies demonstrated that remodeling preferentially occurs in older regions of bones that have presumably accumulated more damage than younger bone (Frost, 1973; Bouvier and Hylander, 1981; Currey, 1984), and that loading significantly increases remodeling rates (Hert et al., 1972; Bouvier and Hylander, 1981, 1996; Burr et al., 1985; Schaffler and Burr, 1988; Mori and Burr, 1993; Lieberman and Crompton, 1998). However, the effectiveness of Haversian

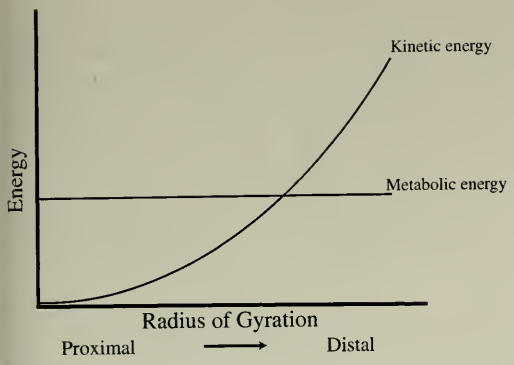

Figure 1. Predicted variation in kinetic versus metabolic energy costs of adding mass as a function of moment arm length (radius of gyration). Kinetic energy costs increase exponentially as a function of moment arm, but the metabolic energy cost of growing or repairing bone is predicted to be constant.

remodeling for counteracting functional strains has three major constraints. The basic multicellular unit through which Haversian remodeling occurs requires blood supply and cannot take place in avascular bone (de Ricqlès et al., 1991). Haversian remodeling also weakens bone by increasing porosity, although presumably less so than the effects of microfracture accumulation (Parfitt, 1988a; Schaffler and Burr, 1988; Martin, 1995). Finally, Haversian remodeling is an ineffective short-term solution to high in vivo strains because the remodeling sequence time of a basic multicellular unit is approximately 30–40 days from activation to termination (Martin and Burr, 1989).

Trade-Off Model

Modeling and remodeling are the most labile osteogenic responses to mechanical loading that generate phenotypically plastic variations in bone shape and strength. However, the effects of modeling and remodeling on limb bones are predicted to vary because of different costs and benefits, the most important of which are the energetic costs of moving bone tissue and the metabolic costs of growing new bone tissue (illustrated in Fig. 1). The dominant long-term cost of adding bone mass through modeling is most likely the kinetic energy (E_k) of accelerating and decelerating the added mass. During the swing phase, limbs function like pendulums in which E_k increases exponentially in more distal bones as a function of $m_i R_i^2$, where m_i is the mass of a given bone, i, and R_i is its radius of gyration (Hildebrand, 1985). In particular, limb acceleration becomes increasingly costly as the frequency of locomotion diverges more from the natural frequency of oscillation of the limb in which gravitational potential energy at the beginning of swing phase is converted to kinetic energy at midswing and then back to gravitational potential energy at the end of the swing phase. Therefore, the energetic costs of weight increments are influenced both by the location of added mass and by the divergence of stride frequency from the natural oscillation frequency of the limb. Thus, at a given speed, modeling responses to strain are more expensive (to the second power) in terms of kinetic energy in distal than in proximal elements (Myers and Steudel, 1985; see also Taylor et al., 1974). Such costs may be considerable in some species. Taylor and colleagues estimate that approximately 66% of E_k required for a horse to run at 15 m/s is spent to accelerate and decelerate the three distal limb segments, whose mass is approximately 80% bone tissue (Fedak et al., 1982, Heglund et al., 1982a,b).

An additional cost of modeling and remodeling is the metabolic energy cost (E_m) of growing and repairing bone tissue. Although cortical bone is probably expensive to synthesize, E_m for both primary and Haversian bone is likely to be constant regardless of skeletal location (see Fig. 1). However, Haversian remodeling is predicted to incur long-term higher metabolic costs than modeling because it leaves a bone insufficiently strong to resist further strain damage; in such cases, Haversian remodeling must reoccur regularly. Therefore, where mass and size do not impose high kinetic energetic costs, changes in cross-sectional geometry generated by modeling are probably more effective re-

sponses to loading than Haversian remodeling because they leave the bone permanently stronger and avoid any potential increases in porosity that Haversian remodeling causes. Further research is necessary to establish the metabolic costs of cortical bone growth and turnover.

On the basis of the above-defined costs and benefits, Lieberman and Crompton (1998) proposed a trade-off model to predict variations in modeling and Haversian remodeling rates in response to mechanical loading with respect to the nature of the applied forces (exercise) and skeletal location. In order to compare functionally comparable (homotypic) sites, the model focuses solely on bone midshafts, which are usually the location of highest bending forces (Biewener et al., 1986; Biewener and Taylor, 1986). Although both modeling and Haversian remodeling rates at bone midshafts are predicted to be higher in animals whose limbs experience more loading, the relative frequency of modeling and Haversian remodeling rates are expected to vary as a function of their radius of gyration (R; see Fig. 2). Because the energetic cost of modeling increases exponentially with increasing R, but the energetic cost of remodeling is hypothesized to remain constant, midshafts of more proximal elements are predicted to respond to applied forces with proportionately higher modeling rates than midshafts of more distal elements. In contrast, midshafts of more distal elements are predicted to respond to applied forces with proportionately higher Haversian remodeling rates than midshafts of more proximal elements.

Although Lieberman and Crompton (1998) provided preliminary data in support of the trade-off model, their sample size was small and their analysis did not include kinematic or kinetic data. This study tests the model more completely by comparing the cross-sectional geometry and histology of the midshaft femur, tibia, and metatarsal in a larger sample of exercised and sedentary control subjects. Two specific hypotheses are tested with kinematic, kinetic, and morphometric data. First, osteogenic responses to strains are predicted to vary according to loading and to position within the skeleton. In particular, higher rates of both modeling and Haversian remodeling are predicted to occur at homotypic sites in exercised animals than in matched controls. Second, a trade-off is predicted between modeling and Haversian remodeling responses, with proportionately higher Haversian remodeling rates at distal than at proximal midshafts, and proportionately higher modeling rates at proximal than at distal midshafts (standardized by body mass and element length). Forthcoming publications will present data on variations in peak strains at distal and proximal midshafts, and differences in trade-off responses between juvenile, subadult, and adult subjects.

MATERIALS AND METHODS

Subjects and Exercise Training

Eleven juvenile rams (*Ovis aries*; Dorset) were divided into control (n = 5) and exercise (n = 6) groups. One animal in the exercise group (lamb 10) had a respiratory infection for 4 weeks and was excluded from all calculations because it gained almost no weight during that period. Subjects were 40 days old at the start of the experiment, which lasted 89 days. For 1 week before the start of the experiment, the exercise group animals were habituated to run in an enclosed box on a Marquette 1800 treadmill (GE Medical Systems, Milwaukee, WI). Exercise group animals ran every day at a horizontal inclination for 60 minutes at a Froude speed of 0.5 (approximately 4 km/h), generating approximately 6,000 loading cycles per day per limb. At this speed, which is well below maximum running speed, the sheep's gait is a slow trot. Subjects were housed in raised 1.0-m^2 cages, limiting additional loading to minor locomotor activity and sedentary weight support. All subjects were fed the same quantity of hay per day

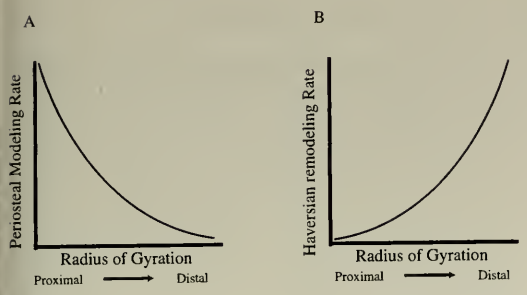

Figure 2. Predicted trade-off between periosteal growth (modeling) and Haversian remodeling (repair) rates in cortical bone as a function of the radius of gyration.

and water ad libitum. Fluorescent dyes that incorporate into bone mineral were administered by intraperitoneal injection at the start of the experiment (calcein, 20 mg/kg), on day 30 (oxytetracyline, 50 mg/kg), and on day 63 (xylenol orange, 25 mg/kg). Body mass was measured weekly. At the end of the experiment, total limb length from the greater trochanter of the femur to the ground was measured for each subject. The subjects were then euthanized, and their limbs bones were removed and defleshed. The radii of gyration from the femoro-acetabular joint to the midshaft of the femur, tibia, and metatarsal were measured at simulated midstance using a plastic tape measure (accurate to 1 mm) on each animal after death. Articular lengths of the femur, tibia, and metatarsal were measured using digital calipers (accurate to 0.01 mm). Femoral length was measured from the most proximal point on the femoral head to the line connecting the two distal condyles. Tibial length was measured from the center of the lateral condylar surface to the center of the distal articular surface. Metatarsal length was measured from the center of the proximal articular surface to the most distal point of the distal articular surface.

Cross-Sectional Geometry and Histologic Analysis

A 2-cm section was cut from the limb midshaft of each left femur, tibia, and metatarsal, and the marrow was removed. After measuring their densities, sections were fixed in 100% ethanol, and then simultaneously stained and dehydrated in a solution of 1% basic fuchsin in denatured ethanol under 20 mm Hg vacuum. Sample solution was changed every 24 hours for 1 week. Samples were then embedded in poly-methyl methacrylate polymer (Osteobed™, Polysciences Inc, Warrington, Pennsylvania). Two sections were cut from each embedded midshaft using an Isomet™ 1000 low-speed saw (Buehler Ltd., Lake Bluff, Illinois), affixed to glass slides with Epotek™ 301 epoxy (Epoxy Technology Inc., Billerica, Massachusetts), ground to approximately 100 μm thick using a Hillquist™ 1005 thin-section machine (Hillquist Inc, Fall City, Washington), polished using a Hillquist™ 900 grinder, and cover-slipped.

Cross-sections were analyzed using an Olympus™ SZH 10 stereozoom microscope with cross-polarized light and a Highlight™ 3000 Fluorescence (Olympus America, Mellville, New York). Digitized images were captured using a Pro-Series™ CCD technical video camera (Media Cybernetics, Silver Spring, Maryland) connected to a Macintosh™ 4440 computer with a Scion™ LG-3 capture board (Scion Corp., Frederick, Maryland). A version of NIH Image, v. 1.61 (W. Rasband, National Institutes of Health) with a macro written by M. Warfel (Cornell University), was used to calculate cortical area, medullary area, the maximum and minimum second moment areas (I_{max}, I_{min}), and the polar moment of inertia (J). These measurements were averaged for the two sections from each midshaft.

Haversian systems were counted and measured using NIH Image. Only complete secondary osteons with reversal lines were counted. Haversian density was computed as the total number of complete secondary osteons divided by cortical bone area. Linear periosteal growth was measured along the anterior, posterior, medial, and lateral axes of each section as the distance from the line of the calcein dye (ad-

ministered on day 1 of the experiment, see above) to the periosteal surface. Periosteal modeling rate (PMR) was calculated as the average of periosteal growth from the four axes divided by the number of days in the experiment. Haversian density and PMR were averaged for the two sections from each midshaft.

Kinematic Analysis

To acquire data on limb element orientation and angular velocity, three subjects were recorded at the end of the experiment (after surgery in which strain gauges were attached to the limbs; strain data are reported in a forthcoming paper). The subjects were videotaped in lateral view using a SONY™ DCR VX-1000 Handycam (Sony Corp., Tokyo, Japan) at 60 fields/s. Subjects were recorded approximately 4 and 24 hours after surgery, and ran with a normal gait (e.g., with full weight-bearing on all limbs and no signs of favoring one limb over another, showing no signs of lameness, distress, or discomfort). At least five complete gait cycles were digitized for each animal at 4.0 km/h. NIH Image was used to measure the orientation of the longitudinal axes of the femur, tibia, and metatarsal relative to the horizontal plane of the treadmill in each frame. These data were used to calculate angular velocity (ω) following the method of Winter (1990).

Analysis

All cross-sectional dimensions were standardized by body mass (calculated as mean mass during the final 3 weeks), and second moment areas were standardized by both body mass and element length. In order to evaluate osteogenic responses to mechanical loading in terms of kinetic energy costs, the area-normalized inertial cost (ANIC) of each midshaft cross-section (i) was estimated (following Winter, 1990) in joules as

$$\text{ANIC} = 0.5 I_i \cdot \omega_i^2$$

where

$$I_i = R_i^2 \cdot \text{CA} \cdot D$$

in which ω is the angular velocity in radians, R_i is the radius of gyration in meters, CA is cortical area expressed in m^2, and D is bone density in kg/m^3. Note that ANIC is not an estimate of the kinetic energy cost of accelerating the limb segment as a whole, but instead estimates the kinetic energy cost of accelerating the midshaft of each limb segment.

Because of the small sample sizes, and to avoid assuming normal distribution of the data, all tests of significance between elements and between groups were calculated using nonparametric methods (in most cases, Wilcoxon two-sample test).

RESULTS

Cross-Sectional Geometry

Cross-sectional properties of the femur, tibia, and metatarsal in the exercised and control sheep are summarized in Table 1, along with data on body mass and element length at the end of the experiment used to standardize comparisons. Little difference in element length and body mass (less than 1% in all cases) was found between exercise and control groups. No significant effects were found of exercise on overall cross-sectional area and shape: mass-adjusted medullary area (MA), CA, and midshaft shape as measured by I_{max}/I_{min} did not differ significantly between groups; CA/kg in the tibia was nearly significant at the $\alpha = 0.05$ level ($P = 0.08$). The value of I differed significantly between exercise and control groups in certain elements: distal elements had absolutely smaller and weaker midshafts than the femur, and the difference in I between exercise and control groups was more pronounced in the tibia and metatarsal than it was in the femur. When standardized for element length and body mass, I_{max}, I_{min}, and J were 25–29% higher in the exercised than in control groups in the tibia ($P < 0.05$); 20% higher in the metatarsal ($P = 0.05$–0.08); and 13–16% higher in the femur ($P = 0.17$–0.25).

TABLE 1. STANDARDIZED CROSS-SECTIONAL PROPERTIES.

Variable*	Controls		Exercised		% Difference†	*P* (Wilcoxon)
	n	Mean ± 1 SD	*n*	Mean ± 1 SD		
Body mass (kg)‡	5	38.56 ± 3.50	5	38.82 ± 2.20	0.7	0.60
Femur						
Articular length (mm)	5	174.3 ± 6.8	5	174.8 ± 3.0	0.3	0.60
MA/kg	5	2.77 ± 0.79	5	2.73 ± 0.79	−1.3	0.92
CA/kg	5	3.45 ± 0.42	5	3.57 ± 0.21	3.5	0.75
I_{max}/kg·L	5	0.57 ± 0.09	5	0.66 ± 0.08	16.2	0.25
I_{min}/kg·L	5	0.43 ± 0.07	5	0.49 ± 0.05	12.5	0.25
I_{max}/I_{min}	5	1.31 ± 0.09	5	1.35 ± 0.06	3.1	0.35
J/kg·L	5	0.99 ± 0.16	5	1.15 ± 0.12	14.6	0.17
Tibia						
Articular length (mm)	5	194.3 ± 7.6	5	193.7 ± 3.9	−0.3	0.92
MA/kg	5	0.94 ± 0.3215	5	1.05 ± 0.1224	11.8	0.60
CA/kg	5	3.17 ± 0.2474	5	3.55 ± 0.3204	11.9	0.08
I_{max}/kg·L	5	0.29 ± 0.0376	5	0.38 ± 0.0529	29.3	0.03
I_{min}/kg·L	5	0.22 ± 0.0258	5	0.27 ± 0.0387	24.9	0.03
I_{max}/I_{min}	5	1.36 ± 0.0575	5	1.41 ± 0.1029	3.7	0.60
J/kg·L	5	0.51 ± 0.0625	5	0.65 ± 0.0889	27.4	0.03
Metatarsal						
Articular length (mm)	5	135.1 ± 4.5	5	135.8 ± 3.0	0.5	0.75
MA/kg	5	0.87 ± 0.3030	5	1.01 ± 0.18	15.4	0.46
CA/kg	5	2.50 ± 0.2597	5	2.66 ± 0.26	6.0	0.17
I_{max}/kg·L	5	0.25 ± 0.0313	5	0.30 ± 0.05	20.7	0.08
I_{min}/kg·L	5	0.22 ± 0.0287	5	0.27 ± 0.04	20.5	0.05
I_{max}/I_{min}	5	1.14 ± 0.0453	5	1.14 ± 0.07	0.2	0.92
J/kg·L	5	0.47 ± 0.0593	5	0.57 ± 0.09	20.6	0.08

* MA, mass-adjusted medullary area; CA, cortical area; I_{max}, maximum second moment area; L, articular length; I_{min}, minimum second moment area; J, polar moment of inertia.

† Calculated as [(exercised group mean − control mean)/control mean] × 100.

‡ Average of the last 3 weeks of body mass.

Energetic Costs

The ANIC of each midshaft cross-section is useful for evaluating osteogenic responses to mechanical loading in terms of energetic costs (see above). This estimate requires data on cortical area (see Table 1) as well as D, R_i, and ω for each element (summarized in Table 2). As Table 2 indicates, no significant differences existed in D between runners and controls for any elements. Peak ω in the femur was considerably lower than that of the tibia and metatarsal, which were roughly similar. Maximum angular excursion was approximately 47° for the femur, 68° for the tibia, and 62° for the metatarsal; these ranges are similar to those of other midsized ungulates (e.g., cervids) but are considerably greater than those reported for larger cursorially specialized mammals such as horses (Gambaryan, 1974; Biewener et al., 1988). The above-described differences in ω, combined with the substantial differences in CA (see Table 1) and R_i (Table 2) resulted in estimates of area normalized inertial cost that were roughly 10 times higher for the tibia than for the femur, and roughly twice as high in the metatarsal as in the tibia. No statistically significant differences in ANIC were detected between the exercise and control groups.

Modeling and Haversian Remodeling

Table 3 summarizes histologic data on average periosteal growth rates (PGR) in μm/d for the femur, tibia, and metatarsal.

TABLE 2. KINEMATIC AND DENSITY DATA USED TO CALCULATE INERTIAL COST OF MIDSHAFT CROSS SECTIONS

Group	Density (kg/m³)			Angular velocity (ω, radians/s)		
	Femur	Tibia	Metatarsal	Femur	Tibia	Metatarsal
Controls (n = 5)	1,976 ± 66	1,995 ± 83	1,897 ± 152	NA†	NA	NA
Exercised (n = 5)	1,974 ± 104	1,902 ± 119	1,846 ± 186	6.89 ± 1.3	12.6 ± 1.8	11.2 ± 0.7

° ANIC, area-normalized inertial cost, calculated as 0.05·CA·density·R_i^2·ω^2 using average value of ω for the three exercised animals. CA, cortical area; R_i, radius of gyration of a given bone, i.

† NA, not available.

Analysis of these data indicated that PGR is significantly higher in the exercised than the in control group for all three elements. In addition, although PGR for the femur is significantly higher ($P < 0.05$) than for the tibia in both groups, PGR is significantly higher in the tibia than in the metatarsal in the exercised ($P = 0.02$) but not in the controls ($P = 0.31$), largely because of the markedly higher tibial PGR in the exercised versus control groups. Therefore, modeling in response to exercise occurs more rapidly at the midshaft in proximal versus distal elements of the limb in proportion to the kinetic energy cost of accelerating added mass, with an especially pronounced effect on the tibial midshaft. This relationship is illustrated in Figure 3A, which shows that midshaft modeling rates in the hind limb are inversely proportional to estimates of midshaft ANIC. Analysis of data on Haversian remodeling rates in Table 3 also indicated that secondary osteon density is higher in distal than in proximal midshafts, with more pronounced differences between exercised and control groups in distal than in proximal midshafts. Analysis of these results indicated that Haversian remodeling in response to exercise occurs at higher levels at the midshaft in distal versus proximal elements of the limb in proportion to estimates of midshaft ANIC, as shown in Figure 3B.

DISCUSSION

Growing sheep that exercised at moderate levels for 90 days had significantly higher periosteal modeling rates than controls at the midshaft of the femur, tibia, and metatarsal; these animals also had significantly higher secondary osteonal densities than controls at the midshaft of the tibia and metatarsal, but not the femur. Therefore, this study supports the findings of previous studies that indicated that growth (periosteal modeling) and repair (Haversian remodeling) in cortical bone occur in response to the functional strains generated by mechanical loading (e.g., Lanyon et al., 1982; Lanyon and Rubin, 1984; Rubin and Lanyon, 1984a,b, 1985; Burr et al., 1985; Biewener et al., 1986; Raab et al., 1991; Bouvier and Hylander, 1996). However, further research is necessary to establish the nature of the strain signal that induces these responses (e.g., magnitude, frequency), and the extent to which osteogenic responses to mechanical loading change with age. These results additionally support the trade-off model for growing animals of Lieberman and Crompton (1998). Cortical bone growth and repair mechanisms in juvenile sheep vary inversely at homotypic sites as a function of the kinetic energy cost of accelerating additional mass. In particular, midshaft periosteal growth rates are significantly higher in proximal than in distal elements in inverse proportion to the estimated ANIC of accelerating mass, and midshaft Haversian remodeling rates are significantly higher in distal than in proximal elements in proportion to the same energetic cost.

Optimization of modeling and remodeling responses in distal and proximal elements in growing animals is a probable

TABLE 2. EXTENDED.

Radius of gyration (m)			ANIC (joules)*		
Femur	Tibia	Metatarsal	Femur	Tibia	Metatarsal
0.09 ± 0.01	0.20 ± 0.01	0.33 ± 0.03	0.05 ± 0.01	0.20 ± 0.01	0.33 ± 0.03
0.09 ± 0.00	0.20 ± 0.01	0.33 ± 0.02	0.05 ± 0.01	0.19 ± 0.01	0.32 ± 0.02

adaptation for limb-bone tapering to enable distal elements to remain lighter than proximal elements, thereby reducing the kinetic energy costs of locomotion (Hildebrand, 1985). By modulating growth and repair responses to loading between proximal and distal elements, animals save kinetic energy, albeit at the expense of higher metabolic energy costs over the long term. Currently, no data exist on the metabolic cost of Haversian remodeling, but this cost is predicted to be less in the long term than the kinetic energy cost of accelerating additional distally located mass that might otherwise be necessary. One important limitation of the trade-off model tested here is that differential modeling versus Haversian remodeling responses to mechanical loading may not occur in all regions of the skeleton or in trabecular bone, and are likely to change with age. As animals mature, periosteal growth rates in response to a given strain stimulus decline, although endosteal growth may increase, leading to stenosis (Woo et al., 1981; Ruff et al., 1994), and Haversian remodeling rates probably increase regardless of skeletal location. These hypothesized effects can be tested by comparing the above results with modeling and remodeling responses in adult sheep subjected to the same mechanical loads.

The variable responses to mechanical loading documented here suggest that any relationships between loading and bone cross-sectional dimensions are more complex than is sometimes assumed. In particular, the higher periosteal growth rates of the exercised juvenile sheep influenced overall midshaft *I* more than cortical or medullary areas (see Table 1), providing experimental support for comparative studies that indicate that *I* and not cortical areas should be used to estimate biomechanical adaptations from bone cross sections (Jungers and Minns, 1979; Ruff and Hayes, 1983; Ruff, 1989; Ruff and Runestad, 1992; Lieberman, 1997). In addition, proximodistal differences in modeling versus Haversian remodeling rates suggest that inferences about biomechanical adaptations to loading from cross-sectional

TABLE 3. HISTOLOGIC DATA.

Element or variable	Controls		Exercised		% Difference*	*P* (Wilcoxon)
	n	Mean ± 1 SD	*n*	Mean ± 1 SD		
Femur: average growth rate† (μm/d)	3	11.03 ± 0.71	5	13.92 ± 1.59	26.1	<0.05
Tibia: average growth rate† (μm/d)	4	6.99 ± 0.72	5	11.04 ± 1.07	58.0	<0.05
Metatarsal: average growth rate† (μm/d)	4	6.43 ± 0.96	5	8.28 ± 1.14	28.8	<0.05
Femur osteon density‡	5	0.42 ± 0.45	5	0.51 ± 0.51	21.4	NS
Tibia osteon density‡	5	2.34 ± 1.13	5	4.67 ± 2.79	99.6	<0.05
Metatarsal osteon density‡	5	7.89 ± 2.26	5	16.31 ± 4.71	206.7	<0.05

* Calculated as [(exercised group mean − control mean)/control mean] × 100.

† Average growth rate (periosteal modeling rate) calculated as mean growth rate (μm/d) of anterior, posterior, medial, and lateral cortices.

‡ Osteon density was calculated as the total number of secondary osteons in the entire section divided by the cortical area (mm^2).

geometry of the midshaft may be less reliable in distal elements, especially the metatarsal, than in more proximal elements. One unexpected result from this study is that *I* discriminates better between exercise and control groups at the tibial midshaft than in the femur or metatarsal. The greater percent difference between treatment groups in the tibia than in the femur or metatarsal may be a function of different local muscle forces, differences in element orientation, or because the femur has a higher safety factor than more distal elements. Bertram and Biewener (1992) also found more variation in limb bone curvature relative to body mass in the femur than in more distal elements among a wide range of mammals, possibly suggesting that the femur may be relatively stronger and therefore experiences lower strains than more distal elements. This hypothesis needs to be tested with in vivo strain data.

Perhaps the most important problem raised by the trade-off between modeling and Haversian remodeling documented here is the mechanism by which bones modulate proximodistal differences in osteogenic responses to mechanical loading. Several hypotheses merit further study. First, different modeling and Haversian remodeling responses to mechanical loading may be a function of differences in strain magnitude, strain polarity, or other aspects of strain energy history. Frost (1990) and Martin and Burr (1989) proposed that remodeling and modeling are mutually exclusive responses below or above specific strain thresholds (minimum effective strains). However, preliminary data (to be presented in a subsequent paper) on cross-sectional strains normal to the tibia and metatarsal midshaft in the sheep indicate that the tibia and metatarsal experience either similar bending strains, or that the metatarsal experiences slightly more bending in the sagittal plane than the tibia. Another hypothesis is that Haversian remodeling rates may be positively correlated with strain magnitudes or strain energy history. Secondary osteonal bone is not as strong as primary osteonal and circumlamellar bone (Currey, 1959; Carter and Hayes, 1977a; Vincentelli and Grigorov, 1985), so any differential response to elevated strain levels might actually exaggerate the apparent trade-off between modeling and remodeling in proximal versus distal bones. However, these and other hypotheses can only be evaluated with in vivo strain data from the midshaft of the femur, tibia, and metatarsal in conjunction with histologic data on growth and remodeling rates.

Another possibility is that variations in vascular or cellular density may modulate growth versus repair responses to loading in different limb elements. Bone vascular density must constrain remodeling responses to some extent because bone morphogenetic units require arteries to supply nutrients and cells (Winet et al., 1990; Singh et al., 1991). Avascular cortical bone tissue is rarely if ever reconstructed by osteoclasts (de Ricqlès et al., 1991), and thus has little potential to respond to loading through Haversian remodeling. Moreover, the vascular density of bone may be partly rate-dependent (de Ricqlès, 1975), possibly explaining the correlation between remodeling rates and vascular density (Green et al., 1987). Further research is needed to test if a correlation exists between the density of vascular channels in the primary cortex of the femur, tibia, and metatarsal and Haversian remodeling rates. An additional possibility is that osteocytes act as strain transducers (Lanyon, 1993; Turner et al., 1994, 1995), potentially limiting Haversian remodeling responses in primary compact bone in proportion to their density. Osteocytes possibly play a role in sensing and transducing information on strains and/or microcracks to precursor stem and mesenchymal cells (Lanyon, 1993), which may limit the ability of acellular cortical bone to undergo Haversian remodeling. Differences in osteocyte density have been implicated as a possible contributing factor to osteoporosis

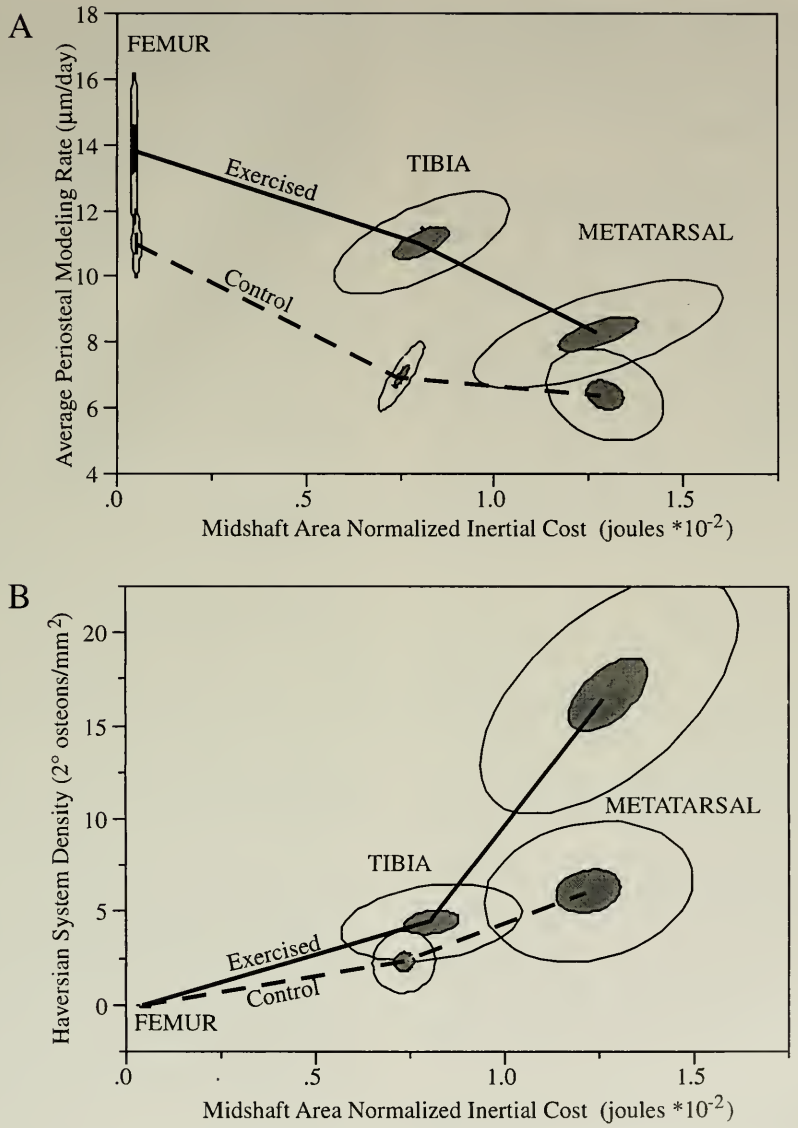

Figure 3. Observed trade-off between modeling (A) and Haversian remodeling (B) in the hindlimb as a function of area-normalized inertial cost of accelerating mass at the midshaft of the femur, tibia, and metatarsal. Density ellipses are plotted for 10% (shaded) and 65% (unshaded) within-group variation for exercised (solid line) and control (dashed line) groups.

(Mullender et al., 1996), but these remain to be tested in the sample here.

The observed trade-off between modeling and remodeling in cortical bone suggests that a more complete understanding of Wolff's law will require integration of both intraindividual as well as interindividual variations in the mechanisms by which bones respond dynamically to their functional environment. In particular, further research needs to address the effects of age, variations in strain levels, and the intermediary factors that modulate the apparent trade-off between growth and re-

pair processes that occurs between proximal and distal elements in the limb and presumably elsewhere in the skeleton.

ACKNOWLEDGMENTS

Thank you, Fuzz, for inspiring the senior author's interest in experimental skeletal biology and functional morphology, and for many years of training, support, and humorous encouragement. We also thank Andy Biewener, Brigitte Demes, Brian Richmond, and Bernard Wood for comments on the manuscript; Robin Bernstein for helping to make the thin sections; and Mike Toscano for running the sheep. This research was supported by National Science Foundation IBN 96-03833 and by funding from the American Federation for Aging Research.

LITERATURE CITED

ALEXANDER, R. MCN. 1977. Terrestrial locomotion, pp. 168–203. *In* R. McN. Alexander and G. Goldspink (eds.), Mechanics and Energetics of Animal Locomotion. London: Chapman and Hall. xii + 346 pp.

———. 1980. Optimum walking techniques for quadrupeds and bipeds. Journal of the Zoological Society (London), **173:** 549–573.

———. 1981. Factors of safety in the structure of animals. Science Progress, Oxford, **67:** 109–130.

———. 1996. Optima for Animals. Princeton, New Jersey: Princeton University Press. viii + 169 pp.

———. 1998. Symmorphosis and safety factors, pp. 28–35. *In* E. Weibel, C.R. Taylor and L. Bolis (eds.), Principles of Biological Design: The Optimization and Symmorphosis Debate. Cambridge: Cambridge University Press. xx + 314 pp.

BERTRAM, J. E. A., AND A. A. BIEWENER. 1988. Bone curvature: sacrificing strength for load predictability? Journal of Theoretical Biology, **131:** 75–92.

———. 1992. Allometry and curvature in the long bones of quadrupedal mammals. Journal of the Zoological Society (London), **226:** 455–467.

BERTRAM, J. E. A., AND S. M. SWARTZ. 1991. The 'Law of Bone Transformation': a case of crying Wolff? Biological Review, **66:** 245–273.

BIEWENER, A. A. 1983a. Allometry of quadrupedal locomotion: the scaling of duty factor, bone curvature and limb orientation to body size. Journal of Experimental Biology, **105:** 147–171.

———. 1983b. Locomotory stresses in the limb bones of two small mammals: the ground squirrel and the chipmunk. Journal of Experimental Biology, **103:** 131–154.

———. 1989. Scaling and body support in mammals: limb posture and muscle mechanics. Science **245:** 45–48.

———. 1990. Biomechanics of mammalian terrestrial locomotion. Science, **250:** 1097–1103.

BIEWENER, A. A., S. M. SWARTZ, AND J. E. A. BERTRAM. 1986. Bone modeling during growth: Dynamic strain equilibrium in the chick tibiotarsus. Calcified Tissue International, **39:** 390–395.

BIEWENER, A. A., AND C. R. TAYLOR. 1986. Bone strain: a determinant of speed and gait? Journal of Experimental Biology, **123:** 383–400.

BIEWENER, A. A., J. J. THOMASON, AND L. E. LANYON. 1988. Mechanics of locomotion and jumping in horse *Equus*; in vivo stress in the tibia and metatarsus. Journal of Zoology (London), **214:** 547–565.

BOUVIER, M., AND W. L. HYLANDER. 1981. Effect of bone strain on cortical bone structure in macaques *Macaca mulatta*. Journal of Morphology, **167:** 1–12.

———. 1996. The function of secondary osteonal bone: mechanical or metabolic? Archives of Oral Biology, **41:** 941–950.

BURR, D. B. 1993. Fatigue and bone remodeling. Calcified Tissue International, **53:** S75–S81.

BURR, D. B., R. B. MARTIN, M. B. SCHAFFLER, AND E. L. RADIN. 1985. Bone remodeling in response to in vivo fatigue microdamage. Journal of Biomechanics, **18:** 189–200.

CARTER, D. R., W. E. CALER, D. M. SPENGLER, AND V. H. FRANKEL. 1981a. Fatigue behavior of adult cortical bone—the influence of mean strain and strain range. Acta Orthopaedica Scandinavica, **55:** 481–490.

———. 1981b. Uniaxial fatigue of human cortical bone. The influence of tissue physical characteristics. Journal of Biomechanics, **14:** 460–470.

CARTER, D. R., AND W.C. HAYES. 1976a. Fatigue life of compact bone. I. Effects of stress amplitude, temperature and density. Journal of Biomechanics, **9:** 27–34.

———. 1976b. Bone compressive strength: the influence of density and strain rate. Science **194:** 1174–1176.

———. 1977a. Compact bone fatigue damage—a microscopic examination. Clinical Orthopedics and Related Research, **127:** 265–274.

———. 1977b. Compact bone fatigue damage I. Residual strength and stiffness. Journal of Biomechanics, **10:** 323–337.

CARTER, D. R., W. C. HAYES, AND D. J. SCHURMAN. 1976. Fatigue life of compact bone—II. Effect of microstructure and density. Journal of Biomechanics, **9:** 211–218.

CHAMAY, A., AND P. TCHANTZ. 1972. Mechanical influences in bone remodeling. Experimental research on Wolff's law. Journal of Biomechanics, **5:** 173–180.

CURREY, J. D. 1959. Differences in the tensile strengths of bone of different histological types. Journal of Anatomy, **93:** 87–95.

———. 1970. The mechanical properties of bone. Clinical Orthopedics and Related Research, **73:** 210–231.

———. 1984. The Mechanical Adaptations of Bones. Princeton, New Jersey: Princeton University Press. viii + 294 pp.

FEDAK, M. A., N. C. HEGLUND, AND C. R. TAYLOR. 1982. Energetics and mechanics of terrestrial locomotion 2. Kinetic energy changes of the limbs and body as a function of speed and body size in birds and mammals. Journal of Experimental Biology, **79:** 23–40.

FROST, H. M. 1963. Bone Remodeling Dynamics. Springfield, Illinois: Charles C. Thomas. 175 pp.

———. 1973. Bone Remodeling and Its Relationship to Metabolic Bone Diseases. Springfield, Illinois: Charles C. Thomas. ix + 210 pp.

———. 1990. Skeletal structural adaptations to mechanical usage SATMU: 2. Redefining Wolff's law: the remodeling problem. The Anatomical Record, **226:** 414–422.

GAMBARYAN, P. P. 1974. How Mammals Run: Anatomical Adaptations. New York: Wiley. xiv + 367 pp.

GOODSHIP, A. E., L. E. LANYON, AND J. H. MACFIE. 1979. Functional adaptation of bone to increased stress. Journal of Bone and Joint Surgery, **61A:** 539–546.

GREEN, J. R., J. REEVE, M. TELLEZ, N. VEALL, AND R. WOOTTON. 1987. Skeletal blood flow in metabolic disorders of the skeleton. Bone, **8:** 293–297.

HEGLUND, N. C., G. A. CAVAGNA, AND C. R. TAYLOR. 1982a. Energetics and mechanics of terrestrial locomotion. III. Energy changes of the center of mass as a function of speed and body size in birds and mammals. Journal of Experimental Biology, **79:** 41–56.

———. 1982b. Energetics and mechanics of terrestrial locomotion. IV. Total mechanical energy changes as a function of speed and body size in birds and mammals. Journal of Experimental Biology, **79:** 57–66.

HERT, J., E. PRYBYLOVÁ, AND M. LISKOVA. 1972. Reaction of bone to mechanical stimuli, part 3. Microstructure of compact bone of rabbit tibia after intermittent loading. Acta Anatomica, **82:** 218–230.

HILDEBRAND, M. 1985. Walking and running, pp. 38–57. *In* M. Hildebrand, D. M. Bramble, K. F. Liem, and D. B. Wake (eds.), Functional Vertebrate Morphology. Cambridge, Massachusetts: Harvard University Press. 430 pp.

JUNGERS, W. J., AND R. J. MINNS. 1979. Computed tomography and biomechanical analysis of fossil long bones. American Journal of Physical Anthropology, **50:** 285–290.

LANYON, L. E. 1993. Osteocyte, strain detection, bone modeling and remodeling. Calcified Tissue International, **53:** S102–S107.

LANYON, L. E., A. E. GOODSHIP, C. J. PYE, AND H. MACFIE. 1982. Mechanically adaptive bone remodeling. Journal of Biomechanics, **15:** 141–154.

LANYON, L. E., AND C. T. RUBIN. 1984. Static versus dynamic loading as an influence on bone remodeling. Journal of Biomechanics, **17:** 897–906.

———. 1985. Functional adaptation in skeletal structures, pp. 1–25. *In* M. Hildebrand, D. M. Bramble, K. F. Liem, and D. B. Wake (eds.), Functional Vertebrate Morphology. Cambridge, Massachusetts: Harvard University Press. 430 pp.

LIEBERMAN, D. E. 1997. Making behavioral and phylogenetic inferences from fossils: considering the developmental influence of mechanical forces. Annual Review of Anthropology, **26:** 185–210.

LIEBERMAN, D. E., AND A. W. CROMPTON. 1998. Responses of bone to stress, pp. 78–86. *In* E. Weibel, C. R. Taylor, and L. Bolis (eds.), Principles of Biological Design: The Optimization and Symmorphosis Debate. Cambridge: Cambridge University Press. xx + 314 pp.

MARTIN, R. B. 1995. Mathematical model for repair of fatigue damage and stress fracture in osteonal bone. Journal of Orthopedic Research, **13:** 309–316.

MARTIN, R. B., AND D. B. BURR. 1982. A hypothetical mechanism for the stimulation of osteonal remodeling by fatigue damage. Journal of Biomechanics, **5:** 137–139.

———. 1989. Structure, Function, and Adaptation of Compact Bone. New York: Raven Press. xii + 275 pp.

MCMAHON, T. A. 1975. Using body size to understand the structural design of animals: quadrupedal locomotion. Journal of Applied Physiology, **39:** 619–627.

MORI, S., AND D. B. BURR. 1993. Increased intracortical remodeling following fatigue damage. Bone, **16:** 103–109.

MULLENDER, M. G., D. D. VAN DER MEER, R. HUISKES, AND P. LIPS. 1996. Osteocyte density changes in aging and osteoporosis. Bone, **18:** 109–113.

MYERS, M. J., AND K. STEUDEL. 1985. Effect of limb mass and its distribution on the energetic cost of running. Journal of Experimental Biology, **116:** 363–373.

PARFITT, A. M. 1988a. Bone remodeling: relationship to the amount and structure of bone, and the pathogenesis and prevention of fractures, pp. 45–93. *In* B. L. Riggs and L. J. Melton (eds.), Osteoporosis: Etiology, Diagnosis and Management. New York: Raven Press. xii + 501 pp.

———. 1988b. Osteonal and semi-osteonal remodeling: the spatial and temporal framework for traffic signal in adult human bone. Journal of Cell Biomechanics, **55:** 273–286.

PAUWELS, F. 1980. Biomechanics of the Locomotor Apparatus: Contributions on the Functional

Anatomy of the Locomotor Apparatus. Berlin: Springer-Verlag. viii + 518 pp.

RAAB, D. M., T. D. CRENSHAW, D. B. KIMMEL, AND E. L. SMITH. 1991. A histomorphometric study of cortical bone activity during increased weight-bearing exercise. Journal of Bone and Mineral Research, **6:** 741–749.

DE RICQLÈS, A. 1975. Evolution of endothermy: histological evidence. Evolutionary Theory, **1:** 51–80.

DE RICQLÈS, A. J., F. J. MEUNIER, J. CASTANET, AND H. FRANCILLON-VIEILLOT. 1991. Comparative microstructure of bone, pp. 1–78. *In* B. K. Hall (ed.), Bone. Vol. 3: Bone Matrix and Bone Specific Products. Boca Raton, Florida: CRC Press. x + 333 pp.

RUBIN, C. T., AND L.E. LANYON. 1984a. Dynamic strain similarity in vertebrates: an alternative to allometric limb bone scaling. Journal of Theoretical Biology, **107:** 321–327.

———. 1984b. Regulation of bone formation by applied dynamic loads. Journal of Bone and Joint Surgery, **66:** 397–402.

———. 1985. Regulation of bone mass by mechanical strain magnitude. Calcified Tissue International, **37:** 411–417.

RUFF, C. B. 1989. New approaches to structural evolution of limb bones in primates. Folia Primatologica, **53:** 142–159.

RUFF, C. B., AND W. C. HAYES. 1983. Cross-sectional geometry of Pecos Pueblo femora and tibiae—a biomechanical investigation: I. Method and general patterns of variation. American Journal of Physical Anthropology, **60:** 359–381.

RUFF, C. B., AND J. A. RUNESTAD. 1992. Primate limb bone structural adaptations. Annual Review of Anthropology, **21:** 407–433.

RUFF, C. B., A. WALKER, AND E. TRINKAUS. 1994. Postcranial robusticity in *Homo* III: ontogeny. American Journal of Physical Anthropology, **93:** 35–54.

SCHAFFLER, M. B., AND D. B. BURR. 1988. Stiffness of compact bone: effects of porosity and density. Journal of Biomechanics, **21:** 13–16.

SCHAFFLER, M. B., E. L. RADIN, AND D. B. BURR. 1989. Mechanical and morphological effects of strain rate on fatigue of compact bone. Bone, **10:** 207–214.

———. 1990. Long-term fatigue behavior of compact bone at low strain magnitude and rate. Bone, **11:** 321–326.

SINGH, I. J., H. S. SANDHU, AND M. S. HERSKOVITS. 1991. Bone vascularity, pp. 141–164. *In* B. K. Hall (ed.), Bone. Vol. 3: Bone Matrix and Bone Specific Products. Boca Raton, Florida: CRC Press. xii + 333 pp.

SMITH, J. M., AND R. J. G. SAVAGE. 1956. Some locomotory adaptations in mammals. Zoological Journal of the Linnaean Society, **42:** 603–622.

TAYLOR, C. R., A. SHKOLNIK, R. DMI'EL, D. BAHARAV, AND A. BORUT. 1974. Running in cheetahs, gazelle and goats: energy costs and limb configuration. American Journal of Physiology, **227:** 848–850.

TURNER, C. H., M. R. FORWOOD, AND M. W. OTTER. 1994. Mechanotransduction in bone: do bone cells act as sensors of fluid flow? FASEB Journal, **8:** 875–878.

TURNER, C. H., I. OWAN, AND Y. TAKANO. 1995. Mechanotransduction in bone: role of strain rate. American Journal of Physiology, **269:** E438–E442.

VINCENTELLI, R., AND M. GRIGOROV. 1985. The effect of Haversian remodeling on the tensile properties of human cortical bone. Journal of Biomechanics, **18:** 201–207.

WAINWRIGHT, S. A., W. D. BIGGS, J. D. CURREY, AND J. M. GOSLINE. 1976. Mechanical Design in Organisms. Princeton, New Jersey: Princeton University Press. xii + 423 pp.

WINET, H., J. Y. BAO, AND R. MOFFAT. 1990. A control model for tibial cortex neovascularization in the bone chamber. Journal of Bone and Mineral Research, **5:** 19–30.

WINTER, D. A. 1990. Biomechanics and Motor Control of Human Movement, second edition. New York: Wiley. xiii + 227 pp.

WOO, S. L. Y., S. C. KUEI, D. AMIEL, M. A. GOMEZ, W. C. HAYES, F. C. WHITE, AND W. H. AKESON. 1981. The effect of prolonged physical training on the properties of long bone: a study of Wolff's law. Journal of Bone and Joint Surgery, **63:** 780–787.

MUSCLE FORCE AND STRESS DURING RUNNING IN DOGS AND WILD TURKEYS

THOMAS J. ROBERTS[1]

ABSTRACT. The function of the avian hind limb during running has received considerable attention, particularly as a potential analog for locomotor function in extinct bipeds. Comparisons of limb kinematics in avian runners and mammalian quadrupeds have revealed consistent differences in the pattern of joint excursions, presumably related to the constraints of bipedal support in birds. The present study asks whether these kinematic differences are paralleled by differences in muscle forces and stresses developed in hind limb locomotor muscles in birds and quadrupedal mammals. High-speed video and force-plate analyses along with anatomical measurements were used to estimate muscle forces and stresses in the locomotor muscles of small dogs and wild turkeys during running. Turkeys and dogs developed remarkably similar patterns of force in hind limb muscles, despite large differences in the magnitude of ground reaction force moments. It was expected that differences in absolute muscle force in hind limb muscles would be matched by differences in cross-sectional area of muscle available to produce force, to maintain similar muscle stress. Instead, muscle stresses varied widely between homologous joints in dogs and turkeys, and between joints within species. The distribution of muscle stress between joints may reflect differences in the design of the avian and mammalian limb for high-power locomotor activities.

INTRODUCTION

Avian and mammalian runners move their limbs in very different ways. Mammalian runners and most quadrupeds retract their hind limbs during stance phase primarily by a large extension of the femur at the hip; the knee flexes and extends over only a small angle (Goslow et al., 1981). Hip extension in birds is negligible at low speeds and increases with running speed (Gatesy, 1999a). At all speeds, the knee undergoes substantial flexion in birds and accounts for a greater angle change than the hip, providing most of the movement for retraction of the limb (Storer, 1971; Jacobson and Hollyday, 1982; Gatesy, 1999a). The suggestion has been made that these differences in limb movement patterns are necessitated by the constraints of balance in bipedal birds (Storer, 1971; Gatesy, 1990). The horizontally oriented femur of birds positions the foot beneath the center of mass for standing and slow movement. The result is that the restricted movement of the avian femur leaves the knee to act, at least kinematically, as the functional equivalent of the mammalian hip (Gatesy and Biewener, 1991).

It is unclear how these kinematic differences, or the requirements of balance in a biped, are reflected in the pattern of force development in locomotor muscles. Because muscle forces are critical to the energetics of running and the mechanical stresses on muscles, tendons, and bones, the most important consequence of variation in limb morphology may be variation in timing and magnitude of muscle forces (Biewener, 1989; Kram and Taylor, 1990; Roberts et al., 1998). It has recently been shown that dogs and wild turkeys produce similar total muscle forces per unit ground reaction force (GRF) during running (Roberts et al., 1998). The present study addresses two questions about the design of the avian and mammalian hind limb for locomotor force production: is the timing of flexor and extensor forces the same at homologous joints in dogs and turkeys, and are the stresses developed in the lo-

[1] Oregon State University, Department of Zoology, 3029 Cordley Hall, Corvallis, Oregon 97331-2914.

comotor muscles equivalent at equivalent speeds?

The muscle forces required to balance gravitational and inertial forces during running are determined primarily by the mechanical advantage for force production against the ground. The mechanical advantage at any given joint can change significantly during the stance phase, as the position of the GRF, and its leverage, changes with respect to the joint (Biewener, 1989; Carrier et al., 1998). These changes in muscle mechanical advantage mean that the timing of the maximum muscle force may be independent of the timing of the GRF. Forces at all joints must be carefully coordinated during running to maintain balance. Presumably, the significant differences in limb posture and running kinematics in bipedal birds and quadrupeds might be associated with distinct differences in the timing and coordination of joint moments and muscle forces.

One possible morphologic indicator of the forces that are developed during locomotion is the cross-sectional area of extensor muscles at a joint. The range of possible joint forces is limited by the total cross-sectional area of muscle available and the maximum stress that can be developed by vertebrate skeletal muscle. It has been hypothesized that locomotor muscles should undergo the same peak stresses during equivalent movements in terrestrial runners (Perry et al., 1988). This hypothesis is based upon the idea that the muscular system, like the skeletal system, should be neither over- nor underbuilt, but rather that the capacity for force generation should be matched to the demand (Biewener, 1990). Because the maximum stress that can be developed is a nearly invariant property of skeletal muscle, the equivalent stress hypothesis states that a similar fraction of the capacity for force production in the extensors of a joint should be used at equivalent speeds. Thus, any differences in force requirements at a joint in different species will be matched by a proportional difference in cross-sectional area of muscle to maintain similar stress. The similar stress hypothesis is supported by the observation that kangaroo rats and white rats maintain the same level of peak stress in their ankle extensors, despite a fourfold difference in peak GRF per limb (Perry et al., 1988).

In the present study, GRF-based joint moments are measured in dogs and turkeys running over a force plate. These data are combined with anatomical data to calculate the required muscle forces and the total stress in major locomotor muscles at homologous joints in dogs and turkeys. Higher hind limb muscle forces are to be expected in turkeys compared with dogs because they support their weight on two limbs rather than four. To maintain similar stress, turkeys should have a greater cross-sectional area of hind limb muscle in proportion to higher absolute muscle forces.

MATERIALS AND METHODS

Animals

Three small terriers (*Canis familiaris*) and three wild turkeys (*Meleagris gallopavo*) were used in these studies. These species were chosen because they were approximately the same body mass, 4.5 ± 1.0 kg and 5.3 ± 2.3 kg for the dogs and turkeys, respectively. The methods for animal training and the data collection methods for dogs and turkeys have been described in detail previously (Roberts et al., 1998), and will be presented only briefly here.

Muscle Force Measurements

High-speed video and force-plate measurements were made as animals ran freely over a 15-m track. Measurements were made at the speeds that were initially freely chosen by the animals, approximately 3.5 m/s for the turkeys and 2.0 m/s for the dogs. Joint moments of force were calculated from the magnitude and position of the GRF vector relative to the joint centers of rotation as determined by force-plate and high-speed video analysis (Rob-

erts et al., 1998). Moments were determined for the hip, knee, and ankle (dog and turkey), as well as the shoulder, elbow, and wrist (dogs only). Measurements included only the GRF-based moments. Moments due to accelerations of limb segments relative to the center of mass also contribute to the required muscle force. Limb inertia–based moments are usually small in birds and quadrupedal mammals (Clark and Alexander, 1975; Pandy et al., 1988), but may be significant at more proximal joints. Muscle forces (F_m) were calculated from the measured joint moments and the average muscle moment arm measured at each joint:

$$F_m = F_g \cdot \frac{R}{\bar{r}} \quad (1)$$

where the joint moment is the product of GRF magnitude F_g (N) and moment arm R (m), and $\bar{r}$ (m) is the average muscle moment arm at that joint.

Calculation of muscle force and stress requires anatomical measurements of muscle moment arms and cross-sectional areas for muscles active during support. The average moment arm ($\bar{r}$) was calculated for the extensor muscles at a joint from an average weighted by the cross-sectional area of each individual muscle (Roberts et al., 1998). This measure assumed that the relative contribution of a given muscle to the total force produced at a joint was proportional to the muscle's force-generating capacity. Muscle physiologic cross-sectional area (A_{cs}) was calculated as:

$$A_{cs} = \frac{m \cdot \cos \theta}{\rho \cdot \ell} \quad (2)$$

where m is the mass of the muscle (g), θ is the fiber pinnation angle, ρ is the density of muscle (g/cm^3) , and ℓ is muscle fascicle length (cm).

Measurements were included for muscles that are primarily extensors of the joint (or flexors in the case of the wrist), and are active during stance phase based on electromyographic activity (Tokuriki, 1973; Goslow et al., 1981; Gatesy, 1999b). Muscles included for turkeys were iliotibialis lateralis pars postacetabularis, iliofibularis, flexor cruris lateralis, flexor cruris medialis, puboischiofemoralis, and ischiofemoralis (hip extensors); femorotibiales (knee extensors); and gastrocnemius, fibularis longus, flexor hallucis longus, flexor digitorum longus, flexor perforatus digiti II and III, and flexor perforans et perforatus digiti II, III, and IV (ankle extensors). Muscles included for dogs were gluteus medius, gluteus superficialis, biceps femoris, and semimembranosus (hip extensors); vastus lateralis, medialis, and intermedius (knee extensors); gastrocnemius, plantaris, and deep digital flexors (ankle extensors); supraspinatus (shoulder extensor); triceps brachii (elbow extensor); and flexor digitorum profundus, flexor digitorum superficialis, flexor carpi ulnaris, and flexor carpi radialis (wrist flexors). Some of the anatomical measurements were taken from specimens available from unrelated experiments. These animals were of similar weight and condition. Small corrections to the muscle dimension measurements were made for differences in the body mass of the experimental subjects by assuming geometric scaling (Roberts et al., 1998).

Contribution of Biarticular Muscles to Extensor Muscle Forces

In addition to the muscle forces required to overcome GRF based moments, extensor muscles must produce force to balance antagonist flexor muscle forces. Cocontraction of muscles that are primarily joint flexors was assumed to be negligible during stance. However, many biarticular (or multiarticular) extensor muscles also act as flexors. The flexor forces produced by biarticular extensor muscles active during stance were included as part of the calculation of total muscle force required at a joint. Thus, part of the calculated extensor moment at several joints includes a component of force necessary to

counteract cocontraction of multiarticular muscles. The contribution of a biarticular muscle to a joint flexor moment was calculated from the extensor force it developed at its extensor articulation, assuming that force was distributed among extensor muscles in proportion to their cross-sectional area. The flexor moment was then calculated from the force produced in the biarticular muscle and its flexor moment arm.

Flexor forces in dogs included gastrocnemius flexion of the knee and flexion of the shoulder by the long head of triceps brachii. In turkeys, extensor muscle forces were required to balance flexor moments produced at the knee by the hip extensors flexor cruris lateralis and medialis, and iliofibularis. The following ankle extensors also produced a flexor moment at the knee in turkeys: gastrocnemius lateralis and medialis, and the digital flexors flexor hallucis longus, flexor perforatus digiti II, III, and IV, and flexor perforans et perforatus digiti II and III. Mulitiarticular muscles also acted to reduce extensor forces in two cases. Some of the digital flexors that contribute to flexion of the wrist also act to extend the elbow in dogs (flexor digitorum profundus, flexor digitorum superficialis, flexor carpi radialis, and flexor carpi ulnaris). In turkeys, iliotibialis lateralis pars postacetabularis was included primarily as a hip extensor but it also contributes an extensor moment at the knee.

The presence of multiple biarticular muscles that both flex and extend the knee and the hip makes calculation of muscle forces an indeterminate problem, because it is impossible to know the degree of cocontraction of antagonist muscle groups (Winter, 1990). This problem was avoided in the present study by omitting the contribution of the rectus femoris to knee extension and hip flexion in dogs. Electromyographic studies suggest that this muscle is active during the second two thirds of stance phase in trotting dogs (Tokuriki, 1973). Rectus femoris is approximately 35% of the total cross-sectional area of the extensor muscles at the knee; omission of this muscle may lead to an underestimate of hip extensor forces late in stance and a small overestimate of knee muscle stress in dogs.

Muscle Stress Measurements

Muscle stress was determined by dividing the peak measured muscle force by the total physiologic cross-sectional area of extensor muscles at a joint. This measure is equivalent to the muscle stress in each individual muscle at a joint only if the force is evenly distributed among muscles in proportion to each muscle's cross-sectional area. Although this assumption has proven accurate for hopping kangaroo rats (Biewener et al., 1988), force buckle measurements in cats suggest that the relative contribution of individual ankle extensors to total extensor force can change with speed of movement and locomotor activity (Walmsley et al., 1978). Although variation in distribution of muscle force between muscles may make it difficult to calculate stresses in individual muscles, the measure of muscle stress of a whole muscle group will still reflect the fraction of the capacity for force production that is being used in the muscle group.

Statistical Analyses

To calculate an average force versus time plot for all of the trials it was necessary to normalize for variation in both stride time and total force between individual trials. Moment and force measurements in an individual trial were divided by the peak GRF for that trial. To control for variation in ground contact time, each original stance period was interpolated to a wave of 30 points using the cubic spline interpolation function in the computer software application Igor (Wavemetrics, Lake Oswego, OR). The interpolation also applied a smoothing function to the data. Average muscle moment and force curves are represented as the means and standard deviations for all of the running trials.

Analysis of variance was used to test for

significant differences at $P < 0.05$. Values presented are means ± one standard deviation unless indicated otherwise. All indicated differences are significant at $P < 0.05$.

RESULTS

Muscle Forces

Dogs and turkeys produce remarkably similar patterns of force at homologous joints in the hind limb. Figure 1 presents joint moments ($F_g \cdot R$) during stance phase normalized to the peak GRF produced during the step. Hip moments were greatest early in stance and relatively small during the second half of stance in both dogs and turkeys. Ankle moments were also at their maximum early in the stance phase. In both the dog and the turkey, the knee musculature produced a net flexor moment early in stance, followed by an extensor moment. This cyclic flexor–extensor moment pattern also occurred at the shoulder of the dog. The highest knee moments occurred during the second half of stance phase in both dogs and turkeys. The peak GRF, indicated by an arrow, occurs earlier in stance in the turkey hind limb than in the dog hind limb or forelimb.

The hind limb muscles of turkeys produce greater joint moments per unit GRF compared with dogs (Fig. 1). Hip moments per unit GRF were 3.1-fold greater in the turkey (turkey, 0.085 ± 0.013; dog, 0.027 ± 0.013), knee moments were greater by a factor of 2.4 (turkey, 0.034 ± 0.012; dog, 0.014 ± 0.004), and ankle moments were 1.8-fold greater in the turkey (turkey, 0.082 ± 0.012; dog, 0.046 ± 0.006). These differences suggest that the turkey's relatively horizontally oriented femur and long tibiotarsus and tarsometatarsus result in greater GRF moment arms (R) at the hip, knee, and ankle.

Despite the large differences observed in muscle moments (Fig. 1), muscle forces produced per unit GRF were similar in the knee and the hip in dogs and turkeys (Fig. 2). Muscle forces presented in Figure 2 were calculated from joint moments by dividing by the average muscle moment arm ($\bar{r}$; Equation 1), and including moments produced by biarticular agonists or antagonists. This similarity in muscle forces at the knee and hip indicates that muscle moment arms ($\bar{r}$) at these joints are proportionately larger in the turkeys to compensate for the higher moments resulting from differences in limb posture. The average muscle moment arm at the ankle was similar in dogs and turkeys; muscle forces were larger in turkeys, as were the muscle moments.

The contribution of biarticular muscle agonists and antagonists to the extensor muscle forces calculated at the knee, elbow, and shoulder is represented in Figure 2 by the difference between the total calculated extensor force (bold line) and the extensor muscle force calculated neglecting the contribution of biarticular muscles (dotted line). Interestingly, flexor forces produced by biarticular muscles seem to provide the flexor moment necessary to balance the GRF early in stance at the knee and shoulder. Later in stance the extensor force necessary is increased by the action of two-joint muscles, assuming that these muscles are fully active throughout stance.

Muscle Stresses

Muscle stresses were quite variable between joints in dogs and turkeys (Fig. 3) running at the speeds measured in this study. The values presented in Figure 3 were obtained by dividing the peak force produced by the total physiologic cross-sectional area of the extensor muscles at a joint. Stress varied by more than fivefold between joints in dogs, from 59 ± 28 kN/m^2 in the hip extensors to 309 ± 59 kN/m^2 in the shoulder extensors. Generally, hind limb stresses were lower than forelimb stresses, and stresses were higher moving distally in the dog hind limb. Turkeys showed less variation in muscle stress between joints and generally operated

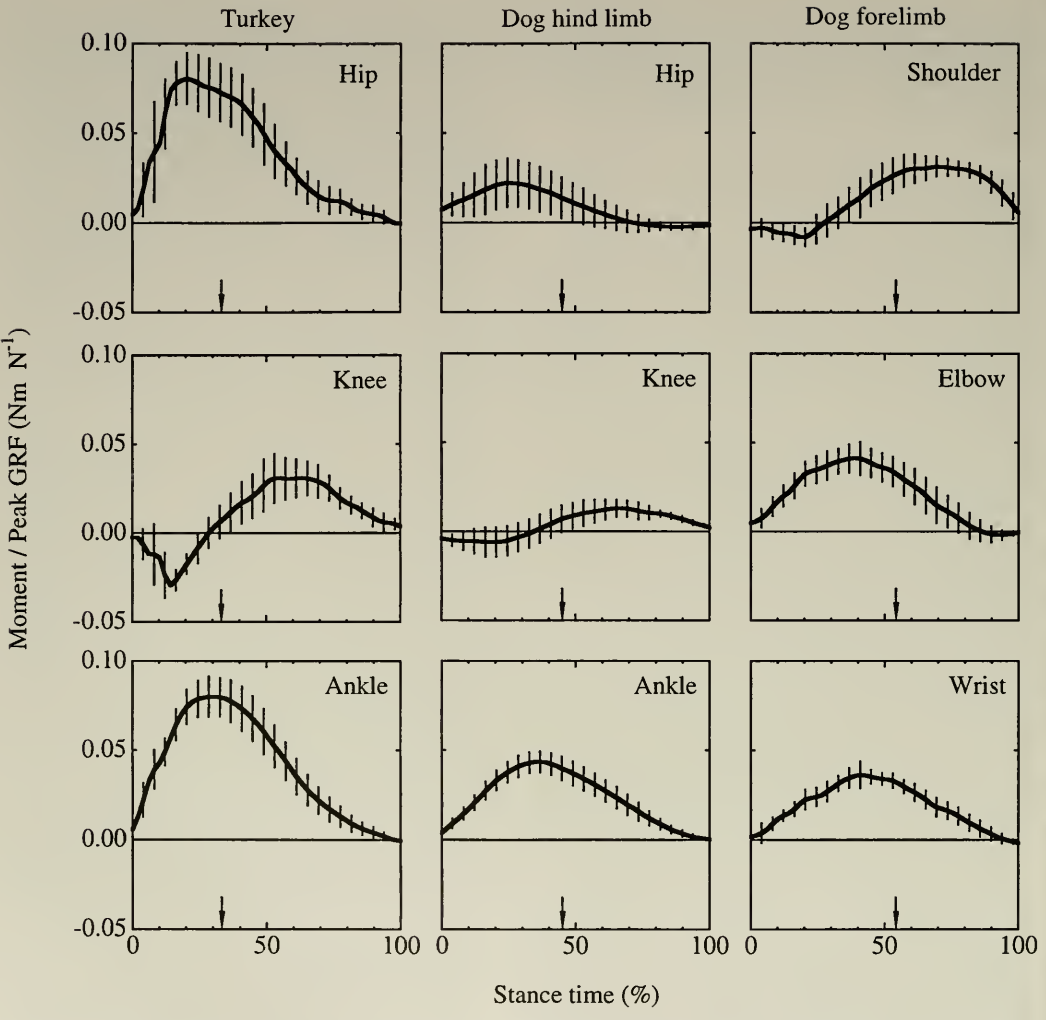

Figure 1. Muscle moments during the stance phase normalized to the peak ground reaction force (GRF). Mean values and standard deviations are presented for 12 strides of three animals. Positive moments represent extensor muscle moments, with the exception of the wrist; wrist flexor muscle moments are represented as positive. Arrows indicate the time of the peak GRF.

with higher hind limb muscle stresses than did dogs.

Higher muscle stresses at a joint can be due to either higher muscle forces or a smaller cross-sectional area of muscle available. Table 1 allows a comparison of the contribution to differences in muscle stress of muscle mechanical advantage, the total GRF produced, and muscle cross-sectional area. The muscle force produced per peak GRF is determined by the muscle mechanical advantage, and is significantly different in the dog and turkey only at the ankle. The peak GRF on a single hind limb in turkeys was equal to 2.4 × body weight. Dogs developed a total peak GRF of 2 × body weight, but only 41% of this was developed by the hind limbs; therefore, the dog hind limb GRF was 0.8 × body weight. When this difference in hind limb GRF is included, it is apparent that, at equivalent speeds, turkeys produce

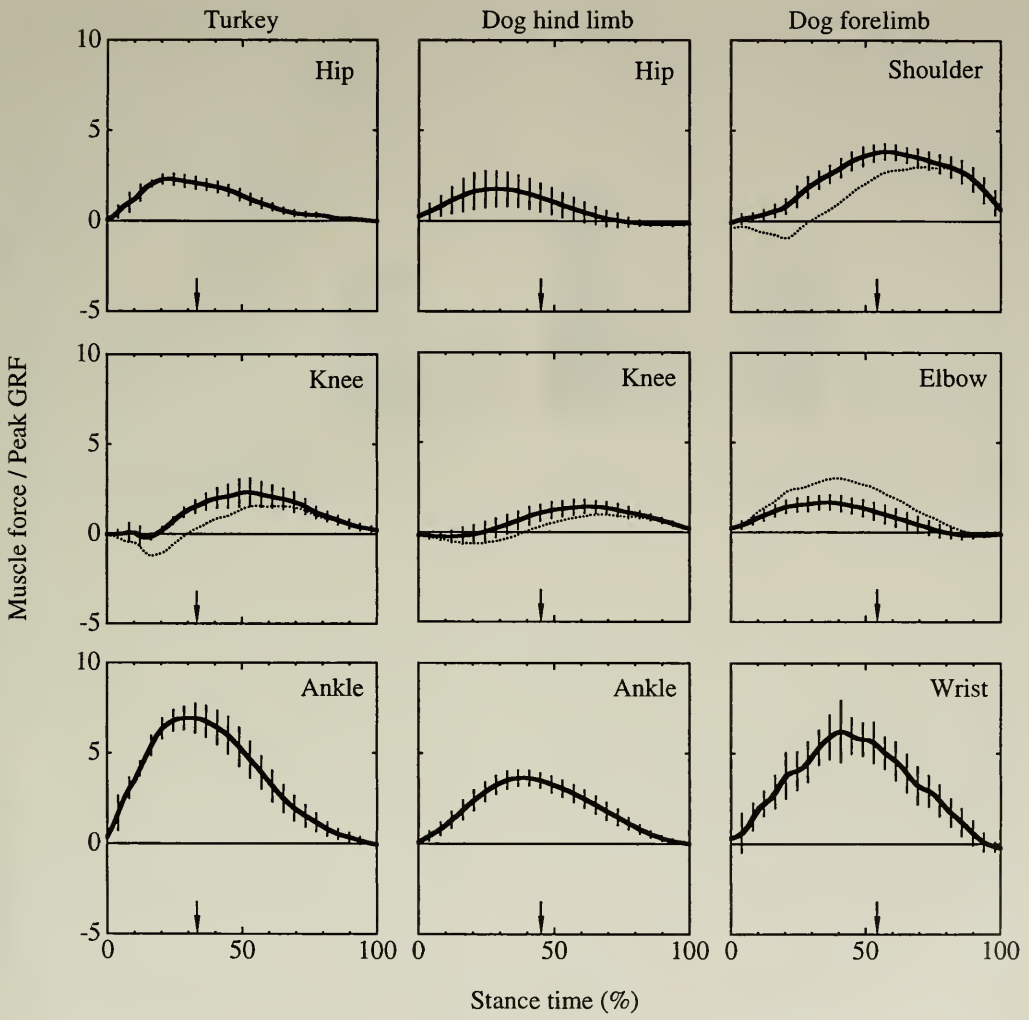

Figure 2. Muscle forces during the stance phase in dogs and turkeys. Muscle force values are normalized to the peak ground reaction force (GRF) developed during the stance phase to give a dimensionless ratio. Solid lines represent the muscle forces necessary to balance the GRF moment and to balance flexor moments produced by two-joint muscles. Dotted lines indicate the muscle forces required to balance GRF moments only. Arrows indicate the time of peak GRF. Means and standard deviations are presented for 12 runs of three animals.

much higher absolute muscle forces at all joints than do dogs (Table 1). At the ankle, for example, turkeys produced muscle forces equivalent to 16.9 × body weight, whereas dogs produce only 3 × body weight with ankle extensor muscles. At the knee and the hip, the differences in muscle cross-sectional area are too small to compensate for the large differences in force, and therefore stresses in turkey muscles are much higher. However, at the ankle, the large difference in muscle cross-sectional area compensates for both the turkey's higher hind limb GRFs and its poorer mechanical advantage; despite a 5.6-fold difference in muscle force, stresses are not significantly different at the ankle in dogs and turkeys.

The speeds measured in this study were approximately 2.0 m/s in the dogs and 3.5

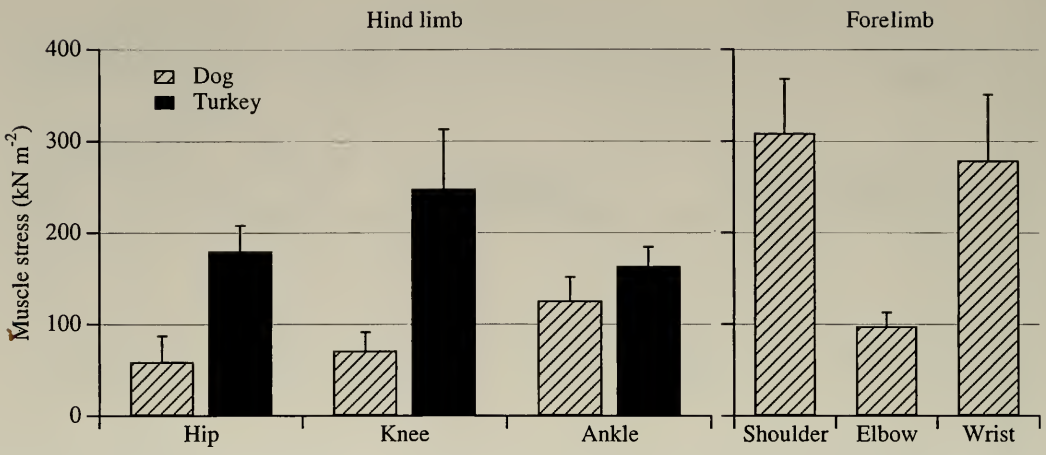

Figure 3. Stress (force/cross-sectional area [A_{cs}]) developed in limb muscles of dogs and turkeys. Stresses are presented for the extensors at the joint indicated, with the exception of the wrist values, which represent flexor stresses. Values are means and standard deviations.

m/s in the turkeys. Despite the large difference in absolute speed, the average GRF developed during stance was similar in the two species, 1.3 ± 0.1 × body weight in the bird and 1.1 ± 0.1 × body weight in the dog. This suggests that the animals were operating at similar duty factors, one of the criteria that has been used to determine equivalent speeds in running mammals (Biewener, 1983). The turkeys were able to run at faster speeds with duty factors similar to those of dogs because they have longer legs. The small difference in average GRF at the speeds used in this study indicates that some of the difference in estimated muscle stress may be due to a 15–20% difference in the magnitude of GRF between the dogs and turkeys.

DISCUSSION

Patterns of Force Development and Limb Design

The results of the present study demonstrate that the timing of muscle force

TABLE 1. MUSCLE FORCE PER UNIT PEAK GROUND REACTION FORCE (GRF), TOTAL GRF AND MUSCLE FORCE IN MULTIPLES OF BODY WEIGHT (BW), MUSCLE CROSS-SECTIONAL AREA (A_{CS}), AND MUSCLE STRESS FOR DOG AND TURKEY HIND LIMBS.

	Muscle force per GRF	Peak GRF per BW	Muscle force per BW	A_{cs} (cm²)	Muscle stress (kN/m²)
Hip					
Turkey	2.3 ± 0.3	2.4 ± 0.2	5.8 ± 0.8	15.9 ± 1.0	180 ± 28
Dog	1.8 ± 1.0	0.8 ± 0.1	1.6 ± 0.8	12.8 ± 2.0	59 ± 28
Ratio	1.3	3.1*	3.6*	1.2	3.1*
Knee					
Turkey	2.3 ± 0.8	2.4 ± 0.2	5.7 ± 2.0	11.0 ± 0.6	248 ± 65
Dog	1.4 ± 0.4	0.8 ± 0.1	1.2 ± 0.3	7.8 ± 0.7	71 ± 20
Ratio	1.6	3.1*	4.8*	1.4*	3.5*
Ankle					
Turkey	6.9 ± 0.7	2.4 ± 0.2	16.9 ± 2.3	50.6 ± 8.4	163 ± 21
Dog	3.6 ± 0.5	0.8 ± 0.1	3.0 ± 0.5	11.4 ± 1.5	125 ± 26
Ratio	1.9*	3.1*	5.6*	4.4*	1.3

* Denotes significant difference between dogs and turkeys, $p < 0.05$.

development is remarkably similar at homologous joints in the hind limbs of dogs and turkeys. This similarity exists despite differences in the timing and magnitude of joint angular excursions in bipedal birds and quadrupedal mammals (Gatesy and Biewener, 1991), as well as differences in limb posture. Both dogs and turkeys produce peak net extensor muscle moments early in the stance phase at the ankle and the hip, and late in the stance phase at the knee. In both species, the knee musculature produces a net flexor moment early in stance, followed by a net extensor moment for approximately the last two thirds of stance phase. The similarity in joint moment timing between animals that have significantly different limb morphology and have independently evolved cursoriality tempts the speculation that this pattern of joint moments is a common feature of hind limb dynamics in runners. However, human runners exhibit patterns of joint moments different from those observed in the present study. In particular, the knee musculature produces an extensor moment throughout stance and a net flexor muscle moment is produced at the hip during the second half of stance phase (Winter, 1983). Also, studies of larger dogs have found that, at the hip, the net muscle extensor moment during early stance is followed by a significant net muscle flexor moment during the second half of stance (Carrier et al., 1998).

The suggestion has been made that the differences in limb posture and joint excursion patterns during locomotion between bipedal birds and quadrupedal mammals are associated with the problem of bipedal support in birds (Storer, 1971; Gatesy, 1990). The horizontally oriented femur in birds allows them to position the point of support under the center of mass during standing or slow movement (Storer, 1971). The present study demonstrates that in turkeys, this difference in limb orientation results in greater muscle moments per unit GRF compared with quadrupedal dogs. However, muscles forces produced per unit GRF were similar at the knee and the hip in dogs and turkeys. Turkeys produced higher joint moments at the knee and hip because they have larger muscle moment arms, rather than higher muscle forces. Thus, differences in musculoskeletal anatomy can compensate for differences in limb posture to achieve similar mechanical advantage for force production. It has recently been demonstrated that the pattern of joint excursions changes markedly with increases in walking or running speed in guinea fowl (Gatesy, 1999a). There appears to be little change with speed in the average mechanical advantage with which muscles generate force in running quadrupedal mammals (Biewener, 1989), but it remains to be seen whether significant changes in the pattern of force development occur across speed in running bipeds.

Biarticular Muscles and Joint Moment Patterns

Several functional advantages have been proposed for muscles that articulate across two or more joints. Two-joint muscles can operate to maintain a uniform length due to compensating displacements at two joints (Goslow et al., 1973; McClearn, 1985), and can function to transfer power from distal to proximal limb segments (Gregoire et al., 1984). It has also been shown that two-joint muscles play an important role in controlling the orientation of the GRF during various movements in humans (Jacobs and van Ingen Schenau, 1992; van Ingen Schenau et al., 1992). At the same time, it can be argued that most biarticular muscles are energetically disadvantageous because they produce flexor forces that must be balanced by cocontraction of antagonist extensor muscles. The present results suggest that two-joint muscles, in both birds and dogs, provide an important mechanism for balancing alternating flexion and extension moments at a joint. The flexor moments produced at the knee in dogs and turkeys appear to be quantitatively matched to the knee flexion

forces contributed by biarticular hip and ankle extensors (Fig. 2). Thus, early in stance biarticular muscles at the knee produce force that supports body weight at both the joint they act to extend (hip or ankle) and the joint they act to flex. The long head of triceps brachii also appears to function early in stance to provide support through both its flexor function at the shoulder and its extensor function at the elbow. Later in the stride biarticular muscles tend to increase the extensor force required at the knee and shoulder. However, electromyographic studies indicate that most of the biarticular muscles considered in the present study are most active early in stance in dogs (Tokuriki, 1973; Goslow et al., 1981), allowing for the possibility that energetically disadvantageous cocontraction may be reduced during the second half of the stance phase. It may be that the important role that biarticular muscles appear to play in maintaining the proper orientation of the GRF (Jacobs and van Ingen Schenau, 1992; van Ingen Schenau et al., 1992) explains in part the similarity in joint moment patterns at the knee in dogs and turkeys.

Muscle Stress and Strategies for Force and Power Development

Many of the muscle stresses estimated in the present study are near the upper end of the range of muscle stresses typically measured in vitro for vertebrate skeletal muscle. Peak isometric stress measurements typically range from 100 to 300 kN/m^2 (Josephson, 1993). Muscles can develop stresses above peak isometric when actively lengthening (Katz, 1939), and stress is reduced as relative shortening velocity increases (Hill, 1938). Thus, differences in muscle stress between joints are proportional to differences in fraction of recruited cross-sectional area only if the muscles are operating at similar relative shortening velocities. The high stresses estimated in the present study at the knee of the turkey and the wrist and shoulder of the dog suggest that these muscles may be operating near their limit of force production, or undergoing sufficient lengthening to operate at high active muscle stresses. Stresses measured at the wrist likely overestimate actual muscle stresses, because some of the wrist moment is balanced by force produced in stretched ligaments (Alexander, 1974). Shoulder stress measurements may also overestimate actual muscle stress if moments due to limb inertia are significant. Previous measurements of stresses in running quail reported lower values than those reported here for turkeys (80–100 kN/m^2; Clark and Alexander, 1975). However, the low speed and GRF (approximately 1.3 × body weight peak GRF) measured in quail make direct comparison of stress values with the present study difficult. It is important to note that the present measurements of muscle cross-sectional areas do not account for the volume of noncontractile elements within muscle (mitochondria, capillaries, and so on), which can be as much as 40% of the muscle volume in bird pectoralis muscle (James and Meek, 1979; Conley et al., 1987). Differences in noncontractile element components between muscles or between species represent a potential source of error in comparisons of muscle stress. However, the variation in volume of nonmyofibrillar components between these largely oxidative muscles is unlikely to be very large, and could not account for the several-fold differences in muscle stress found between muscle groups within dogs and between dogs and turkeys.

The similar stress hypothesis for muscle was originally formulated upon the idea that animals should operate their limb muscles with the same reserve capacity for force development at equivalent speeds (Perry et al., 1988). The hypothesis was supported by observations of similar stress in the ankle extensors in a bipedal hopper, the kangaroo rat, and a quadrupedal runner, the white rat (Perry et al., 1988). The similar scaling of locomotor forces and muscle cross-sectional area across body size also supports the similar stress hy-

pothesis (Biewener, 1990). The results from the present study for the ankle joint provide another example of how large differences in muscle morphology can compensate for differences in muscle forces to produce similar stress in different animals. However, a comparison of stresses between joints in the dog reveals that the similar stress hypothesis is not supported for comparisons between different muscle groups operating at different joints.

Why do some muscle groups operate with a greater reserve capacity for force development (i.e., low stress) during running? This variation in reserve capacity may reveal a specialization of some muscles for locomotor activities that involve high mechanical power outputs. The cross-sectional area of active muscle required to produce force during high-power–output activities such as acceleration, jumping, or incline running can be greater than that required during level running because of an increase in GRF or a change in muscle mechanical advantage. Perhaps more importantly, the cross-sectional area of active muscle must also increase if the relative shortening velocity of the muscle increases, as has been demonstrated for the lateral gastrocnemius muscle in turkeys running on an incline (Roberts et al., 1997). It might be expected that muscle groups that operate with a high reserve capacity during level running are the most important power producers during acceleration or jumping. It has been generally assumed that it is the muscles that articulate between the limb and the body (extrinsic muscles), and particularly those in the hind limb, that are the primary sources of power for acceleration (Gray, 1968). Likewise, it has been shown that jumping dogs produce the greatest muscle work and power at the hip with a smaller contribution at the knee and almost no change in ankle muscle function from running to jumping (Alexander, 1974). Alexander (1974) suggested that differences in muscle architecture in proximal versus distal muscles reflects a specialization for power versus force development. The large mass of largely parallel-fibered muscles located proximally in the limb is well suited to providing high power outputs, whereas the short pinnate fibers of the ankle in conjunction with their long tendons function well as springs (Alexander, 1974).

If differences in muscle stress between joints reflect specializations of different muscle groups for power versus force development, then a comparison of muscle stresses in dogs and turkeys may provide insight into how avian and mammalian limbs are designed to provide work for high-power activities. Turkeys operate with the same reserve capacity for force at the hip and the ankle. Furthermore, the muscle mass distribution is strikingly different in birds compared with mammals. The muscle mass available to extend the ankle in birds is greater than that available to extend the hip (compared with a hip muscle mass greater than three times the ankle muscle mass in dogs; Roberts et al., 1998). The mechanical power that can be developed at a joint is proportional to the muscle mass (assuming equivalent muscle properties); thus the large muscle mass at the ankle in birds represents a significant potential source of power for movement. The present measurements of muscle stress suggest that turkeys may power accelerations and jumps as much with the ankle musculature as with the hip. In fact, measurements of turkeys running uphill suggest that the gastrocnemius increases muscle shortening, recruitment, and power output to provide the power to run uphill (Roberts et al., 1997). Thus, differences in muscle mass distribution and limb design between running birds and mammals may reflect differences in strategies for powering accelerations, rather than differences in muscle function during steady-speed running.

ACKNOWLEDGMENTS

I thank M. S. Chen for help with experiments and data analysis, and the late C. R. Taylor for his help and support with

the project. The project was supported in part by National Institutes of Health grant RO1 AR18140.

LITERATURE CITED

Alexander, R. McN. 1974. The mechanics of jumping by a dog (*Canis familiaris*). Journal of Zoology, London, **173:** 549–573.

Biewener, A. A. 1983. Allometry of quadrupedal locomotion: the scaling of duty factor, bone curvature and limb orientation to body size. Journal of Experimental Biology, **105:** 147–171.

———. 1989. Scaling body support in mammals: limb posture and muscle mechanics. Science, **245:** 45–48.

———. 1990. Biomechanics of mammalian terrestrial locomotion. Science, **250:** 1097–1103.

Biewener, A. A., R. Blickhan, A. K. Perry, N. C. Heglund, and C. R. Taylor. 1988. Muscle forces during locomotion in kangaroo rats: force platform and tendon buckle measurements compared. Journal of Experimental Biology, **137:** 191–205.

Carrier, D. R., C. S. Gregersen, and N. Silverton. 1998. Dynamic gearing in running dogs. Journal of Experimental Biology, **201:** 3185–3195.

Clark, J. and R. McN. Alexander. 1975. Mechanics of running quail (*Coturnix*). Journal of Zoology, London, **176:** 87–113.

Conley, K. E., S. R. Kayar, K. Rosler, H. Hoppeler, E. R. Weibel, and C. R. Taylor. 1987. Adaptive variation in the mammalian respiratory system in relation to energetic demand. IV. Capillaries and their relationship to oxidative capacity. Respiration Physiology, **69:** 47–64.

Gatesy, S. M. 1990. Caudofemoral musculature and the evolution of theropod locomotion. Paleobiology, **16:** 170–186.

———. 1999a. Guineafowl hind limb function. I: cineradiographic analysis and speed effects. Journal of Morphology, **240:** 115–125.

———. 1999b. Guineafowl hind limb function. II: electromyographic analysis and motor pattern evolution. Journal of Morphology, **240:** 127–142.

Gatesy, S. M., and A. A. Biewener. 1991. Bipedal locomotion: effects of speed, size and limb posture in birds and humans. Journal of Zoology, London, **224:** 127–147.

Goslow, G. E. J., R. E. Reinking, and D. G. Stuart. 1973. The cat step cycle: hind limb joint angles and muscle lengths during unrestrained locomotion. Journal of Morphology, **141:** 1–42.

Goslow, G. E., H. J. Seeherman, C. R. Taylor, M. N. McCutchin, and N. C. Heglund. 1981. Electrical activity and relative length changes of dog limb muscles as a function of speed and gait. Journal of Experimental Biology, **94:** 15–42.

Gray, J. 1968. Animal Locomotion. New York: W. W. Norton and Company. vii + 479 pp.

Gregoire, L., H. E. Beeger, P. A. Huijing, and G. J. van Ingen Schenau. 1984. Role of mono- and bi-articular muscles in explosive movements. International Journal of Sports Medicine, **5:** 301–305.

Hill, A. V. 1938. The heat of shortening and the dynamic constants of muscle. Proceedings of the Royal Society of London, B, **126:** 136–195.

Jacobs, R., and G. J. van Ingen Schenau. 1992. Control of external force in leg extensions in humans. Journal of Physiology, **457:** 611–626.

Jacobson, R. D., and M. Hollyday. 1982. A behavioral and electromyographic study of walking in the chick. Journal of Neurophysiology, **48:** 238–256.

James, N. T., and G. A. Meek. 1979. Stereological analyses of the structure of mitochondria in pigeon skeletal muscle. Cell Tissue Research, **202:** 493–503.

Josephson, R. K. 1993. Contraction dynamics and power output of skeletal muscle. Annual Review of Physiology, **55:** 527–546.

Katz, B. 1939. The relation between force and speed in muscular contraction. Journal of Physiology, **96:** 45–64.

Kram, R., and C. R. Taylor. 1990. Energetics of running: a new perspective. Nature, **346:** 265–267.

McClearn, D. R. 1985. Anatomy of raccoon (*Procyon lotor*) and coati (*Nasua narica* and *N. nasua*) forearm and leg muscles: relations between fiber length, moment-arm length, and joint-angle excursion. Journal of Morphology, **83:** 87–115.

Pandy, M. G., V. Kumar, N. Berme, and K. J. Waldron. 1988. The dynamics of quadrupedal locomotion. Journal of Biomechanical Engineering, **110:** 230–237.

Perry, A. K., R. Blickhan, A. A. Biewener, N. C. Heglund, and C. R. Taylor. 1988. Preferred speeds in terrestrial vertebrates: are they equivalent? Journal of Experimental Biology, **137:** 207–219.

Roberts, T. J., M. S. Chen, and C. R. Taylor. 1998. Energetics of bipedal running II: limb design and running mechanics. Journal of Experimental Biology, **201:** 2753–2762.

Roberts, T. J., R. L. Marsh, P. G. Weyand, and C. R. Taylor. 1997. Muscular force in running turkeys: the economy of minimizing work. Science, **275:** 1113–1115.

Storer, R. W. 1971. Adaptive radiation in birds, 149–188. *In* D. S. Farner and J. R. King (eds.), Avian Biology. New York: Academic Press. xiii + 586 pp.

Tokuriki, N. 1973. Electromyographic and joint-mechanical studies in quadrupedal locomotion II: trot. Japanese Journal of Veterinary Science, **35:** 525–535.

VAN INGEN SCHENAU, G. J., P. J. M. BOOTS, G. DE GROOT, R. J. SNACKERS, AND W. W. L. M. VAN WOENSEL. 1992. The constrained control of force and position in multi-joint movements. Neuroscience, **46:** 197–207.

WALMSLEY, B., J. A. HODGSON, AND R. E. BURKE. 1978. Forces produced by medial gastrocnemius and soleus muscles during locomotion in freely moving cats. Journal of Neurophysiology, **41:** 1203–1216.

WINTER, D. A. 1983. Moments of force and mechanical power in jogging. Journal of Biomechanics, **16:** 91–97.

———. 1990. Biomechanics and Motor Control of Human Movement, 2nd Edition. New York: John Wiley & Sons. 296 pp.

REGULATION OF SKELETAL MUSCLE REGENERATION AND BONE REPAIR IN VERTEBRATES

URI ORON[1]

ABSTRACT. The aim of the present study was to investigate the effect of low-energy laser irradiation (LELI) on the process of skeletal muscle regeneration and bone repair in toads and rats. Defined injuries (partial excision or cold injury) to the gastrocnemius muscle and hole injury to the tibia in rats were performed. The rate of regeneration in skeletal muscles was analyzed by quantitative histomorphometric methods, and bone repair was determined using histomorphometric methods. Low-energy laser irradiation (He-Ne laser) was applied directly to the injured sites for 2 minutes at different time intervals postinjury. The rate of skeletal muscle regeneration was enhanced two- and eightfold in the rat and toad, respectively, whereas bone repair was enhanced twofold by the LELI. Although mechanism of the laser irradiation is not yet clearly understood, it is associated with gene activation in the cell and the triggering of a cascade of intracellular events initiating changes in physiologic processes in the cell.

INTRODUCTION

The process of skeletal muscle regeneration after injury has been well documented and reviewed in mammals (Allbrook, 1981; Carlson and Faulkner, 1983), and to a much lesser extent in amphibians (Carlson, 1970). The possible regulatory mechanisms associated with the process of muscle regeneration, and the stimulation of the dormant satellite cells after injury are not yet fully understood.

Osteogenesis and bone repair after trauma are regulated by such mechanisms as growth factors and hormones, among others (Marks and Popoff, 1988). Several experimental models have followed the healing of osseous defects (usually fractures) in long bones in rats (Markel et al., 1991). In other models, bone repair was investigated in the medullary cavity of the tibia after ablation or removal of marrow from long bones. In this model, regeneration was found to be preceded by a local phase of endosteal bone formation (Liang et al., 1992). Promotion of the process of bone repair has been achieved in the past by autogenous bone grafting, application of various growth factors (mainly bone morphogenetic proteins [Spencer et al., 1991]), use of low-intensity pulsed ultrasound and electromagnetic fields (Cane et al., 1993), and by low-energy laser irradiation (LELI) in vivo (Kusakari et al., 1992).

Low-energy laser irradiation has recently been found to modulate various biological processes in tissue cultures and animal models (Belkin et al., 1988; Karu, 1989, 1998; Galletti et al., 1992; Conlan et al., 1996). For example, laser irradiation was found to increase mitochondrial respiration and adenosine triphosphate (ATP) synthesis (Morimoto et al., 1994; Zhu et al., 1997) and to modulate oxidative metabolism in the mitochondria (Yu et al., 1997). Low-energy laser irradiation also was demonstrated to elevate activity of antioxidant enzymes such as superoxide dismutase and catalase (Zhu et al., 1997) and to enhance nitric oxide (NO) production in rat lymphocytes (Chi et al., 1995). The biostimulatory effect of LELI was also investigated in several experimental animal models after injury. Helium–neon laser irradiation was demonstrated to elevate compound action potential after crush in-

[1] Department of Zoology, George S. Wise Faculty of Life Sciences, Tel Aviv University, Ramat Aviv 69978, Israel.

jury to the ischiadic nerve (Rochkind et al., 1987), as well as slow Wallerian degeneration in the injured optic nerve (Schwartz et al., 1987; Assia et al., 1989). The inflammatory response after cold injury to toad muscle also was demonstrated to be markedly decreased by laser irradiation (Bibikova and Oron, 1993), and neoformation of blood vessels in the injured zone was demonstrated to be elevated by laser irradiation (Bibikova et al., 1994). Recently, we have shown that LELI causes induction of cell cycle regulatory proteins in satellite cells from skeletal muscles due to activation of early cell cycle regulatory genes (Ben-Dov et al., 1999).

The aim of the present study was to investigate the effect of LELI on skeletal muscle regeneration in rats and toads and bone repair in rats.

MATERIALS AND METHODS

Surgical Procedures

Forty-nine male toads (*Bufo viridis*) and 30 mature male laboratory rats (Charles River) were used for the experiments. Partial excision to the gastrocnemius muscle of the rats was performed as previously described (Roth and Oron, 1985). Cold injury to the toads' muscles was performed by placing the end of a copper rod (1.8-mm diameter), prechilled in liquid nitrogen, against the muscle for 10 seconds. This created an injured zone of about 4 mm in diameter. Four to six injured experimental (laser-irradiated) and control (injured and irradiated by red light) toads or rats were used for each time interval (9, 14, and 30 days for toads; 3, 8, and 11 days for rats) postinjury. In brief, after removal of the skin and biceps femoris muscle the gastrocnemius was exposed. A special device with two fixed scalpel blades was applied to create a fixed excision (5 × 2 mm) in the middle part of the lateral belly of the gastrocnemius muscle. The biceps femoris and the skin were then closed.

Surgery to create a fixed injury to the tibia was performed on a total of 52 mature (3–4 months old, 300–350 g body weight) Sprague-Dawley male rats (Levinstein Inc., Yoknean, Israel). Rats were anesthetized with Avertin (1 ml/100 g body weight intraperitoneally). A longitudinal incision was made through the skin and muscles to expose the tibia on its proximal and medial surfaces about 10–15 mm distal to the knee joint. A hole was drilled in the cortical bone of the tibia in the center of its medial aspect about 9 mm distal to the knee joint (diaphyseal region) using hand-driven dental drills of increasing diameter in order to obtain a final hole diameter of 1.6 mm. The hole was created in such a manner as to penetrate the cortical bone and damage the trabeculae in the medullary canal, but not to damage the contralateral cortical bone. Care was taken not to injure the periosteum in the vicinity of the hole. After the muscles and skin were sutured, the rats were injected intramuscularly with Penicillin G Sodium (Teva, Petach-Tikva, Israel) at a dose of 100 U/g body weight, followed by 3 days of bioxin (Solmycin 500, Teva, Petach-Tikva, Israel) in the drinking water (1 g/L). In the above model a spontaneous partial healing of the gap injury (probably due to its low diameter relative to the tibia width) occurs at about 3 weeks after injury, and a complete healing occurs at longer time intervals.

Laser Irradiation

An He-Ne laser (Ealing, Electro-Optics, Holliston, Massachusetts, USA) was employed at 632 nm, 5.3-mW power output, and 1.9-mm beam diameter. Laser irradiation was always applied directly on the injured zones of the skeletal muscles of the toads and rats after removal of the skin and muscle. In order to cover the total area of the injured zone (which was larger than the laser beam diameter) in the muscles, the laser was applied several times to each of the visibly injured zones. Laser irradiation to toad injured zones in the muscles was applied every alternate day, from 4 days until 14 days post–cold injury, for

2.3 minutes each time (31 J/cm^2). Laser irradiation to the rats' skeletal muscles was applied as for the toad, but only on the second and third day postinjury. In the case of the hole injury in the tibia, laser irradiation was applied on days 5 and 6 postinjury once a day for 2.3 minutes (31 J/cm^2) directly on the hole injury after careful removal of the sutures in the skin and muscles above it. In all control (sham-operated) experimental animals, the laser was applied but was not connected to a power source.

Histology and Histomorphometry

At various time intervals postinjury the rats were anesthetized with chloroform, and the gastrocnemius muscle exposed, removed, fixed in Bouin's fixative, and embedded in paraffin. Serial sections were prepared from each muscle and stained with hematoxylin and eosin and Masson's trichrome stain. Morphometric measurements were performed on the entire injured zones of four to six randomly chosen sections per each muscle, using the point mounting method. The volume fraction (% of the total volume of injured zone) was calculated for each of the structures analyzed. The results were finally statistically analyzed using the three-level nested analysis of variance.

Injured tibial bone from six rats was taken at each time interval (10, 13, and 15 days) postinjury. This bone was fixed, decalcified, and processed for histology as described above. Histomorphometry was performed to determine the area fraction of various structures (woven bone, compact bone, and so on) in the gap created in the tibia out of the total area of the gap (injured) zone. This process was performed with a microscope and the aid of a video camera and screen using Sigma Scan software.

RESULTS

The process of muscle regeneration in control muscles after cold injury was characterized by sequential changes in the volume fraction of typical structures such as mononucleated cells, myotubes, and young myofibers in the injured area. The laser irradiation during the process of muscle regeneration caused a significant change in the volume fraction of these structures in the traumatized area at all time intervals after injury. Young myofibers populated 15.5 ± 7.9% and 65.0 ± 9.5% of the muscle regenerates in the injured zone in the laser-irradiated toad muscles at 9 and 14 days, respectively; whereas in control nonirradiated muscle regenerates young myofibers were not evident at 9 days postinjury, and comprised only 5.3 ± 2.9% of the area at 14 days (Figs. 1, 2a). The process of muscle regeneration in toads was almost completed after 30 days (90% of the regenerated area was occupied by mature muscle fibers) in the laser-treated muscles, whereas in control muscles only young myofibers still populated a large part (75.7 ± 13.2%) of the injured zone (Fig. 2b). In the case of the rat gastrocnemius muscle, young myofibers were not evident in the injured zone of either experimental or control muscles at 3 days postinjury. Their volume fraction was twofold significantly higher in LELI-treated rat muscles as compared to control muscles at 8 and 11 days postsurgery, respectively (data not shown).

The morphometric analysis of the tissue components of the hole in the rat tibia indicated that at all time intervals (10, 13, and 15 days) the relative areas occupied by compact bone in the hole injury were higher in the LELI-treated rats than in the control (Figs. 3, 4). At 15 days postinjury to the tibia, this value comprised 92 ± 9% in the LELI-treated rats, which was significantly ($P < 0.01$) higher than the area that the compact bone occupied (58 ± 8%) in the control nonirradiated rats.

DISCUSSION

The results of the present study clearly indicate that the process of muscle regeneration after partial excision injury or cold injury is markedly promoted by direct ex-

Figure 1. Light micrographs of regenerated area in control nonirradiated (a) and laser-irradiated (b) toad gastrocnemius muscle 14 days postinjury. Note mainly myotubes (MT) and mononucleated (MN) cells in (a) as compared to mainly young myofibers (YU) with large diameter in (b). ×40.

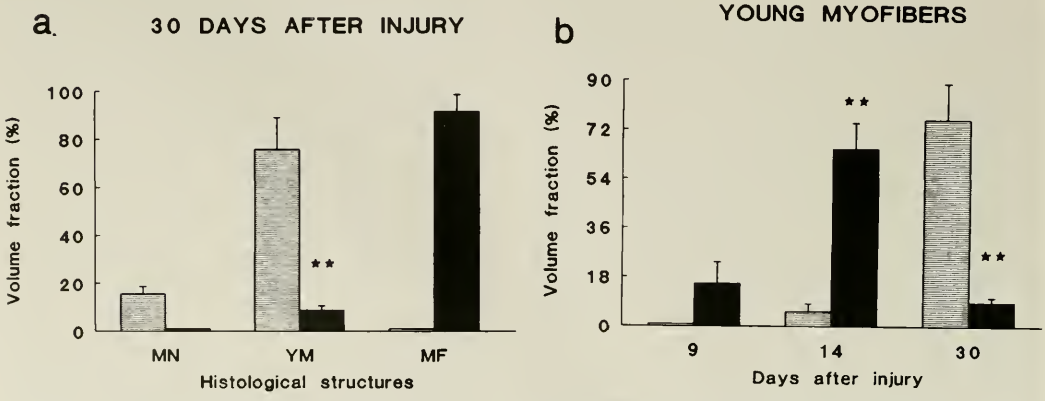

Figure 2. Volume fraction of young myofibers at various time intervals post–cold injury to the toad gastrocnemius muscle injury (a) and of mononucleated cells (MN), young myofibers (YM), and mature myofibers (MF) at 30 days postinjury (b). Values are mean ± SEM of control nonirradiated (dashed columns) and laser-irradiated (solid columns) muscles.

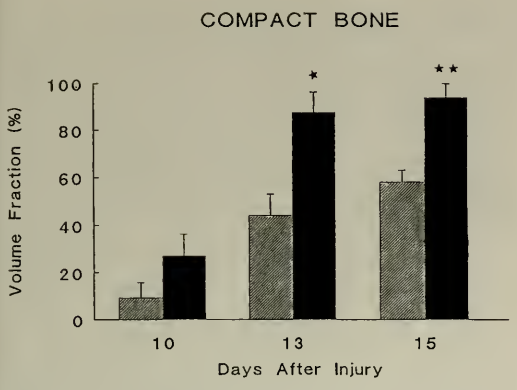

Figure 3. Volume fraction of compact bone at the site of injury to the rat tibia at different time intervals postinjury. Note less compact bone in the control nonirradiated rats (dashed columns) as compared to low-energy laser–irradiated rats (solid columns). $*P < 0.05$; $**P < 0.01$.

posure to He-Ne laser irradiation (during the regeneration process) in both toads and rats, although in the toads the promotion effect was higher. We have recently shown that LELI promotes proliferation of satellite cells from skeletal muscle origin grown in culture (Ben-Dov et al., 1999). These cells are considered to be the stem cells for muscle regeneration and, therefore, their enhanced proliferation by LELI in vitro may explain the enhanced kinetics of regeneration in vivo, as demonstrated in the present study. Because we have previously found that LELI also promotes new blood vessel formation (angiogenesis) at the site of skeletal muscle regeneration (Bibikova et al., 1994), it might be postulated that a better oxygen and nutrient supply will also contribute to enhancement of the regeneration. Assia et al. (1989) suggested that in the case of optic nerve regeneration after crush injury, LELI acts to slow degenerative processes rather than promoting regeneration, and that the effect of laser irradiation is transient and subsides markedly when irradiation ceases. In the present work, the effect of laser irradiation was not transient because the amount of newly formed young myofibers was twofold higher in the injured zone of experimental rats after two subsequent laser irradiations. Tissue reaction to injury in cranial nerves and skeletal muscles is most probably entirely different and they may react differently to laser irradiation. The results of the present study also indicate

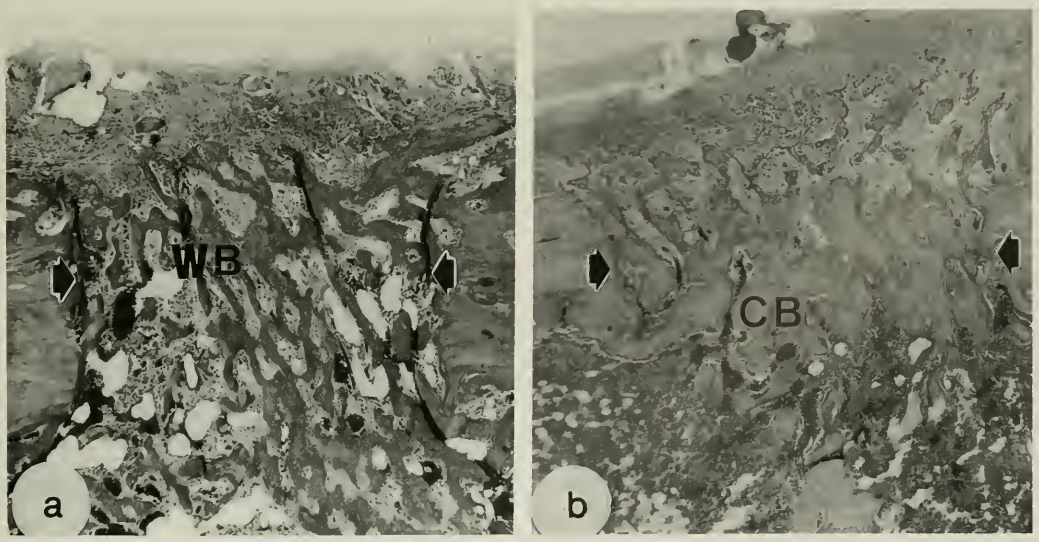

Figure 4. Light micrographs of longitudinal section of the injured zone in the tibia of control (a) and laser-irradiated (b) rat at 13 days postinjury. Note the gap in the tibia (marked by arrows) that is filled only with woven bone (WB) in the control nonirradiated rat and partially filled with compact bone (CB) that bridges the gap in the laser-irradiated rat. ×120.

that LELI may promote, to a much higher extent, biological processes in cells with lower metabolic rates such as in the toads (as compared to the rats). These results corroborate the notion that during a high state of metabolism and proliferation, cells are affected to a lesser extent by laser irradiation (Karu, 1989, 1998).

This communication also indicates by direct measurements that the rate of bone repair in the cortical part of the tibia in an experimental model in the rat is enhanced by LELI. Kusakari et al. (1992) previously reported stimulation of DNA and protein synthesis, and alkaline phosphatase activity in osteoblastlike tissue culture by LELI. These results corroborate the results of the present study indicating that the enhancement of bone repair may be caused by enhanced proliferation of osteoblasts at the injured site.

The present study demonstrates that LELI can promote skeletal muscle regeneration as well as bone repair, indicating that the biostimulation may have a common mechanism that triggers certain cell processes that, in turn, will enhance cell proliferation and differentiation in the skeletal tissues. Thus, it may be hypothesized that the mechanism of biostimulation by LELI may be general for various tissues and in different groups of vertebrates. However, parameters such as energy, wavelength, and timing of laser may differ for different tissues and according to the physiologic state of the cells to be biostimulated.

The precise regulatory mechanisms associated with biostimulatory effects of LELI are not yet fully understood. Laser irradiation probably induces changes in cellular homeostasis, initiating a whole cascade of reactions. A number of respiratory chain components (i.e., cytochromes, flavine dehydrogenases, and so on) may be primary photoacceptors or chromophores of laser photons and thus able to absorb laser light at the proper wavelengths. This causes short-term activation of the respiratory (cytochrome) chain that, in turn, enhances synthesis of ATP. Changes in plasma membrane conduction and transient increase of calcium flux into the cells have also been observed in cells irradiated in vitro by low energy lasers (Lubart et al., 1997). These changes are photochemical in nature; the energy is probably absorbed in intracellular chromophores and converted into metabolic energy involving the respiratory (cytochrome) chain (Karu, 1989, 1998; Galletti et al., 1992).

We have recently shown (Ben-Dov et al., 1999) that LELI causes induction of cell cycle regulatory proteins in satellite cells from skeletal muscles, due to activation of early cell cycle regulatory proteins. Furthermore, it was recently found (unpublished data, this laboratory) in the same system that LELI induces activation of receptors on the cell plasma membrane and other components associated with cell proliferation (kinase enzymatic activity) in a certain signal transduction pathway in the cell. Thus, it may be postulated that the LELI biostimulates the cell via certain mechanisms at the molecular level. However, the precise interaction of the laser irradiation with cellular components or molecules that trigger a cascade of intracellular processes that eventually lead to changes in physiologic processes in the cells will have to be elucidated by further studies.

LITERATURE CITED

ALLBROOK, D. 1981. Skeletal muscle regeneration. Muscle and Nerve, **4:** 234–245.

ASSIA, E. M., M. ROSNER, M. BELKIN, A. SOLOMON, AND M. SCHWARTZ. 1989. Temporal parameters of low energy laser irradiation for optimal delay of post traumatic degeneration of rat optic nerve. Brain Research, **476:** 205–212.

BELKIN, M., B. ZATURUNSKY, AND M. SCHWARTZ. 1988. A critical review of low energy laser bioeffects. Laser Light Ophthalmology, **2:** 63–71.

BEN-DOV, N., G. SHEFER, A. IRINTCHIEV, A. WERNIG, U. ORON, AND I. O. HALEVY. 1999. Low energy laser irradiation affects cell proliferation and differentiation in vitro. Biochimica et Biophysica Acta, **1448:** 372–380.

BIBIKOVA, A., A. BELKIN, AND U. ORON. 1994. Enhancement of angiogenesis in regenerating gastrocnemius muscle of the toad (*Bufo viridis*) by

low energy laser irradiation. Anatomy and Embryology, **190:** 597–602.

Bibikova, A., and U. Oron. 1993. Promotion of muscle regeneration in the toad (*Bufo viridis*) gastrocnemius muscle by low energy laser irradiation. Anatomical Record, **235:** 374–380.

Cane, V., P. Botti, and S. Soana. 1993. Pulsed magnetic fields improve osteoblast activity during the repair of an experimental osseous defect. Journal of Orthopaedic Research, **11:** 664–670.

Carlson, B. M. 1970. Histological observations in the regeneration of mammalian and amphibian muscle, and myogenesis, pp. 38–74. *In* A. Mauro, S. A. Shafiq, and A. T. Milhorat (eds.), Regeneration of Striated Muscle, and Myogenesis; Proceedings of the International Conference convened by the Muscular Dystrophy Associations of America at the Institute of Muscle Disease, New York, March 28–29, 1969. Amsterdam: Excerpta Medica. x + 299 pp.

Carlson, B. M., and J. A. Faulkner. 1983. The regeneration of skeletal muscle fiber following injury. A review. Medical Sciences in Sports and Exercise, **15:** 107–198.

Chi, L. H., W. Yu, J. O. Naim, and R. J. Lanzafame. 1995. Increased synthesis of nitric oxide by laser irradiation in sepsis. Lasers in Surgery and Medicine, **7**(Suppl.): 19.

Conlan, M. J., J. W. Rapley, and C. M. Cobb. 1996. Biostimulation of wound healing by low energy laser irradiation. A review. Journal of Clinical Periodontics, **23:** 492–496.

Galletti, G., L. Bolognani, and G. Ussia. 1992. Laser Applications in Medicine and Surgery. Bologna: Monduzzi Editore. 552 pp.

Karu, T. 1989. Photobiology of low power laser effects. Health Physics, **56:** 691–704.

Karu, T. 1998. Photobiology of Low Power Laser Therapy. Amsterdam: Gordon and Breach Publications. 282 pp.

Kusakari, H., N. Orisaka, and H. Tani. 1992. Effects of low lasers on wound healing of gingiva and bone, pp. 49–56. *In* G. Galletti, L. Bolognani, and G. Ussia (eds.), Laser Applications in Medicine and Surgery. Bologna: Monduzzi Editore. 552 pp.

Liang, C. T., J. Barnes, J. G. Seeder, H. A. Quartuccio, M. Bolander, J. J. Jeffrey, and G. A. Rodan. 1992. Impaired bone activity in aged rats: alternation and the cellular and molecular levels. Bone, **13:** 435–441.

Lubart, R., H. Friedman, N. Grossman, N. Cohen, and H. Breitbart. 1997. Reactive oxygen species and photobiostimulation. Trends in Photobiology, **4:** 277–283.

Markel, M. D., M. A. Wikenheiser, and E. Y. S. Chao. 1991. Formation of bone in tibial defects in a canine model. Journal of Bone and Joint Surgery, **73A:** 914–923.

Marks, S. C., and S. N. Popoff. 1988. Bone cell biology: the regulation of development structure and function in the skeleton. American Journal of Anatomy, **183:** 1–44.

Morimoto, Y., T. Arai, M. Kikuchi, S. Nakajima, and H. Nakamura. 1994. Effect of low intensity argon laser irradiation on mitochondria respiration. Lasers in Surgery and Medicine, **15:** 191–199.

Rochkind, S., L. Barr Nea, A. Bartal, M. Nissan, R. Lubart, and N. Razon. 1987. New methods of treatment of severely injured sciatic nerve and spinal cord. Acta Neurochirurgia, **43:** 91–93.

Roth, D., and U. Oron. 1985. Repair mechanisms involved in muscle regeneration following partial excision of the rat gastrocnemius muscle. Experimental Cell Biology, **53:** 107–114.

Schwartz, M., A. Doron, M. Ehrlich, V. Lovic, S. Benbasat, M. Belkin, and S. Rochkind. 1987. Effect of low energy He-Ne laser irradiation on post traumatic degeneration of adult rabbit optic nerve. Lasers in Surgery and Medicine, **7:** 51–55.

Spencer, F. M., C. C. Liu, R. C. C. Si, and G. A. Howard. 1991. In vivo action of insulin-like growth factor 1 (1GF-1) on bone formation and resorption in rats. Bone, **12:** 21–26.

Yu, W., M. McGowan, K. Ippolito, and R. J. Lanzafame. 1997. Photomodulation of oxidative metabolism and electron chain enzymes in rat liver mitochondria. Photochemistry Photobiology, **66:** 866–871.

Zhu, Q., W. Yu, X. Yang, G. L. Hicks, R. J. Lanzafame, and T. Wang. 1997. Photo-irradiation improved functional preservation of the isolated rat heart. Lasers in Surgery and Medicine, **20:** 332–339.